



Effects of global changes on microbioeroding communities living in massive corals from the Western Indian Ocean over long term

Diego Alaguarda

► To cite this version:

Diego Alaguarda. Effects of global changes on microbioeroding communities living in massive corals from the Western Indian Ocean over long term. Ocean, Atmosphere. Sorbonne Université, 2023. English. NNT : 2023SORUS237 . tel-04227119

HAL Id: tel-04227119

<https://theses.hal.science/tel-04227119>

Submitted on 3 Oct 2023

HAL is a multi-disciplinary open access archive for the deposit and dissemination of scientific research documents, whether they are published or not. The documents may come from teaching and research institutions in France or abroad, or from public or private research centers.

L'archive ouverte pluridisciplinaire **HAL**, est destinée au dépôt et à la diffusion de documents scientifiques de niveau recherche, publiés ou non, émanant des établissements d'enseignement et de recherche français ou étrangers, des laboratoires publics ou privés.



THÈSE DE DOCTORAT
DE SORBONNE UNIVERSITÉ

Spécialité : Océanographie Biologique - Écologie Récifale

École doctorale : Sciences de l'Environnement d'Île-de-France

réalisée au

Laboratoire d'Océanographie et du Climat
Expérimentations et Approches Numériques

présentée par

Diego ALAGUARDA

pour obtenir le grade de

DOCTEUR DE SORBONNE UNIVERSITÉ

Effects of Global Changes on Microbioeroding Communities Living in Massive Corals from the Western Indian Ocean Over Long Term.

date de soutenance prévue le 29 Juin 2023

devant le **jury** composé de

Pr. Damien CARDINAL

Pr. Max WISSHAK

Dr. Paolo MONTAGNA

Dr. Aline TRIBOLLET

Dr. Sakina DOROTHEE-AYATA

Dr. Joanna KOLASINSKI

Dr. Stéphanie RAYNAUD

Dr. Julien BRAJARD

Sorbonne Université, LOCEAN, Paris

Senckenberg am Meer, Marine Dept, Wilhelmshaven,

Istituto di Scienze Marine, ISMAR, CNR, Bologna

IRD, Sorbonne Université, LOCEAN, Paris

Sorbonne Université, LOCEAN, Paris

UMR ENTROPIE, Saint-Denis, La Réunion

Centre Scientifique de Monaco, CSM, Monaco

NERSC, Bergen, Norway

Président

Rapporteur

Rapporteur

Directrice de thèse

Examinatrice

Examinatrice

Invitée

Co-Directeur de thèse



Acknowledgments

I want to start by thanking all the jury members Paolo Montagna, Max Wisshak, Damien Cardinal, Stéphanie Reynaud, and Sakina Dorothée-Ayata for being part of this process. I also want to acknowledge Paolo and Max for agreeing to review this thesis. I appreciate your time and energy and look forward to the inspiring discussion ahead for the defense.

Cette thèse s'est construite et a pu voir sa réalisation avec l'aide de beaucoup de personnes que j'aimerais prendre le temps de remercier.

J'aimerais tout d'abord remercier très sincèrement mes deux directeur-e-s de thèse, Aline Tribollet et Julien Brajard, pour m'avoir soutenu, encouragé tout au long de ce doctorat. Aline, merci de m'avoir donné l'opportunité de démarrer dans la recherche, d'avoir pu m'approprier ce projet tant complexe et d'avoir pu rencontrer tellement de personnes passionnées et stimulantes. Merci pour ton investissement et le temps que tu m'as donné. Merci aussi de m'avoir poussé dans les moments difficiles, d'avoir su me redonner confiance quand je doutais. Julien, malgré la distance, merci pour ton temps, ta patience, ton expertise, mais surtout pour ta pédagogie. Ce n'était pas gagné au départ pour moi de faire mes débuts dans le milieu « obscur » que pouvait représenter le Machine Learning. Merci pour tout ce que tu m'as transmis, même s'il me reste tant à apprendre encore, et de m'avoir communiqué ta passion pour ce domaine de recherche.

Un grand merci aussi à Nicolas Chevalier, tu as aussi été une part intégrante de ce projet et de sa réussite. Merci pour ton temps, ces discussions et aussi tes mots qui ont aussi su me rassurer quand j'en avais le plus besoin et me permettre de prendre du recul et de la hauteur.

J'aimerais dédier ce paragraphe à une équipe incroyable et que je remercie de tout mon cœur : Vous, cette équipe de BONDY. Vous avez été une des plus belles rencontres professionnelles de cette thèse. Je ne sais comment vous remercier pour votre temps, énergie, ces moments de rires, tous ces cafés, ces discussions, vos retours sur mon travail et vos mots encourageants et motivants. Chaque venue à Bondy a été du pur plaisir. Malgré la prochaine fermeture du centre, le cœur de BONDY ce sont ces personnes, c'est vous. J'ai eu vraiment beaucoup de chance de vous connaître professionnellement, mais surtout humainement.

J'aimerais maintenant dédier ce paragraphe à mon doux couloir. Cette belle équipe du 46-00. Au sein du LOCEAN, il semble caché, éloigné de tout, mais pourtant il y abrite de bien belles personnes que j'ai eues la chance de pouvoir rencontrer, avec qui échanger, et surtout rigoler. Merci pour ces 3 ans, avec des sacrés moments de rire, des pots de thèses bien musclés comme on les aime, de la bonne rigolade, alors pour tout ça encore Merci.

Merci aussi à toutes les personnes qui ont aussi permis la réussite de ce projet de thèse. Merci à Khanh-Vi Tran pour ton investissement et ta patience lors de l'extraction du bore et leurs analyses. Merci à Gninyo E. Coulibaly pour ton implication dans mon projet de recherche. Un Merci tout spécial aussi à Marine Canesi pour tes mots et soutien dans cette épreuve de fin de thèse qui ont su me rassurer.

Comment ne pas remercier mon tendre S, ce noyau si fort qui m'a tant apporté. Alors à vous, Léa, Coraline, Marcellin et ce bon Lulu. La Team, je ne sais comment vous remercier pour tout ce que vous m'avez donné. Merci surtout pour les souvenirs. Tous ces moments, ces rires, ces soirées, ces échanges, ces debriefs ONE PIECE qui ont toujours régalié Coco, ces doux potins qui ont toujours été d'une excellente qualité. Mais essentiellement, merci pour tous les moments à venir qui seront tout aussi légendaires. Cette thèse n'est que la fin d'un arc avant le début du prochain que je nous souhaite de partager ensemble, avec vous. Malgré nos parcours professionnels nous éloignant,

je sais que nous nous reverrons. Merci d'être vous ne changez rien, vous êtes des personnes exceptionnelles qui m'avaient tant apportés. Si j'en suis là aujourd'hui c'est en partie grâce à vous alors merci.

J'aimerais dédier ce paragraphe aux gens merveilleux que j'ai pu rencontrer à la Réunion : David, Marion, Jo, Romain, Merlene, Helena, Felix, Alex et Nico. Quel séjour rempli de souvenirs. Venir pour la rédaction de la thèse dans un endroit inconnu sans repère était risquée et pourtant, ce fut tout le contraire. Vous m'avez accueilli tellement à bras ouverts, moi ce « bobo parisien », et adopté si vite. Tant de moments de rire, d'échanges passionnants, vous avez rendu cette période si stressante, compliquée, remplis de doutes et de remises en questions, tellement plus douce. Grâce à vous, j'ai pu prendre de la hauteur et relativiser sur ce que représenter ce travail. J'avais besoin de cet « électrochoc », changer d'endroit pour pouvoir en prendre conscience et tout ceci, c'est grâce à vous alors encore une fois Merci. Je vous souhaite à tous le meilleur pour la fin de vos thèses/projets respectif. Je ne doute pas à l'avenir une seule seconde que vous réussirez tous vos différents projets et espère bien entendu vous revoir prochainement.

Ce paragraphe, il est pour vous. Ma famille KLEY. Vous avez été une des plus belles rencontres de mon arrivée à Paris. Je changeais encore complètement de vie et arrivé dans cette nouvelle résidence, j'y ai fait la rencontre de personnes magnifiques et inestimables. Pour certains, nous avons passé le confinement ensemble, 2 mois enfermés qui ont donné naissance à une amitié que je ne souhaite perdre pour rien au monde. En chemin, des nouveaux sont arrivés et votre rencontre m'ont aussi permis de me construire et de devenir une meilleure personne au quotidien. Grâce à notre diversité d'horizons, nous avons su créer une alchimie tellement forte et je vous remercie d'être qui vous êtes. Je vous souhaite tant de futurs moments ensemble, ne changez pas, car vous êtes des personnes exceptionnelles et je vous souhaite tout le meilleur, parce que vous ne méritez que l'excellence.

J'aimerais maintenant pouvoir dédier ce paragraphe à mon cercle proche : les Pouletos. Vous qui m'avez tant apporté, construit. Les amis, c'est la deuxième famille qu'on possède, mais surtout, c'est celle que l'on choisit. Et je suis tellement fier d'avoir choisi et de pouvoir faire partie d'un groupe comme celui-ci. L'homme que je suis aujourd'hui

ne serait absolument rien sans tous ces moments de joies, de rires, de colères, de tristesses, mais essentiellement d'amour et de partage. Je ne peux compter le nombre de souvenirs, d'expériences et aventures passés ensemble sur les 10 dernières années qui ont été si riche. Si je pouvais les revivre, je ne changerais absolument rien. Je me souviens de cette décision quand je vous ai annoncé la thèse, quand je doutais de me lancer ou pas dans cette aventure à un moment de ma vie où j'étais perdu et c'est vous qui m'avez donné ce surplus de courage pour me lancer et arriver où j'en suis à cet instant. Alors pour tous ces moments et pour tous ceux à venir, car l'aventure ne s'arrête pas là, je vous dis merci mille fois.

Bien entendu, j'aimerais remercier la Familia, le Padre, la Madre, ma Sœur, mes Tantes, Cousin(e)s, ma Grand-mère, mais ceux aussi déjà partis pour votre soutien inconditionnel. Pour m'avoir supporté dans tous mes choix qui m'auront amené ici. Pour le support moral tout autant que financier qui m'a permis de pouvoir réaliser mes études, de me développer professionnellement et aussi humainement grâce à toutes ces rencontres. Malgré la complexité du sujet, vous avez toujours su m'écoutez, être là quand j'en avais besoin et aussi de me supporter quand j'ai pu avoir des sautes d'humeurs. Petite mention spéciale pour Los Padres et toi Emma. Qui aurait cru que j'en arriverai là 29 ans plus tard. C'est grâce à vous, votre éducation, patience, ouverture d'esprit, ces moments de rire, de pleurs présent par milliers, votre générosité, humilité, et surtout tout cet amour. Je suis devenu la personne que je suis grâce à vous, grâce à vos expériences de vies qui m'ont tant inspiré et donné envie de rêver en grand et de vouloir accomplir de grandes choses, alors pour tout ça encore Merci. Maintenant ce n'est que le début d'une nouvelle aventure, un nouvel Arc.

Enfin Merci à toi, Alizée. Toi qui as pris le navire en cours d'aventure, mais qui aura été la personne la plus importante de sa réussite. Je ne pense pas que je pourrais trouver assez de mots pour te remercier et surtout montrer tout ce que tu m'as apporté durant cette thèse, mais surtout en dehors. Tu as été d'un soutien infaillible, d'une patience extraordinaire, d'une générosité sans limites, mais surtout, tu as toujours su trouver les mots pour me rassurer, me sortir de mes moments de doutes, me redonner confiance quand j'étais au plus bas. Et je sais que cette aventure a été si dure aussi pour toi. J'ai pu être bien pénible par certains moments et sans toi, je n'aurais pu réussir cette thèse. Alors Merci. Une grande partie de ce travail, il est grâce à toi. Merci d'être toi, si at-

tentionnée, ouverte, tellement intéressé par ce que je fais. J'ai tant appris sur moi à tes côtés pendant cette aventure et si j'en suis là aussi aujourd'hui comme toutes les personnes auparavant, c'est aussi grâce à ta grande touche, ta personnalité, ton humilité, tout ce que tu représentes et qui font de toi une personne unique, si importante à mes yeux, alors encore une fois mille fois Merci !

Merci à tous ceux que j'ai pu rencontrer, croiser, avec qui j'ai pu échanger au cours de cette aventure. Je suis partisan du fait que chaque rencontre nous apporte un plus, nous change, et apporte un nouveau regard sur ce que nous faisons et qui nous sommes. Alors pour une ultime fois, encore Merci.

And as someone said:

" Last but not least, I wanna thank me. I wanna thank me for believing in me. I wanna thank me for doing all this hard work. I wanna thank me for never quitting. I wanna thank me trying to be a better version of myself. Finally, I wanna thank me for just being me at all times." S.D.



Scientific Activities and Communications

Publications in Peer-Reviewed Scientific Journals

[1] **Alaguarda D.**, Brajard, J., Coulibaly, G., Canesi, M., Douville, E., Le Cornec, F., Lelabousse, C., and Tribollet, A. (2022) *54 years of microboring community history explored by machine learning in a massive coral from Mayotte (Indian Ocean)*, *Frontiers in Marine Sciences*, DOI: <https://doi.org/10.3389/fmars.2022.899398>

[2] **Alaguarda D.**, Tribollet, A., Lguenstat, R., and Brajard, J. *Validation and optimization of a machine learning approach to understand microbioeroding assemblage dynamics in different massive corals* [To be submitted in *Limnology and Oceanography*]

[3] **Alaguarda D.**, Chevalier, N., Klein, V., and Tribollet, A. *Variations of the Abundance of Microbioeroding Communities through Lipid Biomarker Concentrations in Living Massive Corals Over the Long-Term* [In Preparation for *Organic Geochemistry*]

[4] **Alaguarda D.**, Brajard, J., Le Cornec, F., Douville, E., Lelabousse, C., and Tribollet, A. *Intercomparison of the Assemblage of Microbioeroding Communities from two Massive Corals of the Island of Mayotte* [In preparation]

Courses

Seminar "Changement climatique et Impacts", *LOCEAN* (21h)

Courses "Statistics for Weather and Climate Science", *University of Reading* (20h)

Courses "Regression non linéaire par réseau de neurones", *LOCEAN* (40h)

MOOC "Scientific Writing", *ED 129* (24h)

MOOC "LateX for Beginners", *ED 129* (12h)

Scientific Communications

Internation Conferences

Alaguarda D., Brajard, J., Coulibaly, G., Canesi, M., Douville, E., Le Cornec, F., Lelabousse, C., and Tribollet, A. (2021) *Colonization dynamics of a massive coral by microborers over the last 50 years: Use of a machine learning approach and effects of temperature (Mayotte, WIO)* (Poster Session) 14th International Coral Reef Symposium, Bremen, Germany (Online)

Alaguarda D., Brajard, J., Coulibaly, G., Canesi, M., Douville, E., Le Cornec, F., Lelabousse, C., and Tribollet, A. (2022) *Indian Ocean microborers in a living coral: How explore their abundance's variability over 50 years?* (Oral Talk) EGU General Assembly 2022, Vienna, Austria

Alaguarda D., Brajard, J., Coulibaly, G., Canesi, M., Douville, E., Le Cornec, F., Lelabousse, C., and Tribollet, A. (2022) *Indian Ocean microborers in a living coral: How to explore their abundance's variability over 50 years?* (Poster Session) 15th International Coral Reef Symposium, Bremen, Germany

Outreach

[1] Changement Climatique et Récifs Coralliens, Diego Alaguarda, Interview, *Media VRACC*, May 2021

[2] Fête de la Science, Booth with experiences related to climate systems, *Paris - Sorbonne Université*, September 2021

[3] Future Maores Reef, Talk for a school on coral reef, presentation of Mayotte and the Ph.D. Project *Bondy - IRD*, March 2022

[4] Fête de la Science, Talk on climate change, introduction to coral reefs *Bondy - IRD*, Octobre 2022



Abstract

Coral reefs are increasingly threatened by global changes that affect both accretion and erosion processes. Among these processes, reef bioerosion is a major natural degradation process resulting from the action of various organisms on and in carbonate substrates. Recently, particular attention has been given to a better understanding of the roles played by bioeroding (or perforating) microflora, including cyanobacteria, microalgae, and fungi, in the functioning of coral reefs, especially in the carbonate budget, because of their important role in the dissolution of dead carbonates in the short term (day, month, year). Therefore, this thesis's main objective was to study the effect of environmental factors, including long-term (decade) ocean warming and acidification, on the composition, distribution, and abundance of reef microbioeroding communities. Since long-term experiments with dead corals are not feasible, several coral cores from two slow-growing massive coral genera (*Diploastrea* sp. and *Porites* sp.) were collected along the Mozambique Channel, particularly in Mayotte, covering the last decades (30 to 50 years). These massive corals are known to be natural geological archives largely colonized by microbioeroding communities that create traces by dissolving CaCO_3 . To study the dynamics of microbioeroding community in the two targeted coral genera, two innovative methods were developed: machine learning to quickly and accurately analyze thousands of microbioeroding traces, within images taken with a Scanning Electron Microscope (SEM) along three vertical transects parallel to the main growth axis of the two coral genera, and the study of lipid biomarkers along a coral core (only *Diploastrea* sp.). The machine learning method based on a CNN model was first developed on the coral *Diploastrea* sp. with an accuracy of 93%,

then adapted to *Porites* sp. by modifying a hyperparameter (95% accuracy). The geochemical approach tried identifying specific lipid markers of the microalga *Ostreobium* sp. and the coral *Diploastrea* sp. during the last decades. The results showed that the abundance of microbioeroding traces is 3 to 4 times higher in the coral *Diploastrea* sp. than in *Porites* sp and has decreased in all coral genera over the last decades. In *Diploastrea* sp., the decrease is 90% over the last 54 years and is coupled with a very important change in community composition between 1985-1986. The density (bulk) of *Diploastrea* sp. has also dropped significantly over the last 5 decades. Logistic regressions showed that temperature, wind speeds, and internal pH of the coral, more or less coupled, are correlated to the abundance of microbioeroding traces. The geochemical approach also highlighted the significant decrease of a lipid biomarker group, the amides, over the last decades. Although it is difficult to attribute amides to a specific taxon or species in the coral skeleton, I hypothesize that they could potentially reflect the presence of microbioeroding communities. To confirm or refute the observed trends, there is a need to study a more significant number of coral cores, but also in length. In addition, other factors could be studied to understand better the decrease in the abundance of microbioeroding communities, such as trace metals and other carbonate system variables, and its implication in coral health and resilience.

Key-Words: Microbioeroding Assemblages - Euendoliths - Community Shift - Green Bands - Massive Corals - Mayotte - Global Changes - Machine Learning - Organic Geochemistry - Lipid Biomarkers



Résumé

Les récifs coralliens sont de plus en plus menacés par les changements globaux qui affectent à la fois les processus d'accrétion et d'érosion. Parmi ces processus, la bioérosion récifale est un processus de dégradation naturelle majeur résultant de l'action de divers organismes sur et dans les substrats carbonatés. Depuis peu, une attention particulière est portée sur la meilleure compréhension des leurs rôles joués par les microflores bioérodantes (ou perforantes) comprenant des cyanobactéries, microalgues et fungi, dans le fonctionnement des récifs coralliens, notamment le bilan carbonaté, du fait de leur rôle important dans la dissolution récifale des carbonates morts à court terme (jour, mois, année). La présente thèse avait donc pour objectif principal d'étudier l'effet de certains facteurs environnementaux, dont le réchauffement et l'acidification des océans à long terme (décennie) sur à la fois la composition, la distribution et l'abondance de communautés microperforantes récifales. Etant donné que des expériences à long terme avec des coraux morts sont peu envisageables, plusieurs carottes coralliennes issues de deux genres coralliens massifs (*Diploastrea* sp. et *Porites* sp.) à croissance lente, ont été collectés le long du Canal du Mozambique et en particulier à Mayotte, permettant de couvrir les dernières décennies (30 à 50 ans). Ces coraux massifs sont connus pour être de véritables bioarchives géologiques largement colonisées par les microflores perforantes qui en dissolvant le CaCO_3 créent des galeries. Pour étudier la dynamique des microflores perforantes dans les deux genres coralliens ciblés, deux méthodes innovantes ont été développées: le machine learning pour analyser rapidement et précisément des milliers d'images de galeries microperforantes prises au Microscope Électronique à Balayage (MEB), le long de trois

transects verticaux parallèle à l'axe principal de croissance des deux genres coralliens, et l'étude de biomarqueurs lipidiques le long d'une carotte corallienne (uniquement *Diploastrea* sp.). La méthode du machine learning basée sur un model CNN a d'abord été développée sur le corail *Diploastrea* sp. avec une précision de 93%, puis adaptée au *Porites* sp. en modifiant notamment un hyperparamètre (précision de 95%). L'approche géochimique a consisté à tenter d'identifier des marqueurs lipidiques spécifiques de la microalgue *Ostreobium* sp. et du corail *Diploastrea* sp. au cours des dernières décennies. Les résultats ont montré que l'abondance des galeries microperforantes est 3 à 4 fois plus importante dans le corail *Diploastrea* sp. que dans le *Porites* sp. et qu'elle a diminué quelque soit le genre corallien, au cours des dernières décennies. Chez *Diploastrea* sp., la diminution est de 90% en 54 ans et est couplée à un changement très important dans la composition des communautés entre 1985-1986. La densité (bulk) du *Diploastrea* sp. a également chuté de manière significative au sur les 5 dernières décennies. Des régressions logistiques ont montré que la température, les vitesses de vents, le pH interne du corail, plus ou moins couplés, sont corrélés à l'abondance des traces microperforantes. L'approche géochimique a également mis en évidence la diminution importante d'un biomarqueur lipidique, les amides, au cours des dernières décennies. Bien qu'il soit difficile d'attribuer les amides à un taxon ou une espèce en particulier présente dans le squelette corallien, j'émet l'hypothèse que potentiellement ces dernières pourrait refléter la présence de communautés microperforantes. Pour confirmer ou infirmer les tendances observées, il est nécessaire d'étudier un plus large nombre de carotte coralliennes ainsi qu'un longueur. En outre, d'autres facteurs pourraient être étudiés pour mieux comprendre la diminution de l'abondance des communautés microperforantes tels que les métaux traces, d'autres variables du système des carbonates, et son implication dans la santé et la résilience des coraux.

Mots-Clés: Assemblage Traces Microperforantes - Euendolithes - Shift de Communautés - Bandes Vertes - Coraux Massifs - Mayotte - Changement Globaux - Machine Learning - Géochimie Organique - Biomarqueurs Lipidiques



Contents

List of Figures	20
List of Tables	28
1 An Overview of Coral Reefs Functioning and the Role of Microbioeroding Communities	33
1.1 Coral Reef Ecosystems	35
1.1.1 Ecological Importance and Major Threats	35
1.1.1.1 Why Are These Ecosystems so Important?	35
1.1.1.2 A Jewel in Perish	36
1.1.1.2.1 Local Disturbances and Anthropogenic Impacts	37
1.1.1.2.2 Global Changes: Focus on Ocean Acidifica- tion and Warming	38
1.1.2 Reefs Functioning: A Balance of Forces	44
1.1.3 Massive Corals: Natural Bio-Archives	47
1.2 Reef Bioerosion	50
1.2.1 Bioerosion Processes	50
1.2.2 Bioeroding Microflora	52
1.2.2.1 Definition and History	52
1.2.2.2 Colonization of Bioeroding Microflora	55
1.2.2.3 Environmental Effects on Bioeroding Microflora	58
1.2.2.4 Major Role of Bioeroding Microflora in Living Corals . .	60

1.2.3	Known Methodologies to Study Microbioeroding Communities and their Bioeroding Traces	61
1.3	Ph.D. Objectives	67
2	Materials and Methodologies	69
2.1	Study Geographical Area: The Western Indian Ocean	71
2.1.1	Mayotte Island	73
2.1.1.1	Environmental Products Acquisition	74
2.1.2	Reunion Island	76
2.1.3	Scattered Island	77
2.1.3.1	Juan De Nova	78
2.1.3.2	Europa	78
2.2	Coral Data Acquisition	79
2.2.1	Coral Core Sampling	79
2.2.2	Coral Growth Variables	80
2.2.3	Temperature and pH Reconstructions from Coral Cores	83
2.2.3.1	Known Proxies for SST and pH	83
2.2.3.2	SST Dataset Acquisition	84
2.2.3.3	pH Geochemical Analysis	85
2.3	Microbioeroding Communities Investigation	86
2.3.1	Identification of Microbioeroding Organisms: Microscopy Approach	86
2.3.2	Sampling Design to Study Microbioerodings' Abundance and Green Bands	89
2.3.3	Quantification of Microbioeroding Traces: Machine Learning Application	91
2.3.4	Determination of Potential Specific Lipid Biomarkers of Bioeroding Microflora: Geochemistry Approach	91
3	How to Accurately and Efficiently Study the Decadal Variability of Microbioeroding Communities' Composition and Abundance? Development of a Specific and Innovative Approach	93
3.1	What is Machine Learning ?	94
3.2	Machine Learning for Segmentation Task of Classes	95
3.3	Application of Machine Learning on Microbioeroding Communities	96

4	What Are the Effects of Biotic and Abiotic Factors on the Composition and Abundance of Microbioeroding Communities in the massive coral <i>Diploastrea</i> sp over the last 54 years?	143
4.1	Preface	145
4.2	Variability of the Abundance, Shift of Microbioeroding Community Composition and Green Bands Investigation in <i>Diploastrea</i> sp.	146
4.3	Effects of pH on the Abundance and Composition of Microbioeroding Communities in <i>Diploastrea</i> sp.	168
4.3.1	Introduction	168
4.3.2	Methodologies	171
4.3.3	Results	172
4.3.3.1	Evolution of the internal pH of <i>Diploastrea</i> over 54 years	172
4.3.3.2	Internal pH and Abiotic Variables	173
4.3.3.3	Internal pH and Biotic Variables	174
4.3.4	Discussion	176
4.3.4.1	Comparison of Instrumental and Paleo-Proxy pH Reconstructions	176
4.3.4.2	<i>Diploastrea</i> sp. Internal pH : A Particular Signal ?	177
4.3.4.3	Internal pH and the Evolution of the Abundance of Microbioeroding Traces	180
4.4	Conclusion	182
5	Is the Composition and Abundance of Microbioeroding Communities in Massive Corals Genus Dependant?	185
5.1	Introduction	187
5.2	Material and Methodologies	191
5.2.1	Study Site	191
5.2.2	Coral Sampling	191
5.2.3	Coral Growth Variables	191
5.2.4	Observation and Estimation of Microbioeroding Traces	192
5.2.5	Machine Learning Application	193
5.2.6	Statistical Analysis	194
5.3	Results	194
5.3.1	Variability of Environmental Conditions in Mayotte Over the Last 30 Years Among the Two Studied Coral Genera	194

5.3.2	Comparison of Coral Growth Parameters between <i>Diploastrea</i> sp. and <i>Porites</i> sp. Over the Last 30 Years	196
5.3.3	Microbioeroding Community Composition in <i>Porites</i> sp.	197
5.3.4	Effects of the Coral Genus on the Abundance of Microbioeroding Traces over the Last 30 Years	199
5.3.5	Main Factors Influencing the Abundance of Microbioeroding Traces Over the last 30 Years in Massive Corals	200
5.3.5.1	Main Factors Influencing the Abundance of Microbioeroding Traces in <i>Diploastrea</i> sp.	200
5.3.5.2	Main Factors Influencing the Abundance of Microbioeroding Traces in <i>Porites</i> sp.	202
5.4	Discussion	203
5.4.1	Effect of Abiotic Parameters on the Abundance of Microbioeroding Traces in Massive Corals	203
5.4.2	Effect of Skeletal Properties on the Abundance of Microbioeroding Traces in Massive Corals	205
5.4.3	Evolution of the Abundance and Composition of Microbioeroding Traces in Massive Corals	207
5.5	Conclusion	208
6	A Lipid Biomarker Approach to Identify Potential Molecules Indicative of Changes in Microbioeroding Community Composition and Abundance?	211
6.1	Why Use Lipid Biomarkers in Marine Ecology?	213
6.1.1	What is a Biomarker?	213
6.1.2	Corals and Known Lipid Composition	215
6.1.3	Objectives	218
6.2	Materials and Methods	219
6.2.1	Sampling Strategy	220
6.2.2	Samples Preparation	221
6.2.3	Extraction and Separation Procedure	222
6.2.4	Identification and Quantification of Lipid Biomarkers on Gas Chromatography-Mass Spectrometry (GC-MS)	223
6.3	Results	225
6.3.1	Lipid biomarkers Composition: Monoalgal Culture <i>Ostreobium</i> sp. O10	225

6.3.1.1	F1 Fraction: Hydrocarbons Composition	225
6.3.1.2	F3 Fraction: Alcohols and Sterols Composition	225
6.3.1.3	FA Fraction: Fatty Acids Composition	226
6.3.2	Lipid biomarkers Composition: <i>Diploastrea</i> sp.	227
6.3.2.1	F1 Fraction: Hydrocarbons Composition	227
6.3.2.2	F3 Fraction: Alcohols and Sterols Composition	227
6.3.2.3	FA Fraction: Fatty Acids Composition	229
6.4	Discussion	231
6.4.1	Lipid Biomarkers Profile: Monoalgal Strain O10	231
6.4.2	Lipid Biomarkers Profile: <i>Diploastrea</i> sp.	234
6.4.3	Amide Lipid Biomarkers: Proxies of microborers ?	236
6.5	Conclusion	239
7	General Conclusions and Perspectives	241
7.1	Synthesis	242
7.2	Perspectives	249
7.2.1	Machine Learning Application	249
7.2.2	Additional Results of a Coral Core of La Réunion	250
7.2.3	Additional Results from Coral Cores of the Scattered Islands	251
7.2.4	Further Investigations	253
8	Appendix	255
8.1	Cast-Embedding Protocol	255
8.2	Supplementary Materials <i>Diploastrea</i> sp. Coral Investigation	258
8.3	Supplementary Materials <i>Porites</i> sp. Coral Investigation	276
8.4	Supplementary Chromatograms	287
8.5	Curriculum Vitae and Scientific Communications	287
	Appendix	292
	References	293



List of Figures

- 1.1 The geographical distribution of tropical coral reefs worldwide from 30°N to 30°S. Data are from Burke et al., [2011](#). 36
- 1.2 Side-by-side comparison of a coral reef before and after bleaching. Credit: Chasing Coral. 40
- 1.3 Conceptual figure showing the effect of increasing CO₂ concentration on acid-base chemical species present in seawater. Atmospheric CO₂, taken up by the ocean, combined with water to produce carbonic acid, which releases a proton that combines with a carbonate ion, decreasing the concentration of carbonate ions, and making it unavailable to marine calcifiers such as corals. For additional information, refer to Hoegh-Guldberg et al., [2007](#) showing the acidification process and its impact on corals. 42
- 1.4 Figure modified from Mahwren et al. (2021) showing the details of the key ocean circulations over the MC. SEMC South-East Madagascar Current, NEMC North-East Madagascar Current, SEC South Equatorial Current, and Agulhas Current. Red and blue circles illustrate idealized anticyclonic and cyclonic eddies, respectively. Orange shading highlights the distribution of warm-water coral reefs. Colorbar represents the bathymetry. 44
- 1.5 The developmental sequence of coral reefs, from young fringing reefs (left) to barrier reefs (center), and finally to atolls (right). 45

- 1.6 Ternary diagram showing different carbonate production states determined by variations in the relative importance of primary (coral) and secondary (calcareous encruster) carbonate production and carbonate breakdown to sediment/dissolution by bioerosion. Figure modified from C. Perry et al., 2008. 47
- 1.7 (A) Massive *Porites* colony that measures about 13 m across, 6.5 m in height, and 41 m in circumference at the base. Credit Photo: Wendy Cover/NOAA. (B) Typical massive *Diploastrea* colony observed in Indonesia. Credit Photo Gerry Allen. 47
- 1.8 (A) Distribution of one species of massive *Porites* colony: *Porites lutea* (B) Distribution of the massive coral *Diploastrea heliopora*. Both maps obtain from Corals of the World (<http://www.coralsoftheworld.org/page/home/>). . . 49
- 1.9 The bioerosion loop shows a simplified model of interactions between the main bioeroder groups. Figure from Schönberg et al., 2017. 50
- 1.10 Schematic presentation of various types of endoliths that can colonize a substrate. Figure adapted from Golubic et al., 1981. 52
- 1.11 Illustrations and presentation of morphological characteristics of some microborers. 54
- 1.12 (A) Fractured *Goniastrea perisi* with a distinctive green band of endoliths "e" underneath the coral tissue "ct". (B) Fractured *Porites lutea* with a distinctive green band. (C) Close-up of the coral colony *Paragoniastrea* sp. with green boring algae inside the skeleton. (D) Colonized orange *Stylaster* sp from Siladen Island appearing pink-orange in the base. (E) White *Stylaster* sp from Siladen Island with a pink base. (F) *Stylaster* sp from Siladen Island with an apical branch colonized by euendoliths (arrow). Colorations represent colonization from euendolith identified as a cryptic stage of the rhodophyte *Porphyra* (Conchocelis stage). Photographs A and B were extracted from Gutner-Hoch and Fine, 2011. Photograph C was extracted from Verbruggen and Tribollet, 2011. Photographs D to F were extracted from Pica et al., 2016. 57

- 1.13 **(A)** Colored semitransparent visualization of a corallite of the cold-water coral *Lopheliapertusa* with the sponge cavity (orange) and an embedded epibiontic worm (blue). **(B)** Anaglyph 3D visualization of another corallite with heavy sponge infestation (requires anaglyph glasses with left eye red and right eye blue). For further details, refer to Wisshak, 2012. **(C and D)** Visualization of micro-computed tomography (μ CT) scan of an experimental block of *Porites* sp. coral before (C) and after (D) 1 yr deployment in Coconut Island, Hawaii. Further details are available through a movie of the full 3D visualization of the different μ CTCT images within their Supplement 2 from Silbiger et al., 2014. 63
- 1.14 Selected regions of shells from the bivalve *Delectopecten vitreus* infested by different euendoliths and stained with fluorescent dye Sybr Green I. Further details for the different microborers are available from Figure 4 of Schätzle et al., 2021. 64
- 1.15 Figure extracted from Wisshak, 2012 showing different microbioerosion traces in thin petrographic sections. (A) displayed boring traces from ichnotaxa *Eurygonum nodosum* and *Scolecia filosa* in a recent bivalve shell from the Azores. (B) displayed fungal trace of *Orthogonum lineare* in a Pleistocene cold-water coral from Rhodes, Greece. (C) Same assemblage as in A, but from the Carboniferous Buckhorn Asphalt Lagerstätte, USA. (D) displayed a fungal trace of *Saccomorpha clava*, well preserved in a brachiopod shell from the Silurian of Gotland, Sweden. 65
- 2.1 Map of the WIO, obtained from B. N. Alliance, 2020. 71
- 2.2 **(A)** Bathymetry and major circulatory features in the Mozambique Channel and around Madagascar. Shaded areas show the extent of the continental shelf to a depth of 200 m. Green ellipses denote upwelling areas. **(B)** Monthly mean chlorophyll concentrations for February 2003. Intermediate values beyond the continental shelf edge highlight areas of elevated productivity off the Mozambique and Madagascar coasts that are primarily upwelling-driven. Figures from Vinayachandran et al., 2021. 72

- 2.3 Circulation patterns within the northern part of the WIO show the Somali Current (SC), South Equatorial Countercurrent (SECC), East African Coastal Current (EACC), South Equatorial Current (SEC), and Northeast Madagascar Current (NMC). Green ellipses denote upwelling areas. Dark grey shading denotes depths within the 200m isobath. Figure from Vinayachandran et al., 2021. 73
- 2.4 Climate context of Mayotte island showing the interannual variability of the different environmental parameters at Mayotte between 1964 and 2018. **(A)** SST in °C **(B)** SSTA in °C. **(C)** Maximum instantaneous wind speed (km*h-1). **(D)** Precipitation rate (mm). **(E)** Annual cumulative insolation period (hours). Each variable's error bars (SE) were calculated after averaging monthly data. 76
- 2.5 Climate context of Reunion island showing the interannual variability of the different environmental parameters at Mayotte between 1994 and 2015. **(A)** SST in °C **(B)** SSTA in °C. **(C)** Maximum instantaneous wind speed (km*h-1). **(D)** Precipitation rate (mm). **(E)** Annual cumulative insolation period (hours). Each variable's error bars (SE) were calculated after averaging monthly data. 77
- 2.6 Interannual variability of the SST and SSTA from the island of Juan de Nova between 1972 and 2018 (coral growth reconstruction) 78
- 2.7 Interannual variability of the SST and SSTA from the island of Europa between 1993 and 2018 (coral growth reconstruction) 79
- 2.8 **(A)** Location of the different coral samplings corresponded to the different missions CARBODISS and CLIM-EPARSEs. **(B)** Mayotte in the WIO. **(C)** Reef ecosystems around Mayotte. The blue line and black lines represent the different isobaths around the island. The green star indicates the sampling location in the northeastern part of the lagoon. 80
- 2.9 Linear regression between measured Hounsfield Median values (voxels measured in HU) and their experimental measured densities (g.cm-3). Blue dots represent the 11 different coral block standards from *Porites* sp. corals (n=6) and *Diploastrea* sp. corals (n=5). Red dots represent the three standards used for the calibration and the linear regression. 82

2.10	Studied <i>Diploastrea</i> sp. coral colony at Mayotte. (A) <i>Diploastrea</i> sp. colony at 15 m depth. The black arrow indicates where the colony was sampled. (B) <i>Diploastrea</i> sp. core with visible green bands (green arrows). (C) X-ray radiograph of one middle slab cut out of the <i>Diploastrea</i> core measuring 19.5 cm long showing the annual density banding pattern. The white rectangle indicates the studied area. (D) Ten samples were cut from the radiographed slab of the <i>Diploastrea</i> sp. core. Only the first nine samples from the top were analyzed to estimate the microborer traces' abundance. Green arrows indicate green bands. (E) Resin impregnation of the 9 samples. Horizontal white and green arrows represent the horizontal transects where measurements of microbioerodings abundance were realized (i.e., within white vs. green bands). The black arrows represent the vertical transects studied in each sub-sample. (F, G) Different resin casts of microbioerodings observed under a scanning electron microscope after resin impregnation of coral samples and partial decalcification.	87
2.11	Cast Embedding protocol for coral samples. Figure adapted from Wisshak, 2012.	88
2.12	(A) Scanning Electron Microscope (SEM) Zeiss EVO-LS15, Alysés Platform, Sorbonne University-IRD-Region, Ile-de-France, Bondy. (B) Schematic representation of the functioning of the SEM. (C and D) Fragments of coral skeletons for the SEM observations before and after gold metalization.	89
2.13	Schematic representation of vertical and horizontal sample transects across the surface of the radiographed slab of the <i>Diploastrea</i> coral core to estimate the abundance of microborers comparing white and green bands	90
2.14	Schematic representation of the objectives and methodologies for investigating coral cores.	92
3.1	(A) Original MET images showing the different cell wall structures. (B) Prediction of the U-NET model for segmenting the different cell walls in the image.	96
4.1	Interannual variability of the internal pH_{CF} of <i>Diploastrea</i> sp. at Mayotte between 1964 and 2018 reconstructed based on the instrumental SST (red line) and the paleo-proxy (blue line). The black dotted line indicates the pH_{CF} breakpoint.	172

- 5.1 (A) X-Radiograph showing the coral *Diploastrea* sp. (B) X-Radiograph showing the coral *Porites* sp. (C to E) SEM photographs of the colony *Diploastrea* with its corallite and micro-structure. (F) SEM photograph on the studied *Diploastrea* sp. from Mayotte showing one skeletal unit colonized by microbioeroding traces. Image taken at 150x magnification. (G to I) SEM photographs showing the coral colony, corallites structures of *Porites lutea*. (J to L) SEM photographs showing the coral colony, corallites structures of *Porites lobata*. (M to N) SEM photographs showing the coral colony, corallites structures of *Porites solida*. (O) SEM photograph on the studied *Porites* sp. from Mayotte showing multiple skeletal unit colonized by microbioeroding traces. Image taken at 150x magnification. 188
- 5.2 Studied slab of *Porites* sp. coral from Mayotte. (A) The X-ray radiograph of one middle slab cut out of the *Porites* sp. core measuring 29.5 cm long shows the annual density banding pattern. (B) and (C) 14 samples were cut from the radiographed slab of *Porites* sp. core. (D) Example of an SEM image collected from the *Porites* sp. core showing microbioeroding traces colonizing the coral skeleton. Scale is 100 μ m 192
- 5.3 Interannual variability of the internal pH_{CF} of *Diploastrea* and *Porites* sp. at Mayotte between 1990 and 2018. 195
- 5.4 Evolution of the different coral growth parameters of the studied *Diploastrea* sp. and *Porites* sp. colony over the last 29 years. The different panels compared each different growth parameter between both corals. 197
- 5.5 SEM pictures presenting the diversity of microbioeroding traces observed along the coral core of *Porites* sp. (A) SEM image from the top of the core showing traces measuring less than 2 μ m, most probably belonging to fungi. (B) SEM image from the middle of the core showing traces measuring between 2 and 5 μ m, orientated within the coral growth axis. (C) Picture from the bottom of the core showing traces measuring between 5 and 10 μ m, organized in a patch, also orientated towards the coral growth axis. (D) Zoom of C showing the network of microbioeroding traces with a morphology indicative of the potential ichnotaxa *Rhopalia*. 198

5.6	Variability of the percentage of coral skeleton colonized by microbioeroding communities over the last 29 years. (A) Histogram reporting the variability averaged (%) of the thin and wide microbioeroding traces and obtained along the <i>Diploastrea</i> sp. core. (B) Histogram reporting the variability (%) of the total microbioeroding traces obtained along <i>Porites</i> sp. core.	199
6.1	Schematic representation of the organic geochemistry protocol applied on samples of the coral core <i>Diploastrea</i> sp from Mayotte and the monoalgal strain of <i>Ostreobium</i>	219
6.2	Schematic representation of the slab's cutting pattern <i>Diploastrea</i> coral core for quantification of the lipid biomarkers of microborers comparing white and green band.	220
6.3	(A) Photograph of the Agilent 7890 A GC-MS used for the quantification and identification of the lipid biomarkers. (B) Example of a chromatograph showing the relative intensity compared to the retention time of lipid biomarkers from the FA fraction of <i>Ostreobium</i>	223
6.4	Chromatogram of the alcohol/sterol fraction (F3) from the monoalgal strain culture <i>Ostreobium</i> O10 free-living form	226
6.5	Chromatogram of the FA fraction from the monoalgal strain culture <i>Ostreobium</i> O10 free-living form	227
6.6	Chromatogram of the F3 fraction from the top of the coral core of <i>Diploastrea</i> sp.	228
6.7	Histogram of the concentration of total amides lipid biomarker group among the coral core of <i>Diploastrea</i> . Green arrows indicate the position of the green bands within the coral core. CS for the x-axis stands for "Coral Sample".	229
6.8	Chromatogram of the FA fraction from the top of the coral core of <i>Diploastrea</i> sp.	230
7.1	Schematic summary of the Ph.D. project.	248
7.2	Histogram showing the variability of the percentage of the <i>Porites</i> sp. coral skeleton colonized by microbioeroding communities in la Reunion. The variability of the microbioeroding traces were obtained along the 3 vertical transects (same methodology as described in corals from Mayotte).	250
7.3	Evolution of the different coral growth parameters of the studied <i>Porites</i> sp. colony from Juan De Nova.	251

7.4	Evolution of the different coral growth parameters of the studied <i>Porites</i> sp. colony from Europa.	252
8.1	Variability of the abundance of microbioeroding traces among the three different vertical transects for <i>Diploastrea</i> sp. and <i>Porites</i> sp.	276
8.2	Chromatogram of the F3 fraction from one coral sample of the bottom of the core	287
8.3	Chromatogram of the FA fraction from one coral sample of the bottom of the core	287



List of Tables

- 2.1 Considered environmental parameters that could potentially influence microborers abundance over the last decades in both living coral *Diploastrea* and *Porites* sp. (Mayotte). 75
- 4.1 Pearson's correlations between the raw reconstructed pHs_{CF} and the environmental variables over the last 54 years, per period before or after the breakpoint investigated by Alaguarda et al., 2022. Code for significance: *# < 0.1; * < 0.05; ** < 0.01; *** < 0.001; NS is for non significant. 173
- 4.2 Pearson's correlations between the detrended pH reconstructions and the detrended environmental variables over the last 54 years, per period before or after the breakpoint investigated by Alaguarda et al., 2022. *# < 0.1; * < 0.05; ** < 0.01; *** < 0.001; NS is for non significant. 174
- 4.3 Pearson's correlations between the raw pH reconstructions and the abundance of microborers (wide, thin, or total) and coral growth variables over the last 54 years, per period before or after the breakpoint investigated by Alaguarda et al., 2022. *# < 0.1; * < 0.05; ** < 0.01; *** < 0.001; NS is for non significant. 175
- 4.4 Pearson's correlations between the detrended pH reconstructions and the detrended abundance of microborers (wide, thin, or total), coral growth variables over the last 54 years, per period before or after the breakpoint investigated by Alaguarda et al., 2022. *# < 0.1; * < 0.05; ** < 0.01; *** < 0.001; NS is for non significant. 176

5.1	Pearson's correlations between the raw abundance of total microborers and raw environmental or coral growth variables over the last 30 years within <i>Diploastrea</i> sp., (upper part of the table). Pearson's correlations between the detrended abundance of total microborers and detrended environmental or coral growth variables over the last 30 years within <i>Diploastrea</i> sp., (lower part of the table). Code for significance: *** < 0.001; ** < 0.01; * < 0.05; *· < 0.1.	201
5.2	Pearson's correlations between the raw abundance of total microborers and raw environmental or coral growth variables over the last 30 years within <i>Porites</i> sp., (upper part of the table). Pearson's correlations between the detrended abundance of total microborers and detrended environmental or coral growth variables over the last 30 years within <i>Porites</i> sp., (lower part of the table). Code for significance: *# < 0.1; * < 0.05; ** < 0.01; *** < 0.001; NS is for non significant.	202
6.1	Main classes of lipid biomarkers and their interest in marine geochemistry.	214
6.2	Lipid biomarkers studied within the different coral compartments, their known functional roles, and the degree of attention, they received.	216
6.3	Dry-weight of each sample used for the lipid biomarker analysis.	221
6.4	Sterols composition and their respective concentrations observed in the monoalgal culture strain <i>Ostreobium</i> O10 free-living form.	226
6.5	Sterols composition and their respective concentrations observed in the monoalgal culture strain <i>Ostreobium</i> O10 free-living form.	227
6.6	Main sterols and their respective concentrations observed along the different samples of the coral core of <i>Diploastrea</i> sp. The green color in the values corresponds to the green bands.	228
6.7	Main amides and their respective concentrations observed along the different samples of the coral core of <i>Diploastrea</i> sp, here presented in ng/g. The green color in the values corresponds to the green bands.	229
6.8	Main detected Fatty Acids and their respective concentrations calculated along the different samples of the coral core of <i>Diploastrea</i> sp. The green color in the values corresponds to the green bands.	230



List of Acronyms

WIO: Western Indian Ocean
CNN: Convolutional Neural Network
ML: Machine Learning
OA: Ocean Acidification
SST: Sea Surface Temperature
TSM: Temperature de Surface de la Mer
SSTA: Sea Surface Temperature Anomalies
ppm: Part Per Million
IPCC: International Panel for Climate Change
pH: Potential Hydrogen
DIC: Dissolved Inorganic Carbon
 Ω : Aragonite Saturation State
CF: Calcifying Fluid
IOD: Indian Ocean Dipole
ENSO: El Niño Southern Oscillation
CO₂: Carbon Dioxide
O₂: Dioxygen
H⁺: Hydrogen proton
CaCO₃: Calcium Carbonate
H₂CO₃: Carbonic Acid
H₂O₂: Peroxyde Hydrogen
NH₄OH: Hydroxyde Ammonium

CT: Computed-Tomography

MC: Mozambique Channel

INSEE: Institut National de la Statistique et des Études Économiques

JDN: Juan De Nova

EUR: Europa

TAAF: Terres Australes et Antarctiques Françaises

LSCE: Laboratoire des Sciences du Climat et de l' Environnement

LOCEAN: Laboratoire d'Océanographie et du Climat Expérimentations et Approches Numériques

IRD: Institut de Recherche pour le Développement

NOAA: National Oceanic and Atmospheric Administration

IPSL: Institut Pierre et Simon Laplace

CEA: Centre d' Énergie Atomique

SEM: Scanning Electron Microscope

GMM: Gaussian Mixture Model

HU: Hounsfield Units

ERSST: Extended Reconstructed Sea Surface Temperature

OISST: Optimum Interpolation Sea Surface Temperature

ICP-MS: Inductively Coupled Plasma Mass Spectrometry

GC-MS: Gas Chromatography-Mass Spectrometry

CE: Cross Entropy

WCE: Weighted Cross Entropy

FL: Focal Loss

TL: Tversky Loss

FTL: Focal Tversky Loss

An Overview of Coral Reefs

Functioning and the Role of

Microbioeroding Communities

Contents

1.1	Coral Reef Ecosystems	35
1.1.1	Ecological Importance and Major Threats	35
1.1.1.1	Why Are These Ecosystems so Important?	35
1.1.1.2	A Jewel in Perish	36
1.1.1.2.1	Local Disturbances and Anthropogenic Impacts	37
1.1.1.2.2	Global Changes: Focus on Ocean Acidification and Warming	38
1.1.2	Reefs Functioning: A Balance of Forces	44
1.1.3	Massive Corals: Natural Bio-Archives	47
1.2	Reef Bioerosion	50
1.2.1	Bioerosion Processes	50
1.2.2	Bioeroding Microflora	52
1.2.2.1	Definition and History	52
1.2.2.2	Colonization of Bioeroding Microflora	55
1.2.2.3	Environmental Effects on Bioeroding Microflora	58
1.2.2.4	Major Role of Bioeroding Microflora in Living Corals	60

1.2.3	Known Methodologies to Study Microbioeroding Communi- ties and their Bioeroding Traces	61
1.3	Ph.D. Objectives	67

1.1 Coral Reef Ecosystems

1.1.1 Ecological Importance and Major Threats

1.1.1.1 Why Are These Ecosystems so Important?

Present for more than 240 million years (Middle Triassic), scleractinians corals represent the main order of hard skeleton corals (Veron, 1996; Stanley Jr and Fautin, 2001; Stolarski et al., 2011). Scleractinian corals, also known as reef-builders corals, are the principal agent for the most prominent biomineral construction of the world: coral reefs. Coral reefs represent one of the most complex, dynamic, and highly productive ecosystems found on the planet (Odum and Odum, 1955; Connell, 1978). Coral reefs are the equivalent of primary tropical forests for the marine ecosystem. Their distributions and structures represent an ideal location providing nurseries, spawning places, and gathering food sources for many species, including humans. They are an essential ecosystem resource for the subsistence of populations and society (Moberg and Folke, 1999; Woodhead et al., 2019). Corals form natural barriers that protect islands and coastal cities against physical erosion due to the destructive forces of waves, cyclones, and tsunamis by absorbing more than 90% of this energy (S. Wells and Ravilious, 2006). Coral reefs also provide a large panel of ecosystemic services. More than 500 million people rely on resources provided by coral reefs (Woodhead et al., 2019). The estimated value the latter returns is around 24 billion euros each year (P.-Y. Chen et al., 2015). Coral reefs also have a significant role to play within human fisheries as they represent around 12% of the overall fisheries around the globe and more than 90% of the fisheries for the southeastern Asian countries (Moberg and Folke, 1999; Sinclair et al., 2002). Reefs also represent valuable resources and significant economic incomes, primarily due to tourism activities, but also proving sand, essential for facilities such as road and buildings (C. R. Alliance, 2010). Coral reefs are also a significant source of molecules used in the cosmetic and medical fields, and for example, can be used as biological models to understand better immune mechanisms (Spurgeon, 1992; Moberg and Folke, 1999). Corals can be found in many places around the world. From cold to temperate and tropical waters, tropical coral reefs represent the core of the coral diversity of the world's coral reef ecosystems. Tropical coral reefs thrive primarily in shallow waters within the euphotic zone of the ocean, which comprises the first 30 to 50 meters of the water column. Tropical reefs are mainly distributed within the regions between

the 30° North and 30° South, where their thermal optimum is comprised between 21 to 29.5°C (Kleypas et al., 1999; Teh et al., 2013; **Figure 1.1**).

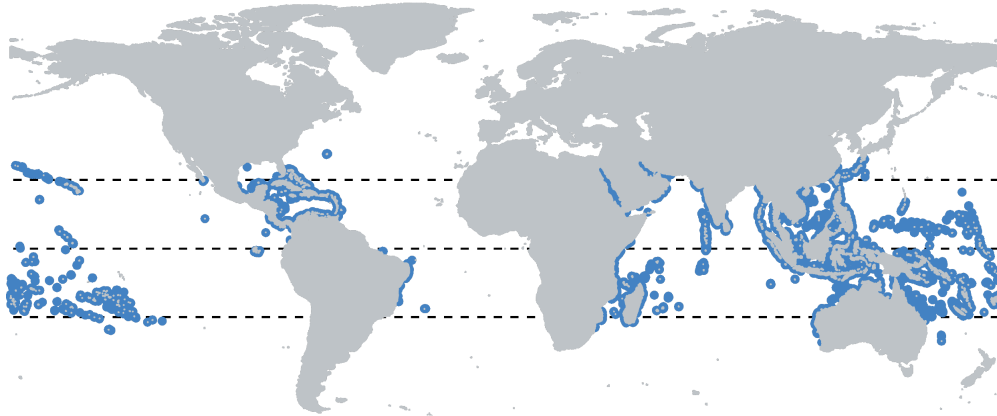


Figure 1.1: The geographical distribution of tropical coral reefs worldwide from 30°N to 30°S. Data are from Burke et al., 2011.

While coral reefs represent less than 1% of the total surface of the ocean, they gather one of the highest biodiversity found on the planet representing more than 25 to 30% of the ocean diversity (Spalding et al., 2001), considered as important biodiversity hotspots (Gove et al., 2016; Wagner et al., 2020). Reef species diversity has been estimated at 600,000 to more than 9 million species worldwide (Reaka-Kudla, 1997; Bouchet, 2006). The world's coral reefs are broadly categorized into six reef zones representing 284,300 km² of ocean area (S. M. Wells, 2008). Coral reefs are found primarily in Southeast Asia (28% of the world's reefs), the Pacific Ocean (25%), Australia (17%), the Western Indian Ocean (WIO; 16%), the Atlantic Ocean (9%), and the Middle East (5%) (Burke et al., 2011; D. Obura et al., 2017). Kitahara et al., 2016 reported 1500 living species of scleractinian corals, divided among 31 families and approximately 240 genera. At least 845 species of corals are known to build reef frameworks in the photic zone (Carpenter et al., 2008), with a wide diversity of coralline algae and invertebrates also contributing to building reef structures.

1.1.1.2 A Jewel in Perish

Despite their extraordinary biodiversity and many ecosystemic services, coral reefs represent one of the world's most endangered and vulnerable ecosystems. Coral reefs could disappear at the end of this century (Allan et al., 2021) and are widely regarded as one of the top conservation and science priorities globally (Klein et al., 2010; Hughes et al., 2017). Corals are very sensitive to their environment. The main disturbances that

can modify those environmental conditions are local and global perturbations (e.g., ongoing climate change).

1.1.1.2.1 Local Disturbances and Anthropogenic Impacts

A wide range of stressors describes local perturbations for coral reef ecosystems. Destructive fishing, overfishing, coastal development of cities, dredging within reef areas, mass tourism, increased sedimentation associated with the runoff of land-based activities, and eutrophication (enrichment of nutrient concentrations, concern phosphate and nitrogen) directly affect the stability and health of coral reefs (Hughes, 1994; Edinger et al., 1998; Szmant, 2002). Coral reefs are found in oligotrophic waters, poor in nutrients such as nitrogen and phosphate (N, P). Despite the low nutrient concentrations, coral reefs exhibit high gross primary productivity rates (Hatcher, 1990; Gattuso et al., 1999; Leclercq et al., 2002; McLaughlin et al., 2023). Massive input of nutrients (especially nitrogen or phosphorus) can degrade reefs through different mechanisms (Dubinsky and Stambler, 1996; Szmant, 2002; Fabricius, 2005). For instance, eutrophication is known to increase the rates of macrobioerosion and microbioerosion (Risk et al., 1995; Edinger et al., 2000; Holmes et al., 2000; Tribollet et al., 2002; Tribollet and Golubic, 2005). Rates of macrobioerosion observed at the Great Barrier Reef (GBR, Australia) were three to ten times higher at inshore eutrophic reefs than at offshore oligotrophic reefs (Risk et al., 1995; Tribollet and Golubic, 2005). On the other hand, Carreiro-Silva et al. (2005) showed that after adding nutrients, microbioerosion rates were five to ten times higher under eutrophic conditions (depending on the grazing pressure) than under oligotrophic conditions at Belize Reef. Chazottes et al. (2002) also showed a similar trend of amplification rates of carbonate dissolution from the different agents (grazers, macroborers, microborers) subject to various levels of eutrophication (exert primary control). Also, nutrient enrichment might be responsible for trophic changes and might increase turbidity and cause light loss, which might affect photosynthesis rates. Finally, sedimentation might cause reduced larval settlement and enhanced mortality (Fabricius, 2011). Nonetheless, some studies described positive coral calcification responses to increase nutrient availability and that nutrient-enriched corals might be less sensitive to acidification (Atkinson et al., 1995; Langdon and Atkinson, 2005; Holcomb et al., 2010) or vice versa where dissolved inorganic carbon (DIC) added to seawater could mitigate the detrimental effect of nutrient enrichment (Marubini and Thake, 1999). Chauvin et al. (2011) also suggested

that nutrient-enriched might positively affect coral calcification in scenarios with and without a pCO₂ increase. Overall, it is inappropriate to discount the detrimental effects of increased nutrient concentrations on coral reefs, reducing coral diversity and recruitment by enhancing macro-algae settlement. Several authors (McCook, 1999; T. McClanahan et al., 1999; Cheroske et al., 2000) have suggested that nutrient loading alone is unlikely to lead directly to macro-algal overgrowth of corals. Phase shifts from abundant coral to abundant macroalgae might appear to involve the combined effects of eutrophication, physical disturbances, and reductions in herbivory (Wanders, 1976; Russ and McCook, 1999; Vermeij et al., 2010). Enrichment of nutrients might also lead to the apparition of invasive species such as the starfish *Acanthaster planci* (Messmer et al., 2013), the main predator of corals. This organism can be responsible for destroying entire reefs, as it has affected the Great Barrier Reef (De'Ath et al., 2012). Additionally, chemical pollution like "antifouling" paints, the discharge of detergents within coastal areas (Sheikh et al., 2009), fertilizers and pesticides (West and Van Woessik, 2001), sunscreens (Corinaldesi et al., 2018; Fel et al., 2019), or the increased and massive discharge of plastic waste through rivers (Lebreton et al., 2017; Reichert et al., 2018) wash directly to the ocean and represent important threats to corals. For instance, marine debris and chemical product exposure can reduce corals' prey acquisition and growth rates (Mouchi et al., 2019; Nama et al., 2023). Plastic debris might deprive corals of light and oxygen exchange, which gives pathogens and makes the reef more vulnerable to disease (Lamb et al., 2018). Corals can also be exposed to high concentrations of heavy metals (e.g., Zn, Pb, Ni, Co, Cu, Mn) that can directly affect and impact their metabolism (T.-R. Chen et al., 2010; Biscere et al., 2015; Jafarabadi et al., 2017). Coral reefs are also subjected to tanker traffic, shipping, the petrochemical industry, coastal and urban development (Abdolahpur Monikh et al., 2013). Moreover, it has recently been highlighted that light and noise pollution might affect coral development and other organisms present within these ecosystems (Ayalon et al., 2019; Garrett et al., 2020; Ferrier-Pagès et al., 2021). When these local anthropogenic pressures are combined with more global pressures (i.e., temperature increase, acidification), these multi-stress factors accumulate and strongly threaten the future of coral ecosystems.

1.1.1.2.2 Global Changes: Focus on Ocean Acidification and Warming

Since the mid 19th century, expansion of industrialization and human demography led to excessive consumption and utilization of fossil fuel energies (coal, petroleum, gas).

Additionally, such consumption was also coupled with fast and intense territorial development and massive deforestation of primary forests (second largest anthropogenic source of carbon dioxide (CO₂) to the atmosphere; Van der Werf et al., 2009; Song et al., 2015, Allan et al., 2021). These activities have led to massive emissions of CO₂ into the atmosphere over the last 150 years and therefore significantly altered the global carbon cycle of the Earth system (Cox et al., 2000; Dufresne et al., 2002; Friedlingstein et al., 2003). The concentration of CO₂ atmospheric has drastically increased from 280 parts per million (ppm) in 1850, before the industrial revolution, to more than 410 ppm in 2020 (Hashimoto, 2019; Dlugokencky and Tans, 2020; Friedlingstein et al., 2022). In consequence, the global atmospheric temperature has increased by 0.8 to 1.2°C since 1850 (Allan et al., 2021). However, this increase in temperature did not only warm the atmosphere but also significantly increased the temperature of the global ocean. The ocean plays a central role in the Earth's climate. On the one hand, it absorbs 93% of the extra heat caused by the anthropogenic emissions of greenhouse gases, on the other hand, it acts as a strong carbon sink by absorbing approximately 30% of anthropogenic CO₂ from the atmosphere (Sarmiento and Sundquist, 1992; Hoegh-Guldberg et al., 2014). Nevertheless, the efficiency of the ocean to absorb the excess of CO₂ from the atmosphere is disrupted by the ongoing climate change (Fung et al., 2005). In tropical regions, as a consequence of the global warming, coral reefs are subject to stressing events called "bleaching" events (see **Figure 1.2**). Coral bleaching by nature describes a succinct event that coral can recover after. Survival rates of corals depend on the intensity of the warming (e.g., Marine Heatwaves), its duration, and the influence of other co-perturbations. Nonetheless, over the last five decades, the intensity and severity of bleaching events have dramatically increased, leading to global bleaching events and have led to massive coral mortality across the world's coral reefs (Hoegh-Guldberg, 1999; Kleypas and Langdon, 2006; Hoegh-Guldberg et al., 2014; Hughes et al., 2018; Sully et al., 2019). This phenomenon involves the breakdown of the symbiosis between the scleractinian corals and their symbiont, a dinoflagellate protist from the genus *Symbiodinium*, also called "zooxanthellae" (Odum and Odum, 1955; Muscatine and Porter, 1977; Hoegh-Guldberg, 1999). This symbiosis is very sensitive to corals' physical and chemical environment changes. Several factors can drive the disruption of the symbiosis and the loss of symbionts, such as short periods of high or low temperature and/or light, exposure to toxins, chemical pollution, changes in pH, and salinity (Hoegh-Guldberg et al., 2017).



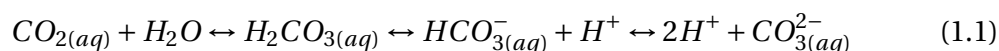
Figure 1.2: Side-by-side comparison of a coral reef before and after bleaching. Credit: Chasing Coral.

In addition to the overall warming, the stability of oceans is also threatened by another crisis called "ocean acidification" (OA), a significant process that affects and changes the seawater carbonate chemistry (Kleypas and Langdon, 2006; Guinotte and Fabry, 2008; Feely et al., 2009). Predictions and scenarios displayed by the IPCC establish a pH reduction from 0.2 to 0.4 units (Allan et al., 2021) at the end of the century. A pH change of this magnitude probably has not occurred for more than 20 million years of Earth's history (Feely et al., 2004). The rate of this change is cause for serious concern, as many marine organisms, particularly those that calcify, may not adapt quickly enough to survive these changes. Guinotte and Fabry (2008) reviewed and attempted to provide a general synthesis of known and/or hypothesized biological and ecosystem responses of several taxa, particularly those that build skeletons, shells, and tests of biogenic calcium carbonate, to increase OA. The scientific knowledge base surrounding the biological effects of OA is still in its infancy, and the long-term consequences of changing seawater chemistry on marine ecosystems can only be theorized. Some studies allowed the identification of "tipping points" or "thresholds" of seawater carbonate chemistry when OA will cause net calcification rates to be less than net dissolution rates in coral reef systems (Yates and Halley, 2006; Hoegh-Guldberg et al., 2007). Reduction in calcification could fundamentally alter the current structure and function of coral reef ecosystems' growth depending on their ability to accrete faster than erosional processes can break them down. On the other hand, few studies have investigated the effects of OA on CaCO_3 dissolution rates and how it could enhance

bioerosion processes from different agents. For instance, Tribollet et al. (2009) experimentally demonstrated increased bioerosion rates under high-CO₂ conditions. When exposing dead coral blocks of *Porites lobata* colonized with natural euendolithic and epilithic communities to different seawater pCO₂ conditions, bioerosion rate under the high-CO₂ conditions was significantly higher than in ambient conditions. Additionally, Enochs et al. (2016) deployed dead coral blocks (*Porites* sp.) for roughly 2 years at two reefs in Papua New Guinea, each experiencing volcanically enriched CO₂ concentrations and showed that OA conditions were correlated with decreased calcification and increased macroboring activities primarily by annelids. Recently, Schonberg et al. (2017) reviewed and attempted to provide information on how erosion and its biological associated agents relate to the OA "problem". Their work summarizes definitions and concepts in bioerosion research and knowledge regarding the context of OA, providing case examples and meta-analyses. Nonetheless, the physiological responses of bioeroders and their interactions with environmental factors are insufficiently studied. OA research and its effects on bioerosion are also in their infancy. Further investigations are needed to obtain more data for reliable general prognoses. Global trends suggest that growing environmental changes (e.g., eutrophication, coral mortality, OA) might elevate bioerosion in the near future. Changes harmful to calcifiers may not be as severe for bioeroders (e.g., warming); and factors facilitating bioerosion often reduce calcification rates (e.g., OA).

One of the most important components of the chemical perspective of oceanography is the carbonate system, primarily because it controls the acidity of seawater. Also, the carbonate system of the ocean plays a key role in controlling the pressure of CO₂ in the atmosphere, which helps regulate the planet's temperature (Emerson and Hedges, 2008). Before the industrial revolution, the mean ocean's pH was around 8.18 (Cao and Caldeira, 2008), while today, pH has decreased to around 8.1. This reduction in the pH system might appear insignificant, but this translates to an increase of nearly 30% of the concentration in ions H⁺ in the seawater surfaces, increasing seawater acidity and modifying the whole carbonate system. Dissolved compounds that make up the carbonate system in the ocean occur in three principal forms: dissolved carbon dioxide (CO₂ (aq)), bicarbonate ion (HCO₃⁻), and carbonate ion (CO₃²⁻). The dissolution of atmospheric CO₂ in seawater forms carbonic acid (H₂CO₃), a weak acid that, at equilibrium, releases protons (H⁺) and bicarbonate ions (HCO₃⁻) but reduces the number

of carbonate ions (CO_3^{2-}) available (**Equation 1.1**).



This reduction in carbonate ion concentration (CO_3^{2-}) also leads to a reduction in the calcium carbonate saturation state (Ω), significantly impacting marine calcifiers. A reduction in the number of carbonate ions available will make it more difficult and/or require marine calcifying organisms to use more energy to form biogenic calcium carbonate (CaCO_3 ; **Figure 1.3**)

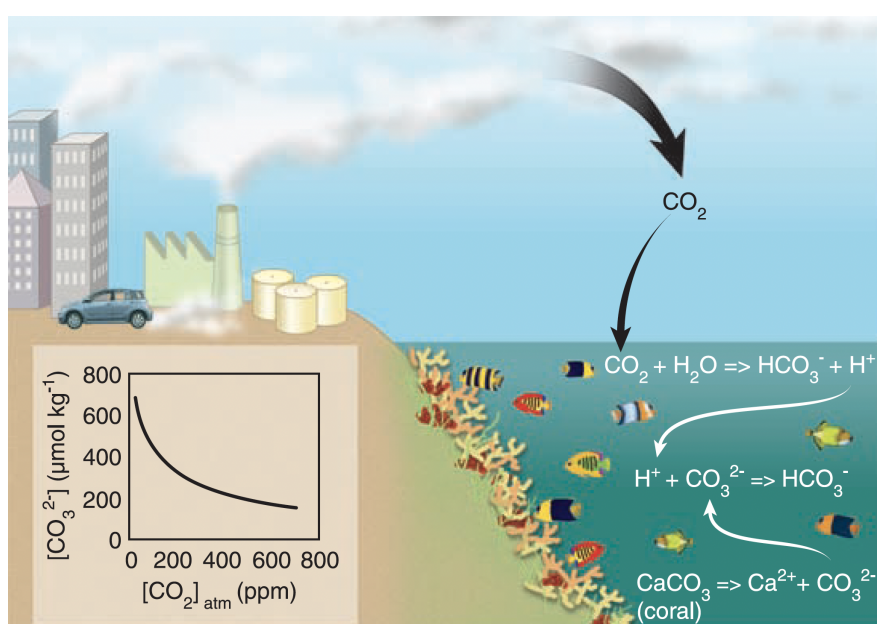


Figure 1.3: Conceptual figure showing the effect of increasing CO_2 concentration on acid-base chemical species present in seawater. Atmospheric CO_2 , taken up by the ocean, combined with water to produce carbonic acid, which releases a proton that combines with a carbonate ion, decreasing the concentration of carbonate ions, and making it unavailable to marine calcifiers such as corals. For additional information, refer to Hoegh-Guldberg et al., 2007 showing the acidification process and its impact on corals.

Corals are one of the most endangered ecosystems facing OA, leading to an overall change in their physiology and growth conditions. The overall documented impacts are the lowering of their skeletal density (soft calcareous skeleton), reduced rates of their calcification or their vertical extension (Gattuso and Hansson, 2011; M. McCulloch et al., 2012; Gattuso et al., 2013; T. M. DeCarlo et al., 2015; D'Olive et al., 2019). Nonetheless, all corals have not been affected the same way by increased levels of OA or warming with more tolerant taxa than sensitive ones (e.g., massive vs. branching corals, Hughes et al., 2017; T. M. DeCarlo et al., 2019).

Ocean circulation features and water masses associated result from various processes across many spatial and temporal scales. All these processes interact together to transport physical, chemical, or biological properties that create the ocean circulation structures observed on the planet and control biodiversity settlement in the different oceanic regions. Therefore, warm-water coral reefs largely depend on the physical and chemical changes that are occurring at the ocean's surface (Freiwald et al., 2004; Eakin et al., 2010), which are different across the planet. Differences also translate into trajectories regarding near and long-term projections of planetary oceans warming and OA. Over the last 70 years, enhanced anthropogenic CO₂ concentrations have increased SSTs of the Indian, Atlantic, and Pacific oceans, respectively of 0.65 °C, 0.41 °C and 0.31 °C (Hoegh-Guldberg et al., 2014). Long-term ocean temperature records show continuous, intense, and fast warming in the Indian Ocean, at about 1.2 °C from 1901–2012 (Roxy et al., 2014). These different SST changes across the disparate oceanic regions impact coral reef ecosystems differently, showing the world's coral heterogeneous variability and resilience facing the ongoing climate change (Hoegh-Guldberg et al., 2017). For instance, the Indian Ocean presents unique features in many respects (e.g., boundary currents) compared to the Atlantic and Pacific oceans (Schott and McCreary Jr, 2001; R. Hood et al., 2015). Unusual attributes, including large alongshore-propagating meanders and eddies, can substantially modify surface currents, upwelling, and downwelling circulations, mainly observed within the WIO (Lutjeharms, 2006; Fig.1 in R. R. Hood et al., 2017; Vinayachandran et al., 2021), affecting in return primary production rates, and the marine diversity within this area. Within the WIO, the Mozambique Channel (MC) is a region of high biodiversity, important fisheries, and a coastal area that supports pristine ecosystems, estuaries and mangroves, high biological diversity, and endangered species, as well as being home to the second most biodiverse area for coral species in the Indo-Pacific (D. Obura et al., 2022). The MC is a highly dynamic region characterized by southward migrating mesoscale eddies most prominent in the western half (Roberts et al., 2014; Halo et al., 2014). These eddies are formed around the Comoros Islands (in the northern MC; **Figure 1.4**) due to the baroclinic instability of the South Equatorial Current (SEC) (Backeberg and Reason, 2010; Mawren, Hermes, et al., 2022) or can be shed off the southwest coast of Madagascar (de Ruijter et al., 2004) from the East Madagascar Current (EMC) as large pairs of counter-rotating eddies. As cyclonic and anticyclonic eddies separate from the mean flow, they may trap cool or warm waters anomalously in their center. For Instance, Mawren et al.,

2020 investigated SST differences between cyclonic eddies and ambient waters in the northern MC in April 2019 that were of 1 °C and slightly less for anticyclonic eddies and are even larger SST differences in eddies associated with the southern part of the MC. Therefore, the temperature gradient between the eddies and the surrounding water can significantly impact the different ecosystems distributed within the MC differently.

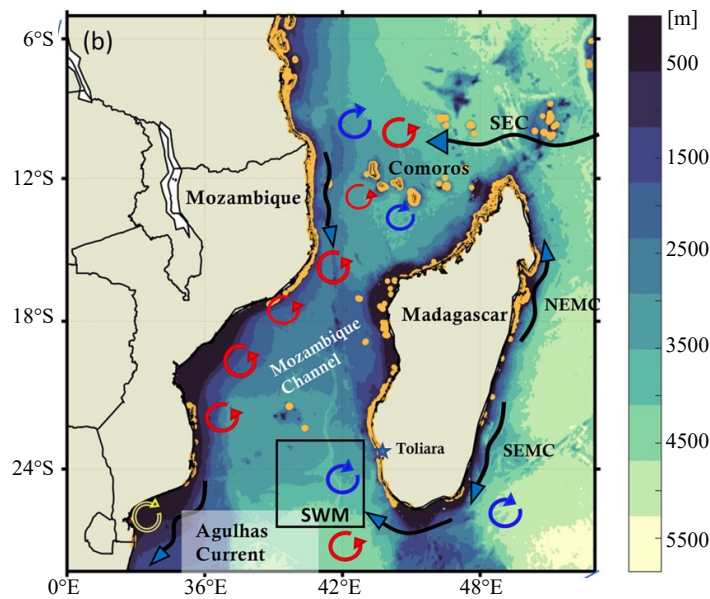


Figure 1.4: Figure modified from Mahwren et al. (2021) showing the details of the key ocean circulations over the MC. SEMC South-East Madagascar Current, NEMC North-East Madagascar Current, SEC South Equatorial Current, and Agulhas Current. Red and blue circles illustrate idealized anticyclonic and cyclonic eddies, respectively. Orange shading highlights the distribution of warm-water coral reefs. Colorbar represents the bathymetry.

1.1.2 Reefs Functioning: A Balance of Forces

Corals are the most important of several reef-building organisms compared to the others, like crustose coralline algae, sponges, and mollusks. First, coral larvae settle on submerged rocks or hard substrate surfaces along the edges of islands or continents to form diverse reef structures. When corals grow and expand in cover, three major reef structures can be observed: fringing, barrier, or atoll reefs (Friedlingstein et al., 2003). Fringing reefs, the most common and widely distributed reefs, develop in shallow waters around islands. They project from the shore toward the sea surrounding islands and form borders along the shoreline. Barrier reefs, as fringing ones, border shorelines but are present at an even greater distance from the shore. Barrier reefs are isolated by an open (often deep) lagoon and separated from their adjacent land mass. Atoll reefs are described as circular or oval reef structures with a lagoon within their center

(**Figure 1.5**). Reef platforms may emerge, and passes in the reef provide access to the central lagoon. Barrier reefs and atolls represent one of the oldest and most spectacular biologically and productive habitats in the ocean (**Figure 1.5**). All three reef types: fringing, barrier, and atoll display different environmental conditions characterized by differences in depth, wave energy, current strength, light, temperature, different bottom topography, and different suspended sediment materials that drive distinct zones for coral settlement, algae, and other tropical species.

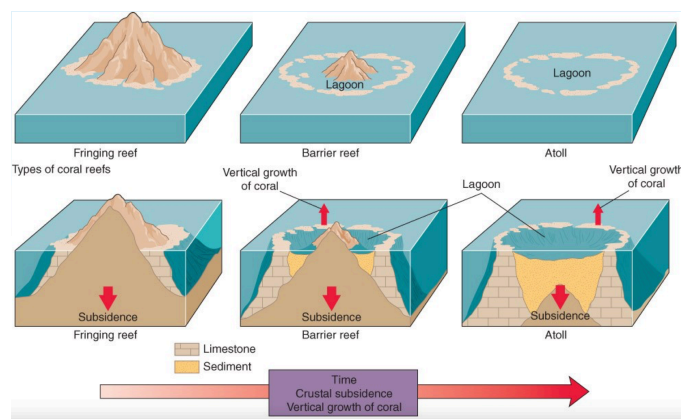


Figure 1.5: The developmental sequence of coral reefs, from young fringing reefs (left) to barrier reefs (center), and finally to atolls (right).

Reef systems are defined as a balance where different forces come along. The production and accumulation of reef framework carbonate are controlled by the relative rates and the interactions between ecologically, physically, and chemically driven production and erosion processes (constructive vs. destructive forces; T. Scoffin, 1992). The primary framework from corals, the secondary framework from calcareous encrusting communities, sedimentation burial, and marine cementation represents constructive forces. On the other hand, destructive processes, which remove or degrade primary (and secondary) framework carbonate, are mainly associated with the effects of either physical (mainly storm) or biological disturbances (erosion forces). Erosion of coral reefs is defined through three forces governed by interrelated physical, chemical, and biological processes (Tribollet and Golubic, 2011). Physical erosion includes seismic events, storm damage, wave, and current action that can cause severe structural damage to coral reefs and export large quantities of CaCO_3 sediments to deeper water (T. P. Scoffin, 1993; Andersson and Gledhill, 2013). Abiogenic chemical erosion is characterized by the thermodynamically driven, passive dissolution of carbonates

through acidity or undersaturation ($\Omega < 1$; e.g., Trudgill, 1976; Morse et al., 2007; Andersson and Gledhill, 2013). Biological erosion or bioerosion—processes is defined through the action of living organisms that degrade hard materials such as wood, bone, cement, siliceous rock, and foremost different CaCO_3 substrates (Neumann, 1966; Scott and Risk, 1988; Wisshak and Tapanila, 2008; Tribollet and Golubic, 2011). Among erosion processes, bioerosion represents the main force of reef degradation (T. Scoffin et al., 1980; Tribollet and Golubic, 2011; Schönberg et al., 2017). Reef bioerosion affects sedimentary and skeletal carbonate substrates. It plays an important role in reef sedimentation and diversity maintenance (creation of habitats and food resources), is involved in biogeochemical cycles (recycling of dissolved Ca^{2+} and C), and thus represents an integral part of the coral reef carbonate balance (Tribollet and Golubic, 2011). Within bioerosion, different processes are described with chemical and mechanical erosion. Formerly, they were named bio-corrosion, which refers to the destruction of carbonates by chemical means, and bio-abrasion, which refers to the mechanical removal of carbonates by organisms (Golubic and Schneider, 1979; Schneider and Torunski, 1983; Tribollet and Golubic, 2011; Schönberg et al., 2017). The path of bioerosion depends on the type of organisms involved in the dissolution process (Andersson and Gledhill, 2013; Schönberg et al., 2017). Overall, chemical etching or leaching dissolves hard material (e.g., microborers) and is contrasted by mechanical fracturing, rasping, biting, and removal of particles (e.g., grazers). Many organisms even combine both modes (e.g., macroborers). These processes, taken in the broadest sense of the term ‘reef taphonomy’ (T. Scoffin, 1992; C. Perry and Hepburn, 2008), define the carbonate budget of reef production or dissolution states. A carbonate budget is the sum of gross carbonate production from corals and calcareous encrusters mainly, as well as sediment produced within or imported into the reef, minus that lost through biological, physical, and chemical erosion, dissolution, or sediment export. Net accretion occurs when this budget is positive with carbonate production and the extension of the coral cover. Net erosion occurs when this budget is negative with carbonate dissolution and reduction of the coral cover. When the budget is neutral, the reef is maintained at equilibrium (stasis) (**Figure 1.6**).

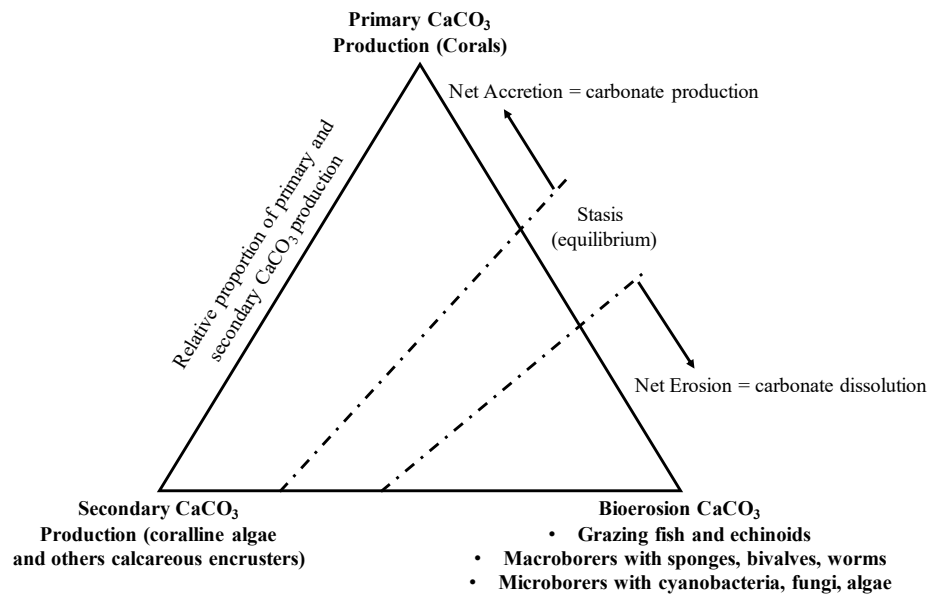


Figure 1.6: Ternary diagram showing different carbonate production states determined by variations in the relative importance of primary (coral) and secondary (calcareous encruster) carbonate production and carbonate breakdown to sediment/dissolution by bioerosion. Figure modified from C. Perry et al., 2008.

1.1.3 Massive Corals: Natural Bio-Archives

Scleractinian corals present very diversified morphologies, isolated or colonial, that can form massive, hemispherical, or domed colonies. For instance, massive corals can live for several centuries and thus measure a few meters in diameter. In this thesis, the focus is on two massive coral genera *Porites* and *Diploastrea* (Figure 1.7).

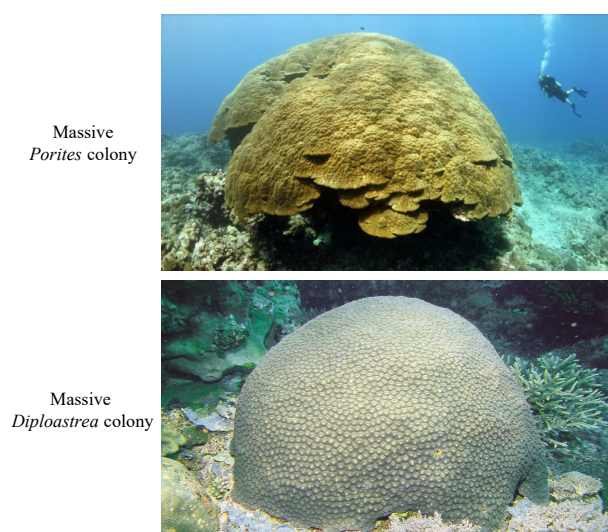


Figure 1.7: (A) Massive *Porites* colony that measures about 13 m across, 6.5 m in height, and 41 m in circumference at the base. Credit Photo: Wendy Cover/NOAA. (B) Typical massive *Diploastrea* colony observed in Indonesia. Credit Photo Gerry Allen.

Their massive form offers them a specific resistance over a long period and prevents them from substantial physical erosion (waves, current energy). They grow around a few mm to a few cm annually. As observed with dendrochronology, the study of annual rings in trees, corals display a similar pattern of annual density banding. Sclerochronology represents the analysis of this pattern, the physical and chemical variations in the accretionary hard tissues of organisms, and the temporal context in which they formed. Sclerochronology focuses primarily on growth patterns reflecting annual, monthly, fortnightly, tidal, daily, and sub-daily increments of time and aims at reconstructing past environmental variability (Hudson et al., 1976; Buddemeier, 1978; Watanabe et al., 2019). These massive corals live in shallow waters (the first 60 m) and are relatively accessible. The genus *Porites* (Link, 1807) has a repartition between 2 and 60 m in depth. The genus *Porites* is easily identifiable, presenting a considerable logistical advantage during the sampling phase. Nonetheless, species identification within the genus *Porites* is not easy and can imply the use of different techniques that can be costly (Scanning Electron Microscope (SEM), optical microscopic, metabarcoding). *Porites* corallites are small, irregular, and highly variable, making it challenging to be identified both in the field and the laboratory (Darke and Barnes, 1993; Forsman et al., 2015). Thus, comparing cores from the same genus but not automatically from the same species can add biases to the different analyses, which need to be considered later on. For instance, in this thesis, massive *Porites* corals collected between the different sites might be different species (e.g., *P. lutea* or *P. lobata*), which could influence differently microbioeroding communities colonizing the coral skeleton, even if corals are from the same genus (species effect). Massive *Porites* generally present a growth around 1 to 1.5 cm.yr⁻¹ (J. Lough, 2008; Cantin and Lough, 2014). The genus *Diploastrea* (Matthai, 1914) also forms massive colonies, denser and generally slower growing (2 to 6 mm.yr⁻¹) producing continuous paleoclimatic records potentially extending over 1000 years (Bagnato et al., 2004; Wu et al., 2018). *Diploastrea heliopora* (Lamarck, 1816) is the only living species assigned to the genus throughout its taxonomic history (Wijsman-Best, 1980), thus eliminating the possibility of inter-species effects on geochemical paleo-proxies (Bagnato et al., 2004; Budd et al., 2012; D. Huang et al., 2014). Budd et al. (2012) supported that *Diploastrea heliopora* had a distinct lineage and only species of its genus (clade XV) amongst living coral species, sister to *Montastraea cavernosa* (see Figure 2 in D. Huang et al., 2014). The presence of the *Porites* genus (here an example of the massive species *P. lutea*) extends to the Pacific Ocean, the Atlantic and

Indian Ocean, and the Caribbean. *Porites* is present within the WIO with a confirmed presence within the Scattered Islands, la Reunion, Comoros Archipelago, and along the eastern African coast. On the other hand, *Diploastrea* is widely distributed on reefs of the Indo-Pacific and absent eastwards from Hawaii. Its presence within the WIO is less confirmed than *Porites*, essentially for la Reunion and the Scattered Islands (e.g., Europa, at the northern part of the MC). Overall, *Diploastrea* is less distributed than the massive *Porites* with main differences in the WIO and the Pacific Ocean (Figure 1.8).

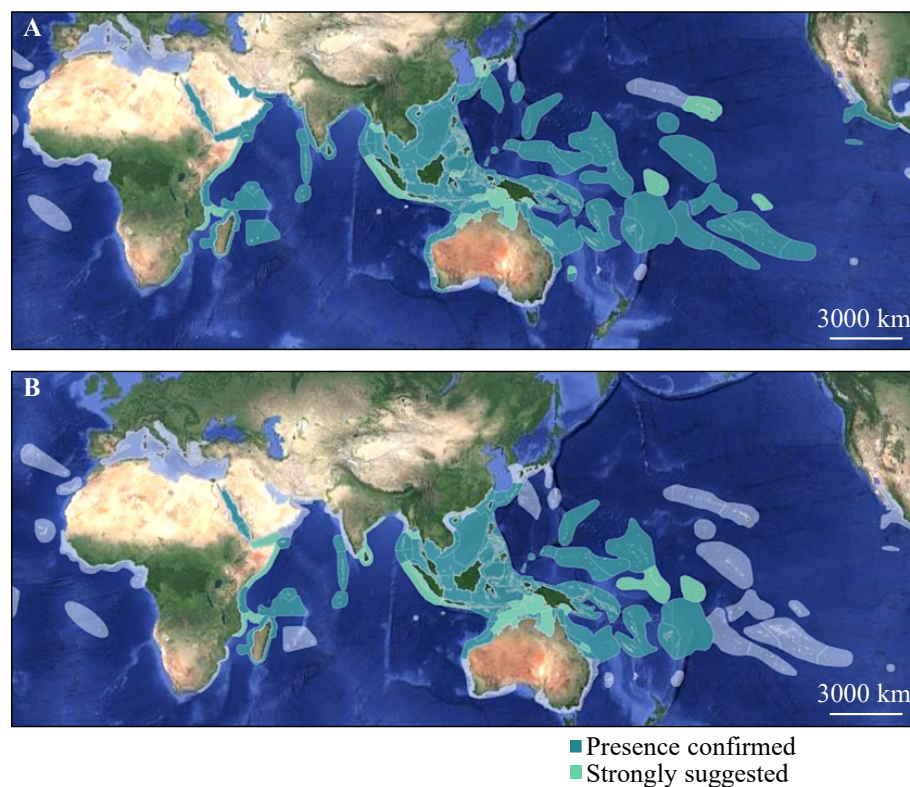


Figure 1.8: (A) Distribution of one species of massive *Porites* colony: *Porites lutea* (B) Distribution of the massive coral *Diploastrea heliopora*. Both maps obtain from Corals of the World (<http://www.coralsoftheworld.org/page/home/>).

Over the last decades, geochemical tools called geochemical tracers (i.e., "proxies") have been developed. Massive tropical corals have been natural archives used in paleoclimatology, paleoceanography, or past environmental sciences for many years (J. Lough, 2008; J. Lough and Cantin, 2014; Wu et al., 2018; Reed et al., 2021). During their development, corals continuously secrete calcium carbonate (CaCO_3) to form their skeleton. Its chemical composition depends on environmental factors (temperature, light, salinity, pH, carbonate chemistry, nutrients, pollutants) and the elemental or isotopic composition (Li, B, Sr, Nd, Pb, Mg, Ca...) (Gagnon et al., 2007; Montagna et al., 2014; Ram and Erez, 2021).

1.2 Reef Bioerosion

1.2.1 Bioerosion Processes

Natural biological erosion (termed bioerosion; Neumann, 1966) can be defined as the corrosion of hard substrates by living organisms. Bioerosion is an essential mechanism of CaCO_3 recycling, especially true in shallow, warm-water habitats such as coral reefs. It is almost precisely the antagonistic counterpart of biological calcification and the main pathway of erosion (Tribollet and Golubic, 2011; Schönberg et al., 2017). Bioerosion, the major force of reef degradation, also aggravates the effects of physical erosion (cyclones, storms) by increasing material porosity, weakening reef substrates (living and dead corals) from the inside and the outside, leading to an overall increase in fragility of coral reefs (Highsmith et al., 1983; Scott and Risk, 1988; Tribollet and Golubic, 2011). Bioerosion is due to the actions of a natural diversity of bioeroding agents (Figure 1.9).

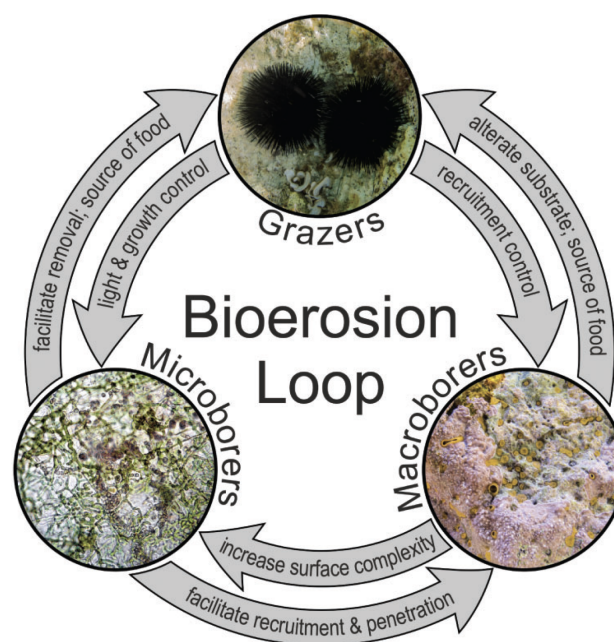


Figure 1.9: The bioerosion loop shows a simplified model of interactions between the main bioeroder groups. Figure from Schönberg et al., 2017.

It is divided into different categories based on their pathway of erosion (chemical vs. mechanical erosion) (internal vs. external erosion). Firstly, the diversity of bioeroding agents is composed of organisms such as cyanobacteria, chlorophytes, rhodophytes, and fungi, constituting the group of microborers. Microborers represent internal bio-

eroders ($<100\ \mu\text{m}$) that live within the substrate and employ mainly chemical bioerosion processes. Secondly, organisms like bivalves, worms (e.g., polychaetes), and sponges constitute the macroborers group. Macroborers are internal bioeroders ($>100\ \mu\text{m}$), employing both pathway of chemical and mechanical erosion processes. Finally, the last group of eroding agents gathers the activities from fishes, urchins, and snails and represents the grazers. Grazers are external bioeroders and remove material from the substrate surface employing mainly a mechanical erosion process (Odum and Odum, 1955; Golubic et al., 1981; Tribollet, 2008; Schönberg et al., 2017). Overall, bioeroders (micro and macroborers and grazers) all interact with each other and with their environment constituting the "bioerosion loop" (**Figure 1.9**). These biological eroding agents have critical roles in reef systems. As mentioned, by directly degrading the primary and secondary framework produced by carbonate producers (e.g., corals, CCA), they increase the susceptibility of coral reefs to physical and chemical erosion. In turn, the physical breakdown of CaCO_3 structures and substrates to smaller sizes can further promote biological and chemical dissolution because of the resulting increase in the ratio of surface area to volume (Andersson and Gledhill, 2013), thus strongly influencing carbonate budgets (dissolution, production, and recycling of CaCO_3). Under normal conditions, borers and grazers do not contribute just to bioerosion by dissolving and fragmenting CaCO_3 substrate but also deliver valuable ecosystem services and sustain and maintain reef health. Microborers are major primary producers on reefs that support many food webs and trophic interactions (e.g., predation) and share nutrients with corals (e.g., Schlichter et al., 1995; Fine and Loya, 2002; Tribollet et al., 2006). Microborers represent a renewable food source for grazers and facilitate the process of grazing by weakening the superficial substrate layer. Besides weakening CaCO_3 for grazers, microborers prepare the substrate for macroborer settlement, e.g., for polychaetes and sponges (e.g., Hutchings, 1986; Mao Che et al., 1996; Schönberg et al., 2017). In turn, they increase the surface area, substrate porosity, light penetration, and thus available microhabitat for microborers (Chazottes et al., 1995; Tribollet and Golubic, 2005; Schönberg et al., 2017; Fordyce et al., 2020). Macroborers are efficient filter feeders that purify the water and recycle nutrients (e.g., Rose and Risk, 1985; Yahel et al., 2009; Mueller et al., 2014). Macroborers also facilitate grazing efficiency by weakening the substrates for parrotfishes, urchins, and mollusks and cause significant calcareous sediments production (Akpan and Farrow, 1985). In addition, many grazers do not only control turf biomass and various euendoliths but are also thought to reg-

ulate macroalgal abundances, thus indirectly reinforcing coral cover (e.g., Sammarco, 1982; Mumby and Harborne, 2010). However, Clements et al., 2017 reviewed herbivorous reef fishes' (parrotfishes) trophodynamics with the first assumption that parrotfishes were primary consumers of macroscopic algae. Instead, the data were consistent with the hypothesis that most parrotfishes were microphages and target cyanobacteria and other protein-rich autotrophic microorganisms that live on (epilithic) or within (endolithic) calcareous substrata. The novel view provided by the authors of parrotfish (grazers) feeding biology provides a unified explanation for the disparate range of feeding substrate used by parrotfishes and further integrates parrotfish nutrition and their ecological roles in reef bioerosion and sediment transport.

1.2.2 Bioeroding Microflora

1.2.2.1 Definition and History

Difficulties and understanding in some research areas sometimes arise from misdefinitions and misusing terms. Regarding bioerosion agents, Golubic et al. (1981) clarified the term "endolith" (microorganisms that inhabit the interior of a substrate) and distinguished different organisms. First, when studying microflora, there is a distinction between microorganisms that inhabit the rock's surface, "epiliths," and those that inhabit the fissures in the rock, "endoliths." Endoliths include organisms that colonize existing fissures (chasmo-endoliths) or cavities in porous substrates (cryptoendoliths), as well as those which actively penetrate carbonate substrates in which they live, such as euendoliths (Golubic et al., 1981). Euendoliths comprise various organisms of different sizes. Microbial euendoliths are often referred to as microborers (bioeroding microflora) (Tribollet and Golubic, 2011) (**Figure 1.10**).

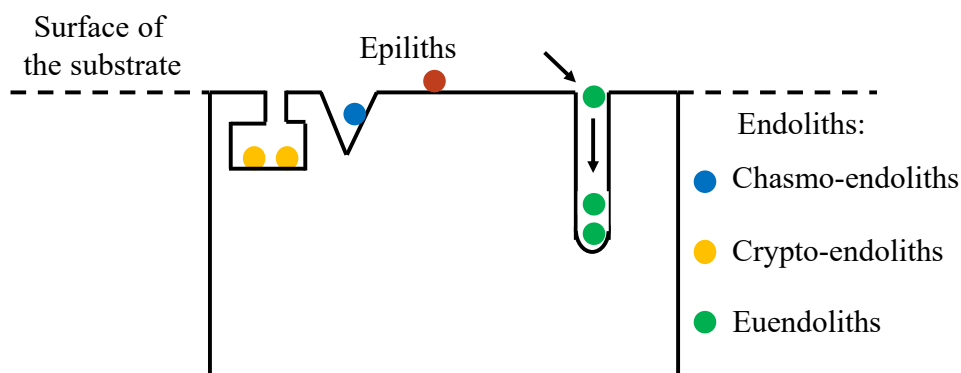
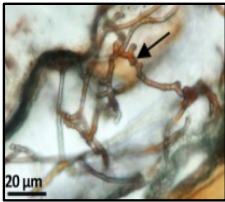
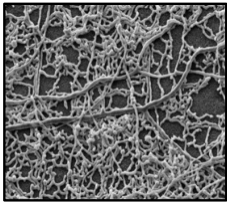
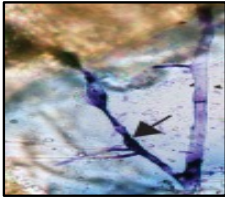
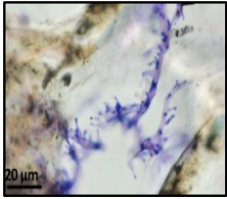
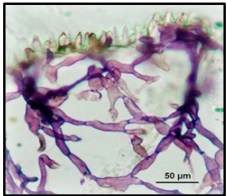
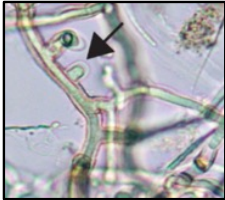




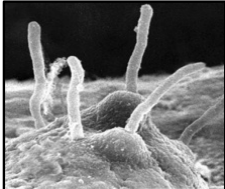
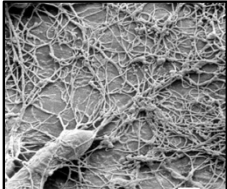


Figure 1.10: Schematic presentation of various types of endoliths that can colonize a substrate. Figure adapted from Golubic et al., 1981.

Bioeroding microflora regroup autotrophic (cyanobacteria, red, and green microalgae) and heterotrophic (fungi) organisms. Microborers organisms have long geological histories and have been present on Earth since the Mesoproterozoic, 1.5 billion years ago (Zhang and Golubic, 1987; Golubic and Schneider, 2003) and have played a significant role in the development and evolution of life as well as the production and destruction of carbonates (Schneider and Le Campion-Alsumard, 1999; Sánchez-Baracaldo et al., 2022). The most common genera of autotrophic euendoliths observed in coral reef substrates (microscopy observations) around the world are the chlorophytes *Ostreobium* (Bornet and Flahault, 1888), and *Phaeophila* (Hauck, 1876), the rhodophyte *Porphyra* (Agardh, 1826) (Conchocelis stage), the cyanobacteria *Hyella* (Bornet and Flahault, 1888), *Mastigocoleus* (Lagerheim, 1886), and *Plectonema* (Bornet and Flahault 1889). Heterotrophic euendoliths are mainly composed of fungi. A brief morphological description and microscopic observations of the main microborers are described in the following **Figure 1.11**. Bioeroding microflora taxonomy has been studied since the 19th century (Bornet and Flahault, 1888) and more widely over the last decades (Lukas, 1973; Golubic et al., 1975; Le Campion Alsumard et al., 1995; Priess et al., 2000; Tribollet, 2008; Tribollet and Golubic, 2011; Golubic et al., 2019).

Algae		
		<p><i>Ostreobium</i> sp. (Chlorophyte)</p> <ul style="list-style-type: none"> Siphonous filaments with variable diameter Polymorphic branched with typical swellings, zigzag branching pattern <p>Description: Lukas, 1973, 1974 Illustration: Massé et al., 2018, Tandon et al., 2022</p>
		<p><i>Phaeophila dendroides</i> (Chlorophyte)</p> <ul style="list-style-type: none"> Branched filaments and elongated cell, separated by cross-walls Thick lamellated crosswalls <p>Description: Nielsen, 1987 Illustration: Grange et al., 2015 and Massé et al., 2018</p>
		<p>Conchocelis stage of Bangiales (Rhodophyte)</p> <ul style="list-style-type: none"> Branched septate filaments Cylindrical cells Euendolith (cryptic stage) <p>Description: Pica et al., 2016 Illustration: Pica et al., 2016</p>
Cyanobacteria		
		<p><i>Mastigocoleus testarum</i></p> <ul style="list-style-type: none"> Cylindrical and thick walls Short lateral branches, terminal heterocysts (black arrow) <p>Description: Golubic and Le Campion-Alsumard, 1973 Illustration: Ramirez-Reinat and Garcia Pichel, 2012, Grange et al., 2015</p>
		<p><i>Plectonema tenebrans</i></p> <ul style="list-style-type: none"> Separated cylindrical cells, mainly unbranched Elongated cells, wide (1 to 1.5 µm) and long (2 to 6 µm) <p>Description: D'Hont and Coppejans, 1988; Wisshak et al., 2011 Illustration: Grange et al., 2015</p>
		<p><i>Hyella caespicio</i></p> <ul style="list-style-type: none"> Cylindrical cells, apical is the longest Large cells (4 to 10 µm) <p>Description: D'Hont and Coppejans, 1988 Illustration: Prusina et al., 2015</p>
Fungi		
		<ul style="list-style-type: none"> Visible (sometimes) reproductive organs (bag shape) Perpendicular, dichotomously branched, ramifications Fungal hyphae isodiameter (µm) <p>Description: Golubic et al., 2005 Illustration: Golubic et al., 2005</p>

54 Figure 1.11: Illustrations and presentation of morphological characteristics of some microborers.

Thanks to the advance of molecular and genetic approaches in the last ten years, much information has been obtained on the diversity of these communities. For instance, sequencing approaches have recently shown massive biodiversity of the green algal euendolith *Ostreobium* in coral skeletons, including a lineage of about 80 different *Ostreobium* species and several other entirely unknown family-level lineages (Sauvage et al., 2016; Del Campo et al., 2017; Ricci et al., 2019). Euendoliths are ubiquitous, found in almost every environment, geographical location, and depth, where the appropriate substratum (e.g., relatively soluble carbonate and phosphate substrates) is available, and their biological requirements are met (Golubic et al., 1975; Friedmann et al., 1988; Gaylarde et al., 2006). They are observed in terrestrial (Ascenso et al., 1998; Golubic and Schneider, 2003), freshwater (Schneider and Torunski, 1983), and marine ecosystems, including the Adriatic Sea (Ghirardelli, 2002), the Mediterranean Sea (Le Campion-Alsumard, 1979), cold temperate coasts (Wisshak et al., 2005), Antarctic (De Los Rios et al., 2005). Over the years, attention has been given to euendoliths infestation in tropical waters such as coral reefs (Le Campion Alsumard et al., 1995; C. T. Perry, 1998; Priess et al., 2000; Tribollet, 2008), as they are believed to have played one of the major roles in the production and destruction of carbonate including reef frame-builders over long periods of geological time.

1.2.2.2 Colonization of Bioeroding Microflora

Despite their microscopic size, euendoliths, main agents of reef bioerosion, can colonize each available micrometer of carbonate surface area from carbonate sand, bivalve shells, the thalli of crustose coralline algae to the skeletons of dead and live hard corals. Infestation within dead substrates is always higher than in their live counterparts due to the new colonization of their surface by euendoliths (Le Campion Alsumard et al., 1995; Tribollet and Payri, 2001). However, the penetration depth of euendolithic filaments in dead substrates corresponds to their bathymetric distribution, depending on the species. For instance, species requiring high light intensities such as *Mastigocoleus testarum* do not penetrate deep into substrates (less than 1 mm in dead *Porites lobata*; Chazottes et al., 1995). In contrast, oligophotic species such as *Plectonema tenebrans* and *Ostreobium quekettii* shows a depth of compensation of 2 to 4 mm in dead *Porites lobata* (Chazottes et al., 1995). Heterotrophic fungal filaments are independent of light and use the euendolithic chlorophytes and the residual organic matter in coral skeletons as a source of food (Bentis et al., 2000; Golubic et al., 2005).

In live corals, living tissue/cell layers can prevent colonization by microborers from the external environment (e.g., water column) (tissues form a sort of anti-fouling layer (Bentis et al., 2000; Le Campion-Alsumard et al., 1995; Tribollet, 2008). Photoautotrophic euendoliths can colonize the coral skeleton from its base as soon as the larvae settle on an already-infested substrate. Massé et al. (2018) showed that microborers colonize branching corals as soon as the carbonate basal plate of the primary polyp is formed (within seven days after metamorphosis). In living corals, the species composition of microbial euendoliths is mainly phototrophic microorganisms dominated by *Ostreobium* sp., that keep up following the growth of their coral host to maintain their access to light and thus their metabolic activity (Le Campion Alsumard et al., 1995; S. H. Magnusson et al., 2007; Massé et al., 2018). Only a few euendolithic organisms have adapted to the low-light and extreme conditions provided by the coral skeleton environment. Light requirement selects only microborers present (positive phototropism, i.e., the ability to move towards the light), such as the cyanobacterium *Plectonema terebrans*, the chlorophyte *Ostreobium quekettii*, and less frequently, some conchocelis stages of Bangiales rhodophytes (Lukas, 1974; Laborel and Le Campion-Alsumard, 1979; Ralph et al., 2007; Gutner-Hoch and Fine, 2011), and fungi. Living calcifying organisms' structure, porosity, and skeletal mineralogy greatly influence euendolith infestation (C. T. Perry, 1998). The great variety of coral growth forms and skeletal features are likely to contribute to shaping the colony's physico-chemical characteristics, thus controlling the level of euendoliths infestations. Recently, Fordyce et al. (2022) investigated the possible correlations between coral inter-specific patterns in skeletal morphology and the variability in the biomass of the endolithic biofilm (dominated by *Ostreobium* sp.). They proposed that the specific density of a coral's skeleton and its capacity for capturing and scattering incident light are the main correlates of endolithic microbial biomass. Overall, studies suggested that variations in the macro- and microstructure of the coral skeleton might be a key characteristic highlighted as a potentially important factor affecting euendolithic taxa distribution, composition, and, therefore, overall microbial biomass inside the skeleton (Golubic et al., 1975; Vogel et al., 2000; Reyes-Nivia et al., 2013; Iha et al., 2021).

As the chlorophyte *Ostreobium* sp is described as the most abundant microborer in coral hosts, several studies showed that it forms dense, visible green bands underlying the coral tissue in slow-growing corals such as massive *Porites* sp. (Lukas, 1974; S. H. Magnusson et al., 2007; Verbruggen and Tribollet, 2011; Ricci et al., 2019; **Figure 1.12 A to C**).

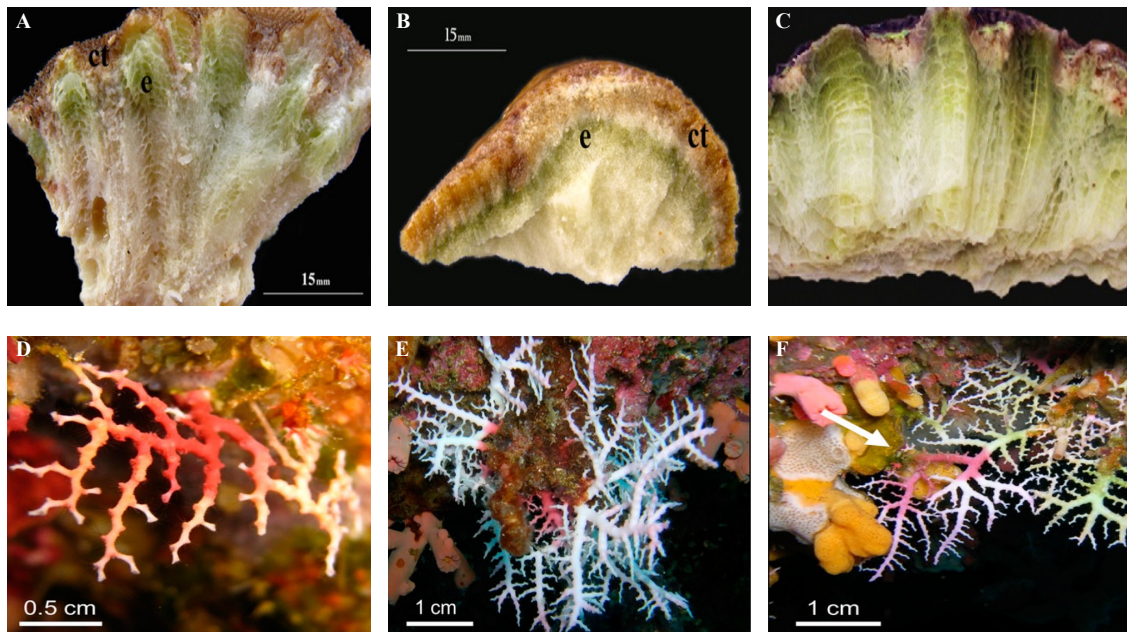


Figure 1.12: (A) Fractured *Goniastrea perisi* with a distinctive green band of endoliths "e" underneath the coral tissue "ct". (B) Fractured *Porites lutea* with a distinctive green band. (C) Close-up of the coral colony *Paragoniastrea* sp. with green boring algae inside the skeleton. (D) Colonized orange *Stylaster* sp from Siladen Island appearing pink-orange in the base. (E) White *Stylaster* sp from Siladen Island with a pink base. (F) *Stylaster* sp from Siladen Island with an apical branch colonized by euendoliths (arrow). Colorations represent colonization from euendolith identified as a cryptic stage of the rhodophyte *Porphyra* (Conchocelis stage). Photographs A and B were extracted from Gutner-Hoch and Fine, 2011. Photograph C was extracted from Verbruggen and Tribollet, 2011. Photographs D to F were extracted from Pica et al., 2016.

Additionally, black bands or red coloration can sometimes be observed in living scleractinian corals and are attributed to microboring fungi (Bak and Laane, 1987; Priess et al., 2000, in coral of the genus *Porites*) or the Conchocelis stage of some rhodophytes (Bangiales; Laborel and Le Campion-Alsumard, 1979; Pica et al., 2016; **Figure 1.12 D to F**). In branching corals, microboring communities dominated by *Ostreobium* sp. do not form green bands as the host growth is too fast and 'dilute' filaments (Godinot et al., 2012; Massé et al., 2018). To the best of our knowledge, only Lukas (1973), Le Campion-Alsumard et al. (1995), and Priess et al. (2000) truly quantified the abundance of microborers in white (= raw coral skeleton) versus green or black bands in living corals. They showed a greater abundance of filaments or microbioeroding traces and chlorophyll

b characteristic of *Ostreobium* sp., in colored bands than in white ones. Le Campion et al. (1995) stated that a green band comprises a dense growth of branched *Ostreobium quekettii* filaments loaded with chloroplasts and starch grains. In such areas of high filament concentration, over 25% of skeletal carbonate could be dissolved (bor-ing). However, the distribution of euendolithic organisms is not limited to the colored bands as they can be present in most regions of the skeleton, although in low densities to be visible (Le Campion Alsumard et al., 1995). Le Campion et al. (1995) suggested that the pattern of green bands in adult colonies of the massive *Porites* could correlate with areas of dense euendolithic growth and are often correlated with areas of slower growth in corals, as shown by the patterns of colored bands in massive, slow-growing corals (Duerden, 1902; Highsmith, 1981; Le Campion Alsumard et al., 1995).

1.2.2.3 Environmental Effects on Bioeroding Microflora

For recall, bioeroders are divided into different erosion processes (chemical vs. mechanical; internal vs. external). Known biology of a given bioeroder taxon and its mode of bioerosion enhance the comprehension of how environmental factors may shape their distribution patterns and biological success implying their bioerosion rates (e.g., Hutchings, 1986; Schönberg, 2008; Tribollet and Golubic, 2011; Wisshak, 2012). Bioeroding communities and their bioerosion rates are highly heterogeneous across space and time (Chazottes et al., 1995; Tribollet and Golubic, 2005; Färber et al., 2015). Caution must be exercised in extrapolating bioerosion rates because they are likely, not constant, and vary between reef habitats (Hutchings, 1986; Wisshak and Tapanila, 2008; Glynn and Manzello, 2015). Bioerosion rates for any particular organism may vary significantly depending on the environment, the density and hardness of the substrate, and competition from other bioeroders different from one location to another (Trudgill, 1976; Hutchings, 1986; Andersson et al., 2007; see Table 1 in Andersson and Gledhill, 2013). In dead corals, environmental parameters (e.g., eutrophication, OA, SST) can positively drive the activity of some bioeroding agents (e.g., micro and macroborers). As most endolithic bioeroders are either phototrophs or filter feeders, they either benefit from elevated levels of nutrients in dissolved or particulate form in the water column (Chazottes et al., 2002; Carreiro-Silva et al., 2009; Carreiro-Silva and McClanahan, 2012). Nutrients can significantly control microbioerosion rates and the abundance of endolithic algae over fungi in carbonate substrate but also initiate a feedback loop where bioerosion processes reinforce one another (e.g., actions of graz-

ers and macroborers), leading to accelerated reef framework erosion (Carreiro-Silva et al., 2009). Additionally, as microborers employ exclusively chemical bioerosion, OA is thought to directly ease this latter process via reduced alkalinity and pH. It is furthermore assumed to indirectly accelerate bioerosion by stimulating energy capture in phototrophic bioeroders and making mechanical bioerosion more effective by “softening” the carbonate substrate (e.g., Tribollet et al., 2009). Nonetheless, investigations on dead carbonate substrates and how environmental parameters affect the bioeroding activities of the different agents bear the limitation of short-term data (a few months to a few years) due to the complexity of deploying experimental blocks in the ocean for multiple years.

On the other hand, the distribution of euendolith organisms in living coral skeletons is mainly controlled and limited by the environmental parameter of light availability within the skeleton. Different factors may influence the light regime available for euendolithic organisms (Highsmith, 1981). Initially, between 0.1 and 10% of the photosynthetically active radiation (PAR) penetrates and reaches the zone of the euendolithic algae, as most of the PAR is absorbed by the coral tissue’s symbionts (zooxanthellae; Halldal, 1968; Shibata and Haxo, 1969; Fine and Loya, 2002). Secondly, the light transmission within the coral skeleton is affected by the skeletal architecture of this latter. Corallites on the top of coral colonies guide light deeper into the coral skeleton. In contrast, in corallites on the side of the colony, light enters at an angle, reducing its penetration into the skeleton (Highsmith, 1981). Finally, the depth of the water column and how far the light can go directly drive the phototropism of euendoliths in living coral skeletons. With future projections of pCO₂ scenarios (e.g., Tribollet et al., 2009; Enochs, Manzello, Tribollet, et al., 2016), microborers could present bioerosion rates about 150% of present-day bioerosion (Figure 5a in Schönberg et al., 2017). The main consequences in reef systems will be observing a shift of the accretion/dissolution balance toward net positive dissolution toward 2100, dramatically impacting coral carbonate budgets. Overall, the physiological responses of bioeroders and their interactions with environmental factors are insufficiently studied. Bioeroders’ threshold responses to pCO₂, temperature, and other environmental factors need to be explored more systematically. There is an urgent need to obtain high-quality bioerosion data in the short and long run. Environmental parameters, their potential influences, and interactions with bioeroding agents (e.g., regulation of the abundance of organisms, increased bioerosion rates) over the long term must be studied in detail to un-

derstand better how carbonate systems such as coral reefs may respond in the coming decades, and how carbonate budget might be affected (net dissolution vs. net accretion) in this changing environment. Global trends suggest that growing environmental change (eutrophication, coral mortality, OA) is expected to elevate bioerosion in the future. Changes harmful to calcifiers may not be as severe for bioeroders (e.g., warming). Factors facilitating bioerosion often reduce calcification rates (e.g., OA). The combined result means that the natural process of bioerosion could become an important “stress factor” for coral reef health and resilience.

1.2.2.4 Major Role of Bioeroding Microflora in Living Corals

To date, interactions between the photoautotrophic euendoliths (e.g., *Ostreobium*) and the coral host remain unclear. In the early 1950s, Odum and Odum suspected another relationship between photoautotrophic euendolith *Ostreobium* and their live coral hosts. This relation was described as positive and mutualistic rather than negative, which they termed ‘ectosymbiosis’ (Odum and Odum, 1955). They suggested that the coral host’s nutrients (via its metabolism) can reach the coral skeleton and, therefore, the euendolith filaments. Overall, the species composition, distribution, and abundance of microbioeroding communities in living corals remain poorly known, and most studies focused only on communities located within the first few centimeters below coral tissues of adult colonies (Lukas, 1973; Fordyce et al., 2021; Galindo-Martinez et al., 2022). Very little is known about microborers’ abundance variability over the life course of the coral host, especially in massive long-lived corals. In addition, sometimes alternating white and colored bands are observed within the skeleton of living massive corals, which indicate the presence of bioeroding microflora (Le Campion-Alsumard et al., 1995; Priess et al., 2000; Carilli et al., 2010). Priess et al. (2000) suggested that most colored bands observed in massive *Porites* from the Indo-Pacific could be due to a limited coral growth rate occurring at the end of the rainy (summer) season. Carilli et al. (2010), who also studied the alternating pattern of white and green bands, suggested that the presence of green bands may be due to microbioeroding phototrophs’ blooms during coral paling episodes (i.e., bleaching events) as they did not find any correlation with coral growth. They suggested that local-scale forcing factors are likely at play but found no significant relationship between physical parameters such as Sea Surface Temperature (SST) and the presence of green bands. Nevertheless, one question remains to understand the possible influence green bands can have on the coral host (e.g., on the

coral development, and its physiology). Besides serving as a food source for grazers such as parrotfish and urchins, euendolith can facilitate coral survival during bleaching events (e.g., boring algae *Ostreobium*; (Fine and Loya, 2002). As zooxanthellae are expelled from the tissue, coral growth slows down, and more light reaches the underlying layer of *Ostreobium*, boosting these algae's photosynthesis and growth. Fine and Loya (2002) showed that the translocation of photoassimilates from euendolithic algae to the coral host was higher in bleached coral colonies than in healthy colonies. This alternative energy source during bleaching events could improve coral colonies' survival chances in case of thermal stress, extending the time corals can survive without zooxanthellae. Overall, euendoliths have important functions in reef ecosystems and will surely influence how coral reef ecosystems cope with climate change and OA in the near future. However, we cannot yet decide whether they will act as a buffer against these environmental changes or worsen the situation as we lack data on the evolution of these communities (e.g., abundance, composition) over long-term environmental changes (e.g., SST, pH) in living carbonates such as corals. Thus, it is important to better understand euendolith ecological characteristics in coral environments to improve the knowledge of past environmental conditions to better predict the future of coral ecosystems over the next decades.

1.2.3 Known Methodologies to Study Microbioeroding Communities and their Bioeroding Traces

Diverse methods are available to visualize microborer organisms or their traces within different carbonate substrates. However, methods that allow quantifying the microbioeroding communities (biotaxa, organisms that bioerode) or quantifying their bioerosion traces (ichnotaxa) created by a bioeroder or trace maker are sparsely used, and respective publications are rare. Different techniques have been used to assess the quantification of microbioeroding communities.

One method investigated by Lukas, 1973 consisted of decalcifying pieces of living coral skeletons to count the number of microborer filaments under a light microscope. Furthermore, Lukas investigated the difference between the number of microborer filaments and chlorophyll "b" concentration by comparing areas of a coral skeleton of a green band, just underneath the coral tissue and a white band. A green band witnessed the presence of the main microborer *Ostreobium*. Her results highlight a greater

concentration of filaments and chlorophyll "b" on a green band than in a white one. Nevertheless, this technique is tedious and loses information regarding microborers' original spatial distribution within the substrate. Also, this method does not inform on the bands' position within coral samples or the period when they formed. Also, there was no estimation of the number of filaments related to a specific moment of the coral host, and to potentially relate a higher abundance of filaments in a green band to a slow period of coral growth as suggested by the author.

Another technique, investigated by Fordyce et al. (2021), analyzed the endolithic biomass (comprising crypto, chasmo, and euendoliths) from five different species of tropical hard coral. Coral carbonate samples were decalcified and extracted as an ash-free dry weight to measure the endolithic biomass (Fordyce et al., 2021). In their work, the authors aimed to identify whether coral skeletal characteristics correlated with variability in the biomass and chlorophyll concentrations of the endolithic microbiome. Nonetheless, such a technique results in a potential overestimation of microborer biomass as it cannot exclude the organic matrix of carbonates such as corals, sponges, mollusks, and bacteria (Mao Che et al., 1996; Cuif et al., 2004; Yang and Tang, 2019).

Over this last decade, X-ray computed tomography (CT), particularly micro-CT, has become an increasingly popular 3D visualization tool for paleontological investigations of various kinds (Sutton, 2008), including the study of macroborers (e.g., Enochs, Manzello, Kolodziej, et al., 2016). The highest resolution is achieved with synchrotron micro-tomography that utilizes monochromatic X-ray with very high beam intensity that allows a voxel size well below 1 μm (Tafforeau et al., 2006). The potential of all these technologies grounds that they are non-destructive, preserving external and internal structures of solid objects (e.g., coral skeletons). They can characterize sediment-filled fossil borings otherwise inaccessible for the vacuum cast-embedding technique. CT technology's major advantage is presenting results in printable and/or screenable 3D formats such as colored semitransparent views (**Figure 1.13 A and B**). This technique was recently investigated by Silbiger et al., 2014, which allowed them to calculate a very accurate rate for net accretion-erosion and to account for and digitally remove the effect of any pre-existing borings in the experimental substrate. This technique allows for visualizing new erosion scars by external and internal eroders and new growth

by secondary calcifiers in 3D, information that cannot be acquired from traditional buoyant weight techniques and precisely quantified the volume of CaCO_3 removed or accreted by comparing before and after images (**Figure 1.13 C and D**). Besides, their volumetric analysis measures changes at the voxel scale of $50\ \mu\text{m}$, which was then averaged to $100\ \mu\text{m}$, and therefore, cannot estimate erosion from microborers that make erosion traces between 1 and $100\ \mu\text{m}$ (most of them comprise traces between 1 and $30\ \mu\text{m}$). Same comments apply to the study of Enochs et al. (2016) with a resolution of the micro-CT set in their study at $65\ \mu\text{m}$.

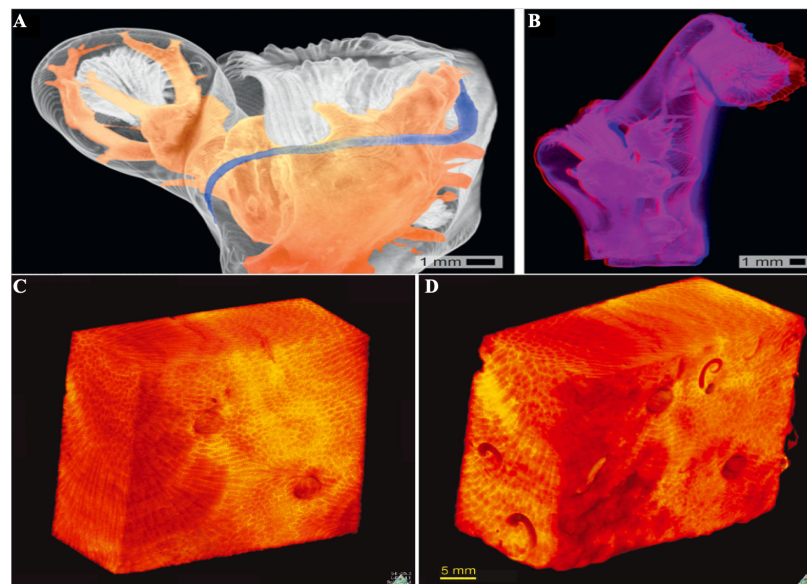


Figure 1.13: (A) Colored semitransparent visualization of a corallite of the cold-water coral *Lophelia pertusa* with the sponge cavity (orange) and an embedded epibiontic worm (blue). (B) Anaglyph 3D visualization of another corallite with heavy sponge infestation (requires anaglyph glasses with left eye red and right eye blue). For further details, refer to Wisshak, 2012. (C and D) Visualization of micro-computed tomography (μCT) scan of an experimental block of *Porites* sp. coral before (C) and after (D) 1 yr deployment in Coconut Island, Hawaii. Further details are available through a movie of the full 3D visualization of the different μCTCT images within their Supplement 2 from Silbiger et al., 2014.

A new technique developed by Schätzle et al., 2021 aimed at visualizing the endolith in situ, addressed as biotaxon (biological trace maker) as far as identification was feasible. Also based on the morphology of the traces, that is the distinct excavation caused by the activity of the boring organism, addressed by an ichnotaxon (trace fossils). Their techniques combine specific fluorescent dyes to study fungal euendoliths in situ in partly translucent mollusk shells with confocal laser scanning microscopy (CLSM). Euendoliths often contain pigments that show auto-fluorescence when stimulated with UV light and can be visualized with fluorescence microscopy. A major ben-

enefit of fluorescence staining and CLSM for the study of marine euendoliths is the differentiation of certain components of the euendoliths, such as cell nuclei for instance, if dyes with specificity to certain biomolecules are applied. A considerable advantage of this technique is the preservation of the three-dimensional configuration of the microborings inside the substrate of their ‘hosts’ due to the in-situ examination (**Figure 1.14 A to C**). Nonetheless, based on the **Figure 1.14 D and E**, the abundance of microborings might be underestimated as there is some ‘unspecific binding’ of the dyes, explained by the authors as probably caused by stained DNA of bacterial epigrowth. Such a technique can also be utilized for euendoliths, such as chlorophytes in corals. For instance, Försterra et al., 2005 used fluorescence microscopy for euendoliths investigation in a shallow cold-water azooxanthellate coral *Desmophyllum dianthus* from the Chilean fjord region. Nonetheless, this technique has not yet been tested within tropical massive corals.

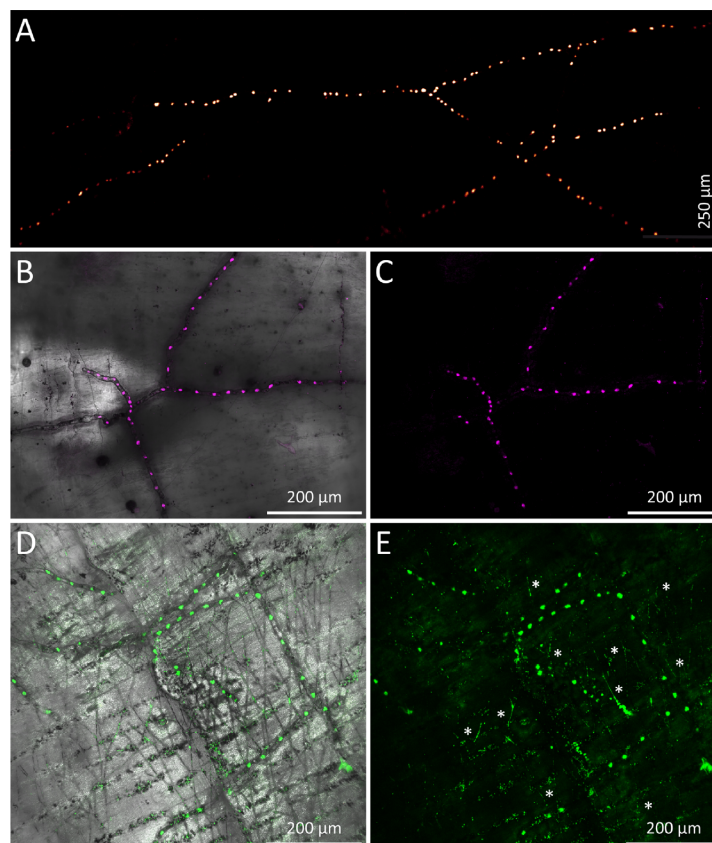


Figure 1.14: Selected regions of shells from the bivalve *Delectopecten vitreus* infested by different euendoliths and stained with fluorescent dye Sybr Green I. Further details for the different microborers are available from Figure 4 of Schätzle et al., 2021.

One technique is based on analyzing petrographic thin sections for microbioero-

sion investigations (bio and ichnotaxa (Wisshak, 2012). Microbioerosion traces can be visualized together with the surrounding matrix. The penetration depth of microbioerodings, as well as secondary mineralization, can easily be determined, which does not imply realizing the costly and standard cast-embedding technique (Figure 1.15). Nevertheless, this technique bears the main limitations adherent to any two-dimensional projections (2D) for the visualization of three-dimensional (3D) objects (e.g., the spatial distribution of microborings). For instance, light microscopy can allow studying microboring structures (e.g., external surface aspects of boreholes, Golubic et al., 1975). Thin sections can be colored with Toluidine blue to reveal live euendolithic filaments, determine the euendolithic species composition (biotaxa), the relative abundance of live filaments, and their depth of penetration inside coral skeletons (Tribollet et al., 2009). Also, the limitations of this technique are an incomplete presentation of the overall microboring network and work only for limited magnifications.

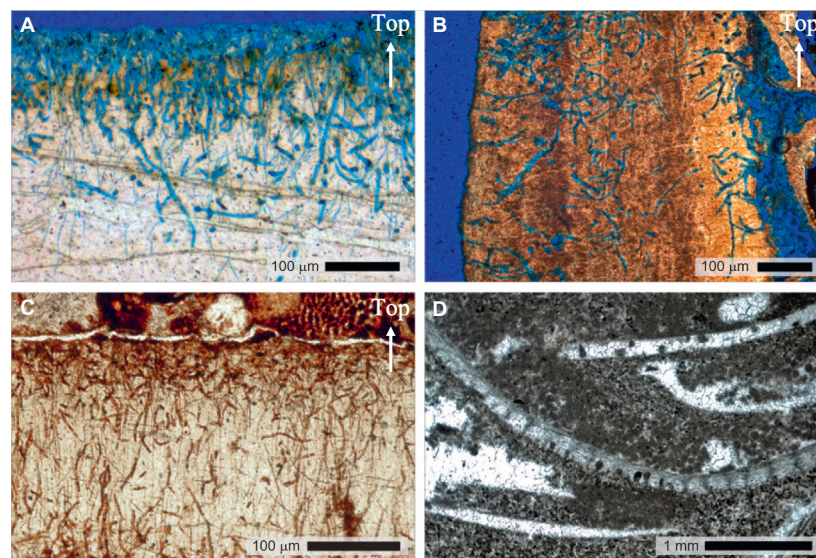


Figure 1.15: Figure extracted from Wisshak, 2012 showing different microbioerosion traces in thin petrographic sections. (A) displayed boring traces from ichnotaxa *Eurygonum nodosum* and *Scolecia filosa* in a recent bivalve shell from the Azores. (B) displayed fungal trace of *Orthogonium lineare* in a Pleistocene cold-water coral from Rhodes, Greece. (C) Same assemblage as in A, but from the Carboniferous Buckhorn Asphalt Lagerstätte, USA. (D) displayed a fungal trace of *Saccomorpha clava*, well preserved in a brachiopod shell from the Silurian of Gotland, Sweden.

One of the most approved methods for investigating microbioerosion structures (e.g., filaments, traces, boreholes) is the vacuum cast-embedding technique that produces polymer resin casts of the substrate investigated that can be visualized and studied under an SEM to display even the most delicate morphological features (Tribollet et

al., 2009; Wisshak and Rüggeberg, 2006; Grange et al., 2015). One prerequisite for this technique is that the borings are empty or filled only with resin epoxy. Thin sections embedded in resin also allow the same observations performed with light microscopy (e.g., estimation of the abundance of filaments/traces, maximal depth of penetration of euendolithic filaments in the substrates) but also assess the biogenic dissolution rates, represented by the surface area bioeroded from euendoliths (Tribollet et al., 2009). Carbonate dissolution rates are calculated following the equation:

$$CD = \frac{DP \times BSA \times CSD}{SAB} \times \frac{1}{1000} \quad (1.2)$$

where the CD is the carbonate dissolution rate (kg.CaCO₃.m².month or year), DP is the depth of penetration (cm), BSA is the bioeroded surface area and is the percent of bioeroded surface area per the picture (%), SAB is the surface area of the bloc exposed to colonization (cm²), CSD is the coral skeleton density in g.cm³, and the ratio 1/1000 converts grams into kilograms (Tribollet et al., 2009). Nonetheless, when quantified boreholes left by microborers, ramifications of microbioeroding filaments are not considered, which can lead to underestimating the actual volume of CaCO₃ dissolved by microbioeroding communities (see also Tribollet et al., 2019). Furthermore, the manual analysis of hundreds of SEM images of carbonate substrates (e.g., corals) for the investigation of microbioerosion structures (filaments, traces, boreholes) is highly time-consuming (e.g., more than 600 SEM by Tribollet et al., 2009) and costly (e.g., in this thesis one session of SEM cost around 100€). This technique depends on the area of the substrate investigated that might underestimate the actual abundance present within the coral (e.g., live corals, Le Campion Alsumard et al., 1995; Priess et al., 2000) or the actual coral surface eroded by euendoliths (e.g., dead corals, Golubic et al., 1975; Carreiro-Silva et al., 2005; Tribollet et al., 2009). Moreover, this technique mostly relies on the eye observer, to identify the microbioerosion structures and its ability to discriminate taxa or ichnotaxa based on the size of their filaments or traces (e.g., diversity and composition). Intricate networks of microborings (e.g., very thin with a diameter of 1 µm) make their identification difficult, and thus their real abundance estimation is complicated for the human eye. Hence, developing a new technique that quantifies microborers (e.g., microbioeroding traces) rapidly, efficiently, accurately, and continuously within the substrate is needed to provide more information on their assemblages, diversity (ichnotaxa), and abundance to enhance the comprehension of this group within coral skeletons.

1.3 Ph.D. Objectives

Microbioeroding communities' spatial evolution and variability over time remain to be studied. To date, no methodologies continuously quantify the real abundance of microbioeroding traces (reflection of the filaments) in coral skeletons over a long-term period. The comprehension of these communities, their biogenic dissolution activities, and how environmental influences can control this latter have been investigated mainly over the short term and in dead coral substrates. A gap remains on what occurs over the long term on how these communities thrive over the lifespan of the coral host. Also, as the environment regulates and controls corals' metabolism, another question remains on how these environmental factors can impact the microbioeroding communities living within. Therefore, the central objective of this Ph.D. project is to understand **the impacts of environmental changes on the composition and the abundance of microborers over the long term in living massive corals**. As long-term in situ experiments are challenging to conduct in dead carbonate substrates, an exciting alternative is studying microbioeroding communities in massive living coral colonies to understand their assemblage composition and the potential relationship between the abundance of microborers and green bands visible upon the skeleton of massive corals. Moreover, studying massive living coral colonies allows for assessing the variability of these communities over decades and identifying which biotic (coral) and abiotic (environmental) parameters could influence microbioeroding communities' abundance, distribution, and assemblage composition over time. Therefore, this thesis was structured around different main research objectives:

- The first objective is **to develop and validate a methodology for studying microbioeroding communities in living slow-growing corals over a long-term period (decadal variability)**. An efficient approach is needed to address this first question and will be presented in **Chapter 3**.

- Once this first objective is achieved, I apply this methodology on a massive coral core of *Diploastrea* sp. from Mayotte to understand **the influence of biotic or abiotic factors, or the combination of those two, that could explain the decadal variability of the composition and abundance of microbioeroding communities observed within *Diploastrea* sp.** Here, the focus is on studying the influence of coral and environmen-

tal variables on the variability of the abundance of microborers in the massive coral *Diploastrea*.sp and will be presented in **Chapter 4**.

- A third objective is to confirm the first trends observed in *Diploastrea* sp. in another massive coral genus such as *Porites* sp. and to evaluate if the same factors were responsible for the trends. The objective here is to understand if **the evolution of the composition and abundance of microbioeroding communities change from one coral to another. Moreover, it is to investigate the influence of biotic and abiotic factors on microbioeroding communities from *Porites* sp. and to determine similarities or differences with *Diploastrea* sp.** and will be presented in **Chapter 5**.

- For the last chapter, two objectives are addressed. Firstly, one objective is to investigate **the lipid biomarker composition of one strain of *Ostreobium*, the main microborer colonizing living corals. The second objective is to study the lipid biomarkers composition within the massive coral core *Diploastrea* that might be specific to microbioeroding communities and specifically *Ostreobium* sp.** If this approach is validated, lipid biomarkers could be used as a proxy informing on the presence and, to an extent, on the abundance of these communities in living massive coral skeletons. This approach and its results will be presented in **Chapter 6**.

- Finally, the last chapter will address the general Conclusions and Perspectives of this thesis and will be presented in **Chapter 7**.

Materials and Methodologies

Contents

2.1	Study Geographical Area: The Western Indian Ocean	71
2.1.1	Mayotte Island	73
2.1.1.1	Environmental Products Acquisition	74
2.1.2	Reunion Island	76
2.1.3	Scattered Island	77
2.1.3.1	Juan De Nova	78
2.1.3.2	Europa	78
2.2	Coral Data Acquisition	79
2.2.1	Coral Core Sampling	79
2.2.2	Coral Growth Variables	80
2.2.3	Temperature and pH Reconstructions from Coral Cores . . .	83
2.2.3.1	Known Proxies for SST and pH	83
2.2.3.2	SST Dataset Acquisition	84
2.2.3.3	pH Geochemical Analysis	85
2.3	Microbioeroding Communities Investigation	86
2.3.1	Identification of Microbioeroding Organisms: Microscopy Approach	86
2.3.2	Sampling Design to Study Microbioerodings' Abundance and Green Bands	89

2.3.3	Quantification of Microbioeroding Traces: Machine Learning Application	91
2.3.4	Determination of Potential Specific Lipid Biomarkers of Bioeroding Microflora: Geochemistry Approach	91

2.1 Study Geographical Area: The Western Indian Ocean

The WIO region comprises the Eastern African coastal states of Kenya, Mozambique, Somalia, South Africa, and Tanzania, as well as the island states of Comoros, Madagascar, Mauritius, Seychelles, and the French overseas territories of Mayotte and Reunion, and finally the Eparses Islands within the MC (**Figure 2.1**).

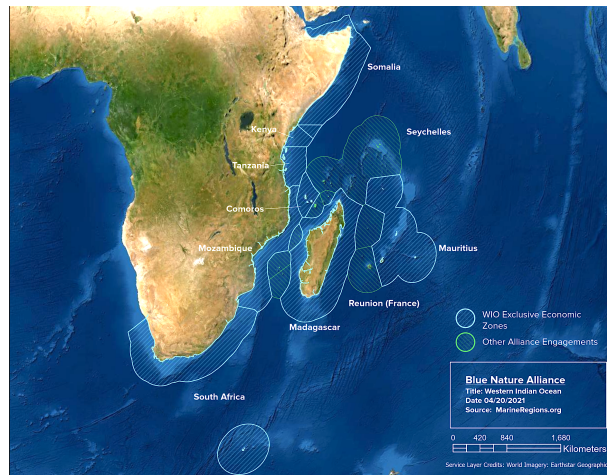


Figure 2.1: Map of the WIO, obtained from B. N. Alliance, 2020.

Its environmental gradient from tropical to temperate conditions and ocean current systems provides a unique opportunity to study climate change impacts on marine ecosystems (T. R. McClanahan et al., 2011). The WIO has a tropical to sub-tropical climate with water surface temperatures between 20 and 30 °C and air temperatures rarely falling below 20 °C. The climate is strongly affected by monsoons, where the northern monsoon generates light, steady winds of 5 m.s⁻¹ from November to March. The southern monsoon generates stronger winds (up to averages of 9 m.s⁻¹ in southern parts of the region) from June to September (Richmond, 2011; Hammar et al., 2012). The northern part of the MC is influenced by the monsoonal wind system, with wind stress predominantly from the north to northeast during austral summer and the south to southeast during austral winter (Saetre and Da Silva, 1982; Schott et al., 2009). The influence of the monsoon winds in the MC is halted at about 20°S (Tomczak and Godfrey, 2003; Schott et al., 2009). South of this latitude, the winds are southeasterly (known as the trade winds) almost all year round and are unfavorable for Ekman upwelling along the Mozambican coast. In the northern sector, upwelling develops at Angoche, off the coast of Nampula between 15 and 18°S around the narrows of the channel. Upwelling in the southern sector of the MC is more variable concerning location, but sev-

eral hotspot regions are evident. Seasonal wind-driven coastal upwellings result in elevated chlorophyll *a* signatures over areas within the MC (**Figure 2.2**).

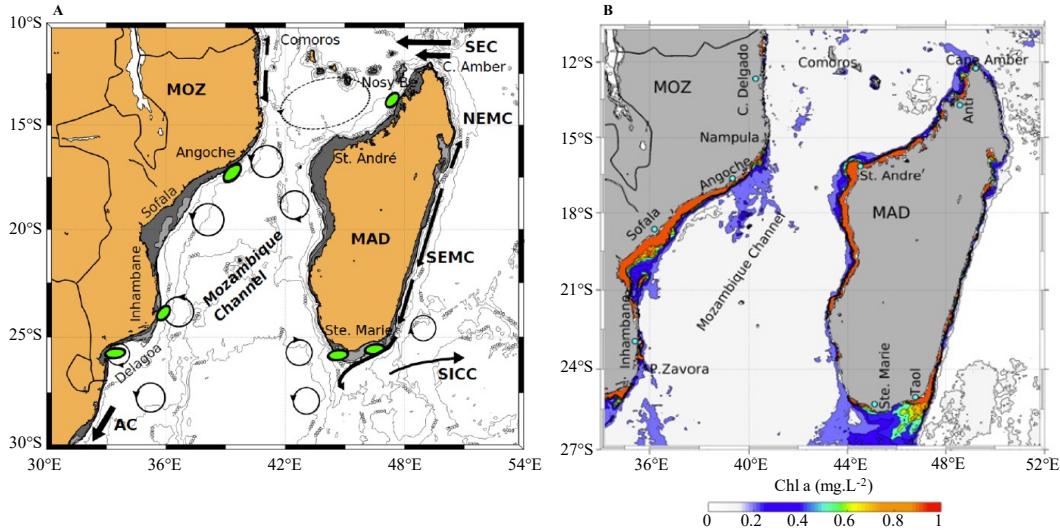


Figure 2.2: **(A)** Bathymetry and major circulatory features in the Mozambique Channel and around Madagascar. Shaded areas show the extent of the continental shelf to a depth of 200 m. Green ellipses denote upwelling areas. **(B)** Monthly mean chlorophyll concentrations for February 2003. Intermediate values beyond the continental shelf edge highlight areas of elevated productivity off the Mozambique and Madagascar coasts that are primarily upwelling-driven. Figures from Vinayachandran et al., 2021.

The WIO is globally acknowledged for its rich biodiversity and significant socio-economic value. The coral reefs, mangroves, seagrasses, rocky and sandy shorelines with associated dune systems, coastal forests, and deep-sea features such as seamounts, ridges, and abyssal plains contribute substantially to the biodiversity and the socio-economic growth of the region. Nonetheless, the reef-building coral fauna of the WIO is one of the least known globally (D. O. Obura, 2005). The WIO contains 16% of the world's coral reefs, and the region is now thought to host the second peak of coral reef biodiversity globally (D. Obura et al., 2017). Coral reef structure in the WIO is predominantly made up of fringing reefs around islands and continental coasts, with narrow lagoons (D. Obura et al., 2022). WIO coral reefs cover an area representing 11,919 km², where 5% of the global total coral reef ecosystems of this area are vulnerable and at risk of collapse (D. Obura et al., 2022). The most critically endangered coral reefs ecoregions in the WIO are represented by the Comoros Archipelago, Eastern, and Southern Madagascar, and the Mascarenes Islands (Reunion and Mauritius (D. Obura et al., 2022), therefore represent areas with an urgent need of crucial protection policies and studies interest. Therefore, during this thesis, the objectives focused on different locations across the MC. In the northern part of the MC, coral cores were collected within

the Comoros archipelago on the island of Mayotte. Coral cores were collected from the southern and central parts of the channel with the Scattered Islands (Europa and Juan de Nova). Both locations within the MC offer the opportunity to study a longitudinal gradient of the abundance of microbioeroding communities within contrasted reefs from a location heavily influenced by anthropogenic impacts (Mayotte, INSEE) to locations supposedly non-impacted by anthropogenic influences with no human presence (Scattered Islands). Finally, the last location investigated was outside the channel, with the island of La Réunion, offering a better understanding of the distribution, abundance, and composition of microbioeroding communities at a regional scale within the WIO.

2.1.1 Mayotte Island

Mayotte is located approximately around the 13°S and 45°E, about 300 km northwest of Madagascar in the northern part of the MC and about 450 km from the African continent. Mayotte is also located at the northern part of the vortex zone generated in the MC (C. Chevalier et al., 2017) and on the northwest extension of the South Equatorial Current (SEC). This current branches out northward into the East African Coastal Current (EACC) and southward into the Northeast Madagascar Current (NMC) (**Figure 2.3**; Schott and McCreary Jr, 2001; Vinayachandran et al., 2021).

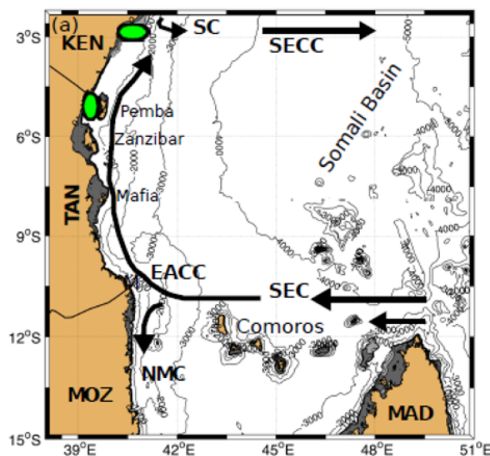


Figure 2.3: Circulation patterns within the northern part of the WIO show the Somali Current (SC), South Equatorial Countercurrent (SECC), East African Coastal Current (EACC), South Equatorial Current (SEC), and Northeast Madagascar Current (NMC). Green ellipses denote upwelling areas. Dark grey shading denotes depths within the 200m isobath. Figure from Vinayachandran et al., 2021.

In the Comoros archipelago, Mayotte is a French tropical island with an area of 374 km², composed of two main volcanic islands, Grande Terre and Petite Terre, culminat-

ing at a peak elevation of 660 m. Mayotte also comprises about 30 islets of volcanic or coral reef origin spread out in a lagoon behind a ring of coral reef barriers, with a circumference of 157 km and an additional 40 km of submerged reefs where this ring is perforated. Mayotte lagoon is 3–15 km wide, up to 80 m deep, and, with an area of nearly 1500 km², is one of the largest reef lagoons in the Indian Ocean. Mayotte's volcanic and tropical context and the vast reef-lagoon system have resulted in remarkable coastal geomorphic diversity. The total shoreline length of Mayotte is 265 km and is an intricate alternation of cliffs separating variably indented pocket beaches of sand and sandy mud. Other ecosystems, such as mangroves, colonize many sheltered low-energy back shores (Jeanson et al., 2014). Due to its location on the continental slope and the dominant coral reef structures, only weak water exchanges occur with the open ocean. According to some studies, the circulation is mainly driven by tides, winds, and waves breaking on the reef (Schott and McCreary Jr, 2001; Schouten et al., 2003; De Ruijter et al., 2005). A monsoonal wind system dominates the island, although two seasons can be distinguished: a hot, windy, and rainy monsoon season from November to April and a dry season from May to October (Zinke et al., 2008; Jeanson et al., 2014).

2.1.1.1 Environmental Products Acquisition

For the island of Mayotte, a range of environmental parameters was collected to assess the potential impacts of abiotic factors on the coral host but primarily how they can influence the distribution, abundance, and diversity of the microbioeroding communities present within both corals. Details regarding the different variables and products and how they relate to microbioeroding communities are presented in the **Table 2.1**. Most of the following parameters were obtained from open databases. Monthly SSTs (i.e., absolute temperatures) were extracted from the National Oceanic and Atmospheric Administration (NOAA) database from the “Extended Reconstructed Sea Surface Temperature” v5 (ERSST) (<https://www.ncei.noaa.gov/products/extended-reconstructed-sst>), then averaged to get yearly dataset at a spatial resolution of 2.0° x 2.0°. SST monitoring is long established, can be remotely sensed in various ways, and continues to increase in accuracy and spatial resolution. SST data are already used to predict coral bleaching and disease events (e.g., Coral Reef Watch; Liu et al., 2006). SSTAs were then reconstructed from *in situ* measurements of SST from buoys, Argo observations, then subtracted with the calculated SST climatology (1971-2000) (baseline temperature), also

at a resolution of $2^\circ \times 2^\circ$ (B. Huang et al., 2015; B. Huang et al., 2017).

Table 2.1: Considered environmental parameters that could potentially influence microborers abundance over the last decades in both living coral *Diploastrea* and *Porites* sp. (Mayotte).

Parameter	Unit	Definition	microborer Context
Sea Surface Temperature (SST)	$^\circ\text{C}$	The measure of the temperature close to the ocean's surface, also defined as absolute temperature. ERSST (v5) is representative of SST measured at a nominal depth of 0.2 m.	Known as a stress factor (Reyes-Nivia et al., 2013).
Sea Surface Temperature Anomalies (SSTA)	$^\circ\text{C}$	A temperature anomaly is the difference from an average or baseline temperature. SSTA is computed by subtracting the absolute temperature from the SST monthly climatology (1971-2000). Monthly climatology is realized by averaging all absolute temperatures for the monthly interval of 1971-2000. Climatology generally covers 30 years. SSTA are obtained with a spatial resolution of $2^\circ \times 2^\circ$ horizontal grid with statistically enhanced spatial completeness and at a monthly scale	Known a stress factor (Reyes-Nivia et al., 2013).
Precipitation Rate	mm	Rainfall rate measures rainfall intensity over a given interval of time expressed in millimeters.	Indicator of the rainy season, a potential proxy of nutrient influx, turbidity, low salinity, and pH from terigenous inputs, which are known as stress factors (Tribollet, 2008; Carreiro-Silva et al., 2009; Tribollet et al., 2009).
Max Instant Wind Speed	km.h^{-1}	The instantaneous wind is measured at concise time intervals (half a second, for example). The maximum instantaneous wind speed measures an instantaneous peak in speed taken into account if it exceeds at least 10 knots (19 km.h^{-1}).	Indicator of potential mixing and nutrient transport in the water column.
Cumulative Insolation Period	Hours	Insolation is the amount of solar radiation received on a given surface in a given period (W.m^{-2}). The term cumulative insolation is commonly used to designate the overall time intervals during which an object is subjected to insolation.	Light availability (and intensity) is the main stress factor (Tribollet, 2008; Galindo-Martinez et al., 2022).
pH	No Unit	pH is a scale used to specify the acidity or basicity of an aqueous solution. Acidic solutions are measured to have lower pH values than basic solutions. pH scale is logarithmic and inversely indicates the concentration of hydrogen ions in the solution	Known as a stress factor impacting the coral host, microbioeroding community, and activity (Hall-Spencer et al., 2008; Reyes-Nivia et al., 2013; Tribollet et al., 2019).

Positive anomalies indicate that SST is warmer than the baseline temperature, while negative anomalies indicate that SST is cooler than the baseline. Temperature is fundamental to determining coral health and survival, especially thermal anomalies. For instance, a 1°C anomaly lasting over a few weeks can cause bleaching (Hughes et al., 2017). Therefore, monitoring temperature anomalies is important for reef surveys (Yap, 2004). The following variables, as the precipitation rate, the max instant wind speed, and the cumulative insolation period, were collected from around the island of Mayotte via the databases from Météo France (<https://publitheque.meteo.fr/okapi/accueil/okapiWebPubli/index.jsp>). The climate variability over the last five decades of the island of Mayotte is presented in **Figure 2.4**. Data were obtained from two different stations: one at the meteorological station of M'Tsamboro, in the northern part of

Mayotte, near our study site. However, data from this station only covered the period 1993-2018. Thus, one other station located at the meteorological station of Pamandzi, was used as it represented the only station recording environmental data for the other considered period 1964-1992, in the northeastern part of Mayotte for *Diploastrea* and 1990-1992 for *Porites* sp. (**Figure 2.4**).

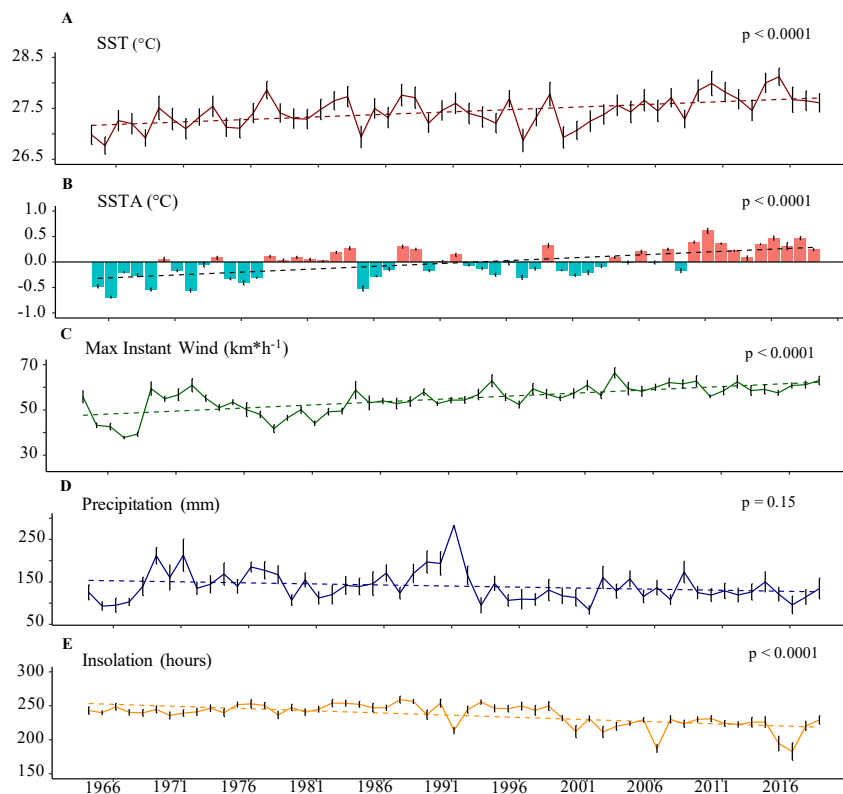


Figure 2.4: Climate context of Mayotte island showing the interannual variability of the different environmental parameters at Mayotte between 1964 and 2018. **(A)** SST in °C **(B)** SSTA in °C. **(C)** Maximum instantaneous wind speed (km*h⁻¹). **(D)** Precipitation rate (mm). **(E)** Annual cumulative insolation period (hours). Each variable's error bars (SE) were calculated after averaging monthly data.

2.1.2 Reunion Island

Reunion Island is a French overseas territory that lies at 21° S and 55° E. Due to its location and tropical climate, annual sunshine is in the range of 1400–2500 h and can reach the value of 2900 h for an altitude lower than 400 m. Average temperatures oscillate from 25 to 32 °C for coastal regions and 15 to 22 °C for regions above an altitude of 1500 m in the island's interior. La Reunion is a mountainous island with a very complex topography. Because of heterogeneous and rapidly changing cloudiness, tropical islands, such as Reunion Island in the South-West Indian Ocean, have a significant solar resource that is a highly variable daily (intermittency). It has a tropical climate with

two seasons: hot and humid (November to May) and cool and dry (June to October). Coral reefs lie along the driest western coast of the island. They are exposed to solid hydrodynamic conditions, mainly due to swells generated by the southeast tradewinds (dry season) and tropical cyclones (humid season). The narrow (maximal width: 520 m) fringing coral reefs form a discontinuous belt along a 25 km section of the island's 210 km circumference (Montaggioni and Faure, 1980). From the open ocean towards land, the reef can be divided into an outer slope, flat reef, and back reef zone. The climate variability over the island of la Reunion over the last two decades is presented in **Figure 2.5**.

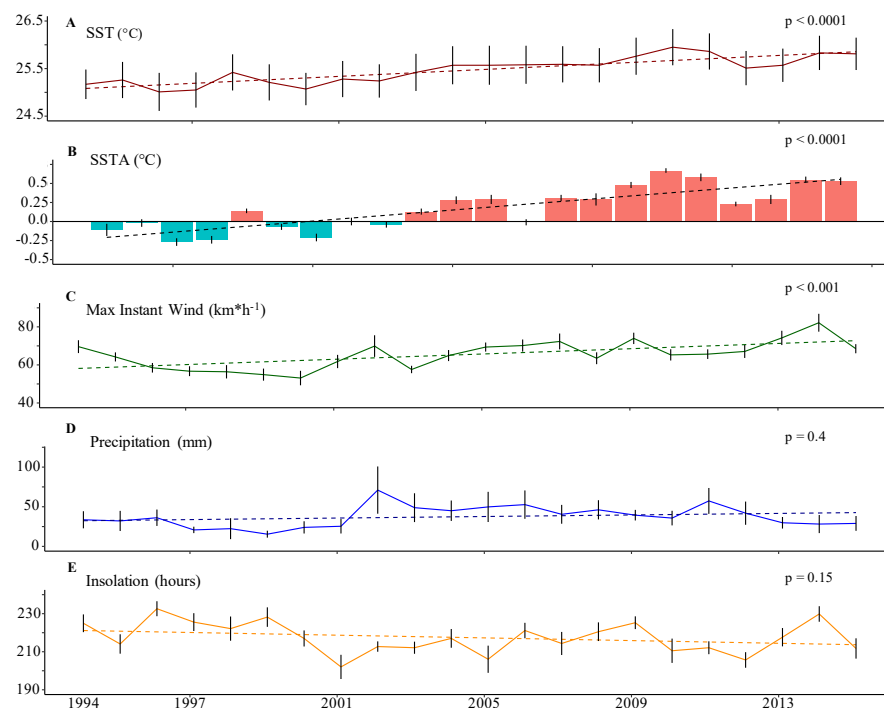


Figure 2.5: Climate context of Reunion island showing the interannual variability of the different environmental parameters at Mayotte between 1994 and 2015. **(A)** SST in °C **(B)** SSTA in °C. **(C)** Maximum instantaneous wind speed (km*h⁻¹). **(D)** Precipitation rate (mm). **(E)** Annual cumulative insolation period (hours). Each variable's error bars (SE) were calculated after averaging monthly data.

2.1.3 Scattered Island

The "Iles Eparses" (Europa, Bassas da India, Juan de Nova, Glorieuses, Tromelin) are spread around Madagascar in the Southwest Indian Ocean. These are French territories administered by the program French Southern Lands and Antarctica "Terres Australes et Antarctiques Françaises" (TAAF) and represent an Exclusive Economic Zone of nearly 650,000 km² (Quod et al., 2007). These islands have been classified as natural reserves since 1975 (Le Corre and Safford, 2001), and very recently for Juan de Nova in

2019 (Pressé, 2022). Apart from Tromelin, the other islands are located along a north-south gradient in the MC. Europa, Bassas da India, Juan de Nova, and the Glorieuses include 2% of the diversity of reef structures worldwide and 7% of the western and central Indian Ocean islands with a total coral reefs area within the four islands of 517 km² (Andréfouët et al., 2008). These islands present two major reef structures: banks (Juan de Nova and the Glorieuses) and atolls (Bassas da India and Europa). Both atolls and banks can be subdivided into three habitats: forereef, reef flat (adjacent to the prominent reef rim), and inner terrace with the development of a lagoon in atolls (shallow or deep with or without coral construction).

2.1.3.1 Juan De Nova

Juan de Nova (17°03 S, 42°45 E) is located 175 km from Madagascar and 285 km from Mozambique, in the narrowest portion of the MC. As the result of the dominant SE trade winds, the contour of the island is that of an arc whose convex side faces the wind, with east and west ends prolonged by sand banks. The island's length between these two points is 6 km, and the maximum width is 1700 m. The emergent land is about 5 km², while the overall coral reef structure covers 207 km². The evolution of Juan de Nova temperatures' variability over the last decades is presented in the **Figure 2.6**.

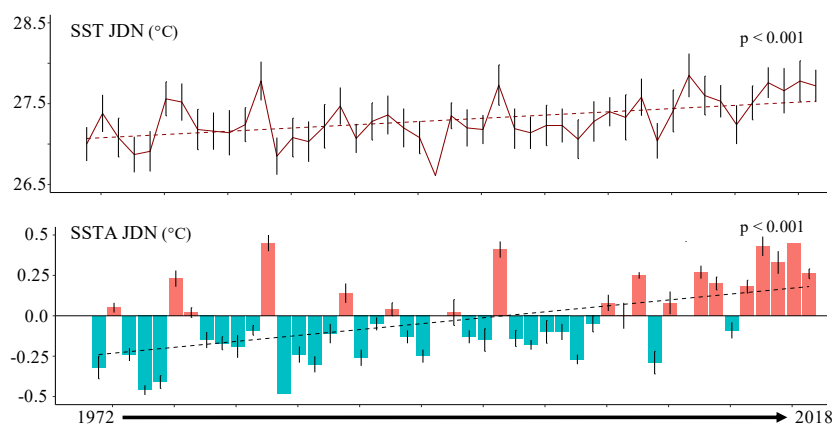


Figure 2.6: Interannual variability of the SST and SSTA from the island of Juan de Nova between 1972 and 2018 (coral growth reconstruction)

2.1.3.2 Europa

Europa (22°22 S, 40°22 E) is located approximately 355 km west-northwest of Madagascar and 529 km east-northeast of Mozambique. The island measures 7 km by 6 km. It is a former atoll, uplifted to a maximum altitude of 7 m, leaving the fossil coral reefs dry.

The emergent land is about 35 km², while the overall coral reef structure has a total area of 18 km². A fringing reef surrounds it with a narrow, shallow lagoon, which only widens towards the north of the island, where there is also the entrance of an extensive inland lagoon system ringed by mangroves. The evolution of Europa temperatures' variability over the last decades is presented in the **Figure 2.7**.

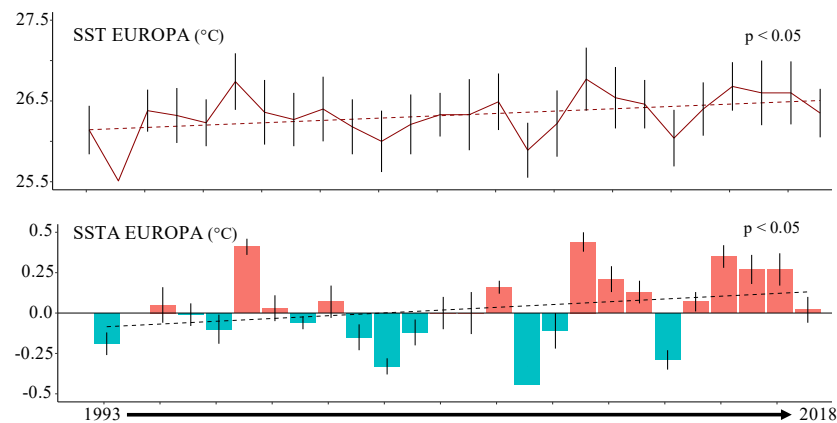


Figure 2.7: Interannual variability of the SST and SSTA from the island of Europa between 1993 and 2018 (coral growth reconstruction)

2.2 Coral Data Acquisition

2.2.1 Coral Core Sampling

This Ph.D. project emerged from two multidisciplinary projects, **CARBODISS**, and **CLIM-EPARSEs**, in 2018-2019, led by **Dr. Aline Tribollet**. During this Ph.D., five coral cores in total were analyzed. Two coral cores from the Scattered Islands (one core for each island) were investigated (from the genus *Porites* sp.), two coral cores from the island of Mayotte (one *Diploastrea* sp. and one *Porites* sp.) and finally one coral core from the island of la Reunion (*Porites* sp.; **Figure 2.8 A**). Within this project, the focus was mainly on coral cores collected from two massive slow-growing corals of the genus *Diploastrea* and *Porites* sp. on the outer slope of the barrier reef at 15 m depth near the M'Tsambo pass (northeastern part of the lagoon of Mayotte (Lat. 12°37'19.4" S - Long. 45°06'42.7" E; **Figure 2.8 B and C**) in October 2018. Preliminary results regarding the Scattered Islands and La Réunion coral cores are presented in the **Chapter 7: Conclusions and Perspectives**.

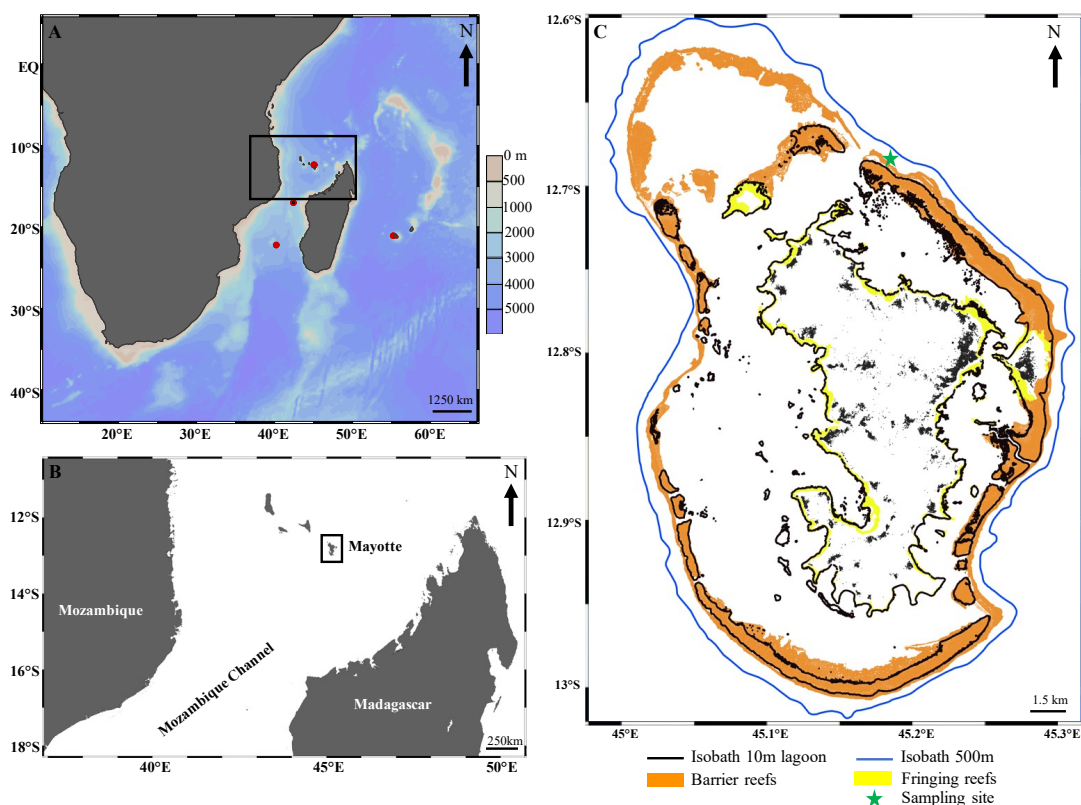


Figure 2.8: (A) Location of the different coral samplings corresponded to the different missions CAR-BODISS and CLIM-EPARSEs. (B) Mayotte in the WIO. (C) Reef ecosystems around Mayotte. The blue line and black lines represent the different isobaths around the island. The green star indicates the sampling location in the northeastern part of the lagoon.

This site was selected to focus on the influence of oceanic conditions on microbio-eroding assemblages in living corals instead of local disturbances, although these cannot be discarded. The coral cores were collected with an 8 cm compressed air driller and measured 19.5 cm long for the *Diploastrea* and 29.5 cm long for the *Porites* sp. It presented ten green bands visible by the naked eye for the *Diploastrea* coral, while no green bands were identified for the *Porites* sp. core. Therefore, quickly after cutting the coral core, each green band's position and thickness along the core of the *Diploastrea* coral were recorded with a Vernier caliper under a dissecting microscope (NIKON Eclipse LV100, Bondy, France). Also, as both corals present different growth rates, two different chronologies were obtained, with *Diploastrea* coral going from 1964 to 2018 and *Porites* sp. coral going from 1990 to 2018.

2.2.2 Coral Growth Variables

As mentioned in the previous sections, massive corals are indeed known to be good bio-archives, recording environmental changes over decades and centuries (Zinke et

al., 2008; Montagna et al., 2014; Wu et al., 2018; Cuny-Guirriec et al., 2019). Continuous, high-resolution (annual to seasonal) information from such corals is provided by various measures, including their growth characteristics. It can document coral responses to unusual environmental conditions and various geochemical tracers whose incorporation into the skeleton is mediated by ambient seawater characteristics. Three different variables characterizing the coral growth were measured here: the vertical linear extension (mm.y^{-1}), the skeletal bulk density (g.cm^{-3}), and the coral calcification rate ($\text{g.cm}^{-2}.\text{y}^{-1}$) which was calculated as the product of the linear extension rate by the skeletal bulk density (P. D. Taylor and Jones, 1993; T. M. DeCarlo et al., 2017). Before measurements, both cores were sliced along the main vertical growth axis into four slabs (the middle slabs being ≈ 1 cm thick). All slabs were well preserved as no diagenetic, nor macrobioerosion traces were observed either by eye or under Scanning Electron Microscopy (SEM), except in one area in the bottom part of the core for the *Diploastrea* coral core (i.e., the last 4.5 cm of the core). Thus, this area was avoided and only the first 15 cm on this core were studied to investigate microbioeroding communities. For the slab of *Porites* sp., some macrobioerosion traces were identified and were thus avoided to study the entire core. The four slabs were scanned together on a Discovery CT750 HD CT scanner (GE Healthcare) set at 120 kV at the DOSEO 'Radiography and Imaging Technology Platform R and D center' (CEA-Saclay, Paris) with three coral standards to obtain a 3D image of the coral core (reconstructed from hundreds of 2D images). The 3D image revealed the pattern of the coral skeleton structure and its density variation over time.

To estimate the skeletal density of the different corals, an approach was developed by the LSCE and used within this thesis. Originally, eleven coral standards were prepared from various fragments of massive coral *Porites* ($n=6$) and *Diploastrea* ($n=5$) skeletons present at the LSCE. Those coral standards were selected as they showed significant density differences (alternating black and white density bands). The 11 coral fragments were cut into geometric forms like cubes, parallelepiped rectangles, and cylinders of a few centimeters. The bulk density of those coral standards was measured using the buoyant weight technique (Bucher et al., 1998). The bulk density of coral standards varied between 0.98 and 1.7 g.cm^{-3} with an uncertainty of 2% (assuming a negligible bias from weighing). Coral density was estimated with a recently developed method applying a Gaussian Mixture Model (GMM; Coulibaly, 2021, master student). On the obtained 3D scan of the coral slabs and our three coral standards, three types of voxels

were obtained (i.e., a pixel in 3 dimensions with a length, width, and thickness). Voxels corresponded to either one of the following categories: 'coral,' 'air' (entrapped in coral pores, for instance), or 'table' (on which the core was placed in the CT scanner). Coral standards were large enough to keep density variations due to (micro-) structures in each massive coral genus or their seasonal bands' alternation. Standards were used for calibration to obtain Gaussian distributions of the different voxels categories in Hounsfield units (HU). The median HU values of the voxel distribution in coral standards measured ranged between 540 and 1400 HU were calculated and enabled to obtain the corresponding density, thanks to a calibration curve. By comparing coral bulk densities of standards measured by buoyant weight vs. the GMM, the following linear regression was obtained:

$$Density = 0.00084 \times HU + 0.51 \quad (2.1)$$

where HU is the Gaussian distribution of voxels corresponding to the 'coral' in Hounsfield units (**Figure 2.9**; $r = 0.99$, $p\text{-value} < 0.001$). When the uncertainties related to the calibration (linear regression) and measurement reproducibility for a confidence interval of 95% are combined, the density measurement uncertainty was estimated to be less or equal to 1%. However, this is only true when the GMM is applied to samples of massive *Porites* sp. or *Diploastrea* sp. with skeletal densities comprised between 1.0 and 1.7 $\text{g}\cdot\text{cm}^{-3}$ (Coulibaly, 2021).

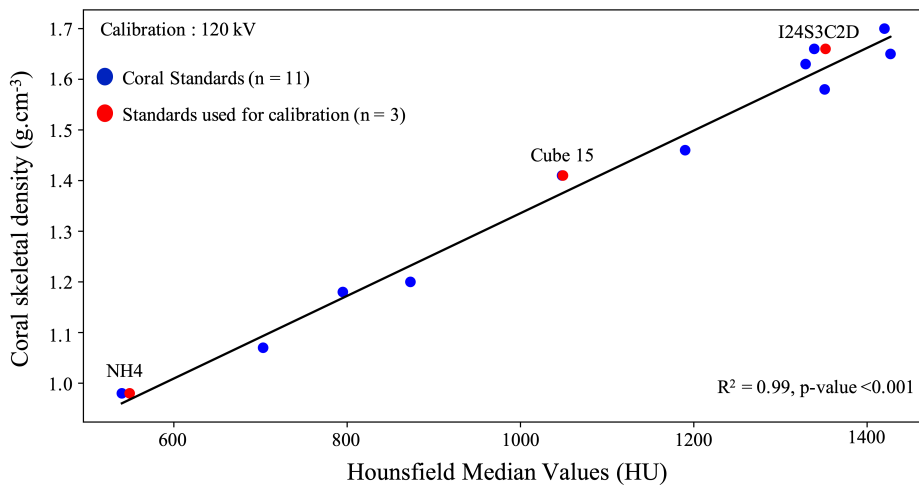


Figure 2.9: Linear regression between measured Hounsfield Median values (voxels measured in HU) and their experimental measured densities ($\text{g}\cdot\text{cm}^{-3}$). Blue dots represent the 11 different coral block standards from *Porites* sp. corals ($n=6$) and *Diploastrea* sp. corals ($n=5$). Red dots represent the three standards used for the calibration and the linear regression.

Thus, the GMM was applied every 0.625 mm on the 3D image on both coral cores and then applied the linear regression to determine its annual bulk density. To estimate the vertical extension rate along the central growth axis of the coral core, a 2D image of one of the two middle slabs (image obtained by CT scan) was analyzed. An eye-visible low-density band together with a high-density band was assumed to correspond to one year of growth (Knutson et al., 1972; Buddemeier, 1978). The estimated vertical extension rate was confirmed by analyzing a 2D X-radiograph of the same middle slab obtained with a scanner VERITON-CT at the Jean-Verdier hospital (Bondy, France).

2.2.3 Temperature and pH Reconstructions from Coral Cores

2.2.3.1 Known Proxies for SST and pH

Paleo-SST reconstructions derived from corals have typically been based on $\delta^{18}O$, Sr/Ca, and less frequently, U/Ca and Mg/Ca (Min et al., 1995; Mitsuguchi et al., 1996). Among these geochemical proxies, the most commonly used in tropical corals is the Sr/Ca ratio (DeLong et al., 2007; Zinke et al., 2014). However, biases on SST estimates from coral Sr/Ca have been reported due to the activity of the coral-associated algal symbionts (Cohen et al., 2002), skeletal heterogeneity (e.g., Cohen et al., 2001), diagenetic modifications (e.g., Hendy et al., 2007) and biomineralization processes, commonly known as “vital effects” (Corrège, 2006; DeLong et al., 2013). Recently, the development of new paleo-thermometers such as Li/Ca (Hathorne et al., 2013) or Li/Mg (Montagna et al., 2014; Cuny-Guirriec et al., 2019) contributed to improve the reliability of the coral-based SST reconstructions. Unlike Sr/Ca, the Li/Mg SST calibration can be extended to an extensive range of zooxanthellate and azooxanthellate coral species covering a wide temperature range (from sub-freezing to tropical temperatures). However, the uncertainty of the Li/Mg equation is relatively high ($\pm 2.6^\circ\text{C}$ at 25°C) for tropical corals (e.g., *Siderastrea*, *Porites* or *Diploastrea* sp.) compared to cold-water corals ($\pm 0.9^\circ\text{C}$ at 1°C), due to the asymptotic behavior at higher temperatures (see Equation (5) in Cuny-Guirriec et al., 2019; due to the exponential relationship, the uncertainty become larger at higher T°). Few studies have thus developed and applied a multi-proxy approach, which combines different temperature-sensitive elements (e.g., Li, Mg, Sr, U) into a multi-regression model that reduces the temperature uncertainty (T. M. DeCarlo et al., 2016; S. E. Fowell et al., 2016; D’Olivo et al., 2018; Zinke et al., 2019). Further studies are required to evaluate their caveats and constraints. Unlike temperature, how-

ever, *in situ* records of changing carbonate chemistry are sparse in the oceans and, at most, only span the last 4 decades (e.g., HOTS, BATS=longest until 1984, ESTOC, CARI-ACO records, Trotter et al., 2011; Tarique and Rahaman, 2022). One of the few ways to overcome this limitation is by using geochemical records of environmental change preserved within the carbonate skeletons of long-lived marine organisms. The boron isotopic composition ($\delta^{11}B$) of marine biogenic carbonates and the B/Ca ratio of aragonite skeletons can be used as a key quantitative proxy to determine and reconstruct carbonate chemistry changes in the calcifying fluid (CF) (e.g., pH_{CF} , DIC_{CF} , Ω_{CF}), by using established relationships between the different variables, and determined long-term pre-instrumental records of ambient seawater pH (M. McCulloch et al., 2012; Holcomb et al., 2014; T. DeCarlo et al., 2018). Thus, massive tropical corals have been successfully utilized to reconstruct ocean pH at seasonal to millennial timescales (Wu et al., 2018; X. Chen et al., 2019).

2.2.3.2 SST Dataset Acquisition

For the present study, two approaches were investigated. Firstly, instrumental temperature data from different datasets were collected. Instrumental SST signals represent direct measurement of seawater temperature at an instant time. Therefore, one objective was to understand the effect of SST on the variability of the abundance of microbioeroding communities. For the *Diploastrea* sp. coral core in Mayotte, long-term SSTs were retrieved from the ERSST(v5) dataset at $2^\circ \times 2^\circ$ spatial resolution in the grid 12-14°S, 42-44°E, covering 1964-2018. For the *Porites* sp. coral core, I additionally collected instrumental data from the AVHRR-OISST(v2) dataset at $0.25^\circ \times 0.25^\circ$ representing a more accurate spatial resolution measurement. Finally, some SSTs could be obtained from the "Parc Marin de Mayotte" and were collected to obtain direct *in situ* SST measurements at the studied location. Their measurements go from 2010-2018, and unfortunately, due to logger losses, only the last four years were entirely usable. SSTs were compared between the *in situ* measurements of the Parc Marin and the different instrumental datasets (ERSST and OISST) to determine potential offsets. After comparing the different measurements, offsets were applied to correct ERSST and OISST datasets based on SSTs measured with the Parc Marin. For the other reef locations (Reunion and Eparses Islands), instrumental SSTs based only on the ERSST were collected. Based on the instrumental temperatures, only SST from the ERSST corrected with the offset from the Parc Marin was considered. The OISST dataset only allows SST

data until 1982, while coral chronology (i.e., *Diploastrea* reconstruction goes further. Correlations between the SSTs of both OISST and ERSST dataset was calculated at $r = 0.85$ for the period 1982-2018. On the other hand, paleo-reconstructions of SSTs from the coral will also be investigated to see if instrumental SSTs and SST from the coral micro-environment differ and may impact different microbioeroding communities. Corals offer a rich archive of past climate variability in tropical ocean regions with limited instrumental data and incomplete knowledge of multi-decadal climate sensitivity (Gagan et al., 2000). Satellite-based data represent the surface temperature (10-20 μm below the surface to 1 mm). For recall, ERSST (v5) is a dataset representative of SST measured at a nominal depth of 0.2 m. At the same time, zooxanthellate corals can live up to 100 m water depth from the surface, suggesting potential differences in SST with satellite measurements (Canesi, 2022). For the present study, a multi-element SST calibration for multi-genera *Porites* sp. and *Diploastrea* sp. developed by Canesi (2022) at the LSCE was used. The calibration is defined with the proxy Sr/Ca and Li/Mg because the variability of the prediction accuracy on the calculated SST was better compared to single Sr/Ca or Li/Mg calibrations. The calibration is defined by the following equation:

$$SST = 68.5 - 3.47 \times Sr/Ca - 7.09 \times Li/Mg \quad (2.2)$$

2.2.3.3 pH Geochemical Analysis

For this thesis, B/Ca, and ($\delta^{11}\text{B}$) ratios were measured within our different coral skeletons to reconstruct long-term variations of their CF compositions (pH_{CF}) and to assess its potential influence on the variability of the abundance and composition of microbioeroding communities. The geochemical analysis regarding boron isotopic measurements was realized by Eric Douville at the LSCE (Paris Saclay). The protocol regarding isotopic measurements was based using the protocol previously developed for carbonates (Bourdin et al., 2011; Montagna et al., 2014) and recently updated by Cuny-Guirriec et al.(2019) and Canesi (2022). Before any isotopic measurements, coral powders were systemically cleaned with a 15% H_2O_2 solution buffered with 0.5 M NH_4OH at 60 °C for 20 min, rinsed three times with MilliQ water, and dried at 50 °C overnight to remove the potential organic matter. Elemental (Li, Mg, Ca, Sr, U...) concentrations were determined using a Quadrupole ICP-MS X-SeriesII at LSCE (Gif-sur-Yvette, France). Samples and standards were prepared to process approximately 2.5 to 5 μg

of B (Bore). Around 100 to 200 mg of powdered aragonite per sample (coral skeleton) were collected for boron geochemical analyses. Coral powders were dissolved in NORMATOM® 4 wt% nitric acid. Around 15 μL of each solution were pipetted and diluted in HNO_3 0.5N to obtain Ca-100 ppm solutions ready for element analysis. The boron isotope measurements ($\delta^{11}\text{B}$) were performed using the previously prepared nitric solutions containing each sample $\sim 5 \mu\text{g}$ of boron ($\sim 100 \text{ mg}$ of dissolved powder) with the LSCE's Thermo Scientific Multi-Collector ICP-MS Neptune^{Plus}. The isotopic composition of boron $\delta^{11}\text{B}$ determined for each sample is calculated from the average of three measurements. The mean values and the standard deviations at 95% level of confidence determined for the standard *Porites* sp. standard M1P-p (reference standard powder used by the LSCE) were $25.17 \pm 0.22 \text{ ‰}$ ($n=22$), mean isotopic ratio, and reproducibility in good agreement with expected $\delta^{11}\text{B}$ value. Elemental concentrations were measured and then reported on the chronology reconstruction for the investigated corals. The pH_{CF} is calculated from the coral skeletal boron isotopic composition ($\delta^{11}\text{B}_{\text{coral}}$) according to the following equation (Hemming and Hanson, 1992; Zeebe and Wolf-Gladrow, 2001):

$$\text{pH}_{\text{CF}} = \text{pK}_B - \log \left(\frac{\delta^{11}\text{B}_{\text{SW}} - \delta^{11}\text{B}_{\text{coral}}}{\alpha_B \delta^{11}\text{B}_{\text{coral}} - \delta^{11}\text{B}_{\text{SW}} + 1000(\alpha_B - 1)} \right) \quad (2.3)$$

where $\delta^{11}\text{B}_{\text{SW}}$ is the B isotopic composition of seawater (39.61 ‰, Foster et al., 2010) and the B isotopic fractionation factor (α_B) is 1.0272 (Klochko et al., 2006). The dissociation constant of boric acid (pK_B) in seawater (Dickson, 1990) is defined by the temperature and salinity of the seawater.

2.3 Microbioeroding Communities Investigation

2.3.1 Identification of Microbioeroding Organisms: Microscopy

Approach

A sub-slab of 1.5 cm width was cut along the middle slab of the different coral cores and then cut into 10 and 14 coral samples for both *Diploastrea* sp. and *Porites* sp. corals, respectively. The **Figure 2.10** shows how the *Diploastrea* sp. coral core was collected and investigated for the growth rate reconstruction. Then, the cast-embedding protocol was to study the diversity and abundance of microbioeroding traces and their distribution within their coral skeletons with the same methodology performed for the *Porites*

core. Before SEM observations, each coral sample was bleached using concentrated sodium hypochlorite (8%) for three days to remove all traces of organic matter, rinsed with Milli-Q water for three days, and dried at 50°C for an additional 48h. Dried coral samples were then embedded in the Specifix-40 epoxy resin from Struers Inc. (Cleveland, United States, 2 parts of resin: 1 part of curing agent) to allow the observation of resin casts of microbioerodings (traces) under SEM (**Figure 2.10**).

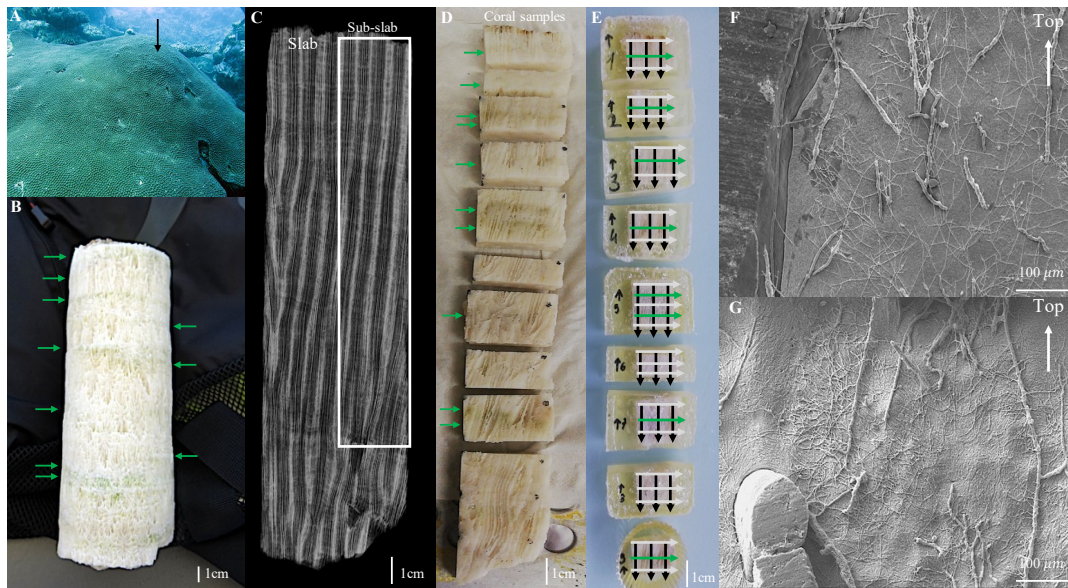


Figure 2.10: Studied *Diploastrea* sp. coral colony at Mayotte. (A) *Diploastrea* sp. colony at 15 m depth. The black arrow indicates where the colony was sampled. (B) *Diploastrea* sp. core with visible green bands (green arrows). (C) X-ray radiograph of one middle slab cut out of the *Diploastrea* core measuring 19.5 cm long showing the annual density banding pattern. The white rectangle indicates the studied area. (D) Ten samples were cut from the radiographed slab of the *Diploastrea* sp. core. Only the first nine samples from the top were analyzed to estimate the microborer traces' abundance. Green arrows indicate green bands. (E) Resin impregnation of the 9 samples. Horizontal white and green arrows represent the horizontal transects where measurements of microbioerodings abundance were realized (i.e., within white vs. green bands). The black arrows represent the vertical transects studied in each sub-sample. (F, G) Different resin casts of microbioerodings observed under a scanning electron microscope after resin impregnation of coral samples and partial decalcification.

Samples were placed in a Cytovac vacuum chamber (Struers) for several minutes before polymerization to perform good resin impregnation (Wisshak, 2012; Golubic et al., 2019). Resin polymerization occurred at 40°C in an oven for at least 24h. Embedded coral samples were then sectioned (about 1 cm thick) along the vertical growth axis of the coral with a diamond saw (Isomet1000 from Buehler) and sonicated to remove potential sediments from sectioning for a few seconds. The surface of each thin section (n=9 and n = 14, i.e., one per coral section) was then etched with a 10% hydrochloric acid solution for 15 seconds to remove tens of micrometers of coral carbonate, then rinsed in Milli-Q water for a few seconds and dried at 40°C in the oven prior gold met-

alization for the observation of resin casts of microbioerodings under SEM (**Figure 2.11**).

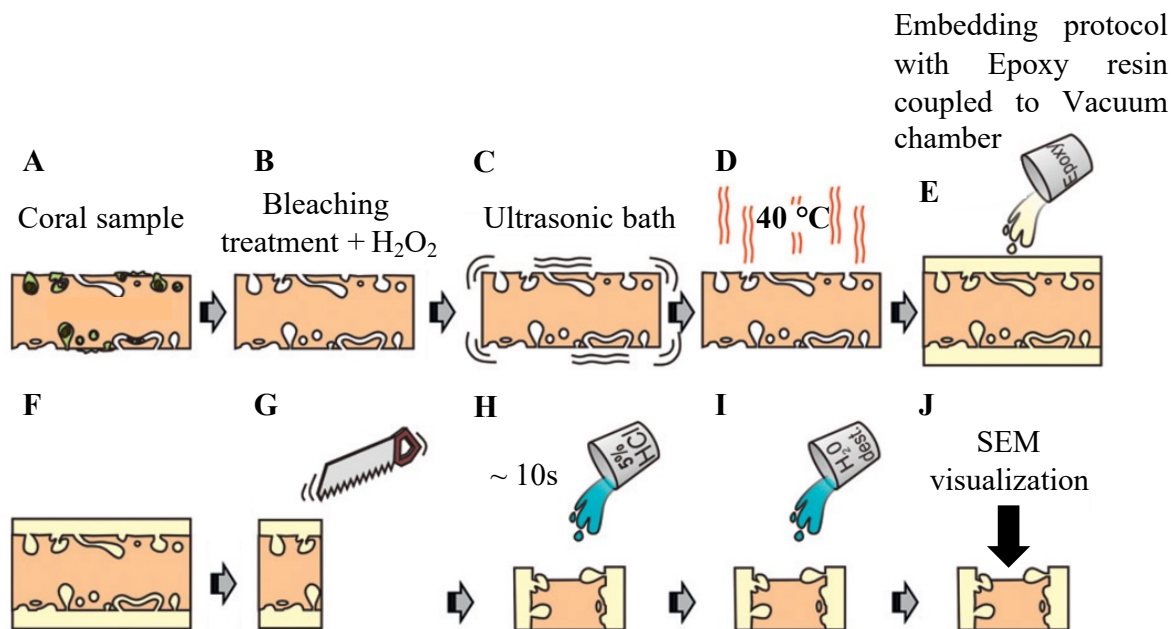


Figure 2.11: Cast Embedding protocol for coral samples. Figure adapted from Wisshak, 2012.

For a detailed and explained version of the embedding resin protocol for coral samples and microborers' visualization under SEM, please refer to **Appendix Section 8**. The different types of microbioerodings were determined based on their diameter, morphology, and distribution within the coral skeleton. Along the *Diploastrea* sp. coral core, 4 SEM images were randomly selected per coral section (n=36 images per sample) within the pool of SEM images taken to analyze microbioerodings abundance. The diameter of the different types of microbioerodings was measured using the ImageJ software (<https://imagej.nih.gov/v1.53>) and also to observe their distribution within the coral skeleton. Ten measurements of diameter (μm) were performed per type of trace and SEM image. This analysis unveiled to distinguish three types of microbioerodings based on their diameter for applying our machine-learning approach to estimate the percentage of coral skeleton colonized by microborers (proxy of their abundance). Those with a diameter comprised between 1 and 2 μm , others comprised between 2 and 5 μm , and finally, some with a diameter higher than 5 μm (**Figure 2.10 F and G**). This approach was not performed within the *Porites* sp. coral core, as only the total microbioeroding traces were determined and estimated. Thus, the first 9 for *Diploastrea* sp. and all 14 coral samples for *Porites* sp. were observed under an SEM operating at 15 kV (Zeiss EVO LS15) on the platform ALYSES (**Figure 2.12**; Bondy, France).

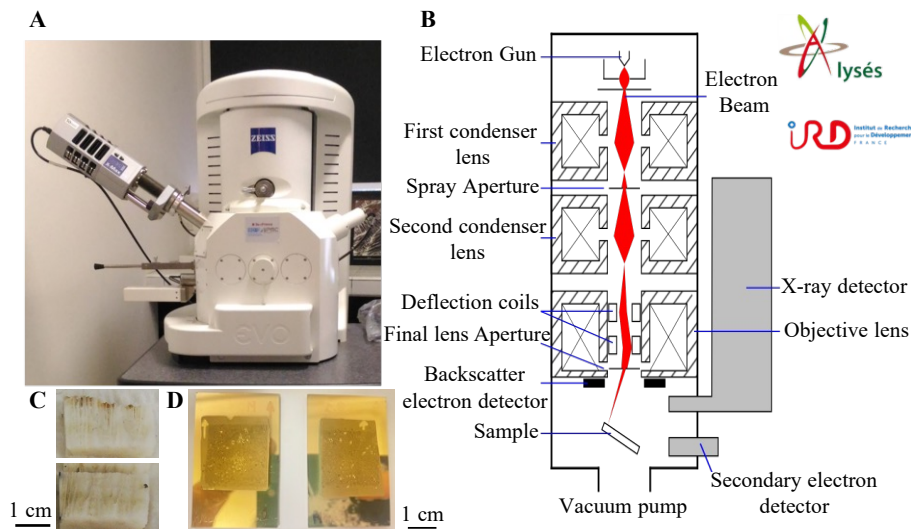


Figure 2.12: **(A)** Scanning Electron Microscope (SEM) Zeiss EVO-LS15, Alysés Platform, Sorbonne University-IRD-Region, Ile-de-France, Bondy. **(B)** Schematic representation of the functioning of the SEM. **(C and D)** Fragments of coral skeletons for the SEM observations before and after gold metalization.

2.3.2 Sampling Design to Study Microbioerodings' Abundance and Green Bands

To investigate the variability of the relative abundance of the different types of microbioerodings composing the assemblage and the percentage of the coral skeleton they colonized (ratio between the surface area of microborer traces in a given coral skeleton section and the total surface area of the coral skeleton section $\times 100$; a proxy of microborer abundance) over the last decades, two complementary approaches were applied to the studied thin sections collected along the *Diploastrea* sp. coral core: a 'vertical approach' comprising the study of SEM images taken continuously along three vertical transects parallel to the central coral growth axis, and a 'horizontal approach' (perpendicular to the central coral growth axis) comprising the study of SEM images taken continuously within 8 out of 10 visible green bands and 10 white bands selected along the *Diploastrea* sp. coral core (detailed in **Figure 2.10**, grey and green arrows). Green bands on coral samples 3 and 9 were too close to each other or merged to separate them properly, so one green band was considered in each of these samples. For the *Diploastrea* sp. coral core, 16 to 55 SEM images were taken per vertical transect, depending on the height of the coral section. In comparison, in the *Porites* sp coral core, 17 to 58 SEM images were taken per vertical transect. Only the vertical approach was performed for the *Porites* sp. coral core, as no green bands were spotted or visible before SEM anal-

ysis. In contrast, about 30 SEM images were taken on each horizontal transect in the *Diploastrea* sp. coral core. At several periods along the coral core, the vertical transects crossed the horizontal transects (**Figure 2.13** and also shown in **Figure 2E** from Alaguarda et al., 2022), allowing a comparison of the estimated average percentages of coral skeleton colonized by microborers obtained by the two approaches. This comparison was meaningful as the estimated average percentages of the coral skeleton colonized by microborers via the vertical approach were based on the analysis of 3 SEM images per period (corresponding to the 3 vertical transects), while that obtained via the horizontal approach was based on the analysis of 30 SEM images (**Figure 2.13**).

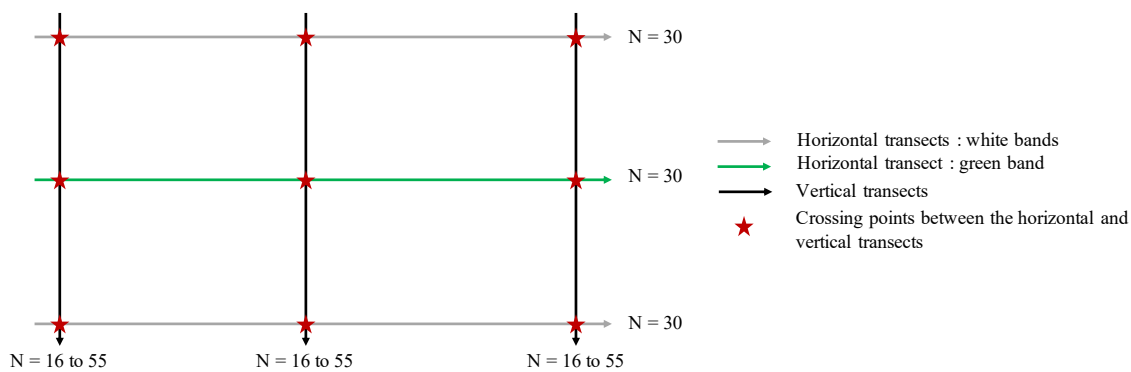


Figure 2.13: Schematic representation of vertical and horizontal sample transects across the surface of the radiographed slab of the *Diploastrea* coral core to estimate the abundance of microborers comparing white and green bands

More importantly, as the primary goal of the vertical approach was to highlight possible assemblage shifts, the variability in microborers' abundance over the last decades, and the possible influence of abiotic and biotic factors, it was crucial to show that trends obtained based on the vertical approach were reliable and accurate. On the other hand, the horizontal approach aimed at determining the possible link between the presence of green bands and certain microborers and their abundance. As the studied physical factors and coral parameters were calculated yearly, the average percentages of the coral skeleton colonized by microborers were calculated along the vertical growth axis yearly to highlight the possible influence of abiotic and biotic factors. It involved estimating the rate of the vertical extension of the coral colony over the past decades and adjusting the number of SEM images collected along the vertical transects to match each year of coral growth.

2.3.3 Quantification of Microbioeroding Traces: Machine Learning Application

To determine the relative abundance of the different types of microbioeroding traces and the area of the coral skeleton they colonized (based on thousands of SEM images taken manually along our coral core), the Convolutional Neural Network (CNN) model called U-NET was modified. This type of neural network belongs to the family of deep learning methods which allows the recognition of various cellular structures in biomedical images (Ronneberger et al., 2015), producing systems with interconnected nodes that can recognize patterns and correlations in datasets and classify them. It is commonly applied to two-dimensional images (Krizhevsky et al., 2017). Here, our modified CNN model comprised 10 convolutional layers, each representing a linear operation involving the product of a set of parameters with a 2D input feature map. The various parameters in our CNN model were optimized to improve the identification of different defined categories between our corals. The classes defined were: 'resin', 'coral skeleton', and 'microbioeroding traces'. Two classes of microbioeroding traces were investigated in *Diploastrea* sp. and only one in *Porites* sp. A maximum of two microbioeroding classes were considered due to the difficulty of distinguishing some microbioeroding traces by the CNN model (Alaguarda et al., 2022). The method was limited by the grayscale SEM images reducing the ability of the CNN model to distinguish various types of traces properly. Further details of each component of the model are provided on the **Chapter 3 Section 3.3** for the description of the CNN neural model structure and its three main steps (dataset constitution step, training step and model tuning and post-processing step).

2.3.4 Determination of Potential Specific Lipid Biomarkers of Bioeroding Microflora: Geochemistry Approach

During this Ph.D., I also investigated an approach and methodology based on geochemistry. The main objective was to investigate lipid biomarkers that might be specific to microbioeroding communities, especially from *Ostreobium* sp., the main microborer present within corals. All details and information regarding this approach, methodology, and investigation protocol are detailed in **Chapter 6**. To summarize both methods and objectives performed on the different coral cores, see **Figure 2.14**.

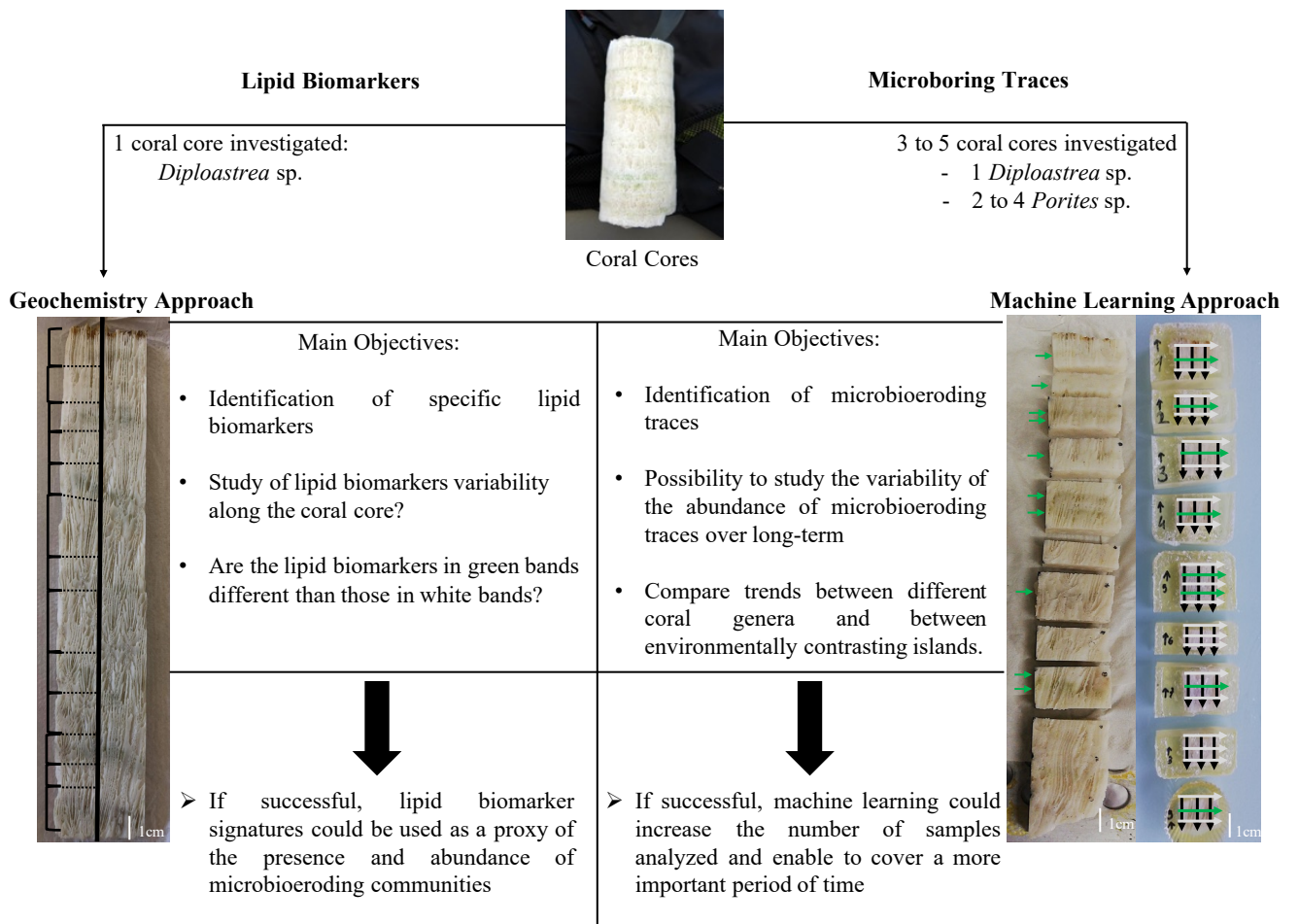


Figure 2.14: Schematic representation of the objectives and methodologies for investigating coral cores.

How to Accurately and Efficiently Study the Decadal Variability of Microbioeroding Communities' Composition and Abundance? Development of a Specific and Innovative Approach

Contents

3.1	What is Machine Learning?	94
3.2	Machine Learning for Segmentation Task of Classes	95
3.3	Application of Machine Learning on Microbioeroding Communities	96

3.1 What is Machine Learning ?

Machine learning (ML) is an evolving branch of computational algorithms designed to emulate human intelligence by learning from the surrounding environment that can solve problems efficiently and rapidly (Mitchell and Mitchell, 1997; Silva et al., 2022). They are the working horse in the new era of big data. Techniques based on ML have been applied successfully in diverse fields ranging from pattern recognition, computer vision, spacecraft engineering, finance, entertainment, and computational biology to biomedical and medical applications. The rapidly developing ML applies algorithms (artificial neural networks) that can quickly solve complex problems by processing big datasets, sometimes achieving better performance than human experts. Scientists have started to look towards supervised ML methods and algorithms that learn to classify new data from a set of human-generated training examples to expedite classification efforts (Irisson et al., 2022). Given ML's opportunities, its integration into marine science and marine resource management is inevitable (Beyan and Browman, 2020). ML approaches have great potential to improve the quality and extent of marine research by identifying latent patterns and hidden trends, particularly when studying large datasets which could not be investigated otherwise (Sun and Scanlon, 2019). Recently, aquatic ecologists have started applying popular deep-learning techniques that have surpassed the previous state-of-the-art classification performance on specific datasets (LeCun et al., 2015; Ellen et al., 2019; Orenstein et al., 2022) which enhanced the comprehension of marine systems. Yet accurate automated technology to monitor the health of our oceans exist only on a limited scale (Mahmood et al., 2016). Over the last decades, data imagery acquisition from coral reefs has facilitated the scientific investigation of these intricate ecosystems (Beijbom et al., 2012; Hopkinson et al., 2020). Nonetheless, manual annotation is a labor-intensive and time-consuming task requiring an expert to process each image manually. For instance, accurate annotation of coral imagery would enable access to diverse information such as species counting, sizing, movement tracking of specific marine organisms within a coral reef, and even identifying different micro-organisms colonizing the coral skeleton (e.g., microbioeroding communities). ML-based techniques present significant advantages and can potentially automate the annotation of specific objects within images, reducing the time consumed in manual processing (Bishop and Nasrabadi, 2006). Nonetheless, the accuracy of these techniques directly relies on the availability of high-quality

and expertly annotated training and testing data (e.g., identification of different microbioeroding traces within the image). As explained in the **section 1.3**, the objective was to assess the long-term variability of microbioeroding communities, which need the process of thousands of SEM images. Long-term data on microbioeroding communities within living corals are scarce, even inexistent, as manual processing of SEM images is very time-consuming and costly. To reduce the manual processing time of these images, ML was proposed as a solution to automate the analysis and process of large datasets of images within a few minutes.

3.2 Machine Learning for Segmentation Task of Classes

Automatic segmentation is an important task in processing images for visualizing a wide range of structures. A common approach to automatic segmentation is supervised pixel classification, where a classifier is trained to assign a class label to each pixel (Moeskops, Wolterink, et al., 2016). Within automatic segmentation, Convolutional Neural Networks (CNN) automatically extract features optimized for the classification task at hand. For instance, CNNs have been successfully applied to medical image segmentation (de Brebisson and Montana, 2015; Moeskops, Viergever, et al., 2016). CNNs have not only been used for processing medical images and can be designed for image classification in natural images (Krizhevsky et al., 2017). CNNs have shown great generalisability for divergent tasks such as image segmentation (Long et al., 2015), object detection (Girshick et al., 2015), and object localization (De Vos et al., 2016). Hence, CNN architectures may have the flexibility to be used for different tasks and within different areas. In this thesis, I used a CNN architecture called, U-Net, that was developed for Biomedical Image Segmentation (Ronneberger et al., 2015). The U-Net is an optimized convolutional network architecture that can work with very few training images (training set = 30 images in Ronneberger et al., 2015 and achieve very good performance on very different biomedical segmentation applications (**Figure 3.1**; Long et al., 2015). Therefore, the U-Net architecture was modified and extended to fit the different objectives of this work: to enable the analysis of the large dataset of SEM images rapidly and to segment the different classes accurately. Regarding how microbioeroding communities were investigated and to prevent further repetitions, please refer to the **section 2.3**.

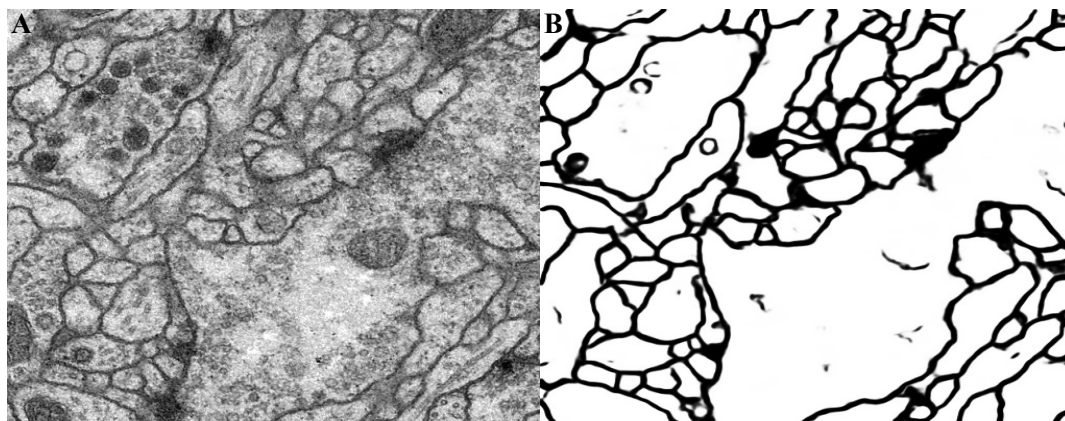


Figure 3.1: (A) Original MET images showing the different cell wall structures. (B) Prediction of the U-NET model for segmenting the different cell walls in the image.

3.3 Application of Machine Learning on Microbioeroding Communities

Originally, Alaguarda et al. 2022 developed a machine-learning approach that was applied to a slow-growing massive coral *Diploastrea* sp. from Mayotte to determine the variability of the abundance of microborings over the last five decades (to be presented in **Chapter 4**). One main objective of this ML approach is to extend its application to further different corals (e.g., massive and branching) from contrasted reefs to estimate rapidly and efficiently the surface of coral skeleton colonized by microbioeroding traces and enable a better understanding of the distribution, composition, and abundance of these communities. Therefore, this approach needs validation with other coral genera to verify that it can identify microbioerosion traces. Thus, in this chapter, the first step was to directly apply the CNN model developed by Alaguarda et al. (2022) trained on the coral *Diploastrea* sp. from Mayotte on another coral genus, based on massive *Porites* sp. from Mayotte and la Reunion to validate if the ML application works on different corals. We also especially improved the treatment of class unbalanced representations by testing various loss functions. The present work highlights the differences between the two procedures and how a dedicated, optimized loss function can significantly improve the CNN model's accuracy. This approach could appear as a powerful tool allowing the accurate and rapid quantification of the abundance of microbioeroding traces in a large number of samples (along a single long coral core, for instance, or in different coral samples) and in different types of coral skeletons.

Article to be submitted in 2023

in the Journal: *Limnology and Oceanography: Methods*

Machine learning approach to quantify microboring assemblage dynamics in two living massive corals

Authors: D. Alaguarda¹, A.Tribollet², R. Lguensat¹, J. Brajard³

Affiliations:

¹ Laboratoire LOCEAN-IPSL, Sorbonne Université-IRD-CNRS-MNHN, 4 Place Jussieu, 75005 Paris Cedex

² Laboratoire LOCEAN, IRD-Sorbonne Université-CNRS-MNHN, Institut de recherche pour le développement, CS 41095 - 2 rue J. Wetzell – PTU – 97 495 Sainte Clotilde cedex – Réunion, France

³ NERSC, Jahnebakken 3, 5007, Bergen, Norway

Keywords: Machine learning approach – Semantic segmentation - Unbalanced dataset – Loss functions – Microboring traces abundance - Massive corals.

Abstract (Need for 250 Words and here 250)

The coral microbiome comprises various micro-organisms located in its tissues, mucus, and skeleton. Within this latter, microboring communities comprise mainly filamentous cyanobacteria, algae and hyphae of fungi,. They produce specific traces by dissolving CaCO_3 skeletons through various metabolic processes. Those traces are of importance as they can be seen as instant fossil traces which are well preserved during the lifespan of their coral host. The study of the variability of their abundance within skeletons of living massive slow growing corals has been overlooked but is of great interest to better understand long term effects of climate change on those microborers and on coral resilience. Microboring traces can be observed using scanning electronic microscopy (SEM). To date, only a few highly time-consuming methods relying on the observer allow their quantification . This limits greatly the number of samples that can be analyzed. Recently, a machine-learning approach based on a Convolutional Neural Network (CNN) model was developed to study accurately and quickly microboring traces' abundance along a core of the very slow-growing massive coral *Diploastrea* sp. (Mayotte). We first tested it on another massive coral, *Porites* sp. and found that the accuracy which was initially 93% dropped down to 88%. We then adapted the initial CNN model for the study of microboring traces in *Porites* sp. and show that optimized loss function can significantly improve the accuracy (from 88% to 95.2%). We then suggest improvements of our models for allowing the analysis of microboring traces in all kinds of living coral skeletons.

Introduction

Since two decades, there is a rising interest for better understanding microboring communities' diversity in both living and dead reef carbonate substrates, implications in the reef carbonate budget and corals' resilience (del Campo et al. 2017; Marcelino and Verbruggen, 2016; Schönberg et al. 2017; Tribollet et al. 2019; Galindo-Martinez et al. 2022). Tribollet et al. (2006, 2019) showed that those cryptic microorganisms play an important role in reef primary production and dissolution, and are strongly stimulated by ocean acidification over a few months or years (see also Tribollet et al. 2009; Reyes-Nivia et al. 2013; Färber et al. 2015; Enochs et al. 2016). Carreiro-Silva et al. (2005, 2009) and Reyes-Nivia et al. (2013) also showed that some microboring organisms are stimulated by eutrophication and global warming over short term (see also Grange 2015). The study of the dynamics of microboring communities in a changing environment over long term remain however unexplored limiting the predictions of the future of coral reefs. Due to experimental and methodological limitations, the long term (decade, century) dynamics of reef microboring communities is extremely difficult to study using dead carbonate substrates as they tend to be completely eroded (reduced in sand particles and dissolved CaCO_3) over more than ten years (Tribollet's pers. obs). Cores of living massive coral colonies which are known as well-preserved bio-archives (Wu et al. 2018; Cuny-Guirriec et al. 2019) appear thus as a good alternative to better understand the long-term effects of climate change and local disturbances on microboring communities (composition and abundance). To date, only three methods were developed to quantify the abundance of microboring filaments or traces in living corals (Lukas, 1973; Le Campion Alsumard et al., 1995a; Priess et al., 2000). Lukas (1973)'s method consisted of decalcifying pieces of living coral skeletons using Perenyi's solution to count the number of microborer filaments under a light microscope. This method was applied only on a few samples located within the first centimeters of the coral colonies. This method is highly time-consuming and does not allow

studying microborers' original spatial distribution within the substrate. It can also underestimate microborers' biomass due to loss or degradation of filaments during the decalcification process. Le Campion-Alsumard et al. (1995)'s method combined observations under light and scanning electron microscopes (SEM) to identify and to count the number of filaments or traces (respectively) among different areas of the coral skeleton but only within the first few cm of coral skeletons. The method of Priess et al. (2000) also combined light microscopy and SEM but focused on the composition and abundance of microboring traces within white versus colored bands in the coral skeletons of the massive *Porites* sp. Those methods were all observer dependent and highly time-consuming. They cannot allow investigating the dynamics of microboring communities over decades or centuries as many samples need to be studied and images to be analyzed. To reach this goal, Alaguarda et al. 2022 developed a new approach relying on a machine learning (ML) technique, reducing the processing of thousands of SEM images to few minutes. Thanks to this approach, the authors reconstructed the abundance variability of microboring traces colonizing a living coral skeleton of a massive *Diploastrea* sp. in Mayotte over the last 54 years. The ML technique performed with 93% of accuracy, which represent the ability of the model to attribute a pixel in the image to its suitable class (e.g., microboring traces, coral skeleton). Four classes were previously described in their SEM images: the resin used to embed the samples, the coral skeleton and two classes of microboring traces divided among their diameter. These classes were not equally balanced in all images. The For instance, the resin or the coral skeleton were the abundant classes while the microboring traces were poorly represented. This scenario represent what we call an “unbalanced dataset problem” (see Prati et al. 2009; Lemaitre et al. 2016; Johnson and Khoshgoftaar, 2019). To tackle such unbalanced effect, Alaguarda et al. (2022) attributed more weights to under-represented classes (e.g., microboring traces). Therefore, this approach makes it a promising tool for quantifying microboring traces in coral skeletons and for continuous reconstruction

over decades. However, their technique could also benefit from improvements for applications on other corals but also lead to refine and better estimations of the colonization of microborers in living coral skeletons. In this work: (i), we present results obtained on a coral core of a massive *Porites* sp. using the model developed on *Diploastrea* sp., (ii) then results obtained from the model after modifications and optimization procedure of the model developed for *Diploastrea* sp., and (iii) the results obtained when combining SEM images obtained from both massive coral for training the model. The possible extend application of our approach to all coral skeleton morphotypes (encrusting, branching..) is then discussed.

Materials and Procedures

1) Coral samples and Treatment

In order to extend the ML approach developed by Alaguarda et al. (2022) could be applied to other coral cores of massive corals than *Diploastrea* sp., two cores of *Porites* sp. were investigated. One core was sampled in a healthy coral colony of *Porites* sp. on the outer slope of the NE barrier reef of Mayotte at 15m depth next to the *Diploastrea* sp. studied by Alaguarda et al. (2022). The other core was collected in a healthy coral colony of *Porites* sp. in the shallow lagoon (1m depth) at La Saline in Reunion Island (Western Indian Ocean). The first core from Mayotte had a diameter of 8 cm and a length of 29.5 cm, while the core from Reunion had a diameter of 8 cm and a length of 40 cm. The age chronologies reconstructed for both corals went from 1990 to 2018 for the *Porites* sp. from Mayotte and 1993 to 2015 for the *Porites* sp. from la Réunion. Coral cores were preserved and then treated using the same methodology as for the *Diploastrea* sp. coral (Alaguarda et al. 2022). Prior measurements, the *Porites* sp. cores were sliced along the main vertical growth axis into four different slabs. A sub-slab of 1.5 cm width were cut along the middle slab of each *Porites* core and then cut into 14 coral samples. Those 14 samples were then embedded in an epoxy resin (see details of the resin inclusion in

Alaguarda et al 2022). Each embedded sample was observed under a SEM operating at 15kv (Zeiss EVO LS15) on the platform ALYSES (Bondy, France) to study the diversity (ichnotaxa) and the abundance of microboring traces as well as their distribution within the coral samples. A total of 1422 images were taken on the *Porites* sp. coral from Mayotte and 1589 on the *Porites* sp. from la Reunion ($n_{\text{total}} = 3011$ SEM images).

2) Dataset constitution step

A reference dataset (also sometimes called a labeled dataset) was first needed. The reference dataset comprised a total of 74 SEM images randomly selected among the 3011 SEM images. 37 SEM images were taken per *Porites* coral core (to be equally present in our database). Those 74 SEM images from both corals constituted a global dataset for *Porites* corals, later called in the study *Porites* sp. The reference dataset ($n = 74$) was then randomly split into three sub-datasets. The training set of 67 images used to determine, optimize, and fit the trainable parameters of the Convolutional Neural Network (CNN). Then, the validation set of 4 images was used to tune the hyper-parameters of the CNN. Finally, the test set comprises 3 SEM images that are neither part of the training nor the validation dataset. It can be considered a reliable, independent test for the capacity of the model to generalize the classification to new SEM images. For technical reasons, the original SEM images of 1024x768 pixels were cut into 12 sub-images of size 256x256 (called patches hereafter). The output patches per SEM image were then reunited after treatment to produce a final image of the same size as the original SEM image (Fig. 2). The total number of test patches was thus 36 (3x12). To further increase the number of patches in the training set (which is critical for the ML approach), we applied a data augmentation technique that increased the number of training patches by applying a rotation of 0°, 90°, 180°, and 270°. Therefore, this procedure allowed the production of 3312 training patches (67 images used for training x 12 patches/image x 4 rotations/patch). The manual

classification of the different objects present in each image was performed using the software GIMP (v2.10) with the following methodology: each image was carefully inspected by an expert human operator, manually associating each pixel to one of the predetermined classes for ground truthing: "resin," "coral skeleton," and "the microboring traces" (= our class of interest; Fig.1). To the contrary to Alaguarda et al. (2022), no distinction was made among the different types of microboring traces (thin vs wide traces based on their diameter). Such visual inspection would indeed be too time-consuming and is beyond the aim of this study.

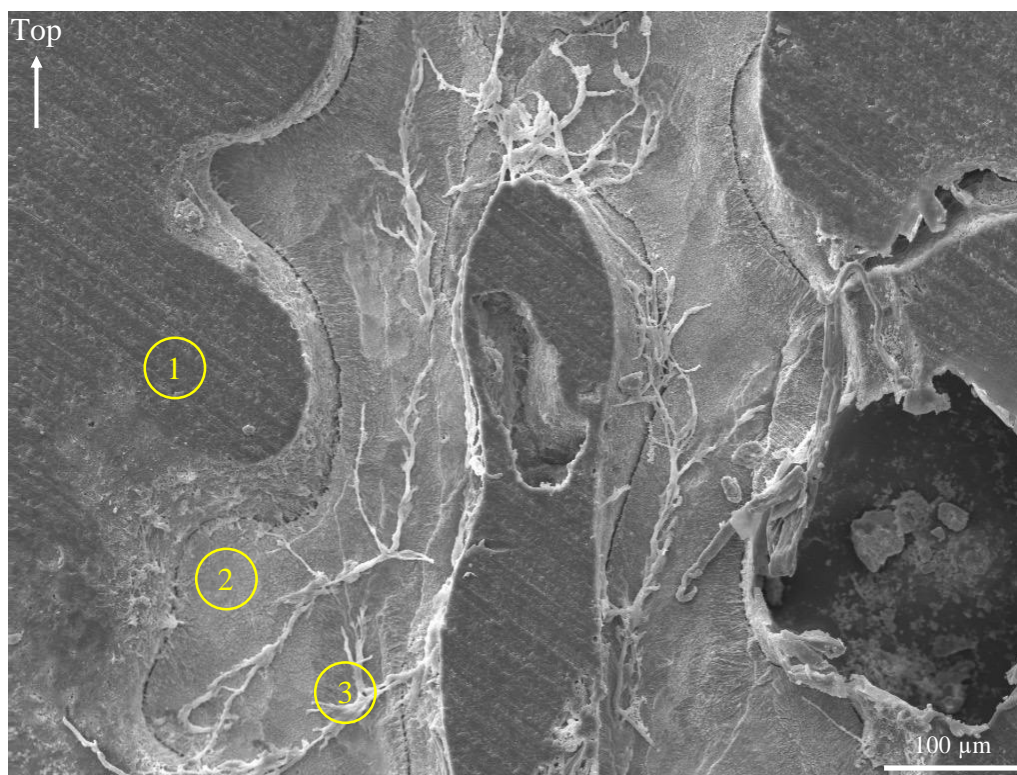


Figure 1: Illustration of an original SEM image from the coral *Porites* sp. displaying the three different classes studied within the coral that the Convolutional Neural network model had to recognize: (1) resin, (2) coral skeleton, and (3) microboring traces. This image was taken in the coral core from la Reunion at the middle of the core.

3) Machine Learning

Neural network architecture

The architecture of an existing CNN model called U-NET (Ronneberger et al. 2015) was adapted for the study. For a detailed visualization of the CNN architecture, please refer to the Suppl Fig.1 from Alaguarda et al. (2022) as the same architecture was used in this study. This type of neural network belongs to the family of deep learning methods and is commonly applied to two-dimensional images (Krizhevsky et al. 2017). Here, for each pixel of the input SEM patch, the CNN model associated a class among three modalities: resin, skeleton, and the microboring traces. The CNN takes the SEM patch as an input and iteratively transforms it to a succession of intermediate features. Each transformation uses a parametrized function whose output is called a layer. The CNN model was built with 10 convolutional layers, one convolution representing a linear operation involving the convolution product of a 3D kernel with the 3D input feature map. A kernel is a tensor of parameters that must be determined in a training phase. Note that convolutional layers are invariant by translation, which means, in our case, that the classification of a microboring trace, for instance, does not depend on its location in the SEM image, which is a desired behavior. Convolutional layers make the CNN model more stable and prevent overfitting, which occurs when a model gives results fitted to the dataset used in the training phase but fails to predict any other inputs correctly. In addition to the convolutional layers that contain most of the trainable parameters, the CNN model contains batch normalization layers, a method used for training CNNs faster through the normalizations of the layers' input (re-centering and scaling, see Ioffe and Szegedy, 2015). Batch normalization also makes training more robust and enables higher learning rates. Moreover, max-pooling layers are added and represented an operation that down-sampled feature map (Nagi et al., 2011) to reduce their size. Then, rectified linear units were applied after each convolutional layer (ReLU; Romanuke, 2017). ReLU is a non-linear function that will output the input directly if it is positive, and zeros otherwise:

$$f(x) = \max(0, x) \quad (1)$$

The last layer, defined as a softmax function, converts output values of the previous layer into probabilities, i.e., positive and sum to 1 (Goodfellow et al. 2016). The model attributes a probability for each pixel to belong to each predetermined class (skeleton, resin, or microboring traces). The final class attributed corresponds to the one with the highest predicted probability. The trainable parameters of the convolutional layers were thus optimized during the training process in which a loss function was minimized. The output predicted by the CNN model corresponded to the closest output to reference (the input data). See the dedicated section for more details about the loss function. Once the parameters of the CNN model are optimized, the CNN model can be used to process any input SEM images.

Model assessment

Four metrics were computed on the test dataset to validate the outcome of the CNN model and verify that it can be used on new images. The first metric is the accuracy of the classification. It corresponds to the ratio between correctly classified pixels and the total number of pixels (100% corresponds to a perfect classification). An excellent way to better understand is to look at the confusion matrix (Fig.2).

		Actual	
		Positive	Negative
Predicted	Positive	True Positive (TP)	False Positive (FP) Type I error
	Negative	False Negative (FN) Type II error	True Negative (TN)

Figure 2: Definition of the confusion matrix showing the different possibilities when classifying pixels

Four possibilities are available: (A) The model predicts a pixel belonging to the class “microboring,” and the reality is the presence of “microboring” (True Positives =TP); (B) The

model does not predict a pixel belonging to the class “microboring,” and the reality is the absence of “microboring” (True Negatives= TN); (C) The model predicts a pixel belonging to the class “microboring,” and the reality is the absence of “microboring” (False Positives= FP); (D) The model does not predict a pixel belonging to the class “microboring,” and the reality is the presence of “microboring” (False Negatives =FN). In a binary classification, the accuracy is defined as:

$$Accuracy = \frac{TP+TN}{TP+FP+TN+FN} \quad (2)$$

which correspond to the total correct predictions (TP+TN) out of the total predictions (TP+FP+TN+FN). The same reasoning is also valid for a multi-class scenario. In this case, the accuracy returns the proportion of correctly classified cases from the total number of object in the dataset. Besides the global accuracy, other scores were looked into and dedicated to the class of interest: the microboring traces.

First, we defined the precision (also called Positive Predictive Value) which is represented in a binary classification as:

$$Precision = \frac{TP}{TP + FP} \quad (3)$$

which corresponds to the rate of correct predictions among the positive predictions. It measures the capacity of the model of a non-error during a positive prediction.

We also defined recall (also called Sensitivity or Hit Rate) as:

$$Recall = \frac{TP}{TP + FN} \quad (4)$$

which corresponds to the rate of positive individuals detected by the model. It measures the capacity of the model to detect all the positive individuals (microboring traces).

Finally, we used the F1-score metric which is the harmonic means of precision and recall:

$$F1 = 2 \cdot \frac{precision \cdot recall}{precision+recall} \quad (5)$$

The four metrics used gave values between 0 (the model is always wrong) and 1 (the model is always right).

Loss Function

As mentioned previously, the training process consists of adjusting the parameters of the CNN model by minimizing a loss function representing the mismatch between the targeted output and the simulated output. This loss function is computed on each pixel of the output patch and then sum over all the pixels of the output patch to obtain a total value over the whole patch. Suppose the loss function gives equal importance to pixels labeled in a majority class as those labeled in the minority class, the loss function's total value, which considers all the pixels of the image, is mainly determined by the majority class. Consequently, the training is biased toward giving the best accuracy to the majority class, which can be detrimental to the minority. To tackle this challenge, we define the loss function of CNN to assign higher costs to the minor-represented classes. The choice of the loss function can significantly impact the result as it is the criteria used to determine the final parameter of the model. In the study of Alaguarda et al. (2022), the authors used only one loss function: the Weighted Cross Entropy (WCE). This loss function efficiently tackled the unbalanced class problem and identified clearly the proportion of the different classes in the coral *Diploastrea* sp. Nonetheless, this loss function was classifying too many pixels “microboring traces”, making them thicker than reality, therefore over-estimating slightly their real abundance colonizing the coral skeleton. In the following, several loss functions were considered to assess the sensitivity to this choice for the model's accuracy and to propose the optimal choice given evaluation metrics defined in the previous section, "model assessment". We define different variables for the following equations regarding the different loss functions. Within the different equations, N represents the number of classes with i comprised between 1 and N , P represents the number of pixels with j

comprised between 1 and P, p_i represents the probability for the truth label and g_i is the probability for the class i predicted by the model. For a 3-classes classification problem, 3 possible values are defined for the vector (p_1, p_2, p_3) : [1,0,0], [0,1,0], and [0,0,1], respectively, for classes 1, 2, and 3. For example, giving a pixel belonging to class 2, we obtained: $p_1 = 0$, $p_2 = 1$, and $p_3 = 0$.

a) *Cross entropy loss function*

Cross-Entropy (CE) is the standard loss function for classification problems (Goodfellow et al. 2016, Chapter 6). CE can be defined as:

$$CE = - \sum_{i=1}^N \sum_{j=1}^P \cdot p_{i,j} \cdot \log (g_{i,j}) \quad (6)$$

CE loss is calculated as the pixel level. CE can be unsuitable for an unbalanced dataset, leading to decision boundaries biased toward the majority class as explained above.

b) *Weighted cross entropy loss function*

The Weighted Cross Entropy loss function is designed to tackle issues of the unbalanced dataset. This loss function is adapted from the negative log cross-entropy, a standard procedure used for classification, and defined for each set of training samples by:

$$WCE = - \sum_{i=1}^N \sum_{j=1}^P \cdot w_i \cdot p_{i,j} \cdot \log (g_{i,j}) \quad (7)$$

The coefficient w_i is a weighted factor to compensate for the fact that classes are highly unbalanced by attributing more important weights to under-represented classes. The factor was set with a weight of 0.7 for the microboring traces , 0.15 for the skeleton and 0.15 for the resin.

c) *Dice loss function*

Dice Loss (DL) comes from the Sørensen–Dice coefficient, a statistical approach to calculating the similarity between two images and used for class segmentation tasks (Salehi et al., 2017; Zhang et al. 2021), and allows to avoid re-weighting as in WCE. The function is defined as:

$$D = \frac{2 \cdot \sum_{i=1}^N \sum_{j=1}^P (p_{i,j} \cdot g_{i,j})}{\sum_{i=1}^N \sum_{j=1}^P (p_{i,j} + g_{i,j})} \quad (8)$$

DL typically outperforms CE in unbalanced image segmentation problems (Milletari et al. 2016, 2017; Wong et al. 2018) and performs well within models.

d) *Focal loss function*

The Focal Loss (FL) addresses scenarios with an extreme imbalance between foreground and background classes during the training. FL works as an improvement of the version of Cross Entropy. It handles the imbalance classes problem by assigning more weights to complex or easily misclassified examples and to down weights the easily classified examples (Lin et al. 2018). The FL equation is defined as:

$$FL = \sum_{i=1}^N \sum_{j=1}^P \cdot \alpha \cdot (1 - p_{i,j})^\gamma \cdot p_{i,j} \cdot \log(g_{i,j}) \quad (9)$$

α is a hyperparameter designed to handle the class imbalance problem. In our case, α is set up at 0.25. The parameter γ smoothly adjusts the rate at which easy examples (i.e. easily recognizable, class resin for example) are down-weighted and is a focusing parameter for the modulating factor $(1 - p_i)$. When $\gamma = 1$, FL is equivalent to CE. When γ is increased the effect of the modulating factor is likewise increased. Setting $\gamma > 0$ reduces the relative loss for well-classifications (Lin et al., 2018). Here, γ is set up at 2.

e) *Tversky loss function*

Tversky Loss (TL) is based on the Tversky similarity index (Tversky, 1977). The Tversky similarity index can be evaluated as a generalization of the Dice coefficient, adding weights to the FPs and FNs through the help of a coefficient. TL can be defined as:

$$TL = \sum_{i=1}^N \sum_{j=1}^P \frac{p_{i,j} \cdot g_{i,j}}{p_{i,j} \cdot g_{i,j} + \Delta (p_{i,j}(1-g_{i,j})) + \beta (g_{i,j} (1-p_{i,j}))} \quad (10)$$

The Tversky index adds two hyperparameters, Δ and β , where $\Delta + \beta = 1$. In the case where $\Delta = \beta = 0.5$, it is equivalent to the dice coefficient. Δ and β control the magnitude of FPs and FNs (Salehi et al. 2017). Adjusting hyperparameters like Δ and β permits higher tradeoffs between FPs and FNs, allows to weight FNs and enhances model performances in a highly unbalanced dataset (α defined in (8)). For our study Δ and β were set up at 0.3 and 0.7 respectively.

f) *Focal Tversky loss function*

The Focal Tversky Loss (FTL) function is a variant of the FL and a modulation of the Tversky similarity index, better suited for identifying small structures segmentation. Therefore, the FTL function works for highly unbalanced data segmentation. As observed in the FL function, FTL attempts to weights more the minor represented examples, with the help of the precedent coefficient defined in (9):

$$FTL = \sum_{i=1}^N \sum_{j=1}^P \left(1 - \frac{p_{i,j} \cdot g_{i,j}}{p_{i,j} \cdot g_{i,j} + \Delta (p_{i,j}(1-g_{i,j})) + \beta (g_{i,j} (1-p_{i,j}))} \right)^\gamma \quad (11)$$

Finally, an average coefficient was calculated from each Tversky loss coefficient calculated for each different class. TL indicates the Tversky Index, the parameter γ is the hyper-parameter previously defined in (9) but was set up at $\frac{4}{3}$ for this loss function. α and β were again set up at 0.3 and 0.7 respectively (Abraham and Khan, 2018). The number of pixels associated for each class was very heterogenous, making our dataset unbalanced where the minority class (microboring traces) represents the class of interest (Table.1).

Total Training set	Number of total Pixels	Pixels attributed to traces	Pixels attributed to skeleton	Pixels attributed to resin
67 Training Images	100%	2,3%	29,3%	68,4%
7 Validation and Test Images	100%	4,1%	26,7%	69,2%

Table 1. Pixel classification between the different classes regarding the training dataset, validation, and test set shows the typical unbalanced dataset problem between the different classes.

Training and Validation step

The training phase of the CNN model aims at optimizing the trainable parameters of the model. It was performed by minimizing one of the mentioned loss functions on the training dataset using the Adam algorithm based on a gradient descent technique (Kingma et al. 2014). Hyperparameters of the model were set similarly as investigated by Alaguarda et al (2022) for the coral *Diploastrea* sp. for comparison with this latter later on. The only difference was setting a maximum of 80 epochs to reduce the time calculation. We assured that it had no impact on the model's predictions. An epoch in ML indicates one complete passage of the training dataset into the model during the training. The training was stopped if the loss computed over the validation set (not used to optimize the trainable parameter) stopped improving for more than 10 epochs. This procedure, known as early stopping, aims at avoiding overfitting (Goodfellow et al. 2016). The duration of the training was between 1 and 2 hours by connecting to the IPSL MESRI Mesocenter using its GPU with two graphic cards, NVIDIA GeForce RTX 2080 Ti (11Go), using TensorFlow (version 2.6.0). After the training, the CNN model takes only a few minutes to analyze the entire SEM dataset of 3011 images from both corals. For each model, the metrics described in the "Model assessment" section were computed on the validation dataset. The score for each metric was relatively sensitive to the choice of the loss function considered. The model gathering the best performance (highest F1-score) is available online (<https://gist.github.com/brajard/ad809dbbcf9ba723320a47b89d26e1d4>).

Post-processing steps

The final quantity of interest x_{est} represents the abundance of microboring traces colonizing the coral skeleton in the SEM images, calculated as:

$$x_{est} = \frac{m_a}{(m_a + s_a)} \cdot 100 \quad (12)$$

Where m_a represents the number of pixels attributed to the class “microboring traces” for an image a and s_a the number of pixels attributed to the class “coral skeleton”. Equation (12) applies to segmentations estimated from CNNs and manual processing. Overall, the CNN model overestimated the surface area of microboring traces (see paragraph 1 in Assessment). Thus, a correcting factor was applied to the collection of SEM images to correct the bias. The corrected factor C was computed by linear regression between the true abundance in the training set and the abundance reconstructed by the CNN model following the formula:

$$C = \frac{\sum_{i=1}^Z (x_{est} - X_{est}) \cdot (x_{ref} - X_{ref})}{\sum_{i=1}^Z (x_{est} - X_{est})^2} \quad (13)$$

where x_{ref} represent the abundance of microboring traces estimated from the manual processing calculated based on (12) for an image i , Z being the number of training images. X_{est} and X_{ref} represents the mean area of microboring traces estimated from one of the different CNN models and the manual processing respectively over the all training set. The coefficient factor (computed on the training set) was then applied to all the images as follow:

$$X_{cor} = X_{est} * C + B_{mean} \quad (14)$$

where B_{mean} is the y-intercept computed for all the images from the training set.

Assessments**1) Application of the *Diploastrea* model on *Porites* SEM images**

We first applied the Alaguarda et al. (2022) model developed for the massive coral *Diploastrea* sp. to the dataset of SEM images used for the present study ($n = 74$) from both *Porites* sp. corals. The objective was to assess whether this model could be performant and could accurately identify the microboring traces colonizing this type of coral skeleton. The model used by Alaguarda et al. (2022) was trained using a WCE loss function with weights set up at 0.7 for the class “microboring traces”, 0.15 for the class “resin” and 0.15 for the class “coral skeleton”. When applying the *Diploastrea* sp. CNN model to SEM images belonging to *Porites* sp. corals, we noticed errors in the identification of the different classes in the images and a decreasing accuracy from 93% to 88%. More significant decreases could be observed when focusing on the class “microboring traces” looking at the other metrics. The precision of the model *Diploastrea* sp., applied to the dataset of SEM images from *Porites* sp. corals decreased from 68% to 50%, the recall from 90% to 72%, and the F1-score from 80% to 59%. One SEM image from the test dataset from *Porites* corals (Fig.3A) was first manually analyzed (Fig.3B) and then analyzed using the model CNN developed initially for *Diploastrea* sp. by Alaguarda et al. (2022) (Fig.3C).

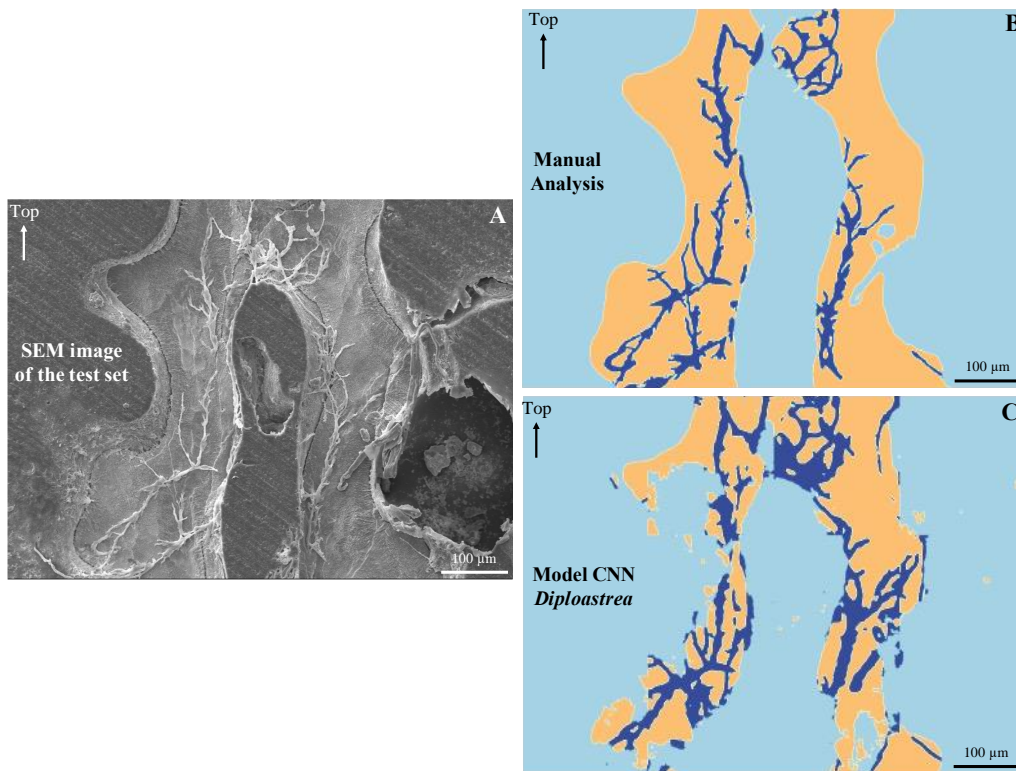


Figure 3: A comparison of the different outputs between manual processing and model predictions on the test image presented in Figure 1. **A.** SEM validation image. **B.** Manual processing of the same image. **C.** Model estimation based on the *Diploastrea* coral from Alaguarda et al. (2022).

By looking at the Figure 3B and 3C, the microboring traces estimated with the CNN model developed on *Diploastrea* sp. appeared thicker conducting to the over-estimation of their surface area compared to the manual estimation. This was expected as shown and corrected by Alaguarda et al. (2022). In the following we will refer to the “**raw model**” if the correction was not performed, and to the “**bias corrected model**” if the correction was performed (from Eq. 13 and 14). Estimations of the “raw model” *Diploastrea* sp. and the “bias corrected model” of the percentage of coral skeleton colonized by microboring traces, from the SEM images of *Porites* sp. were compared with the manual processing (Fig. 5). The estimation from the “bias corrected model” *Diploastrea* sp. was realized with the corrected factor $C = 0.64$ and $B_{mean} =$

−0.023 (Eq. 14) computed on the *Porites* sp. training set ($n = 67$). One relevant point is that the estimation of the “raw model” *Diploastrea* sp. shows a similar general variability of the surface of the coral skeleton colonized by microboring traces compared to the manual processing estimation (Fig.4). Nonetheless, the estimation of the “raw model” *Diploastrea* sp. always overestimated the real coral surface area colonized by microboring traces compared to the manual processing (Fig.4). When correcting the model, the estimation of the surface of the coral skeleton colonized by microboring traces, almost fit the estimation from the manual processing, even if some variability can be observed (Fig.4, not significant on 74 SEM images). To be more accurate, we trained a model based on the dataset of SEM images obtained from *Porites* corals to investigate if the accuracy would be better in estimating the coral surface colonized by microboring traces.

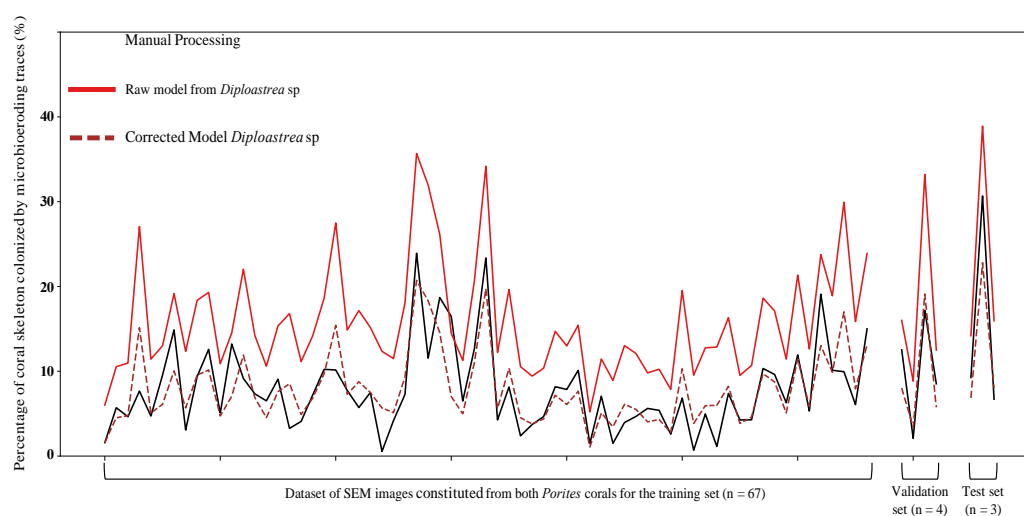


Figure 4: A comparison of the colonized surface by microboring communities estimated by manual processing vs. estimations of the raw and bias corrected model of *Diploastrea* sp. on the dataset of images from *Porites* sp. The black line represents manual processing. The “red” dotted line represents the estimation with the “raw model” of *Diploastrea* sp. developed by Alaguarda et al. (2022). Finally, the “brown” dotted line represents the estimation with the “bias corrected model” *Diploastrea* sp.

2) Loss Functions Investigations for *Porites* sp.

The following investigations were based on the dataset of SEM images of two *Porites* corals to enhance the model's predictions for analyzing microboring traces in a different massive coral, compared to the predictions from the CNN model *Diploastrea* sp. Several loss functions were optimized during the training phase to tackle the unbalanced dataset problem in the SEM images. Different metrics for models' performances assessed how was the identification of the class “microboring traces” on the validation dataset (Fig. 5).

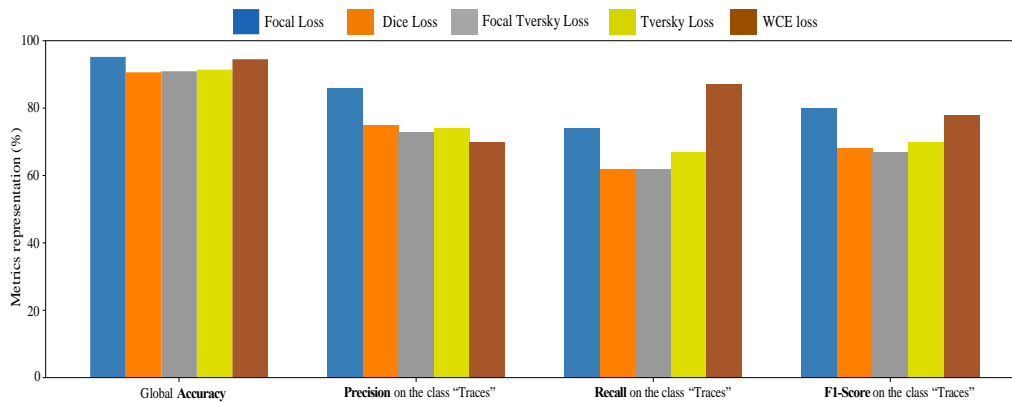


Figure 5: Barplots of the different metrics representative of the performance of our CNN models on the validation set. Here, four different metrics are described: Global accuracy (the number of correct predictions divided by the number of total predictions). The second metric described is the Precision over the “microboring traces” class (= Type 1 Error). The third metric represents the Recall over the “microboring traces” class (= Type 2 Error). The last one is the F1-Score, which combines Precision and Recall (harmonic mean of the Precision and Recall metrics).

Considering the CE loss function, the model's performance was significantly lower than the other loss functions. Such results demonstrate that the CE can lead to biased estimates when trained on unbalanced datasets. Using dedicated loss functions tailored to the unbalanced data

problem can significantly improve the model's performance. Considering the WCE loss function, the model's overall accuracy was 94.5%, the second most performant model in global accuracy (Fig.5; Table.2). Nevertheless, this model presented the lowest precision (if we exclude CE) regarding the “microboring traces” class (70%), classifying more pixels within this class that were not correctly identified and leading to thicker traces.

Training ID	Loss Functions	Weight on the class “Traces”	Global Accuracy	Precision on the class “Traces”	Recall on the class “Traces”	F1-Score on the class “Traces”
1	Cross Entropy loss	Equal Weights	89.2%	75%	51%	61%
2	Weighted loss	Weight = 0.7	94.5%	70%	87%	78%
3	Dice loss	Weight = 0.6	90.6%	75%	62%	68%
4	Tversky loss	$\Delta = 0.3$; $\beta = 0.7$	91.4%	74%	67%	70%
5	Focal Tversky loss	$\alpha = 0.3$; $\gamma = \frac{4}{3}$; $\beta = 0.7$	90.9%	73%	62%	67%
6	Focal loss	$\alpha = 0.25$; $\gamma = 2$	95.2%	86%	74%	80%

Table 2. Summary of models' training for each loss function, with the associated weight for the "microboring traces" class. Also, metrics used to assess the model performance on the validation dataset displayed for each model for the "microboring traces" class.

Compared to the CE, the model trained with the WCE displayed the highest performances in discriminating the different classes (Table.2), demonstrating that weighted cross-entropy was more efficient in tackling unbalanced class problems than the standard CE. Considering the model trained with DL, TL, and FTL functions, the model's accuracy, precision, recall, and F1-score had very close results (1 to 2% differences for all metrics, Table.2). The model trained with the FL function presented the highest value for precision, accuracy, and F1 score and the second highest for recall (Fig.5, Table.2), representing the proportion of correctly attributed real traces. Thus, the trained model with the FL function represented the model selected for identifying the microboring traces. Differences between the loss functions could also be visualized when zooming on a specific area of one SEM image of the test dataset (Fig.6A and

B). This figure showed the variability of the model's accuracy when identifying the microboring traces between the different loss functions and the manual processing (Fig.6C and D). When classifying with the WCE, microboring traces appeared thicker, leading to an overestimation of the area of the coral skeleton colonized by microboring traces (Fig.6E and F). The training with the DL function struggled with the identification of some microboring trace pixels and misclassifying them into resin pixels. Such misclassification can lead to potential underestimation of the surface of the coral skeleton colonized by microboring traces (Fig.6G and H). The TL model also misidentified microboring trace pixels and classed them into resin pixels, leading again to potential underestimation of the real coral surface occupied by these traces (Fig.6I and J). As previously mentioned with the DL and TL models, the FTL model under-estimated the coral surface occupied by microboring traces by attributing some pixels to the resin class (Fig.6K and L). The FL model predictions for the different classes and mainly for the microboring traces class, were the closest to fitting the manual processing estimation (Fig.6M and N).

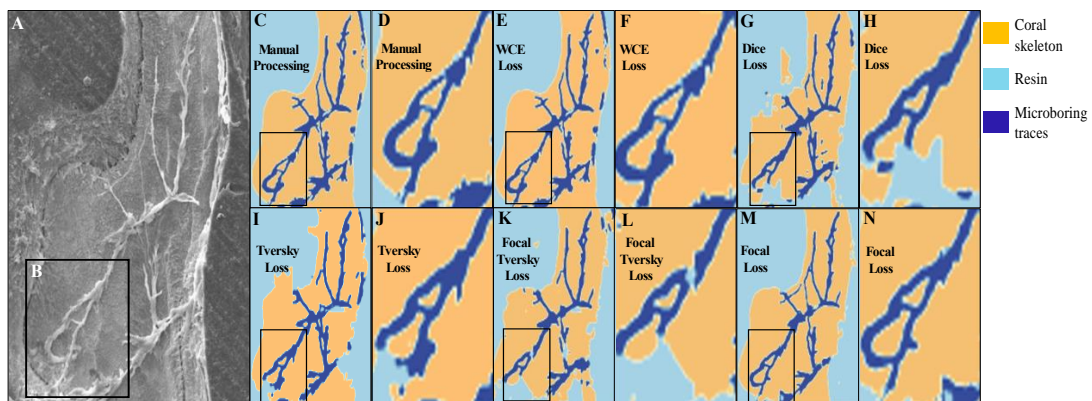


Figure 6: Illustration of a zoomed part of the SEM image shown in Figure.1 (lower left part) displaying the comparison between the models' predictions trained with different loss functions and the manual processing. **A.** Zoom within one of the validation SEM images showing the three different classes. **B.** Square shows a zoom within a specific location to witness the three different classes used to assess differences between manual processing and the model's predictions. **C and D.** Images from the manual processing of the

validation (= desired output). **E and F.** Prediction from the model trained with Weighted Cross Entropy loss function. **G and H.** Prediction from the model trained with Dice Loss function. **I and J.** Prediction from the model trained with Focal Loss function. **K and L.** Prediction from the model trained with Tversky Loss function. **M and N.** Prediction from the model trained with the Focal Tversky Loss function.

To summarize, the DL, TL, and FTL performed similarly regarding model predictions with overall underestimations regarding the class microboring traces. WCE showed good performances in predicting the different classes with a slight overestimation of the surface occupied by the microboring traces class. Overall, with these findings, different dedicated loss functions tailored to the unbalanced data problem can significantly improve the model's performance in identifying the class of interest, and here the FL model showed the highest performances.

3) Comparison of *Diploastrea* and *Porites* sp. models

To compare the predictions from the model developed by Alaguarda et al. (2022) on the coral *Diploastrea* sp., with the selected CNN model trained with the FL function on the dataset of *Porites* sp., one SEM image from the test set (Fig.7A) was first manually analyzed (Fig.7B), then analyzed using the model CNN developed initially for *Diploastrea* sp. (Fig.7C) and finally analyzed with the newly trained model CNN with the FL function (Fig.7D). By looking at 7C and 7D, the microboring traces estimated with the model *Diploastrea* sp. appeared thicker. Differences were highlighted in estimating the percentage of coral skeleton colonized by microboring traces between the CNN models of *Diploastrea* sp. and *Porites* sp.

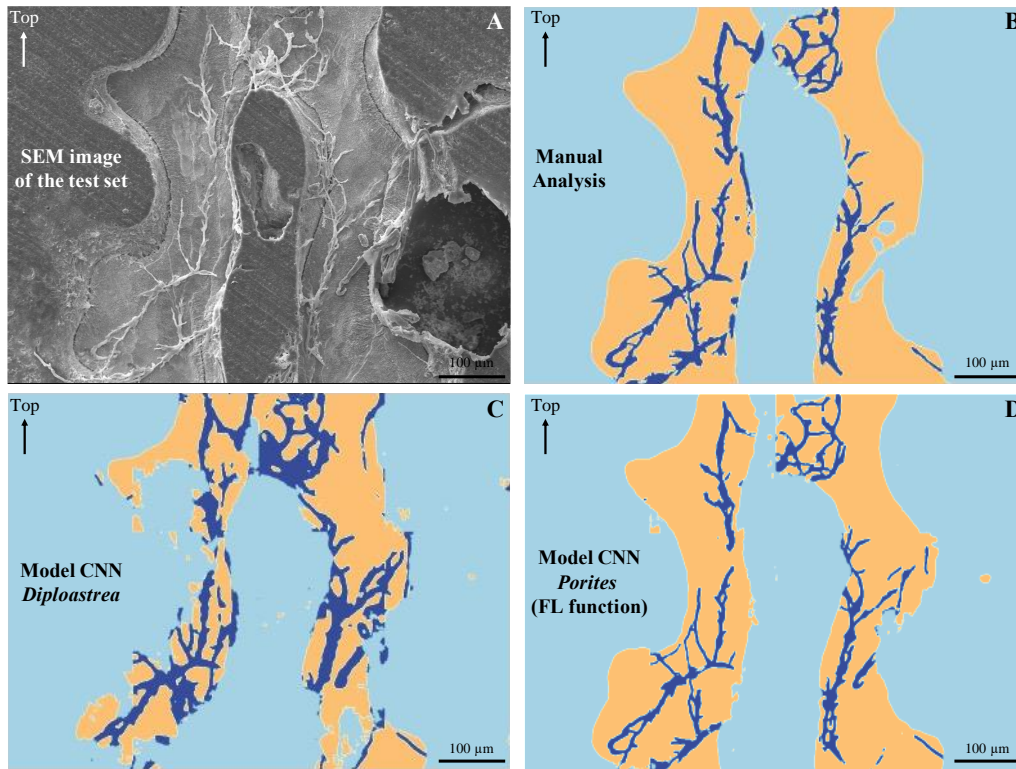


Figure 7 : A comparison of the different outputs between manual processing and model predictions on the test image presented in Figure 1. **A.** SEM validation image. **B.** Manual processing of the same image. **C.** Model estimation based on the *Diploastrea* sp. coral from Alaguarda et al. (2022). **D.** Model FL estimation based on the *Porites* sp. coral developed in this study.

The dataset constituted from SEM images of both *Porites* sp. corals ($n=74$) was processed manually, then by the CNN “raw model” from *Diploastrea* sp. and then by the CNN “raw model” trained with the FL function developed in this study (Fig.8). The dataset was also processed with the CNN “bias corrected model” *Diploastrea* sp. and the CNN “bias corrected model” trained with the FL function developed in this study (Eq. 13 and 14). The correction was computed on the *Porites* sp. training set ($n = 67$). The estimation from the “bias corrected model” trained with the FL function was realized with the corrected factor $C = 1.04$ and $B_{mean} = 0.001$ (Eq.14), also computed on the *Porites* sp. training set ($n = 67$). Spearman's correlations

were realized between the CNN models and the manual processing. Between the "raw model" *Diploastrea* sp. and the manual processing, we obtained a correlation of 0.81 ($p < 0.001$). In contrast, with the "raw model" trained on the *Porites* sp. dataset trained with the FL function and the manual processing, we obtained a correlation of 0.99 ($p < 0.001$). Differences were highlighted in estimating the percentage of coral skeleton colonized by microboring traces between CNN model of *Porites* and *Diploastrea* sp (Wilcoxon Test, p -value < 0.001). Correlations with the bias corrected model and the manual processing did not change significantly. The correlation validates the variability observed between models estimation from *Diploastrea* and *Porites* sp. Besides, the "bias corrected model" trained on the *Porites* sp. dataset trained with the FL function nearly perfectly fits the manual processing estimation compared to the "bias corrected model" *Diploastrea* sp. However, one relevant point was that the estimations from the "raw model" *Diploastrea* sp. showed a similar general variability of the surface of the coral skeleton colonized by microboring traces, compared with the estimation of the "raw model" trained on the *Porites* sp. dataset trained with the FL function (Fig.8).

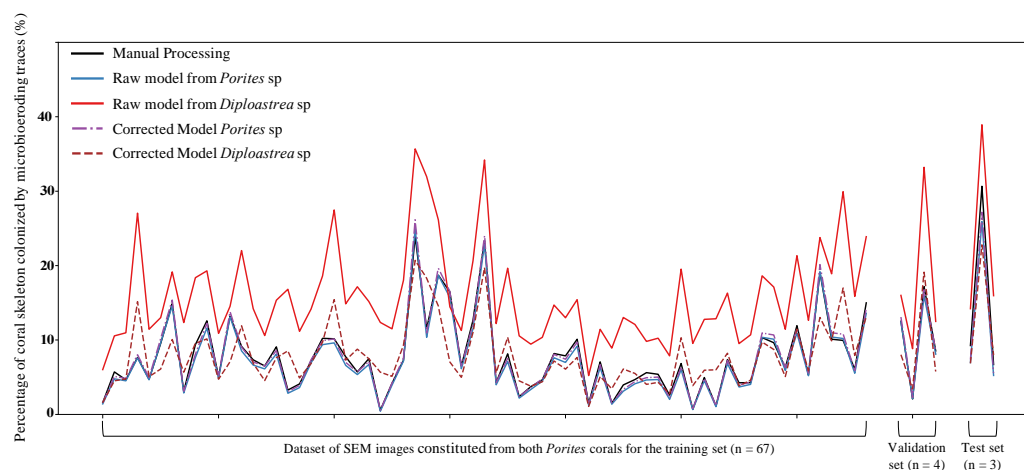


Figure 8 : Comparison of the manual processing estimation of the colonized surface by microboring communities vs. estimations from different models on *Porites* sp. images. The black line represents manual processing. The “blue” dotted line represents the estimation with *Porites* sp.'s “raw model” with the Focal Loss Function. The “red” dotted line represents the estimation with the “raw model” of *Diploastrea* sp.

developed by Alaguarda et al. (2022). The “purple” dotted line represents the estimation with the “bias corrected model” of *Porites* sp with the Focal Loss Function. Finally, the “brown” dotted line represents the estimation with the “bias corrected model” *Diploastrea* sp.

Nonetheless, the estimation of the "raw model" *Diploastrea* sp. overestimated the real coral surface colonized compared to the "raw model" trained on the *Porites* sp. dataset trained with the FL function. These findings showed that the model *Diploastrea* sp. from Alaguarda et al. (2022) could identify the different classes in another dataset of SEM images from another massive coral *Porites* sp. but errors may be introduced and mainly concerning the "microboring traces". These latter were corrected to eliminate the biases from the "raw model" estimations (Fig. 8). Moreover, these findings showed that the FL model explicitly trained on the dataset better predicted and discriminated the different classes than the estimations from the model *Diploastrea* sp.

4) A Multi CNN model: combination of SEM images from both massive corals

A final objective was to merge SEM images for both corals and assess if the training of a multi coral model based on SEM images from both corals would identify microboring traces in either of these two massive corals, and be as good as the model trained with the FL function for *Porites* sp. and the first model developed for *Diploastrea* sp. SEM images (n = 52) from the coral *Diploastrea* sp. were used from Alaguarda et al. (2022) and from *Porites* corals of this study (n = 53). Images were merged together to constitute a new dataset (n = 105). This dataset was again randomly split into three sub-datasets: the training set of 90 images, the validation set of 5 images and finally the test set comprises 10 SEM images of each massive coral. For these experimentations, models were trained with three main loss functions: the WCE, the DL and the FL (Table.3). The metrics were evaluated first on the test dataset of the coral *Diploastrea* sp. alone (n=10), then the coral *Porites* sp. alone(n=10) and finally the combination of both test

sets (n=20). For the following, we present only the best results from the multi coral model trained with the DL function. The overall accuracy of the multi coral model trained with the DL function reached more than 94.2% for all different test set scenarios. The Recall and F1-score were higher than the *Porites* sp. model trained with the FL function, with an increase of 5% and 2% in average respectively. The precision was the same (see Table.3).

Training ID	1	2	3
Loss Functions	Weighted loss	Dice loss	Focal loss
Weight on the class Traces	Weight = 0.7	Weight = 0.6	$\alpha = 0.25; \gamma = 2$
Accuracy on test images of <i>Diploastrea</i> sp. (n=10)	88%	94.2	93.9%
Precision on test images of <i>Diploastrea</i> sp. (n=10)	54%	87%	83%
Recall on test images of <i>Diploastrea</i> sp. (n=10)	89%	81%	69%
F1-score on test images of <i>Diploastrea</i> sp. (n=10)	67%	84%	76%
Accuracy on test images of <i>Porites</i> sp. (n=10)	94.6%	96.4%	96.5
Precision on test images of <i>Porites</i> sp. (n=10)	54%	84%	78%
Recall on test images of <i>Porites</i> sp. (n=10)	86%	78%	77%
F1-score on test images of <i>Porites</i> sp. (n=10)	67%	81%	77%
Accuracy on combine test images of both corals (n=20)	91.5%	95.3%	95.2%
Precision on combine test images of both corals (n=20)	54%	86%	81%
Recall on combine test images of both corals (n=20)	88%	80%	72%
F1-score on combine test images of both corals (n=20)	67%	83%	76%

Table 3. Summary of metrics performance for each multi coral model with the associated loss function and selected weight for the "microboring traces" class. Metrics are calculated on a test set of only 10 images from the coral *Diploastrea* sp, then 10 images from the coral *Porites* sp and the combination of those two.

Predictions from the model developed by Alaguarda et al. (2022) on the coral *Diploastrea* sp., the selected model trained with the FL function on the dataset of *Porites* sp., and the multi coral model trained with the DL function were compared from one SEM image of the test set of *Porites* sp. (refer to figure 7.A for the original SEM image, and see Fig.9A to D). By looking at Fig.9D, predictions from the multi coral model of the class microboring traces were nearly

exactly similar to the analysis from the manual processing (Fig.9A) or the estimation from the CNN *Porites* sp. model trained with the FL function (Fig.9C). Errors came from the misclassification of pixels belonging to the class coral skeleton replaced by resin pixels.

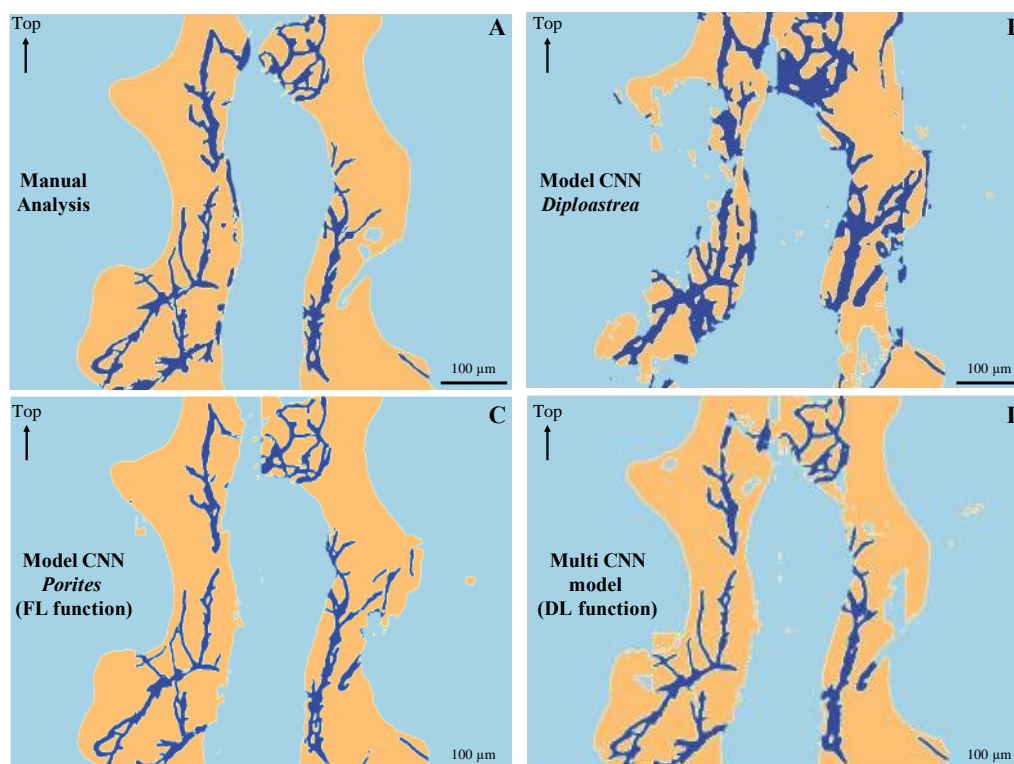


Figure 9 : A comparison of the different outputs between manual processing and model predictions on the validation image is presented in Figure 1. **A.** Manual processing of the test image presented in Fig.1. **B.** Model estimation based on the *Diploastrea* sp. coral from Alaguarda et al. (2022). **C.** Model FL estimation based on the *Porites* sp. coral developed in this study. **D.** Multi coral model estimation based on SEM images of both corals

The same reasoning was also performed on a SEM image of the coral *Diploastrea* sp. (see Fig.10A to 10.D). This image was the same as investigated by Alaguarda et al. (2022; see their Figure 3). By looking at Fig.10D, predictions from the multi coral model of the class microboring traces were almost close to the result of the manual processing (Fig.10A), even

better than the predictions of the *Diploastrea* sp. CNN (Fig.10B). The estimation from the CNN *Porites* sp. model trained with the FL function (Fig.10C) also nearly fit the estimation from the manual processing, nonetheless with errors pixels belonging to the class coral skeleton replaced by resin pixels.

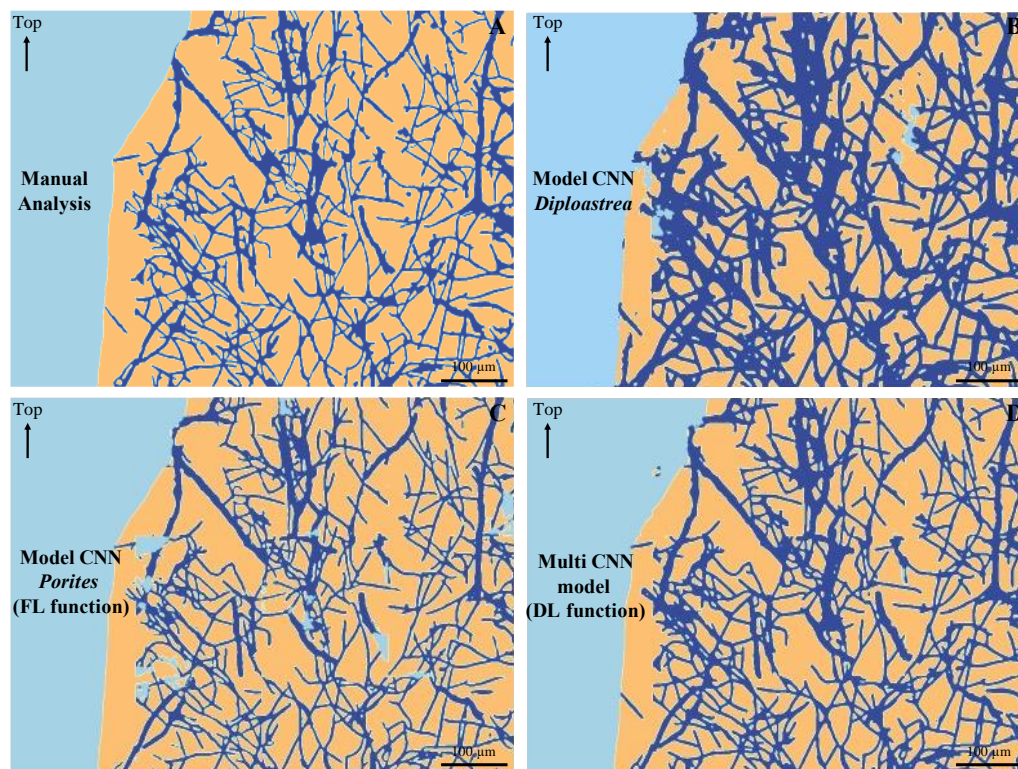


Figure 10 : A comparison of the different outputs between manual processing and model predictions on one test image from the coral *Diploastrea* sp. investigated by Alaguarda et al. (2022). **A.** Manual processing of the test image of the coral *Diploastrea* sp. **B.** Model estimation based on the *Diploastrea* sp. coral from Alaguarda et al. (2022). **C.** Model FL estimation based on the *Porites* sp. coral developed in this study. **D.** Multi coral model estimation based on SEM images of both corals

Finally, a last experience was performed to compare all CNN between each other, the CNN model *Diploastrea* sp. from Alaguarda et al. (2022), the CNN model trained with the FL function on *Porites* sp. and finally the CNN model trained with the DL function on both corals

(Fig.11). Estimations for all CNN were performed on 100 randomly chosen new SEM images for each coral. This new dataset of images was processed by each “raw model” and each “corrected model” (with Eq. 13 and 14). The dataset constituted from SEM images of the coral *Diploastrea* sp. (n=100) was processed by the CNN “raw model” *Diploastrea* sp., then by the CNN “raw model” from the *Porites* sp. trained with the FL function developed in this study and finally by the “raw multi coral model” (Fig.11A). The dataset was also processed with the CNN “bias corrected model” *Diploastrea* sp., the CNN “bias corrected model” *Porites* sp. trained with the FL function developed in this study and finally the “corrected multi coral model” (Eq. 13 and 14; Fig.11B). Spearman's correlations were realized between the estimations of the CNN *Diploastrea* sp. and the estimations from the CNN *Porites* sp. and the CNN of the multi coral model. For the correlations between the “raw CNN *Diploastrea* sp.” and the “raw CNN *Porites* sp.”, we obtained a correlation of 0.96 ($p < 0.001$). For the correlations between the “raw CNN *Diploastrea* sp.” and the “raw CNN multi coral”, we obtained a correlation of 0.99 ($p < 0.001$). Correlations with bias corrected models did not change significantly. Then, the dataset constituted from SEM images of the coral *Porites* sp. (n=100) was processed by the CNN “raw model” *Porites* sp., then by the CNN “raw model” from the *Diploastrea* sp. trained with the FL function developed in this study and finally by the “raw multi coral model” (Fig.11C). The dataset was also processed with the CNN “bias corrected model” *Diploastrea* sp., the CNN “bias corrected model” *Porites* sp. trained with the FL function developed in this study and finally the “corrected multi coral model” (Eq. 13 and 14; Fig.11D). Spearman's correlations were realized between the estimations of the CNN *Porites* sp. and the estimations from the CNN *Diploastrea* sp. and the CNN of the multi coral model. For the correlations between the “raw CNN *Porites* sp.” and the “raw CNN *Diploastrea* sp.”, we obtained a correlation of 0.86 ($p < 0.001$). For the correlations between the “raw CNN *Porites*

sp.” and the “raw CNN multi coral., we obtained a correlation of 0.97 ($p < 0.001$). Correlations with bias corrected models did not change significantly.

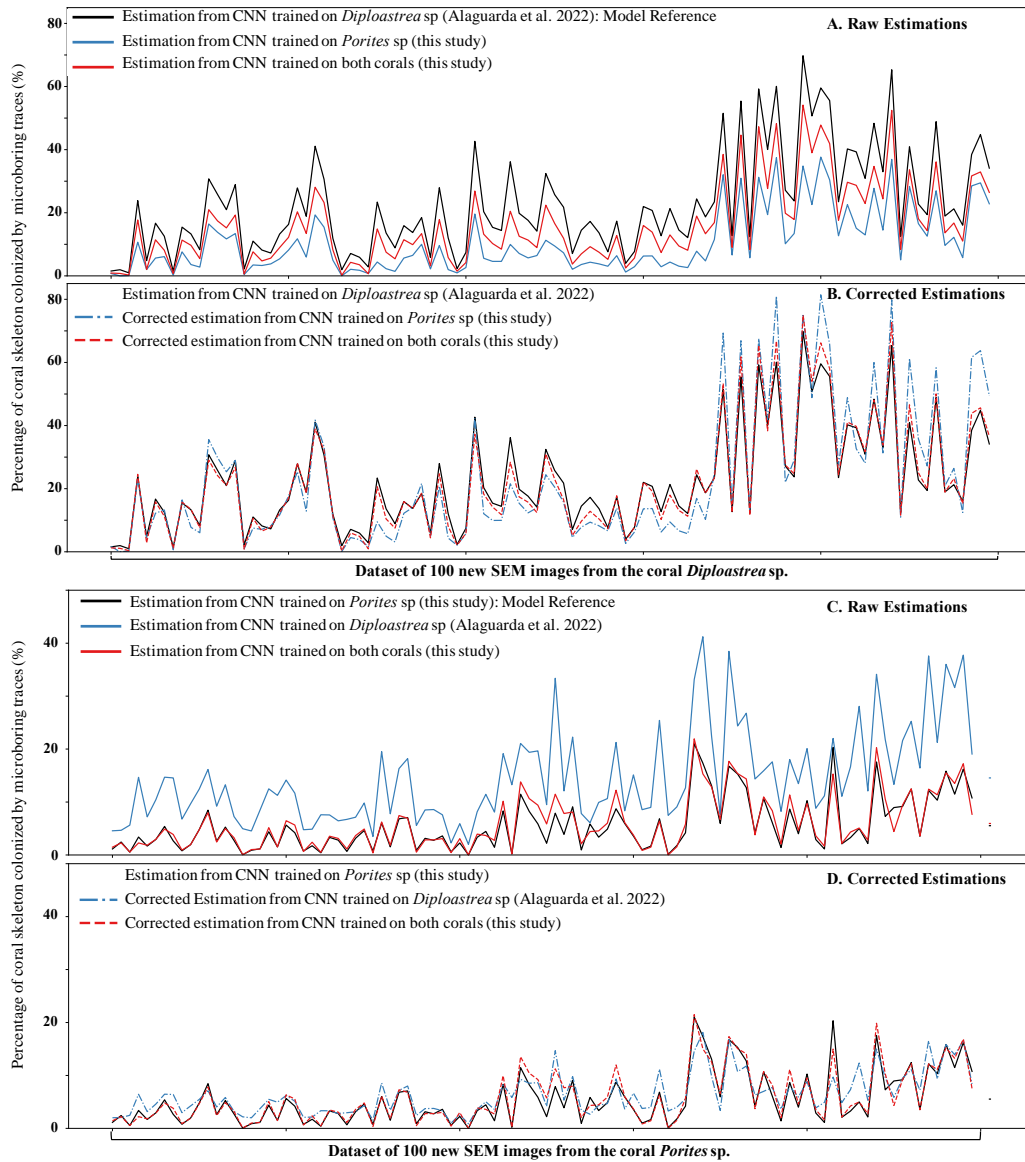


Figure 11 : Comparison of models predictions based on 100 new SEM images of each massive coral *Diploastrea* and *Porites* sp. **A.** Raw estimations for each model on 100 SEM images of the coral *Diploastrea* sp. The black line is the reference model and represents the estimation from the model of the coral *Diploastrea* sp. developed by Alaguarda et al. (2022). The blue line represents the estimation from the model of the coral *Porites* sp. trained with the Focal loss function developed in this study. The red line represent the

multi coral model trained with the Dice loss function on SEM images from both *Diploastrea* and *Porites* sp.

B. Corrected estimations for each model based on the estimated reference from the model of the coral *Diploastrea* sp. (specific model). Same legend for the dotted line. **C.** Raw estimations for each model on 100 SEM images of the coral *Porites* sp. The black line is the reference model and represents the estimation from the model of the coral *Porites* sp. trained with the Focal loss function developed in this study. The blue line represents the estimation from the model of the coral *Diploastrea* sp. developed by Alaguarda et al. (2022). The red line represent the multi coral model trained with the Dice loss function on SEM images from both *Diploastrea* and *Porites* sp. **D.** Corrected estimations for each model based on the estimated reference from the model of the coral *Porites* sp. (specific model). Same legend for the dotted line.

Discussion

1) Machine Learning and microboring assemblage in massive corals

To this date, the ML application represents the fastest method than any other known quantitative method for analyzing microboring filaments/traces (ichnotaxa). Manual processing of one SEM image can take 3 to 5 hours to properly delimit the contour of the different microboring traces, depending on the assemblage of the traces (patchy or not), making their identification even more difficult for human-eye identification. Alaguarda et al. (2022) and the present study manually labeled 142 SEM images representing more than six months of analysis. In comparison, analyzing the same amount of SEM images with the ML approach took only a few minutes and could significantly enable the number of samples that can be processed. With the ML application, we can now provide a continuous and accurate estimation of the coral surface colonized by the different microboring traces (i.e., communities). Alaguarda et al. (2022) investigated two different classes of traces based on their diameter with ML, while three classes were identified. A maximum of two classes identified is not representative of the overall diversity of microboring communities that colonize living coral skeletons (Lukas, 1973; Le Campion-Alsumard et al., 1995; Tribollet, 2008; Tribollet et Golubic, 2011), but still provide first indications of the type of communities present within the coral skeleton. The first machine-learning application developed by Alaguarda et al. (2022) allowed identifying microboring

traces in the massive coral *Diploastrea* sp. with an accuracy of 93% in a few hours. This model was initially trained with a weighted cross-entropy loss function to tackle the unbalanced dataset problem firstly encountered in the SEM images of *Diploastrea* sp. In the present study, we first applied this model to another massive coral, *Porites* sp., to test whether identifying microboring traces in a different coral would be accurate. When applying the model *Diploastrea* sp. to the collection of SEM images from *Porites* sp., the overall accuracy decreased from 93% to 88%. However, more significant decreases in the precision, recall, and F1-score were observed when focusing on the microboring traces class. Applying the model *Diploastrea* sp. to the coral *Porites* sp. has highlighted two potential disadvantages. Firstly, as observed previously by Alaguarda et al. (2022), microboring traces estimated by the model appear thicker than usual (Fig. 8C), leading to potential overestimation of the actual surface of the coral skeleton occupied by the different microboring traces. Nonetheless, such overestimations can be corrected (Eq. 13 and 14). Secondly, the model *Diploastrea* sp. struggled with identifying some coral skeleton pixels, often misclassified as resin pixels (Fig. 8C), leading to an underestimation of the actual surface of the coral skeleton in the image. In return, it accentuates the overestimation of the coral surface occupied by microboring traces because less proportion of coral skeleton is present in the images. Overall, the level of accuracy when applying directly the *Diploastrea* sp. model to *Porites* SEM images is still largely acceptable and depends on the objectives of the practitioner behind. If one overview is to have a general trend of the variability of the abundance of microboring communities over time, applying directly the *Diploastrea* sp. model would directly work and provide enough precision to this objective. . Nonetheless, if one objective is to obtain precise measurement of such variability, a more suited model that *Diploastrea* sp. will be needed.

2) What can explain differences between CNN of both massive corals ?

Massive corals such as *Diploastrea* sp. and *Porites* sp. which are important reef framebuilders and are spread across the Indo-Pacific Ocean, are slow growing corals. *Diploastrea* sp. presents an annual growth rate of a few mm while *Porites* sp grows at an average rate of 1 cm per year (Watanabe et al., 2003; Bagnato et al., 2004; Lough et al. 2008; Cantin et Lough et al., 2014).

One potential reason for such differences in the model's predictions might be the skeletal architecture that differs between both massive corals (Veron, 2000). *Porites* sp. corals present a less dense skeletal structure than *Diploastrea* sp. corals, are less porous, and present thin polyps and corallites (Watanabe et al., 2003; Bagnato et al., 2004). Corallites in *Porites* sp. have a typical diameter comprising between 0.8 to 2 mm depending on the species (Veron, 1986; Darke and Barnes, 1993), while corallites in *Diploastrea* sp. are typically between 7.1 and 9.3 mm in diameter (Todd et al., 2004; Budd et al., 2011). *Diploastrea* sp. corallites are therefore 4 to 5 times larger than *Porites* sp. (Todd et al., 2004), which affect the coral skeleton's capacity to scatter light (Enriquez et al., 2005, 2017) and can influence microboring communities which are generally dominated by phototrophs such as the chlorophyte *Ostreobium* sp (Tribollet 2008; Fordyce et al. 2021; Galindo-Martinez, 2022). Differences in the skeletal architecture of both massive corals might translate into differences regarding the proportion of the classes (e.g., coral skeleton class) within the different SEM images of *Diploastrea* and *Porites* sp. The obtention of the different SEM images was taken under the same conditions and with the same strategy for both corals. Images were the same size (e.g., 1024x768), taken at the same magnification (x150), limiting biases attributing to the image SEM strategy. Nonetheless, biases might have been introduced when preparing the coral samples before observations. The quality of resin casts of coral samples and time exposure to the acid dissolution of the carbonate skeleton might influence the level of contrast and luminosity for observation and can lead to low-quality SEM images (Wisshak, 2012; Salamon et al., 2019). These steps can make the identification of microboring traces difficult for the human eye observer but also for the CNN. Apart from protocol biases and differences in corallites structure, within the same SEM image, the cover of the coral skeleton (i.e., its proportion) is different from one coral to another. Such differences modify the unbalance between the classes of both corals. They might need readjustments when training models to identify the different classes better, underlining why predictions with the model trained on *Diploastrea* sp. decrease when applied to the massive coral skeleton *Porites* sp. Differences in skeletal architecture might also explain potential differences in the level of infestation of microboring communities in living corals (Fordyce et al., 2021). In return, it could increase CNN's difficulties in identifying microboring traces from

one coral to another. For instance, assemblages in patches of microboring traces observed in the images from the *Porites* sp. can be a real problem for the CNN (i.e., the model *Diploastrea* sp.) for delimiting the shape of the different traces and often lead to overestimations of the actual coral surface occupied (Fig.8C).

3) Exportation of the technique: Microboring estimations in other massive corals ?

As explained earlier, if one objective is to rapidly analyze different massive coral cores with a global accuracy of more than 80%, applying the *Diploastrea* sp. model fulfil this task. The value of the coral surface occupied by microboring traces predicted by the CNN would be biased but can be corrected if the objective is only to compare general trends from one core to another. Therefore, there might be no need to train a new and more specific model for identifying microboring traces in a different massive coral genus. Based on the predictions from the model *Diploastrea* sp. on a new collection of SEM images belonging to a different massive coral, the choice was to develop a new model exclusively trained on a set of manually labeled SEM images from *Porites* sp. corals. The objective was to assess if its predictions would be better than the model *Diploastrea* sp. Additionally, compared to the model *Diploastrea* sp. developed by Alaguarda et al. (2022)., it was performed to tackle the unbalanced dataset problem better and reduce the overestimations observed with the model *Diploastrea* sp. trained with the WCE loss function. An interesting result is that either on *Diploastrea* sp. or *Porites* sp., and when training the model with the WCE loss function, both CNN displays an accuracy of more than 93% when identifying the different classes. This finding supports that the WCE can represent a suitable loss function for an unbalanced dataset problem, even if overestimations are observed. On the other hand, the investigations on the choice of a suitable loss function have shown that general performances of the model for the identification of the different classes can be enhanced and significantly reduce the overestimations (e.g., on the microboring traces class; Fig. 5 and 6). The accuracy of both CNN models (i.e., *Diploastrea* and *Porites*) represented more than 90% of accuracy, corresponding to a high level of confidence within the model to analyze the different classes within the images. The optimal accuracy for training is around 85% (Wilson et al., 2019), as an accuracy of 100% would correspond to overfitting and

only adapted to the training set (Goodfellow et al., 2016). One promising investigation was the multi coral model that presented more than 94.2% accuracy. For instance, its predictions were close to the ones from the specific *Porites* sp., CNN model when classifying microboring traces from the SEM dataset of *Porites* corals. The same conclusion was observed with the *Diploastrea* sp. CNN model (Fig.10 and 11). These findings show that the multi coral model trained on SEM images of both corals can identify similarly the different classes in either of the massive corals (Fig.12). Such multi coral model could be now used to assess colonization of microboring traces in massive corals and essentially on *Diploastrea* and *Porites* as training occurred on those corals. Therefore, one suggestion for further investigations would be to apply this multi coral model to the set of images of the coral *Diploastrea* sp. that were analyzed by Alaguarda et al. (2022) and see if the variability they found would be the same or different using the new multi coral model. Additionally, another suggestion would be to increase the number of classes the model can recognize, but it will require manual labeling of these different classes and additional training for the model. Successful estimations of the method require careful consideration and highly rely on specialized, diverse, and annotated data to build an appropriate set of images the model will train on. Nevertheless, developing and training CNN models requires much processing time and power calculations. The dataset constitution step does not need any power calculations. Nevertheless, one major procedure with direct and elevated costs concerns sampling coral cores and manually processing the SEM images. Taking more than 3000 SEM images represents hundreds of hours and weeks of analysis which is very time-consuming but essential, and SEM sessions also represent high economic costs (100€/day/session). Future works with automatized SEM would greatly help in accessing long images dataset. Regarding the technical energy cost for running the CNN, using a standard personal laptop to run the CNN model could be tricky, even impossible, as they often present low random-access memory (RAM) and computing limitations. Thus, power from GPU servers is highly recommended as training is very fast and gathers high-power calculations.

Comments and Recommendations

In this study, several loss functions has been tested. However, a practitioner interested to apply the method could only focus on WCE, DL or FL. Thanks to the present study and the model developed by Alaguarda et al. (2022), two robust and specific CNN models applied on SEM database for each type of massive coral, are now fully developed and operational at high levels of accuracy when identifying microboring traces colonizing coral skeletons. These two CNN models that worked with more than 93% accuracy for the coral *Diploastrea* sp. and 95% for the coral *Porites* sp. for identifying the coral surface occupied by microboring traces. On another aspect and very interestingly, the multi coral model based on SEM images of both massive corals gather the ultimate “goal” with outstanding predictions either considering one of the coral genus. Indeed, this model could now be used to identify accurately microboring traces colonizing the skeleton of those two massive coral, even if they present differences in skeletal architecture influencing the distribution and colonization of these communities. Finally, in order to estimate the coral surface colonized by microboring traces in other corals, if the SEM images acquisition follows the one described in Alaguarda and al. (2022), the quantification of microboring traces can be summarized as the following procedure:

- 1) Apply our model directly and assess the performance of limited samples of manually labeled images. If the abundance estimation is highly biased:
- 2) Correct for a potential bias (no need to retrain) following Eq. 13 and 14. There will be a need of additional manually labeled images. After 2) the variability can be satisfactory (e.g. 0.81 when applying on *Porites* using the model trained on *Diploastrea*), or not accurate enough and will need to:
- 3) Re-train the model on a manually labeled dataset using the FL or DL function. After 3), we assume that the estimations are likely to be accurate enough, but in the case of the outputs’ estimations are not satisfactory, it is possible to:

- 4) Re-train the model and tune the different hyperparameters (other loss functions, number of iterations, learning rate).

Overall, this study aimed to confirm and provide the effectiveness of the machine-learning approach developed by Alaguarda et al. (2022) in identifying accurately microboring traces. It also confirmed that through investigations and optimization regarding the choice of a suitable loss function, the performance of a CNN model can significantly be improved, making the image segmentation task easier and tackle better unbalanced dataset issues. To further push this method and extend its utilization, additional coral cores should be studied to better understand the possible implications of microborers abundance in living corals such as *Porites* or *Diploastrea*. In the future, this approach could also be improved to identify more classes of microboring communities and give a better representation of the diversity of microboring communities colonizing living corals. It could also include different coral morphotypes such as other massive corals but also branching corals, in order to study the variability of the abundance of these communities in the latter. It could also be applied to other geographical areas, in order to compare whether this decline and/or shift in communities that Alaguarda et al. (2022) observed in Mayotte was limited to a regional phenomenon or can be generalized to the global scale.

References

- Abraham, Nabila, and Naimul Mefraz Khan. 2018. "A Novel Focal Tversky Loss Function with Improved Attention U-Net for Lesion Segmentation," October. <http://arxiv.org/abs/1810.07842>.
- Alaguarda, D., J. Brajard, G. Coulibaly, M. Canesi, E. Douville, F. Le Cornec, C. Lelabousse, and A. Tribollet. 2022. "54 Years of Microboring Community History Explored by Machine Learning in a Massive Coral from Mayotte (Indian Ocean)." *Frontiers in Marine Science* 9 (December). <https://doi.org/10.3389/fmars.2022.899398>.

- Bak, RPM, and RWPM Laane. 1987. "Annual Black Bands in Skeletons of Reef Corals (Scleractinia)." *Marine Ecology Progress Series* 38: 169–75.
<https://doi.org/10.3354/meps038169>.
- Campion Alsumard, T. Le, S. Golubic, and P. Hutchings. 1995. "Microbial Endoliths in Skeletons of Live and Dead Corals: Porites Lobata (Moorea, French Polynesia)." *Marine Ecology Progress Series* 117 (1–3): 149–58. <https://doi.org/10.3354/meps117149>.
- Campo, Javier del, Jean-François Pombert, Jan Šlapeta, Anthony Larkum, and Patrick J Keeling. 2017. "The 'Other' Coral Symbiont: *Ostreobium* Diversity and Distribution." *The ISME Journal* 11 (1): 296–99. <https://doi.org/10.1038/ismej.2016.101>.
- Carreiro-Silva, M., T. R. McClanahan, and W. E. Kiene. 2005. "The Role of Inorganic Nutrients and Herbivory in Controlling Microbioerosion of Carbonate Substratum." *Coral Reefs* 24 (2): 214–21. <https://doi.org/10.1007/s00338-004-0445-3>.
- . 2009. "Effects of Inorganic Nutrients and Organic Matter on Microbial Euendolithic Community Composition and Microbioerosion Rates." *Marine Ecology Progress Series* 392: 1–15. <https://doi.org/10.3354/meps08251>.
- Chazottes, V., T. Le Campion-Alsumard, and M. Peyrot-Clausade. 1995. "Bioerosion Rates on Coral Reefs: Interactions between Macroborers, Microborers and Grazers (Moorea, French Polynesia)." *Palaeogeography, Palaeoclimatology, Palaeoecology* 113 (2–4): 189–98. [https://doi.org/10.1016/0031-0182\(95\)00043-L](https://doi.org/10.1016/0031-0182(95)00043-L).
- Darke, W. M., and D. J. Barnes. 1993. "Growth Trajectories of Corallites and Ages of Polyps in Massive Colonies of Reef-Building Corals of the Genus *Porites*." *Marine Biology* 117 (2): 321–26. <https://doi.org/10.1007/BF00345677>.
- Eyre, Bradley D., Tyler Cyronak, Patrick Drupp, Eric Heinen De Carlo, Julian P. Sachs, and Andreas J. Andersson. 2018. "Coral Reefs Will Transition to Net Dissolving before End of Century." *Science* 359 (6378): 908–11. <https://doi.org/10.1126/science.aao1118>.

- Golubic, S., Brent, G., LeCampion, T. 1970. "Scanning Electron Microscopy of Endolithic Algae and Fungi Using a Multipurpose Casting-Embedding Technique." *Lethaia* 3 (2): 203–9. <https://doi.org/10.1111/j.1502-3931.1970.tb01858.x>.
- Golubic S; Friedmann I.E; Schneider J. 1981. "The Lithobiontic Ecological Niche, with Special Reference to Microorganisms." *Journal of Sedimentary Research* Vol. 51 (2): 475–78. <https://doi.org/10.1306/212F7CB6-2B24-11D7-8648000102C1865D>.
- Golubic, Stjepko, Gudrun Radtke, and Therese Le Campion-Alsumard. 2005. "Endolithic Fungi in Marine Ecosystems." *Trends in Microbiology* 13 (5): 229–35. <https://doi.org/10.1016/j.tim.2005.03.007>.
- Goodfellow, Ian, Yoshua Bengio, and Courville Aaron. 2016. *Deep Learning*. MIT Press. the MIT Press, Cambridge, MA, USA.
- Hughes, Terry P., Kristen D. Anderson, Sean R. Connolly, Scott F. Heron, James T. Kerry, Janice M. Lough, Andrew H. Baird, et al. 2018. "Spatial and Temporal Patterns of Mass Bleaching of Corals in the Anthropocene." *Science* 359 (6371): 80–83. <https://doi.org/10.1126/science.aan8048>.
- Hughes, Terry P., James T. Kerry, Mariana Álvarez-Noriega, Jorge G. Álvarez-Romero, Kristen D. Anderson, Andrew H. Baird, Russell C. Babcock, et al. 2017. "Global Warming and Recurrent Mass Bleaching of Corals." *Nature* 543 (7645): 373–77. <https://doi.org/10.1038/nature21707>.
- Ioffe, Sergey, and Christian Szegedy. 2015. "Batch Normalization: Accelerating Deep Network Training by Reducing Internal Covariate Shift." <https://doi.org/10.48550/arXiv.1502.03167>.
- Johnson, Justin M., and Taghi M. Khoshgoftaar. 2019. "Survey on Deep Learning with Class Imbalance." *Journal of Big Data* 6 (1): 27. <https://doi.org/10.1186/s40537-019-0192-5>.
- Kervadec, Hoel, Jihene Bouchtiba, Christian Desrosiers, Eric Granger, Jose Dolz, and Ismail

- Ben Ayed. 2020. "Boundary Loss for Highly Unbalanced Segmentation," December. <https://doi.org/10.1016/j.media.2020.101851>.
- Kingma, Diederik, Danilo Rezende, Shakir Mohamed, and Max Welling. 2014. "Semi-Supervised Learning with Deep Generative Models." *Advances in Neural Information Processing Systems*.
- Krizhevsky, Alex, Ilya Sutskever, and Geoffrey E. Hinton. 2017. "ImageNet Classification with Deep Convolutional Neural Networks." *Communications of the ACM* 60 (6): 84–90. <https://doi.org/10.1145/3065386>.
- Lemaitre, Guillaume, Fernando Nogueira, and Christos K. Aridas. 2016. "Unbalanced-Learn: A Python Toolbox to Tackle the Curse of Unbalanced Datasets in Machine Learning," September. <http://arxiv.org/abs/1609.06570>.
- Lin, Tsung-Yi, Priya Goyal, Ross Girshick, Kaiming He, and Piotr Dollár. 2018. "Focal Loss for Dense Object Detection," August. <http://arxiv.org/abs/1708.02002>.
- Lukas, Karen J. 1973. "Taxonomy and Ecology of the Endolithic Microflora of Reef Corals, with a Review of the Literature on Endolithic Microphytes." University Rhode Island.
- Marcelino, Vanessa Rossetto, and Heroen Verbruggen. 2016. "Multi-Marker Metabarcoding of Coral Skeletons Reveals a Rich Microbiome and Diverse Evolutionary Origins of Endolithic Algae." *Scientific Reports* 6 (1): 31508. <https://doi.org/10.1038/srep31508>.
- Milletari, Fausto, Seyed-Ahmad Ahmadi, Christine Kroll, Annika Plate, Verena Rozanski, Juliana Maiostre, Johannes Levin, et al. 2017. "Hough-CNN: Deep Learning for Segmentation of Deep Brain Regions in MRI and Ultrasound." *Computer Vision and Image Understanding* 164 (November): 92–102. <https://doi.org/10.1016/j.cviu.2017.04.002>.
- Milletari, Fausto, Nassir Navab, and Seyed-Ahmad Ahmadi. 2016. "V-Net: Fully Convolutional Neural Networks for Volumetric Medical Image Segmentation," June.

<http://arxiv.org/abs/1606.04797>.

- Perry, Chris T., Robert S. Steneck, Gary N. Murphy, Paul S. Kench, Evan N. Edinger, Scott G. Smithers, and Peter J. Mumby. 2014. "Regional-scale Dominance of Non-framework Building Corals on Caribbean Reefs Affects Carbonate Production and Future Reef Growth." *Global Change Biology* 21 (3): 1153–64. <https://doi.org/10.1111/gcb.12792>.
- Prati, R, G. E Gustavo, and M. C Monard. 2009. "Data Mining with Unbalanced Class Distributions: Concepts and Methods." *Indian International Conference Artificial Intelligence*, 359–76.
- Priess, K., T. Le Campion-Alsumard, B. A. Thomassin, S. Golubic, and F. Gadel. 2000. "Fungi in Corals: Black Bands and Density-Banding of *Porites Lutea* and *P. Lobata* Skeleton." *Marine Biology* 136 (1): 19–27. <https://doi.org/10.1007/s002270050003>.
- Romanuke, Vadim. 2017. "Appropriate Number and Allocation of RELUS in Convolutional Neural Networks." *Research Bulletin of the National Technical University of Ukraine "Kyiv Politechnic Institute,"* no. 1 (March): 69–78. <https://doi.org/10.20535/1810-0546.2017.1.88156>.
- Ronneberger, Olaf, Philipp Fischer, and Thomas Brox. 2015. "U-Net: Convolutional Networks for Biomedical Image Segmentation." In *Medical Image Computing and Computer-Assisted Intervention*, edited by Frangi A Navab N, Hornegger J, Wells W, Vol. 9351:234–41. https://doi.org/10.1007/978-3-319-24574-4_28.
- Sadler, James, Gregory E. Webb, Luke D. Nothdurft, and Belinda Dechnik. 2014. "Geochemistry-Based Coral Palaeoclimate Studies and the Potential of 'Non-Traditional' (Non-Massive *Porites*) Corals: Recent Developments and Future Progression." *Earth-Science Reviews* 139 (December): 291–316. <https://doi.org/10.1016/j.earscirev.2014.10.002>.
- Salamon, Klaudiusz, Bogusław Kołodziej, and Vadim L. Stefanskyi. 2019. "Simple Methods

- for Detection of Microborings Produced by Coral-Associated Microendoliths.” *Facies* 65 (2): 1–13. <https://doi.org/10.1007/s10347-019-0560-9>.
- Salehi, Seyed Sadegh Mohseni, Deniz Erdogmus, and Ali Gholipour. 2017. “Tversky Loss Function for Image Segmentation Using 3D Fully Convolutional Deep Networks,” June. <http://arxiv.org/abs/1706.05721>.
- Salvo, L. H. Di. 1969. “Isolation of Bacteria from the Corallum of *Porites Lobata* (Vaughn) and Its Possible Significance.” *American Zoologist* 9 (3): 735–40. <https://doi.org/10.1093/icb/9.3.735>.
- Sammarco, Paul W., Michael J. Risk, and Christopher Rose. 1987. “Effects of Grazing and Damsel Fish Territoriality on Internal Bioerosion of Dead Corals : Indirect Effects.” *Journal of Experimental Marine Biology and Ecology* 112 (2): 185–99. [https://doi.org/10.1016/0022-0981\(87\)90116-X](https://doi.org/10.1016/0022-0981(87)90116-X).
- Schönberg, Christine H.L., James K.H. Fang, Marina Carreiro-Silva, Aline Tribollet, and Max Wisshak. 2017. “Bioerosion: The Other Ocean Acidification Problem.” *ICES Journal of Marine Science* 74 (4): 895–925. <https://doi.org/10.1093/icesjms/fsw254>.
- Spalding M.D, and Brown B.E. 2015. “Warm-Water Coral Reefs and Climate Change.” *Science* 350 (6262): 769–77.
- Todd, PA, RJ Ladle, NJI Lewin-Koh, and LM Chou. 2004. “Genotype × Environment Interactions in Transplanted Clones of the Massive Corals *Favia Speciosa* and *Diploastrea Heliopora*.” *Marine Ecology Progress Series* 271: 167–82. <https://doi.org/10.3354/meps271167>.
- Tribollet, A., A. Chauvin, and P. Cuet. 2019. “Carbonate Dissolution by Reef Microbial Borers: A Biogeological Process Producing Alkalinity under Different PCO₂ Conditions.” *Facies* 65 (2): 1–10. <https://doi.org/10.1007/s10347-018-0548-x>.
- Tribollet, Aline. 2008. “The Boring Microflora in Modern Coral Reef Ecosystems: A Review

- of Its Roles.” *Current Developments in Bioerosion*, no. 1974: 397–413.
<https://doi.org/10.1007/978-3-540-77598-0>.
- Tversky, Amos. 1977. “Features of Similarity.” *Psychological Review* 84 (4): 327–52.
<https://doi.org/10.1037/0033-295X.84.4.327>.
- Veron, J. E. N. 2000. *Corals of the World*. Townsville, Australia: Australian Institute of Marine Science.
- Wong, Ken C. L., Tanveer Syeda-Mahmood, and Mehdi Moradi. 2018. “Building Medical Image Classifiers with Very Limited Data Using Segmentation Networks,” August.
<https://doi.org/10.1016/j.media.2018.07.010>.
- Wu, Henry C., Delphine Dissard, Eric Douville, Dominique Blamart, Louise Bordier, Aline Tribollet, Florence Le Cornec, Edwige Pons-Branchu, Arnaud Dapoigny, and Claire E. Lazareth. 2018. “Surface Ocean PH Variations since 1689 CE and Recent Ocean Acidification in the Tropical South Pacific.” *Nature Communications* 9 (1).
<https://doi.org/10.1038/s41467-018-04922-1>.
- Yamaguchi, K., K Sakamoto, T Akabane, and Y Fujimoto. 1990. “A Neural Network for Speaker-Independent Isolated Word Recognition.” *Computer Science*.
- Zhang, Yue, Shijie Liu, Chunlai Li, and Jianyu Wang. 2021. “Rethinking the Dice Loss for Deep Learning Lesion Segmentation in Medical Images.” *Journal of Shanghai Jiaotong University (Science)* 26 (1): 93–102. <https://doi.org/10.1007/s12204-021-2264-x>.

Authors Contribution Statement

AT designed, coordinated, and funded the project. AT collected the coral core in Mayotte and la Reunion and trained DA at the methodologies to study microboring communities. DA, JB, and RL developed the machine learning approach. DA obtained and analyzed the SEM images,

managed the statistical analysis. DA, AT, RL and JB interpreted the results and also contributed to the writing of the article.

Data Availability Statement

The original data are presented here. Any further inquiries should be sent to the corresponding authors.

Acknowledgements:

We want to thank the following people for their help and assistance: Michel Guillemard, head of the company TSMOI (Reunion Island), for helping us collect the coral core in Mayotte in October 2018, Pascale Cuet, Joanna Kolasinski, and Lionel Bigot as part of the LABEX Corail and the grant “MARG-1” project for helping us collecting the coral core in la Reunion in 2015, Sandrine Caquineau (IRD-France Nord) for SEM training and collection and Thierry Pilorge (IRD-France Nord) for his help cutting the coral core and preparing samples for the observation of resin casts of microborings.

What Are the Effects of Biotic and Abiotic Factors on the Composition and Abundance of Microbioeroding Communities in the massive coral *Diploastrea* sp over the last 54 years?

Contents

4.1	Preface	145
4.2	Variability of the Abundance, Shift of Microbioeroding Community Composition and Green Bands Investigation in <i>Diploastrea</i> sp.	146
4.3	Effects of pH on the Abundance and Composition of Microbioeroding Communities in <i>Diploastrea</i> sp.	168
4.3.1	Introduction	168
4.3.2	Methodologies	171
4.3.3	Results	172
4.3.3.1	Evolution of the internal pH of <i>Diploastrea</i> over 54 years	172
4.3.3.2	Internal pH and Abiotic Variables	173
4.3.3.3	Internal pH and Biotic Variables	174
4.3.4	Discussion	176

4.3.4.1	Comparison of Instrumental and Paleo-Proxy pH Reconstructions	176
4.3.4.2	<i>Diploastrea</i> sp. Internal pH : A Particular Signal ? .	177
4.3.4.3	Internal pH and the Evolution of the Abundance of Microbioeroding Traces	180
4.4	Conclusion	182

4.1 Preface

In recent years there has been a rising interest in better understanding the diversity and the functional roles of bioeroding microflora (cyanobacteria, algae, fungi) in reef carbonate budget and scleractinian corals health (Schönberg et al., 2017; Tribollet et al., 2019; Ricci et al., 2019). Microbioeroding communities have been known to be part of the coral holobiont microbiome since the early 20th century and be potentially an important ecto-symbiont (e.g., Odum and Odum, 1955), and have only recently attracted considerable attention. Nonetheless, the species composition, distribution, and abundance of microbioeroding communities in living corals remain poorly known. Most studies focused only on communities within the first few centimeters below coral tissues. Thus, very little is known about microborers' abundance variability over the life course of their coral host, especially in massive long-lived corals. Massive corals have a critical interest in paleo-climatology, offer long-term climate reconstructions, and here the possibility to study microborers' abundance variability over the long term for the first time. In this chapter, I addressed different questions by studying a remarkably well-preserved coral core of a slow-growing colony of *Diploastrea* sp. from Mayotte (WIO), presenting several green bands and covering the last 54 years to:

- 1) Identify the main types of microborers and if traces of assemblage composition shifts could be observed over time.
- 2) Determine the variability of the abundance of microborers over the last five decades.
- 3) Identify the main abiotic and/or biotic factors that could influence such variability.
- 4) Better understanding of the relationship between microborer abundance and green bands' presence.

The innovative approach based on ML presented in the **Chapter 3** was used to reach those goals. For this study, the ML model *Diploastrea* sp. was coupled to a weighted cross-entropy loss function and represented an accuracy of 93%. This approach allowed the identification of the different main types of microbioeroding traces, an accurate, continuous, and rapid quantification of the area of the coral skeleton they colonized along the massive coral core of *Diploastrea* sp.

4.2 Variability of the Abundance, Shift of Microbioeroding Community Composition and Green Bands Investigation in *Diploastrea* sp.

Article published in 2022

in the Journal: *Frontiers in Marine Sciences*

How to cite:

Alaguarda D, Brajard J, Coulibaly G, Canesi M, Douville E, Le Cornec F, Lelabousse C and Tribollet A. (2022). 54 years of microboring community history explored by machine learning in a massive coral from Mayotte (Indian Ocean). *Frontiers Marine Sciences* 9:899398. DOI: <https://doi.org/10.3389/fmars.2022.899398>



OPEN ACCESS

EDITED BY
Ana Santos,
University of Oviedo, Spain

REVIEWED BY
Max Wisshak,
Senckenberg am Meer Wilhelmshaven,
Germany
Christine Schoenberg,
National Sun Yat-sen University,
Taiwan

*CORRESPONDENCE
D. Alaguarda
diego.alaguarda@locean.ipsl.fr
A. Tribollet
aline.tribollet@ird.fr

SPECIALTY SECTION
This article was submitted to
Marine Biology,
a section of the journal
Frontiers in Marine Science

RECEIVED 18 March 2022
ACCEPTED 08 November 2022
PUBLISHED 22 December 2022

CITATION
Alaguarda D, Brajard J, Coulibaly G,
Canesi M, Douville E, Le Cornec F,
Lelabousse C and Tribollet A (2022) 54
years of microboring community
history explored by machine learning
in a massive coral from Mayotte
(Indian Ocean).
Front. Mar. Sci. 9:899398.
doi: 10.3389/fmars.2022.899398

COPYRIGHT
© 2022 Alaguarda, Brajard, Coulibaly,
Canesi, Douville, Le Cornec, Lelabousse
and Tribollet. This is an open-access
article distributed under the terms of
the [Creative Commons Attribution
License \(CC BY\)](https://creativecommons.org/licenses/by/4.0/). The use, distribution
or reproduction in other forums is
permitted, provided the original
author(s) and the copyright owner(s)
are credited and that the original
publication in this journal is cited, in
accordance with accepted academic
practice. No use, distribution or
reproduction is permitted which does
not comply with these terms.

54 years of microboring community history explored by machine learning in a massive coral from Mayotte (Indian Ocean)

D. Alaguarda^{1*}, J. Brajard², G. Coulibaly³, M. Canesi³,
E. Douville³, F. Le Cornec⁴, C. Lelabousse⁵ and A. Tribollet^{4*}

¹Sorbonne Université (CNRS-IRD-MNHN), Laboratoire LOCEAN-IPSL, Paris Cedex, France, ²Nansen Environmental and Remote Sensing Center, Bergen, Norway, ³CEA (CNRS-UVSQ), Laboratoire LSCE-IPSL, Université Paris-Saclay, Gif-sur-Yvette, France, ⁴IRD (Sorbonne Université/UPMC-CNRS-MNHN), Laboratoire LOCEAN-IPSL, Paris Cedex, France, ⁵Parc National Marin de Mayotte, Aéroport de Dzaoudzi, Petite Terre, Mayotte, France

Coral reefs are increasingly in jeopardy due to global changes affecting both reef accretion and bioerosion processes. Bioerosion processes dynamics in dead reef carbonates under various environmental conditions are relatively well understood but only over a short-term limiting projections of coral reef evolution by 2100. It is thus essential to monitor and understand bioerosion processes over the long term. Here we studied the assemblage of traces of microborers in a coral core of a massive *Diploastrea* sp. from Mayotte, allowing us to explore the variability of its specific composition, distribution, and abundance between 1964 and 2018. Observations of microborer traces were realized under a scanning electron microscope (SEM). The area of coral skeleton sections colonized by microborers (a proxy of their abundance) was estimated based on an innovative machine learning approach. This new method with 93% accuracy allowed analyzing rapidly more than a thousand SEM images. Our results showed an important shift in the trace assemblage composition that occurred in 1985, and a loss of 90% of microborer traces over the last five decades. Our data also showed a strong positive correlation between microborer trace abundance and the coral bulk density, this latter being particularly affected by the interannual variation of temperature and cumulative insolation. Although various combined environmental factors certainly had direct and/or indirect effects on microboring species before and after the breakpoint in 1985, we suggest that rising sea surface temperature, rainfall, and the loss of light over time were the main factors driving the observed trace assemblage change and decline in microborer abundance. In addition, the interannual variability of sea surface temperature and instantaneous maximum wind speed appeared to influence greatly the occurrence of green bands. We thus stress the importance to study more coral cores to confirm the decadal trends observed in the *Diploastrea* sp. from Mayotte and to better identify the main factors influencing microboring

communities, as the decrease of their abundance in living massive stress tolerant corals may have important consequences on their resilience.

KEYWORDS

coral growth, microborers abundance, euendolith traces, assemblage shift, green bands, Mayotte, machine learning, global change

1 Introduction

In recent years there has been a rising interest in better understanding the diversity and the functional roles of bioeroding microflora (cyanobacteria, algae, fungi) in reef carbonate budget and scleractinian corals health (Marcelino and Verbruggen, 2016; Del Campo et al., 2017; Schönberg et al., 2017; Tribollet et al., 2019; Ricci et al., 2019). This became particularly an emerging topic since the frequency of periods of thermal stress and marine heat waves has increased, affecting dramatically coral reefs worldwide (Hughes et al., 2018; Wernberg et al., 2021). The last IPCC report (2019) estimated that up to 99% of corals and reefs may disappear with +2°C of global warming before the end of the century if nothing is done to both reduce considerably CO₂ emissions into the atmosphere and local disturbances (see also Perry et al., 2014; Schönberg et al., 2017; Eyre et al., 2018; Tribollet et al., 2019). Nevertheless, to better predict the fate of coral reefs there is still a crucial need to understand the long-term dynamics of reef bioerosion processes, especially that of biogenic dissolution of carbonates by microboring flora as it is one of the main processes of reef dissolution (Schönberg et al., 2017; Tribollet et al., 2019) and the ability of corals to adapt and to be resilient to changes owing to their microbiome (Hughes et al., 2003; Ainsworth et al., 2017; McManus et al., 2021). To date, only a few bioerosion studies focused on the effects of hypersedimentation, eutrophication and ocean acidification and warming on microboring communities colonizing dead carbonate substrates (mostly dead corals) over short periods, i.e. over a few months or years (Carreiro-Silva et al., 2005; Tribollet, 2008a; Tribollet et al., 2009; Reyes-Nivia et al., 2013; Grange et al., 2015; Enochs et al., 2016; Tribollet et al., 2019). Those studies showed that ocean acidification, warming and eutrophication stimulate the growth of phototrophic microborers and therefore increase rates of biogenic dissolution of dead carbonates in short-term (Carreiro-Silva et al., 2005; Carreiro-Silva et al., 2009; Tribollet et al., 2009; Reyes-Nivia et al., 2013; Enochs et al., 2016; Tribollet et al., 2019) while hypersedimentation limits greatly microboring community development due to light limitation (Tribollet, 2008b). As long-term *in situ* experiments are difficult to conduct, an interesting alternative to study the

effects of environmental changes on microboring communities over decades is to study those communities in slow-growing corals. Those latter are indeed known to be good bio-archives recording environmental changes over decades and centuries (Zinke et al., 2008; Montagna et al., 2014; Zinke et al., 2015; Wu et al., 2018; Cuny-Guirriec et al., 2019). While microborer communities have been known to be part of the coral holobiont microbiome since the early 20th century and to be potentially an important ecto-symbiont (e.g. Odum and Odum, 1955), they have only recently attracted considerable attention (see review by Ricci et al., 2019). Within the past few years, several studies have thus investigated the genetic diversity of the endolithic microbiome, and especially that of the dominant euendolith, the chlorophyte *Ostreobium* sp. (Marcelino and Verbruggen, 2016; Sauvage et al., 2016; Yang et al., 2016; Del Campo et al., 2017; Massé et al., 2020) and its possible implications in coral growth, physiology and photoprotection (Sangsawang et al., 2017; Massé et al., 2018; Galindo-Martínez et al., 2022). Conversely, the species composition, distribution and abundance of microboring communities in living corals remain poorly known and most studies focused only on communities located within the first few centimeters below coral tissues of adult colonies (Odum and Odum, 1955; Lukas, 1973; Kühl and Polerecky, 2008; Fordyce et al., 2021; Galindo-Martínez et al., 2022). Massé et al. (2018) were the first to show that microborers colonize branching corals from the substrate of fixation as soon as the primary polyp forms its carbonate basal plate (within 7 days after metamorphosis). Then, microborers which are mainly phototrophic microorganisms dominated by *Ostreobium* sp., keep following the growth of their coral host to maintain their access to light and thus their metabolic activity (Le Campion-Alsumard et al., 1995a; Magnusson et al., 2007; Massé et al., 2018). In branching corals, microboring communities dominated by *Ostreobium* sp. do not form green bands as the host growth is too fast and 'dilute' filaments (Godinot et al., 2012; Massé et al., 2018). In contrast, a more or less intense green band is usually seen just below the coral host tissue layer in slow-growing massive corals (Le Campion-Alsumard et al., 1995a; see for instance Figure 1 in Verbruggen and Tribollet, 2011). Sometimes alternating white and colored bands can be observed in massive corals indicating the past presence of

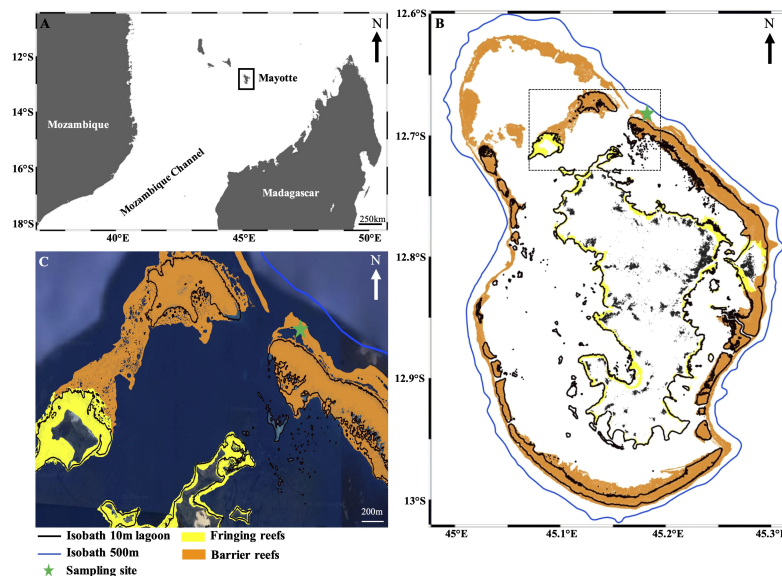


FIGURE 1

Location of the sample site. (A) Mayotte in the Western Indian Ocean (WIO). (B) Reef ecosystems around Mayotte. The blue line and black lines represent the different isobaths around the island. The green star indicates the sampling location in the northeastern part of the lagoon (C) Details of the northeastern part of the lagoon showing the barrier reef near the M'Tsambo pass and the sampling location on the outer slope (green star).

boring microflora (Le Campion-Alsumard et al., 1995a; Le Campion-Alsumard et al., 1995b; Priess et al., 2000; Carilli et al., 2010). But very little is known about microborers' abundance variability over the life course of their coral host, especially in massive long-lived corals. To the best of our knowledge, only Lukas (1973), Le Campion-Alsumard et al. (1995a) and Priess et al. (2000) truly quantified the abundance of microborers in white *versus* green or black bands in living corals and showed a greater abundance of traces, and chlorophyll *b* characteristic of *Ostreobium* sp., in colored bands than in white ones. Priess et al. (2000) suggested that most colored bands observed in massive *Porites* from the Indo-Pacific could be due to a limited coral growth rate occurring at the end of the rainy (summer) season. Carilli et al. (2010) who studied the pattern of alternating white and green bands without quantifying microborers in several massive corals like *Montastrea faveolata* over the last century, suggested that the presence of green bands may be due to microboring phototrophs' blooms during coral paling episodes as they did not find any correlation with coral growth. They also suggested that local-scale forcing factors are likely at play but found no significant relationship between physical parameters such as sea surface temperature and the presence of green bands. Therefore, the origin of the variability of microborers

abundance in massive corals remain to be understood. Here, we studied a very well preserved coral core of a slow-growing colony of *Diploastrea* sp. from Mayotte (Western Indian Ocean) presenting several green bands and covering the last 54 years to: (i) identify the main types of microborers and if shifts in their trace assemblage composition could be observed over time, (ii) better understand the relationship between the abundance of microborers and the presence of green bands, (iii) determine microborers abundance variability over the last five decades, and (iv) identify the main abiotic and/or biotic factors that could influence such variability. To reach those goals, we developed an innovative approach based on machine learning, allowing the identification of the different main types of microborings (microborer traces), the estimation of their relative abundance, and a precise, continuous, and rapid quantification of the area of the coral skeleton they colonized along the core (proxy of their abundance). To determine the possible abiotic and biotic factors influencing the variability of microborers abundance over the last decades, we also measured the main coral skeleton parameters (vertical extension and bulk density) along the core and collected the following environmental data from available databases: Sea Surface Temperature (SST), Sea Surface Temperature Anomalies (SSTA), precipitations, instantaneous maximum

wind speed (instant max wind speed), and the cumulative insolation duration over the last 54 years.

2 Material and methods

2.1 Study site

Mayotte, a french tropical island located in the northern part of the Mozambique Channel (Western Indian Ocean, Figure 1), is dominated by a monsoonal wind system although two seasons can be distinguished: a hot windy and rainy monsoon season from November to April, and a dry season from May to October (Zinke et al., 2008; Jeanson et al., 2014; Vinayachandran et al., 2021). Vinayachandran et al. (2021) showed that Mayotte experiences hot and humid winds stress predominantly from the north to northeast during the austral summer and cool, dry winds from south to southeast winds during the austral winter. Mayotte is also located at the northern part of the vortex zone generated in the Mozambique Channel (Chevalier et al., 2017), and on the northwest extension of the South Equatorial Current (SEC) that branch out northward into the East African Coastal Current (EACC) and southward into the Northeast Madagascar Current (NMC, Schott and McCreary, 2001; Vinayachandran et al., 2021). Historically, Mayotte island is subject to temperatures around 26.4 to 27.6°C in winter and 27.5 to 29°C in summer (Zinke et al., 2008). To determine the possible main abiotic drivers that could influence microborers abundance in the studied coral core, the following environmental parameters were collected: Monthly SST (in °C), SSTA (in °C), precipitation rate (in mm), the maximum instantaneous wind speed (in km·h⁻¹

¹) and the cumulative insolation (in hours; see Table 1). Monthly SST were extracted from the National Oceanic and Atmospheric Administration (NOAA) database from the “Extended Reconstructed Sea Surface Temperature” v5 (ERSST) (<https://www.ncei.noaa.gov/products/extended-reconstructed-sst>), and then averaged to get yearly dataset at a spatial resolution of 2.0° x 2.0°. SSTAs were reconstructed from SST measured *in situ* by buoys and ships, and Argo observations (<https://argo.ucsd.edu/>) also at a resolution of 2° x 2° (Table 1, Huang et al., 2015; Huang et al., 2017). The other environmental data were collected *via* Météo France, at two different stations: one located at the meteorological station of M^oTsambo for the period 1993–2018 (northern part of Mayotte near the study site) and one located at the meteorological station of Pamandzi for the period 1964–1992 as it was the only station which recorded environmental data for the considered period in the northeastern part of Mayotte (<https://publitheque.meteo.fr/okapi/accueil/okapiWebPubli/index.jsp>).

2.2 Coral sampling

The studied coral core was collected from a massive slow-growing coral of the genus *Diploastrea* (Figure 2A) on the outer slope of the barrier reef at 15 m depth near the M^oTsambo pass (northeastern part of the lagoon of Mayotte Lat. 12°37'19.4"S - Long. 45°06'42.7"E; Figure 1) in October 2018. We selected this site to focus on the influence of oceanic conditions on microboring assemblages in living corals instead of local disturbances, although these cannot be discarded. The coral core was collected with an 8 cm compressed air driller and

TABLE 1 Considered environmental parameters that could potentially influence microborers abundance over the last five decades (1964–2018) in the living coral *Diploastrea* sp. (Mayotte).

Parameter	Unit	Definition	Microborer Context
Sea Surface Temperature (SST)	°C	Measure of the temperature close to the ocean's surface. The surface is defined between 1 mm and 20 m below the sea surface.	Known as a stress factor (Reyes-Nivia et al., 2013)
Sea Surface Temperature Anomalies (SSTA)	°C	Temperature anomaly refers to a departure from the long-term average temperature value. SSTA are obtained by subtracting the SST climatology (1971–2000) from the <i>in situ</i> SST location, with a spatial resolution of 2° × 2° horizontal grid with statistically enhanced spatial completeness and at a monthly scale (Huang et al., 2015; Huang et al., 2017)	Putative stress factor
Precipitation Rate	mm	Rainfall rate is the measure of the intensity of rainfall over a given interval of time expressed in millimeters.	Indicator of the rainy season, potential proxy of nutrient influx, turbidity, low salinity and pH from terrigenous inputs which are known as stress factors (Tribollet, 2008b; Carreiro-Silva et al., 2009; Tribollet et al., 2009)
Max Instant Wind Speed	km·h ⁻¹	The instantaneous wind is measured at very short time intervals (e.g. half a second for example). The maximum instantaneous wind speed measures an instantaneous peak in speed when it exceeds at least 10 knots (19 km·h ⁻¹).	Indicator of potential mixing and nutrient transport in the water column
Cumulative Insolation Period	hours	Insolation is the amount of solar radiation received on a given surface in a given time period (W·m ⁻²). The term cumulative insolation is commonly used to designate the overall time during an object is subjected to insolation.	Light availability (and intensity) is a main stress factor (Tribollet, 2008a; Galindo-Martinez et al., 2022)

Averages and standard deviations were calculated for each parameter per year.

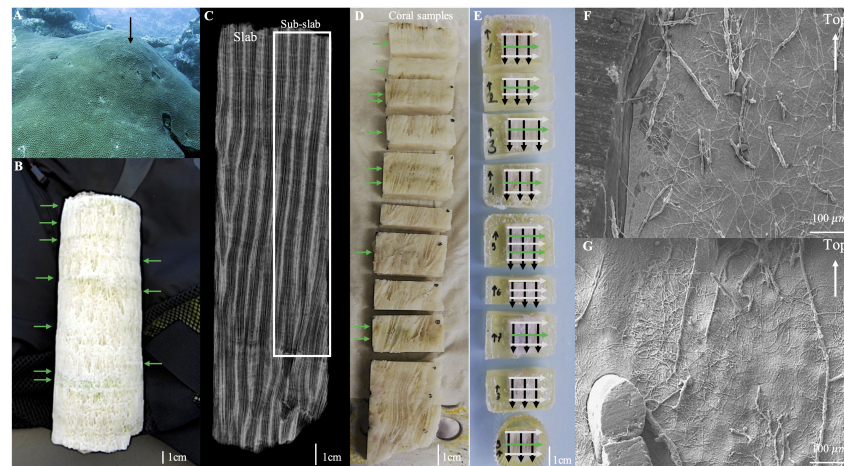


FIGURE 2

Studied *Diploastrea* coral colony at Mayotte. (A) *Diploastrea* colony at 15 m depth. The black arrow indicates where the colony was sampled. (B) *Diploastrea* core with visible green bands (green arrows). (C) X-ray radiograph of one middle slab cut out of the *Diploastrea* core measuring 19.5 cm long showing the annual density banding pattern. The studied area is indicated by the white rectangle. (D) Ten samples were cut from the radiographed slab of *Diploastrea* core. Only the first nine samples from the top were analyzed to estimate the microborer traces' abundance. Green arrows indicate green bands. (E) Resin impregnation of the 9 samples. Horizontal white and green arrows represent the horizontal transects where measurements of microborings abundance were realized (i.e. within white vs green bands). The black arrows represent the vertical transects studied in each sub-sample. (F, G) Different resin casts of microborings observed under scanning electron microscope after resin impregnation of coral samples and partial decalcification.

measured 19.5 cm in length. It presented 10 green bands visible by the naked eye (Figure 2B). Quickly after cutting the coral core, the position and the thickness of each green band along the core were recorded with a Vernier caliper under a dissecting microscope (NIKON Eclipse LV100, Bondy, France)

2.3 Coral growth variables

Two coral variables were measured along the coral core: the vertical linear extension ($\text{mm} \cdot \text{y}^{-1}$) and the skeletal bulk density ($\text{g} \cdot \text{cm}^{-3}$). Prior to measurements, the *Diploastrea* core was sliced along the main vertical growth axis into four different slabs (the middle slabs being ~ 1 cm thick). All slabs were well preserved as no diagenetic nor macrobioerosion traces were observed either by eye or under Scanning Electron Microscopy (SEM), except in one area in the bottom part of the core (i.e. the last 4.5 cm of the core). We thus avoided this area and studied only the first 15 cm of the core (see Figure 2C). The 4 slabs were scanned together on a Discovery CT750 HD CT scanner (GE Healthcare) set at 120 kV at the DOSEO 'Radiography and Imaging Technology Platform R and D center' (CEA-Saclay, Paris) with three coral standards to obtain a 3D image of the coral core (reconstructed from hundreds of 2D images). The 3D image revealed the pattern of the coral skeleton structure and its density variation over time.

Three coral standards cut from massive colonies of *Porites* sp. ($n = 2$) and *Diploastrea* sp. ($n = 1$) were prepared manually with a band saw to produce coral geometric blocks (cubes and cylinders) of different sizes. The bulk density of those coral standards was measured with both the buoyant weight technique (Bucher et al., 1998) and a recently developed method applying a Gaussian Mixture Model (Coulibaly, 2021). The GMM model allowed distinguishing the different voxels of the 3D image of the coral standards. Voxels corresponded to either one of the following categories: 'coral', 'air' (entrapped in coral pores for instance), or 'table' (on which the core was placed in the CT scanner). Coral standards were thus used for calibration to obtain Gaussian distributions of the different categories in Hounsfield units (HU). By comparing coral bulk densities of standards measured by buoyant weight vs the GMM, the following linear regression was obtained: $\text{Density} = 0.00084 \cdot \text{HU} + 0.51$ where HU is the Gaussian distribution of voxels corresponding to the 'coral' in Hounsfield units ($r = 0.99$, $p\text{-value} < 0.001$). The uncertainty of the bulk density measurement with this method was less than 1%. This is only true when the GMM is applied to samples of massive *Porites* sp. or *Diploastrea* sp. with skeletal densities comprised between 1.0 and 1.7 $\text{g} \cdot \text{cm}^{-3}$ (Coulibaly, 2021). We thus applied the GMM every 0.625 mm on the 3D image of our *Diploastrea* coral core, and then applied the linear regression to determine its annual bulk density. To estimate the

vertical extension rate along the main growth axis of the coral core, a 2D image of one of the two middle slabs (image obtained by CT scan) was analyzed. We assumed that an eye visible low-density band together with a high-density band corresponded to one year of growth (Figure 2C, Knutson et al., 1972; Buddemier, 1974). The estimated vertical extension rate was then confirmed by the analysis of a 2D X-radiograph of the same middle slab obtained with a scanner VERITON-CT at the Jean-Verdier hospital (Bondy, France). Finally, the annual coral calcification rate ($\text{g}\cdot\text{cm}^{-2}\cdot\text{y}^{-1}$) was calculated by multiplying the estimated annual bulk density by the annual vertical extension rate (see Taylor and Jones, 1993 and DeCarlo and Cohen, 2017).

2.4 Observation and estimation of the abundance of microborer traces

A sub-slab of 1.5 cm width (Figure 2C; white rectangle) was cut along the middle slab of the coral core and then cut into 10 coral samples (Figure 2D). The first 9 coral samples were observed under an SEM operating at 15kv (Zeiss EVO LS15) on the platform ALYSES (Bondy, France), to study the diversity and abundance of microborer traces as well as their distribution within the coral skeleton. Before SEM observations, each coral sample was bleached using concentrated sodium hypochlorite (8%) for 3 days to remove all traces of organic matter, rinsed with Milli-Q water for 3 days, and then dried at 50°C for an additional 48h. Dried coral samples were then embedded in the Specifix-40 epoxy resin from Struers Inc. (Cleveland, United States, 2 parts of resin: 1 part of curing agent, Figure 2E) to allow the observation of resin casts of microborings (traces) under SEM (Figures 2F, G). To perform good resin impregnation, samples were placed in a Cytovac vacuum chamber (Struers) for several minutes prior to polymerization (Wisshak, 2012; Golubic et al., 2019). Resin polymerization took place at 40°C in an oven for at least 24h. Embedded coral samples were then sectioned (sections of about 1 cm thick) along the vertical growth axis of the coral with a diamond saw (Isomet1000 from Buehler) and sonicated to remove potential sediments from sectioning for a few seconds. The surface of each thin section ($n=9$ i.e. one per coral section) was then etched with a 10% hydrochloric acid solution for 15 seconds to remove tens of micrometers of coral carbonate, then rinse in Milli-Q water for a few seconds and dried at 40°C in the oven prior gold metallization for the observation of resin casts of microborings under SEM (Figures 2F, G). The different types of microborings were determined based on their diameter, their morphology and their distribution within the coral skeleton. Along the coral core, 4 SEM images were randomly selected per coral section ($n=36$ images per sample) within the pool of SEM images taken for the analysis of microborings abundance, to measure the diameter of the different types of microborings using the ImageJ software (<https://imagej.nih.gov>, v1.53) and to observe their

distribution within the coral skeleton. Ten measurements of diameter (μm) were performed per type of trace and per SEM image. This analysis allowed us to distinguish a total of three types of microborings based on their diameter for the application of our machine learning approach to estimate the percentage of coral skeleton colonized by microborers (proxy of their abundance): those with a diameter comprised between 1 and 2 μm , those with a diameter comprised between 2 and 5 μm , and those with a diameter higher than 5 μm .

2.5 Innovative approach to study microboring assemblages in living corals

2.5.1 Data collection design

To study the variability of the relative abundance of the different types of microborings composing the assemblage and the percentage of coral skeleton they colonized (ratio between the surface area of microborer traces in a given coral skeleton section and the total surface area of the coral skeleton section $\times 100$; a proxy of microborer abundance) over the last decades, two complementary approaches were applied to the studied thin sections collected along the coral core: a 'vertical approach' comprising the study of SEM images taken continuously along 3 vertical transects parallel to the main coral growth axis (Figure 2E, black arrows), and a 'horizontal approach' (perpendicular to the main coral growth axis) comprising the study of SEM images taken continuously within 8 out of 10 visible green bands and 10 white bands selected along the coral core (Figure 2E, white and green arrows). Green bands on coral samples 3 and 9 were too close to each other to separate them so we considered one green band in each of these samples. Per vertical transect, 16 to 55 SEM images were taken depending on the height of the coral section while on each horizontal transect, about 30 SEM images were taken. At several periods along the coral core, the vertical transects crossed the horizontal transects (intersections shown in Figure 2E) allowing a comparison of the estimated average percentages of coral skeleton colonized by microborers obtained by the two approaches. This comparison was important as the estimated average percentages of the coral skeleton colonized by microborers *via* the vertical approach were based on the analysis of 3 SEM images per period (corresponding to the 3 vertical transects) while that obtained *via* the horizontal approach was based on the analysis of 30 SEM images. More importantly, as the main goal of the vertical approach was to highlight possible assemblage shifts, the variability in microborers abundance over the last decades, and the possible influence of abiotic and/or biotic factors, it was crucial to show that trends obtained based on the vertical approach were reliable and accurate. In addition to validating the vertical approach, the horizontal approach aimed at determining the possible link between the presence of green bands and certain microborers and their abundance. To

highlight the possible influence of abiotic and/or biotic factors, the average percentages of coral skeleton colonized by microborers were calculated along the vertical growth axis per year as the physical studied factors and coral parameters were calculated per year. This involved first estimating the rate of the vertical extension of the coral colony over the past decades and adjusting the number of SEM images collected along the vertical transects to match each year of coral growth.

2.5.2 Machine learning

To determine the relative abundance of the different types of microborings and the area of the coral skeleton they colonized per period of time (based on hundreds of SEM images taken along our coral core), we modified the Convolutional Neural Network (CNN) model called U-NET, which allows the recognition of various cellular structures in biomedical images (Ronneberger et al., 2015). This type of neural network belongs to the family of deep learning methods producing systems with interconnected nodes that can recognize patterns and correlations in datasets and can classify them. It is commonly applied to two-dimensional images (Krizhevsky et al., 2017). Here, our modified CNN model comprised 10 convolutional layers with each layer representing a linear operation involving the product of a set of parameters with a 2D input feature map (see Supplementary Figure 1 and Supplementary Material). The various parameters involved in our CNN model were optimized to improve the identification of the four defined categories: 'resin', 'coral skeleton', 'thin microborings', 'wide microborings' (Figure 3). Here only two types of microborings were considered due to the difficulty to distinguish some galleries

by the CNN model (see Supplementary Material). This approach led to the highest probability of the neural network correctly attributing a pixel to its right class (=accuracy, 93%). Providing all details of each component of the model would be out of the scope of this article, so we invite the reader to refer to Goodfellow et al. (2016) for a detailed explanation and to Supplementary material for the description of our CNN neural model structure and its three main steps (dataset constitution step, training step and model tuning and post-processing step, Supplementary Figure 2).

2.6 Statistical analysis

The present machine learning approach was conducted using Python (v3.8) through JupyterLab (<https://jupyter.org>). The manual analysis of a set of SEM images (n=60) used for the training step was performed with the image manipulation software GIMP (v2.10.14; <https://www.gimp.org>) and ImageJ (v1.53a; <https://imagej.nih.gov/ij/>) to detour shapes and then measure the area of coral skeleton colonized by microborers per SEM image. Coral bulk densities over time were calculated through the GMM model on Python, then averaged to be consistent with the coral growth rate per year. Linear regressions on environmental data and coral variables were generated from the library *ggpubr* on RStudio (v1.4.17; <https://www.rstudio.com>). The Non-parametric Mann-Kendall test was then performed to assess if the observed trend on each time series was significant. The areas of coral skeleton colonized by microborers (thin + wide microborings) measured along the

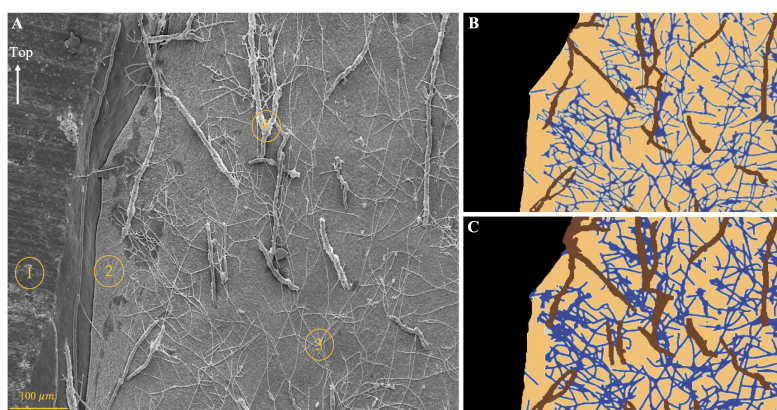


FIGURE 3
Illustration of the manual vs machine learning image analysis. (A) Original SEM image displaying the four classes of items that the Convolutional Neural Network model had to recognize: resin, coral skeleton, thin microborings, and wide microborings. (B) Result of the manual quantification of the area of coral skeleton colonized by thin (dark blue) and wide microborings (brown), uncolonized coral skeleton (orange), and resin (black). (C) Result of the machine learning approach.

three vertical transects were compared using an ANCOVA. Although no significant differences were obtained between two pairs of two transects (p -values > 0.2) the third one showed a significant difference (p -value < 0.001). Despite such slight variability, and because the three transects showed the same trend over the studied period (i.e. 54 years), we chose to average values from the 3 vertical transects per period (year) to determine the possible main factors driving the overall temporal variability of microborers abundance. Pearson correlations were carried out to detect the potential effects of the environmental and/or coral variables studied on the traces' abundance (i.e. the abundance of thin microborings, wide, or all microborings) obtained over the last five decades (vertical transects). These correlations were performed on detrended variables to focus on their possible interannual and decadal variability and to avoid spurious correlations due to linear trends. To estimate the possible differences between means of the area of the coral skeleton colonized by microborers (microborings' abundance) obtained on vertical vs horizontal transects (at the intersections in Figure 2E), a student t-test was performed. A non-parametric Pettitt test was then applied to means to determine a potential breakpoint in the trend over the last 54 years. Finally, binary logistic regressions were generated using the library *glm* in RStudio (generalized linear models) to determine the possible factors influencing the presence or absence of green bands along the coral core. The selection of these factors was done using a so-called backward procedure: first, the binary logistic regressions were carried out using all studied variables over the period 1964–2018 (i.e. the area of coral skeleton colonized by all microborers or just thin or wide trace makers, coral growth variables and environmental data). When a nonsignificant link between the presence of green bands and any of our variables was observed, the variable presenting the highest p -value from the dataset was removed. This was done until all remaining variables were significant (i.e. presented a significant effect on the presence or absence of green bands).

3 Results

3.1 Mayotte's environmental conditions over the last 54 years

The SST and SSTA which are dependent variables showed a similar and significant annual variability over the last five decades ($p < 0.0001$, Mann Kendall test, Table 1 in Supplementary Material). SST varied between $25.2^{\circ}\text{C} \pm 0.7$ and 26.7 ± 0.6 in winter and $28.1^{\circ}\text{C} \pm 0.2$ and $29.7^{\circ}\text{C} \pm 0.4$ in summer. Since the 60's, Mayotte reefs experienced significant warming with an estimated SST increase of $+0.11^{\circ}\text{C}$ per decade ($p < 0.0001$, Mann Kendall test; Figure 4A and Supplementary Figure 3A). They also experienced increasingly positively SSTA over time, especially in the recent years (down to -0.84°C in winter 1964

towards up to $+0.9^{\circ}\text{C}$ in summer 2016, $p < 0.0001$; Figure 4B and Supplementary Figure 3B). Similarly, the max instant wind speed increased significantly since the 60's by a factor of 0.3 per year ($p < 0.0001$, Mann Kendall test; Figure 4C and Supplementary Figure 3C). In contrast, precipitations did not change significantly over time (Figure 4D and Supplementary Figure 3D) and the duration of the insolation period significantly decreased by 6.4 hours per decade over the last 54 years (15% diminution over the considered period, $p < 0.0001$, Mann Kendall test; Figure 4E and Supplementary Figure 3E).

3.2 Coral growth parameters

Based on the density bands of the *Diploastrea* coral core which allowed the reconstruction of the colony vertical linear extension rate, we estimated that our study covered a period of 54 years from 1964 to 2018 (Table 2 in Supplementary Material). The vertical extension rate did not vary significantly over time and was comprised between 2.1 (in 1997–1998) and $4.9 \text{ mm} \cdot \text{yr}^{-1}$ (in 2017), with an average of $2.6 \text{ mm} \cdot \text{yr}^{-1} \pm 0.5$ (Figure 5A). In contrast, the coral bulk density decreased significantly and nonlinearly since the 60's (40% decrease, $p < 0.001$, Mann Kendall test; Figure 5B). The calcification rate also varied slightly significantly ($p < 0.05$, Mann Kendall test) and was comprised between 0.25 ± 0.002 in 2009 and 0.55 ± 0.023 in 2017 $\text{g} \cdot \text{cm}^{-2} \cdot \text{yr}^{-1}$ (Figure 5C). A strong negative correlation was found between the detrended data of bulk density and the cumulative insolation period whatever the considered period ($p < 0.01$ with a Pearson correlation coefficient $r = -0.39$ for the whole studied period) and to a lesser extent to SSTA ($p < 0.05$, $r = -0.39$, Table 2). When considering the raw data sets (both coral and environmental parameters), SSTA was again negatively correlated to the bulk density, especially after the breakpoint (Table 3 in Supplementary Material). Precipitations were the only other environmental factor with a significant correlation with both the vertical coral extension (before the breakpoint) and calcification rates (after the breakpoint) whether we considered raw or detrended data sets (Tables 2, 3 in Supplementary Material).

3.3 Diversity of microborings

Based on morphological criteria including the diameter of microborer traces, and their distribution within the coral skeleton, we were able to identify three different types of microborings. Most microborings with a diameter comprised between 1 and $2 \mu\text{m}$, with branches perpendicular to the main traces and with a random distribution within the coral skeleton were indicative of fungi. However, within those thin traces, some appeared to follow the main coral growth axis and therefore could be attributed to other trace makers such as the cyanobacterium *Plectonema* (Figure 6A) or exploratory

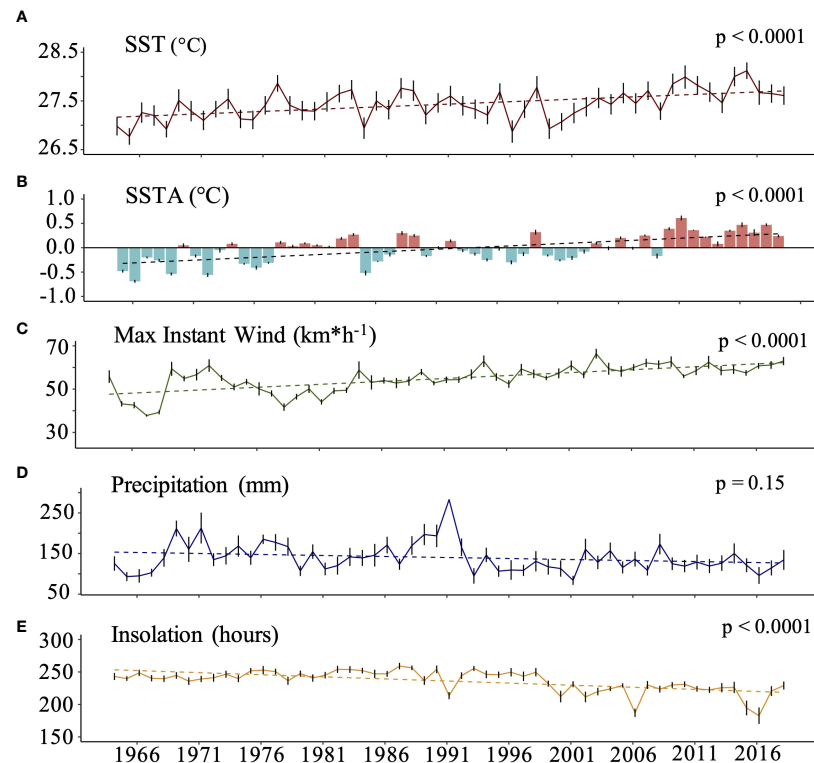


FIGURE 4
Interannual variability of the different environmental parameters at Mayotte between 1964 and 2018. (A) Sea Surface Temperature (SST in °C) (B) Sea surface temperature anomalies (SSTA in °C). (C) Maximum instantaneous wind speed ($\text{km}\cdot\text{h}^{-1}$). (D) Precipitation rate (mm). (E) Annual cumulative insolation period (hours). Errors bars (SE) for each variable were calculated after averaging monthly data.

filaments of the chlorophyte *Ostreobium* sp. (Wisshak et al., 2011). Microborings with a diameter between 5 and 10 μm were either in the form of a zigzag pattern typical of *Ostreobium quekettii* (chlorophyte; Figure 6B), or in the form of vertical tubules parallel to the main growth axis of the coral with specific branching, a few bulges and club-shaped apices indicating the presence of other chlorophytes such as *Epicladia testarum* or *Gomontia* sp. (Figures 6B, C; Bornet and Flahault, 1888; see Figure 5I in Wisshak et al., 2011). Finally, very large traces with bulges, cross-wall constrictions and branches were observed with sometimes a diameter higher than 30 μm , indicating the presence of another microboring chlorophyte. They were mainly distributed along the main coral growth axis (Figure 6D). The analysis of a few SEM images randomly chosen along the coral core revealed that microborings with the largest diameters were more often observed in the bottom part of the coral core, i.e. between the 60's and the early 80's, than near the coral tissues where microborings with the smallest diameter dominated (Figure 7). The composition

change in the trace assemblage lasted about ten years (Figure 7). In the most recent years (2014–2018), trace makers of thin microborings clearly dominated the assemblage.

3.4 Variability of microborings abundance over the last 54 years

3.4.1 Representativeness of data obtained along the main vertical coral growth axis

Comparison of means of the percentage of coral skeleton colonized by microborings, a proxy of microborers abundance, at the intersections between vertical and horizontal transects along the coral core revealed no significant differences (paired Student test, $p > 0.05$; Figure 8). Both approaches highlighted a significant decrease of microborings abundance over the last 50 years ($p < 0.001$, Mann Kendall test). Although the variance on vertical transects was higher than that of means obtained on

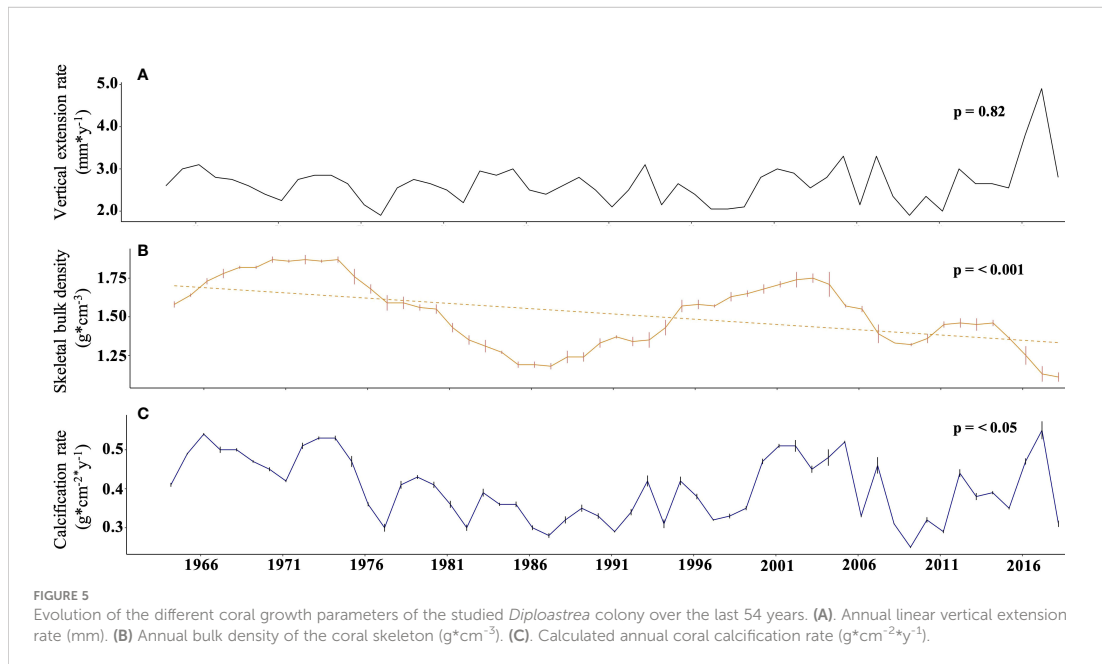


TABLE 2 Pearson's correlations between the detrended coral growth variables and detrended environmental variables over the last 50 years and per period before or after the breakpoint.

VARIABLES	WHOLE DATASET (1964 – 2018)		
	Vertical extension rate	Skeletal bulk density	Calcification rate
SST	NS	NS	NS
SSTA	NS	NS	NS
Precipitations	$r = -0.324^*$	NS	$r = -0.379^*$
Max Instant Wind Speed	NS	NS	NS
Cumulative insolation	NS	$r = -0.391^{**}$	$r = -0.378^{**}$
VARIABLES	DATASET between 1964 and 1985		
	Vertical extension rate	Skeletal bulk density	Calcification rate
SST	NS	NS	NS
SSTA	NS	NS	NS
Precipitations	$r = -0.563^{**}$	NS	NS
Max Instant Wind Speed	NS	NS	NS
Cumulative insolation	NS	$r = -0.639^{**}$	$r = -0.567^{**}$
VARIABLES	DATESET between 1986 and 2018		
	Vertical extension rate	Skeletal bulk density	Calcification rate
SST	NS	NS	NS
SSTA	NS	$r = -0.385^*$	NS
Precipitations	NS	$r = -0.328^{*#}$	$r = -0.423^*$
Max Instant Wind Speed	NS	NS	NS
Cumulative insolation	NS	$r = -0.318^{*#}$	$r = -0.320^{*#}$

*#: p-value < 0.1; *: p < 0.05; **: p-value < 0.01; NS, non-significant.

horizontal transects due to the difference in the number of measurements per approach (3 versus 30, respectively), our results showed that means of microborings abundance calculated from 3 measurements along the vertical coral growth axis were well representative of those obtained on a horizontal band of about 1.5 cm width of the coral sub-slab (Figure 2C). To study the interannual variability of microborings abundance and to identify the main factors that may influence it, we thus chose to focus on data obtained continuously along the vertical coral growth axis.

3.4.2 Variability of microborings abundance and assemblage shift

Based on data obtained along the main vertical coral growth axis, we estimated that the decrease in microborings abundance was 91% over the last 54 years. The highest abundance of microborings (thin + wide) was observed in the mid 70's ($51\% \pm 3.9\%$ of the coral skeleton was colonized by microborers), while the lowest was found in the very recent years 2017-2018 ($1.3\% \pm 1.2\%$; Table 4 in Supplementary Material). This trend was confirmed by the horizontal approach although this latter did not cover the whole coral core, with the highest abundance estimated in 1972-1973 ($45.6\% \pm 3.5\%$) and the lowest abundance in 2015-2016 ($4.3\% \pm 1.2\%$; Table 5 in Supplementary Material). We also noticed a major step in the 80's. This breakpoint was identified between 1985 and 1986 (Pettit test, $p < 0.001$). Comparing separately the two periods, 1964-1985 and 1986-2018, our results showed that not only the abundance of microborings drastically decreased after the breakpoint, but a shift in the assemblage composition was also observed. Before 1985-86, the trace assemblage was dominated by borers making wide traces and to a lesser extent thin traces, while in recent years it was clearly dominated by microborers making thin traces (Figures 7, 9). Interestingly during the shift which lasted a few years, the diversity of microborings increased as shown by the more important diversity of measured trace diameters (Figure 7).

3.4.3 Main factors influencing microborings abundance over time

Considering raw data sets, our results showed that the decrease of microborings abundance (total abundance as well as the abundance of both thin and wide microborings; see Table 3) was positively correlated to the decrease of both the coral bulk density and the cumulative insolation. In contrast, microborings abundance was negatively correlated to SST, SSTA and the max instant wind speed (Table 3). When focusing on the period before the breakpoint, we could observe that the

abundance of thin trace makers was for instance positively correlated to SST and precipitations ($p < 0.05$), while the abundance of wide trace makers was negatively correlated to the max instant wind speed ($p < 0.05$; Table 3). After the breakpoint (1986-2018), thin trace makers were surprisingly negatively correlated to precipitations and to the vertical coral growth extension rate ($p < 0.05$). In contrast, the wide trace makers were positively correlated to precipitations and the cumulative insolation but negatively correlated to SSTA ($p < 0.05$; Table 3). A similar analysis was conducted but on detrended data sets to reveal the main biotic and abiotic factors that could affect the interannual variability of the microboring assemblage. This analysis confirmed that the coral bulk density was significantly correlated to microborings' abundance (total, wide, and thin microborings' abundance, Table 4). It also confirmed the positive correlation between the decreasing cumulative insolation and the abundance of the thin trace makers ($p < 0.05$, Table 4). SST had also a relatively positive effect on the abundance of the thin trace makers ($p < 0.1$). Interestingly, after the breakpoint, precipitations had the opposite influence. The analysis of detrended data also confirmed the negative correlation between the abundance of the wide trace makers and precipitations, especially before the breakpoint as well as the strong influence of the max instant wind speed (Table 4).

3.5 Characteristics, drivers and occurrence of green bands

We distinguished a total of 10 green bands extending in parallel to the coral tissue within the upper 15 cm of the coral core. Their thickness varied between 3 and 5 mm (Figures 2B, D, and Table 5) covering on average a period of 1.5 years. The largest green bands were observed between 1991 and 1997. In general, green bands appeared during the winter season or at the end of the summer season. While only 3 green bands were observed between 1964 and the mid-80's, 7 bands were observed between the mid-80's and 2018 indicating an increase in the occurrence of these events by 233% after the breakpoint. The interval between two green bands over the studied period varied greatly with a remarkable long period of 8 years and 4 months without any green band between the early 80's and early 90's (Table 5). A binary logistic regression on the detrended data showed that the variability of SSTA and the max instant wind speed seemed to be the most significant parameters influencing the green bands' presence ($p = 0.028$ and $p = 0.021$, respectively). This model presented an accuracy of 65% and was better at predicting the absence of green bands than their presence (Figure 10). The model confidence was also greater before the

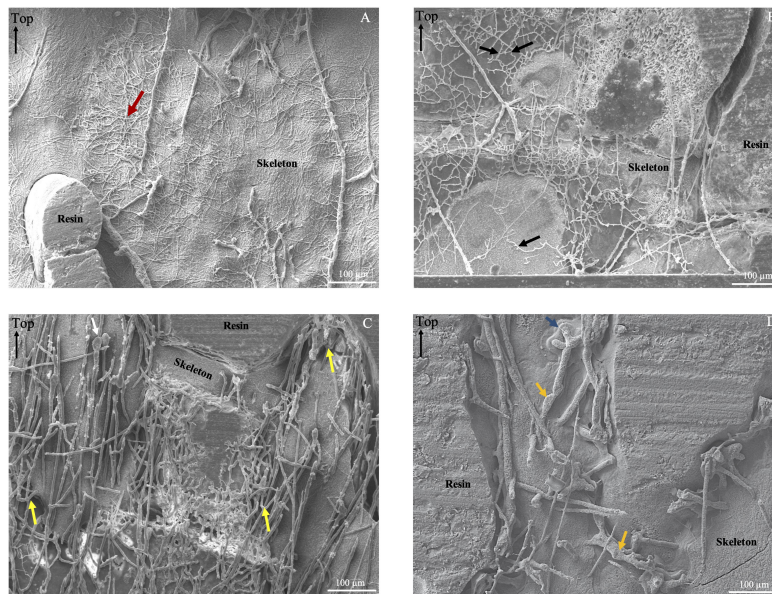


FIGURE 6

SEM pictures presenting the diversity of traces (microborings) observed along the coral core. (A) SEM image from the top of the core showing traces of *Scolecia filosa* (produced by the cyanobacterium *Plectonema* sp.; red arrow). (B) Picture from the bottom of the core showing a great abundance of the typical *Ichnoreticulina elegans* trace (work of the chlorophyte *Ostreobium* sp. *quekettii*; black arrows). (C) Picture from the bottom of the core showing wide microborings oriented towards the coral tissue layer. Tubules presenting branches (yellow arrow) and club shape apices (white arrow) indicative of microboring algae. In the center of the picture, traces of *Ichnoreticulina elegans* can be observed. (D) Picture from the middle of the core showing very wide microborings (> 20 μ m) oriented towards the coral tissue layer. Those traces are cylindrical tubules, sometimes with bulges and visible cross-wall constrictions (yellow arrows), as well as branches (blue arrow).

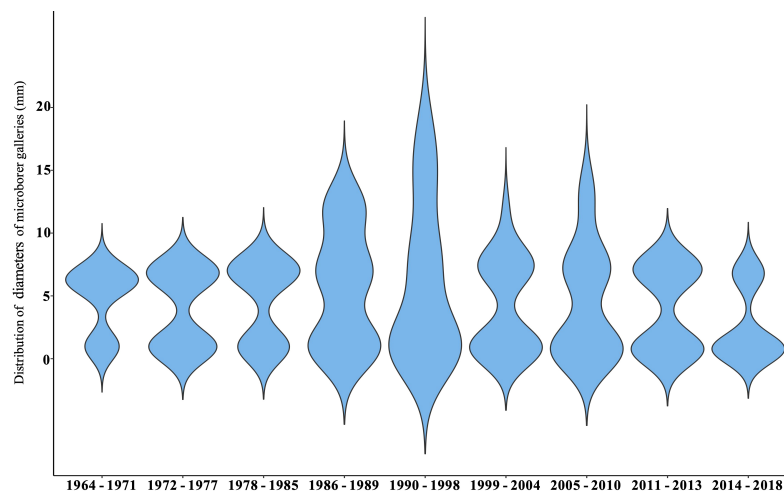
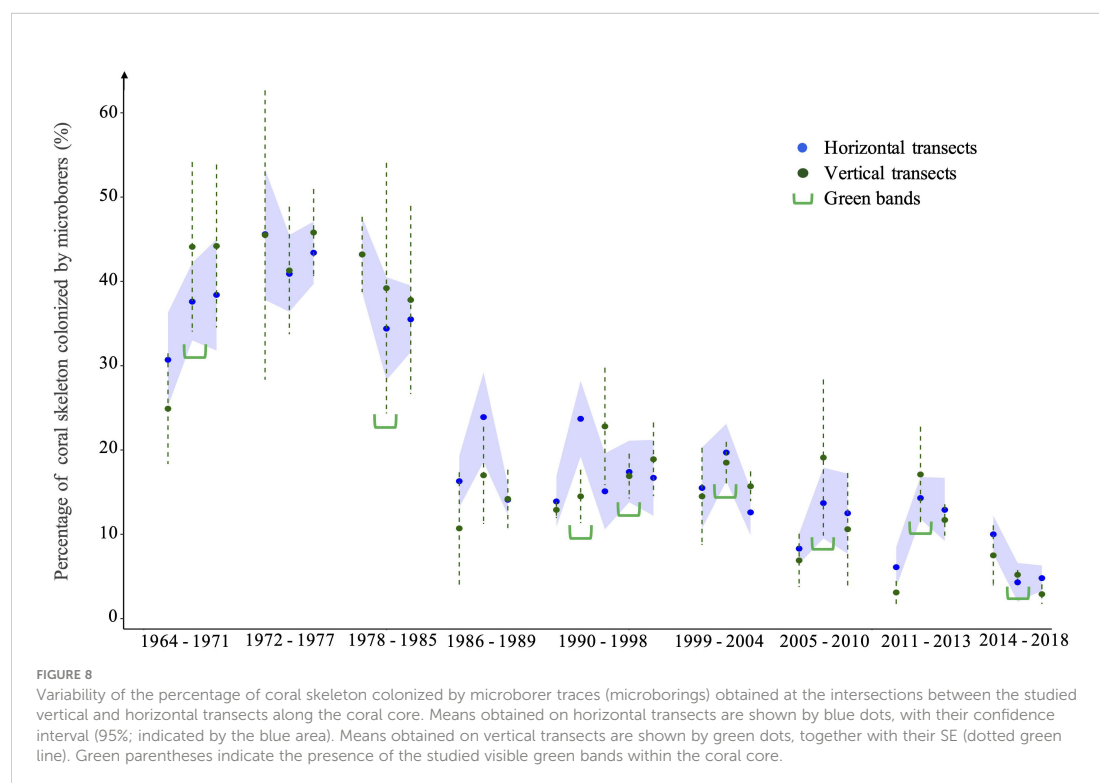


FIGURE 7

Violin plot showing the temporal variability in microborer traces' diversity identified based on their diameter.



breakpoint (black dotted box) than after as it identified only 3 green bands out of 7 after 1985 (Figure 10).

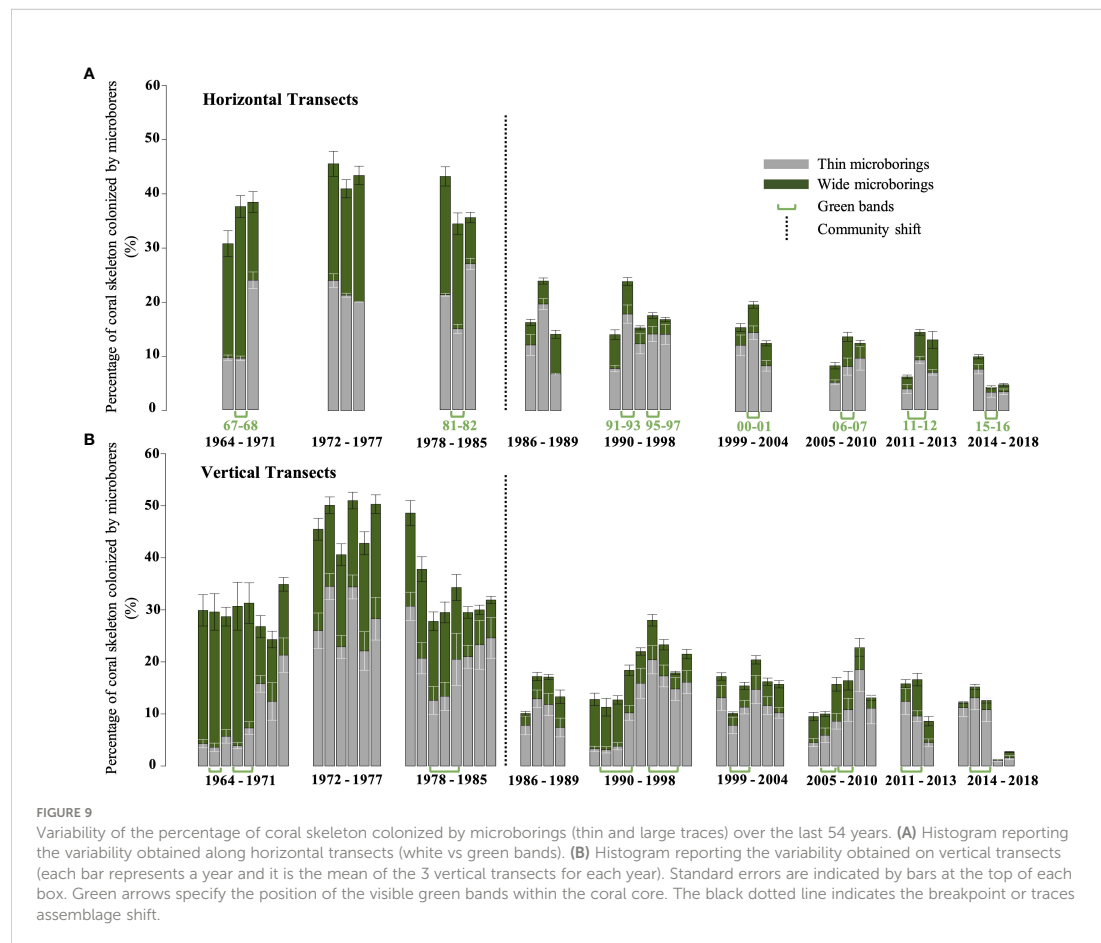
4 Discussion

4.1 Microboring assemblage of *Diploastrea* sp.: Study method and composition

The machine learning approach developed here to quantify the abundance of microborers in a living coral colony over the last 54 years allowed the study of thousands of SEM images in a few hours with an accuracy of 93%. This is noteworthy because other quantitative methodologies including the total decalcification of coral skeleton to estimate the ash-free dry weight of endoliths (Fordyce et al., 2021) or the number of microboring filaments (Lukas, 1973) implied several biases and/or were time-consuming. Measurements of endolith dry weight include the biomass of the organic matrix of the coral skeleton (about 1%; Cuif et al., 2004) and potentially that of other organisms such as boring sponges, mollusks and/or other endolithic microorganisms (Golubic et al., 1981; Cuif et al., 2004; Kobayashi and Samata, 2006; Tribollet and Golubic, 2011; Yang and Tang, 2019), conducting to an

overestimation of microborers biomass. Moreover, such method do not allow microborers observation in their original spatial orientation. The estimation of microborer filaments (Lukas, 1973; Priess et al., 2000) or traces (Chazottes et al., 1995; Carreiro-Silva et al., 2005) depends also on the observer, thus limiting comparisons of results. In the light of the new techniques developed recently by Salamon et al. (2019) and Schätzle et al. (2021) which combine specific fluorescent dyes and SEM or Confocal Laser Scanning Microscopy (CLSM) we believe that our method could be improved to quantify the abundance of a larger variety of microboring traces as here only two types were studied with the machine learning approach. Our method was limited by the grayscale SEM images reducing the ability of the CNN model to distinguish properly the various types of traces. Other hyperparameters of the machine learning process, such as different loss functions, could furthermore improve the accuracy of the analysis but were not tested in the present study.

Although only three types of traces were determined based on their diameter and orientation along the main coral growth axis, we were able to identify the main common trace makers colonizing live coral skeletons, i.e. *Ostreobium quekettii* with its typical zigzag pattern, *Plectonema* sp. with its typical 'spaghetti-like' pattern and very narrow fungi (Lukas, 1973; Le Campion-Alsumard et al., 1995a; Massé et al., 2018). In addition to those ubiquitous



microborers, we observed wide traces (10–30 μm) in abundance forming tubules with specific ramifications, bulges, and/or cross-wall constrictions and club shape apices, all of them mainly oriented towards coral tissues in the central and bottom part of the coral core (light; Figures 6B, D). The trace makers of those tubular microborings were most probably eukaryotic phototrophs due to their shapes and orientation (light-dependent organisms; see also Kolodziej et al., 2012). They could be attributed to other *Ostreobium* species (Lukas, 1974; Marcelino and Verbruggen, 2016) or other chlorophytes such as *Ulvella* sp., *Gomontia* sp., *Phaeophila* sp., or *Epicladia testarum* (Bornet and Flahault, 1888; Wisshak et al., 2011; Nielsen et al., 2013; Marcelino and Verbruggen, 2016). We do not believe that they were traces of the *Conchocelis* stage of bangialean red algae as the typical reddish color was not observed when the coral core was collected (Pica et al., 2016) and the large tubules lasted over decades. The *Conchocelis* stage is known to be a transient phenomenon in the life cycle of bangialean red macroalgae (Tribollet et al., 2017). Large

tubular traces and filaments similar to ours were observed by Kolodziej et al. (2012) and Salamon and Kolodziej (2021) in fossil corals from Eastern Europe (from Paleogene to Jurassic) and were interpreted as those of *Ostreobium* sp., suggesting that such pattern was maintained over millions of years. We cannot exclude however that some of the observed large traces were made by fungi as they are well known in marine carbonates including coral skeletons (Le Campion-Alsumard et al., 1995b; Benthis et al., 2000; Priess et al., 2000; Wisshak et al., 2011) but based on our observations, the majority of tubules presented a typical shape and orientation of eukaryotic phototrophs.

4.2 Microboring assemblage shift and abundance decrease

For the first time here, we highlight a major shift in the microboring assemblage composition over the life span of a

TABLE 3 Pearson's correlations between the raw abundance of microborers (wide, thin or total) and raw environmental or coral growth variables over the last 50 years and per period before or after the breakpoint.

WHOLE DATASET (1964 – 2018)			
VARIABLES	Wide microborings	Thin microborings	Total microborings
Vertical Extension Rate	NS	NS	NS
Skeletal Bulk Density	$r = 0.538^{***}$	$r = 0.311^*$	$r = 0.529^{***}$
Calcification Rate	$r = 0.360^{**}$	NS	$r = 0.245^{*#}$
SST	$r = -0.440^{***}$	NS	$r = -0.251^{*#}$
SSTA	$r = -0.536^{***}$	NS	$r = -0.393^{**}$
Precipitations	NS	NS	NS
Max Instant Wind Speed	$r = -0.736^{***}$	NS	$r = -0.524^{***}$
Cumulative insolation	$r = 0.422^{**}$	$r = 0.359^{**}$	$r = 0.492^{***}$
DATASET between 1964 and 1985			
Vertical Extension Rate	NS	NS	NS
Skeletal Bulk Density	0.455*	NS	NS
Calcification Rate	NS	NS	NS
SST	NS	$r = 0.458^*$	NS
SSTA	NS	NS	NS
Precipitations	$r = -0.382^{*#}$	$r = 0.425^*$	NS
Max Instant Wind Speed	$r = -0.558^{**}$	$r = 0.416^{*#}$	NS
Cumulative insolation	NS	NS	NS
DATESET between 1986 and 2018			
Vertical Extension Rate	NS	$r = -0.414^*$	$r = -0.485^{**}$
Skeletal Bulk Density	NS	$r = 0.388^*$	$r = 0.411^*$
Calcification Rate	NS	NS	NS
SST	NS	NS	NS
SSTA	$r = -0.396^*$	NS	NS
Precipitations	$r = 0.362^*$	$r = -0.355^*$	NS
Max Instant Wind Speed	NS	NS	NS
Cumulative insolation	$r = 0.403^*$	NS	$r = 0.350^*$

*#: p-value< 0.1 ; *: p< 0.05 ; ** : p-value< 0.01 ; *** : p-value< 0.001 ; NS , non-significant.

slow-growing massive coral in the Western Indian Ocean (Figures 7, 9). This shift occurred around 1985 and was coupled with a decrease of more than a half of the initial microborer's abundance (Figure 9). Before the identified breakpoint in 1985-86, the microboring assemblage was dominated by wide tubular traces, and to a less extent by thin ones. After the breakpoint, the assemblage became more diversified over about 10 years and increasingly dominated by thin traces. We strongly suggest here that the decreasing cumulative insolation together with rainfall and rising SST over the studied period (Figure 4 and Table 4) selected thin trace makers at the expense of wide trace makers. Before 1985, wind stress and rainfall may have enhanced the general reduction of light reaching the wide trace makers within the coral skeleton by re-suspending sediments on the barrier reef (Vacelet et al., 1996) and/or increasing terrigenous inputs in the

lagoon (Risk et al., 1995; Tribollet, 2008b) accelerating the assemblage shift. Moreover, terrigenous inputs enriched in nutrients in the northern lagoon of Mayotte (Vacelet et al., 1996) may have also enhanced the growth of the thin trace makers. Carreiro-Silva et al. (2009) showed indeed that inorganic nutrients stimulate *Ostreobium*'s growth as well as that of other bioeroding green algae and cyanobacteria. Although we did not study the genetic diversity of microborers in our coral core, we strongly suggest that the advantaged thin trace makers were dominated by the phototrophic *Ostreobium* sp. Those bioeroding algae are known to be sciaphile phototrophs, i.e. low-light extremophiles (Shashar and Stambler, 1992; Gektidis, 1999; Tribollet et al., 2006; Tribollet, 2008a), to form green bands in living corals (Odum and Odum, 1955; Lukas, 1973; Le Campion-Alsumard et al., 1995a; Fine and Loya, 2002; Carilli et al., 2010) and to be also stimulated by

TABLE 4 Pearson's correlations between the detrended abundance of microborers (wide, thin or total) and detrended environmental or coral growth variables over the last 50 years and per period before or after the breakpoint.

WHOLE DATASET (1964 – 2018)			
VARIABLES	Wide microborings	Thin microborings	Total microborings
Vertical Extension Rate	NS	NS	NS
Skeletal Bulk Density	$r = 0.243^{*#}$	NS	$r = 0.268^{*}$
Calcification Rate	$r = 0.252^{*#}$	NS	NS
SST	NS	$r = 0.255^{*#}$	$r = 0.251^{*#}$
SSTA	NS	NS	NS
Precipitations	$r = -0.291^{*}$	NS	NS
Max Instant Wind Speed	$r = -0.404^{**}$	NS	NS
Cumulative insolation	$r = -0.263^{*#}$	NS	NS
DATASET between 1964 and 1985			
Vertical Extension Rate	NS	NS	NS
Skeletal Bulk Density	NS	NS	NS
Calcification Rate	NS	NS	NS
SST	NS	$r = 0.370^{*#}$	NS
SSTA	NS	NS	NS
Precipitations	$r = -0.476^{*}$	$r = 0.462^{*}$	NS
Max Instant Wind Speed	$r = -0.565^{**}$	NS	NS
Cumulative insolation	NS	$r = 0.559^{**}$	$r = 0.475^{*}$
DATESET between 1986 and 2018			
Vertical Extension Rate	NS	$r = -0.305^{*}$	NS
Skeletal Bulk Density	$r = 0.365^{*}$	$r = 0.429^{*}$	$r = 0.523^{**}$
Calcification Rate	$r = 0.404^{*}$	NS	NS
SST	NS	NS	NS
SSTA	NS	NS	NS
Precipitations	NS	$r = -0.485^{**}$	$r = -0.444^{**}$
Max Instant Wind Speed	NS	NS	NS
Cumulative insolation	$r = -0.293^{*#}$	NS	NS

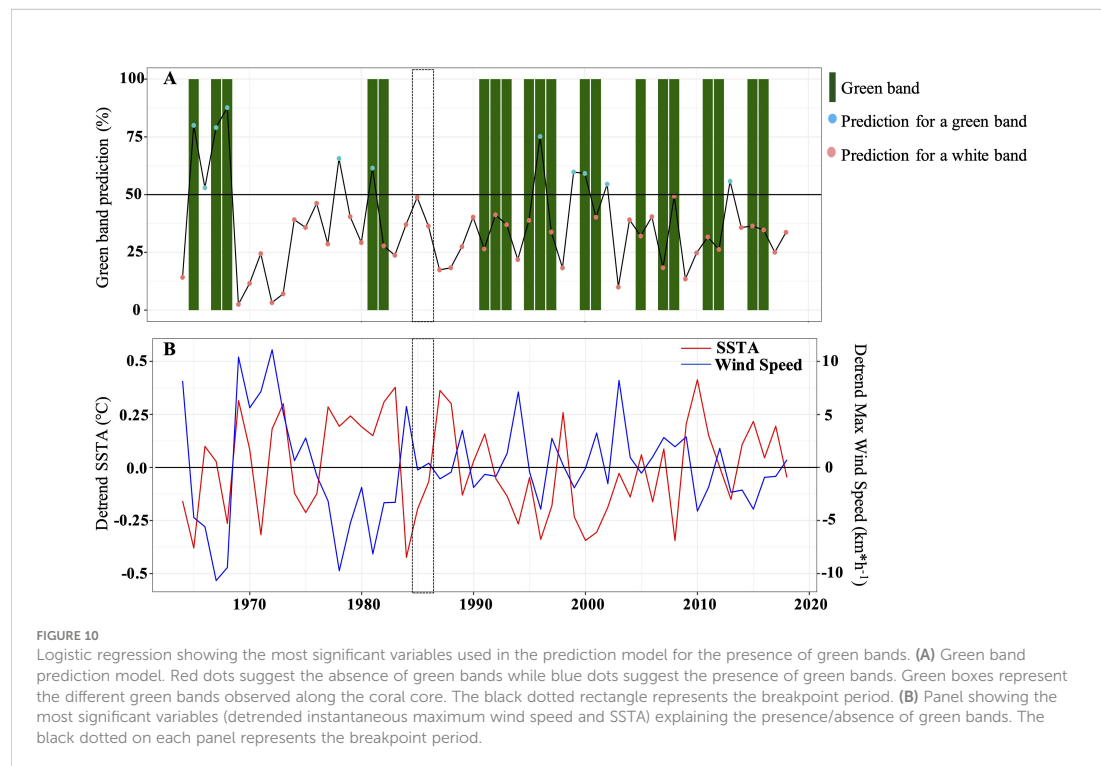
*#: p-value < 0.1 ; *: p < 0.05 ; **: p-value < 0.01; NS, non-significant.

elevated SST in dead corals (Reyes-Nivia et al., 2013; Grange and Tribollet, unpubl.data). If thin fungi were stimulated instead of

TABLE 5 Periods at which eye visible green bands were observed along the 15 cm coral core of *Diploastrea* sp. (Mayotte).

Periods of presence of green bands	Starting season	Period covered by a green band (year)	Interval between two green bands(year)
June 2015 – November 2016	Winter	1.4	2.91
March 2011 – July 2012	End of Summer	1.3	2.58
September 2007 – July 2008	Winter	0.8	0.08
March 2006 – July 2007 *	End of Summer	1.3	4.33
August 2000 – September 2001	Winter	1.08	2.66
September 1995 – October 1997	Winter	2.08	2
April 1991 – September 1993	End of Summer	2.4	8.25
December 1980 – December 1982	Summer	2	2
June 1967 – November 1968	Winter	1.33	1.5
May 1964 – October 1965	Start Winter	1.4	

*: Two green bands with only one month interval. They were considered as one green band.



thin phototrophic microborers, black bands would have been eventually observed (Priess et al., 2000).

The positive correlation between bulk density and microborers abundance over decades, especially after 1985, appears counterintuitive as the active removal of calcium carbonate by microborers (dissolution process driven by photosynthesis; Garcia-Pichel et al., 2010; Tribollet et al., 2019) would normally conduct to a less dense coral skeleton. Here such an inverse relationship was not seen probably because the bulk density was studied instead of the microdensity. Fordyce et al. (2021) reported that corals with a low skeletal microdensity are more colonized by phototrophic microboring communities as they would benefit from greater and easier access to nutrients (organic matrix: see Massé et al., 2020; Iha et al., 2021) than corals with a high density. Interestingly and similarly to microborers abundance, the coral bulk density, calcification and linear extension rates in our study were strongly correlated to SSTA, rainfall and cumulative insolation (Table 2); factors reported previously by Lough and Barnes (1997) and Lough and Cantin (2014). Ocean acidification might have also been involved in the *Diploastrea* bulk density decrease (Mollica et al., 2018) but this factor was not studied here. Tribollet et al. (2009), Tribollet et al. (2019) and Reyes-Nivia et al. (2013) showed that *Ostreobium* sp. growth is stimulated by elevated $p\text{CO}_2$ in dead corals, so we hypothesize

that this factor might have also contributed to the selection of the thin trace makers (mainly *Ostreobium* sp.) over the last 54 years, especially over the last two decades as Lo Monaco et al. (2021) reported accelerated acidification in the Mozambique channel. The unclear relationship between the coral bulk density and microborers abundance needs further investigation as it may not be a direct causal and effect relationship or it could vary depending on the coral species, microboring assemblage, and environmental conditions. In the very recent years (2015–2017) when major consecutive positive SSTA occurred (Hughes et al., 2017), the accelerated decrease of microborers abundance probably resulted from the suddenly important vertical extension rate of *Diploastrea* sp. ($4.9 \text{ mm}\cdot\text{yr}^{-1} \pm 1.05$). Lough and Barnes (1997) and Kleypas and Langdon (2006) showed that corals can invest more in their vertical extension rate than in their skeletal strength (bulk density) under thermal stress (see Figure 5). The average vertical extension rate for the studied *Diploastrea* sp. was $2.6 \text{ mm}\cdot\text{y}^{-1}$ over the last 54 years, which is similar to that measured on *Diploastrea* sp. from Palau ($2.7 - 6.0 \text{ mm}\cdot\text{yr}^{-1}$; Canesi, 2022) and in New Caledonia ($2.68 \pm 0.64 \text{ mm}\cdot\text{yr}^{-1}$; Wu et al., 2018). But between 2015 and 2017 the coral growth extension of our *Diploastrea* sp. was twofold more important ($4.9 \text{ mm}\cdot\text{yr}^{-1}$) while the bulk density was reduced by about 40% ($1.13 \text{ g}\cdot\text{cm}^{-3}$ while in the 60's it was above $1.6 \text{ g}\cdot\text{cm}^{-3}$). Godinot et al. (2012) showed that a rapid vertical coral

growth can 'dilute' microborers as they cannot keep up with their host's fast growth. The possible consequences of such a drastic decrease in microborers' abundance in massive corals such as *Diploastrea* sp. may be important as several authors suggested that *Ostreobium* sp. may play a key role in coral health, especially during coral bleaching recovery, by both providing photoprotection (Galindo-Martinez et al., 2022) and photoassimilates (Schlichter et al., 1995; Schlichter et al., 1997; Sangsawang et al., 2017; Massé et al., 2020; Iha et al., 2021). More coral cores should thus be studied to confirm the observed trends in order to better understand the possible implications of an important decrease of microborers abundance in living corals especially the stress-tolerant ones such as *Porites* sp. (Schoepf et al., 2019; DeCarlo et al., 2019).

4.3 Possible explanatory factors for green bands

Interestingly, our logistic regression model highlighted that the absence of green bands was strongly correlated to an increase in max instant wind speed and positive SSTA (Figure 10). Due to the low number of green bands in our coral core, it was not possible to run our logistic regression model on detrended data before and after the breakpoint to reveal the possible role of different factors on green band formation. However, although no significant correlation was found between the abundance of microborers and the presence of green bands over the studied period (due to the continuous decrease of microborers abundance over the last 54 years), we suggest that wide trace makers before 1985 were a major component of green bands as their abundance was also strongly negatively correlated to the interannual variability of the max instant wind speed (Table 4). Lukas (1973) showed that green bands result from both a greater abundance of microborers, especially *Ostreobium* sp., and pigment content compared to white bands (see also Fine and Loya, 2002; Galindo-Martinez et al., 2022). Although we cannot exclude that green sulfur bacteria or other endolithic phototrophic microbes may have contributed to green band formation (Yang and Tang, 2019), our correlations computed on raw data tended to confirm the assumption of the influence of the temperature warming on the abundance of microborers, (Table 3). Nevertheless, this should be considered with caution, as the existence of a trend can induce significant correlations with no direct causal links. After 1985 the occurrence of green bands greatly increased, similarly to positive SSTA. The SSTA can either be the trigger for green bands, but with some delay as green bands seem to have formed generally during the winter season, or limit their expansion as most green bands have stopped when the summer season started. Anomalously warm temperatures are known to cause major coral bleaching events (Hughes et al., 2017). In the Western Indian Ocean, several

bleaching events have been reported: in 1983, 1998, 2005, 2007, 2010, and 2016 (Obura et al., 2018). It is interesting to note here that no green band was recorded at those periods except in 2016 (Table 4). The hypothesis stating that more light reaching boring microflora in corals during bleaching periods would lead to a bloom of these microorganisms and thus the formation of green bands (Fine and Loya, 2002; Carilli et al., 2010), is not supported by our results. The time scale is also different since bleaching events occurred over a few weeks while green bands lasted several months or years (Table 4). More coral cores from contrasted environments should be investigated to better understand the controlling factors of microborers abundance, their community composition, and the presence of green bands in living corals. Environmental factors such as seawater pH, DIC, and metal trace pollution could be good targets as these factors are known to affect microborer's abundance in dead carbonates (Tribollet et al., 2009; Cherchi et al., 2011; Reyes-Nivia et al., 2013).

5 Conclusion

The study of a coral core of the very slow-growing massive coral *Diploastrea* sp. revealed an unprecedented decrease in microborers abundance and a major shift in community composition over the last decades. Possible explanatory factors are ocean warming (both SST and SSTA), wind stress, precipitations, and cumulative insolation more or less combined, as well as the bulk density of the coral host. The direct or indirect effects of those factors on microboring communities need to be explored, especially that of global warming. The main cause of the shift and major decrease in microborers abundance in 1985 needs also to be determined. Mayotte showed a rapid increase in its demography since the 80's, especially since 2012 (+3.8%/year; INSEE), which may have greatly impacted the quality of the lagoon. Additionally, Gupta et al. (2020) reported an important marine heat wave in the Mozambique Channel around 1983. Other factors such as seawater pH and metal trace pollution which influence microborers abundance could also be involved. More coral cores of *Diploastrea* sp. and other massive species such as *Porites* from contrasted environments in the Western Indian Ocean should be studied to confirm the general trends observed here and to better understand their possible implications for coral health and resilience.

Data availability statement

The original data are presented here and in [Supplementary Material](#). Any further inquiries should be sent to the correspondent authors.

Author contributions

AT designed, coordinated and funded the project. AT and CL collected the coral core in Mayotte. DA and JB developed the innovative machine learning approach. DA prepared samples from the coral core, and obtained and analyzed the SEM images. He also collected all the environmental data and managed the statistical analyses with the help of AT and JB. GC, ED and MC developed a new approach to measure the skeleton density of massive corals. MC also prepared and analyzed coral standards. DA and FC measured the coral growth rate on both the X-ray radiograph (acquired by DA) and CT scan. DA, AT and JB interpreted the results and wrote the manuscript with the help of all co-authors. All authors contributed to the article and approved the submitted version.

Funding

The presented work was made possible thanks to several funding agencies which supported the project: INSU-CNRS-EC2CO-LEFE (program CARBODISS 2018-2020), IRD support through the laboratory LOCEAN (2019-2021), The University of Sorbonne (UPMC, Paris 6), the Marine Park Authority of Mayotte (2019-2020), The Belmont Forum International program (project OA-ME) and France Relance through The Office Français de la Biodiversité for the program Future Maore Reefs (2021-2023).

Acknowledgments

We would like to thank the following people for their help and assistance: Michel Guillemard, head of the company TSMOI (Reunion Island) for helping us collecting the coral core in Mayotte in October 2018, Sandrine Caquineau (IRD-France

Nord) for SEM training and collection, Thierry Pilorge (IRD-France Nord) for his help cutting the coral core and preparing samples for the observation of resin casts of microborings, Anne-Catherine Simon and Mathieu Agelou (CEA Gif-sur-Yvette) for the CT-scan of the coral core. Finally, we thank the Marine Park Authority of Mayotte and local authorities in Mayotte for making fieldwork possible, Antonella Pellecchia from the University of Bologna (Italy) for her contribution to the preparation of the first coral samples for SEM analysis, and François Guilhaumon for his suggestions regarding the statistical analyses.

Conflict of interest

The authors declare that the research was conducted in the absence of any commercial or financial relationships that could be construed as a potential conflict of interest.

Publisher's note

All claims expressed in this article are solely those of the authors and do not necessarily represent those of their affiliated organizations, or those of the publisher, the editors and the reviewers. Any product that may be evaluated in this article, or claim that may be made by its manufacturer, is not guaranteed or endorsed by the publisher.

Supplementary material

The Supplementary Material for this article can be found online at: <https://www.frontiersin.org/articles/10.3389/fmars.2022.899398/full#supplementary-material>

References

- Ainsworth, T. D., Fordyce, A. J., and Camp, E. F. (2017). The other microeukaryotes of the coral reef microbiome. *Trends Microbiol.* 25 (12), 980–991. doi: 10.1016/j.tim.2017.06.007
- Bentis, C. J., Kaufman, L., and Golubic, S. (2000). Endolithic fungi in reef-building corals (order: Scleractinia) are common, cosmopolitan, and potentially pathogenic. *Biol. Bull.* 198 (2), 254–260. doi: 10.2307/1542528
- Bornet, E., and Flahault, C. (1888). Note sur deux nouveaux genres d'algues perforantes. *J. Botanique Morot* 2, 161–165.
- Bucher, D. J., Harriott, V. J., and Roberts, L. G. (1998). Skeletal micro-density, porosity and bulk density of acroporid corals. *J. Exp. Mar. Biol. Ecol.* 228 (1), 117–136. doi: 10.1016/S0022-0981(98)00020-3
- Buddemier, R. W. (1974). Environmental controls over annual and lunar monthly cycles in hermatypic coral calcification. *Proc. Second Int. Coral Reef Symposium* 2, 259–267.
- Canesi, M. (2022). *Impacts of global change on massive porites and diploastrea corals across the pacific ocean* (Cambridge: University of Paris-Saclay), 212 pp.
- Carilli, J. E., Godfrey, J., Norris, R. D., and Sandin, S. A. (2010). Periodic endolithic algal blooms in *Montastraea faveolata* corals may represent periods of low-level stress. *Bull. Mar. Sci.* 86 (3), 709–718.
- Carreiro-Silva, M., McClanahan, T. R., and Kiene, W. E. (2005). The role of inorganic nutrients and herbivory in controlling microbioerosion of carbonate substratum. *Coral Reefs* 24 (2), 214–221. doi: 10.1007/s00338-004-0445-3
- Carreiro-Silva, M., McClanahan, T. R., and Kiene, W. E. (2009). Effects of inorganic nutrients and organic matter on microbial euendolithic community composition and microbioerosion rates. *Mar. Ecol. Prog. Ser.* 392, 1–15. doi: 10.3354/meps08251
- Chazottes, V., Le Campion-Alsumard, T., and Peyrot-Clausade, M. (1995). Bioerosion rates on coral reefs: Interactions between macroborers, microborers and

- grazers (Moorea, French Polynesia). *Palaeogeography Palaeoclimatology Palaeoecol.* 113 (2–4), 189–198. doi: 10.1016/0031-0182(95)00043-L
- Cherchi, A., Alessandri, A., Masina, S., and Navarra, A. (2011). Effects of increased CO₂ levels on monsoons. *Climate Dynamics* 37 (1–2), 83–101. doi: 10.1007/s00382-010-0801-7
- Chevalier, C., Devenon, J. L., Pagano, M., Rougier, G., Blanchot, J., and Arfi, R. (2017). The atypical hydrodynamics of the Mayotte lagoon (Indian ocean): Effects on water age and potential impact on plankton productivity. *Estuarine Coast. Shelf Sci.* 196 (September), 182–197. doi: 10.1016/j.ecss.2017.06.027
- Coulbaly, G. (2021). Développement de la mesure quantitative de la densité du squelette corallien par 3D-Tomographie à différentes résolutions spatiales. *Université de Paris*. (Paris) 42pp.
- Cuif, J. P., Dauphin, Y., Berthet, P., and Jegoudez, J. (2004). Associated water and organic compounds in coral skeletons: Quantitative thermogravimetry coupled to infrared absorption spectrometry. *Geochemistry Geophysics Geosystems* 5 (11), GC000783. doi: 10.1029/2004GC000783
- Cuny-Guirrec, K., Douville, E., Reynaud, S., Allemand, D., Bordier, L., Canesi, M., et al. (2019). Coral Li/Mg thermometry: Caveats and constraints. *Chem. Geology* 523 (September), 162–178. doi: 10.1016/j.chemgeo.2019.03.038
- DeCarlo, T. M., and Cohen, A. L. (2017). Dissepiments, density bands and signatures of thermal stress in *Porites* skeletons. *Coral Reefs* 36 (3), 749–761. doi: 10.1007/s00338-017-1566-9
- DeCarlo, T. M., Harrison, H. B., Gajdzik, L., Alaguarda, D., Rodolfo-Metalpa, R., D'Olive, J., et al. (2019). "Acclimatization of massive reef-building corals to consecutive heatwaves". *Proc. R. Soc. B: Biol. Sci.* 286 (1898), 20190235. doi: 10.1098/rspb.2019.0235
- Del Campo, J., Pombert, J. F., Šlapeta, J., Larkum, A., and Keeling, P. J. (2017). The 'other' coral symbiont: *Ostreobium* diversity and distribution. *ISME J.* 11 (1), 296–299. doi: 10.1038/ismej.2016.101
- Enochs, I. C., Manzello, D. P., Kolodziej, G., Noonan, S. H. C., Valentino, L., and Fabricius, K. E. (2016). Enhanced macroboring and depressed calcification drive net dissolution at high CO₂ coral reefs. *Proc. R. Soc. B: Biol. Sci.* 283 (1842), 20161742. doi: 10.1098/rspb.2016.1742
- Eyre, B. D., Cyronak, T., Drupp, P., De Carlo, E. H., Sachs, J. P., and Andersson, A. J. (2018). Coral reefs will transition to net dissolving before end of century. *Science* 359 (6378), 908–911. doi: 10.1126/science.aao1118
- Fine, M., Fine, E. F., and Hoegh-Guldberg, O. (2005). Tolerance of endolithic algae to elevated temperature and light in the coral *Montipora monasteriata* from the southern great barrier reef. *J. Exp. Biol.* 208 (1), 75–81. doi: 10.1242/jeb.01381
- Fine, M., and Loya, Y. (2002). Endolithic algae: An alternative source of photoassimilates during coral bleaching. *Proc. R. Soc. B: Biol. Sci.* 269 (1497), 1205–1210. doi: 10.1098/rspb.2002.1983
- Fordyce, A. J., Ainsworth, T. D., and Leggat, W. (2021). Light capture, skeletal morphology, and the biomass of corals' boring endoliths. *MSphere* 6 (1), e00060-21. doi: 10.1128/msphere.00060-21
- Galindo-Martinez, C. T., Weber, M., Avila-Magaña, V., Enriquez, S., Kitano, H., Medina, M., et al. (2022). The role of the endolithic alga *Ostreobium* spp. during coral bleaching recovery. *Sci. Rep.* 12 (1), 2977. doi: 10.1038/s41598-022-07017-6
- García-Pichel, F., Ramírez-Reinat, E., and Gao, Q. (2010). Microbial excavation of solid carbonates powered by p-type ATPase-mediated transcellular Ca²⁺ transport. *Proc. Natl. Acad. Sci. United States America* 107 (50), 21749–21754. doi: 10.1073/pnas.1011884108
- Gektidis, M. (1999). Development of microbial euendolithic communities: The influence of night and time. *Bull. Geological Soc. Denmark* 45, 147–150. doi: 10.37570/bgnd-1998-45-18
- Godinot, C., Tribollet, A., Grover, R., and Ferrier-Pagès, C. (2012). Bioerosion by euendoliths decreases in phosphate-enriched skeletons of living corals. *Biogeosciences* 9 (7), 2377–2384. doi: 10.5194/bg-9-2377-2012
- Golubic, S., Friedmann, I. E., and Schneider, J. (1981). The lithobiontic ecological niche, with special reference to microorganisms. *J. Sedimentary Res.* 51 (2), 475–478. doi: 10.1306/212F7CB6-2B24-11D7-8648000102C1865D
- Golubic, S., Schneider, J., Le Campion-Alsumard, T., Campbell, S. E., Hook, J. E., and Radtke, G. (2019). Approaching microbial bioerosion. *Facies* 65 (3), 25. doi: 10.1007/s10347-019-0568-1
- Goodfellow, I., Bengio, Y., and Courville, A. (2016). *Deep learning* (Cambridge, MA, USA: the MIT Press).
- Grange, J. S., Rybarczyk, H., and Tribollet, A. (2015). The three steps of the carbonate biogenic dissolution process by microborers in coral reefs (New Caledonia). *Environ. Sci. Pollut. Res.* 22 (18), 13625–13637. doi: 10.1007/s11356-014-4069-z
- Gupta, A. S., Thomsen, M., Benthuyzen, J. A., Hobday, A. J., Oliver, E., Alexander, L. V., et al. (2020). Drivers and impacts of the most extreme marine heatwave events. *Sci. Rep.* 10 (1), 19359. doi: 10.1038/s41598-020-75445-3
- Huang, B., Banzon, V. F., Freeman, E., Lawrimore, J., Liu, W., Peterson, T. C., et al. (2015). Extended reconstructed Sea surface temperature version 4 (ERSST.v4). part I: Upgrades and intercomparisons. *J. Climate* 28 (3), 911–930. doi: 10.1175/JCLI-D-14-00006.1
- Huang, B., Thorne, P. W., Banzon, V. F., Boyer, T., Chepurin, G., Lawrimore, J. H., et al. (2017). Extended reconstructed Sea surface temperature, version 5 (ERSSTv5): Upgrades, validations, and I-intercomparisons. *J. Climate* 30 (20), 8179–8205. doi: 10.1175/JCLI-D-16-0836.1
- Hughes, T. P., Anderson, K. D., Connolly, S. R., Heron, S. F., Kerry, J. T., Lough, J. M., et al. (2018). Spatial and temporal patterns of mass bleaching of corals in the anthropocene. *Science* 359 (6371), 80–83. doi: 10.1126/science.aan8048
- Hughes, T. P., Baird, A. H., Bellwood, D. R., Card, M., Connolly, S. R., Folke, C., et al. (2003). Climate change, human impacts, and the resilience of coral reefs. *Science* 301 (5635), 929–933. doi: 10.1126/science.1085046
- Hughes, T. P., Kerry, J. T., Álvarez-Noriega, M., Álvarez-Romero, J. G., Anderson, K. D., Baird, A. H., et al. (2017). Global warming and recurrent mass bleaching of corals. *Nature* 543 (7645), 373–377. doi: 10.1038/nature21707
- Iha, C., Dougan, K. E., Varela, J. A., Avila, V., Jackson, C. J., Bogaert, K. A., et al. (2021). Genomic adaptations to an endolithic lifestyle in the coral-associated alga *Ostreobium*. *Curr. Biol.* 31 (7), 1393–1402.e5. doi: 10.1016/j.cub.2021.01.018
- IPCC (2019). *Special report on the ocean and cryosphere in a changing climate* (Intergovernmental Panel on Climate Change). Available at: <https://www.ipcc.ch/srocc/chapter/summary-for-policymakers/>.
- Jeanson, M., Anthony, E. J., Dolique, F., and Cremades, C. (2014). Mangrove evolution in Mayotte island, Indian ocean: A 60 year synopsis based on aerial photographs. *Wetlands* 34 (3), 459–468. doi: 10.1007/s13157-014-0512-7
- Kleypas, J. A., and Langdon, C. (2006). *Coral reefs and changing seawater carbonate chemistry*. (Washington: American Geophysical Union) 73–110. doi: 10.1029/61CE06
- Knutson, D. W., Buddemeier, R. W., and Smith, S. V. (1972). Coral chronometers: Seasonal growth bands in reef corals. *Science* 177 (4045), 270–272. doi: 10.1126/science.177.4045.270
- Kobayashi, I., and Samata, T. (2006). Bivalve shell structure and organic matrix. *Materials Sci. Engineering: C* 26 (4), 692–698. doi: 10.1016/j.msec.2005.09.101
- Kolodziej, B., Golubic, S., Bucur, I. I., Radtke, G., and Tribollet, A. (2012). Early cretaceous record of microboring organisms in skeletons of growing corals. *Lethaia* 45 (1), 34–45. doi: 10.1111/j.1502-3931.2011.00291.x
- Krizhevsky, A., Sutskever, I., and Hinton, G. E. (2017). ImageNet classification with deep convolutional neural networks. *Commun. ACM* 60 (6), 84–90. doi: 10.1145/3065386
- Kühl, M., and Polerecky, L. (2008). Functional and structural imaging of phototrophic microbial communities and symbioses. *Aquat. Microbial Ecol.* 53 (September), 99–118. doi: 10.3354/ame01224
- Le Campion-Alsumard, T., Golubic, S., and Hutchings, P. (1995a). Microbial endoliths in skeletons of live and dead corals: *Porites lobata* (Moorea, French Polynesia). *Mar. Ecol. Prog. Ser.* 117 (1–3), 149–158. doi: 10.3354/meps117149
- Le Campion-Alsumard, T., Golubic, S., and Priess, K. (1995b). Fungi in corals: Symbiosis or disease? interaction between polyps and fungi causes pearl-like skeleton biomineralization. *Mar. Ecol. Prog. Ser.* 117, 137–147. doi: 10.3354/meps117137
- Lo Monaco, C., Metzl, N., Fin, J., Mignon, C., Cuet, P., Douville, E., et al. (2021). Distribution and long-term change of the sea surface carbonate system in the Mozambique channel (1963–2019). *Deep Sea Res. Part II: Topical Stud. Oceanography* 186–188 (May), 104936. doi: 10.1016/j.dsr2.2021.104936
- Lough, J. M., and Barnes, D. J. (1997). Several centuries of variation in skeletal extension, density and calcification in massive *Porites* colonies from the great barrier reef: A proxy for seawater temperature and a background of variability against which to identify unnatural change. *J. Exp. Mar. Biol. Ecol.* 211 (1), 29–67. doi: 10.1016/S0022-0981(96)02710-4
- Lough, J. M., and Cantin, N. E. (2014). Perspectives on massive coral growth rates in a changing ocean. *Biol. Bull.* 226 (3), 187–202. doi: 10.1086/BBLv226n3p187
- Lukas, K. J. (1973). *Taxonomy and ecology of the endolithic microflora of reef corals, with a review of the literature on endolithic microphytes* (Rhode Island: University Rhode Island), 318 pp.
- Lukas, K. J. (1974). Two species of the chlorophyte genus *Ostreobium* from skeletons of atlantic caribbean reef corals. *J. Phycology* 10 (3), 331–335. doi: 10.1111/j.1529-8817.1974.tb02722.x
- Magnusson, S. H., Fine, M., and Kühl, M. (2007). Light microclimate of endolithic phototrophs in the scleractinian corals *Montipora monasteriata* and *Porites cylindrica*. *Mar. Ecol. Prog. Ser.* 332 (March), 119–128. doi: 10.3354/meps332119
- Marcelino, V. R., and Verbruggen, H. (2016). Multi-marker metabarcoding of coral skeletons reveals a rich microbiome and diverse evolutionary origins of endolithic algae. *Sci. Rep.* 6 (1), 31508. doi: 10.1038/srep31508
- Massé, A., Domart-Coulon, I., Golubic, S., Duché, D., and Tribollet, A. (2018). Early skeletal colonization of the coral holobiont by the microboring ulvophyceae *Ostreobium* sp. *Sci. Rep.* 8 (1), 1–11. doi: 10.1038/s41598-018-20196-5

- Massé, A., Tribollet, A., Meziane, T., Bourguet-Kondracki, M., Yéprémian, C., Sève, C., et al. (2020). Functional diversity of microboring *Ostreobium* algae isolated from corals. *Environ. Microbiol.* 22 (11), 4825–4846. doi: 10.1111/1462-2920.15256
- McManus, L. C., Forrest, D. L., Tekwa, E. W., Schindler, D. E., Colton, M. A., Webster, M. M., et al. (2021). Evolution and connectivity influence the persistence and recovery of coral reefs under climate change in the caribbean, southwest pacific, and coral triangle. *Global Change Biol.* 27 (18), 4307–4321. doi: 10.1111/gcb.15725
- Mollica, N. R., Cohen, A. L., Alpert, A. E., Barkley, H. C., Brainard, R. E., Carilli, J. E., et al. (2018). Skeletal records of bleaching reveal different thermal thresholds of pacific coral reef assemblages. *Coral Reefs* 38 (6), 743–757. doi: 10.1007/s00338-019-01834-4
- Montagna, P., McCulloch, M., Douville, E., López Correa, M., Trotter, J., Rodolfo-Metalpa, R., et al. (2014). Li/Mg systematics in scleractinian corals: calibration of the thermometer. *Geochimica Cosmochimica Acta* 132 (May), 288–310. doi: 10.1016/j.gca.2014.02.005
- Nielsen, R., Petersen, G., Seberg, O., Daugbjerg, N., O'Kelly, C. J., and Wysor, B. (2013). Revision of the genus *Ulvella* (Ulvellaceae, ulvophyceae) based on morphology and *tufA* gene sequences of species in culture, with *Acrochaete* and *Pringsheimella* placed in synonymy. *Phycologia* 52 (1), 37–56. doi: 10.2216/11-067.1
- Obura, D. O., Bigot, L., and Benzon, F. (2018). Coral responses to a repeat bleaching event in Mayotte in 2010. *PeerJ* 6 (August), e5305. doi: 10.7717/peerj.5305
- Odum, H. T., and Odum, E. P. (1955). Trophic structure and productivity of a windward coral reef community on eniwetok atoll. *Ecol. Monogr.* 25 (3), 291–320. doi: 10.2307/1943285
- Perry, C. T., Steneck, R. S., Murphy, G. N., Kench, P. S., Edinger, E. N., Smithers, S. G., et al. (2014). Regional-scale dominance of non-framework building corals on caribbean reefs affects carbonate production and future reef growth. *Global Change Biol.* 21 (3), 1153–1164. doi: 10.1111/gcb.12792
- Pica, D., Tribollet, A., Golubic, S., Bo, M., Camillo, C. G. D., Bavestrello, G., et al. (2016). Microboring organisms in living stylasterid corals (Cnidaria, hydrozoa). *Mar. Biol. Res.* 12 (6), 573–825. doi: 10.1080/17451000.2016.1169298
- Priest, K., Le Campion-Alsumard, T., Thomassin, B. A., Golubic, S., and Gadel, F. (2000). Fungi in corals: Black bands and density-banding of *Porites lutea* and *Porites lobata* skeleton. *Mar. Biol.* 136 (1), 19–27. doi: 10.1007/s002270050003
- Reyes-Nivia, C., Diaz-Pulido, G., Kline, D., Hoegh-Guldberg, O., and Dove, S. (2013). Ocean acidification and warming scenarios increase microbioerosion of coral skeletons. *Global Change Biol.* 19 (6), 1919–1929. doi: 10.1111/gcb.12158
- Ricci, F., Marcelino, V. R., Blackall, L. L., Kühl, M., Medina, M., and Verbruggen, H. (2019). Beneath the surface: Community assembly and functions of the coral skeleton microbiome. *Microbiome* 7 (1), 159. doi: 10.1186/s40168-019-0762-y
- Risk, M. J., Sammarco, P. W., and Edinger, E. N. (1995). Bioerosion in *Acropora* across the continental shelf of the great barrier reef. *Coral Reefs* 14 (2), 79–86. doi: 10.1007/BF00303427
- Ronneberger, O., Fischer, P., and Brox, T. (2015). "U-Net: Convolutional networks for biomedical image segmentation," in *Medical image computing and computer-assisted intervention* (Cham: Springer), vol. 9351, , 234–241. doi: 10.1007/978-3-319-24574-4_28
- Salamon, K., and Boguslaw, K. (2021). Unravelling the microbiome of fossil corals: A message from microborings. *Historical Biol.* 00 (00), 1–12. doi: 10.1080/08912963.2021.1971213
- Salamon, K., Boguslaw, K., and Vadim, L. S. (2019). Simple methods for detection of microborings produced by coral-associated microendoliths. *Facies* 65 (2), 1–13. doi: 10.1007/s10347-019-0560-9
- Sangsawang, L., Casareto, B. E., Ohba, H., Vu, H. M., Meekaew, A., Suzuki, T., et al. (2017). ¹³C and ¹⁵N assimilation and organic matter translocation by the endolithic community in the massive coral *Porites lutea*. *R. Soc. Open Sci.* 4 (12), 171201. doi: 10.1098/rsos.171201
- Sauvage, T., Schmidt, W. E., Suda, S., and Fredericq, S. (2016). A metabarcoding framework for facilitated survey of endolithic phototrophs with *tufA*. *BMC Ecol.* 16 (1), 8. doi: 10.1186/s12898-016-0068-x
- Schätzle, P. K., Wisshak, M., Bick, A., Freiwald, A., and Kienke, A. (2021). Exploring confocal laser scanning microscopy (CLSM) and fluorescence staining as a tool for imaging and quantifying traces of marine microbioerosion and their trace-making microendoliths. *J. Microscopy* 284 (2), 118–131. doi: 10.1111/jmi.13046
- Schlichter, D., Kampmann, H., and Conrady, S. (1997). Trophic potential and photoecology of endolithic algae living within coral skeletons. *Mar. Ecol.* 18 (4), 299–317. doi: 10.1111/j.1439-0485.1997.tb00444.x
- Schlichter, D., Zscharnack, B., and Krisch, H. (1995). Transfer of photoassimilates from endolithic algae to coral tissue. *Naturwissenschaften* 82 (12), 561–564. doi: 10.1007/BF01140246
- Schoepf, V., Carrion, S. A., Pfeifer, S. M., Naugle, M., Dugal, L., Bruyn, J., et al. (2019). Stress-resistant corals may not acclimatize to ocean warming but maintain heat tolerance under cooler temperatures. *Nat. Commun.* 10 (1), 1–10. doi: 10.1038/s41467-019-12065-0
- Schönberg, C. H. L., Fang, J. K. H., Carreiro-Silva, M., Tribollet, A., and Wisshak, M. (2017). Bioerosion: the other ocean acidification problem. *ICES J. Mar. Sci.* 74 (4), 895–925. doi: 10.1093/icesjms/fsw254
- Schott, F. A., and McCreary, J. P. (2001). The monsoon circulation of the Indian ocean. *Prog. Oceanography* 51 (1), 1–123. doi: 10.1016/S0079-6611(01)00083-0
- Shashar, N., and Stambler, N. (1992). Endolithic algae within corals: Life in an extreme environment. *J. Exp. Mar. Biol. Ecol.* 163 (2), 277–286. doi: 10.1016/0022-0981(92)90055-F
- Taylor, P. D., and Jones, C. G. (1993). Skeletal ultrastructure in the cyclostome bryozoan *Hornera*. *Acta Zoologica* 74 (2), 135–143. doi: 10.1111/j.1463-6395.1993.tb01230.x
- Tribollet, A. (2008a). The boring microflora in modern coral reef ecosystems: A review of its roles. *Curr. Developments Bioerosion* 1974, 397–413. doi: 10.1007/978-3-540-77598-0
- Tribollet, A. (2008b). Dissolution of dead corals by euendolithic microorganisms across the northern great barrier reef (Australia). *Microbial Ecol.* 55 (4), 569–580. doi: 10.1007/s00248-007-9302-6
- Tribollet, A., Chauvin, A., and Cuet, P. (2019). Carbonate dissolution by reef microbial borers: A biogeological process producing alkalinity under different pCO₂ conditions. *Facies* 65 (2), 1–10. doi: 10.1007/s10347-018-0548-x
- Tribollet, A., Godinot, C., Atkinson, M., and Langdon, C. (2009). Effects of elevated pCO₂ on dissolution of coral carbonates by microbial euendoliths. *Global Biogeochemical Cycles* 23 (3), n/a–n/a. doi: 10.1029/2008GB003286
- Tribollet, A., and Golubic, S. (2011). "Reef bioerosion: Agents and processes," in *Coral reefs: An ecosystem in transition*, vol. 435–49. (Dordrecht: Springer Netherlands), doi: 10.1007/978-94-007-0114-4_25
- Tribollet, A., Langdon, C., Golubic, S., and Atkinson, M. (2006). Endolithic microflora are major primary producers in dead carbonate substrates of hawaiian coral reefs. *J. Phycology* 42 (2), 292–303. doi: 10.1111/j.1529-8817.2006.00198.x
- Tribollet, A., Pica, D., Puce, S., Radtke, G., Campbell, S. E., and Golubic, S. (2017). Euendolithic conchocelis stage (Bangiales, rhodophyta) in the skeletons of live stylasterid reef corals. *Mar. Biodiversity* 48 (4), 1855–1625. doi: 10.1007/s12526-017-0684-5
- Vacelet, E., Arnoux, A., and Thomassin, B. (1996). Particulate material as an indicator of pearl-oyster excess in the takapoto lagoon (Tuamotu, French Polynesia). *Aquaculture* 144 (1–3), 133–148. doi: 10.1016/S0044-8486(96)01323-3
- Verbruggen, H., and Tribollet, A. (2011). Boring algae. *Curr. Biol.* 21 (21), R876–R877. doi: 10.1016/j.cub.2011.09.014
- Vinayachandran, P. N. M., Masumoto, Y., Roberts, M. J., Huggett, J. A., Halo, L., Chatterjee, A., et al. (2021). Reviews and syntheses: Physical and biogeochemical processes associated with upwelling in the Indian ocean. *Biogeosciences* 18 (22), 5967–6029. doi: 10.5194/bg-18-5967-2021
- Wernberg, T., Smale, D. A., Frolicher, T. L., and Smith, A. J. P. (2021). Climate change increases marine heatwaves harming marine ecosystems. *ScienceBrief Crit. Issues Climate Change Sci.* doi: 10.5281/zenodo.5596820
- Wisshak, M. (2012). Microbioerosion. *Developments Sedimentology* 64, 213–243. doi: 10.1016/B978-0-444-53813-0.00008-3
- Wisshak, M., Tribollet, A., Golubic, S., Jakobsen, J., and Freiwald, A. (2011). Temperate bioerosion: Ichnodiversity and biodiversity from intertidal to bathyal depths (Azores). *Geobiology* 9 (6), 492–520. doi: 10.1111/j.1472-4669.2011.00299.x
- Wu, H. C., Dissard, D., Douville, E., Blamart, D., Bordier, B., Tribollet, A., et al. (2018). Surface ocean pH variations since 1689 CE and recent ocean acidification in the tropical south pacific. *Nat. Commun.* 9 (1), 1–13. doi: 10.1038/s41467-018-04922-1
- Yang, S. H., Lee, S. T. M., Huang, C. R., Tseng, C. H., Chiang, P. W., Chen, C. P., et al. (2016). Prevalence of potential nitrogen-fixing, green sulfur bacteria in the skeleton of reef-building coral *Isopora palifera*. *Limnology Oceanography* 61 (3), 1078–1086. doi: 10.1002/lno.10277
- Yang, S. H., and Tang, S. L. (2019). Endolithic microbes in coral skeletons: Algae or bacteria? *Symbiotic Microbiomes Coral Reefs Sponges Corals*, 43–53. doi: 10.1007/978-94-024-1612-1_4
- Zinke, J., Hoell, A., Lough, J. M., Feng, M., Kuret, A. J., Clarke, H., et al. (2015). Coral record of southeast indian ocean marine heatwaves with intensified western pacific temperature gradient. *Nat. Commun.* 6 (1), 8562. doi: 10.1038/ncomms9562
- Zinke, J., Pfeiffer, M., Timm, O., Dullo, W. C., Kroon, D., and Thomassin, B. A. (2008). Mayotte Coral reveals hydrological changes in the western indian ocean between 1881 and 1994. *Geophysical Res. Lett.* 35 (23), L23707. doi: 10.1029/2008GL035634

4.3 Effects of pH on the Abundance and Composition of Microbioeroding Communities in *Diploastrea* sp.

4.3.1 Introduction

Over the pre-industrial era, one-third of the anthropogenic CO₂ emissions have been absorbed by the ocean, driving a decline of about 0.1 units in seawater pH Feely et al., 2009; Friedlingstein et al., 2022, a phenomenon commonly known as OA, a process that affects and changes the seawater carbonate chemistry (Kleypas and Langdon, 2006; Guinotte and Fabry, 2008). These major changes in seawater carbonate chemistry and saturation state Ω for aragonite (or calcite) would lead to serious damage in calcifying organisms' biomineralization processes that need carbonate ions to secrete their calcareous skeleton. For corals, the overall documented impacts are the lowering of their skeletal density (soft calcareous skeleton), reduced rates of their calcification or their vertical extension (Gattuso and Hansson, 2011; M. McCulloch et al., 2012; T. M. DeCarlo et al., 2015; D'Olive et al., 2019). Nonetheless, all corals are not affected the same way by increased levels of OA with tolerant taxa and sensitive ones (e.g., massive vs. branching corals, Hughes et al., 2017; T. M. DeCarlo et al., 2019). Scleractinian corals precipitate their calcium carbonate skeleton from an extracellular CF (Allemand et al., 2004) located at the interface between the living polyp and the aragonite skeleton (Tambutté et al., 2011; Comeau et al., 2017). Evidence suggests that seawater is the initial source of the CF (Cohen and McConnaughey, 2003; Tambutté et al., 2011; Gagnon et al., 2012), also strongly influenced by biological processes (Ca²⁺ ATP-ase pump) that regulate the carbonate chemistry of the calcifying medium (Cohen and McConnaughey, 2003; Allemand et al., 2004). Skeletal geochemical analyses enable us to evaluate the corals' ability to calcify and grow over time. The CF reflects ambient seawater properties (e.g., temperature, pH), the chemical composition (i.e., boron abundance and speciation), and physiological 'controls' exerted by the coral. Laboratory experiments and field measurements show a wide variation in the response of corals to calcify at species and ecosystem levels (Fabricius, 2011; Chan and Connolly, 2013). This large variability observed at the inter-species level shows that the carbonate chemistry properties of seawater are not the only factors that affect the calcification process in corals. The chemical composition of the coral CF is sensitive but not identical to that of the surrounding seawater due to the species-dependent physiological

regulation (M. McCulloch et al., 2012; Comeau et al., 2018).

The boron isotopic composition ($\delta^{11}B$) and B/Ca ratio of aragonite skeletons can be used as a powerful tool (i.e., proxies) to determine and reconstruct carbonate chemistry changes in the CF (e.g., pH_{CF} , DIC_{CF} , Ω_{CF}) by using established relationships (Holcomb et al., 2014; T. DeCarlo et al., 2018). Tropical corals have been successfully utilized to reconstruct ocean pH at seasonal to millennial timescales (Wu et al., 2018; H.-Z. Wei et al., 2021). Species of massive *Porites* corals have been widely investigated for reconstructing seasonal changes in the composition of their CF since they are long-lived. More importantly, the architecture of their skeleton has a relatively straightforward chronology that facilitates well-constrained timing of their skeletal growth at seasonal resolution (J. Lough and Cantin, 2014; M. T. McCulloch et al., 2017). Only Wu et al. (2018) investigated a very long record of the massive coral *Diploastrea heliopora* of New Caledonia in the South Pacific Ocean, providing more than 300 years of ($\delta^{11}B$) with estimated seawater pH decreasing trend since the Industrial Revolution. Recently, in her thesis, Canesi (2022) investigated the responses of CF composition and growth/-calcification parameters of two genera of massive corals (*Porites* and *Diploastrea*) exposed to various natural seawater changes across the tropical Pacific Ocean over the period 2010-2016. The geochemical analyses of the modern coral skeleton (B/Ca and $\delta^{11}B$) were used to reconstruct the chemical properties of the CF of both massive corals (pH_{CF} , DIC_{CF} , Ω_{CF} ; CO_3^{2-} $_{CF}$). Her results suggest that both genera modulate the chemical composition of their CF compared to ambient seawater carbonate chemistry with biological genus-specific mechanisms (e.g., metabolic efficiency, photosynthetic rates, tissue thickness, reproduction cycles, growth). Such results were also previously mentioned by authors that proved that corals' physiological regulation to modulate their CF chemistry was species or genus-dependent (Ross et al., 2019; Comeau et al., 2019). Though $\delta^{11}B$ pH records were limited to a few oceanic regions/sectors in the Pacific Ocean, the increasing number of coral records in recent years from the Atlantic Ocean and the Indian Ocean offer an excellent opportunity to address OA as regional perspectives between the different oceanic basins vs. global trends (Tarique and Rahman, 2022). For instance, Lauvset et al. (2015) estimated that the fastest seawater pH decline occurred in the Indian Ocean over the 1991-2011 period compared to the different oceanic basins (i.e. -0.0024.yr). Additionally, Lo Monaco et al. (2021) observed a large decrease in seawater pH (mean decrease of -0.104, period 1963-2019) for all sectors of the MC (e.g., Mayotte), including near coral reef areas in the Eparses

Islands (Europa, Juan de Nova), which might put coral reef ecosystems of the area at risk. Therefore, as the chemical properties of the CF are coral genus-dependent, they are also dependent on the seawater carbonate chemistry of the oceanic region considered.

Scleractinian corals have diverse ecological micro-niches shaped by physico-chemical gradients across the various tissue and skeleton compartments (Shashar and Stambler, 1992; Kühl et al., 2008; M. Magnusson et al., 2010). These gradients are affected by the environment surrounding the coral holobiont (Reyes-Nivia et al., 2013; Massé et al., 2018), the skeletal microstructure (Falini et al., 2015; L. A. Marcelino et al., 2013), and the physiology of holobiont members, such as microbioeroding communities. For instance, the autotrophic metabolism of photosynthetic endoliths such as *Ostreobium* sp. can be responsible for increasing pH in the medium. This process substantially influences the internal skeletal pH more than the outside environment (Shashar and Stambler, 1992), where the dissolution process of the calcium carbonate by microbioeroding communities increases pH and the total alkalinity of the system (Tribollet et al., 2019). Recently, Alaguarda et al., 2022 investigated a well-preserved coral core of the slow-growing coral *Diploastrea* sp. from Mayotte in the WIO but did not look into the carbonate chemistry of the coral (e.g., pH_{CF}). Based on the investigations of seawater pH in the Indian Ocean, and mainly from the MC, one primary hypothesis would be to find a decrease within the internal pH_{CF} of the *Diploastrea* sp. coral due to the increased OA observed over the years in the area (Monaco et al., 2021). On the other hand, some studies have investigated the effects of OA on CaCO_3 dissolution rates and how it could enhance bioerosion processes from different agents. For instance, in dead carbonate substrates, OA can positively drive the activity of some bioeroding agents (e.g., micro and macroborers (Tribollet et al., 2009; Enochs, Manzello, Tribollet, et al., 2016; Tribollet et al., 2019)). Microborers employ exclusively chemical bioerosion, where OA is thought to ease this latter process via reduced alkalinity and pH directly. It is furthermore assumed to indirectly accelerate bioerosion by stimulating energy capture in phototrophic bioeroders and making mechanical bioerosion more effective by “softening” the carbonate substrate (e.g., Tribollet et al., 2009). Nonetheless, investigations were only performed in dead carbonate substrates and bear the limitation of short-term data. Alaguarda et al. (2022) were the first to provide a long record (i.e. 54 years) of the abundance and composition of microbioeroding traces over the lifespan

of a coral host. The main results were to observe a significant decrease in the abundance of microbioeroding traces over time with a community shift identified. Possible explanatory factors were the combination of various environmental influences (e.g., SST, wind stress, cumulative insolation) and the significant decrease in the coral host bulk density. Therefore, to supplement the findings published by Alaguarda et al., 2022 on the abundance of microbioeroding traces over the last 54 years, the pH_{CF} from the living coral *Diploastrea* sp. from Mayotte was investigated : (i) to determine the evolution of the internal pH_{CF} over time within *Diploastrea* in this context of OA recently assessed within the MC (Monaco et al., 2021) (ii) to identify the interactions of the pH_{CF} with the environment and coral variables previously discussed by Alaguarda et al., 2022 and (iii) to understand the potential effects of the internal pH_{CF} on the decrease of the abundance of microborers in the coral *Diploastrea* sp. over time (e.g., thin, wide or all microbioeroding traces).

4.3.2 Methodologies

Here two paleo pH reconstructions were assessed. One reconstruction was based on the instrumental SST dataset from the ERSST (v5) corrected with an offset of SST of the Parc Marin from Mayotte (**Appendix Section 8.2 Table 6 and 7**). The second pH reconstruction was based on paleo-SST reconstructions developed by Canesi et al. (2022) at the LSCE, defined with the proxy Sr/Ca and Li/Mg (**Equation 2.2**). The methodologies of the reconstruction of pH_{CF} are explained in the **Chapter 2 section 2.2.3** through the boron isotope systems with the equation presented (**Equation 2.3**). Regarding pH investigations, statistical analyses were performed. The non-parametric Mann-Kendall test was performed on each pH_{CF} reconstruction (instrumental and reconstructed) to assess if the observed trend was significant. Linear regressions on pH data were generated from the library *ggpubr* on RStudio (v1.4.17; <https://www.rstudio.com>). Pearson correlations were carried out to detect the potential interactions of pH with the environmental and/or coral variables and the effects with the traces' abundance (i.e., the abundance of thin microborings, wide, or all microborings) obtained over the last five decades. These correlations were performed on un-detrended and detrended variables to focus on their possible interannual and decadal variability and to avoid spurious correlations due to linear trends. Finally, a non-parametric Pettitt test was applied to both pH reconstructions to determine a potential breakpoint in the trend over the last 54 years.

4.3.3 Results

4.3.3.1 Evolution of the internal pH of *Diploastrea* over 54 years

As mentioned in the **Section 2.2.3**, two approaches were investigated for analyzing the variability of the internal pH of the *Diploastrea* sp. coral. First, pH reconstructions were based on instrumental SST from the ERSST dataset(v5) (called pH_{CF} Instrumental later) and then from SST reconstruction with the multi-element SST calibration for multi-genera *Porites* sp. and *Diploastrea* sp. developed by Canesi et al. (2022) (called pH_{CF} Paleo-Proxy later). The internal pH_{CF} of *Diploastrea* sp. coral from both reconstructions showed a similar and significant annual variability over the last five decades ($p < 0.0001$, Mann Kendall test; **Figure 4.1**). Both reconstructed pHs calculated from the different SST products display the same variability over time.

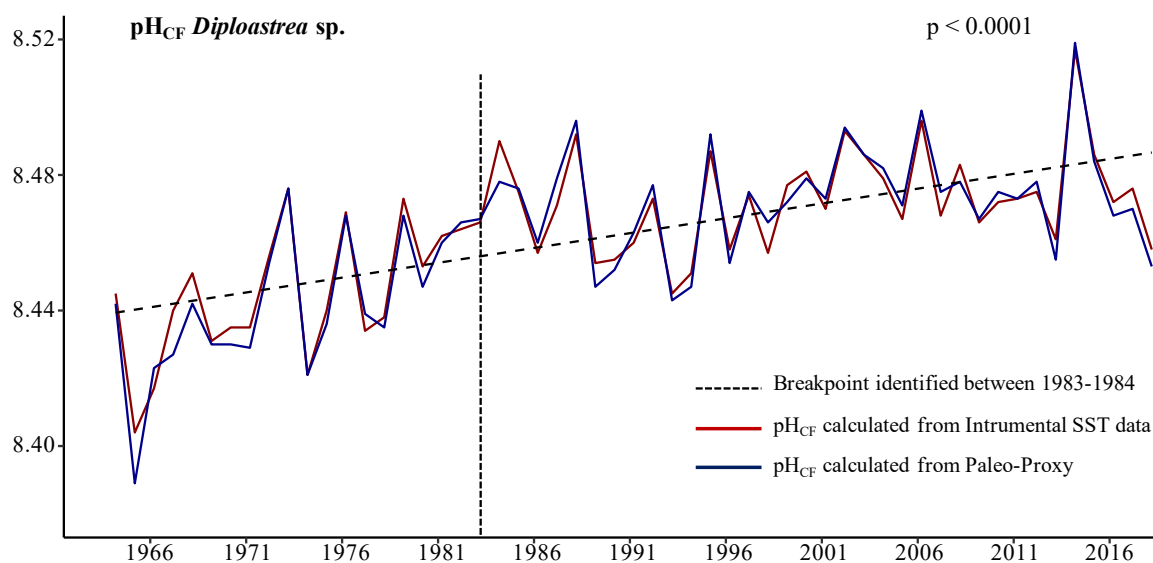


Figure 4.1: Interannual variability of the internal pH_{CF} of *Diploastrea* sp. at Mayotte between 1964 and 2018 reconstructed based on the instrumental SST (red line) and the paleo-proxy (blue line). The black dotted line indicates the pH_{CF} breakpoint.

Mayotte *Diploastrea* sp. coral experienced a significant increase in its pH_{CF} with an estimated pH_{CF} increase of +0.001 per decade ($p < 0.0001$, Mann Kendall test). The pH_{CF} was comprised between 8.39 (in 1965) and 8.52 (in 2014) with an average value of 8.46 ± 0.02 (**Figure 4.1**). Interestingly, a breakpoint in the pH_{CF}' evolution over the last five decades in the *Diploastrea* sp. coral was also highlighted. This breakpoint was identified between 1983 and 1984 (Pettit test, $p < 0.001$).

4.3.3.2 Internal pH and Abiotic Variables

Correlations were investigated between the environmental variables discussed by Alaguarda et al. (2022) and the reconstructed pH_{CF} for different periods based on the breakpoint identified of the community shift of microbioeroding communities. Firstly, the environmental variables' raw dataset (no detrended) was investigated with both reconstructed pH_{CF} . Considering the period 1964-2018, both reconstructed pH_{CF} (instrumental and paleo-proxy) were positively correlated with the instrumental SST/SSTA and the Max Instant Wind Speed ($p < 0.001$). Reconstructed pH_{CF} were also negatively correlated to the Cumulative Insolation ($p < 0.01$ and 0.05) (**Table 4.1**).

Table 4.1: Pearson's correlations between the raw reconstructed pH_{CF} and the environmental variables over the last 54 years, per period before or after the breakpoint investigated by Alaguarda et al., 2022. Code for significance: $\# < 0.1$; $* < 0.05$; $** < 0.01$; $*** < 0.001$; NS is for non significant.

Abiotic Variables	pH_{CF} Instrumental	pH_{CF} Paleo-proxy
	Period 1964-2018	
Instrumental SST (ERSST v5)	0.425**	0.522***
Instrumental SSTA (climatology 1971-2001)	0.439***	0.513***
Precipitations	NS	NS
Max Instant Wind Speed	0.484***	0.496***
Cumulative Insolation	-0.378**	-0.340*
	Period 1964-1985	
Instrumental SST (ERSST v5)	NS	0.458*
Instrumental SSTA (climatology 1971-2001)	NS	0.424*
Precipitations	NS	NS
Max Instant Wind Speed	NS	NS
Cumulative Insolation	0.497*	0.578**
	Period 1986-2018	
Instrumental SST (ERSST v5)	0.326* $\#$	0.395*
Instrumental SSTA (climatology 1971-2001)	NS	NS
Precipitations	NS	NS
Max Instant Wind Speed	NS	NS
Cumulative Insolation	-0.427*	-0.333* $\#$

Interestingly, for the period 1964-1985, reconstructed pH_{CF} were positively correlated to the cumulative insolation ($p < 0.01$ and 0.05). The positive correlation with the instrumental SST/SSTA was still observed but only for the pH_{CF} from the paleo-proxy ($p < 0.05$).

When considering the period 1986-2018, the SST was positively correlated with reconstructed pH_{CF} ($p < 0.05$). Again a negative correlation was observed between the pH_{CF} and the cumulative insolation ($p < 0.05$ and $p < 0.1$). Some events might have happened before and after 1985 that could be responsible for the changing correlation with the cumulative correlation (to discuss later). Surprisingly, no correlations were observed between the Max instant wind speed and pH_{CF} when both periods are considered separately.

A similar analysis was conducted on the detrended environmental variables discussed by Alaguarda et al. (2022) and the detrended reconstructed pH for the different periods. Considering the period 1964-2018, the pH_{CF} instrumental was correlated to neither environmental variables. Only the detrended pH_{CF} instrumental was positively correlated with the detrended instrumental SST ($p < 0.5$).

Interestingly, for the period 1964-2018, a positive correlation was still observed between the detrended cumulative insolation and the detrended reconstructed pH_{CF} ($p < 0.05$). For the period 1986-2018, no correlations were to be observed between detrended environmental variables and the pH_{CF} (see **Table 4.2**).

Table 4.2: Pearson's correlations between the detrended pH reconstructions and the detrended environmental variables over the last 54 years, per period before or after the breakpoint investigated by Alaguarda et al., 2022. $^{\#} < 0.1$; $* < 0.05$; $** < 0.01$; $*** < 0.001$; NS is for non significant.

Abiotic Variables	pH_{CF} Instrumental	pH_{CF} Paleo-proxy
	Period 1964-2018	
Instrumental SST (ERSST v5)	NS	0.275*
Instrumental SSTA (climatology 1971-2001)	NS	NS
Precipitations	NS	NS
Max Instant Wind Speed	NS	NS
Cumulative Insolation	NS	NS
Period 1964-1985		
Instrumental SST (ERSST v5)	NS	NS
Instrumental SSTA (climatology 1971-2001)	NS	NS
Precipitations	NS	NS
Max Instant Wind Speed	NS	NS
Cumulative Insolation	0.534*	0.616*
Period 1986-2018		
Instrumental SST (ERSST v5)	NS	NS
Instrumental SSTA (climatology 1971-2001)	NS	NS
Precipitations	NS	NS
Max Instant Wind Speed	NS	NS
Cumulative Insolation	NS	NS

4.3.3.3 Internal pH and Biotic Variables

Correlations were also investigated between the coral variables, the abundance of the microbioeroding traces (total, wide, and thin) discussed by Alaguarda et al. (2022), and the reconstructed pH_{CF} for different periods based on the breakpoint identified of the community shift of microbioeroding communities. Firstly, the coral and abundance variables' (not detrended) raw dataset was investigated with both reconstructed pH_{CF} . Considering the period 1964-2018, reconstructed pH_{CF} was negatively correlated with the abundance of total microbioeroding traces ($p < 0.01$), even more with the abundance of wide microbioeroding traces ($p < 0.001$) (see **Table 4.3**). No correlations were observed with the abundance of the thin traces or the vertical extension of the coral. A

negative correlation was observed between reconstructed pH_{CF} and the coral skeletal density ($p < 0.01$). A slight negative correlation was also observed with the calcification rate ($p < 0.05$ and $p < 0.1$).

When focusing on the period 1964-1985, the negative correlation between reconstructed pH_{CF} and the abundance of wide microbioeroding traces was still observed ($p < 0.01$ and $p < 0.05$). Interestingly, a slight positive correlation was observed between the reconstructed pH_{CF} and the abundance of the thin microbioeroding traces ($p < 0.05$ and $p < 0.1$). Negative correlations were still present between reconstructed pH_{CF} with the coral skeletal density ($p < 0.01$) and the calcification rate ($p < 0.05$).

When considering the period 1986-2018, no correlations were observed between reconstructed pH_{CF} and coral variables and the abundance of microbioeroding traces.

Table 4.3: Pearson's correlations between the raw pH reconstructions and the abundance of microborers (wide, thin, or total) and coral growth variables over the last 54 years, per period before or after the breakpoint investigated by Alaguarda et al., 2022. $^{*#} < 0.1$; $^{*} < 0.05$; $^{**} < 0.01$; $^{***} < 0.001$; NS is for non significant.

Biotic Variables	pH _{CF} Instrumental	pH _{CF} Paleo-proxy
	Period 1964-2018	
Abundance total microbioerodings traces	-0.430**	-0.424**
Abundance wide microbioerodings traces	-0.662***	-0.676***
Abundance thin microbioerodings traces	NS	NS
Vertical Extension Rate	NS	NS
Skeletal Bulk Density	-0.351**	-0.345**
Calcification Rate	-0.247* [#]	-0.277*
Period 1964-1985		
Total microbioerodings Abundance	NS	NS
Wide microbioerodings Abundance	-0.519*	-0.543**
Thin microbioerodings Abundance	0.396* [#]	0.472*
Vertical Extension Rate	NS	NS
Skeletal Bulk Density	-0.541**	-0.542**
Calcification Rate	-0.444*	-0.474*
Period 1986-2018		
Total microbioerodings Abundance	NS	NS
Wide microbioerodings Abundance	NS	NS
Thin microbioerodings Abundance	NS	NS
Vertical Extension Rate	NS	NS
Skeletal Bulk Density	NS	NS
Calcification Rate	NS	NS

A similar analysis was conducted on the detrended coral and abundance variables discussed by Alaguarda et al. (2022) with the detrended reconstructed pH for the different periods. Considering the period 1964-2018, the pH_{CF} was slightly negatively correlated to the abundance of the wide microbioeroding traces ($p < 0.05$ and $p < 0.1$). The opposite was observed with the abundance of the thin microbioeroding traces, slight negatively correlated with reconstructed pH_{CF} ($p < 0.05$ and $p < 0.1$).

For the period 1964-2018, only a slight positive correlation was observed between re-

constructed pH_{CF} and the abundance of the thin microbioeroding traces ($p < 0.1$). For the period 1964-2018, only a slight negative correlation was observed between reconstructed pH_{CF} and the abundance of the wide microbioeroding traces ($p < 0.1$). Finally, considering all different periods, no correlations were observed between both reconstructed pH_{CF} and any of the coral growth variables (see **Table 4.4**).

Table 4.4: Pearson's correlations between the detrended pH reconstructions and the detrended abundance of microborers (wide, thin, or total), coral growth variables over the last 54 years, per period before or after the breakpoint investigated by Alaguarda et al., 2022. $^{*#} < 0.1$; $* < 0.05$; $** < 0.01$; $*** < 0.001$; NS is for non significant.

Biotic Variables	pH _{CF} Instrumental	pH _{CF} Paleo-proxy
	Period 1964-2018	
Total microbioerodings Abundance	NS	NS
Wide microbioerodings Abundance	-0.253 ^{*#}	-0.285 [*]
Thin microbioerodings Abundance	0.259 ^{*#}	0.290 [*]
Vertical Extension Rate	NS	NS
Skeletal Bulk Density	NS	NS
Calcification Rate	NS	NS
Period 1964-1985		
Total microbioerodings Abundance	NS	NS
Wide microbioerodings Abundance	NS	NS
Thin microbioerodings Abundance	0.390 ^{*#}	0.420 ^{*#}
Vertical Extension Rate	NS	NS
Skeletal Bulk Density	NS	NS
Calcification Rate	NS	NS
Period 1986-2018		
Total microbioerodings Abundance	NS	NS
Wide microbioerodings Abundance	-0.295 ^{*#}	-0.331 ^{*#}
Thin microbioerodings Abundance	NS	NS
Vertical Extension Rate	NS	NS
Skeletal Bulk Density	NS	NS
Calcification Rate	NS	NS

4.3.4 Discussion

4.3.4.1 Comparison of Instrumental and Paleo-Proxy pH Reconstructions

The internal pH_{CF} investigations provided supplemental information regarding the study of Alaguarda et al. (2022) of the coral *Diploastrea* sp. and its possible influence on microbioeroding communities. First, two methods were investigated for the reconstruction of the pH. One was based on instrumental SST of satellite data, and the other from the combination of geochemical proxies Sr/Ca and Li/Mg (Canesi, 2022). Both pH_{CF} signals (instrumental and paleo-proxy) described the same trends and evolution over time with small variations (**Figure 4.1**). The quality of the coral-based calibrations used to reconstruct past seawater temperatures, used later for the pH reconstructions, depends on different factors such as the analytical uncertainty from the machine (ICP-MS), and the choice of the SST database used for the calibrations (here ERSST v5). The

variations observed between both pH_{CF} signals can also be explained by the geochemical signal of the aragonite skeleton of modern corals can be altered by different early and post-depositional diagenetic processes (e.g., bioerosion, dissolution, secondary aragonite, and calcite precipitation, replacement of aragonite by calcite). Also, it can be explained by the presence of organic matter, as in the green bands often observed in massive tropical corals, indicative of microborers (Lukas, 1973; Nothdurft and Webb, 2009; Cuny-Guirriec et al., 2019). For instance, early diagenetic intra-skeletal calcite has a lower Sr/Ca and Li/Mg composition than that of skeletal aragonite (Sayani et al., 2011; Lazareth et al., 2016), which could significantly impact the temperature reconstructions and could explain part of the uncertainties/variations associated with the pH reconstruction via SST estimated with the paleo-proxy compared to the instrumental one. Also, one potential source of error in the proxy calibration is the difference between the real temperature experienced by the coral during its life and the temperature selected for the calibration. The *in situ* temperatures are usually the best approach since the temperature of the sensor is located nearby the coral colony and reflects the ambient temperature of the reef (Castillo and Lima, 2010; Canesi, 2022). Overall, pH reconstructions based on two different SSTs products described the same evolution over time, showing the relevance of the multi-element proxy approach Sr/Ca and Li/Mg for robust paleo reconstructions (Canesi, 2022).

4.3.4.2 *Diploastrea* sp. Internal pH : A Particular Signal ?

Surprisingly, one result that was not expected was to assess an increase of the pH_{CF} of the coral *Diploastrea* sp. from Mayotte over the last 54 years. Such findings represent a very particular signal as oceanic regions around the globe displayed an overall decrease in the seawater pH (Feely et al., 2004; Doney et al., 2009). An even more significant decrease in the seawater pH was estimated within the Indian Ocean compared to the other oceanic regions (Lauvset et al., 2015). Even closely within the area where the coral *Diploastrea* sp. was collected, Lo Monaco et al. (2021) reported oceanic carbonate system observations (pH, alkalinity, DIC, $f\text{CO}_2$) in the MC and estimated long-term pH trends over the period 1963-2019 (in the range of the coral chronology reconstruction). Their results highlighted overall changes in the carbonate system in the MC at a regional scale. They concluded that the anthropogenic CO_2 emissions were responsible for the significant acidification in surface waters. The authors reconstructed pH

changes back to the pre-industrial period and estimated that pH in the MC was about 8.18 (± 0.014), i.e., 0.13 higher than in 2019. Even if the focus of their study was not on the island of Mayotte, they concluded with a general decrease in the seawater pH within the MC. Nonetheless, as a hypothesis, the reconstructed seawater pH would also show an increasing trend over time as seawater pH is estimated through a calculation implying pH_{CF} (D'Olive et al., 2019; X. Chen et al., 2019). Most of the reconstruction of seawater pH is based on massive *Porites* sp. corals (M. McCulloch et al., 2012). In the absence of a general calibration equation, species-specific calibration for *Porites cylindrica* has been used in several studies from the Atlantic, Pacific, and Indian oceans (G. Wei et al., 2015; S. Fowell et al., 2018; Tarique and Rahaman, 2022). On the other hand, reconstruction of seawater pH based on *Diploastrea* sp. is scarce and has only been investigated by Wu et al. (2018) from a coral of the South Pacific Ocean. A preliminary result (not presented here) has consisted in reconstructing the seawater pH based on the equation from Wu et al. (2018) for the *Diploastrea heliophora* of the South Pacific Ocean. The results of the supposed reconstructed seawater pH for the *Diploastrea* sp. of Mayotte ranged from 7.70 and 8.01, characterizing important acidic conditions of the seawater (7.70 being pH prediction for the worst scenario of the IPCC, Allan et al., 2021). Therefore, this calibration and equation for seawater pH based on *Diploastrea heliophora* suggest limitations when applied to the *Diploastrea* sp. from Mayotte. First, calibrations based on *Diploastrea* sp. are too scarce and need further investigations to be robust as *Porites* sp. Such variations observed in the reconstructed seawater pH might also come from the oceanic region considered. As the surface ocean pH is influenced by multiple parameters such as atmospheric CO₂, temperature, biological productivity, the ocean circulation, and oscillations specific to the basin (e.g., ENSO, IOD for the Indian Ocean), upwelling and mixing of the water column, it is imperative to have species-specific calibration in regard of the coral investigated and also adapted to the oceanic region considered, to calculate the seawater pH from the pH_{CF} accurately. The WIO is characterized by a wind-driven circulation where the warming and cooling of SST play an important role in pH seasonality (Cao et al., 2007 Kapsenberg et al., 2017). The dominance of SST in the seasonal pH cycle in this region indicates a clear role of the solubility pump in the carbon cycle as opposed to the biological pump (Valsala et al., 2012). Such regions also display important monthly pH variability from one season to another (+0.04 see R7 in Figure 3 from Madkai et al., 2023). This can be explained by the mixed layer deepening of these regions during austral winter. The

deepening of the mixed layer entrains the subsurface DIC to the surface, modifying the pH seasonal cycle. The maximum enhancement happens in the southernmost regions (Eparses Islands) where mixing is further expected to be important (i.e., eddies circulation, upwelling) (Mawren, Hermes, et al., 2022; Vinayachandran et al., 2021). Nonetheless, such potential explanation here may apply to seasonal/annual pH variations and might differ for decadal and long-term pH' variability (e.g., 54 years), where such changes in pH within this area remain to be further explored. Investigations regarding pH changes in the open ocean of the WIO but also near coastal areas where coral reef ecosystems are present need to be realized to predict the latter's resilience in this rapidly changing climate (i.e., OA and warming).

Hence, one question to address now would be to understand better the reasons for such elevation of the pH_{CF} of the coral *Diploastrea* sp. in Mayotte over the last 54 years. Additionally, to assess if such elevation could have been observed in other oceanic regions. Recently, Chen et al. (2019) investigated century-long temperature (Sr/Ca and Li/Mg) and CF carbonate chemistry ($\delta^{11}\text{B}$ and B/Ca) records for a long-lived (1919 to 2016) *Porites* coral from the Kimberley Region (Eastern Indian Ocean, Australia). They investigate how increasing temperatures and OA were manifested in the carbonate chemistry of coral's CF and the impacts of climate change on calcification processes. Interestingly, they highlighted for the period 2000-2016 between summer and winter that the coral's pH_{CF} and Ω_{CF} remain elevated and even show an increasing trend over this period (only for the pH_{CF}). Therefore, the saturation state and calcification rate exhibited only relatively small disturbances from increasing temperatures (see Figures 5 and 6 in X. Chen et al., 2019). This is consistent with previous field and culture experiment observations that corals can regulate CF carbonate chemistry to maintain a favorable metabolism environment under extreme temperatures or acidic seawater carbonate chemistry conditions (Comeau et al., 2018; Ross et al., 2019). Overall, over the period 1919-2016, the pH_{CF} of *Porites* coral decreased and could be a result of OA, induced by lower pH in the external seawater environment (Holcomb et al., 2014; T. DeCarlo et al., 2018; Kubota et al., 2017). Nonetheless, pH_{CF} remained at an elevated level even under the influence of OA, helping to keep elevated and near constant levels of Ω_{cf} , highlighting the ability of coral to continue to manipulate its physiological control of the internal carbonate chemistry to promote calcification process (see Figures 5 and 6 in X. Chen et al., 2019). Hence, based on these findings from *Porites* sp., regarding the *Diploastrea* sp. coral from Mayotte, one hypothesis could be that the coral

maintains and even elevates its internal pH_{CF} for metabolism purposes (calcification, growth). Maintaining elevated pH in the extracellular CF, where precipitation of calcium carbonate occurs, is a critical step to initiate and sustain the biomineralization process (i.e., calcification) (M. McCulloch et al., 2012). Nonetheless, the skeletal bulk density of *Diploastrea* decreased for more than 40% over the last 54 years as well as the calcification rate of this latter (see Figure 5 in Alaguarda et al., 2022). When looking at the period 1964-1985 of the coral growth parameters of *Diploastrea* sp., a first decrease of skeletal bulk density and calcification rate is observed while this period represents where the pH increased the fastest. From the literature, by elevated level of pH_{CF} , process of calcification can be maintained ; Comeau et al., 2015; T. DeCarlo et al., 2018). Therefore, even if the internal pH of *Diploastrea* sp. rose over this period, other factors seem to have influenced the observed decrease of the coral growth parameters. Further investigations are needed to understand better what might have triggered both the increase in pH_{CF} and the decrease in coral density and calcification of *Diploastrea* sp.

4.3.4.3 Internal pH and the Evolution of the Abundance of Microbioeroding Traces

Based on the reconstructed pH over the last five decades from the coral *Diploastrea* sp., opposite correlations were observed with the abundance and composition of microbioeroding communities. These correlations highlighted that the abundance of wide microbioeroding traces might have been impacted by the increase of the pH_{CF} . In contrast, it might have been more suitable for the abundance of thin microbioeroding traces. Nonetheless, no clear evidence showed that such relations could be established ($p < 0.1$ for both correlations; Table 4.4). Interestingly, the breakpoint identified within the pH occurred one year before the observed breakpoint of the microbioeroding abundance estimated by Alaguarda et al., 2022. This finding could suggest that the potential shift of microbioeroding communities observed in 1985-1986 could have been linked to the pH changes occurring one year before (1983-1984). pH variations are known to be an active parameter that can influence the activity of microbioeroding communities. For instance, in dead coral substrates (*Porites* sp. skeletons), Tribollet et al. (2009) demonstrated that increased levels of seawater $p\text{CO}_2$ enhanced dissolution rates of carbonates. Additionally, Reyes-Nivia et al., 2013 investigated the level of dissolution rates from photosynthetic microborers. They highlighted that the skeletal dissolution was higher in the increased $p\text{CO}_2$ and warming scenarios. She also showed

enhanced dissolution rates were associated with elevated endolithic biomass, mainly dominated by *Ostreobium* sp. Similarly, Tribollet et al. (2019) also showed increased net biogenic dissolution from microborers of dead coral substrates (*Porites lobata*) in New Caledonia under elevated $p\text{CO}_2$. Nonetheless, these studies focused only on dead coral substrates over a few months or a year of experiments focusing on how seawater pH modulations influence microbioeroding communities' activity. They did not consider the implications of the coral physiology (e.g., regulation of its internal pH of the CF generally higher than the pH seawater, its growth parameters..) that may influence the coral holobiont (including microbioeroding communities living within). Among living corals, a dynamic, endolithic microbiome lives within the coral skeleton organized with different gradients of physico-chemical properties (Kühl et al., 2008; Ricci et al., 2019). These gradients might determine the stratification of the endolithic community, where O_2 and pH gradients can be linked to heterotrophic and autotrophic metabolism of microbiome members (Bellamy and Risk, 1982; Shashar and Stambler, 1992; Kühl et al., 2008). Recently, Ricci et al. (2023) investigated how physico-chemical gradients such as O_2 and pH can affect the coral skeleton microbiome of two reef-building corals *Porites lutea* and *Paragoniastrea benhami*. For comparison, the skeleton of *Paragoniastrea benhami* can be similar to *Diploastrea* sp. with its perforated and porous skeleton compared to *Porites* sp. In their study, each coral skeleton was characterized by ecological micro-niches shaped by dynamic O_2 and pH gradients, harboring microbial communities that varied in composition and abundance with depth in the skeleton. Oxygenic phototrophs inhabiting the skeleton can induce oxygenation and alkalization of this latter (an increase of the pH) through photosynthesis, but this is not the only functional group influencing the O_2 and pH gradients through their metabolism. For instance, denitrifiers and sulfate reducers can also induce alkalization (Rust et al., 2000; Tran et al., 2021). Nonetheless, photosynthesis through the alternate cycle of day and night showed important pH variations within the coral skeleton (i.e., CO_2 removal during the day; respiration during the night, Shashar and Stambler, 1992 in *Porites compressa*; Ricci et al., 2019; Iha et al., 2021) is not a potential reason that can explain the increase of the pH_{CF} of *Diploastrea* sp. over the last 54 years. As the abundance of these communities decreases over time (90%, Alaguarda et al., 2022), microbioeroding communities might not be responsible for such an increase in the pH_{CF} of the coral. Overall, no causality can be determined on whether the pH_{CF} directly influenced the microbioeroding communities or whether the coral

holobiont (including microbioeroding communities) has modified the internal coral pH. One suggestion could be that the pH_{CF} might have played an accelerating role in the observed microbioeroding community shift but do not seem to be the primary factor influencing the abundance and composition of these latter. Thus, the significant decrease in the abundance of microbioeroding traces over time, as discussed by Alaguarda et al., 2022, might have been from co-factor influences, including environmental pressures (SST/SSTA, Wind stress, and potentially the internal pH_{CF}) and biotic coral interactions (e.g., skeletal bulk density, calcification rate).

4.4 Conclusion

In this chapter, the machine-learning approach was developed to quantify the abundance of microbioeroding communities in a living coral colony over the last 54 years. While acquiring the SEM images for *Diploastrea* sp. took months, the ML approach allowed the study of thousands of SEM images in a few hours with an accuracy of 93%. This is noteworthy because other quantitative methodologies, including the total decalcification of coral skeleton to estimate the ash-free dry weight of endoliths (Fordyce et al., 2021), or the number of microbioeroding filaments (Lukas, 1973) implied several biases and/or were time-consuming. For the first time here, a major shift in the microbioeroding assemblage composition over the lifespan of a slow-growing massive coral in the WIO was highlighted with a significant decrease in the abundance of microbioeroding traces (90%). Reasons for the major decrease in the abundance of microbioeroding traces could be linked to multiple co-factors influence, including thermal stress (SST/SSTA), wind, insolation, biotic parameters of the coral with its density and calcification rate and potentially the increase of the coral' pH_{CF} over time. Nonetheless, the increase of the internal pH might not be the main reason for the decrease of microbioeroding traces over time in *Diploastrea* sp. It should be further investigated in different coral cores to assess whether this factor can control the variability and distribution of microbioeroding communities in living corals. Overall, such augmentation in the internal pH of the coral underlines the question of the seawater pH in Mayotte, where progressive acidification from 1963 to 2019 has been assessed in the WIO (MC, Monaco et al., 2021). More coral cores should be studied to confirm the observed trends to understand better the possible implications of a significant decrease in microborers abundance in living corals, especially the stress-tolerant ones such as *Porites* sp.

(Schoepf et al., 2019; T. M. DeCarlo et al., 2019). Also, coral cores from contrasted environments should be investigated to understand better the controlling factors of microborers' abundance, their community composition, the presence of green bands in living corals, and their possible implications for coral health and resilience. Environmental factors such as nutrients, DIC, and metal trace pollution could be promising targets as these factors are known to affect microborer's abundance in dead carbonates (Tribollet et al., 2006; Cherchi et al., 2012; Reyes-Nivia et al., 2013). Nowadays, it remains to be understood whether corals living in naturally extreme thermal/acidic environments may be better adapted to withstand the increasing effects of global warming or OA, especially on decadal and longer time-scale warming and acidification occur. Also, a specific need must be addressed to understand better the roles of microbioeroding communities in reef carbonate budgets, coral health, and their resilience states for the following decades.

Is the Composition and Abundance of Microbioeroding Communities in Massive Corals Genus Dependant?

Contents

5.1	Introduction	187
5.2	Material and Methodologies	191
5.2.1	Study Site	191
5.2.2	Coral Sampling	191
5.2.3	Coral Growth Variables	191
5.2.4	Observation and Estimation of Microbioeroding Traces . . .	192
5.2.5	Machine Learning Application	193
5.2.6	Statistical Analysis	194
5.3	Results	194
5.3.1	Variability of Environmental Conditions in Mayotte Over the Last 30 Years Among the Two Studied Coral Genera	194
5.3.2	Comparison of Coral Growth Parameters between <i>Diploastrea</i> sp. and <i>Porites</i> sp. Over the Last 30 Years	196
5.3.3	Microbioeroding Community Composition in <i>Porites</i> sp. . .	197
5.3.4	Effects of the Coral Genus on the Abundance of Microbioeroding Traces over the Last 30 Years	199

5.3.5	Main Factors Influencing the Abundance of Microbioeroding Traces Over the last 30 Years in Massive Corals	200
5.3.5.1	Main Factors Influencing the Abundance of Microbioeroding Traces in <i>Diploastrea</i> sp.	200
5.3.5.2	Main Factors Influencing the Abundance of Microbioeroding Traces in <i>Porites</i> sp.	202
5.4	Discussion	203
5.4.1	Effect of Abiotic Parameters on the Abundance of Microbioeroding Traces in Massive Corals	203
5.4.2	Effect of Skeletal Properties on the Abundance of Microbioeroding Traces in Massive Corals	205
5.4.3	Evolution of the Abundance and Composition of Microbioeroding Traces in Massive Corals	207
5.5	Conclusion	208

5.1 Introduction

The great variety of coral growth forms and skeletal features are likely to contribute to shaping the physico-chemical characteristics of the colony skeleton. Among them, massive corals have been widely used as proxies for paleoclimate studies (Gagan et al., 2000; Watanabe et al., 2003; Bagnato et al., 2004). Most studies have utilized core samples from the genus *Porites* and have been most successful in reconstructing past variability on interannual timescales. On the other hand, the coral genus *Diploastrea* has been less utilized, however, it presents 2 to 3 times as many annual density bands than *Porites*, resulting in a longer paleoclimatic record for the same length of core (Watanabe et al., 2003). *Diploastrea* corals present slower extension rate of few mm/years (Bagnato et al., 2004) compared to few cm/years for *Porites*. For instance, Canesi (2022) estimated averaged growth rate of *Diploastrea* sp. from Palau of 2.7 mm.y^{-1} and an average of 1.2 cm.y^{-1} for the *Porites* sp. *Diploastrea* present also a denser structure than *Porites* corals. Watanabe et al. (2003) showed that *Diploastrea* can have bulk densities of 1.8 g.cm^{-3} , which are 50% greater than densities typical for *Porites* ($1.2 \pm 0.2 \text{ g.cm}^{-3}$, as measured throughout the Great Barrier Reef, Australia (J. Lough and Barnes, 1997). Nonetheless, Tribollet et al. (2002), in her experiments with coral blocks from massive *Porites* sp of Snapper and Lizard Island (GBR, Australia) estimated coral density between 1.15 and 1.73 g.cm^{-3} , in the range of the density of *Diploastrea* sp. Differences between the two massive corals are also noticed in their skeletal architecture, particularly the size of the corallites (Figure 5.1). *Diploastrea* sp., corallites are 4–5 times larger than *Porites* and visible on X-radiographs (Figure 5.1 A and B). Corallites in *Diploastrea* are plocoid and typically between 7.1 and 9.3 mm in diameter (Todd et al., 2004) (Figure 5.1 C to E). The different corallites in *Diploastrea* have their walls separated by a common skeleton (coenosteum) which is more or less developed and sometimes not easily conspicuous (Todd et al., 2004; Budd and Stolarski, 2011; Sadler et al., 2014). On the other hand *Porites* corals have thinner polyps and corallites. Corallites in *Porites* have a typical diameter of 0.8 to 1.1 mm, *P. mayeri*; 1.0 to 1.5 mm, *P. lobata* *P. lutea*; 1.5 to 2.0 mm, *P. solida*, (Veron, 1986; Darke and Barnes, 1993) (Figure 5.1 G to N). The different corallites in *Diploastrea* have their walls separated by a common skeleton (coenosteum) which is more or less developed and sometimes not easily conspicuous (Todd et al., 2004).

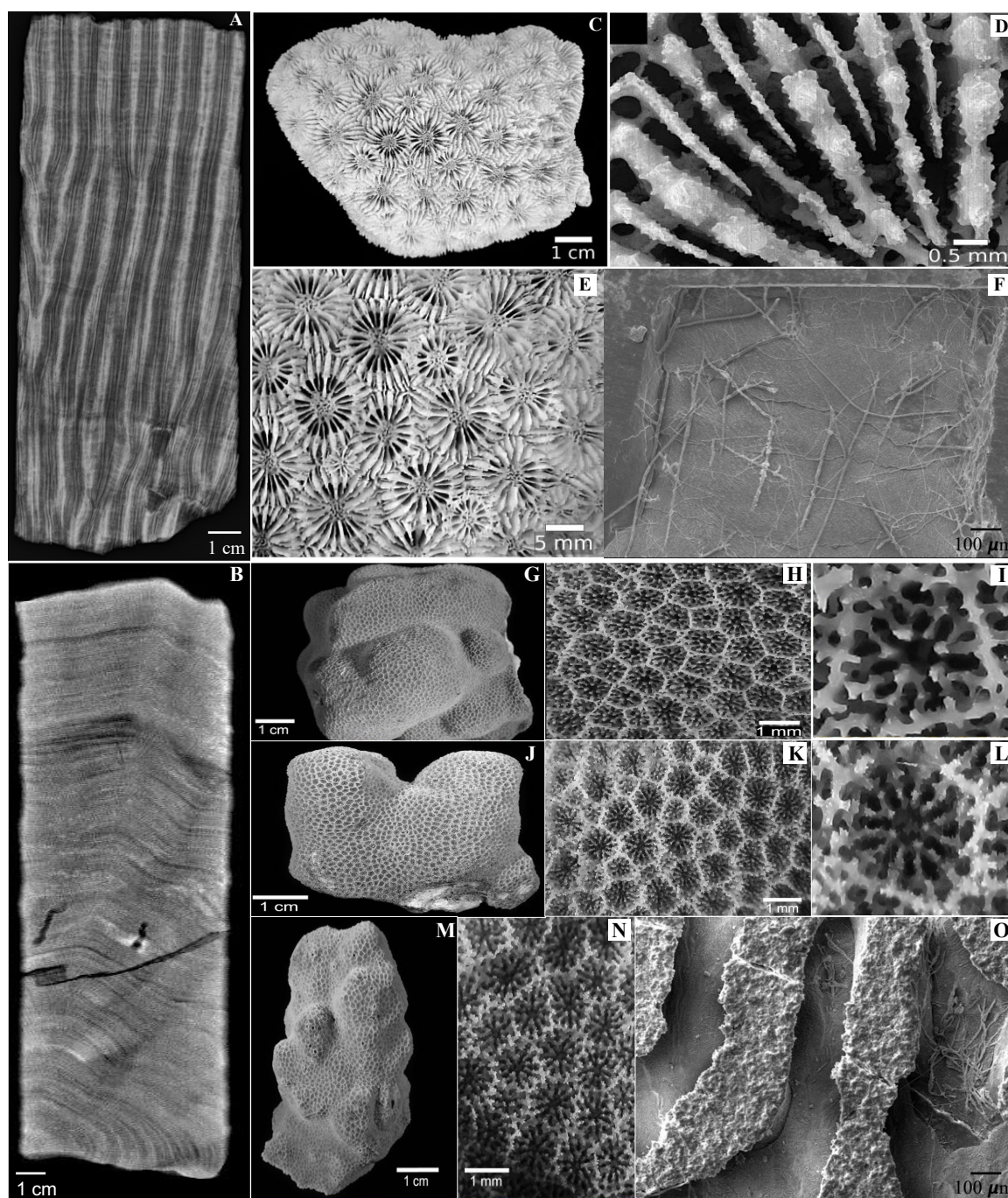


Figure 5.1: (A) X-Radiograph showing the coral *Diploastrea* sp. (B) X-Radiograph showing the coral *Porites* sp. (C to E) SEM photographs of the colony *Diploastrea* with its corallite and micro-structure. (F) SEM photograph on the studied *Diploastrea* sp. from Mayotte showing one skeletal unit colonized by microbioeroding traces. Image taken at 150x magnification. (G to I) SEM photographs showing the coral colony, corallites structures of *Porites lutea*. ((J to L) SEM photographs showing the coral colony, corallites structures of *Porites lobata*. ((M to N) SEM photographs showing the coral colony, corallites structures of *Porites solida*. ((O) SEM photograph on the studied *Porites* sp. from Mayotte showing multiple skeletal unit colonized by microbioeroding traces. Image taken at 150x magnification.

Colonization and distribution of euendolith assemblages are intrinsically influenced by the nature and physical properties of the substrate, such as its mineralogy, poros-

ity, translucency, density, or architecture (C. T. Perry, 1998; Chacón et al., 2006; Massé et al., 2018; Tandon et al., 2023). For instance, Massé et al. (2018) showed colonization of euendoliths in the branching coral *Pocillopora damicornis* as soon as the primary polyp forms its carbonate basal plate. She was the first to show this early colonization of microborers in living young coral recruits and that early colonization did not slow the host extension rates. In fast-growing branching corals, euendoliths abundance decreases from the base towards the tissue layer (Difference of factor 6 described by Massé et al., 2018, also shown by Godinot et al., 2012). Moreover, she did not find any green band upon the skeleton of *Pocillopora damicornis* compared to this pattern of green bands observed in slow-growing massive corals, permitting dense growth of multiply ramified euendolith filaments (e.g., *Ostreobium*; Le Campion Alsumard et al., 1995). She also showed that colonization of euendoliths (i.e., *Ostreobium* was higher in dead skeletons of *Porites* compared to calcite spar (non-porous) or non-carbonates substrates showing a variability of colonization from euendolith depending on the nature (e.g., porosity) of the substrate. Recently, Fordyce et al. (2021) investigated the possible correlations between coral inter-specific patterns in skeletal morphology and the variability in the biomass of endolith (dominated by *Ostreobium* sp., in their study the eundo, crypto, and chasmoendoliths were considered). They showed that massive or mounding corals, whose microbial endoliths are most commonly studied, have a large volume of substrates to colonize leading to a greater biomass of endoliths for these corals. For instance in their study, the massive coral *Goniastrea retiformis* presented a significant and higher biomass of endoliths ($\approx 85 \text{ mg.cm}^{-3}$) than the branching species *Montipora digitata* and *Isopora palifera* ($\approx 28 \text{ mg.cm}^{-3}$; see their Figure 2 in Fordyce et al., 2021). Such findings let suggest that parameters linked to the nature of the coral skeleton, the growth physiology of the coral (e.g., extension rate, skeletal density), variations in the macro and microstructure of the coral skeleton are key factors that can shaped the colonization and distribution of euendolith taxa in this latter (e.g., differences between branching and massive species) (Golubic et al., 1975; Vogel et al., 2000; Reyes-Nivia et al., 2013; Fordyce et al., 2021).

Concomitantly, abiotic factors such as light may control the distribution of euendoliths (e.g., phototrophs) within coral skeletons. Light in the skeleton is scattered and influenced differently by the skeletal microstructure within the different coral species (L. A. Marcelino et al., 2013), impacting the coral symbionts and their associated microbiota

(e.g., phototroph compartment). Enriquez et al. (2005) showed that multiple scattering by the skeleton enhances the local light field efficiency of coral symbionts and plays a key role in the regulation of their internal diffuse light field (also supported by Teran et al., 2010). More recently, Enriquez et al. (2017) investigated the scattering abilities of different coral skeletons for 74 Indo-Pacific species. Their results highlighted that flat, extraplanate, and branching corals showed the most efficient structures for scattering light, while massive-robust species were less efficient (see Figure 2a in Enriquez et al., 2017). Their results also suggest significant differences regarding scattering light properties between forms of corallites (see Figure 2b in Enriquez et al., 2017). Regarding the influence of light on microbioeroding communities, Fordyce et al. (2021) also proposed that the specific density of a coral's skeleton and its capacity for capturing and scattering incident light are the main parameters influencing the biomass of endoliths. Larger and more complex corallites seem to be considered more effective "photon traps," which increase light availability for tissue-associated zooxanthellae and the associated microbiota within the skeleton (Enriquez et al., 2005; L. A. Marcelino et al., 2013; Swain et al., 2018).

Nonetheless, long-term variability of the abundance and composition of euendolithic communities among coral genera or species remains to be understood. Alaguarda et al. (2022) first investigated the variability of the abundance, distribution, and composition of microbioeroding communities in a coral core of a massive *Diploastrea* sp. from Mayotte between 1964 and 2018. Their main results showed an important shift in the trace assemblage composition in 1985 and a loss of 90% of microbioeroding traces over the last five decades. The objective is to confirm or infirm this trend by studying different massive coral: *Porites* sp. Here, a remarkably well-preserved coral core of a slow-growing colony of *Porites* sp. was collected next to the *Diploastrea* sp., in Mayotte (on the outer slope of the NE barrier reef), covering the period 1990-2018 (29 years/3 last decades) to: (i) determine if the same microbioeroding communities colonized *Porites* sp over the last 3 decades, (ii) confirm that the abundance of microbioerodings decreased over time and (iii) identify the main abiotic and/or biotic factors that could influence the variability of the abundance observed in *Porites* sp. The innovative ML approach described in **Chapter 3** trained with the focal loss was used to reach those goals.

5.2 Material and Methodologies

5.2.1 Study Site

Mayotte, a French tropical island located in the northern part of the MC (WIO, see **Figure 2.8**), is dominated by a monsoonal wind system with two seasons identified: a hot, windy and rainy monsoon season from November to April, and a dry season from May to October (Jeanson et al., 2014). Historically, Mayotte island is subject to temperatures around 26.4 to 27.6°C in winter and 27.5 to 29°C in summer (Zinke et al., 2008). To determine the possible main abiotic drivers influencing microborers' abundance in the *Porites* sp. coral core, the same environmental parameters that were collected for the *Diploastrea* sp. (Alaguarda et al., 2022) were analyzed (e.g., SST/SSTA, max instant wind speed, precipitation rate, cumulative insolation and pH_{CF}). The internal pH investigation of *Porites* sp. was studied the same as *Diploastrea* sp with the two approaches (instrumental and multi-proxy) explained in the section 2.2.3. Here, the period considered was 1990-2018.

5.2.2 Coral Sampling

The core studied here from a massive *Porites* sp. was sampled in a healthy coral colony nearby the *Diploastrea* sp. colony, on the outer slope of the NE barrier reef of the M'Tsambo Pass at 15 m depth (Alaguarda et al., 2022; Mayotte, WIO). For recall, this site was selected to focus on the influence of oceanic conditions on microboring assemblages in living corals instead of local disturbances, although these cannot be discarded. The core was collected with an 8 cm compressed air driller and measured 29.5 cm long. Compared to the *Diploastrea* sp., one major difference is that no green bands were identified on the coral skeleton of *Porites* sp.

5.2.3 Coral Growth Variables

The *Porites* sp. core was treated according to the same protocol as the one used for the *Diploastrea* sp. (Alaguarda et al. 2022). Before measurements, the *Porites* core was sliced along the main vertical growth axis into four slabs (the middle slabs being ≈ 1 cm thick). All slabs were well-preserved. Macrobioerosion traces were identified under X-radiographs but were avoided for measurements (red square in **Figure 5.2 A**). Thus, the right part of the core was studied (white square in **Figure 5.2 A**).

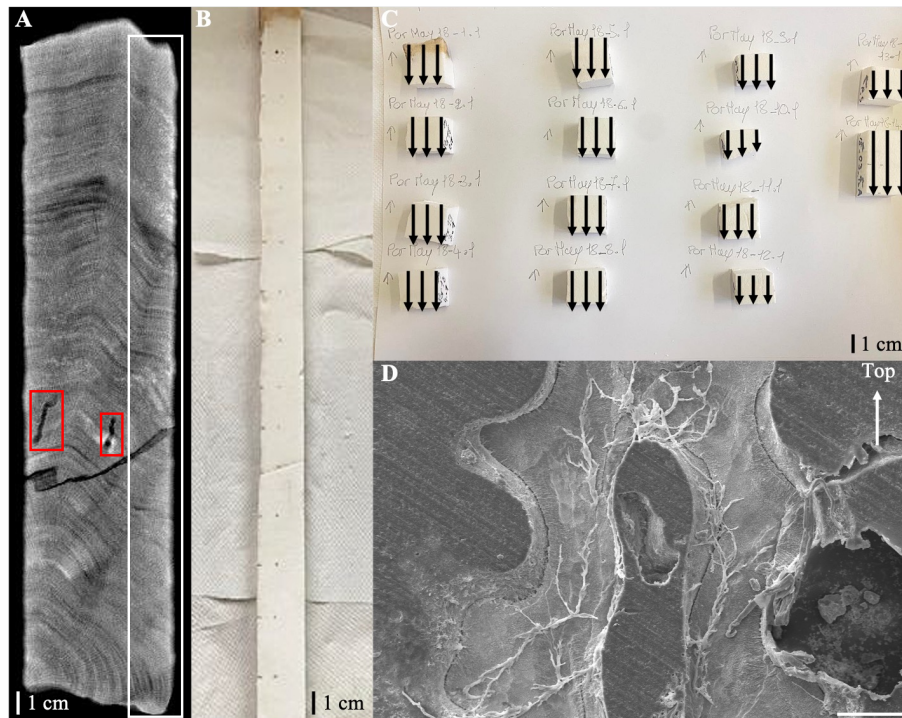


Figure 5.2: Studied slab of *Porites* sp. coral from Mayotte. (A) The X-ray radiograph of one middle slab cut out of the *Porites* sp. core measuring 29.5 cm long shows the annual density banding pattern. (B) and (C) 14 samples were cut from the radiographed slab of *Porites* sp. core. (D) Example of an SEM image collected from the *Porites* sp. core showing microbioeroding traces colonizing the coral skeleton. Scale is 100 μm

The 4 slabs were scanned together on a Discovery CT750 HD CT scanner (GE Healthcare) set at 120 kV at the DOSEO 'Radiography and Imaging Technology Platform R and D center' (CEA-Saclay, Paris) with three coral standards. Two coral variables were measured: The vertical linear extension (mm.y^{-1}) and the skeletal bulk density (g.cm^{-3}). To prevent redundancy, please refer to Alaguarda et al. (2022) or the section 2.2.2 for further details regarding their estimation. The annual coral calcification rate ($\text{g.cm}^{-2}.\text{y}^{-1}$) was calculated by multiplying the estimated annual bulk density by the annual vertical extension rate (P. D. Taylor and Jones, 1993; T. M. DeCarlo et al., 2017). The age chronology reconstructed for *Porites* sp. coral went from 1990 to 2018 (representing the entire core).

5.2.4 Observation and Estimation of Microbioeroding Traces

Then, a sub-slab of 1.5 cm width was cut along the middle slab of the *Porites* sp. core (Figure 5.2 B) and then cut into 14 coral samples (Figure 5.2 C). Then, they were observed under an SEM operating at 15kv (Zeiss EVO LS15) on the platform ALYSES (Bondy, France) to study the diversity and abundance of microbioeroding traces and their dis-

tribution within the coral skeleton (**Figure 5.2 D**). To prevent redundancy, please refer to Alaguarda et al. (2022) or the section 2.3.1 for further details regarding their estimation. To estimate the relative abundance of microbioeroding traces colonizing the coral skeleton of *Porites* sp., I hypothesized that the approaches performed in *Diploastrea* sp. by Alaguarda et al. (2022) could be translocated to the thin coral sections of *Porites* sp. Therefore, here the vertical approach was applied, comprising the study of SEM images taken continuously along 3 vertical transects parallel to the main coral growth axis (black arrows in **Figure 5.2 C**). No horizontal approach was performed for the *Porites* core as no green bands were identified. Per vertical transect, 17 to 58 SEM images were taken depending on the height of the coral section. As investigated in *Diploastrea* sp., the main goal of the vertical approach was to highlight possible assemblage shifts, the variability in microborers' abundance over the last decades, and the possible influence of abiotic and/or biotic factors on this latter. To highlight the possible influence of abiotic and/or biotic factors, the average percentage of the thin sections of coral skeletons colonized by microborers were calculated along the vertical growth axis per year as the physical studied factors and coral parameters were calculated per year. First, this involved estimating the rate of the vertical extension of the coral colony over the past decades and adjusting the number of SEM images collected along the vertical transects to match each year of coral growth.

5.2.5 Machine Learning Application

To estimate the relative abundance of microbioeroding traces colonizing the coral skeleton, I modified the ML application developed for the *Diploastrea* sp. For this study, a CNN was re-trained based on the dataset of SEM images collected from the *Porites* sp. ($n = 1422$ SEM images). The manual analysis of 74 SEM images was used to develop the CNN model of *Porites* sp. 67 SEM images were used for the training set, 4 for the validation, and 3 to test the final parameters of the *Porites* sp. CNN model. The CNN originally developed for *Diploastrea* sp. was modified, adjusting one hyper-parameter of the CNN: the loss function. Here, the *Porites* sp. model was coupled with the Focal loss function. The various parameters involved in this CNN model were optimized to improve the identification of the three defined categories: 'resin', 'coral skeleton', and 'all microborings'. This CNN developed with *Porites* sp. led to the highest probability of the neural network correctly attributing a pixel to its right class (=accuracy, 95%). Further details regarding the structure of the CNN, the investigations of the different loss

functions, and comparisons with the previous model *Diploastrea* sp. are presented in **Chapter 3**.

5.2.6 Statistical Analysis

The image manipulation software GIMP (v2.10.14; <https://www.gimp.org>) was used to detour shapes of the different classes to constitute the dataset (n=74) of *Porites* sp. Coral bulk densities over time were calculated through the GMM model on Python, then averaged to be consistent with the coral growth rate per year. Linear regressions on environmental data and coral variables were generated from the library *ggpubr* on RStudio (v1.4.17; <https://www.rstudio.com>). The Non-parametric Mann-Kendall test was then performed to assess if the observed trend on each time series was significant. Same as investigated within the coral *Diploastrea* sp., the areas of coral skeleton colonized by microborers (total microbioerodings) measured along the three vertical transects were compared using an ANCOVA. Although no significant differences were obtained between the first two transects (p-values > 0.2), the third one showed a significant difference (p-value < 0.001; see **Figure 8.1 in Appendix 8.3**). Despite such variability, and because the three transects showed the same trend over the studied period (i.e., 29 years), we chose to average values from the 3 vertical transects per period (year) to determine the possible main factors driving the overall temporal variability of microborers abundance (see. Pearson correlations were carried out to detect the potential effects of the environmental and/or coral variables studied on the traces' abundance (i.e., the abundance of total microbioerodings) obtained over the last decades (vertical transects). These correlations were performed on detrended variables to focus on their possible inter-annual and decadal variability and to avoid spurious correlations due to linear trends. Finally, a non-parametric Pettitt test was applied to the different variables to determine potential breakpoints in the trend over the last 29 years.

5.3 Results

5.3.1 Variability of Environmental Conditions in Mayotte Over the Last 30 Years Among the Two Studied Coral Genera

As the coral core of *Porites* sp. was collected close to the *Diploastrea* sp., environmental parameters were already presented in Alaguarda et al. (2022). Here, the environmental

parameters were adapted to fit the chronology age reconstruction of *Porites* coral from 1990 to 2018. The objective was to analyze which factors might influence the variability of microbioeroding communities within *Porites* sp. The evolution of the environmental parameters in Mayotte is already presented in the **section 2.1.1.1: Figure 2.4**. Reconstructions of the pH_{CF} from instrumental data (ERSSTv5) and the multi-proxy by Canesi et al. (2022) for the coral *Diploastrea* sp. and *Porites* sp. described the same variability (see **Appendix 8.3 Table 1 and 2**). The correlation between the instrumental and paleo-proxy pH_{CF} was $r = 0.93$ for *Porites* sp. and $r = 0.97$ for the *Diploastrea* sp. Thus, only the signal from the reconstructed pH_{CF} based on the instrumental data ERSST was plotted (instrumental SST is usually the best approach that reflects the ambient temperature of the reef). The variability of the pH_{CF} overtime was too important to identify trends in both corals (Mann Kendall Test $p > 0.05$; **Figure 5.3**). Nonetheless, between 1990 and 2002, pH_{CF} for both corals increased before decreasing and stabilizing until 2018. The average pH_{CF} for *Porites* sp. was 8.48 ± 0.02 and for *Diploastrea* was 8.47 ± 0.015 . Comparison of means of the reconstructed pH_{CF} of both corals revealed significant differences between *Porites* and *Diploastrea* sp. (Student T-Test, $p < 0.05$). Overall, the *Porites* sp. internal pH_{CF} was higher than *Diploastrea* pH_{CF} over the period 1990-2018 (**Figure 5.3**). Interestingly, a breakpoint was found in the evolution of the pH_{CF} over the last three decades in the *Porites* sp. coral. This breakpoint was identified between 1995 and 1996 (Pettit test, $p < 0.1$; black arrow in **Figure 5.3**).

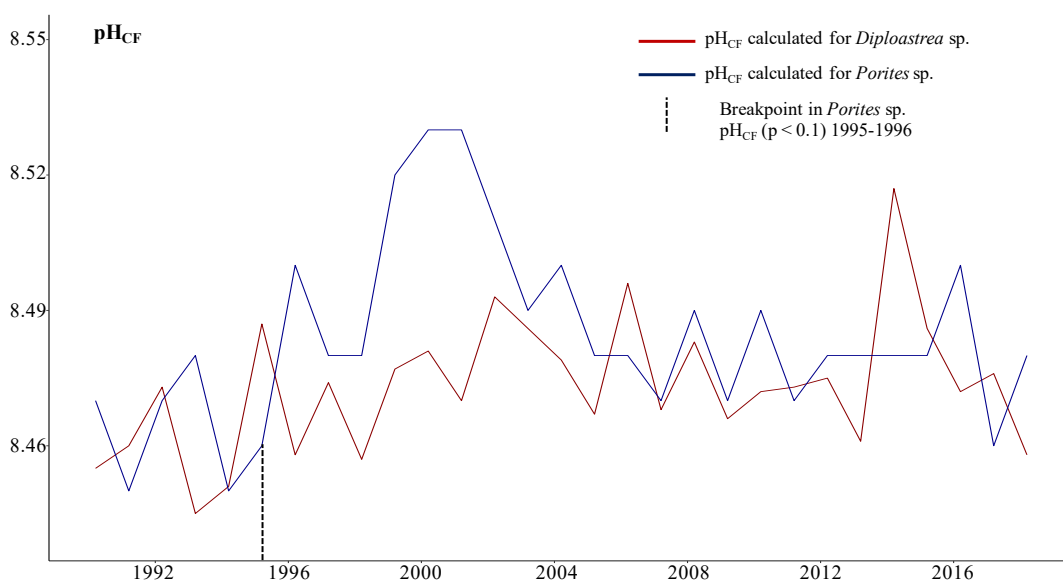


Figure 5.3: Interannual variability of the internal pH_{CF} of *Diploastrea* and *Porites* sp. at Mayotte between 1990 and 2018.

5.3.2 Comparison of Coral Growth Parameters between *Diploastrea* sp. and *Porites* sp. Over the Last 30 Years

When considering the *Diploastrea* sp. coral, all three growth parameters did not vary significantly from 1990 to 2018 (Mann Kendall Test $p > 0.05$). The vertical extension was comprised between 0.19 (in 2009) and 0.49 cm.yr⁻¹ (in 2017). The average growth rate for *Diploastrea* sp. was 0.26 ± 0.06 cm.yr⁻¹. The coral bulk density was comprised between 1.11 ± 0.03 (2018) to 1.75 ± 0.03 (2003), averaging 1.47 ± 0.03 g.cm⁻³. Finally, the calcification rate was comprised between 0.25 ± 0.002 (in 2009) and 0.55 ± 0.023 g.cm⁻².y⁻¹ (in 2017), averaging 0.39 ± 0.01 g.cm⁻².y⁻¹ (**Figure 5.4**). Regarding the correlations between the *Diploastrea* sp. coral growth parameters and environmental variables, the analysis was only performed on the detrended dataset (**Appendix section 8.3 Supp Table 3**). A strong positive correlation was identified between the detrended data of bulk density and the pH_{CF} ($r = 0.530$; $p < 0.01$; see **Appendix section 8.3 Supp Table 3 and Fig.1**). A negative correlation was found between the calcification rate and the precipitations ($r = -0.373$; $p < 0.05$). The vertical extension rate was not correlated to any environmental parameters.

When considering the *Porites* sp. coral, all three growth parameters did not vary significantly over the last three decades (Mann Kendall Test $p > 0.05$). The vertical extension rate was comprised between 0.7 (in 1998) and 1.3 cm.yr⁻¹ (in 2010). The average growth rate for *Porites* sp. was 0.96 ± 0.14 cm.yr⁻¹. The coral bulk density was comprised between 1.01 ± 0.02 (in 2006) to 1.26 ± 0.02 (in 1991), averaging 1.14 ± 0.03 g.cm⁻³. Finally, the calcification rate was comprised between 0.79 ± 0.02 (in 1998) and 1.48 ± 0.03 g.cm⁻².y⁻¹ (in 2010), averaging 1.10 ± 0.03 g.cm⁻².y⁻¹ (**Figure 5.4 and Appendix 8.3 Table 4**). Regarding the correlations between the *Porites* sp. coral growth parameters and environmental variables, the analysis was only performed on the detrended dataset (**Appendix section 8.3 Supp Table 5 and Fig.2**). interestingly, the skeletal bulk density was positively correlated with the precipitation rate for the period ($r = 0.42$; $p < 0.05$; see **Appendix section 8.3 Supp Table 5**). The detrended calcification rate was positively correlated to detrended SST and SSTA ($p < 0.05$, $r = 0.39$). The detrended extension rate was slightly positively correlated to both detrended SST and SSTA ($p < 0.1$; $r = 0.35$).

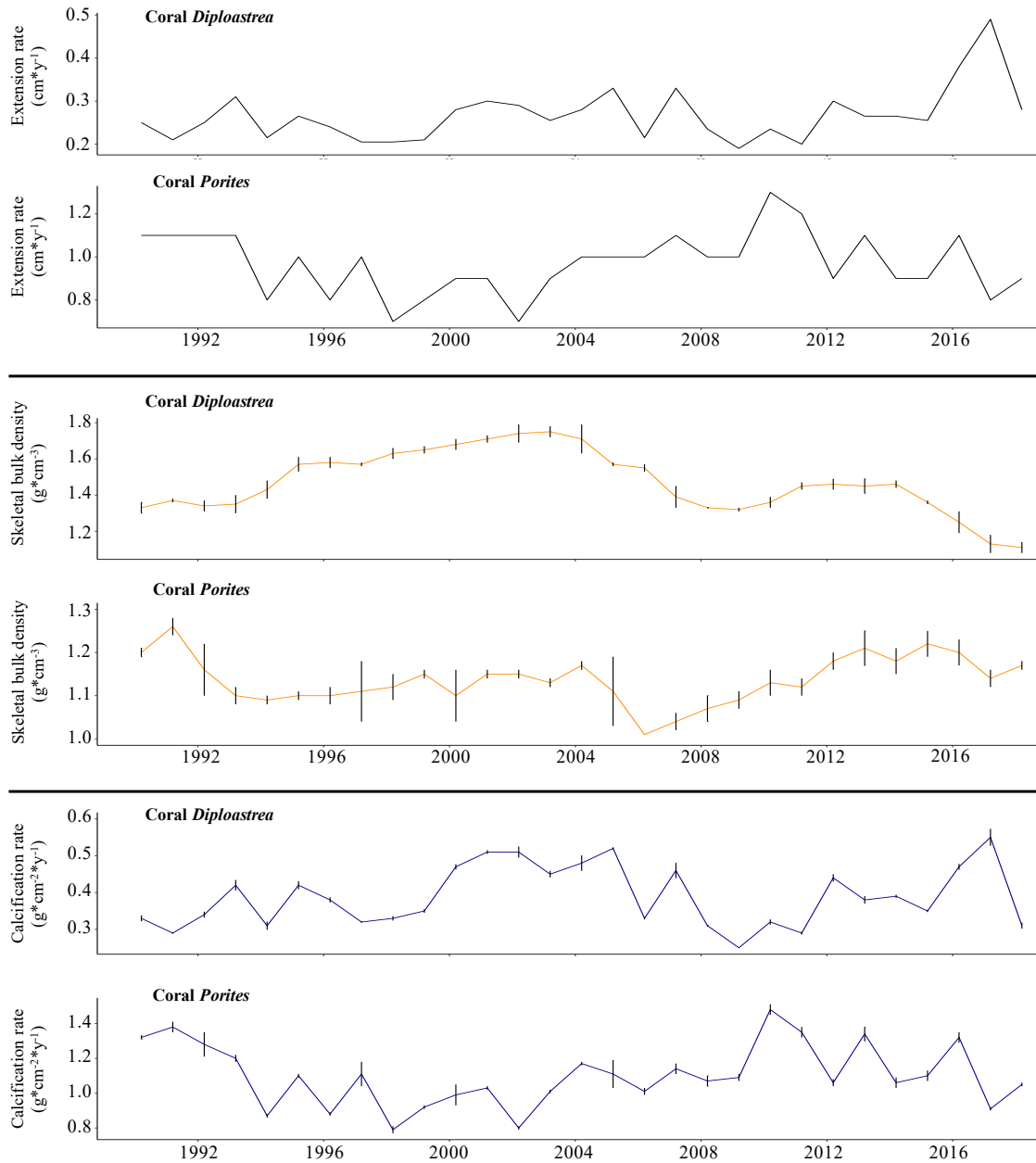


Figure 5.4: Evolution of the different coral growth parameters of the studied *Diploastrea* sp. and *Porites* sp. colony over the last 29 years. The different panels compared each different growth parameter between both corals.

5.3.3 Microbioeroding Community Composition in *Porites* sp.

Based on morphological criteria and their distribution within the coral skeleton of *Porites* sp., three different types of microbioeroding traces could be identified. Microbioeroding traces with a diameter between 1 and 2 μm were identified with a random distribution within the coral skeleton, most probably resulted from the activity of fungi as observed in *Diploastrea* sp (Figure 5.5 A). Then, microbioeroding traces with

a diameter between 2 and 5 μm were observed in the middle part of the core, which was orientated parallel to the coral growth axis (**Figure 5.5 B**). Finally, microbioeroding traces between 5 and 10 μm were mainly observed within the bottom of the core and formed in patches, orientated vertically and parallel to the main growth axis of the coral (**Figure 5.5 C**). When zooming on a particular patch (**Figure 5.5 D**), the network present cell constrictions and ramifications, orientated along the coral growth axis. This particular assemblage suggests the presence of the chlorophytes *Phaeophila* sp. or *Eugomontia* sp. or the ichnotaxa *Rhopalia* (Wisshak et al., 2008).

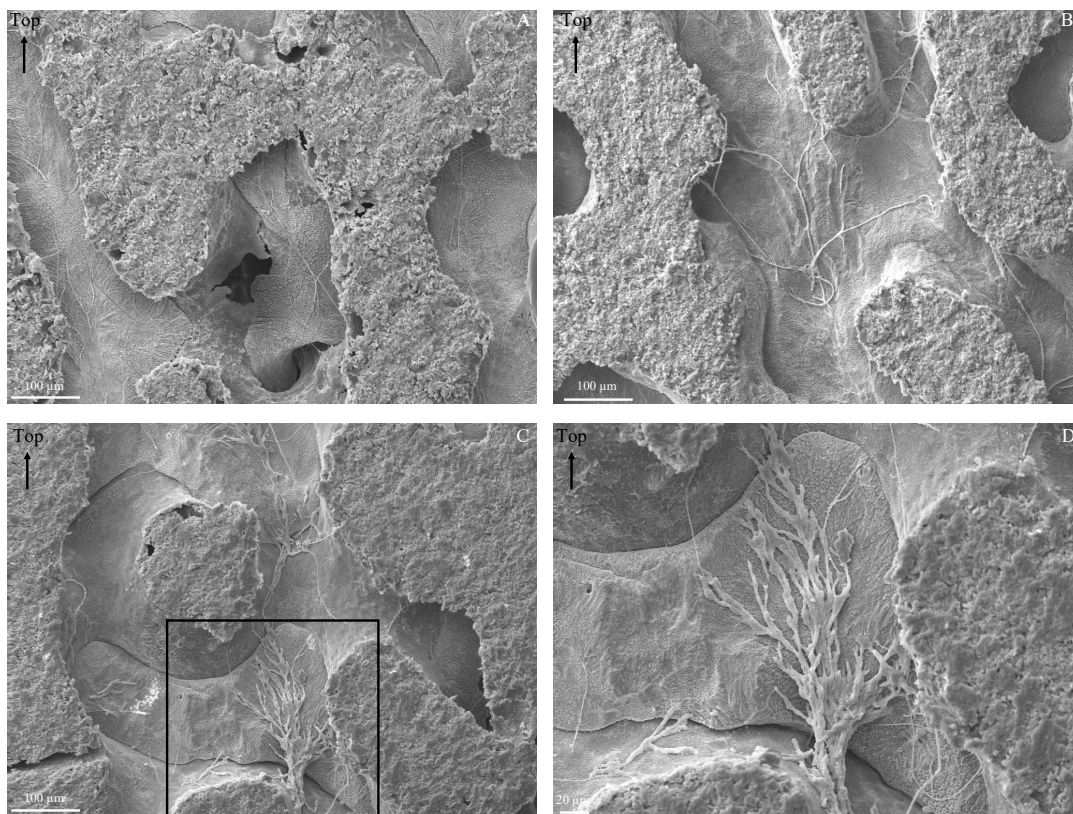


Figure 5.5: SEM pictures presenting the diversity of microbioeroding traces observed along the coral core of *Porites* sp. (A) SEM image from the top of the core showing traces measuring less than 2 μm , most probably belonging to fungi. (B) SEM image from the middle of the core showing traces measuring between 2 and 5 μm , orientated within the coral growth axis. (C) Picture from the bottom of the core showing traces measuring between 5 and 10 μm , organized in a patch, also orientated towards the coral growth axis. (D) Zoom of C showing the network of microbioeroding traces with a morphology indicative of the potential ichnotaxa *Rhopalia*.

Nevertheless, compared to the coral *Diploastrea* sp., no very wide microbioeroding traces with a diameter higher than 30 μm were observed in *Porites* sp (**Figure 5.5**). As previously observed in *Diploastrea* sp., a pattern of succession of communities seems also to occur within *Porites* sp. with larger traces in the bottom of the core and thinner galleries near the top of the core. Nonetheless, compared to *Diploastrea* sp., no

qualitative measurements of the temporal distribution of the different types of traces were assessed for *Porites* sp. (cf Figure 7: Violin Plot in Alaguarda et al., 2022 for the *Diploastrea* sp.).

5.3.4 Effects of the Coral Genus on the Abundance of Microbioeroding Traces over the Last 30 Years

Abundance of microbioeroding traces for *Diploastrea* sp. and *Porites* sp., obtained along the vertical coral growth axis, showed a significant decrease over the last 29 years ($p < 0.05$ Mann Kendall test; **Figure 5.6**).

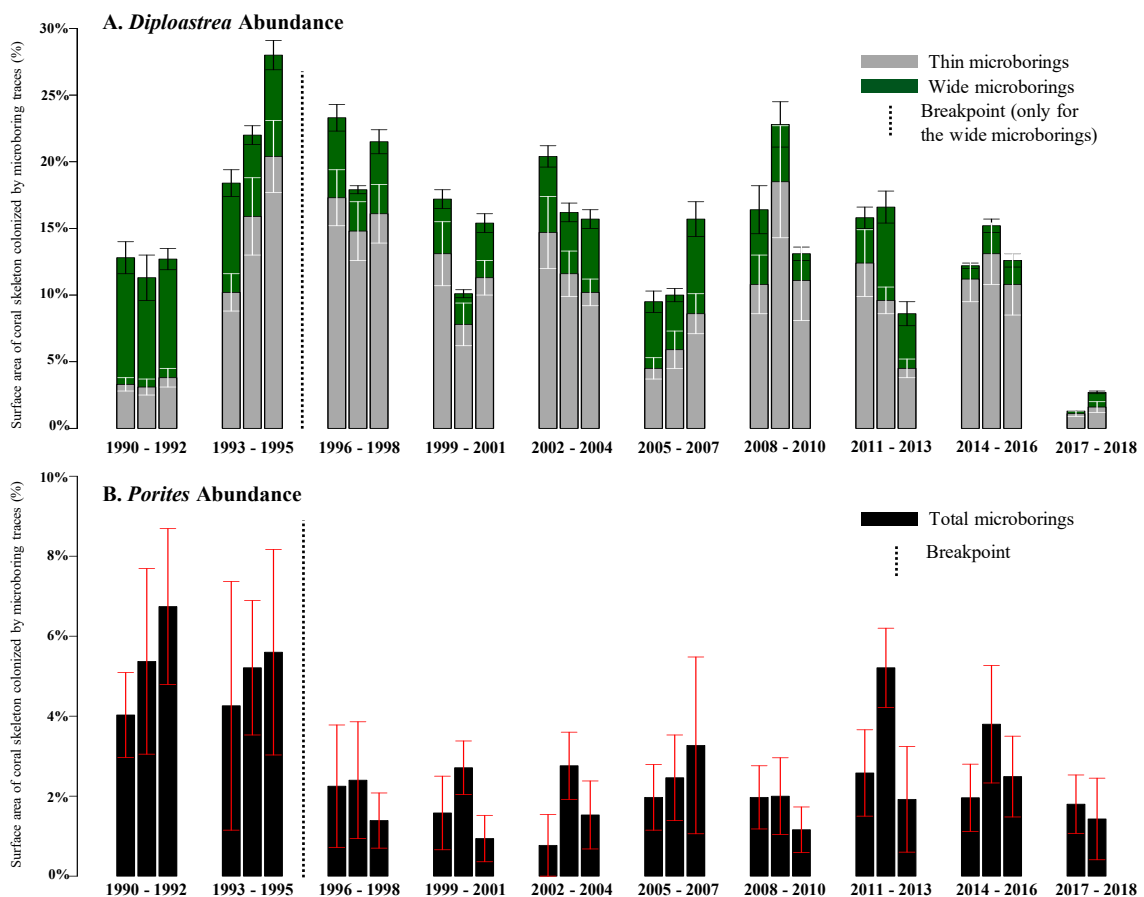


Figure 5.6: Variability of the percentage of coral skeleton colonized by microbioeroding communities over the last 29 years. (A) Histogram reporting the variability averaged (%) of the thin and wide microbioeroding traces and obtained along the *Diploastrea* sp. core. (B) Histogram reporting the variability (%) of the total microbioeroding traces obtained along *Porites* sp. core.

In *Diploastrea* sp., the highest abundances of microbioeroding traces were observed in 1995 ($28\% \pm 3.4\%$ of the coral skeleton colonized by microborers), while the lowest abundances were found in 2017-2018 (1.3 to $2.7\% \pm 0.35\%$; **Figure 5.6 A**). In *Porites* sp.,

the highest abundances of microbioeroding traces were observed in 1991-1992 (5.5 to $7\% \pm 2\%$ of the coral skeleton colonized by microborers) and 1995 ($5.6 \pm 2.5\%$), while the lowest abundances were found in 2001-2002 ($< 1\% \pm 0.7\%$; **Figure 5.6 B Appendix 8.3 Table 6**). The level of infestation of microbioeroding communities in *Diploastrea* sp. reached 3 to 4 times the level observed within the *Porites* sp. core. In *Diploastrea* sp., colonization of the coral surface by microbioeroding communities reached near 30%, while in *Porites* sp., the maximum of colonization was near 7% (**Figure 5.6 A and B**). In both corals, breakpoints were identified. For the *Diploastrea* sp., the identification of a breakpoint occurred in 1996-1997 (Pettit test, $p < 0.05$), concerning only the wide microbioeroding traces, while it occurred in 1995-1996 when considering the total microbioeroding traces in *Porites* sp (Pettit test, $p < 0.05$).

5.3.5 Main Factors Influencing the Abundance of Microbioeroding Traces Over the last 30 Years in Massive Corals

5.3.5.1 Main Factors Influencing the Abundance of Microbioeroding Traces in *Diploastrea* sp.

Considering raw data sets over the last 30 years, results showed that the decrease in the abundance of microbioeroding traces (total and thin abundance) was negatively correlated to the vertical extension rate ($p < 0.01$) but positively correlated to the skeletal bulk density ($p < 0.01$; **Table 5.1 and Appendix 8.3 Supp Fig.3**). Interestingly, the abundance of the wide microbioeroding traces was not correlated to any coral growth characteristics. The abundance of wide microbioeroding traces was negatively correlated to the SSTA, Max instant wind speed, and the pH_{CF} ($p < 0.05$), while positively with the precipitations and the cumulative insolation ($p < 0.05$; **Table 5.1**). On the other hand, the abundance of thin microbioeroding traces was negatively correlated with the precipitations ($p < 0.05$). Overall, compared to the period 1964-2018 investigated by Alaguarda et al. (2022, see their Table.3), correlations with the environmental parameters and the abundance of the different microbioeroding traces were still present or less important. For the correlations with coral parameters, the skeletal bulk density for 1964-2018 presents the same correlations observed in the present study. Alaguarda et al. (2022) highlighted correlations between the abundance of the total and thin microbioeroding traces with the vertical extension rate when considering the period 1986-2018. They were also observed in the present study.

A similar analysis was conducted on detrended data sets to reveal the main biotic and abiotic factors that could affect the inter-annual variability of the different microbioeroding assemblages (see **Appendix 8.3 Supp Fig.4**). This analysis confirmed that the growth rate and the skeletal density were significantly correlated to the total and mainly to the abundance of thin microbioeroding traces in *Diploastrea* sp. Interestingly, the abundance of wide microbioeroding traces showed no correlations to the different variables (growth and environmental). When comparing with the detrended period 1964-2018 investigated by Alaguarda et al. (2022, see their Table.4), the main differences concern the abundance of wide microbioeroding traces where in the present study, no correlations were highlighted.

Table 5.1: Pearson's correlations between the raw abundance of total microborers and raw environmental or coral growth variables over the last 30 years within *Diploastrea* sp., (upper part of the table). Pearson's correlations between the detrended abundance of total microborers and detrended environmental or coral growth variables over the last 30 years within *Diploastrea* sp., (lower part of the table). Code for significance: *** < 0.001; ** < 0.01; * < 0.05; · < 0.1.

Variables	Raw Dataset (1990-2018)		
	Total Microbioerodings	Wide Microbioerodings	Thin Microbioerodings
Vertical Extension Rate	-0.491**	NS	-0.416*
Skeletal Bulk Density	0.491**	NS	0.437*
Calcification Rate	NS	NS	NS
Instrumental SST (ERSSTv5)	NS	NS	NS
Instrumental SSTA (climatology 1971-2001)	-0.323*	-0.440*	NS
Precipitations	NS	0.394*	-0.344*
Max Instant Wind Speed	NS	-0.367*	NS
Cumulative Insolation	0.388*	0.483**	NS
pH _{CF} Instrumental	NS	-0.385*	NS
pH _{CF} Paleo-Proxy	NS	NS	NS
Variables	Detrended Dataset (1990-2018)		
	Total Microbioerodings	Wide Microbioerodings	Thin Microbioerodings
Vertical Extension Rate	-0.370*	NS	-0.370*
Skeletal Bulk Density	0.330*	NS	0.404*
Calcification Rate	NS	NS	NS
Instrumental SST (ERSSTv5)	NS	NS	NS
Instrumental SSTA (climatology 1971-2001)	NS	NS	NS
Precipitations	-0.354*	NS	-0.434*
Max Instant Wind Speed	NS	NS	NS
Cumulative Insolation	NS	NS	NS
pH _{CF} Instrumental	NS	NS	NS
pH _{CF} Paleo-proxy	NS	NS	NS

5.3.5.2 Main Factors Influencing the Abundance of Microbioeroding Traces in *Porites* sp.

Considering raw data sets over the last 30 years, results showed no correlations between the decrease of the total abundance of microbioeroding traces with any coral growth characteristics. The total abundance of microbioerodings was only significantly and negatively correlated to the pH_{CF} (Table 5.2, Appendix 8.3 Supp Fig.5). A similar analysis was conducted on detrended data sets to reveal the main biotic and abiotic factors that could affect the inter-annual variability of the microbioeroding assemblage. Interestingly, the detrended analysis showed a negative correlation between the pH_{CF} and the abundance of total microbioeroding traces (Table 5.2). The detrended analysis revealed a slight positive correlation with the calcification rate and the SST ($p < 0.1$) (see Appendix 8.3 Supp Fig.6).

Table 5.2: Pearson's correlations between the raw abundance of total microborers and raw environmental or coral growth variables over the last 30 years within *Porites* sp., (upper part of the table). Pearson's correlations between the detrended abundance of total microborers and detrended environmental or coral growth variables over the last 30 years within *Porites* sp., (lower part of the table). Code for significance: $\# < 0.1$; $* < 0.05$; $** < 0.01$; $*** < 0.001$; NS is for non significant.

Variables	Raw Dataset (1990-2018)
	Total Microbioerodings
Vertical Extension Rate	NS
Skeletal Bulk Density	NS
Calcification Rate	NS
Instrumental SST (ERSSTv5)	NS
Instrumental SSTA (climatology 1971-2001)	NS
Precipitations	NS
Max Instant Wind Speed	NS
Cumulative Insolation	NS
pH_{CF} Instrumental	-0.566**
pH_{CF} Paleo-proxy	-0.570**
Variables	Detrended Dataset (1990-2018)
	Total Microbioerodings
Vertical Extension Rate	NS
Skeletal Bulk Density	NS
Calcification Rate	0.330 $\#$
Instrumental SST (ERSSTv5)	0.356 $\#$
Instrumental SSTA (climatology 1971-2001)	NS
Precipitations	NS
Max Instant Wind Speed	NS
Cumulative Insolation	NS
pH_{CF} Instrumental	-0.609***
pH_{CF} Paleo-proxy	-0.598***

5.4 Discussion

5.4.1 Effect of Abiotic Parameters on the Abundance of Microbioeroding Traces in Massive Corals

Compared with the results of Alaguarda et al., 2022, the studied period 1990-2018 in the two massive corals highlighted much fewer correlations between the detrended abundance of microbioeroding communities and detrended coral and environmental variables than observed over the period 1964-2018. This might also be because considering a smaller time interval (e.g., 29 years) makes significant links between variables more difficult, whereas a longer timescale can reveal trends more significant. When looking at the coral *Diploastrea* sp., before 1990, the abundance of microbioeroding traces was correlated to the cumulative insolation (positively) and the precipitations essentially (negatively). After 1990, the correlation that lasted was only with the precipitations, and interestingly the sign changed. The major environmental difference between both periods is the influence of cumulative insolation on the abundance of microbioeroding traces. Therefore, the influence of environmental forcings on the abundance of microbioeroding traces in *Diploastrea* sp. differed between periods. Moreover, in *Diploastrea*, the abundance and composition of microbioeroding communities might be influenced by multiple factors such as SST/SSTA and also the precipitations (**Table 5.1**). SSTAs were negatively correlated to the skeletal density ($r = -0.385$, $p\text{-value} < 0.05$), and precipitations both negatively to skeletal density and calcification rate of *Diploastrea* ($r = -0.328$ and -0.425 , $p\text{-value} < 0.05$). In contrast, for *Porites* sp. coral, the skeletal density was positively correlated to the precipitations ($r = 0.383$, $p\text{-value} < 0.05$), and the calcification rate as well with the pair SST/SSTA ($r = 0.390$, $p\text{-value} < 0.05$). These findings suggest that even if both massive corals came from the same location (i.e., Mayotte), under identical environmental forcings, corals and their growth characteristics have responded differently to the environment from 1990-2018. Secondly, one hypothesis would be that microbioeroding communities within both massive corals could be different and adapted to the skeletal environment shaped by the coral, influenced by the environmental parameters. One primary difference concerns the influence of both corals' internal pH_{CF} on the abundance of microbioeroding communities. The significant correlation with the detrended pH_{CF} (**Table 5.2**) indicated that it might be one factor influencing the abundance and composition of microbioeroding communities

in *Porites* sp. In contrast, no correlations were observed with *Diploastrea* sp., (**Table 5.1**). It has been proven that the physiological regulation exerted by corals to modulate their CF chemistry is species or genus-dependent (Ross et al., 2019; Comeau et al., 2019). As pH_{CF} remains always above seawater pH (M. T. McCulloch et al., 2017; Schoepf et al., 2019, the magnitude of the up-regulation seemed species-specific with pH_{CF} significantly different between both corals, and was higher for *Porites* (8.483 ± 0.02) than for *Diploastrea* (8.472 ± 0.015 ; **Figure 5.3**). From the findings of Canesi (2022) of the "Tara Expedition" in the Pacific Ocean, she highlighted higher values of the reconstructed carbonates system (e.g. pH_{CF} , $[\text{CO}_3^{2-}]_{cf}$ and Ω_{cf}) in *Porites* corals compared to the *Diploastrea* corals from the South Pacific Ocean. She hypothesized that *Diploastrea* sp. might be less adapted than *Porites* sp. to important changes (SST, OA) and could consequently impact its skeletal development. In this study, even if both corals seemed to have maintained elevated levels of pH_{CF} (**Figure 5.3**), progressive warming and OA within the area (Lauvset et al., 2015; Monaco et al., 2021) could have led to changes in their physiology and growth conditions, such as decreased skeletal density (i.e., *Diploastrea* sp.) or reduced calcification rates (i.e., *Porites* sp. (see **Figure 5.4**; Anthony et al., 2011; Gattuso et al., 2013). Important differences between corals can be noticed in the period 2006-2018, where each growth characteristic seemed to describe an opposite "trend". This suggests that both corals, due to the influence of the environment, might have been impacted differently in their skeletal compartment, favoring one process compared to another (i.e., skeletal bulk density or calcification process). These biologically species-dependant characteristics and how they are influenced by the environment could be one of the reasons that potentially explain the differences in abundance and composition of microbioeroding communities of both corals. Reyes-Nivia et al. (2013) investigated that euendolithic microborers (e.g., *Ostreobium*) growth and dissolution activities of coral skeletons were stimulated under projected ocean acidification (also supported by Tribollet et al., 2019) and warming scenarios. Nonetheless, even if Mayotte experienced important warming over the years and potentially lower seawater pH conditions (Monaco et al., 2021), no increase in the abundance of microbioeroding traces in both corals was found. It may be possible that massive corals exert genus-specific physiological control that is not only driven by seawater chemistry and temperature but also by other biotic parameters. The metabolic efficiency of corals, photosynthetic rates, and growth characteristics may impact microbioeroding communities in both corals differently and might also explain the differ-

ences observed in their abundance and composition within both corals (Priess et al., 2000; Massé et al., 2018; Pernice et al., 2020; Ricci et al., 2023). Overall, environmental forcings may affect microbioeroding communities differently and are not the same factors between both massive corals over the last two decades. One hypothesis, based on findings from Canesi (2022), could be that values of the other variables of the carbonate system of *Porites* sp. could be higher than the ones of the *Diploastrea* from Mayotte. Therefore, an interesting approach would require further investigations regarding both corals' other carbonate system variables. If validated in another oceanic basin than the Pacific Ocean, these new findings could support that corals from the exact location exert different species-dependent regulation of their calcifying fluid properties and could have a different influence on the microbioeroding communities living within.

5.4.2 Effect of Skeletal Properties on the Abundance of Microbioeroding Traces in Massive Corals

A major finding that differentiated both massive corals was the percentage of colonization by microbioeroding communities. Colonization of the coral surface skeleton by microbioeroding traces within *Porites* sp. reached up 8% at maximum, while it was nearly 30% in *Diploastrea* sp. Differences in colonization might come from differences in the skeletal architecture of massive corals. *Diploastrea* possess large and complex corallite systems that might indicate that they may be more effective "photon traps" than other coral species (Teran et al., 2010; L. A. Marcelino et al., 2013; Swain et al., 2018), and subject to increase in abundance of microbioeroding phototrophs. Even if estimates suggested that up to 99% of the incident PAR were absorbed by the coral symbionts or scattered before reaching the endoliths (Halldal, 1968; Shibata and Haxo, 1969; Schlichter et al., 1997), similar values were derived from more recent *in situ* measurements, with 0.1–10% of incident PAR reaching the endolithic communities (S. H. Magnusson et al., 2007). Internal irradiance scattered within the coral skeleton is strongly influenced by coral species through variations in tissue thickness and skeletal morphology, as well as water depth. Several studies have described the important implications of coral structural complexity for light distribution (Ow and Todd, 2010; Wangpraseurt et al., 2012) and also have demonstrated the effectiveness of two-dimensional models for investigating the interaction between light and coral architecture on a colony scale (Muko et al., 2000; Anthony et al., 2005) and on a single corallite

scale. Fordyce et al. (2021) also found that large corallites and coenostemum width in *Goniastrea retiformis* favored the greatest endolithic biomass. In contrast, in their study, other corals with low corallite complexity and low calice/coenostemum width ratios had significantly lower microbial biomasses. Moreover, the authors found that the coral species with the highest skeletal micro-densities recorded the highest endolithic biomass. Nonetheless, they considered all endoliths and not only the euendoliths organisms.

Recently, Kramer et al., 2022 investigated how the micro-skeletal coral features of the coral *Stylophora pistillata* enhance light capture under low-light environments. They aimed to compare shallow (4–5 m) and mesophotic (45–50 m) corals. They found that microstructural features of corallites from mesophotic corals provided a greater ability to use solar energy under light-limited conditions. In contrast, corals associated with shallow morphotypes avoided excess light through self-shading skeletal architectures. Thus, their results suggest that corals' corallite constitutes a dominant structural component, influencing light harvesting, and is species-specific (Crabbe and Smith, 2006; Studivan et al., 2019). Moreover, as shown by Todd et al. (2004) in *Dipsastraea speciosa* (formerly *Favia speciosa*) and *Diploastrea heliophora*, the corallites expand and deepen, but are more spaced under shallow-water conditions. Thus, light scattering properties differ from one species to another, shaping the coral holobiont and its associated microbiota within the skeleton (Enriquez et al., 2005; L. A. Marcelino et al., 2013). Effective light capture at the external surface of the coral skeleton could either increase the light intensity in the coral skeleton for euendolithic development or decrease it by scattering light more effectively in the photo-symbiont coral tissue. Higher light intensity inside the habitat might increase phototrophic euendolith growth. Hence, despite the higher skeletal density of *Diploastrea* sp. compared to *Porites* sp., one hypothesis could be that the skeletal architecture composition and the structure of its large corallites and coenostemum make it more porous and effective in scattering light in the coral skeletal compartment than *Porites* sp. Such differences in the amount of light penetrating the coral skeleton of *Diploastrea* sp. vs *Porites* sp. may also explain the different microbioeroding community composition with species more adapted to low-light conditions in *Porites* than *Diploastrea*.

5.4.3 Evolution of the Abundance and Composition of Microbioeroding Traces in Massive Corals

Although only the total abundance of microbioeroding traces was quantified within *Porites* sp., different assemblages of trace makers colonizing the coral skeleton were identified. For instance, some microbioeroding traces were assembled in patches at the bottom of the core (**Figure 5.5**). The trace makers of these microbioeroding patches were probably eukaryotic phototrophs due to their shapes and orientation (light-dependent organisms; see also Kołodziej et al., 2012). They could also be attributed to different *Ostreobium* species (Lukas, 1974; V. R. Marcelino and Verbruggen, 2016). Nevertheless, assemblages of those microbioeroding traces were not observed in the *Diploastrea* sp., coral. On the other hand, no wide traces (10-30 μm) with specific ramifications, bulges, and/or cross-wall constrictions were observed in the *Porites* sp., coral. These differences in microbioeroding assemblages could suggest that both corals present different microbioeroding communities in their skeletons.

For the second time here, a significant decrease in the abundance of microbioeroding traces was highlighted over the life span of another slow-growing massive coral in the WIO: *Porites* sp. Also, a breakpoint in the total abundance of microbioeroding traces occurred around 1995-1996, coupled with a decrease of more than half of the initial abundance of microbioeroding traces (**Figure 5.6**). Interestingly, for the coral *Diploastrea* sp., statistical analysis confirmed the significant decrease in the abundance of microbioeroding traces whatever the period considered (here 1990-2018, and see Alaguarda et al., 2022). It also highlighted a second breakpoint (the first breakpoint was 1985-1986 but included 54 years) that occurred in the period 1996-1997 but concerned only the abundance of wide microbioeroding traces. The difference in identifying the breakpoint in both massive corals (i.e., one year difference) could be explained due to the precision when reconstructing the coral growth rate. Therefore, I suggested that both breakpoints for *Porites* sp. and *Diploastrea* sp. might be the same and defined for the period 1995-1997. Also, based on the visual observations of the SEM images from the *Porites* sp., the microbioeroding traces with a diameter comprised between 5 and 10 μm were mainly observed within the bottom of the core associated with the coral samples 14 to 12. From the coral chronology reconstruction, coral sample 12 corresponded to 1995-1996, when the breakpoint was identified in the total abundance of microbioeroding traces in the *Porites* sp. Therefore, one hypothesis could be that the

breakpoint identified at that time was related to a shift in the microbioeroding community. This shift could have concerned the microbioeroding traces with a diameter comprised between 5 and 10 μm toward traces measuring less than 5 μm . Therefore, based on these results, shifts in abundance, distribution, and composition of microbioeroding communities seemed to be identified in both massive corals from Mayotte. Nevertheless, it is necessary to provide a qualitative and accurate characterization of the evolution of microbioeroding communities colonizing *Porites* sp., to understand better the potential shift observed.

5.5 Conclusion

In this chapter, the ML approach from the *Diploastrea* sp. was enhanced to quantify the abundance of microbioeroding communities in another living coral colony *Porites* sp. over the last 29 years. The ML approach allowed the study of thousands of SEM images in a few hours with an accuracy of 95%. The study of a coral core of the very slow-growing massive coral *Porites* sp. confirmed a significant decrease in microborers' abundance and potentially a major shift in community composition over the last decades. Possible explanatory factors regulating the composition and abundance of microborers in *Porites* sp. are essentially the coral's internal pH_{CF} . Comparing both massive corals from the same location showed that the abundance of microbioeroding traces in both massive corals was influenced differently by the environment and the different coral growth characteristics. In both massive corals, a decrease of more than 50% of the initial abundance of microbioeroding traces was highlighted over the last two decades. Species-dependant coral skeletal micro-environments that influence scattering light properties most probably influenced the abundance and composition of microbioeroding traces between *Porites* sp. and *Diploastrea* sp. More coral cores of massive species presented different corallite architecture from contrasted environments should be investigated to understand better the controlling factors of euendoliths' abundance and their community composition to (i) confirm the observed trends found in *Porites* and *Diploastrea* sp. to (ii) understand better the possible implications of a significant decrease in microborers abundance in the health and resilience of living corals. Other environmental factors such as nutrients, DIC, and metal trace pollution could be again promising targets as these factors are known to affect mi-

microbioeroder's abundance in dead carbonates (Tribollet et al., [2006](#); Reyes-Nivia et al., [2013](#); Enochs, Manzello, Tribollet, et al., [2016](#)). Further exploring how and why the abundance and composition of euendolith vary between coral species is vital in defining the role of microbioeroding communities within living corals, both now and in the future, for reef carbonate budgets.

A Lipid Biomarker Approach to Identify Potential Molecules Indicative of Changes in Microbioeroding Community Composition and Abundance?

Contents

6.1	Why Use Lipid Biomarkers in Marine Ecology?	213
6.1.1	What is a Biomarker?	213
6.1.2	Corals and Known Lipid Composition	215
6.1.3	Objectives	218
6.2	Materials and Methods	219
6.2.1	Sampling Strategy	220
6.2.2	Samples Preparation	221
6.2.3	Extraction and Separation Procedure	222
6.2.4	Identification and Quantification of Lipid Biomarkers on Gas Chromatography-Mass Spectrometry (GC-MS)	223
6.3	Results	225
6.3.1	Lipid biomarkers Composition: Monoalgal Culture <i>Ostreo-</i> <i>bium</i> sp. O10	225
6.3.1.1	F1 Fraction: Hydrocarbons Composition	225
6.3.1.2	F3 Fraction: Alcohols and Sterols Composition	225

6.3.1.3	FA Fraction: Fatty Acids Composition	226
6.3.2	Lipid biomarkers Composition: <i>Diploastrea</i> sp.	227
6.3.2.1	F1 Fraction: Hydrocarbons Composition	227
6.3.2.2	F3 Fraction: Alcohols and Sterols Composition	227
6.3.2.3	FA Fraction: Fatty Acids Composition	229
6.4	Discussion	231
6.4.1	Lipid Biomarkers Profile: Monoalgal Strain O10	231
6.4.2	Lipid Biomarkers Profile: <i>Diploastrea</i> sp.	234
6.4.3	Amide Lipid Biomarkers: Proxies of microborers ?	236
6.5	Conclusion	239

Article in prep

for a submission in the Journal: *Organic Geochemistry*

6.1 Why Use Lipid Biomarkers in Marine Ecology?

6.1.1 What is a Biomarker?

A biomarker represents a measurable molecular, biochemical, cellular, or physiological change of an organism, community, or environmental substrate (Depledge and Fossi, 1994). Biomarkers are specific organic molecules that can be traced back to their natural source organism in the environment. During the last few decades, molecular markers revealing polymorphism at the DNA level have been playing an increasing part in environmental sciences and genetics studies (Vignal et al., 2002; Kumar et al., 2009). For instance, molecular genetic analyses can provide important insights into the evolutionary biology of marine organisms and the understanding of the origin and maintenance of biodiversity in marine ecosystems (Junior et al., 2006). In marine ecosystems, chlorophyll *a* (photosynthesis pigment and its degradation products) can be used as a biomarker to estimate phytoplankton biomass and productivity and represents the most frequently performed analysis in aquatic ecology (Mantoura and Llewellyn, 1983; Stauber and Jeffrey, 1988). Nevertheless, pigments undergo chemical changes after the death of the cells in which they were contained. They ultimately oxidize to colorless compounds (Moss, 1968) and are rarely preserved for extended periods (Sanger, 1988). To overcome this constraint, other organic biomarkers in various materials (soils, sediments, and plant/animal products) make it possible to measure and reconstruct geochemical parameters, record past variations of ocean surface properties like salinity, temperature, and redox state in marine sediments (Brocks and Banfield, 2009; Luo et al., 2019). This is the case with lipids, which have been used in many different areas, including petroleum geology, paleoclimatology, oceanography, meteorology, geobiology, environmental science, and food-web dynamics (Alfaro et al., 2006; Luo et al., 2019). Lipids are well preserved over time (= molecular fossil), so they can also be used to reconstruct highly ancient microbial diversity. Lipids also present different functions within living organisms, separated into (i) reserve lipids, (ii) structural lipids, and (iii) metabolic lipids. The lipid biomarker approach refers to structural lipids (e.g., membranous for studying lipid functions in biological processes) and their hydrocarbon derivatives in geological materials containing diverse information such as biotic sources (composition and biomass of dead and/or alive (micro)organisms) or environmental conditions (Luo et al., 2019). In marine ecosystem studies, lipid biomarkers analyses focus on different classes represented by the phospholipids, hydrocarbons

(alkanes), ketones, alcohols and sterols and fatty acids (C. Parrish et al., 2000; **Table 6.1**).

Table 6.1: Main classes of lipid biomarkers and their interest in marine geochemistry.

Lipid Biomarker Class	Source	Interest	Degradation	References
Phospholipids (PL)	Essential components of membranes in plants and animals. Share a structural function with sterol.	Phospholipids can indicate freshly bio-synthesized material. PL may be used to distinguish bacteria and phytoplankton	Intact phospholipids are known to be hydrolyzed within weeks after cell death. Their presence in sediments is thus a good indicator of the presence of alive biomass.	White et al., 1979; Harvey et al., 1986; Goutx et al., 1990; Guérin et al., 1993; De Silva et al., 1998; Rütters et al., 2002
Hydrocarbons (alkanes)	Minor components of zooplanktonic species (3% dry-weight). A major component of certain microalgae. Hydrocarbon markers include alkanes derived from algae or plant leaves.	Hydrocarbons act as suitable markers for distinguishing different source inputs in marine sediments and for investigating the cycling of organic matter in the marine environment.	Alkanes are trace constituents of biological lipids. Alkanes have excellent preservation characteristics (highly resistant).	Lee and Loeblich III, 1971; Barrick et al., 1980; Salot, 1981; Bouloubassi and Salot, 1993; Gonzalez-Vila, 1995; C. Parrish et al., 2000
Ketones	In marine systems, ketones are essentially present in phytoplanktonic algae belonging to the class of the prymnesiophytes (family Coccolithophyceae). Ketones can also be found in higher plants (terrestrial systems).	Interest in their use as paleo-temperature indicators. Ketones could be excellent water column markers of productivity in some areas. For example, alkenones can inform on the paleo-productivity of continental and marine vegetation and animals.	Ketones have excellent preservation characteristics.	Conte and Eglinton, 1993; Sikes and Volkman, 1993; Sicre and Ternois, 2006
Alcohols	Generally minor compounds in the marine environment. Terrestrial higher plants are major sources of wax esters and fatty alcohols.	They can be used as an organic matter source and degradation index.	Alcohols have excellent preservation characteristics.	Sargent et al., 1977; Mudge and Norris, 1997
Sterols	Essential constituents of membranes in all eukaryotes, including microalgae. They share with PL a structural function in membranes (unique hydrophobic and steric properties). They act as specific internal regulators of membrane fluidity and influence various membrane functions and membrane-associated enzymes.	Excellent biomarker compounds due to the stability and diversity of their structures. Sterols can be highly specific to a class of organisms (e.g., dinosterol for dinoflagellates). In algae and many invertebrates, various sterols are used for chemo-taxonomic purposes and food web tracing.	They are known for their chemical resistance to biodegradation in the marine environment (Long term valuable biomarkers = paleoproxies of organisms productivity).	J. K. Volkman, 1986; J. Volkman et al., 1989; Patterson and VanValkenburg, 1991; Teshima, 1991; Barrett et al., 1995
Fatty Acids	Fatty acids are present in animal and vegetable fats and vegetable oils. Fatty acids play a fundamental structural role in all known life forms, structuring all biological membranes (cell membrane, endoplasmic reticulum membrane..). Fatty acid biomarkers are common to determine general micro-organism sources in marine samples (micro-algae, aerobic/anaerobic bacteria).	They are biomarkers to infer trophic relationships in aquatic and soil food webs. FAs are used to determine phytoplankton sources in marine samples. Long-chain (> 24 carbons) fatty acids are often used as terrestrial plant indicators, compare to short ones, which are more characteristic of phytoplankton sources	FA signatures remain adequately reliable for long periods even without preservation in the deep freeze.	Galloway and Budge, 2020; C. Parrish et al., 2000; Budge and Parrish, 1998; J. Taylor and Parkes, 1983; Caudales and Wells, 1991; Nieminen et al., 2018; Claustre et al., 1988

6.1.2 Corals and Known Lipid Composition

Lipids are involved in many biochemical and physiological processes in corals, representing 10 to 40% of their dry biomass (Conlan et al., 2017). Variability in lipid composition reflect thus change in environmental conditions, nutrition or coral health status. Recently, coral lipid investigations have gained attention to understand current and future climate change impacts on coral reefs' physiology (Baumann et al., 2014). Specifically, coral lipid reserves can be used as a universal proxy for coral health status, given their ubiquitous nature (Anthony et al., 2009; Lesser, 2013). Coral lipid profiles vary significantly in response to physiological processes such as photosynthesis, respiration, cell replenishment, and reproduction, and these processes, in turn, are influenced by external physico-chemical factors such as water chemistry, rainfall, temperature, and food availability (Leuzinger et al., 2003; Imbs, 2013). Overall, bibliographic analysis revealed that 560 publications on coral lipids have been published since 1970 (ISI Web of Science; see Table 6.2). Nonetheless, various compartments in the coral holobiont should be distinguished: polyp tissue (which includes the animal itself and all microbes present within tissues), the isolated endosymbionts (i.e., zooxanthellae), which are located in coral tissues, the mucus layer (which comprises organic matter from the coral, zooxanthellae and bacteria) and the aragonite skeleton. The coral holobiont includes dinoflagellates, bacteria, archaea, fungi, and viruses (V. R. Marcelino and Verbruggen, 2016; Hernandez-Agreda et al., 2017; Ricci et al., 2019), but also a range of euendolithic communities (Schönberg et al., 2017; Yang and Tang, 2019). The coral microbiome plays a key role in host health by being involved in energy metabolism, nutrient cycling, immune system formation, and the host's ability to cope with complex and changing marine environments (Foo et al., 2017; Zhang et al., 2021). It was shown that abiotic stressors (e.g., SST) alter the coral holobiont, resulting in a breakdown of host-symbiont relationships and a shift in the diversity of resident microbes (Hoegh-Guldberg, 1999; Banin et al., 2000; Bourne et al., 2008). Within the coral holobiont, the aragonite skeleton is known to comprise a wide range of several taxa (bacteria, archaea, micro-algae, fungi, as well as macroborers), and a broad distinction is made among organisms that can bore into the coral skeletal compartment (Golubic et al., 1981; Tribollet and Golubic, 2011). Chasmo-endoliths can colonize existing cracks and fissures in the coral skeleton. Crypto-endoliths can colonize pre-existing cavities within porous coral skeletons. Euendoliths can actively penetrate carbonate skeletons and reside partially or totally inside cavities of their own making (Golubic et al., 1975);

Tribollet, 2008). Among the coral holobiont, much more attention has been given to studying lipid compositions of polyp tissues and isolated endo-symbionts than other compartment of the coral (Zhukova and Titlyanov, 2003; Tchernov et al., 2004; **Table 6.2**).

Table 6.2: Lipid biomarkers studied within the different coral compartments, their known functional roles, and the degree of attention, they received.

Coral Compartment	Lipid Biomarker Class	Role of Lipids	Investigation	References
Polyp Tissue with symbionts	Triacylglycerols (TG), Wax (WX), Sterol esters (SE)	Storage lipids and determine the energy balance of corals.	+++	Seemann et al., 2013; Towle et al., 2015; Crandall et al., 2016
Isolated Zooxanthellae (<i>Symbiodinium</i>)	Polar lipids (PL), Sterols (ST), Polyunsaturated FA (PuFA).	Polar lipids (PL) and sterols (ST) are the structural basis of cell membranes in corals and their symbionts. Some polyunsaturated FA (PuFA) were shown to be specific biomarkers of zooxanthellae. High PuFA content protects thylakoid membranes from oxidative damage by reactive oxygen species (ROS) during thermal stress. Utility as an indicator of taxonomic sensitivity to thermal stress.	+++	Grottoli et al., 2004; Bachok et al., 2006; Zhukova and Aizdaicher, 1995; Zhukova and Titlyanov, 2003; Tchernov et al., 2004; Imbs, 2013; Kneeland et al., 2013
Coral Mucus Layer (ML)	Composition of the mucus in 1/3 of dry tissue was lipids. Phospholipids constitute a large fraction of lipids in floating mucus aggregates. Sterols are not abundant in the mucus present at the polyp surface. Mucus from various reefs was found to contain wax ester and triglycerides.	Lipids in mucus exuded by corals serve as food resources for many reef organisms, including fishes. Mucus constituents have a role in energy transfer in marine communities	+++	Crossland et al., 1980; Crossland, 1987; Daumas et al., 1981; Johannes, 1967; Coles and Strathmann, 1973; B. Brown and Bythell, 2005; Bythell and Wild, 2011; Rix et al., 2016
Coral Skeleton	Triacylglycerol, Fatty acid, Amino acid composition, proteins (aspartic, glutamic acid).	potential in coral calcification? (known mostly for amino-acids).	+	Isa and Okazaki, 1987; Ingalls et al., 2003; Conlan et al., 2017
Bioeroding microflora: monocultures of free-living vs microbioeroding forms of <i>Ostreobium</i> sp.	Fatty acids with a majority of saturated FA within the microbioeroding forms and a majority of PuFA in the free-living forms.	Involved in biological membranes fluidity, permeability, and cellular signalization. Variability in the membrane FAs composition suggests adjustments due to lifestyle constraints (seawater vs. coral skeleton).	-	Massé et al., 2020 Focus on the physiology of <i>Ostreobium</i> (free-living vs. microbioeroding form)

Comprehensive quantification, identification, and role of lipids retained by the skeleton need to be better documented. Coral skeletons provide an ideal archive to extract climate and environmental information and the physiological responses of corals to changes, as shown in the previous Chapters (4 and 5. While inorganic geochemical approach in coral skeletons are intensively used as paleo-oceanographic and cli-

matic proxies (Druffel, 1997), organic geochemical approach in coral skeletons has been overlooked. The organic matter in coral skeletons can be well preserved over long term. Ingalls et al. (2003) investigated lipid concentrations in 0–300-year-old annual corals from *Montastraea annularis* (Florida Keys) and *Porites lutea* (Red Sea). They highlighted the preservation of lipids in coral aragonite skeletons at concentrations greater than $1 \mu\text{mol C.g}^{-1}$ providing the potential for reconstructing paleo-environmental records. Fatty acids, and sterols, which are often highly specific molecule (e.g., Badwey et al., 1984), have the potential to be preserved as intra-crystalline lipids for centuries (Ingalls et al., 2003). To date, no studies focused on analyzing lipid biomarkers composition of microbioeroding communities within living coral skeletons to understand better the effects of long-term environmental changes on microbioeroding communities. Algae including microalgae, synthesize many specific compounds (long-chain alkanes, distinctive sterols, or unsaturated fatty acids) that can be used as biomarkers for sources of organic matter in marine ecosystems (Han et al., 1968; Jeffries, 1970; J. K. Volkman, 2006). Bacteria and marine fungi can also synthesize specific fatty acids that can be used as biomarkers for micro-organisms' chemotaxonomy (Mukwaya and Welch, 1989; De Silva et al., 1998; Madan et al., 2002). This can give access to information related to germination, sporulation, and physiological processes (Weete and Weber, 1980). Concerning the microbioeroding flora in reef environments, only Massé et al. (2020) published results on fatty acids composition from monoalgal cultures of *Ostreobium* sp., maintained as microbioeroding and free-living forms. Saturated fatty acids (SFA) dominated microbioeroding forms versus PuFA in free-living forms. The major difference between both forms concerned the arachidonic acid that could reach concentrations 30x higher in some free-living lineage of *Ostreobium* sp. compared to microbioeroding ones. This FA is a constituent of phospholipids in biological membranes, involved in fluidity, permeability, and cellular signalization (Maulucci et al., 2016). For instance, variations of arachidonic acid concentrations could be used as an indicator to understand the variability of the abundance of *Ostreobium* sp. among coral skeletons over the long term. In their study, Massé et al. (2020) did not aim to study the chronological evolution of fatty acids composition or other classes of lipid biomarkers of *Ostreobium* sp. over time. Hence, there is still a gap in understanding the lipid biomarker composition of *Ostreobium* sp. and microbioeroding communities in general over the long term.

6.1.3 Objectives

To identify the potential variability of lipid biomarker composition and concentration of the most abundant microbioeroding organism within living corals, the siphonous chlorophyte *Ostreobium* sp. along the coral core, I first analyzed a strain of *Ostreobium* sp. named O10, as a ‘reference’. This strain was provided by Anaïs Massé and Isabelle Domart-Coulon from MNHN (Paris, Massé et al., 2020). It was initially isolated from coral colonies of *Pocillopora acuta* growing in closed-circuit at the Aquarium Tropical du Palais de la Porte Dorée (Paris, France; Massé et al., 2018) and cultivated on a medium of Provasoli Enriched Seawater medium (PES; Provasoli, 1968; see Massé et al., 2020) under non-axenic conditions. The studied monoalgal strain O10 here, was a free-living form (not microbioeroding) of *Ostreobium* sp., conserved at -20°C before analysis. For this study, one main objective was to:

- Analyze the lipid biomarker composition and abundance of a monoalgal strain of a free-living form of *Ostreobium* sp. cultivated under controlled conditions at the MNHN, Paris. I used N. Chevalier et al., 2015 protocol as I wanted to study FA like Massé et al. (2020) but also to focus on other fractions: F1 (hydrocarbons), F3 (alcohols/sterols), and FA (fatty acids). Those different fractions can indicate the presence of various organisms such as bacteria, cyanobacteria and fungi, and are the most represented fraction to study biological precursors that consequently accumulate in environmental substrates (e.g., sediments, carbonates; Meyers, 2003; Ranjan et al., 2015).

Then, I intended to study:

- The variability of the lipid biomarker composition of the skeleton of a living massive slow-growing coral of the genus *Diploastrea*, as it was the only coral core presenting visible green bands upon the skeleton. The lipid fractions investigated were the same as in the mono-algal strain O10 (F1, F3, and FA). This core served as a “test” to estimate if the lipid geochemistry approach would give exploitable and relevant results before applying it to other coral cores.

6.2 Materials and Methods

The approach of lipid biomarker analysis comprised different chemical steps (lyophilization, extraction, separation, visualization...) summarized in the **Figure 6.1**. Each step is described and detailed in the following sections. The analyses were performed at the campus Pierre et Marie Curie (Paris, France) on the organic geochemical platform (GEORG).

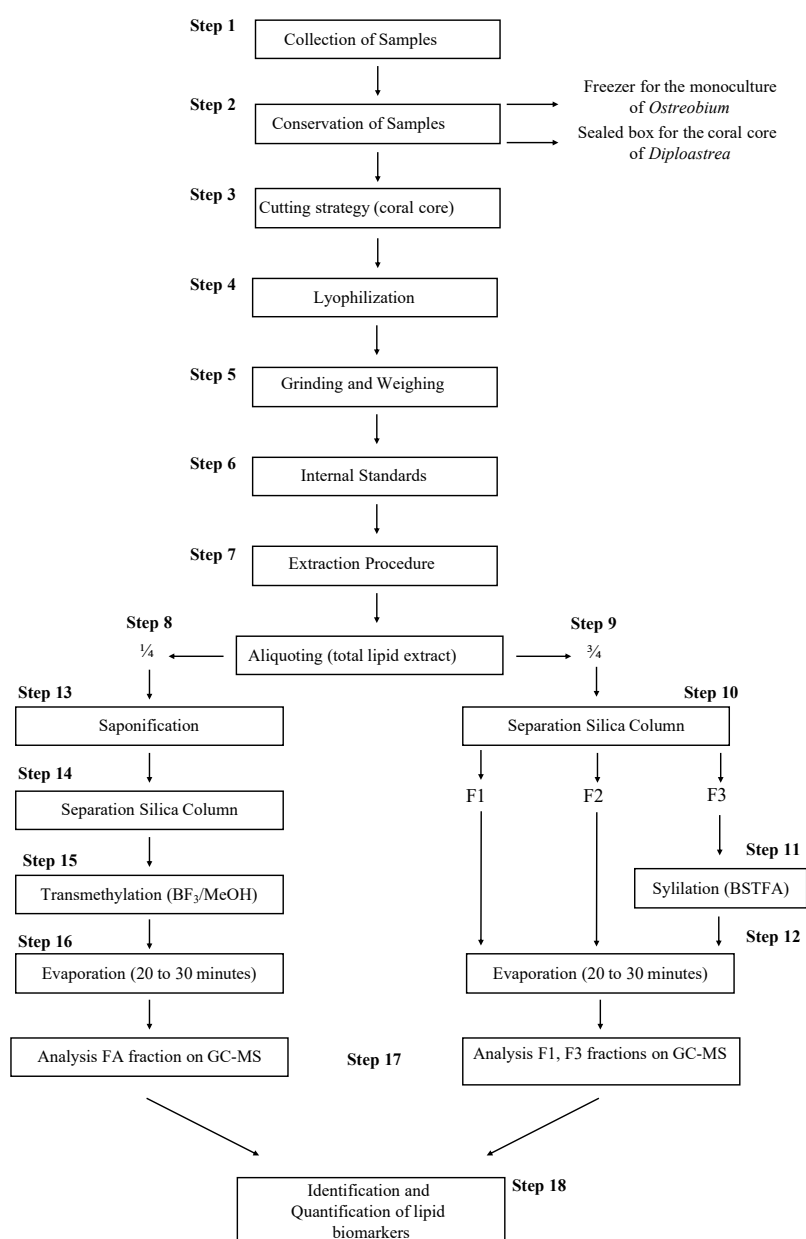


Figure 6.1: Schematic representation of the organic geochemistry protocol applied on samples of the coral core *Diploastrea* sp from Mayotte and the monoalgal strain of *Ostreobium*

6.2.1 Sampling Strategy

The studied coral core was collected from a well-preserved massive slow-growing coral of *Diploastrea* sp (outer slope of the NE Mayotte barrier reef; Lat. 12°37'19.4"S - Long. 45°06'42.7"E; Alaguarda et al., 2022). Among the sampled coral cores, it was the only core presenting an alternate banding pattern of white and green bands. The coral core measured 19.5 cm in length (Figure 6.2). At the sampling time (October 2018), 10 green bands were eye visible. The coral core was preserved and dried under dark conditions in a box at the Center IRD of Bondy (LOCEAN). Nevertheless, at the time of analysis for lipid biomarker investigation, only 7 green bands remained easily eye-visible and were used to collect sub-samples to analyze microbioeroding traces exposing pigments to light (and thus degradation; Figure 6.2). The coral core was thus cut according to the visible alternate banding pattern. Thirteen sub-samples were cut in total (Steps 1 to 3 in Figure 6.1).

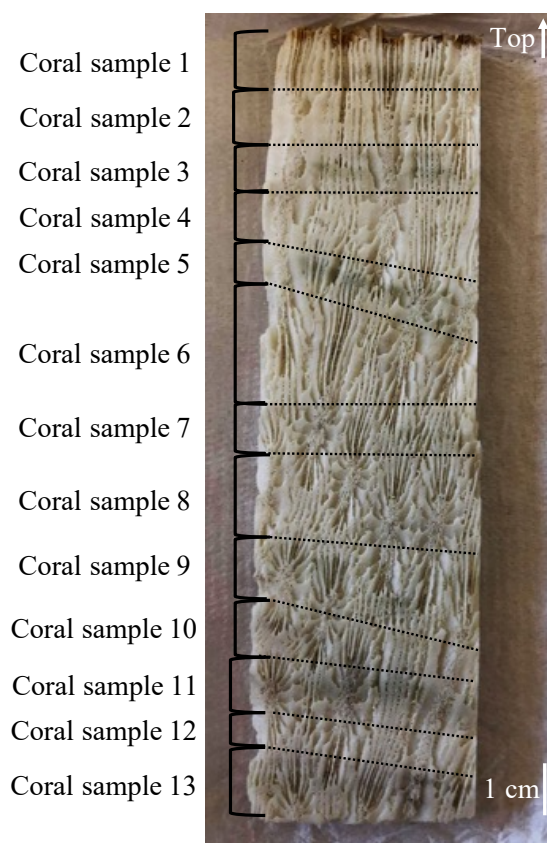


Figure 6.2: Schematic representation of the slab's cutting pattern *Diploastrea* coral core for quantification of the lipid biomarkers of microborers comparing white and green band.

6.2.2 Samples Preparation

The 13 coral sub-samples and the monoalgal strain culture O10 were freeze-dried at -50°C. The lyophilization is essential: Lipids are hydrophobic compounds, so this step eliminates any water molecules within the samples for better organic extraction. Then, each sub-sample of the coral skeleton was ground to obtain a very thin powder. Each grounded sub-sample was then weighed to get a dry-weight of each sub-sample (Steps 4 to 5 in **Figure 6.1**; **Table 6.3**).

Table 6.3: Dry-weight of each sample used for the lipid biomarker analysis.

Sub-sample identification	Band Characteristics	Dry Weights (g)	Sub-sample Length (cm)
Monoalgal strain <i>Ostreobium</i> O10	No bands	3 mg	X
sub-sample 1	Green bands	3.9	1.5
sub-sample 2	White bands	3.7	1.3
sub-sample 3	Green bands	3.2	1.1
sub-sample 4	White bands	4	1.5
sub-sample 5	Green bands	3.4	1.1
sub-sample 6	White bands	6.5	2.3
sub-sample 7	Green bands	3.3	1.2
sub-sample 8	White bands	6.5	2.3
sub-sample 9	Green bands	4.2	1.6
sub-sample 10	White bands	3.2	1.3
sub-sample 11	Green bands	4	1.5
sub-sample 12	White bands	2.3	0.9
sub-sample 13	White bands	4.5	1.8

Before the extraction of total lipids in each sample with the organic solvent, step 6 (**Figure 6.1**) consists of the addition of internal standards.

- A classical external calibration: during an external calibration, a range of standards with a known concentration(s) are prepared for the chemical molecules of interest. The obtained signal of each standard(e.g., intensity of the signal) is thus correlated to the concentration of the standard. A calibration curve is then realized, giving the signal's intensity compared to the standard's concentration. Thanks to the calibration curve (and the calibration equation), the concentration of the studied molecule in a sample can be calculated from the signal intensity. Nonetheless, in our study, uncertainties are possible with external calibration. Imprecision on the volume of the analyzed sample solution may result in potential errors in the real concentration of lipid biomarkers in a sub-sample. Moreover, yield losses can occur during the different steps of the protocol, which would imply an underestimation of lipid concentrations.

- An “internal” quantification was used here to eliminate these biases. This consists of the addition of “internal” standards (lipids here) in a known amount in each sample

at the beginning of the protocol (before extraction, after grinding and weighing, see Step 6 in Fig.6.1). For our study, solutions with internal standards are prepared with a known concentration. For each lipids class, the internal standard's chemical behavior must be equivalent to the lipid biomarkers of interest during all protocol steps. Thus, three different internal standards for the quantification of the different lipid biomarkers were added in the three fractions:

- 1) 10 μ L of Cholestane ($C_{27}H_{48}$) were added for the quantification of lipids in the F1 fraction in (Alkanes).
- 2) 10 μ L of Androstanol ($C_{19}H_{30}O$) were added for the quantification of lipids in the F3 fraction (Alcohols and Sterols).
- 3) 20 μ L of Cholanil Acid ($C_{24}H_{40}O_2$) were added for the quantification of lipids in the FA fraction (Fatty Acids).

6.2.3 Extraction and Separation Procedure

The seventh step consists of extracting the total lipids with organic solvents. Total lipids in each coral sub-sample as well as the monoalgal strain O10 were extracted three times with a mixture of two volumes of Dichloromethane (DCM; CH_2Cl_2) and one volume of methanol (MeOH; ratio 2:1) (Poole and Poole, 2003; Romero and Feakins, 2011) (Step 7 in Figure 6.1). The total lipid extract was then separated into two aliquots: A $\frac{1}{4}$ aliquot (Step 8 in Figure 6.1) was dedicated to the analyze of Fatty Acids (see details below), and the $\frac{3}{4}$ aliquot was dedicated to the analysis of the fractions F1 and F3 (Step 9 in Figure 6.1). The total lipid extract of the $\frac{3}{4}$ aliquot is separated into three different fractions. This separation step was carried out on a silica chromatography column, using different organic solvent solutions characterized by different polarities. First, the total lipid extract of the $\frac{3}{4}$ aliquot was evaporated under a stream of nitrogen and reconditioned with 200 μ L of pure hexane (the most apolar organic solvent) The 200 μ L was deposited on the silica column, and then 4 mL of hexane was eluted on the silica column to obtain the first fraction (F1). Secondly, the sample was reconditioned in 5 mL of a Hexane and DCM mixture (50/50) and deposited on the silica column to obtain a second fraction (F2). Finally, the silica column was washed with a solvent representing a mix of DCM and Acetone (90/10) to elute and obtain the F3 fraction (Step 10 in Figure 6.1). The separation procedure allows obtaining more "clean" fractions: this is a step of purification to decrease the number of lipids detected during the analysis. Indeed, better identification and quantification of the lipids is thus possible in each

fraction compared to the total lipid extract. After the separation in three fractions, the F3 fraction was derivatized (silylation) with N, O-bis(trimethylsilyl) trifluoroacetamide (BSTFA, Thermo Scientific), and pyridine to form trimethylsilyl-(TMS)ethers (Bornstein, 1980). This reaction (Step 11 in **Figure 6.1**) allows for better detection of alcohols and sterols during the analysis on Gas Chromatography-Mass Spectrometry (GC-MS). Concerning the analysis of FA fraction, the aliquot $\frac{1}{4}$ was saponified with 6% KOH in methanol (80 °C, one hour; Step 13 in **Figure 6.1**) to convert esters into carboxylate ions and alcohols. This reaction allows the production of total fatty acids. The total FA fraction was taken, evaporated, and reconditioned in Toluene (solvent). The fraction was deposited on a silica column to obtain a clean fraction with FAs (Step 14 in **Figure 6.1**). FAs were trans-methylated using Boron Trifluoride with Methanol (BF₃/MeOH, Regis; Nordby and Nagy, 1971) (Step 15 in **Figure 6.1**). As for the alcohols and sterols, this reaction allows fatty acid methyl esters to be formed for better detection during the GC-MS analysis (FAMES; Eder, 1995). Finally, all the fractions were evaporated under a stream of nitrogen between 20 to 30 minutes, reconditioned in 100 µl of analysis solvent (hexane or toluene), and stored at -20°C before GC-MS analysis (Steps 12 and 16 in **Figure 6.1**).

6.2.4 Identification and Quantification of Lipid Biomarkers on Gas Chromatography-Mass Spectrometry (GC-MS)

For the identification and quantification of lipid biomarkers, the three fractions (F1, F3, FA) were analyzed on GC-MS using an Agilent 7890 A (**Figure 6.3**).

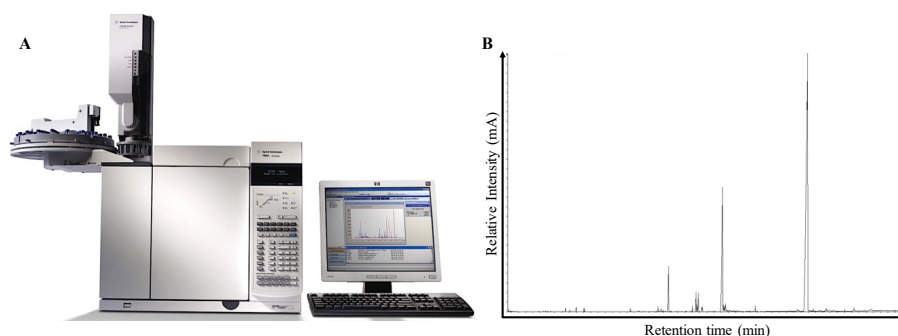


Figure 6.3: (A) Photograph of the Agilent 7890 A GC-MS used for the quantification and identification of the lipid biomarkers. (B) Example of a chromatograph showing the relative intensity compared to the retention time of lipid biomarkers from the FA fraction of *Ostreobium*

GC, equipped with a fused silica capillary column (30m x 0.25mm inner diameter, 0.25 µm film thickness) for separating lipids, was coupled to an Agilent 5975 C MS instru-

ment (for identification) at the laboratory LOCEAN (Step 17 in **Figure 6.1**). The F2 fraction was directly stored at -20°C for later further investigation. GC-MS operated with an ionization energy of 70 eV with a scanning mass range of m/z 50–800. The temperature program of the GC oven was as follows (Akhoudas et al., 2018):

- (i) For alkanes (F1): increase from 50 to 120 °C at a rate of 30 °C/min, then to 320 °C at a rate of 5 °C/min. The temperature was held at 320 °C for 7 min.
- (ii) For alcohols and sterols (F3): increase from 50 to 100 °C at a rate of 30 °C/min, then to 150 °C at a rate of 15 °C/min followed by an increase to 300 °C at a rate of 3 °C/min. The temperature was then kept constant for 45 min.
- (iii) For Fatty acids (FA): increase from 50 to 100 °C at a rate of 30 °C/min, then to 310 °C at 2 °C/min, and finally maintained at 310 °C for 35 min.

A chromatogram is thus obtained for each fraction of the sub-samples. On the axis of retention time of the obtained chromatogram (**Figure 6.3**), one peak generally represents one lipid. Lipids are identified by comparing their mass spectrum and a data bank of mass spectra of known lipids. Quantification of lipid biomarkers is based on the GC response (peak area) relative to internal standards as indicated above (cholestane, androstanol, and cholanolic acid) within the respective lipid fraction. To obtain the mass of a lipid biomarker present in the sub-samples, the following calculation is realized:

$$LBM = \frac{P_{lb} \times m_i}{P_i} \quad (6.1)$$

where LBM represents the lipid biomarker biomass estimated with P_{lb} that represents the peak's area of lipid biomarker identified in the chromatogram, m_i represents the mass of the internal standard (ng), and P_i represents the peak's area of the internal standard. Finally, to obtain the lipid biomarker concentration (per dry weight of the sub-sample considered):

$$LBM_{ps} = \frac{LBM}{DWS} \quad (6.2)$$

LBM_{ps} represents the lipid biomarker biomass per sub-sample and DWS the dry weight of each sub-sample (g). The concentrations of FA were calculated based on the cholanolic acid (internal standard for FA; Equation 6.2). The concentrations of F3 were calculated based on the androstanol (internal standard for F3; Equation 6.2). Regarding statistical analysis used in this study, the non-parametric Mann-Kendall test was

performed to assess the observed trend on each profile of lipid biomarker from the coral core of *Diploastrea* sp was significant. Multiple visible green bands were identified on the coral core of *Diploastrea* sp. (n=7). Concentrations were averaged regarding the band's nature for each lipid biomarker detected. The first two bands (1 green + 1 white) were not used as they might reflect the coral tissue's lipid biomarkers composition and signals from the zooxanthellae and not reflect the lipid biomarker composition of the coral skeleton. Thus, the concentrations of lipid biomarkers identified within the coral skeleton were averaged for all white bands (n=5) and all green bands (n=6). A non-parametric Wilcoxon Mann-Whitney test was adapted to low-size samples to estimate the possible differences in lipid biomarker concentrations between green and white bands.

6.3 Results

6.3.1 Lipid biomarkers Composition: Monoalgal Culture

Ostreobium sp. O10

6.3.1.1 F1 Fraction: Hydrocarbons Composition

No lipid biomarker was detected regarding the lipid biomarkers composition of the F1 fraction of the monoalgal strain O10.

6.3.1.2 F3 Fraction: Alcohols and Sterols Composition

The representative alcohols/sterols profile obtained by gas chromatography (GC-MS) was illustrated in **Figure 6.4**. No alcohol lipid biomarkers were identified in the monoalgal strain O10. In contrast, a total of 4 sterols were detected. The presence of cholesterol and campesterol was detected in relatively low abundance (147 and 151 $\mu\text{g/g}$ respectively) compared to the presence of cholestanol (619 $\mu\text{g/g}$) and β -Sitosterol (1043 $\mu\text{g/g}$) detected in high abundance. The β -Sitosterol was 7x higher than the cholesterol and campesterol (**Table 6.4**).

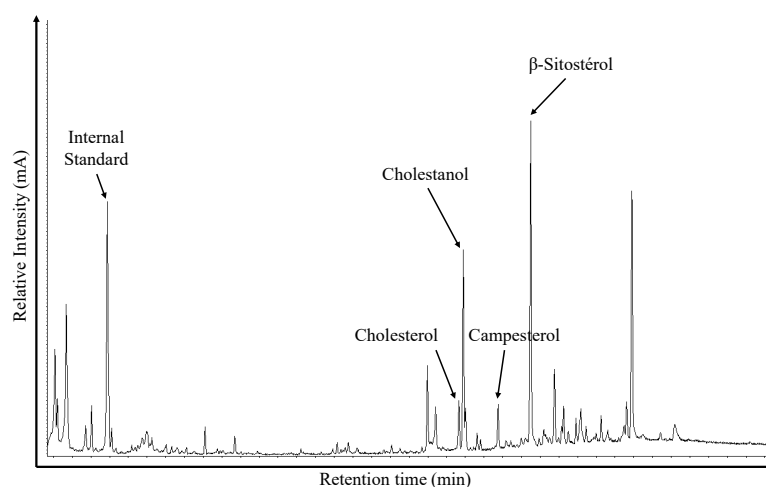


Figure 6.4: Chromatogram of the alcohol/sterol fraction (F3) from the monoalgal strain culture *Ostreobium* O10 free-living form

Table 6.4: Sterols composition and their respective concentrations observed in the monoalgal culture strain *Ostreobium* O10 free-living form.

Sterols Composition (F3)	Sterols Concentration ($\mu\text{g/g}$)
Internal Standard = Androstanol	X
$\text{C}_{27}\text{H}_{46}\text{O}$ = Cholesterol	147
$\text{C}_{28}\text{H}_{48}\text{O}$ = Campesterol	151
$\text{C}_{27}\text{H}_{46}\text{O}$ = Cholestanol	620
$\text{C}_{29}\text{H}_{50}\text{O}$ = β -Sitosterol	1043

6.3.1.3 FA Fraction: Fatty Acids Composition

The representative fatty acid profile obtained by gas chromatography (GC-MS) was illustrated in **Figure 6.5**. A total of 6 FAs were detected in the monoalgal strain culture *Ostreobium* O10 (free-living form). Only two saturated FAs were found ($\text{C}_{16:0}$ at $408 \mu\text{g/g}$ and $\text{C}_{18:0}$ at $20 \mu\text{g/g}$), while unsaturated fatty acids with UFA $18:1$, $18:2$, $18:3$, and $20:4$. A significant observation was due to the high concentration of arachidonic acid content ($20:4\omega6$; $2091 \mu\text{g/g}$), main FA detected in the monoalgal strain culture *Ostreobium* O10 with a concentration 13x higher than the other UFAs, and 5x higher than the $\text{C}_{16:0}$ (**Table 6.5**).

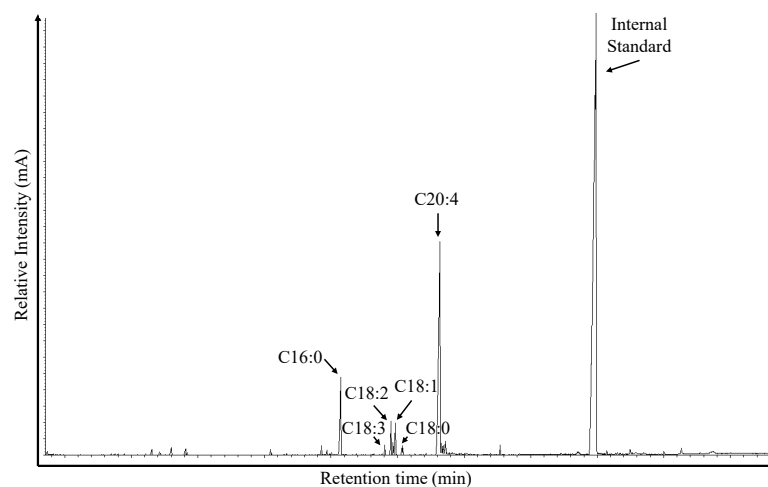


Figure 6.5: Chromatogram of the FA fraction from the monoalgal strain culture *Ostreobium* O10 free-living form

Table 6.5: Sterols composition and their respective concentrations observed in the monoalgal culture strain *Ostreobium* O10 free-living form.

Fatty Acids Composition (FA)	Fatty Acids Concentration ($\mu\text{g/g}$)
Internal Standard = Cholanic Acid	X
C16 (SFA) = Palmitic Acid	408
C18 (SFA) = Stearic Acid	32
C18:1 (UFA) = Oleic Acid	158
C18:2 (PuFA) = Linoleic Acid	124
C18:3 (PuFA) = α -Linolenic Acid	30
C20:4 ω 6 (PuFA) = Arachidonic Acid	2091

6.3.2 Lipid biomarkers Composition: *Diploastrea* sp.

6.3.2.1 F1 Fraction: Hydrocarbons Composition

No lipid biomarker was detected regarding the lipid biomarkers composition of the F1 fraction from the different coral sub-samples of *Diploastrea* sp.

6.3.2.2 F3 Fraction: Alcohols and Sterols Composition

Concerning the alcohol and sterol (F3) composition, no alcohol lipid biomarkers were detected along the coral core of *Diploastrea* sp (Figure 6.6). In contrast, four main sterols (F3) were detected along the coral core of *Diploastrea* sp. cholesterol, campesterol, and β -sitosterol were detected but in lower concentrations (5.41, 4.99, and 12.2 $\mu\text{g/g}$ respectively at the top of the core; Table 6.6), compared to the concentrations

observed in the monoalgal strain O10 (147, 150 and 1043 $\mu\text{g/g}$ respectively). Interestingly, brassicasterol was detected in higher concentrations at the top of the coral core (55.3 $\mu\text{g/g}$). No differences in cholesterol, campesterol and brassicasterol concentrations were identified between green and white bands (Wilcoxon Test; $p = 0.5$). Interestingly, lipid concentrations of β -Sitosterol were significantly different between green and white bands ($p < 0.05$).

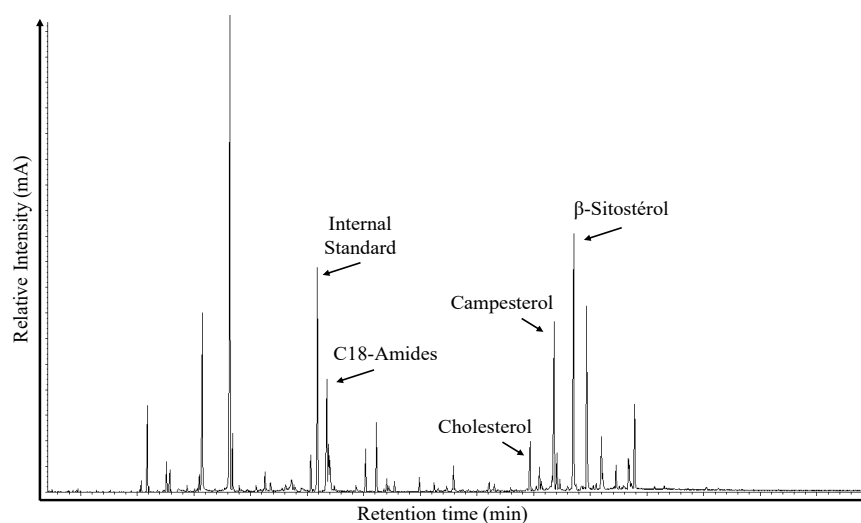


Figure 6.6: Chromatogram of the F3 fraction from the top of the coral core of *Diploastrea* sp.

Table 6.6: Main sterols and their respective concentrations observed along the different samples of the coral core of *Diploastrea* sp. The green color in the values corresponds to the green bands.

Sub-sample identification	Band Characteristics	Cholesterol ($\mu\text{g/g}$)	Campesterol ($\mu\text{g/g}$)	Brassicasterol ($\mu\text{g/g}$)	β -Sitosterol ($\mu\text{g/g}$)
sub-sample 1	Green bands	5.41	4.99	55.3	12.2
sub-sample 2	White bands	0.085	0.026	0.52	0.57
sub-sample 3	Green bands	0.012	0.0	0.06	0.04
sub-sample 4	White bands	0.0	0.0	0.0	0.0
sub-sample 5	Green bands	0.042	0.001	0.03	0.057
sub-sample 6	White bands	0.045	0.0006	0.005	0.0006
sub-sample 7	Green bands	0.009	0.0	0.0	0.0
sub-sample 8	White bands	0.019	0.0007	0.002	0.0
sub-sample 9	Green bands	0.011	0.001	0.0	0.04
sub-sample 10	White bands	0.015	0.001	0.0025	0.0
sub-sample 11	Green bands	0.025	0.003	0.0004	0.001
sub-sample 12	White bands	0.006	0.0002	0.0	0.0
sub-sample 13	Green bands	0.05	0.002	0.006	0.0004

A significant observation in fraction F3 was the detection of the group of amide lipid biomarkers along the coral core that was not detected within the monoalgal strain O10. Four main amides were identified: C16, C18, C18:1, and C20:1. A F3 profile from the coral sub-sample 13 (bottom-core) is illustrated in the **Appendix 8.4 Figure 8.2** showing better the amides group. The amide group of lipid biomarkers (in F3 fraction) was mainly observed at the bottom of the core from the sub-sample 13 to 8 and dominated by the C18:1 (Table 6.7).

Table 6.7: Main amides and their respective concentrations observed along the different samples of the coral core of *Diploastrea* sp, here presented in ng/g. The green color in the values corresponds to the green bands.

Sub-sample identification	Band Characteristics	C16 Amide ($\mu\text{g/g}$)	C18 Amide ($\mu\text{g/g}$)	C18:1 Amide ($\mu\text{g/g}$)	C20:1 Amide ($\mu\text{g/g}$)	Amide Total ($\mu\text{g/g}$)
sub-sample 1	Green bands	0.0	0.0	0.0	0.0	0.0
sub-sample 2	White bands	0.0	0.0	0.133	0.0	0.133
sub-sample 3	Green bands	0.0	0.0	0.0	0.0	0.0
sub-sample 4	White bands	0.0	0.0	0.0	0.0	0.0
sub-sample 5	Green bands	0.0	0.0	0.0	0.0	0.0
sub-sample 6	White bands	0.0	0.0	0.0	0.0	0.0
sub-sample 7	Green bands	0.0	0.0	0.0	0.0	0.0
sub-sample 8	White bands	0.593	0.245	9.93	0.358	11.12
sub-sample 9	Green bands	0.337	0.103	6.26	0.109	6.81
sub-sample 10	White bands	0.508	0.235	9.73	0.374	10.84
sub-sample 11	Green bands	0.641	0.278	11.51	0.410	12.84
sub-sample 12	White bands	0.315	0.147	6.20	0.27	6.93
sub-sample 13	Green bands	0.657	0.403	14.71	0.723	16.5

One major finding from this figure was the significant decrease of the amides' concentration over time (Mann-Kendall test; p -value < 0.01). The **Figure 6.7** described the relative total concentration of the amides groups (C16, C18, C18:1, C20; Fig 6.8) within the coral core. No differences in amides concentrations were identified between green and white bands (Wilcoxon Test; $p = 0.9$)

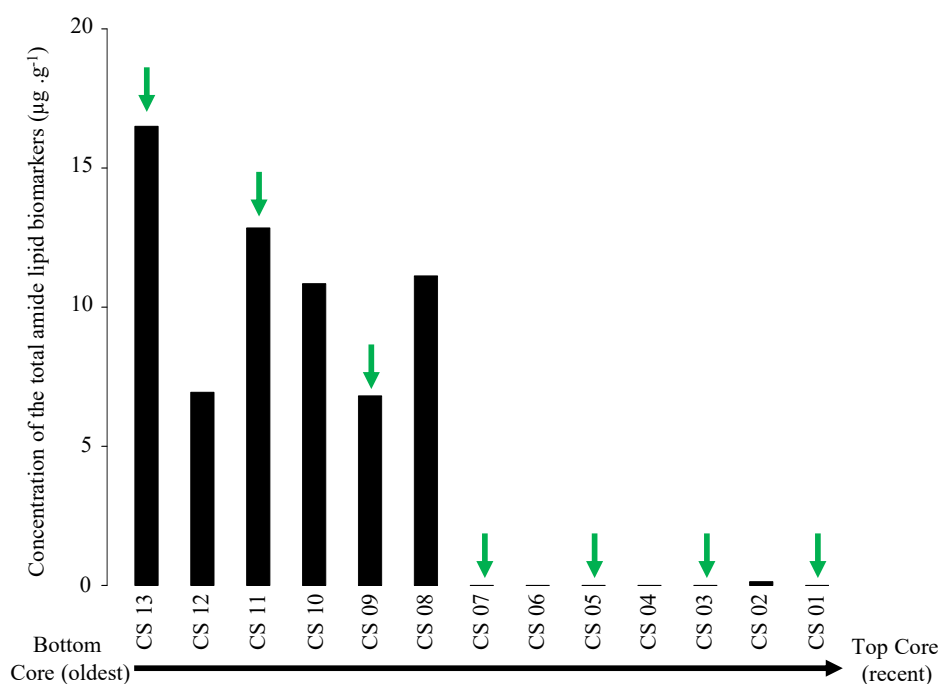


Figure 6.7: Histogram of the concentration of total amides lipid biomarker group among the coral core of *Diploastrea*. Green arrows indicate the position of the green bands within the coral core. CS for the x-axis stands for "Coral Sample".

6.3.2.3 FA Fraction: Fatty Acids Composition

The fatty acid (FA) composition observed among the coral core of *Diploastrea* sp. presented three main FAs (Fig 6.9). Two saturated FAs (16:0, 18:0) and only one unsatu-

rated fatty acid (UFA; 18:1) were detected along the coral core of *Diploastrea* sp. The present study does not provide all representative fatty acid profiles obtained by gas chromatography (GC) along the coral core. For example, a fatty acid profile is represented from the coral sub-sample 2 (top-core; **Figure 6.8**).

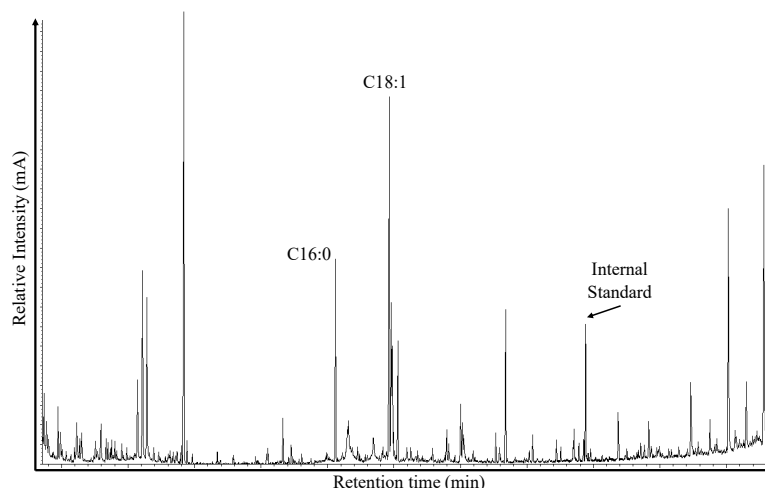


Figure 6.8: Chromatogram of the FA fraction from the top of the coral core of *Diploastrea* sp.

Interestingly, SFA C16 and C18 were most abundant at the top of the core. Concentrations of the C16 and C18:1 were relatively abundant from sample 13 to 7 (between 6 and 29 $\mu\text{g/g}$ for C16, between 30 and 290 $\mu\text{g/g}$ for C18:1; **Table 6.8**). A F3 profile from the coral sub-sample 13 (bottom-core) is illustrated in the **Appendix 8.4 Figure 8.3**. There were no differences in FA lipid biomarkers concentrations between green and white bands (Wilcoxon Test; $p\text{-value} = 0.5$). No significant changes regarding the concentration of the C16 and C18 were identified over time (bottom toward the top of the core; Mann Kendall Test, $p\text{-value} = 0.6$). Interestingly, the concentration of the C18:1 decreased significantly over time (Mann-Kendall test; $p\text{-value} < 0.1$).

Table 6.8: Main detected Fatty Acids and their respective concentrations calculated along the different samples of the coral core of *Diploastrea* sp. The green color in the values corresponds to the green bands.

Sub-sample identification	Band Characteristics	SFA C16 ($\mu\text{g/g}$)	SFA C18 ($\mu\text{g/g}$)	SFA C18:1 ($\mu\text{g/g}$)
sub-sample 1	Green bands	820	107	47.7
sub-sample 2	White bands	7.5	4.0	28.6
sub-sample 3	Green bands	10.5	5.9	67.5
sub-sample 4	White bands	2.0	2.1	12.1
sub-sample 5	Green bands	1.7	1.9	14.2
sub-sample 6	White bands	7.9	4.1	54
sub-sample 7	Green bands	29.5	15.3	287
sub-sample 8	White bands	21.9	9.8	204
sub-sample 9	Green bands	5.8	2.7	31.7
sub-sample 10	White bands	18.4	8.4	145
sub-sample 11	Green bands	25.6	11.2	211
sub-sample 12	White bands	21.7	11.1	190
sub-sample 13	Green bands	13.5	6.8	109

6.4 Discussion

6.4.1 Lipid Biomarkers Profile: Monoalgal Strain O10

The analysis of the monoalgal culture strain of *Ostreobium* O10 showed the presence of the FA arachidonic acid and the sterol β -Sitosterol in important concentrations (**Tables 6.4; 6.5**). In 2020, Massé et al. observed similar results, especially for the arachidonic acid, on the same strain O10 free-living forms, although two different protocols were used. Differences in FA composition might be explained by the different GC-MS parameters used for quantification and identification relative to the detection threshold and differences in dry-weight samples before extraction. Massé et al. (2020) found that free-living forms had 3.5 more arachidonic acid than the bioeroding forms. Such differences in this specific FA between both forms suggest that *Ostreobium* sp. proceed to important adjustments of fluidity and permeability of its membrane, possibly for the adaptation to the extreme environment provided by the coral skeleton. A shifting in arachidonic acid content between both phenotypes may reflect differential signalization activity (De Carvalho and Caramujo, 2018) and a shift in communication with associated microbes. Here, the fatty acid composition of the monoalgal culture strain O10 was typical of chlorophytes. *Ostreobium* belongs to the order Bryopsidales, which is most commonly classified in the Ulvophyceae, a class within the phylum Chlorophyta (Tandon et al., 2022). The *Ostreobium* clade is one of the three main lineages of Bryopsidales and has been assigned to its suborder Ostreobineae (Verbruggen et al., 2017; Cremen et al., 2019). Like Massé et al. (2020), the monoalgal strain O10 displayed a high abundance of palmitic acid (16:0), a saturated FA reported in several green macroalgae (Kumar et al., 2009; Pereira et al., 2012). Also, it displayed high contents of C18 mono-or polyunsaturated FA (PuFA), which are characteristic of chlorophytes (Jamieson and Reid, 1972; Khotimchenko and Svetashev, 1987). Nonetheless, some common FA found in other algae of order Bryopsidales were not detected in the monoalgal strain O10. Indeed, Bryopsidales are characterized by high quantities of 16:3 ω 3 combined with low quantities of 16:4 ω 3 and 18:4 ω 3 (Aknin et al., 1992). The absence of these ω 3 fatty acids in the monoalgal strain O10 supports the statement from Massé et al. (2020) of its absence in the suborder Ostreobineae. Finally, the detection in the culture of C18:1 and C18:2 was surely indicative of fungal presence (Mikola and Setälä, 1998; Méziane et al., 2006; Massé et al., 2018) and confirms that cultures were not axenic as also mentioned by Massé et al. (2020). Indeed, fungi may have

been isolated within the microbiome and the coral skeleton. Moreover, morphological structures as fungal hyphae are indeed known to colonize *Ostreobium* filaments in carbonate substrates (Le Campion-Alsumard et al., 1995; Tribollet and Payri, 2001; Golubic et al., 2005) and may explain the presence of such PuFA in the coral skeleton. Fatty acids are essential for the physiological adaptation of algae to environmental stress, for instance, high PuFA content may provide more protection from temperature changes (De Carvalho and Caramujo, 2018), or salinity (Zhila et al., 2011). Fatty acids can be essential in energy storage, cell membrane structure, and overall fitness (Bergé and Barnathan, 2005; Farre et al., 2010). Within this context, fatty acids may be used to understand the nutritional value of *Ostreobium* to the coral host (suggested by Fine and Loya, 2002) and as a potential trophic marker to trace food sources in reef organisms (Clements et al., 2017). Nonetheless, in this study, only 6 FA were detected in the monoalgal strain O10 whereas Massé et al. (2020) investigated more than 30 FA within the different lineages of *Ostreobium*, suggesting further investigations from these preliminary results to assess better *Ostreobium* FA composition.

From the F1 fraction (hydrocarbons), no lipid biomarker was detected in the monoalgal strain O10. Two explanations are possible. (i) It could be associated with a lack of sensitivity of the GC-MS that cannot detect, even in very low concentrations of hydrocarbon lipid biomarkers, or (ii) it is due to an insufficient quantity of dry samples weighed at the beginning of the protocol. For instance, in sediment, for F1 fraction (alkane analysis), dry weight samples are often between 3 to 15g, and for primary producer biomass, around 0.3 to 1g to obtain enough material for detection and quantification (N. Chevalier et al., 2015). Here, the dry weight of the monoalgal strain O10 was less than 0,005g.

For the first time, our study presents sterol profiles in an *Ostreobium* monoalgal strain O10. Sterols are essential components of lipid membranes and play important roles in signaling molecules (Nes et al., 1990), regulating membrane fluidity (e.g., D. J. Brown and DuPont, 1989), and permeability in microalgae (J. K. Volkman, 2003). The sterol synthesis pathway has been thoroughly studied in vertebrates, fungi with cholesterol, and ergosterol (Desmond and Gribaldo, 2009). On the other hand, a greater variety of terrestrial plant sterols can be found, such as campesterol, sitosterol, and stigmasterol (Desmond and Gribaldo, 2009). Sterols are particularly well-suited as

biomarkers for nutrient acquisition in heterotrophic corals because their origin can be identified (Crandall et al., 2016). Here, cholesterol was detected and is characterized as a lipid biomarker ubiquitous in animal, fungi, and plant cells (Behrman and Gopalan, 2005; Voshall et al., 2021). Thus, it cannot be used as a “specific” biomarker to investigate the abundance of microbioeroding flora, and especially *Ostreobium* sp. in living coral skeletons. At the same concentration, campesterol was detected and is one of the main phytosterols observed in plants/algae, which is coherent to detect it in the micro-alga *Ostreobium*. Still, as it is ubiquitous in many different vegetal systems, like cholesterol, it cannot be used as a “specific” biomarker to investigate the abundance of *Ostreobium* sp. in living coral skeletons as its signal might originate from different sources (e.g., symbionts; Babcock-Adams et al., 2016). Interestingly, in the monoalgal strain O10, the presence of β -sitosterol and cholestanol was detected in high concentrations. Hence, such lipid biomarkers and mostly the β -sitosterol could potentially be used as a biomarker of the presence of *Ostreobium* sp. in living coral skeletons or other micro-alga sources colonizing the coral skeleton. Nonetheless, if high contents were to be observed in the top part of the coral skeleton, the signal might originate both from *Ostreobium* sp. (as it is mainly present underneath the tissue layer, indicated by a green band; Lukas, 1973) and the coral symbionts (C. Parrish, 2013). Overall, based only on these preliminary findings on the sterol composition of one monoalgal strain of *Ostreobium* sp., it is complicated to conclude in the potential use of the sterol fraction as a biomarker for the presence of *Ostreobium* in living coral skeletons and need further investigations. However, the high abundance of the β -sitosterol detected in the monoalgal O10 is interesting. One objective would be to investigate other lineages of *Ostreobium* sp (free-living and bioeroding forms) to detect and quantify concentrations of β -sitosterol to identify it or not as a major sterol. If validated in other lineages, such sterol could represent a potential lipid biomarker characterizing the presence of *Ostreobium* in living coral skeletons. For recall, the monoalgal strain culture of *Ostreobium* O10 was obtained in non-axenic conditions, suggesting that biomarkers detected can also potentially reflect a fungal influence and not *Ostreobium* lipid biomarker composition alone. Finally, mono-strain cultures of other microbioeroding communities should be investigated to be used as reference standards providing information on their lipid biomarker composition (sterols, fatty acids) with the objective of better understanding the lipid biomarker composition observed in living corals’ skeleton and serving as potential proxies of the abundance of these communities.

6.4.2 Lipid Biomarkers Profile: *Diploastrea* sp.

Detailed records of lipid biomarker profiles (FA and sterols) were also investigated for the first time among a coral core of the massive coral *Diploastrea* sp., highlighting their concentration and variability over time. Disparities were observed within the core when focusing on the coral's bottom or top part. The dominant fatty acids identified in *Diploastrea* sp. were the saturated FA (C16:0 and C18:0). These FA presented the highest concentrations at the top of the core. Here, the first top sample was ground in bulk. Thus, the top included a mix of coral tissue (polyp + zooxanthellae + microbes) and organisms from the top green band (e.g. *Ostreobium*). Such concentrations of both compounds might indicate a potential multi-signal from the coral holobiont at the top of the coral core. High concentrations might be more influenced by the coral tissue than the organisms in the skeleton, as it was not observed at important concentrations at the bottom of the core. Previous reports of fatty acids in corals indicate that there is usually more C16:0 (palmitic acid) than C18:0 (stearic acid) in coral tissue (zooxanthellae) and coral skeletons (Meyers et al., 1974; Isa and Okazaki, 1987; Harland et al., 1993). Treignier et al. (2008) showed in the scleractinian coral *Turbinaria reniformis* that C16 FA was predominant in zooxanthellae and that C16, C18, and C20:4:6 were the dominant FAs compounds of the total FAs within the animal tissue. They also represent the main FAs transferred between the zooxanthellae and the animal (for metabolic purposes; Treignier et al., 2008). Interestingly, the FA (C18:1) was observed and detected throughout the entire coral skeleton, with the highest concentrations at the bottom of the core. Specific studies on *Symbiodinium* spp. showed that the most abundant saturated fatty acids were palmitic (C16:0) and stearic (C18:0) acids and the unsaturated fatty acids, including palmitoleic (C16:1), oleic (C18:1) (Zhukova and Tilyanov, 2003; Tchernov et al., 2004; Kneeland et al., 2013). A hypothesis could be that the FA C18:1 might originate from another potential source of the coral holobiont, i.e., from a bacteria origin, as it was mainly observed through the entire coral skeleton and not only the coral tissue (symbionts). Moghrabi et al. (1995) showed an increase in fatty acids from the scleractinian coral *Galaxea fascicularis*, in dark incubation (C16:1, C18:1), which might indicate a microbial source of nutrition. Indeed they showed that oleic acid (C18:1) was considerably in higher concentrations in bacteria, served as a source of energy for the coral, and might be considered a useful marker for bacteria

(Joint and Morris, 1982; Wakeham and Canuel, 1988; Al-Moghrabi et al., 1995). This FA could also originate from euendolithic communities as coral skeletons present an important diversity of associated microborers (Yang and Tang, 2019; see Table 4.1 in their paper). The lipid biomarker investigation of the coral core *Diploastrea* sp. showed that no FA characteristic of *Ostreobium* sp. was found in abundance (e.g., arachidonic acid C20:4) in the coral skeleton, especially in green bands as no difference was identified with white bands, indicating that it might not be a dominant organism within the coral skeleton of *Diploastrea* sp.

No lipid biomarker from the F1 fraction (hydrocarbons) was detected in the massive coral *Diploastrea* sp., with two explanations already mentioned about the lack of sensitivity of the GC-MS or due to the insufficient quantity of dry samples at the beginning of the protocol (cf. amount of dry samples in N. Chevalier et al., 2015). To counter this last limit, one objective could have been to pool samples from the top altogether (e.g., the first 6 samples) and the samples from the bottom of the core to detect lipid biomarkers in the F1 fraction (could also apply to the other fractions). Still, this method was not performed as it did not suit the initial objective to study the lipid biomarker composition between the alternate pattern of green and white bands upon the coral skeleton. One possibility could be to pool samples corresponding to all green bands and, on the other hand, to pool the white bands altogether to understand and quantify differences in lipid biomarkers composition between the two kinds of bands.

Regarding the sterol fraction within the coral core of *Diploastrea* sp., no cholestanol was detected in the coral core, while it was one of the major sterols observed in the monoalgal strain O10 (Table 6.6). Only the β -sitosterol was detected in abundance within the first few centimeters of the top coral core, similarly observed with the monoalgal strain O10. Nevertheless, a hypothesis is that β -sitosterol could originate from the symbionts of the coral (Carreón-Palau et al., 2020) or remains left in the upper part of the coral skeleton as it was nearly not detected in the bottom of the core. Carréon-Palau et al., 2020 showed that shallow tropical cnidarians from the southwest Gulf of Mexico (shallow tropical coral reefs) presented both zooxanthellae sterols in their tissues, mainly campesterol and β -sitosterol. Interestingly, only for the lipid concentration of β -sitosterol, there was a significant difference in concentration between green and white bands ($p < 0.05$). When excluding the first white band (remaining traces of

coral tissue), β -sitosterol concentrations are nearly close to 0, while β -sitosterol is detected in green bands. Such findings suggest that β -sitosterol in the green bands might be synthesized from organisms (e.g., *Ostreobium*) that are possibly not present in white bands or are in higher abundance in green bands than white ones, which permits detection of β -sitosterol. Also, brassicasterol was detected in high abundance only from the top of the coral core (Table 6.6). Babcocks-Adams et al. (2016) showed that cholesterol, campesterol, and brassicasterol were the main sterols observed in zooxanthellae and that the bleaching-resistant clade D symbionts contained higher levels of sterols compared to corals with non-resistant symbionts. This supports that in the findings, the highest abundance of sterols was observed only within the first cm of the coral core and may originate from the coral symbionts. Other sterols might be present within the coral skeleton, but quantities of samples may not be enough to be detected along the coral core. Moreover, the sterol fraction analyzed in the *Diploastrea* coral skeleton, compared with the monoalgal strain O10, confirms that *Ostreobium* presence might be limited within the coral skeleton of *Diploastrea* sp.

6.4.3 Amide Lipid Biomarkers: Proxies of microborers ?

In the coral core of *Diploastrea* sp, one interesting result was the detection of the lipid biomarkers corresponding to the amides. Significant differences existed between the concentrations observed at the core's top and the bottom, as amides were only detected from samples 13 to 8 (**Figure 6.7**; except C18 in sample 2). This significant decrease in lipid biomarker composition, especially in the amides group, over time in the massive slow-growing coral *Diploastrea* sp. could result from a shift in the community composition within the coral skeleton responsible for the synthesis of the amides. Concomitantly, a similar decreasing trend of the estimated abundance of microbioeroding communities within *Diploastrea* sp. (Alaguarda et al., 2022) was estimated along with a rupture over time (1985-1986). Alaguarda et al. (2022) reconstructed the growth rate of the coral belonging to the 15 first cm until 1964. In this study, all core (19.5 cm) was investigated. Thus, for the last 4.5 cm, if an average growth rate of 3 to 4 mm.y⁻¹ (Bagnato et al., 2004; Wu et al., 2018) is considered, the remaining 4.5 could cover up to 15 years (so early 1950s). Based on this assumption and from the coral reconstruction for the period 1964-2018 (Alaguarda et al., 2022), the last concentration observed of the amides group (sample 8 corresponds to 9cm if started from the bottom) could correspond to the period 1982-1984, and match potentially the breakpoint observed

(1985-1986) of the community shift of microbioeroding communities in *Diploastrea* sp. The potential gap between both periods might be explained by the uncertainties of the growth reconstruction of the last 4.5 cm, but it might only be for a few years. Moreover, Alaguarda et al. (2022) investigated only the first 15 cm because the coral core presented a hole below, characteristic of macrobioerosion signs (**Figure 2.10**). One hypothesis could have been to attribute the amides' origin to potential macrobioeroders present at that time within the coral skeleton of *Diploastrea*. Nonetheless, as the macrobioerosion hole was only present at a specific location of the core and the amides signal was present from the bottom of the core until above the macrobioerosion mark, the possible attribution of the amides to macrobioeroding agents could be excluded. Such findings could suggest that the group of amides could represent a potential proxy of microbioeroding communities comprising cyanobacteria, microalgae, and fungi in the coral skeleton. Fatty-acid amides are widespread and synthesized by many organisms and taxa (Hannun et al., 1996). They are incorporated into lipid classes such as ceramides, glycosphingolipids, and N-acylated molecules (Bergé and Barnathan, 2005). For instance, ceramides are fatty acids that usually have an even number (16 to 24) of carbon atoms and are saturated or monounsaturated, corresponding to what was observed in the coral core of *Diploastrea*, suggesting that ceramides could be the lipid biomarkers present within the coral. Such molecules are abundant in cell membranes but can also have lipid signaling functions (Castro et al., 2014). For instance, cyanobacteria of the genus *Lyngbya* are a rich source of bioactive secondary metabolites, including fatty-acid amides (Dembitsky and Srebnik, 2002). Some ceramides were also isolated from epiphytic dinoflagellate (Tanaka et al., 1998), in different bacteria (Keck et al., 2011; Lorenzen et al., 2014) as well as in various marine sponges (Hattori et al., 1998), red algae (Lo et al., 2001), even the starfish *Acanthaster* (Inagaki et al., 1998). Ceramides have also been highlighted in marine-derived endophytic fungi (Sallam et al., 2021). Li et al. (2017) quantified and identified ceramides from 17 strains of microalgae (diatoms, dinoflagellates, and haptophytes). They showed that the composition in ceramides significantly differed among the micro-algal categories highlighting the potential of a new basis for microalgae chemotaxonomy. As many taxa can synthesize amides, their origin within the coral skeleton of *Diploastrea* could originate from a large range of organisms, including the microbioeroding communities such as cyanobacteria, micro-algae or fungi that colonized the coral skeleton. From the findings established by Alaguarda et al. (2022), three main classes of microbor-

ers, regarding their size, were present colonizing the coral skeleton of *Diploastrea* sp. The authors suggested that there were potentially phototrophs with large diameters (up to 30 μm), fungi, the cyanobacteria *Plectonema*, and the presence of *Ostreobium*. Nonetheless, the non-bioeroding euendolithic compartment was not studied in their research. Thus, as the amides were identified and quantified from a bulk signal, it might be that the entire euendolithic compartment (bioeroding and non-bioeroding) could have shifted over some decades with a strong assumption for the microbioeroding communities due to their abundance that also decreased over time. Also, findings from Alaguarda et al. (2022) emitted the hypothesis that a combination of environmental factors (e.g., SST/SSTA, pH, wind ..) had potential effects on the abundance of microbioeroding communities and was responsible for the decrease over time. The authors hypothesized that the massive coral *Diploastrea* sp. might have been under heat stress around 1982-1983 from a critical MHW event in the MC (Sen Gupta et al., 2020; Mawren, Blamey, et al., 2022). Such stress might have triggered the shift in microbioeroding communities' abundance observed by the authors. Another hypothesis could be that the environmental forcings have also impacted the coral microbiome and its lipid biomarker composition, especially in the amides group at that period. Tisthammer et al. (2021) investigated *Porites lobata* corals from near and off-shore reefs and highlighted significant changes in protein profiles and lipid metabolism between near/offshore corals. Nearshore corals presented higher concentrations of lipids such as ceramides and mostly higher concentrations of one enzyme, ceramidase, that might explain the resilience activity of nearshore corals and a higher ability to handle stress conditions than offshore corals. Thus, higher concentrations of ceramides might be related to a better-facing ability of corals to stress conditions such as poor water quality, OA, or increased temperatures (e.g., marine heat waves; Tisthammer et al., 2021). No amides were observed from the top of the core, whereas the last decade, for instance, has surely gathered higher stress conditions for corals than the last decades where the amides were observed. Environmental forcings might have only affected the microbioeroding communities and have not influenced the amide concentrations over time or indirectly through the abundance' decrease of these communities. Suppose a correlation could be established between the decrease in the amides' concentrations and the decrease in the abundance of microborers, such lipids biomarkers could be defined as proxies of the presence, even the abundance of microbioeroding communities in living coral skeletons. However, further studies are needed to understand better the

origin of the amides and why they decreased over time and establish the link between the amides group and microborers.

6.5 Conclusion

The lipid molecular organic geochemical approach allowed identifying and quantifying lipid biomarker composition of a monoalgal strain culture of *Ostreobium* sp. and a massive living coral core of *Diploastrea* sp. Based on a different protocol, this study first confirmed the understanding of the already known fatty acids lipids composition of the monoalgal strain *Ostreobium* O10 (free-living form, Massé et al., 2020), but also provided comprehension of another lipid biomarker fraction, the sterols. As Massé et al. (2020) highlighted, the main dominant FA also found in this study was the arachidonic acid, and for the sterol fraction, the β sitostérol. On the other hand, this study enhanced the understanding of the long-term lipid biomarker composition of a massive coral core of *Diploastrea* sp. for the first time. The different FA and sterols identified in high concentrations were at the top of the coral core, suggesting a potential signature of the coral symbionts and not from microbioeroding communities. For instance, no arachidonic acid was found in the *Diploastrea* sp. Interestingly, the lipid biomarker composition of *Diploastrea* sp. highlighted a specific group of the amides that decreased over time. Moreover, the decrease in the concentration of the amides was found to potentially match the observed community shift in the composition of microbioeroding communities in *Diploastrea* sp. (Alaguarda et al., 2022). Nonetheless, exploring the origin of the amides and the breakpoint observed in the microbioeroding communities from the *Diploastrea* sp. from Mayotte need further investigation. Further information obtained from the analysis of the lipid biomarker composition in the coral holobiont (especially the coral skeleton) could be used to assess the presence/abundance of the coral-associated microbiota and potentially microbioeroding communities within corals. One critical step in this approach would be to access mono-strain cultures of various microborers (going from fungi, algae, and cyanobacteria). Cultures must be obtained for free-living forms and bioeroding strains before any analysis in carbonate materials (corals, shells, sands, rocks) to provide an accurate dataset of the lipid biomarkers composition from those specific organisms. On the other hand, as mentioned for the F1 fraction, the total dry weight of some coral samples was maybe insufficient (less than 5g) for precise detection and quantification

of lipid biomarkers in GS-MS chromatography. Such limitations can also be applied to the other fractions where some lipid biomarkers could not have been detected due to poor carbonate quantity. Also, the threshold of the GC-MS for lipid biomarkers identification could be insufficient to detect the potential presence of lipid biomarkers, even at a low concentration. For instance, no amides lipid biomarkers were found in the monoalgal strain O10 potentially because (1) they are naturally absent or (2) undetected. Despite promising results, this approach was based only on 13 samples and from only one core. The number of samples must be significantly increased to be representative and confident. Nevertheless, I did not pursue the geochemistry analyses of the following coral cores. However, based on these preliminary results, this approach seeks future investigations. It could represent a promising tool for understanding functional diversity, physiology, and traits of microbioeroding communities within massive coral skeletons and should be extended to other massive species.

General Conclusions and Perspectives

Contents

7.1	Synthesis	242
7.2	Perspectives	249
7.2.1	Machine Learning Application	249
7.2.2	Additional Results of a Coral Core of La Réunion	250
7.2.3	Additional Results from Coral Cores of the Scattered Islands	251
7.2.4	Further Investigations	253

My Ph.D. project was motivated and structured to understand the impacts of global environmental changes on the variability of the composition and the abundance of microbioeroding communities over the long term. This work aims to better predict the future of coral reefs over the long term and improve climate models (CMIP-6). Four main questions were raised in the introductory chapter and addressed in the results of the different chapters. I will now attempt a general conclusion of these different results.

7.1 Synthesis

Coral reefs' production and accumulation of reef framework carbonate are controlled by the relative rates and the interactions between ecologically, physically, and chemically driven production and erosion processes (constructive vs. destructive forces) (Tribollet, 2008; Andersson and Gledhill, 2013; Schönberg et al., 2017). Among the erosion processes, natural biological erosion (termed bioerosion) is the main pathway of reefs' erosion. Bioerosion is associated with a natural diversity of bioeroding agents interacting with each other and the environment. Among bioeroders, microbioeroding communities are probably the main agents of reef bioerosion. Bioeroding microflora regroups autotrophic (cyanobacteria, and red and green microalgae) and heterotrophic (fungi) euendolithic microorganisms that actively penetrate the hard substrates in which they live (Golubic et al., 1981). The filamentous green alga *Ostreobium* is described as the dominant microborer in tropical coral reefs (Lukas, 1973; Le Campion Alsumard et al., 1995; Priess et al., 2000; Tribollet, 2008), with more than 99% of presence in living corals (Lukas, 1974), that can form visible green bands upon the skeleton of massive corals. Research on microbioeroding communities has mainly focused on biogenic dissolution rates of dead substrates, the bioerosion loop interactions with grazers and macroborers (Schönberg et al., 2017), the succession of microbioeroding communities over the short-term (Chazottes et al., 1995; Grange et al., 2015), and how environmental forcing can enhance such rates in the context of global changes (Tribollet et al., 2019). Overall, only some authors documented the abundance of microborers such as *Ostreobium* and fungi in living corals to study the alternate pattern of green or black bands and the differences of abundances between colored bands (Lukas, 1973; Le Campion Alsumard et al., 1995; Priess et al., 2000). However, these studies never implied chronological context and investigation of their

variability over time. Massive living corals represent an interesting alternative to studying microbioeroding communities over time. They are sources of valuable information that are characterized as natural archives used in paleoclimatology as they can record environmental variability over time within their skeleton (J. Lough and Cantin, 2014; Wu et al., 2018; Reed et al., 2021). Moreover, such archives are known to be heavily colonized by microbioeroding communities. As no previous quantitative methodologies were available to answer the primary objective of this work, there was a need to develop a tool/application to study the variability of microbioeroding communities within living massive corals.

To address this need, I developed, in collaboration with **Julien Brajard**, a new quantitative application for estimating microbioeroding communities (i.e., their traces) within living massive coral skeletons based on a machine-learning approach. This approach permitted the identification of a maximum of two classes of microbioeroding communities, and its overall accuracy was more than 93% in identifying microbioeroding traces colonizing the coral skeleton. Moreover, through the development of this method, for both corals, I found that tuning some hyper-parameters of the CNN model, such as the loss function, can enhance the overall model performances to identify better the different traces. As the dataset of SEM images between both corals presented heavily imbalanced classes, finding a dedicated and optimized loss function significantly changed the model's capacity to identify the different classes within an image. Thus, two different CNN models, specific to each massive coral, were developed in this study. With this method, I analyzed more than 3000 SEM images to identify the different microbioeroding traces between the *Diploastrea* and *Porites* coral core accurately and continuously. Nonetheless, even if the ML approach saved hours of manual analysis, there was the obligation to take manually the different SEM images for different transects to analyze enough coral surface, which took months of acquisition that still cannot be avoided yet (future automatized SEM acquisition?).

Following the successful development of the ML application, I first studied a remarkably well-preserved coral core of a slow-growing colony of *Diploastrea* sp. from Mayotte (WIO), presenting several green bands and covering the last 54 years. From this first core, I studied the influence of biotic and abiotic factors on the decadal variability of the composition and abundance of microbioeroding communities observed within *Diploastrea* sp. The study of this coral core showed a decrease of the coral bulk density

over the last 5 decades (40%), a significant warming observed over the last 5 decades in Mayotte (+0.11/decade), a significant increase of the internal coral pH_{CF} over the last decades. Overall, within the *Diploastrea* sp. coral core, there was a significant decrease in the abundance of microbioeroding communities over the last 5 decades (90%). Three microbioeroding communities were identified colonizing the coral skeleton of *Diploastrea* sp. Still, the CNN model only identified two classes: the thin and wide microbioeroding traces. Additionally, a community shift was identified in 1985-1986 with a dominance of a mix of thin and wide microbioeroding traces before this period towards a dominance of the thin traces after it, yet in lower abundance. The investigation of the green bands and their potential link to higher microbioeroding abundance was only performed in the coral core *Diploastrea* sp. No green bands were identified within the other coral cores. Based on these findings, there was no direct evidence that green bands may reflect a high abundance of microbioeroding traces, as suggested by previous studies (Lukas, 1973; Le Campion Alsumard et al., 1995; Tribollet, 2008). Instead, green bands may be explained by both the abundance of microbioeroding traces and the influence of environmental factors like SSTA and the maximum instantaneous wind speed (e.g., potential season effect between austral summer and winter) that can trigger the formation of green bands, but this subject needs further investigation. Overall, the findings from this first coral core highlighted that the variability, composition, and abundance of microbioeroding communities within *Diploastrea* sp. might be explained by the co-action of biotic (with the skeletal bulk density, calcification rate) and abiotic (SST/SSTA, pH_{CF}) factors that have impacted both microbioeroding communities differently that live within the *Diploastrea* skeleton.

Concomitantly to the ML application for estimating the abundance of microbioeroding communities in *Diploastrea* sp., this coral was also studied under a geochemistry approach to analyze the lipid biomarkers composition present within the coral skeleton. The goal was to highlight potential specific lipid biomarkers of microbioeroding communities, especially *Ostreobium*, based on the alternate pattern of green and white bands as green bands characterize the presence of *Ostreobium* sp. I expected a potentially higher concentration of lipid biomarkers in green compared to a white band and to identify some lipids that might be considered a proxy of the presence or abundance of *Ostreobium* in the coral skeleton. Within this work, the study of the fatty acid lipid biomarker composition of one monoalgal strain culture of *Ostreobium* sp.

(O10) was similar to what has been observed by Massé et al. (2020), showing that even with different protocols, the main lipid biomarkers within this fraction were similar. On the other hand, I completed information by providing for the first time the sterol composition of one monoalgal strain culture of *Ostreobium* (O10). Nonetheless, no lipid biomarkers of the monoalgal strain culture of *Ostreobium* sp. were to be found in abundance in the coral skeleton of *Diploastrea* sp., suggesting that *Ostreobium* sp. might not be the dominant microborer in the coral skeleton. Overall no differences were found in microbioerodings' abundance between a green and white band. I observed only a significant difference in lipid biomarker concentrations between a green and white band for the β -sitostérol. Overall, the largest differences observed were more between the core's top and bottom, where the highest sterols and fatty acids concentrations were observed essentially at the top of the coral skeleton (Carreón-Palau et al., 2020) but might belong and reflect the signal from the coral symbionts (*Symbiodinium*). One major finding from this approach was the detection and identification of a group of lipid biomarkers: the amides and I showed a significant decrease of the amides biomarkers group among the coral core of *Diploastrea* sp. over time. This decrease in the concentration of the amides could potentially match the decrease in the abundance of microbioeroding communities, and potentially the abundance of the wide microbioeroding traces. Nonetheless, a clear link between both decreases is still hard to establish from the preliminary findings of the geochemistry, as the origin of these lipid biomarkers remains to be explored. More research, specifically analytical chemistry, will be necessary to identify the lipid biomarkers composition compounds in corals to understand their specific roles in regulating the physiology of the coral holobiont and its associated microbiota.

The trends and assumptions obtained from only one coral core are insufficient to identify relevant trends to a larger group of corals. Therefore, I studied the variability of the composition and abundance of microbioeroding communities in another type of massive coral also collected in Mayotte, the *Porites* sp. This *Porites* sp. coral presented no visible green bands upon the skeleton and a mid-term record reconstruction of 29 years. As for *Diploastrea* sp, three microbioeroding communities were identified colonizing the skeleton of *Porites* sp. Nevertheless, differences were observed, as the skeleton of *Porites* sp did not present very wide traces (up to 30 μ m). The investigation focused only on the total abundance of microbioeroding traces as the objective

was first to focus on the total abundance to reconstruct the history of the abundance of microborers in *Porites* sp. I decided to re-train and optimize (through loss function adjustments) a dedicated CNN model for the coral *Porites* sp. because the model trained on *Diploastrea* sp. was introducing errors. Interestingly, I also noticed a decrease in the microbioeroding's abundance over time and in a different massive coral. Nonetheless, the abundance of microbioeroding traces in *Porites* sp. was significantly lower than observed in *Diploastrea* sp. When considering the same period for both corals (1990-2018), one breakpoint was highlighted at the same period (1995-1997), with a decrease in abundance observed then. One very interesting result highlighted from the *Porites* sp. coral core was the significant negative correlation of the abundance of microbioeroding traces with the pH_{CF} indicating that it might be one of the main factors that have regulated the variability of microbioeroding communities in *Porites* sp. over time. In contrast, in *Diploastrea* sp. the observed abundance decrease could be associated with a multi-factor explanation (biotic and abiotic influences). Additionally, differences in the abundance of microbioeroding traces in both corals might be explained by their different skeletal properties. Even if *Diploastrea* sp. presents a denser skeleton than *Porites* sp., it is much more porous. As *Diploastrea* sp. presents bigger corallites, it may allow it to better scatter light in the skeletal compartment than *Porites* sp. This could allow the growth of euendolith phototrophs more easily than in *Porites* sp. skeleton. Overall, investigating two massive distinct coral cores has highlighted a decrease in the microbioeroding communities compartment within the coral skeleton. Despite their known biogenic dissolution activities, some studies highlighted the potential role of microborers acting as ecto-symbionts (e.g., *Ostreobium*; Fine and Loya, 2002) that represent a key-organisms for sustaining the physiology of corals under extreme stress events. Hence, such a decrease in the composition and abundance of microborers over time underlines the question of their role in the holobiont and how they might be involved in corals' health and resilience states in a near future.

Finally, this Ph.D. could be summarized in this schematic representation, presenting our overall first knowledge of microbioeroding communities and how here in this work, I provided for the first time a better understanding of the long-term dynamics of these communities in living massive corals. Environmental archives such as massive corals are key to studying the evolution of the diversity, distribution, and abundance of microbioeroding communities over the coral host's lifespan and provide a better un-

derstanding of which biotic or abiotic factor can control their variability over the long term.

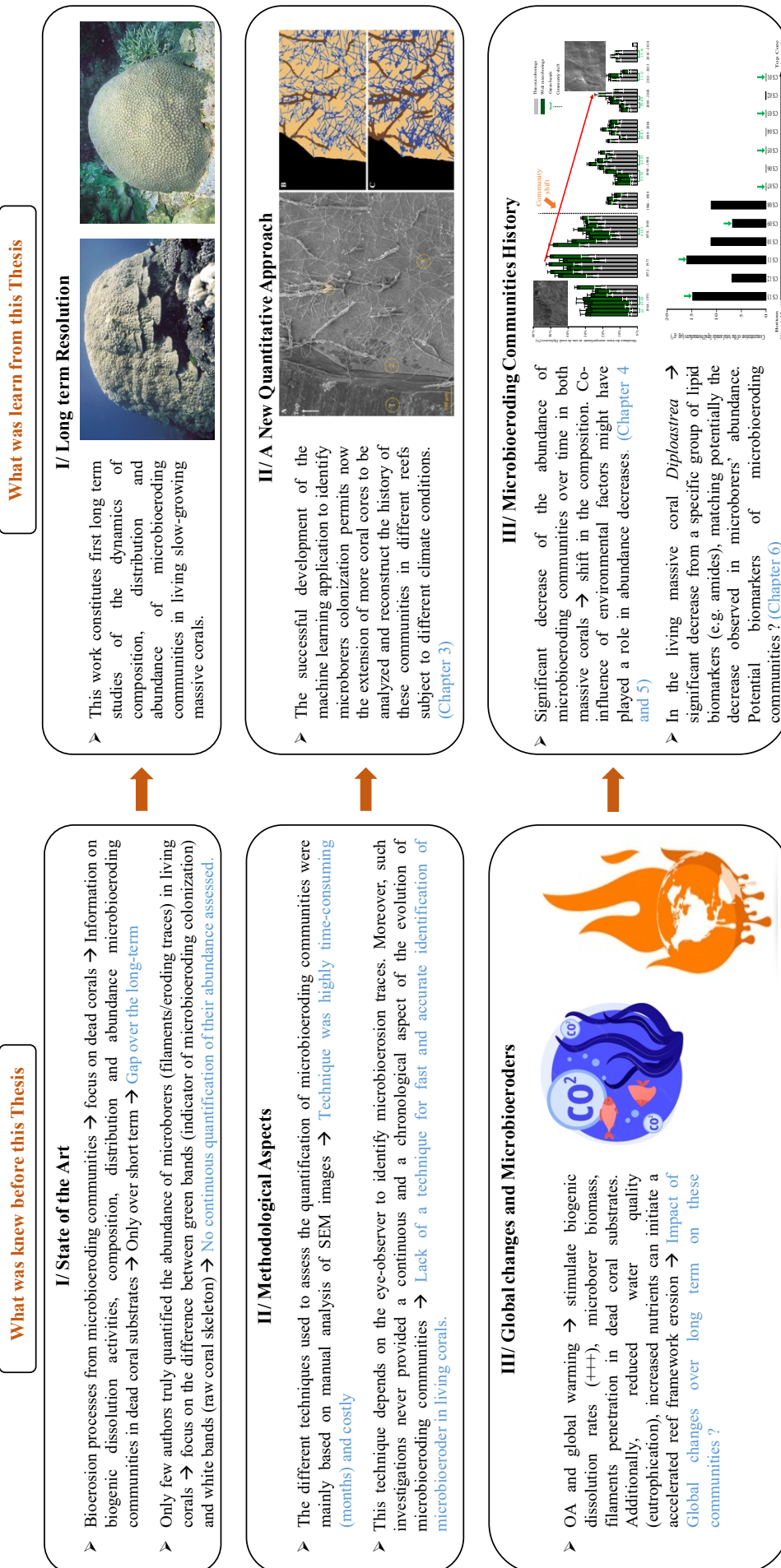


Figure 7.1: Schematic summary of the Ph.D. project.

7.2 Perspectives

The processes between microbioeroding communities and living massive corals are complex, as this work highlights. Thus, from these findings emerge new scientific questions that require future work. This thesis opens the way for many perspectives on the application of the ML method, the identification of more classes of microbioeroding communities, and the inclusion of various types of corals.

7.2.1 Machine Learning Application

In this thesis, developing an ML application allowed me to identify accurately and continuously the colonization of coral skeletons of microbioeroding communities through the lifespan of different massive corals. Within this work, I developed two applications trained on SEM images specific to each massive coral. Both models gathered more than 90% accuracy in identifying microbioeroding traces colonizing the coral skeleton. Nonetheless, this ML application could be improved in many different ways:

- The ML application could be enhanced and trained to identify more different classes of microbioeroding communities. Nonetheless, this will require an important pre-processing period by manually labeling the different microbioeroding classes the application must identify. The more classes to be identified, the more complex and diverse the dataset will need to be for the network to train, which implies a longer training phase.
- Through this work and the will to improve the performances of the ML application, I only focused on modifying one specific hyper-parameter (e.g., loss function) during the training phase. Such modification from one application to another showed better performances at identifying the class of interest. I strongly believe that by modifying other hyper-parameters mentioned in the **Chapter 3**, the performances of the model could be even better than the ones already assessed.

In the future, one interesting objective would be to realize one training that gathers the SEM images collected from both massive corals. It will create one ML application that will identify first the total abundance of microbioeroding traces in massive corals (*Diploastrea* and *Porites*) and then fine-tune the application to identify more communities. To push even further, one objective will be to collect and label SEM images from different branching corals to quantify and identify microbioeroding communities col-

onizing their skeletons. Then, it would be interesting to realize an ML training adapted to branching corals and fit to identify the microbioeroding communities in these types of skeletal architectures. Finally, one key prospect would be to define a multi-coral model application to identify microbioeroding communities in diverse corals, such as massive and branching.

7.2.2 Additional Results of a Coral Core of La Réunion

The coral core of la Reunion offers an understanding of the evolution of microbioeroding communities in a healthy massive coral colony *Porites* sp. It is of great interest as it is located in the very shallow waters ($\approx 1\text{m}$) of the lagoon at la Saline in la Reunion, which might be subject to anthropogenic impacts. I, therefore, analyzed the variability of the total abundance of microbioeroding traces colonizing the *Porites* sp. coral skeleton from la Reunion (**Figure 7.2**).

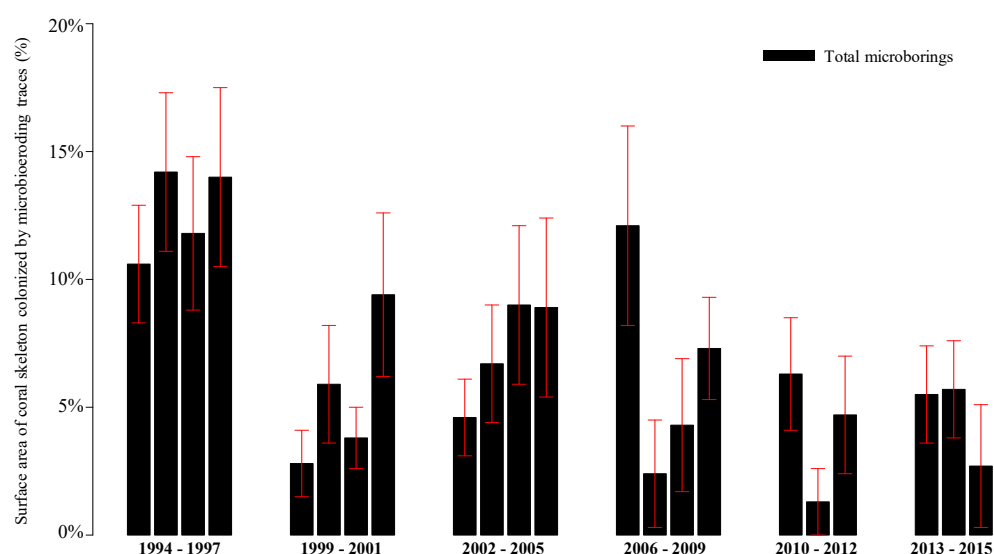


Figure 7.2: Histogram showing the variability of the percentage of the *Porites* sp. coral skeleton colonized by microbioeroding communities in la Reunion. The variability of the microbioeroding traces were obtained along the 3 vertical transects (same methodology as described in corals from Mayotte).

One interesting result is a significant decrease in the total abundance of microbioeroding traces colonizing the coral skeleton of *Porites* in la Reunion (Mann-Kendall test, $p < 0.05$). No breakpoints were identified over the last 20 years regarding the colonization history of microbioeroding communities in the *Porites* sp. Still, between 1997-1998, I observed a sudden decrease in the abundance of microbioeroding traces from 15% to around 3%. This sudden decrease could match the breakpoint period observed in both corals from Mayotte (1-year difference). It may be related to the strong el Niño

observed at that time. Nonetheless, such assumptions must be further investigated to identify which factors could explain the decrease in the abundance of microbioeroding traces in the *Porites* sp. coral from la Reunion.

7.2.3 Additional Results from Coral Cores of the Scattered Islands

Preliminary results have been obtained on two *Porites* sp. coral cores from Juan de Nova (JDN) and Europa, islands located along a north-south gradient in the MC. The coral cores of Scattered Islands offer an understanding of the evolution of microbioeroding communities in massive *Porites* sp. corals, from contrasted reefs supposedly free from anthropogenic activities as no human development is present within these islands and understand the potential environmental effects alone (SST, pH, wind, insolation ...). Moreover, Lo Monaco et al. (2021) observed a large decrease in the seawater pH in all sectors of the MC, including near coral reef areas in the Eparses Islands (Europa, Juan de Nova), with more acidic waters in the southern part of the channel. For both coral cores, I reconstructed the coral growth variables. The *Porites* sp. coral core from Juan de Nova allowed a reconstruction from 1972 to 2018 (**Figure 7.3**).

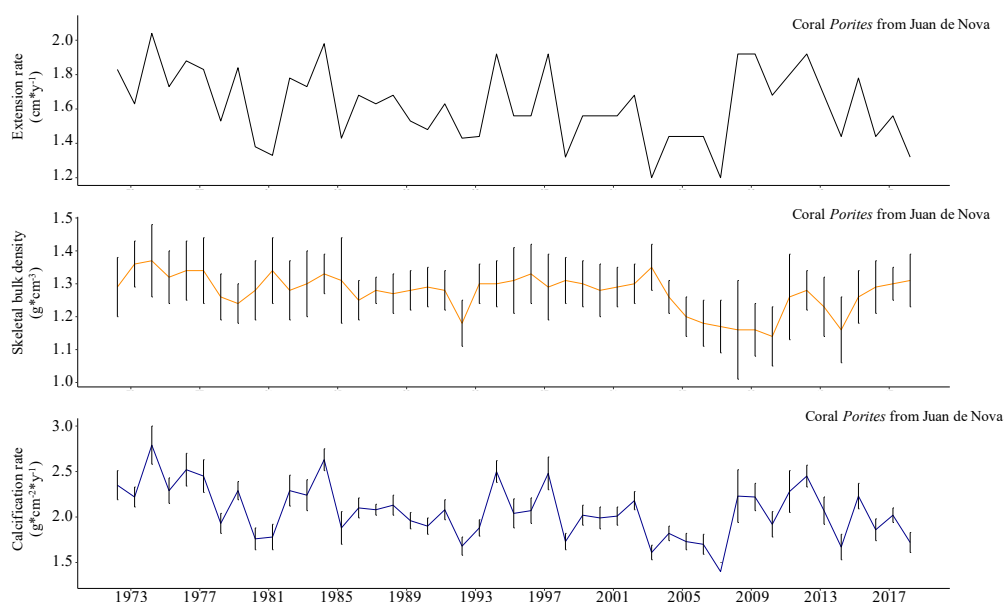


Figure 7.3: Evolution of the different coral growth parameters of the studied *Porites* sp. colony from Juan De Nova.

Analyzing the long coral record of *Porites* sp. from JDN may validate or not the first assumptions observed in the *Diploastrea* sp. from Mayotte that covered nearly the same period. Considering the growth parameters of *Porites* from JDN, the vertical extension

rate did not vary significantly from 1972 to 2018. While the skeletal bulk density and calcification rate decreased significantly over this period (Mann-Kendall test $p < 0.001$) **Figure 7.3**), as also observed in the long record of *Diploastrea* sp. Thus, investigating the composition and abundance of microbioeroding communities on another massive coral presenting similar decreasing patterns in density and calcification than the *Diploastrea* sp. from Mayotte could reveal valuable information and is now under investigation.

The *Porites* sp. coral core from Europa allowed a reconstruction from 1993 to 2018. When considering the *Porites* sp. coral, all three growth parameters did not vary significantly over the last three decades (**Figure 7.4**), which can be potentially explained due to the small interval of time considered (i.e, 25 years). As mentioned, Europa represents the southern area of the cores studied in this project. It might also represent the study site with the most acidic conditions (Monaco et al., 2021). Such a site offers the possibility of studying the variability of the composition and abundance of microbioeroding communities in a changing and decreasing seawater pH environment. Moreover, it is known that their biogenic dissolution activities are greatly enhanced in conditions of OA (Reyes-Nivia et al., 2013; Schönberg et al., 2017; Tribollet et al., 2019).

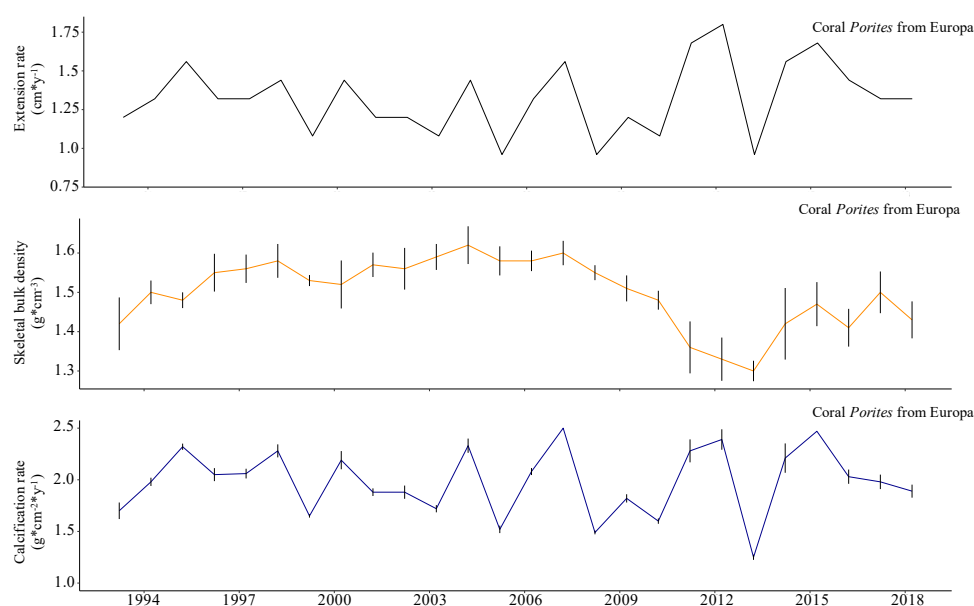


Figure 7.4: Evolution of the different coral growth parameters of the studied *Porites* sp. colony from Europa.

7.2.4 Further Investigations

In this work, I investigated two massive coral cores from Mayotte to study the decadal variability of the composition and abundance of microbioeroding communities over the last three to five decades. As mentioned, additional cores are already under investigation from contrasted reefs of the Indian Ocean. More coral cores from contrasted reefs from others oceanic regions should be studied to confirm the observed trends of the decrease in microborers' abundance. As possible explanatory factors could be ocean warming (both SST and SSTA), OA (pH), wind stress, precipitations, and cumulative insolation more or less combined, as well as the bulk density of the coral host, investigations on coral reefs from different oceanic regions (Eastern Indian Ocean, Tropical Pacific, Caribbean Reefs ...), under a different climate variability than the Indian Ocean, need to be explored to assess how the variability of abundance and composition of microbioeroding communities answer to climate conditions in such regions. Other factors, such as seawater pH, other variables from coral carbonate chemistry, and metal trace pollution, could be involved and explained potentially the variability of microbioeroding communities and need to be further explored. Additionally, long and well-preserved coral cores could be investigated for long-term chronology reconstruction and evolution of microbioeroding communities over centuries. For instance, Wu et al. (2018) studied the massive coral *Diploastrea heliopora* from New Caledonia and reconstructed inter-decadal pH variability from 1689 to 2011 in the South Pacific Ocean. Access to such long records would allow a better understanding of the long-term evolution of microbioeroding communities in living massive corals. If the trends found over the last five decades in our corals were validated on a larger time scale (the last three centuries, for example), with a large abundance of these communities in the past and then a decline, this could potentially highlight the presence of a cycle of the evolution of these communities within living corals. Above all, thanks to these long-term records of the variability of these communities and the understanding of the climate situation at that time, this will allow for improving coral model projections in the future to predict better and forecast coral health and resilience state over the next decades.

Appendix

8.1 Cast-Embedding Protocol

Here is a detailed and explained version of the embedding resin protocol for coral samples and microbioeroders' visualization under SEM.

1) Chronology reconstruction through the estimation of the coral growth rate. Two complementary methods, the geochemistry analysis with the proxy Sr/Ca, record the temperature variations over time. A distance between two peaks indicates a year of growth. The approach is coupled with the X-ray and tomography of the coral core using the annual density banding to validate the growth rate reconstruction. A year of growth is characterized by adding one high and one low-density band.

2) Cutting the coral core in sub-samples in adequation with the chronology reconstruction model. Avoid cutting through the middle of one year. The maximum size for sub-samples does not exceed 2 cm (representing the size of the container for the embedding).

3) Label the sub-samples according to their sampling area and indicate an arrow to show the upward direction of the coral growth (taking pictures can help).

4) Bleaching treatment of the sub-samples with sodium hypochlorite (NaClO) for 3 days to remove all organic matrix (tissue layer of the coral). Sub-samples are placed in

small beakers and under a fume hood.

5) After the 3 days of bleaching, rinse the sub-samples with distilled water (or Milli-Q) for 2-3 days. Importance of changing the bath regularly (use the same beakers after rinsing them well with distilled water to eliminate any bleach left).

6) Dry the sub-samples in the oven at 40°C-50°C. Leave for at least 24 to 48 hours.

7) Impregnation in epoxy resin as shown below:

(A): Several tests were performed to determine the proportion of epoxy resin and curing agent required for a solid and clean sub-sample. The final mix comprises 30 gr epoxy resin and 15 gr curing agent (ratio 1/0.5).

(B): Mix gently for 5 to 10 minutes, avoiding the formation of bubbles. The mixture must be homogeneous.

(C): The mixture is then placed within a mold to create a layer that is not too liquid so that the sub-sample does not touch the bottom (a problem for the following cutting if the sub-sample is at the bottom). Also not too hard so that it does not remain on the surface. Put the mold in the oven at 50°C for about 10 minutes (check every 2 minutes). The resin must remain sticky, allowing the sub-sample to sink within a few millimeters.

(D): Once the mixture is half hardened, put the sub-samples in the molds, and if there is still some mixture (if not, repeat according to A.), immerse the sub-samples completely and note on the edges of the mold the name of each sub-sample, the direction of the upward growth rate, and remove the potential bubble formation using wooden sticks.

(E): Place the molds in the vacuum chamber configured at 0.1 bar. Moisten the edge of the chamber so that the glass pane sticks and the air is drawn out. Open and pop the bubbles as soon as they form on the surface of the embedded sub-samples. Leave under vacuum for about 15-20 minutes.

F): Place the molds in the oven at 50°C for 24 hours (nevertheless, 6 to 7 hours can be enough).

8) Unmold the blocks and cut the included sub-samples with a diamond saw (Isomet1000 from Buehler), and then stick the thin coral section on a microscopic slide. Finally, coral sections are sonicated to remove potential sediments from sectioning for a few seconds.

9) Decalcification with Hydrochloric acid (HCl 10%) for 10 seconds. Put a few drops on the surface of the thin section (Same time for each coral section). Stop the reaction by immersing the samples in a beaker with distilled water.

10) Dry the thin coral sections in the oven at 40°C-50°C. Leave for 1 to 2 hours.

11) Gold metallization of the coral sections for observing the different microboring traces under SEM.

12) Observation of the different microborings depends on the study and objectives of the authors. Here, 3 vertical transects were investigated along each coral section, one on the left, one on the right, and one in the middle, applied over the length of the entire core. Additionally, horizontal transects can be established if the visual presence of green bands is spotted.

Materials for Impregnation:

- Specifix Epoxy Resin
- Specifix Curing Agent
- Rectangular Molds
- Plastic Cups (for the mix)
- Wooden Sticks
- Beakers (2 to 3, 250-500 mL)
- Vacuum chamber
- Aluminium Paper

8.2 Supplementary Materials *Diploastrea* sp. Coral Investigation

Supplementary Material

Supplemental material related to the article entitled “54 years of microborings community history explored by machine learning in a massive coral from Mayotte (Indian Ocean)” by D. Alaguarda, J. Brajard, G. Coulibaly, M. Canesi, E. Douville, F. Le Cornec, C. Lelabousse, A. Tribollet (2022) Front. Mar. Sci. 9:899398. doi: 10.3389/fmars.2022.899398

Machine Learning Approach

We present here the code used to defined the CNN model. The full implementation of the model using the Keras library is provided on an open access database:

<https://gist.github.com/brajard/ad809dbbcf9ba723320a47b89d26e1d4>

```
from tensorflow.keras.models import *
from tensorflow.keras.layers import *
from tensorflow.keras.optimizers import Adam
n_filters = 32
input_size = (256, 256, 1)

inputs = Input(input_size)
conv1 = Conv2D(n_filters, 3, activation='relu', padding='same',
kernel_initializer='he_normal')(inputs)
conv1 = BatchNormalization()(conv1)
conv1 = Conv2D(n_filters, 3, activation='relu', padding='same',
kernel_initializer='he_normal')(conv1)
conv1 = BatchNormalization()(conv1)
pool1 = MaxPooling2D(pool_size=(2, 2))(conv1)

conv2 = Conv2D(2 * n_filters, 3, activation='relu', padding='same',
kernel_initializer='he_normal')(pool1)
conv2 = BatchNormalization()(conv2)
conv2 = Conv2D(2 * n_filters, 3, activation='relu', padding='same',
kernel_initializer='he_normal')(conv2)
conv2 = BatchNormalization()(conv2)
pool2 = MaxPooling2D(pool_size=(2, 2))(conv2)

conv3 = Conv2D(4 * n_filters, 3, activation='relu', padding='same',
kernel_initializer='he_normal')(pool2)
conv3 = BatchNormalization()(conv3)
conv3 = Conv2D(4 * n_filters, 3, activation='relu', padding='same',
kernel_initializer='he_normal')(conv3)
conv3 = BatchNormalization()(conv3)
pool3 = MaxPooling2D(pool_size=(2, 2))(conv3)

conv4 = Conv2D(8 * n_filters, 3, activation='relu', padding='same',
kernel_initializer='he_normal')(pool3)
```

```

conv4 = BatchNormalization()(conv4)
conv4 = Conv2D(8 * n_filters, 3, activation='relu', padding='same',
kernel_initializer='he_normal')(conv4)
conv4 = BatchNormalization()(conv4)
pool4 = MaxPooling2D(pool_size=(2, 2))(conv4)

conv5 = Conv2D(16 * n_filters, 3, activation='relu', padding='same',
kernel_initializer='he_normal')(pool4)
conv5 = BatchNormalization()(conv5)
conv5 = Conv2D(16 * n_filters, 3, activation='relu', padding='same',
kernel_initializer='he_normal')(conv5)
conv5 = BatchNormalization()(conv5)

up6 = Conv2D(8 * n_filters, 2, activation='relu', padding='same',
kernel_initializer='he_normal')(UpSampling2D(size=(2, 2))(conv5))
merge6 = concatenate([conv4, up6], axis=3)
conv6 = Conv2D(8 * n_filters, 3, activation='relu', padding='same',
kernel_initializer='he_normal')(merge6)
conv6 = BatchNormalization()(conv6)
conv6 = Conv2D(8 * n_filters, 3, activation='relu', padding='same',
kernel_initializer='he_normal')(conv6)
conv6 = BatchNormalization()(conv6)

up7 = Conv2D(4 * n_filters, 2, activation='relu', padding='same',
kernel_initializer='he_normal')(UpSampling2D(size=(2, 2))(conv6))
merge7 = concatenate([conv3, up7], axis=3)
conv7 = Conv2D(4 * n_filters, 3, activation='relu', padding='same',
kernel_initializer='he_normal')(merge7)
conv7 = BatchNormalization()(conv7)
conv7 = Conv2D(4 * n_filters, 3, activation='relu', padding='same',
kernel_initializer='he_normal')(conv7)
conv7 = BatchNormalization()(conv7)

up8 = Conv2D(2 * n_filters, 2, activation='relu', padding='same',
kernel_initializer='he_normal')(UpSampling2D(size=(2, 2))(conv7))
merge8 = concatenate([conv2, up8], axis=3)
conv8 = Conv2D(2 * n_filters, 3, activation='relu', padding='same',
kernel_initializer='he_normal')(merge8)
conv8 = BatchNormalization()(conv8)
conv8 = Conv2D(2 * n_filters, 3, activation='relu', padding='same',
kernel_initializer='he_normal')(conv8)
conv8 = BatchNormalization()(conv8)

up9 = Conv2D(n_filters, 2, activation='relu', padding='same',
kernel_initializer='he_normal')(UpSampling2D(size=(2, 2))(conv8))
merge9 = concatenate([conv1, up9], axis=3)
conv9 = Conv2D(n_filters, 3, activation='relu', padding='same',
kernel_initializer='he_normal')(merge9)
conv9 = BatchNormalization()(conv9)
conv9 = Conv2D(n_filters, 3, activation='relu', padding='same',
kernel_initializer='he_normal')(conv9)
conv9 = BatchNormalization()(conv9)
conv9 = Conv2D(3, 3, activation='relu', padding='same',
kernel_initializer='he_normal')(conv9)

conv10 = Conv2D(4, 1, activation='softmax')(conv9)

```

```
model = Model(inputs=inputs, outputs=conv10)

model.compile(optimizer = Adam(lr = 1e-3), loss =
'categorical_crossentropy', metrics = ['accuracy'])

model.summary()
```

Neural network structure

The structure of the CNN model is detailed in the Suppl Fig 2. Each feature map (gray or orange blocks in the figure) represents a 3-dimensional matrix, also called tensor. Each tensor is transformed using a parametrized function whose output is called a layer. Our CNN model was built with 10 convolutional layers, one convolution representing a linear operation involving the product of a set of parameters with the 2D input feature map. Here, the first convolutional layer was related to the input SEM images, i.e. the original images obtained using the SEM ZEISS from the Platform ALYSES in Bondy (Suppl Fig 2). Note that, convolutional layers are invariant by translation, which means in our case that the classification of a microborer trace for instance does not depend on its location on the SEM image, which is the desired behavior. The “trainable” parameters of the convolutional layers need to be optimized during a training process, so the output predicted by the CNN model corresponds to the desired output SEM image. The optimization process involves a reference dataset mapping input SEM images with the desired output classification comprising our four defined categories: ‘resin’, ‘coral’, ‘skeleton’, ‘thin microborings’ and ‘wide microborings’. This reference dataset was here obtained by manually analyzing 68 original SEM images (input, see described below). Once the parameters of the CNN model were optimized during a training phase and some tuning of the model has been performed the CNN model could be used to process any input SEM images in the so-called inference phase. In addition to the convolutional layers that contain most of the trainable parameters, the CNN model contained bath normalization layers (Ioffe and Szegedy, 2015) and max-pooling layers (Supp Fig 2; Yamaguchi et al. 1990; Ioffe and Szegedy, 2015). Those trainable parameters made the CNN model more stable and prevented overfitting. Such

overfitting can occur when a model gives results fitted on the dataset used in the training phase but failed to give a correct prediction for any other inputs. To enable a non-linear model, rectified linear units were applied after each convolutional layer (ReLU; Romanuke, 2017). ReLU is a function that takes a scalar input x and returns $\max(0, x)$. For each image, the CNN model determined thus which pixel was a thin or a wide microboring, part of the coral skeleton or resin. The last layer was defined as a so-called softmax function converting output values of the previous layer into probabilities (the sum of those probabilities equal 1; Goodfellow et al., 2016). The model thus attributed a probability for each pixel to belong to each predetermined category (resin, skeleton, thin or wide microborings). The final category attributes corresponded to the highest determined probability. All the components of our approach were common for a machine learning model used to classify objects.

Dataset constitution step

As explained in the previous section, a reference dataset was needed to determine the best possible model by optimizing the parameters of the CNN model. Two types of parameters were determined: the parameters of each layer and the so-called hyper-parameters that need to be specified beforehand such as the size of the layers and the type of the used optimizer. To constitute this reference dataset, we randomly selected 68 SEM images from our database and processed them manually, i.e. that each pixel was associated to one of the four predetermined categories for ground truthing. This was very time consuming and could not be applied to all the available SEM images (≥ 1500). This dataset was then randomly split into 3 sub-datasets: the training set composed of 60 images and which allowed determining the trainable parameters, the validation set composed of 5 images and which allowed determining the hyperparameters, and the test set composed of the last 3 images in order to assess the performance of the final model (Suppl. Fig. 2A & B). For technical reasons, the original SEM images of 1024x768 pixels, were cut into 12 sub-images of size 256x256. Once the model

analyzed all input sub-images, the original output SEM images were formed again based on their 12 corresponding sub-images. The number of validation sub-images was thus 60 (i.e. 5x12) and the number of test samples was 36 (i.e. 3x12). To further increase the number of samples in the training set (which is critical for the machine learning approach) we applied a data augmentation technique that consisted of multiplying the number of training sub-images by applying a rotation of 0°, 90°, 180° and 270°. This step allowed the production of training set of 2880 sub-images.

Training step

Our network aimed at estimating the relative abundance (%) of thin vs wide microborings on each SEM image via the measurement of the surface area of coral skeleton colonized by each type of microborings. The training phase of the CNN model thus aimed at optimizing the trainable parameters of the model. This step was performed by minimizing a loss function using the Adams algorithm which is based on a gradient descent technique (Kingma et al., 2014). We used the standard configuration of TensorFlow (version 2.6.0) with a loss function adapted from the negative log cross-entropy, a common procedure used for classification (Murphy, 2012). This was defined for each set of training sub-images according to the following

$L = \sum_{n=1}^N \sum_{k=1}^4 w_k p_{n,k} \log \hat{p}_{n,k}$, where $p_{n,k}$ is the true probability of the pixel n for the class k , which equals 1 if the true class is k , otherwise it is 0; $\hat{p}_{n,k}$ is the probability computed by the CNN model when it attributes the right pixel to a given category; and the coefficient w_k is a weighted factor used to as our four categories were highly unbalanced, by attributing more important weights to under-represented classes (here we are much more skeleton pixels than microboring pixels for instance; see Huang and Wu, 2016). We have thus set $w_1 = w_2 = 0.66$ for the two categories of microborings, $w_3 = 0.11$ for the ‘coral skeleton’ and $w_4 = 0.22$ for the ‘resin’. We used a maximum of 130 iterations (epochs). In general we used less iterations

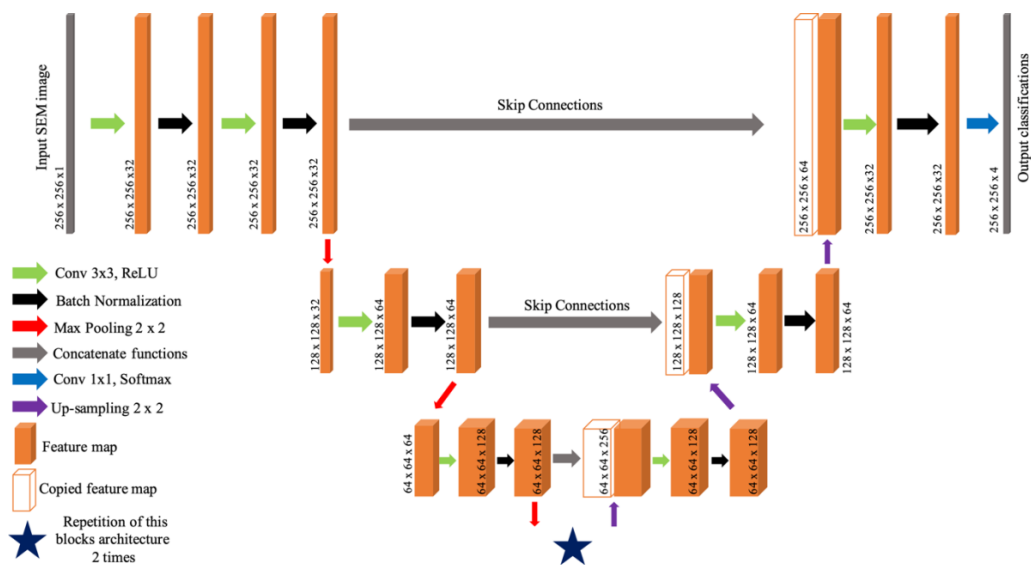
as we could monitored the loss of accuracy in the validation samples to avoid overfitting (Goodfellow et al. 2016). The duration of the training step was between 2 and 3 hours due to a good connection to the IPSL MESRI Mesocenter and the use of its GPU with two graphic cards NVIDIA GeForce RTX 2080 Ti (11Go). Despite the time spent to collect the original SEM images and to set the training step once the CNN model was ready, it allowed a rapid assessment of thousands of original SEM images (a few minutes).

Model tuning and post processing steps

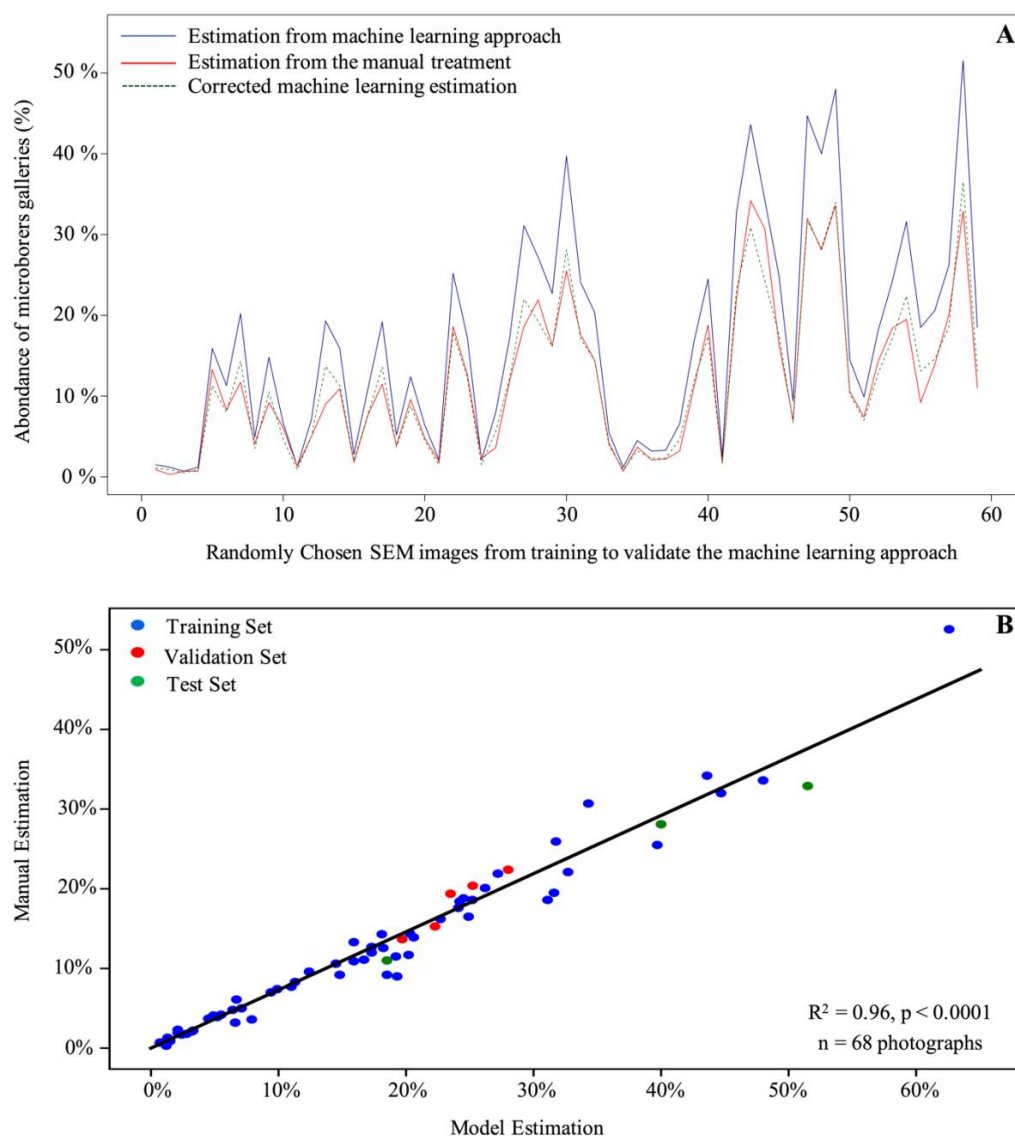
corresponds thus to the best model obtained with the lowest loss during the validation phase Q. To validate the CNN model and to verify that it could be used on new original SEM images, we used two metrics computed on the test dataset. The test dataset was neither part of the training nor of the tuning of the CNN model and could be considered as a reliable independent test for the capacity of the model to generalize the classification to new SEM images. The dataset allowed thus providing two metrics : the accuracy of the classification, which corresponded to the ratio between the number of pixels that were correctly classified and the total number of pixels per SEM image (100% corresponded to a perfect classification), and the % of the surface area of the coral skeleton colonized by thin or wide microborings. For example, the following equation was used to estimate the % of the surface area of coral skeleton colonized by thin galleries : $N_1/(N_1+N_2+N_3)*100$, where N_1 is the number of pixels classified in the class 'thin microborings', N_2 , the number of pixels attributed to 'wide microborings' and N_3 , the number of pixels attributed to 'coral skeleton'). Surprisingly, we observed that our CNN model systematically overestimated the surface area of microborings. We thus applied a correcting factor of 15% to the whole training dataset of SEM images to correct the bias (Fig.3A, Suppl. Fig.3A). A linear regression between the percentages of surface area of coral skeleton colonized by all microborings (thin + wide ones) estimated

manually on the training set, validation set and test set of SEM images and those obtained by the CNN model on the same sets of images after application of the correction factor showed that the correction was efficient ($R^2 = 0.96$, $p < 0.0001$; Suppl Fig.3B). The estimated accuracy of the CNN Model was thus 93%.

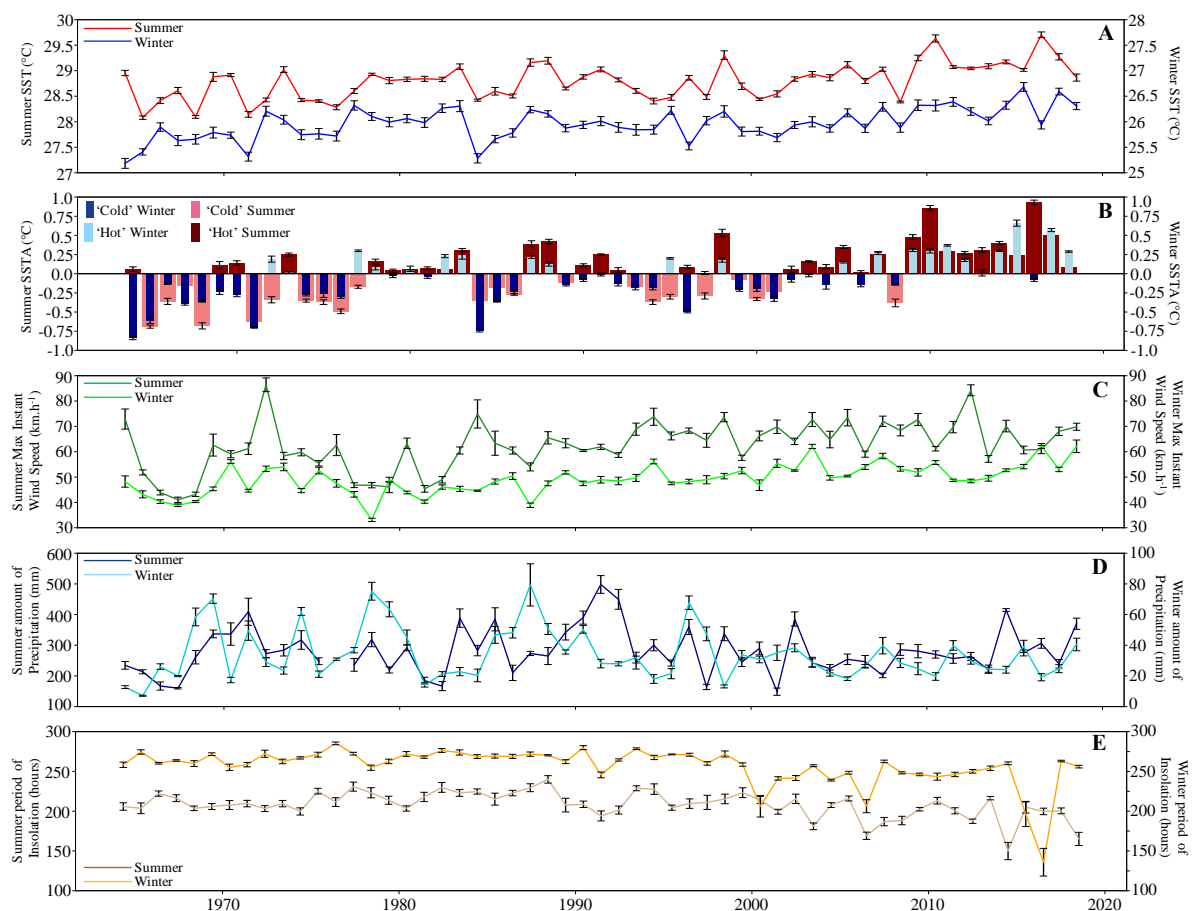
Suppl Figure 1: Convolutional Neural Network architecture used to determine the surface area of coral skeleton colonized by microborers on SEM images. Each box represents an SEM image and its size in pixels is indicated on the side. The two vertical grey boxes indicate the input (original) and output (analyzed) SEM images. The right grey box represents the SEM image that first enters into the CNN (input data). The left grey box represents the SEM image but including the differentiation of the different classes (output data). Each orange box corresponds to multiple channel feature maps. Colored arrows represent the various CNN operation and steps.



Suppl Figure 2: Comparison of the estimated surface area of coral skeleton colonized by microborers (thin + wide ones) obtained manually and by the CNN model (60 SEM images were analyzed here). **A.** The CNN model (blue line) always overestimated the surface area of coral skeleton colonized by microborers. It was thus corrected by a factor (15%) so the estimations provided by the CNN model (green dotted line) were very closed to those obtained manually (red line). **B.** Linear regression showing the correspondence between the manual and model estimation. The regression is based on the 68 images used by the CNN splitted in the 3 different dataset ($R^2 = 0,96$).



Suppl Figure 3: Interannual variability of the different environmental parameters between 1964 and 2018 decoupling the two different seasons at Mayotte: the summer season comprises December to April while the winter season comprises June to October. May and November were considered transition months (interseasons) and thus were not considered here. **A.** Sea Surface Temperature (SST in °C). **B.** Sea surface temperature anomalies (SSTA in °C). **C.** Maximum instantaneous wind speed (km·h⁻¹). **D.** Precipitation rate (mm). **E.** Cumulative insolation period (hours). Mean and SE are presented per year for each variable at each season.



Suppl Table 1. Environmental parameters collected within the area of Mayotte over the last 50 years. Mean and SE were calculated per year.

Year	SST (°C)	SSTA (°C)	Volume of Precipitations (mm)	Max Instand Wind (km*h)	Cumulative Insolation (Hours)
1964	26.98 ± 0.19	-0.48 ± 0.03	125.46 ± 17.82	55.8 ± 2.89	242.97 ± 5.43
1965	26.77 ± 0.17	-0.69 ± 0.03	93.19 ± 11.16	43.2 ± 1.23	239.84 ± 3.56
1966	27.26 ± 0.21	-0.2 ± 0.02	94.99 ± 16.63	42.6 ± 1.46	248.58 ± 4.88
1967	27.2 ± 0.21	-0.26 ± 0.03	102.83 ± 9.67	37.8 ± 0.5	240.32 ± 4.86
1968	26.92 ± 0.17	-0.54 ± 0.03	139.34 ± 21.78	39.3 ± 0.94	239.58 ± 4.93
1969	27.51 ± 0.23	0.05 ± 0.04	211.63 ± 19.52	59.4 ± 3.21	244.59 ± 5.1
1970	27.29 ± 0.21	-0.17 ± 0.03	160.41 ± 30.98	54.9 ± 1.31	235.78 ± 5.81
1971	27.1 ± 0.2	-0.56 ± 0.04	212.75 ± 38.07	56.7 ± 2.67	239.22 ± 4.82
1972	27.33 ± 0.17	-0.05 ± 0.05	134.86 ± 15.72	60.9 ± 2.89	241.08 ± 6.11
1973	27.54 ± 0.21	0.08 ± 0.03	144.43 ± 21.39	55.2 ± 1.4	246.51 ± 5.43
1974	27.13 ± 0.19	-0.33 ± 0.02	168.5 ± 26.16	51 ± 1.56	239.78 ± 5.59
1975	27.11 ± 0.19	-0.41 ± 0.04	139.54 ± 17.37	53.4 ± 1.31	251.68 ± 4.41
1976	27.41 ± 0.19	-0.31 ± 0.02	185.17 ± 11.53	50.1 ± 3.07	252.85 ± 6.28
1977	27.86 ± 0.17	0.11 ± 0.03	177.44 ± 20.5	48 ± 1.42	250.53 ± 4.44
1978	27.41 ± 0.19	0.03 ± 0.03	167 ± 22.46	41.7 ± 1.75	236.43 ± 6.2
1979	27.3 ± 0.2	0.09 ± 0.02	107.25 ± 12.69	46.5 ± 1.34	247.48 ± 4.65
1980	27.29 ± 0.19	0.05 ± 0.02	154.77 ± 17.82	50.1 ± 1.86	240.63 ± 5.61
1981	27.48 ± 0.2	0.02 ± 0.02	112.07 ± 15.62	44.1 ± 1.23	244.99 ± 5.03
1982	27.65 ± 0.18	0.19 ± 0.03	120.3 ± 22.19	49.2 ± 1.46	253.96 ± 5.38
1983	27.73 ± 0.2	0.27 ± 0.03	141.73 ± 22.43	49.5 ± 1.23	253.72 ± 5.21
1984	26.94 ± 0.22	-0.52 ± 0.05	139.24 ± 19.7	58.8 ± 4.02	252.08 ± 4.37
1985	27.5 ± 0.2	-0.28 ± 0.01	145.88 ± 27.88	53.1 ± 3.29	247.1 ± 6.31
1986	27.32 ± 0.2	-0.14 ± 0.04	170.88 ± 20.48	54 ± 1.44	247.08 ± 4.51
1987	27.76 ± 0.21	0.3 ± 0.04	123.72 ± 13.72	52.8 ± 2.38	259.04 ± 4.99
1988	27.71 ± 0.21	0.25 ± 0.03	169.89 ± 22.92	53.7 ± 2.11	256.38 ± 3.56
1989	27.21 ± 0.19	-0.17 ± 0.02	196.93 ± 26.12	57.9 ± 1.42	236.82 ± 6.72
1990	27.46 ± 0.2	0 ± 0.03	193.53 ± 27.79	52.8 ± 1.03	253.99 ± 5.91
1991	27.6 ± 0.21	0.14 ± 0.03	283.01 ± 43.3	54.3 ± 1.5	213.58 ± 5.44
1992	27.4 ± 0.2	-0.06 ± 0.03	165.45 ± 21.77	54.39 ± 1.49	244.25 ± 5.15
1993	27.33 ± 0.2	-0.13 ± 0.03	94.89 ± 19.01	56.82 ± 2.31	255.43 ± 3.86
1994	27.21 ± 0.19	-0.25 ± 0.03	146.64 ± 17.82	62.88 ± 2.67	246.23 ± 5.9
1995	27.69 ± 0.17	-0.02 ± 0.04	106.6 ± 13.83	55.62 ± 1.76	245.73 ± 4.88
1996	26.87 ± 0.23	-0.3 ± 0.04	109.44 ± 24.13	52.38 ± 1.77	249.58 ± 6.48
1997	27.33 ± 0.18	-0.13 ± 0.04	108.61 ± 13.82	59.31 ± 2.33	243.35 ± 7.25
1998	27.78 ± 0.23	0.32 ± 0.05	130.86 ± 25.03	57.06 ± 2.02	249.61 ± 6.51
1999	26.93 ± 0.21	-0.16 ± 0.02	117.38 ± 19.42	55.2 ± 1.07	232.02 ± 4.63
2000	27.07 ± 0.18	-0.26 ± 0.02	113.02 ± 20.05	57.3 ± 2.29	212.07 ± 8.89
2001	27.25 ± 0.21	-0.21 ± 0.04	83.98 ± 11.16	60.9 ± 2.28	231.12 ± 4.56
2002	27.38 ± 0.2	-0.08 ± 0.04	160.42 ± 25.95	56.4 ± 1.35	211.49 ± 4.17
2003	27.56 ± 0.21	0.09 ± 0.03	128.19 ± 16.63	66.4 ± 2.25	219.76 ± 5.8
2004	27.43 ± 0.21	-0.01 ± 0.04	157.14 ± 19.95	59.4 ± 2.77	223.88 ± 3.35
2005	27.66 ± 0.21	0.2 ± 0.03	115.72 ± 14.88	58.2 ± 2.45	229.28 ± 3.28
2006	27.45 ± 0.21	-0.01 ± 0.03	136.36 ± 18.39	60 ± 1.57	187.09 ± 6.37
2007	27.71 ± 0.19	0.25 ± 0.02	108.41 ± 12.65	62.1 ± 1.92	229.98 ± 6.14
2008	27.29 ± 0.18	-0.17 ± 0.05	173.25 ± 25.27	61.5 ± 1.79	223.52 ± 5.32
2009	27.85 ± 0.21	0.39 ± 0.03	124.91 ± 15.59	62.7 ± 2.45	229.98 ± 4.43
2010	27.99 ± 0.24	0.61 ± 0.05	119.06 ± 15.15	55.98 ± 0.84	231.01 ± 4.41
2011	27.82 ± 0.19	0.36 ± 0.01	128.93 ± 18.21	58.5 ± 2.03	224.01 ± 4.38
2012	27.68 ± 0.2	0.22 ± 0.01	119.25 ± 17.36	62.43 ± 2.96	222.41 ± 4.63
2013	27.46 ± 0.21	0.08 ± 0.05	126.34 ± 19.09	58.56 ± 2.19	225.81 ± 7.18
2014	28 ± 0.2	0.35 ± 0.02	150.12 ± 24.88	59.04 ± 2.02	226.18 ± 8.58
2015	28.12 ± 0.17	0.47 ± 0.05	121.1 ± 17.16	57.51 ± 1.32	194.49 ± 11.36

2016	27.67 ± 0.25	0.31 ± 0.07	96 ± 20.82	60.78 ± 1.35	182.61 ± 12.78
2017	27.65 ± 0.19	0.47 ± 0.03	114.56 ± 18.56	61.14 ± 1.78	220.5 ± 7.57
2018	27.61 ± 0.19	0.24 ± 0.03	134.32 ± 24.45	62.97 ± 1.91	229.16 ± 6.2

Suppl Table 2. Coral growth parameters reconstructed in *Diploastrea* sp. over the last 50 years. Mean and SDs were calculated per year.

Year	Growth rate (mm)	Coral bulk density (g*cm ⁻³)	Calcification rate (g*cm ⁻² *y ⁻¹)
1964	2.6	1.58 ± 0.02	0.41 ± 0.005
1965	3	1.64 ± 0.01	0.49 ± 0.002
1966	3.1	1.73 ± 0.02	0.54 ± 0.003
1967	2.8	1.78 ± 0.03	0.5 ± 0.008
1968	2.75	1.82 ± 0.01	0.5 ± 0.004
1969	2.6	1.82 ± 0.01	0.47 ± 0.003
1970	2.4	1.87 ± 0.02	0.45 ± 0.005
1971	2.25	1.86 ± 0.01	0.42 ± 0.003
1972	2.75	1.87 ± 0.03	0.51 ± 0.008
1973	2.85	1.86 ± 0.01	0.53 ± 0.004
1974	2.85	1.87 ± 0.02	0.53 ± 0.006
1975	2.65	1.76 ± 0.05	0.47 ± 0.014
1976	2.15	1.68 ± 0.03	0.36 ± 0.005
1977	1.9	1.59 ± 0.05	0.3 ± 0.01
1978	2.55	1.59 ± 0.04	0.41 ± 0.01
1979	2.75	1.56 ± 0.02	0.43 ± 0.005
1980	2.65	1.55 ± 0.03	0.41 ± 0.008
1981	2.5	1.43 ± 0.03	0.36 ± 0.009
1982	2.2	1.35 ± 0.03	0.3 ± 0.008
1983	2.95	1.31 ± 0.04	0.39 ± 0.01
1984	2.85	1.27 ± 0.01	0.36 ± 0.004
1985	3	1.19 ± 0.02	0.36 ± 0.007
1986	2.5	1.19 ± 0.02	0.3 ± 0.006
1987	2.4	1.18 ± 0.02	0.28 ± 0.006
1988	2.6	1.24 ± 0.04	0.32 ± 0.009
1989	2.8	1.24 ± 0.03	0.35 ± 0.009
1990	2.5	1.33 ± 0.03	0.33 ± 0.007
1991	2.1	1.37 ± 0.01	0.29 ± 0.002
1992	2.5	1.34 ± 0.03	0.34 ± 0.008
1993	3.1	1.35 ± 0.05	0.42 ± 0.014
1994	2.15	1.43 ± 0.05	0.31 ± 0.011
1995	2.65	1.57 ± 0.04	0.42 ± 0.011
1996	2.4	1.58 ± 0.03	0.38 ± 0.007
1997	2.05	1.57 ± 0.01	0.32 ± 0.002
1998	2.05	1.63 ± 0.03	0.33 ± 0.006
1999	2.1	1.65 ± 0.02	0.35 ± 0.005
2000	2.8	1.68 ± 0.03	0.47 ± 0.007
2001	3	1.71 ± 0.02	0.51 ± 0.005
2002	2.9	1.74 ± 0.05	0.51 ± 0.015
2003	2.55	1.75 ± 0.03	0.45 ± 0.009
2004	2.8	1.71 ± 0.08	0.48 ± 0.021
2005	3.3	1.57 ± 0.01	0.52 ± 0.003
2006	2.15	1.55 ± 0.02	0.33 ± 0.003
2007	3.3	1.39 ± 0.06	0.46 ± 0.021
2008	2.35	1.33 ± 0.02	0.31 ± 0.001
2009	1.9	1.32 ± 0.01	0.25 ± 0.002
2010	2.35	1.36 ± 0.03	0.32 ± 0.007
2011	2	1.45 ± 0.02	0.29 ± 0.004

2012	3	1.46 ± 0.03	0.44 ± 0.01
2013	2.65	1.45 ± 0.04	0.38 ± 0.009
2014	2.65	1.46 ± 0.02	0.39 ± 0.004
2015	2.55	1.36 ± 0.01	0.35 ± 0.003
2016	3.8	1.25 ± 0.06	0.47 ± 0.008
2017	4.9	1.13 ± 0.05	0.55 ± 0.023
2018	2.8	1.11 ± 0.03	0.31 ± 0.008

Suppl Table 3. Pearson's correlations between the raw coral growth variables and raw environmental variables over the last 50 years and per period before or after the break point.

*#: p-value < 0.1 ; *: p < 0.05 ; **: p-value < 0.01 ; ***: p-value < 0.001 ; NS : non-significant.

VARIABLES	WHOLE DATASET (1964 – 2018)		
	Vertical Extension Rate	Skeletal Bulk Density	Calcification Rate
SST	NS	$r = -0.405$ **	$r = -0.323$ *
SSTA	NS	$r = -0.451$ ***	$r = -0.277$ *
Precipitations	$r = -0.344$ *	NS	$r = -0.296$ *
Max Instant Wind Speed	NS	NS	NS
Cumulative insolation	NS	NS	NS

VARIABLES	DATASET between 1964 and 1985		
	Vertical Extension Rate	Skeletal Bulk Density	Calcification Rate
SST	NS	NS	$r = -0.446$ *
SSTA	NS	NS	NS
Precipitations	$r = -0.553$ **	NS	NS
Max Instant Wind Speed	NS	NS	NS
Cumulative insolation	NS	$r = -0.537$ **	$r = -0.457$ *

VARIABLES	DATESET between 1986 and 2018		
	Vertical Extension Rate	Skeletal Bulk Density	Calcification Rate
SST	NS	$r = -0.311$ *#	NS
SSTA	NS	$r = -0.388$ **	NS
Precipitations	NS	NS	$r = -0.426$ *
Max Instant Wind Speed	NS	NS	NS
Cumulative insolation	NS	NS	$r = -0.329$ *#

Suppl Table 4. Mean percentages of coral skeleton colonized by microborers estimated per year with the vertical approach. SE are indicated.

Year	Abundance of total traces (%)	Abundance of wide traces (%)	Abundance of thin traces (%)
1964	29.9	25.7 ± 3	4.3 ± 0.8
1965	29.6	26 ± 3.5	3.6 ± 0.8
1966	28.7	23 ± 1.8	5.7 ± 1.3
1967	30.7	26.8 ± 4.6	3.9 ± 0.6
1968	31.3	24.1 ± 3.9	7.3 ± 1.2
1969	26.8	11 ± 2.1	15.8 ± 1.6
1970	24.3	11.9 ± 1.6	12.4 ± 3.6
1971	34.9	13.6 ± 1.3	21.3 ± 3.3
1972	45.5	19.5 ± 2.1	26 ± 3.4
1973	50.1	15.6 ± 1.6	34.5 ± 2.5
1974	40.6	17.7 ± 2.1	22.9 ± 2.2
1975	51	16.6 ± 1.6	34.4 ± 2.3
1976	42.8	20.7 ± 2.2	22.1 ± 3.7
1977	50.3	22 ± 1.8	28.3 ± 4.1
1978	48.6	17.9 ± 2.4	30.7 ± 2.7
1979	37.8	17.1 ± 2.4	20.7 ± 3
1980	27.8	15.1 ± 1.8	12.6 ± 2.7
1981	29.5	16.1 ± 2	13.4 ± 2.7
1982	34.3	13.7 ± 2.5	20.5 ± 5
1983	29.5	8.5 ± 1.1	21 ± 2.2
1984	30	6.7 ± 0.9	23.3 ± 4.7
1985	31.9	7.3 ± 0.7	24.6 ± 3.9
1986	10.1	2.4 ± 0.4	7.8 ± 1.8
1987	17.2	4.2 ± 0.8	12.9 ± 1.7
1988	17.1	5.3 ± 0.5	11.8 ± 2.1
1989	13.3	5.9 ± 1.3	7.4 ± 1.8
1990	12.8	9.5 ± 1.2	3.3 ± 0.5
1991	11.3	8.2 ± 1.7	3.1 ± 0.6
1992	12.7	8.9 ± 0.8	3.8 ± 0.7
1993	18.4	8.2 ± 1	10.2 ± 1.4
1994	22	6.1 ± 0.7	15.9 ± 2.9
1995	28	7.5 ± 1.1	20.4 ± 2.7
1996	23.3	6 ± 1	17.3 ± 2.1
1997	17.9	3.1 ± 0.3	14.8 ± 2.2
1998	21.5	5.4 ± 0.9	16.1 ± 2.2
1999	17.2	4.1 ± 0.7	13.1 ± 2.4
2000	10.1	2.4 ± 0.3	7.8 ± 1.6
2001	15.4	4.1 ± 0.7	11.3 ± 1.3
2002	20.4	5.7 ± 0.8	14.7 ± 2.7
2003	16.2	4.7 ± 0.7	11.6 ± 1.7
2004	15.7	5.5 ± 0.7	10.2 ± 1
2005	9.5	5 ± 0.8	4.5 ± 0.8
2006	10	4.1 ± 0.5	5.9 ± 1.4
2007	15.7	7.1 ± 1.3	8.6 ± 1.5
2008	16.4	5.6 ± 1.8	10.8 ± 2.2
2009	22.8	4.3 ± 1.7	18.5 ± 4.2
2010	13.1	2.1 ± 0.5	11.1 ± 3
2011	15.8	3.5 ± 0.8	12.4 ± 2.5
2012	16.6	7 ± 1.2	9.6 ± 1
2013	8.6	4.2 ± 0.9	4.5 ± 0.7

2014	12.2	1 ± 0.2	11.2 ± 1.7
2015	15.2	2.1 ± 0.5	13.1 ± 2.3
2016	12.6	1.8 ± 0.5	10.8 ± 2.3
2017	1.3	0.2 ± 0	1.1 ± 0.2
2018	2.7	1 ± 0.1	1.6 ± 0.4

Suppl Table 5. Mean percentages of coral skeleton colonized by microborers estimated with the horizontal approach within white vs green bands SE are indicated.

Year	Abundance of total traces (%)	Abundance of wide traces (%)	Abundance of thin traces (%)
1964-1966	30.72	21.09 ± 2.4	9.63 ± 0.49
1967-1968	37.59	28.06 ± 2.02	9.53 ± 0.4
1969-1971	38.4	14.44 ± 1.95	23.96 ± 1.53
1972-1973	45.55	21.54 ± 2.32	24.01 ± 1.24
1974-1975	40.94	19.63 ± 1.67	21.31 ± 0.36
1976-1977	43.4	23.33 ± 1.71	20.07 ± 0.06
1978-1980	43.17	21.9 ± 1.78	21.27 ± 0.25
1981-1982	34.39	19.42 ± 2.02	14.97 ± 0.83
1983-1985	35.55	8.55 ± 0.97	27 ± 1.03
1986	16.27	4.15 ± 0.59	12.12 ± 1.91
1987	23.92	4.24 ± 0.56	19.68 ± 1
1988-1989	14.09	7.33 ± 0.74	6.76 ± 0.15
1990	13.89	6.29 ± 0.89	7.6 ± 0.58
1991-1993	23.71	6.01 ± 0.72	17.7 ± 1.68
1994	15.14	2.94 ± 0.38	12.2 ± 1.86
1995-1997	17.43	3.43 ± 0.53	14 ± 1.39
1998	16.69	2.75 ± 0.4	13.94 ± 1.83
2000 - 1999	15.5	3.26 ± 0.72	12.24 ± 1.9
2002 - 2001	19.7	5.13 ± 0.62	14.57 ± 1.24
2004 - 2003	12.6	4.15 ± 0.47	8.45 ± 0.97
2006 - 2005	8.31	3.07 ± 0.59	5.24 ± 0.45
2008 - 2007	13.67	5.51 ± 0.84	8.16 ± 1.58
2010 - 2009	12.47	2.76 ± 0.54	9.7 ± 2.2
2011	6.07	2.23 ± 0.35	3.84 ± 0.85
2012	14.32	5.12 ± 0.52	9.2 ± 0.66
2013	12.93	6.02 ± 1.56	6.91 ± 0.5
2014	9.95	2.3 ± 0.4	7.65 ± 0.86
2016 - 2015	4.31	0.91 ± 0.27	3.4 ± 0.92
2018 - 2017	4.78	1.3 ± 0.25	3.48 ± 0.52

Supp Table 6. Geochemical analyses realized at LSCE on the *Diploastrea* coral core. Each sample correspond to one year of coral growth for further analysis reconstructing SST or pH.

Year	Samples	Delta 11B/10B	Li	B	Na	Mg	Mn	Sr	Cd	Ba	Pb	U
			$\mu\text{M}/\text{M}$	$\mu\text{M}/\text{M}$	mM/M	$\mu\text{M}/\text{M}$	$\mu\text{M}/\text{M}$	mM/M	$\mu\text{M}/\text{M}$	$\mu\text{M}/\text{M}$	nM/M	nM/M
1964	MAY18D_01.58	23.6	6.6	480.4	21086.3	4484.4	0.1	9.0	2.4	4.5	4.5	1061.8
1965	MAY18D_01.57	22.9	6.4	446.5	20961.0	4591.2	0.1	8.9	2.5	4.5	3.8	1094.1
1966	MAY18D_01.56	23.2	6.6	477.2	20860.3	4259.9	0.1	9.0	2.3	4.4	-1.5	1146.4
1967	MAY18D_01.55	23.5	6.0	456.0	20537.5	4324.6	0.5	8.9	2.4	4.3	4.1	1098.5
1968	MAY18D_01.54	23.6	6.3	485.0	20569.5	4388.3	0.1	8.9	4.2	4.3	3.3	1072.0
1969	MAY18D_01.53	23.4	6.3	482.3	20864.9	4332.3	0.1	8.9	2.7	4.4	1.1	1107.8
1970	MAY18D_01.52	23.5	6.2	478.6	20742.5	4313.7	0.6	8.9	2.3	4.4	26.8	1071.6
1971	MAY18D_01.51	23.4	6.2	473.9	20720.3	4270.3	0.5	8.9	3.3	4.4	109.6	1094.7
1972	MAY18D_01.50	23.8	6.2	483.7	20510.8	4257.9	0.1	8.9	2.0	4.3	4.3	1100.5
1973	MAY18D_01.49	24.1	6.1	487.3	20494.1	4208.5	0.1	8.9	2.9	4.3	3.5	1080.7
1974	MAY18D_01.48	23.2	6.3	483.4	20679.2	4253.1	0.1	9.0	2.6	4.4	5.6	1096.4
1975	MAY18D_01.47	23.5	6.3	467.7	20882.9	4297.2	0.1	8.9	3.5	4.3	3.5	1128.9
1976	MAY18D_01.46	24.0	6.3	492.1	20607.9	4306.6	0.1	8.9	2.0	4.3	11.4	1070.2
1977	MAY18D_01.45	23.6	6.2	482.8	20514.7	4260.1	0.1	9.0	2.8	4.3	5.0	1085.3
1978	MAY18D_01.44	23.5	6.2	476.3	20512.5	4329.4	0.1	8.9	3.3	4.2	-0.6	1082.0
1979	MAY18D_01.43	24.1	6.0	484.9	20411.1	4208.8	0.1	8.9	3.1	4.2	4.6	1076.7
1980	MAY18D_01.42	23.7	6.1	484.2	20451.7	4267.9	0.1	8.9	2.7	4.2	4.0	1052.8
1981	MAY18D_01.41	23.9	6.0	493.5	20202.2	4198.3	0.1	8.9	2.3	4.3	4.8	1074.1
1982	MAY18D_01.40	24.0	6.0	491.1	20395.5	4156.1	0.1	8.9	2.8	4.3	5.8	1092.0
1983	MAY18D_01.39	24.0	6.1	499.3	20264.8	4231.3	0.2	8.9	2.1	4.2	110.1	1071.3
1984	MAY18D_01.38	24.3	6.1	490.4	20621.0	4407.4	0.2	8.9	2.8	4.2	7.1	1040.3
1985	MAY18D_01.37	24.1	6.2	506.3	20556.9	4262.9	0.1	9.0	2.6	4.3	3.5	1079.4
1986	MAY18D_01.36	23.8	6.3	501.9	20457.4	4258.8	0.2	9.0	3.1	4.4	203.7	1073.7
1987	MAY18D_01.35	24.1	6.3	510.1	20328.7	4206.2	0.1	9.0	4.1	4.2	0.6	1085.9
1988	MAY18D_01.34	24.4	6.2	497.9	20810.4	4205.9	0.1	8.9	1.8	4.3	5.9	1079.1
1989	MAY18D_01.33	23.7	6.0	476.4	20325.9	4221.4	0.1	8.9	2.5	4.2	6.0	1073.9
1990	MAY18D_01.32	23.8	6.2	476.8	20387.3	4311.8	0.2	8.9	2.1	4.2	5.8	1075.7
1991	MAY18D_01.31	23.9	6.3	485.6	20771.9	4307.6	0.1	9.0	2.4	4.3	5.7	1077.8
1992	MAY18D_01.30	24.1	6.3	509.9	20551.5	4218.6	0.1	9.0	2.4	4.3	6.0	1068.3
1993	MAY18D_01.29	23.6	6.1	480.7	20348.1	4207.5	0.1	9.0	1.8	4.3	6.9	1091.2
1994	MAY18D_01.28	23.7	6.2	481.4	20538.3	4286.8	0.1	8.9	2.0	4.2	6.6	1087.6
1995	MAY18D_01.27	24.3	6.3	516.3	20491.3	4264.9	0.1	9.0	1.9	4.3	7.9	1072.0
1996	MAY18D_01.26	23.7	6.3	501.8	20497.3	4238.9	0.1	9.0	1.7	4.3	2.2	1100.5
1997	MAY18D_01.25	24.1	6.1	503.3	20437.9	4148.7	0.1	9.0	2.7	4.2	8.4	1107.5
1998	MAY18D_01.24	23.9	6.2	503.6	20437.4	4138.4	0.1	9.0	2.6	4.3	7.0	1114.8
1999	MAY18D_01.23	24.0	6.1	501.9	20577.6	4124.8	0.4	9.0	2.8	4.3	9.5	1101.5
2000	MAY18D_01.22	24.1	6.3	499.1	20661.1	4200.0	0.2	8.9	1.6	4.4	33.7	1057.3
2001	MAY18D_01.21	24.0	6.2	512.7	20488.6	4169.4	0.1	9.0	1.8	4.3	7.9	1122.8
2002	MAY18D_01.20	24.4	6.2	513.5	20446.2	4159.6	0.1	9.0	2.9	4.3	7.5	1070.9
2003	MAY18D_01.18-19	24.3	6.0	511.2	20472.8	4105.1	0.1	8.9	1.3	4.3	9.7	1100.1
2004	MAY18D_01.17	24.2	6.1	528.1	20618.7	4061.5	0.1	9.0	1.9	4.3	7.7	1107.5
2005	MAY18D_01.16	24.0	6.1	516.1	20493.0	4155.9	0.3	8.9	1.9	4.3	3.9	1105.5
2006	MAY18D_01.15	24.4	6.1	495.0	20686.5	4116.0	0.1	9.0	3.1	4.3	9.3	1123.8
2007	MAY18D_01.14	24.1	6.2	507.8	20464.0	4177.4	0.1	9.0	3.3	4.3	9.5	1085.1
2008	MAY18D_01.13	24.2	6.3	502.6	20357.9	4313.8	0.1	8.9	3.8	4.3	10.7	1057.5
2009	MAY18D_01.12	24.0	6.1	493.9	20289.2	4242.6	0.2	8.9	2.9	4.2	10.4	1074.4
2010	MAY18D_01.11	24.2	6.2	509.2	20509.5	4279.9	0.4	8.9	2.6	4.2	31.7	1050.3

2011	MAY18D_01.10	24.1	6.2	511.7	20413.3	4314.2	0.1	8.9	1.5	4.3	3.9	1073.2
2012	MAY18D_01.09	24.2	6.2	510.6	20730.0	4241.8	0.1	9.0	1.6	4.3	11.3	1091.2
2013	MAY18D_01.08	23.9	6.1	486.2	20299.2	4251.9	0.1	8.9	2.2	4.2	9.8	1093.7
2014	MAY18D_01.07	24.9	6.3	523.7	20249.6	4420.8	0.1	8.9	1.4	4.2	7.0	1066.3
2015	MAY18D_01.06	24.4	6.1	498.3	20558.0	4362.3	0.1	8.8	1.9	4.1	13.3	1025.1
2016	MAY18D_01.04	24.2	6.1	500.8	20539.1	4356.6	0.2	8.9	1.5	4.1	14.2	1066.0
2016	MAY18D_01.05	24.0	6.2	495.0	20453.0	4345.2	0.1	8.9	2.1	4.1	9.7	1058.3
2017	MAY18D_01.02-03	24.2	6.1	510.9	20722.3	4396.4	0.1	8.9	1.0	4.1	11.8	1048.7
2018	MAY18D_01.01	23.9	6.1	506.4	20908.9	4386.6	0.2	8.9	4.1	4.2	17.7	1013.9

Supp Table 7. Instrumental SSTs from the ERSST dataset corrected with an offset based on SST of the Parc Marin of Mayotte and reconstructed SST from the multi coral proxy Li/Mg et Sr/Ca (Lefts columns). Calculations of the Pkb (Equation. Dickson, 1990) and pH_{CF} (Equation 2.3 in the Manuscript) for the *Diploastrea* coral core are then realized based on the different SSTs products (Middle and Right Columns).

Year	ERSST_cor	SST_Multi_Proxy	Pkb_ERSST	Pkb_Multi_Proxy	pH_ERSST	pH_Multi_Proxy
1964	26.63	26.96	8.58	8.57	8.45	8.44
1965	26.42	27.70	8.58	8.57	8.40	8.39
1966	26.91	26.35	8.58	8.58	8.42	8.42
1967	26.85	27.90	8.58	8.56	8.44	8.43
1968	26.57	27.31	8.58	8.57	8.45	8.44
1969	27.16	27.25	8.57	8.57	8.43	8.43
1970	26.94	27.37	8.58	8.57	8.44	8.43
1971	26.75	27.25	8.58	8.57	8.43	8.43
1972	26.98	27.13	8.57	8.57	8.46	8.45
1973	27.19	27.15	8.57	8.57	8.48	8.48
1974	26.78	26.83	8.58	8.58	8.42	8.42
1975	26.76	27.14	8.58	8.57	8.44	8.44
1976	27.06	27.13	8.57	8.57	8.47	8.47
1977	27.51	27.08	8.57	8.57	8.43	8.44
1978	27.06	27.33	8.57	8.57	8.44	8.43
1979	26.95	27.42	8.57	8.57	8.47	8.47
1980	26.94	27.43	8.58	8.57	8.45	8.45
1981	27.13	27.37	8.57	8.57	8.46	8.46
1982	27.3	27.19	8.57	8.57	8.46	8.47
1983	27.38	27.30	8.57	8.57	8.47	8.47
1984	26.59	27.62	8.58	8.57	8.49	8.48
1985	27.15	27.06	8.57	8.57	8.48	8.48
1986	26.97	26.78	8.57	8.58	8.46	8.46
1987	27.41	26.71	8.57	8.58	8.47	8.48
1988	27.36	27.02	8.57	8.57	8.49	8.50
1989	26.86	27.50	8.58	8.57	8.45	8.45
1990	27.11	27.31	8.57	8.57	8.45	8.45
1991	27.25	26.99	8.57	8.57	8.46	8.46
1992	27.05	26.69	8.57	8.58	8.47	8.48
1993	26.98	27.16	8.57	8.57	8.45	8.44
1994	26.86	27.25	8.58	8.57	8.45	8.45
1995	27.34	26.90	8.57	8.58	8.49	8.49
1996	26.52	26.79	8.58	8.58	8.46	8.45
1997	26.98	26.91	8.57	8.58	8.47	8.48
1998	27.43	26.61	8.57	8.58	8.46	8.47

1999	26.58	26.96	8.58	8.57	8.48	8.47
2000	26.72	26.90	8.58	8.58	8.48	8.48
2001	26.9	26.70	8.58	8.58	8.47	8.47
2002	27.03	26.89	8.57	8.58	8.49	8.49
2003	27.21	27.13	8.57	8.57	8.49	8.49
2004	27.08	26.77	8.57	8.58	8.48	8.48
2005	27.31	26.99	8.57	8.57	8.47	8.47
2006	27.1	26.86	8.57	8.58	8.50	8.50
2007	27.36	26.78	8.57	8.58	8.47	8.47
2008	26.94	27.33	8.58	8.57	8.48	8.48
2009	27.5	27.45	8.57	8.57	8.47	8.47
2010	27.64	27.38	8.57	8.57	8.47	8.48
2011	27.47	27.49	8.57	8.57	8.47	8.47
2012	27.33	27.11	8.57	8.57	8.48	8.48
2013	27.11	27.67	8.57	8.57	8.46	8.45
2014	27.65	27.49	8.57	8.57	8.52	8.52
2015	27.77	27.91	8.57	8.56	8.49	8.48
2016	27.32	27.65	8.57	8.57	8.47	8.47
2017	27.3	27.84	8.57	8.56	8.48	8.47
2018	27.26	27.71	8.57	8.57	8.46	8.45

8.3 Supplementary Materials *Porites* sp. Coral Investigation

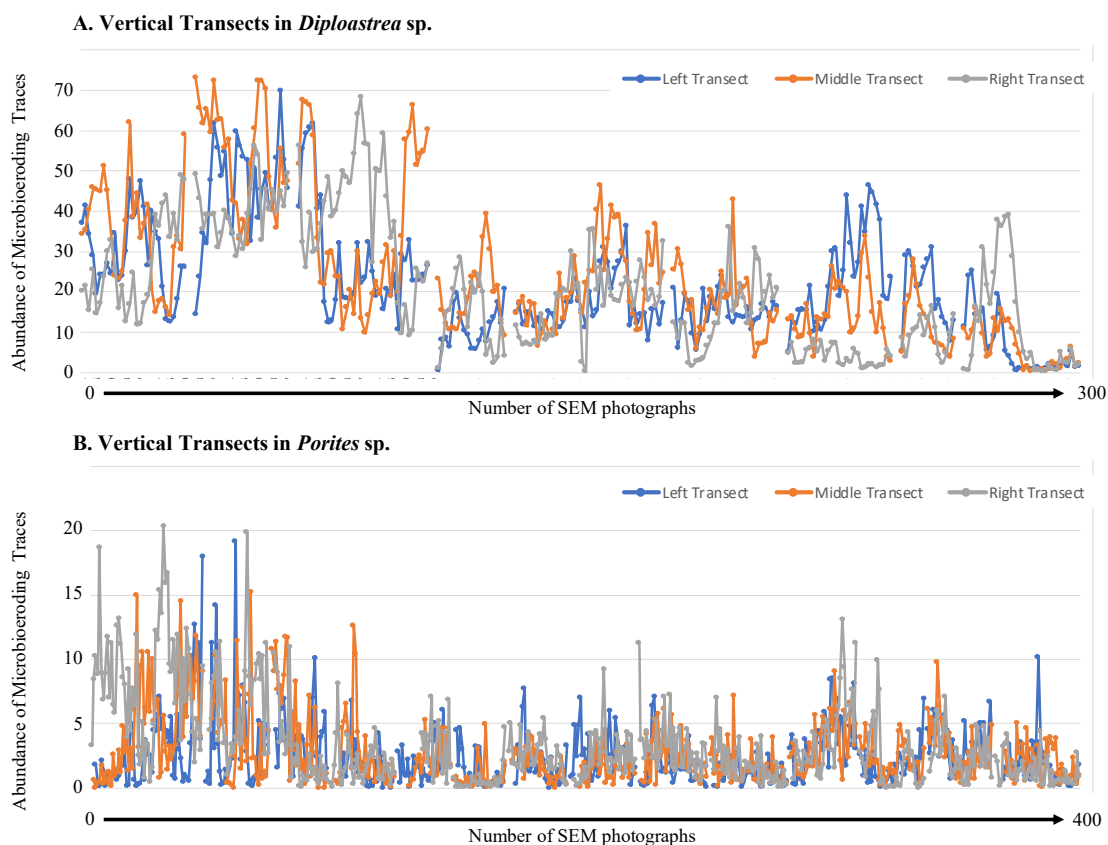


Figure 8.1: Variability of the abundance of microbioeroding traces among the three different vertical transects for *Diploastrea* sp. and *Porites* sp.

Supp Table 1 Geochemical analyses realized at LSCE on the *Porites* coral core. Each sample correspond to one year of coral growth for further analysis reconstructing SST or pH.

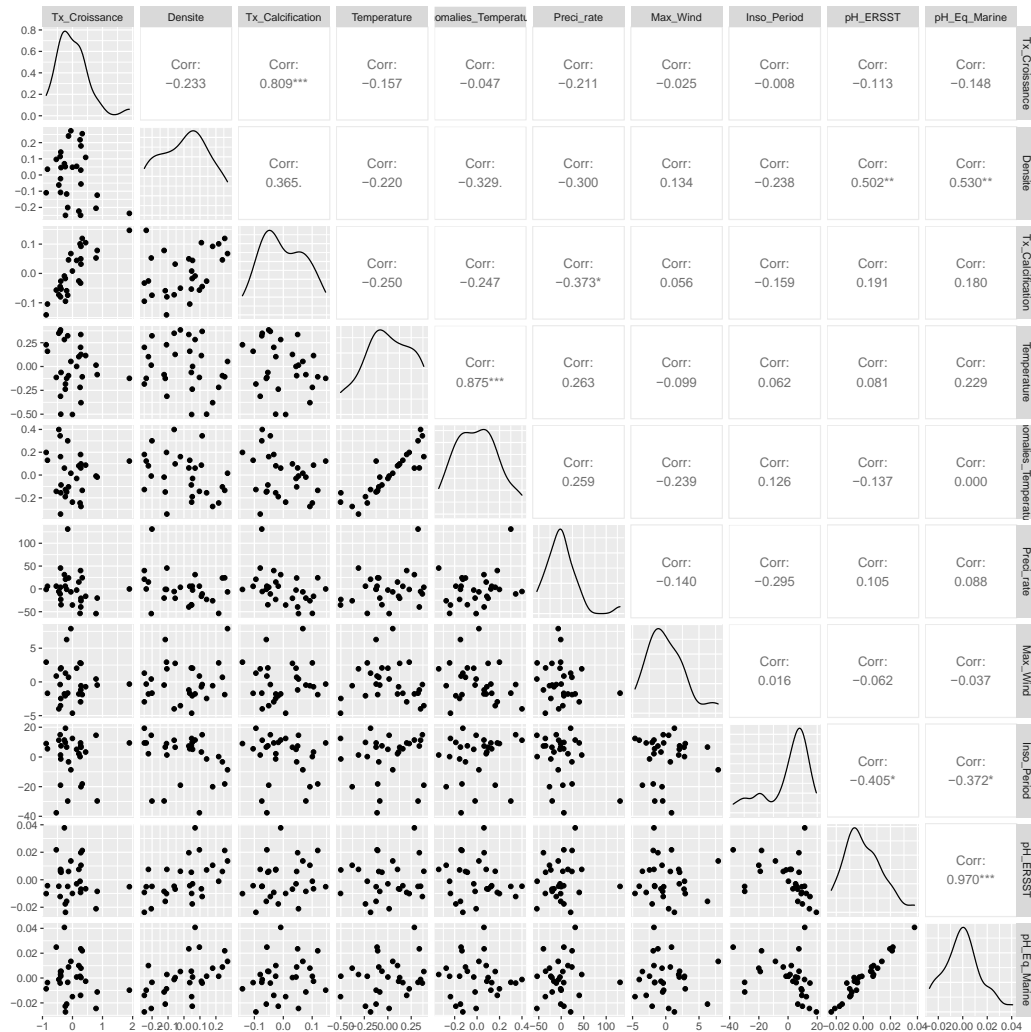
Year	Samples	Delta 11B/10B	Li	B	Na	Mg	Mn	Sr	Cd	Ba	Pb	U
			$\mu\text{M}/\text{M}$	$\mu\text{M}/\text{M}$	mM/M	$\mu\text{M}/\text{M}$	$\mu\text{M}/\text{M}$	mM/M	$\mu\text{M}/\text{M}$	$\mu\text{M}/\text{M}$	nM/M	nM/M
1990	MAY18P_01.57_58	24.0	6.3	439.4	20033.8	4190.8	0.2	8944.5	9.4	4.1	88.0	1110.7
1991	MAY18P_01.55_56	23.7	6.4	436.3	20130.3	4064.3	0.3	8924.1	4.0	4.2	52.7	1113.2
1992	MAY18P_01.53_54	24.1	6.3	457.5	19919.2	3982.2	0.1	8953.3	4.2	4.2	42.0	1114.6
1993	MAY18P_01.51_52	24.2	6.3	458.1	19695.9	3939.6	0.2	8938.5	5.7	4.1	96.9	1120.2
1994	MAY18P_01.49_50	23.7	6.2	419.5	19755.8	4145.9	0.2	8881.0	6.4	4.0	37.5	1076.0
1995	MAY18P_01.47_48	24.0	6.2	440.9	19729.1	4028.4	0.3	8949.0	10.2	4.0	97.7	1108.6
1996	MAY18P_01.45_46	24.4	6.0	454.3	19590.2	3964.4	0.2	8906.2	4.7	4.1	42.0	1082.0
1997	MAY18P_01.43_44	24.1	6.1	449.7	19716.5	3889.6	0.3	8880.3	11.1	4.1	41.9	1096.0
1998	MAY18P_01.41_42	24.2	6.1	474.8	19713.5	3766.0	0.2	8991.3	4.6	4.1	33.1	1132.2
1999	MAY18P_01.39_40	24.7	6.1	485.6	19642.2	3861.2	0.2	9013.6	3.9	4.2	25.1	1157.3
2000	MAY18P_01.37_38	24.9	6.0	494.2	19745.0	3841.3	0.2	8991.4	5.6	4.2	24.9	1163.2
2001	MAY18P_01.35_36	24.9	5.9	490.8	19860.5	3894.8	0.2	8977.0	5.3	4.2	53.1	1142.1
2002	MAY18P_01.33_34	24.6	6.2	482.4	20018.3	3926.1	0.2	8995.8	12.0	4.1	82.1	1124.0
2003	MAY18P_01.31_32	24.4	5.9	460.9	19900.6	4050.9	2.6	8877.4	6.3	4.1	39.2	1073.8
2004	MAY18P_01.29_30	24.5	6.0	468.3	19935.8	3999.2	0.2	8928.7	4.8	4.2	58.8	1100.6
2005	MAY18P_01.27_28	24.3	6.1	462.4	19930.9	4067.0	0.2	8922.0	15.9	4.2	51.4	1096.2
2006	MAY18P_01.25_26	24.1	6.1	448.6	19918.1	4136.7	0.3	8861.7	10.3	4.1	56.1	1073.4
2007	MAY18P_01.23_24	24.1	6.1	444.9	19952.5	4159.6	0.2	8859.7	6.3	4.0	23.7	1061.5
2008	MAY18P_01.21_22	24.2	6.3	458.0	19956.8	4135.1	0.2	8909.1	5.4	4.1	36.4	1072.0
2009	MAY18P_01.19_20	24.1	6.2	459.6	19952.6	4050.7	0.3	8917.5	7.3	4.2	39.7	1084.6
2010	MAY18P_01.17_18	24.4	6.1	484.4	19369.8	3694.0	0.2	8944.8	4.9	4.1	25.2	1141.0
2011	MAY18P_01.15_16	24.0	6.2	466.5	19983.5	4056.3	0.3	8944.2	5.1	4.1	47.8	1084.0
2012	MAY18P_01.13_14	24.2	6.1	448.5	20112.3	4163.2	0.2	8845.5	99.3	4.0	163.4	1051.0
2013	MAY18P_01.11_12	24.2	6.0	468.1	20111.8	4056.4	0.3	8908.2	53.7	4.0	345.6	1079.9
2014	MAY18P_01.9_10	24.3	6.0	459.7	20110.6	4056.3	0.2	8883.3	7.2	4.0	44.2	1069.2
2015	MAY18P_01.7_8	24.3	5.9	453.2	19994.4	4009.4	0.2	8843.0	3.2	4.0	25.7	1064.0
2016	MAY18P_01.5_6	24.6	6.1	482.2	20088.1	3929.0	0.1	8894.9	2.1	4.1	15.9	1096.4
2017	MAY18P_01.3_4	24.0	6.3	444.1	20294.9	4237.1	0.2	8813.9	6.1	4.0	36.4	1047.0
2018	MAY18P_01.1_2	24.2	6.9	462.8	20497.8	4155.0	0.4	8913.7	96.8	4.1	298.7	1069.7

Supp Table 2. Instrumental SSTs from the ERSST dataset corrected with an offset based on SST of the Parc Marin of Mayotte and reconstructed SST from the multi coral proxy Li/Mg et Sr/Ca (Lefts columns). Calculations of the Pkb (Equation. Dickson, 1990) and pH_{CF} (Equation 2.3 in the Manuscript) for the *Porites* coral core are then realized based on the different SSTs products (Middle and Right Columns).

Year	ERSST_cor	SST_Multi_Proxy	PkB_ERSST	PkB_Multi_Proxy	pH_ERSST	pH_Multi_Proxy
1990	27.11	26.83	8.573	8.576	8.47	8.47
1991	27.25	26.43	8.571	8.581	8.45	8.45
1992	27.05	26.16	8.574	8.584	8.47	8.48
1993	26.98	26.16	8.575	8.584	8.48	8.48
1994	26.86	27.15	8.576	8.573	8.45	8.44
1995	27.34	26.53	8.570	8.580	8.46	8.47
1996	26.52	26.78	8.580	8.577	8.50	8.49
1997	26.98	26.64	8.575	8.579	8.48	8.47
1998	27.43	25.80	8.569	8.588	8.48	8.50
1999	26.58	26.07	8.579	8.585	8.52	8.53
2000	26.72	26.22	8.578	8.583	8.53	8.54
2001	26.9	26.60	8.576	8.579	8.53	8.54
2002	27.03	26.17	8.574	8.584	8.51	8.52
2003	27.21	27.31	8.572	8.571	8.49	8.49
2004	27.08	26.96	8.573	8.575	8.50	8.50
2005	27.31	26.84	8.571	8.576	8.48	8.49
2006	27.1	27.32	8.573	8.571	8.48	8.47
2007	27.36	27.29	8.570	8.571	8.47	8.47
2008	26.94	26.83	8.575	8.576	8.49	8.48
2009	27.5	26.63	8.569	8.579	8.47	8.48
2010	27.64	25.75	8.567	8.589	8.49	8.50
2011	27.47	26.56	8.569	8.579	8.47	8.48
2012	27.33	27.41	8.571	8.570	8.48	8.47
2013	27.11	27.08	8.573	8.573	8.48	8.48
2014	27.65	27.13	8.567	8.573	8.48	8.48
2015	27.77	27.44	8.566	8.569	8.48	8.48
2016	27.32	26.61	8.571	8.579	8.50	8.50
2017	27.3	27.32	8.571	8.571	8.46	8.45
2018	27.26	25.76	8.571	8.589	8.48	8.48

Suppl Table 3 and Fig.1. Pearson's correlations between the detrended coral growth variables and detrended environmental variables over the last 29 years for *Diploastrea* sp. coral. #: p-value < 0.1 ; *: p < 0.05 ; ** : p-value < 0.01 ; *** : p-value < 0.001 ; NS : non-significant.

Variables	<i>Diploastrea</i> coral core (1990-2018)		
	Vertical Extension Rate	Skeletal Bulk Density	Calcification Rate
SST	NS	NS	NS
SSTA	NS	R = - 0.329 [#]	NS
Precipitations	NS	NS	R = -0.373 [*]
Max Instant Wind Speed	NS	NS	NS
Cumulative Insolation	NS	NS	NS
pH _{CF} with ERSST	NS	R = 0.502 ^{**}	NS
pH _{CF} with Multi-Proxy	NS	R = 0.530 ^{**}	NS



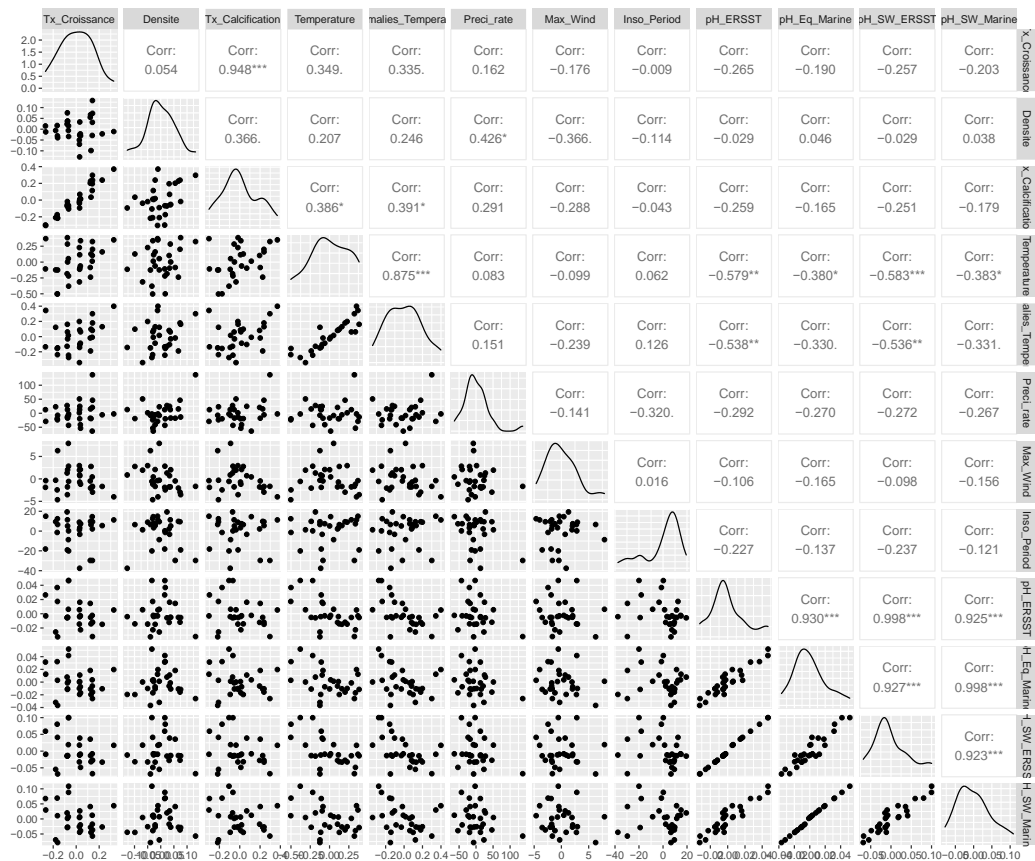
Suppl Table 4. Coral growth parameters reconstructed in *Porites* sp. over the last 29 years. Mean and SDs were calculated per year.

Year	Sample Name	Length	Growth Rate (cm)	Density (g.cm-3)	Coral Calcification (g.cm-2.y-1)
1990	PorMay18 14.1	3.3	1.1	1.20 ± 0.01	1.32 ± 0.01
1991			1.1	1.26 ± 0.02	1.38 ± 0.03
1992			1.1	1.16 ± 0.06	1.28 ± 0.07
1993	PorMay18 13.1	1.85	1.1	1.10 ± 0.02	1.20 ± 0.02
1994			0.8	1.09 ± 0.01	0.87 ± 0.01
1995	PorMay18 12.1	1.6	1	1.10 ± 0.01	1.10 ± 0.01
1996			0.8	1.10 ± 0.02	0.88 ± 0.01
1997	PorMay18	1.6	1	1.11 ± 0.07	1.11 ± 0.07

1998	11.1		0.7	1.12 ± 0.03	0.79 ± 0.02
1999	PorMay18		0.8	1.15 ± 0.01	0.92 ± 0.01
2000	10.1	1.6	0.9	1.10 ± 0.06	0.99 ± 0.06
2001	PorMay18		0.9	1.15 ± 0.01	1.03 ± 0.01
2002	9.1	1.5	0.7	1.15 ± 0.01	0.80 ± 0.01
2003	PorMay18		0.9	1.13 ± 0.01	1.01 ± 0.01
2004	8.1	1.8	1	1.17 ± 0.01	1.17 ± 0.01
2005	PorMay18		1	1.11 ± 0.08	1.11 ± 0.08
2006	7.1	1.95	1	1.01 ± 0.02	1.01 ± 0.02
2007	PorMay18		1.1	1.04 ± 0.02	1.14 ± 0.03
2008	6.1	2	1	1.07 ± 0.03	1.07 ± 0.03
2009	PorMay18		1	1.09 ± 0.02	1.09 ± 0.02
2010	5.1	2.2	1.3	1.13 ± 0.03	1.48 ± 0.03
2011	PorMay18		1.2	1.12 ± 0.02	1.35 ± 0.03
2012	4.1	1.95	0.9	1.18 ± 0.02	1.06 ± 0.02
2013	PorMay18		1.1	1.21 ± 0.04	1.34 ± 0.04
2014	3.1	1.95	0.9	1.18 ± 0.02	1.06 ± 0.03
2015	PorMay18		0.9	1.22 ± 0.03	1.10 ± 0.03
2016	2.1	1.95	1.1	1.20 ± 0.03	1.32 ± 0.03
2017	PorMay18		0.8	1.14 ± 0.02	0.91 ± 0.01
2018	1.1	1.65	0.9	1.17 ± 0.01	1.05 ± 0.01

Suppl Table 5 and Fig.2. Pearson's correlations between the detrended coral growth variables and detrended environmental variables over the last 29 years for *Porites* sp. coral. *#: p-value < 0.1 ; *: p < 0.05 ; ** : p-value < 0.01 ; *** : p-value < 0.001 ; NS : non-significant.

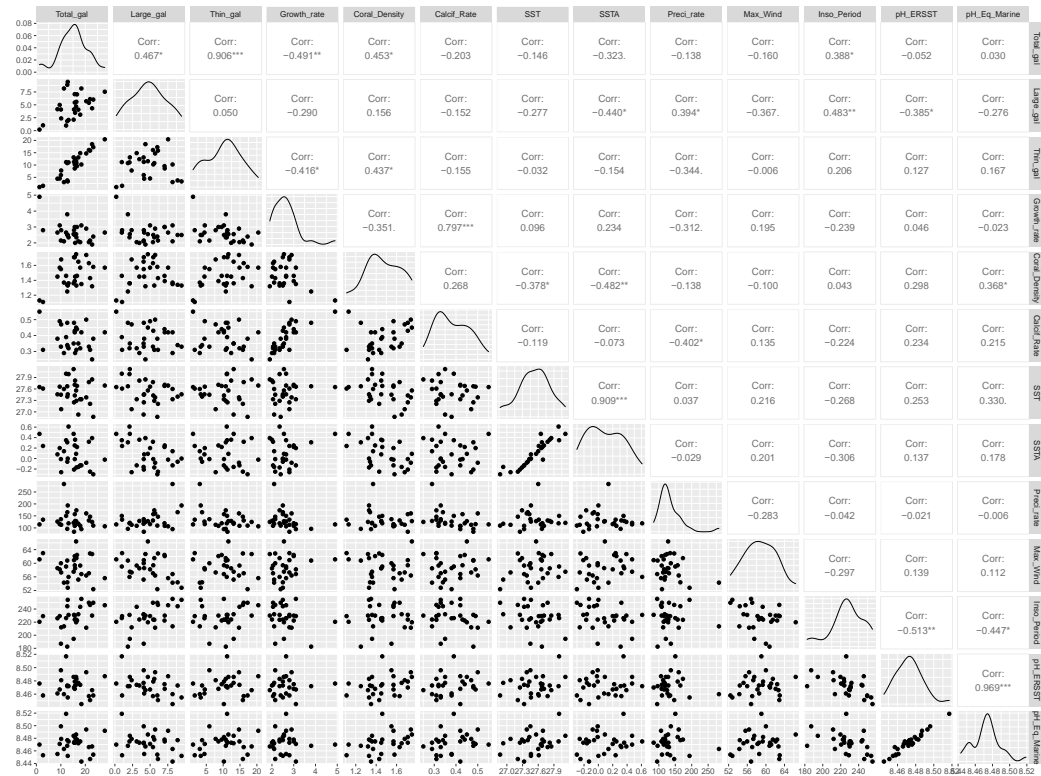
Variables	<i>Porites</i> coral core (1990-2018)		
	Vertical Extension Rate	Skeletal Bulk Density	Calcification Rate
SST	R = 0.349 *#	NS	R = 0.386 *
SSTA	R = 0.335 *#	NS	R = 0.391 *
Precipitations	NS	R = 0.426 *	NS
Max Instant Wind Speed	NS	R = -0.366 *#	NS
Cumulative Insolation	NS	NS	NS
pH _{CF} with ERSST	NS	NS	NS
pH _{CF} with Multi-Proxy	NS	NS	NS



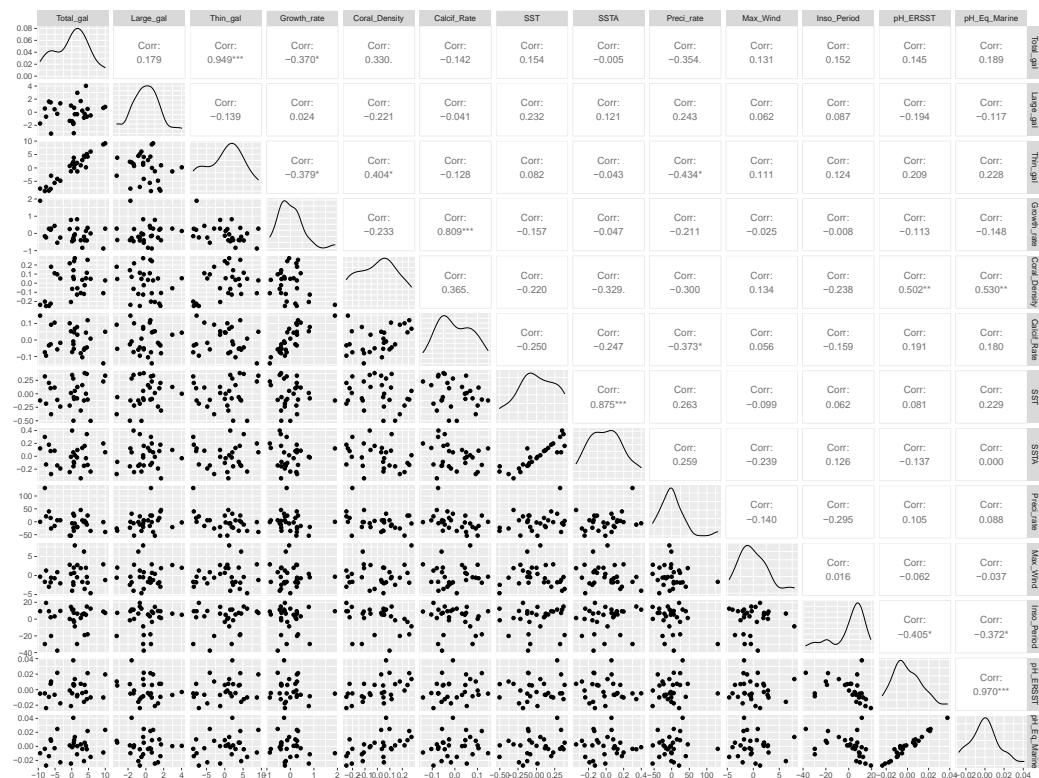
Suppl Table 6. Mean percentages of the *Porites* coral skeleton colonized by microborers estimated per year with the vertical approach. SE are indicated.

Year	Abundance of Total Microbioeroding Traces (%)
1990	4.03 ± 1.06
1991	5.37 ± 2.32
1992	6.74 ± 1.95
1993	4.26 ± 3.11
1994	5.21 ± 1.68
1995	5.60 ± 2.57
1996	2.25 ± 1.53
1997	2.40 ± 1.46
1998	1.39 ± 0.69
1999	1.58 ± 0.92
2000	2.71 ± 0.67
2001	0.94 ± 0.58
2002	0.77 ± 0.67
2003	2.76 ± 0.84
2004	1.53 ± 0.85
2005	1.97 ± 0.82
2006	2.46 ± 1.07
2007	3.27 ± 2.21
2008	1.97 ± 0.79
2009	2.00 ± 0.96
2010	1.16 ± 0.57
2011	2.58 ± 1.08
2012	5.21 ± 0.99
2013	1.92 ± 1.32
2014	1.96 ± 0.84
2015	3.80 ± 1.47
2016	2.49 ± 1.01
2017	1.80 ± 0.73
2018	1.43 ± 1.02

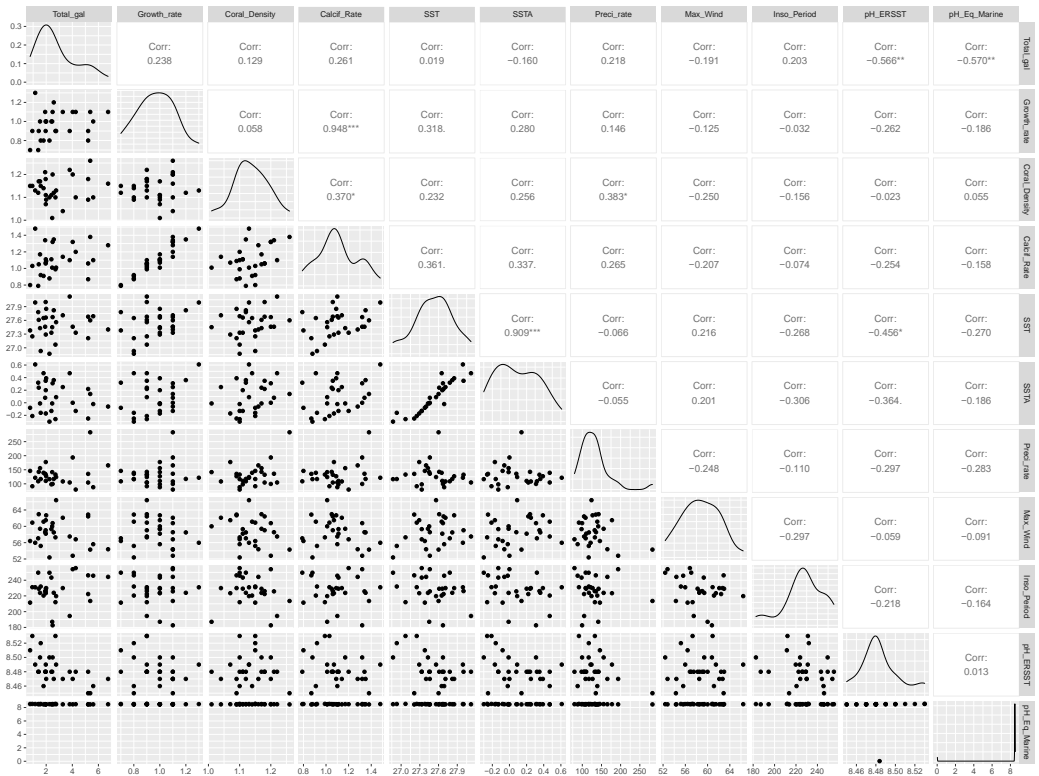
Suppl Fig 3: Pearson's correlations between the raw coral growth variables, microbioeroding abundances and raw environmental variables over the last 29 years for *Diploastrea* sp. coral.
 *#: p-value < 0.1 ; *: p < 0.05 ; ** : p-value < 0.01 ; *** : p-value < 0.001 ; NS : non-significant.



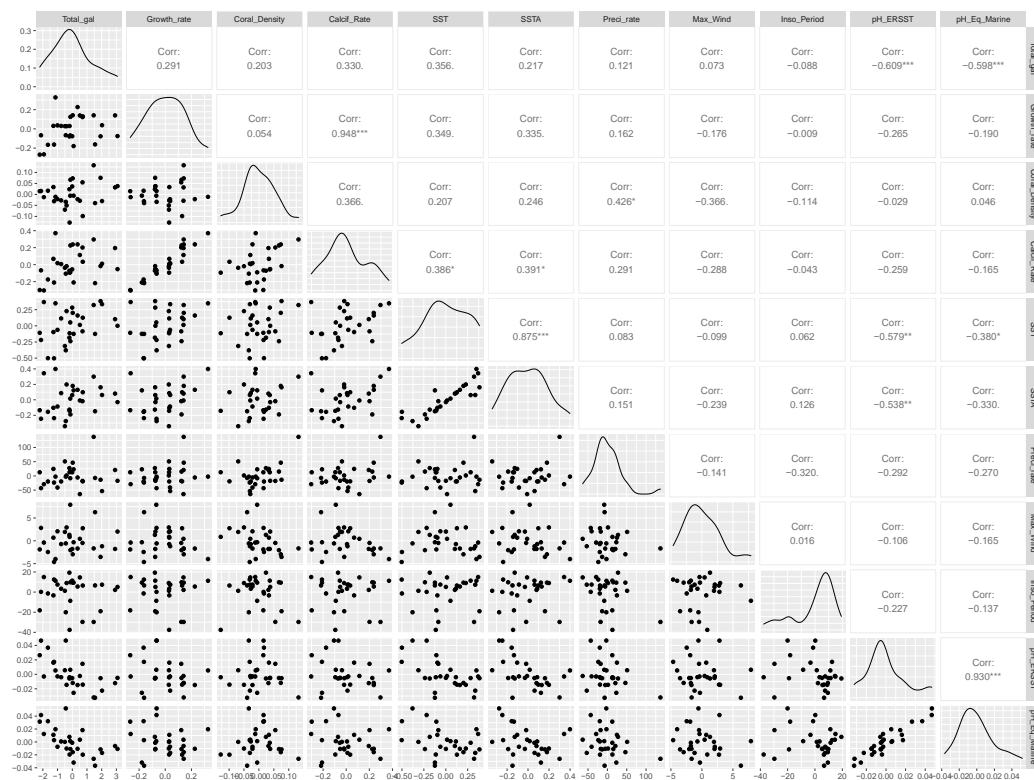
Suppl Fig 4: Pearson's correlations between the detrended coral growth variables, microbioeroding abundances and raw environmental variables over the last 29 years for *Diploastrea* sp. coral. *#: p-value < 0.1 ; *: p < 0.05 ; **: p-value < 0.01 ; *** : p-value < 0.001 ; NS : non-significant.



Suppl Fig 5: Pearson’s correlations between the detrended coral growth variables, microbioeroding abundances and raw environmental variables over the last 29 years for *Porites* sp. coral. ##: p-value < 0.1 ; * : p < 0.05 ; ** : p-value < 0.01 ; *** : p-value < 0.001 ; NS : non-significant.



Suppl Fig 6: Pearson's correlations between the detrended coral growth variables, microbioeroding abundances and raw environmental variables over the last 29 years for *Porites* sp. coral. ##: p-value < 0.1 ; * : p < 0.05 ; ** : p-value < 0.01 ; *** : p-value < 0.001 ; NS : non-significant.



8.4 Supplementary Chromatograms

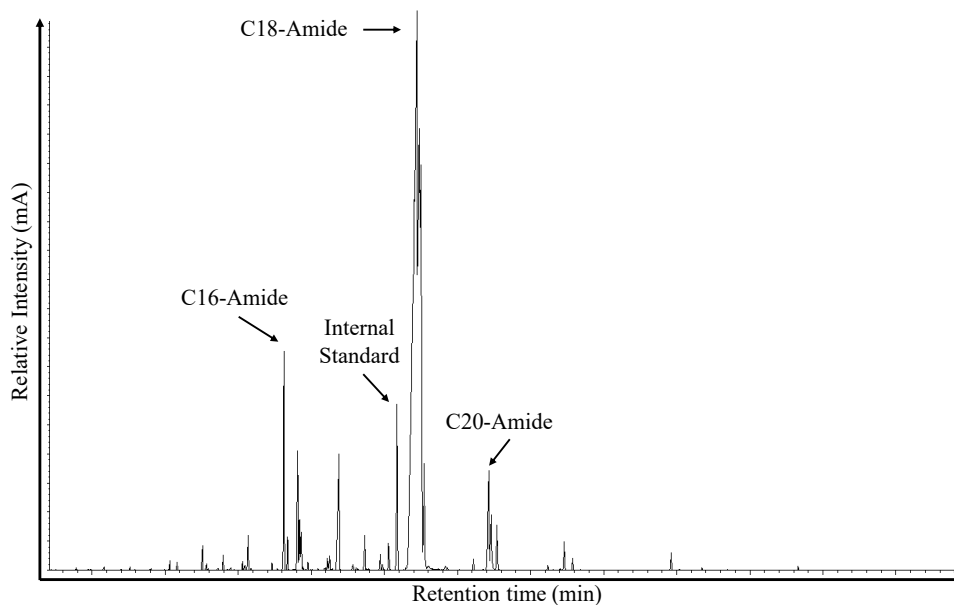


Figure 8.2: Chromatogram of the F3 fraction from one coral sample of the bottom of the core

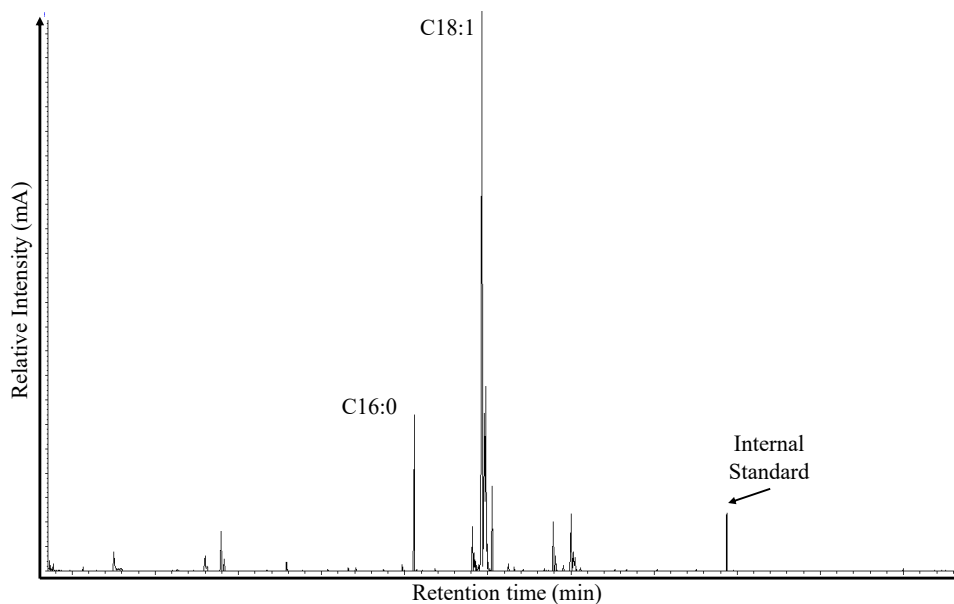
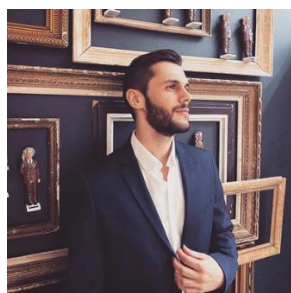


Figure 8.3: Chromatogram of the FA fraction from one coral sample of the bottom of the core

8.5 Curriculum Vitae and Scientific Communications



Diego Alaguarda

Ph.D in Coral Reef Ecology

Coral reef, paleo-oceanography, bioerosion,
LOCEAN, Sorbonne Université, Paris, 75005 – France

☎ +33 6 37 65 27 22

✉ diego.alaguarda@locean.ipsl.fr



22/01/1994

1. Positions & Education

- Ph.D in Coral Reef Ecology** **2020 – 2023**
 LOCEAN, Sorbonne Université, Paris – France *PI: Aline Tribollet, Julien Brajard*
Research Project: “Effect of Global Changes on Microbioeroding Communities Living in Massive Corals from the Island of Mayotte (Western Indian Ocean)”
- M.Sc. in Oceanography** **2016 – 2018**
 Aix Marseille Université, Marseille – France *PI: Thomas DeCarlo, McCulloch Lab*
Research Project: “Skeletal Growth Records of *Porites* corals from the Great Barrier Reef and the Coral Sea during consecutive thermal stress events (2016-2017)”
- B.Sc. in Biology of Organisms, Populations and Ecosystems** **2014 – 2015**
 Université Paul Sabatier, Toulouse – France

2. Publications

- Alaguarda, D.**, J. Brajard, G. Coulibaly, M. Canesi, E. Douville, F. Le Cornec, C. Lelabousse, and A. Tribollet. 2022. “54 Years of Microboring Community History Explored by Machine Learning in a Massive Coral from Mayotte (Indian Ocean).” *Frontiers in Marine Science* 9. <https://doi.org/10.3389/fmars.2022.899398>.
- DeCarlo, T. M., Harrison, H. B., Gajdzik, L., **Alaguarda, D.**, Rodolfo-Metalpa, R., D’Olivo, J., Liu, G., Patalwala, D., and McCulloch, M. T. (2019). “Acclimatization of massive reef-building corals to consecutive heatwaves.” *Proceedings of the Royal Society B: Biological Sciences* 286 (1898). <https://doi.org/10.1098/rspb.2019.0235>.

3. Communications

15 th ICRS International Coral Reef Symposium (<i>Poster</i>)	<i>Bremen (GE) – 2022</i>
EGU General Assembly (<i>Talk</i>)	<i>Vienna (AUT) – 2022</i>
14 th ICRS International Coral Reef Symposium (<i>Poster - Virtual</i>)	<i>Bremen (GE) – 2021</i>
PhD Meeting (<i>Talk</i>)	<i>Paris (FR) – 2021</i>

4. Technical expertise

- **Coral Growth Reconstruction:** X-ray Analysis, Annual density banding reconstruction, Sr/Ca reconstruction, CT-scan analysis, Density and Calcification Reconstruction, paleo-proxies calculations and reconstructions (SST, pH)
 - **Microbioeroding Communities:** Scanning Electron Microscope, Cast-Embedding Protocol, Identification through Machine Learning application
 - **Organic Geochemistry:** Extraction and separation protocol, Lipid biomarker calculation
 - **Data analysis:** Rstudio, Python, Matlab,
-

5. Scientific outreach

- Séminaire BIOECOTROP, la Réunion- (Talk) (February 2023)
 - Fête de la science 2022, Bondy – (Talk and introduction on climate change, coral reefs) (October 2022)
 - Future Maores Reef, Bondy – (Talk for school kids on climate change and introduction to coral reefs) (Mars 2022)
 - Doctoriales 2021 - (Talk) (October 2021)
 - Fête de la science 2021, Paris - (Ocean practical experiments for school kids) (September 2021)
 - Interview for the social media “VRACC” related to the impact of climate change on coral reef ecosystems (https://www.instagram.com/p/COayHq_oWwf/) (May 2021)
-

6. Personal Skills

- **Language:** French (mother tongue), English (professional), Spanish (professional)
- **Dive Certification :** PADI Advanced Water (18 Dives)

Colonization dynamics of a massive coral by microborers over the last 50 years : Use of a machine learning approach and effects of temperature (Mayotte, WIO)

*D. Alaguarda*¹, *J. Brajard*², *F. Le Cornec*¹, *G. Coulibaly*³, *M. Canesi*³, *E. Douville*³, *C. Lelabousse*⁴, *A. Tribollet*¹

1. Lab. LOCEAN-IPSL (IRD-SU-CNRS-MNHN) 4 place Jussieu, Paris France
2. NERSC, Thormøllens gate 47, 5006, Bergen, Norway
3. Lab. LSCE/IPSL (CEA-CNRS-UVSQ), Paris-Saclay, F-91191, Gif-sur-Yvette, France
4. National Marine Park Authority of Mayotte, Centre d'affaires de l'aéroport 97615 Pamandzi, Mayotte



Study Context

Microboring flora are known as one of the main agents of reef dissolution and bioerosion^{1,2}. Their activity in dead carbonates is greatly stimulated by ocean acidification, warming and eutrophication, putting reef resilience at risk^{3,4,5}. The last SROCC report⁶ suggests indeed that 70% to 99% of reefs could disappear by 2100 due to a negative balance between reef accretion and erosion. Nevertheless, the effects of combined environmental factors on microboring communities remain poorly known over long periods. Only a few studies have investigated dynamics of colonization of dead corals by boring floras and their associated dissolution rates over a few months or years⁷. Running experiments with dead coral substrates for more than a few years is difficult. Living colonies of slow growing corals are thus an opportunity to study the effects of various factors on microboring flora (corals being to natural bioarchives recording environmental variability)^{8,9} over several decades. **Here we studied microborer colonization dynamics in a very slow growing coral, *Diplaoxia* sp., over 50 years to determine the possible effects of global warming, as well as coral vital effects (coral growth and skeletal density), on their abundance.**

Conclusions

- Large galleries were probably due to the green algae *Ostreobium* sp. ($\varnothing > 5\mu\text{m}$) as they followed the main axis of coral growth while thin galleries ($\varnothing \sim 1\mu\text{m}$) were probably due to a mix of cyanobacteria and abundant fungi as they showed a more random distribution.
- Dominant large galleries between the 60's and 80's were replaced by thin galleries in the recent years indicating a shift in microboring community composition over the last decades.
- Surprisingly, variability of microborer abundance was not related to *Diplaoxia* coral growth rate to the contrary of what is observed in branching corals¹⁰. It was however positively correlated to the coral skeletal density, similarly to what was found in *Porites* colonies to explain the distribution of black bands¹¹.
- For the first time, we also show a strong negative correlation between microborer abundance and temperature anomalies suggesting that rising temperature may affect differently microborers in live and dead corals. This needs further investigations.

Reference

1. Tribollet, A. (2008) *Current topics in bioerosion*. 2. Tribollet, A. et al. (2019) *Facies* ; 3. Caruso-Silva et al. (2009) *MEPS*; 4. Reyes-Nivia et al. (2013) *GCB* ; 5. Schönberg et al. (2017) *JCES*; 6. SROCC (2019) *IPCC*; 7. Grange, J. et al. (2015), *Environ. Sci. Pollut. Res.*; 8. Wu et al. (2018) *Nature Comm.*; 9. Cui-Guarnie et al. (2019) *Chemical Geol.*; 10. Massé et al. (2018) *Sci. Reports.*; 11. Pruss et al. (2000) *Mar. Biol.*

Material & Methods

- A 15 cm long core was collected in a massive coral *Diplaoxia* sp. at 15 m depth on the outer slope of the MT Tamboro pass (NE Mayotte) in October 2018 (Fig. 1).
- The core was scanned using computed tomography (Discovery CT750, Doseo Platform, CEA-Saclay, Paris) to estimate coral vertical extension (manual analysis) and skeletal density (new image analysis approach, CEA project COR-DENSITÉ, Anne-Catherine Simon & Mathieu Agelou, CEA/DRT/LM2S). The calcification rate was then calculated.
- A subsample core cut in 9 pieces was included in resin epoxy for observations of resin casts of microborings under SEM. SEM images were collected on horizontal transects along the core ($n > 800$ images, ALIZES platform; Fig. 2) covering both white and green bands to determine the abundance variability of microborer galleries, especially that of photophytes (mostly the chlorophyte *Ostreobium* sp. which forms green bands).
- A machine learning approach allowed automatic calculation of surface areas of the 4 defined classes (resin, coral skeleton, large and thin boring galleries, Fig. 2).
- Model II regressions (using R) were used to determine possible correlations between measured variables and environmental parameters (e.g. SST, NOAA ERSST V5).



Fig.1 A&B Study site in Mayotte. 1.C Coral core with visible green bands (green arrows) indicating microboring organisms presence. 1.D Linear extension rate and measured skeletal density (HU) were determined in the area indicated by the yellow scale. 1.E Subsamples embedded in epoxy resin prior SEM observations.

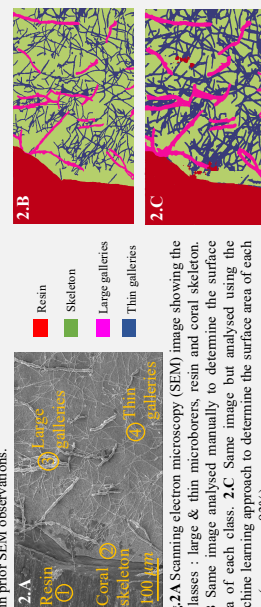


Fig.2 A Scanning electron microscopy (SEM) image showing the 4 classes : large & thin microborers, resin and coral skeleton. 2.B Same image analysed manually to determine the surface area of each class. 2.C Same image but analysed using the machine learning approach to determine the surface area of each class (accuracy = 93%).

Results

- 1/ No direct evidence of a positive correlation between green bands and abundance of microboring galleries was found (Fig. 3). Green bands seem to be due to a high abundance of microboring filaments and/or chlorophyll pigments.
- 2/ Microboring galleries abundance (especially large ones = supposed phototrophic galleries) decreased significantly over the last 50 years (Fig. 4) ($r = -0.83$, $p < 0.05$, decreasing rate around $0.53\% \cdot \text{y}^{-1}$).
- 3/ Global warming may influence negatively microborer abundance and *Diplaoxia* skeletal density ($r = 0.6$, $p < 0.001$ for both); those 2 biological variables being positively correlated ($r > 0.6$, $p < 0.0005$). Coral vertical extension was not correlated to any variables except with the abundance of thin galleries (supposed fungi and/or cyanobacteria) ($r = -0.6$, $p < 0.002$). The calcification rate was slightly negatively correlated to SST ($p = 0.04$).

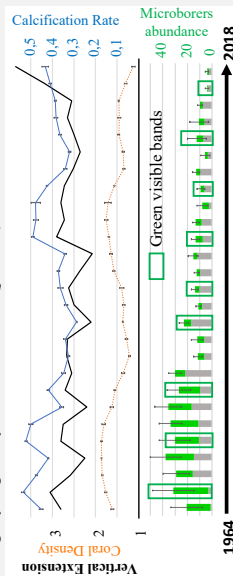


Fig.3 Variability of coral growth parameters (vertical extension in $\text{mm} \cdot \text{y}^{-1}$, skeletal density in $\text{g} \cdot \text{cm}^{-3}$, calcification rate $\text{g} \cdot \text{cm}^{-2} \cdot \text{y}^{-1}$) and the estimated abundance (%) of microboring galleries (large in green; thin in grey) within the coral *Diplaoxia* sp. over the last 50 years.

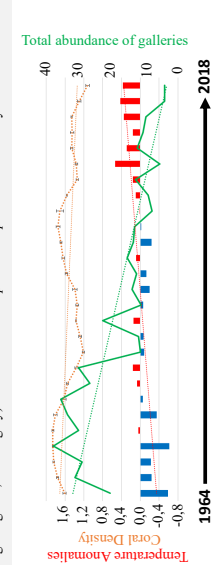


Fig.4 Variability of the abundance (%) of microborers, coral skeletal density ($\text{g} \cdot \text{cm}^{-3}$) and temperature anomalies in Mayotte over the last 50 years.



Indian Ocean microborers in a living coral: How to explore the variability of their abundance over 50 years?

D. Alaguarda¹, J. Brajard², F. Le Cornec¹, G. Coulibaty³, M. Canesi³, E. Douville³, A.C. Simon³,
M. Agelou³, C. Lelabousse⁴, A. Tribollet¹

1. Lab. LOCEAN-IPSL, Sorbonne Université-IRD-CNRS-MNH, 4 place Jussieu, 75005 Paris Cedex,
2. NERSC, Jahnebakken 3, 5007, Bergen, Norway
3. Lab. LSCE/IPSL (CEA-CNRS-UVSQ), Université Paris-Saclay, Gif-sur-Yvette, France
4. National Marine Park Authority of Mayotte, Pamandzi, Petite-Terre, Mayotte



MICROBORERS : WHAT ARE THEY ?

- Microboring flora are known as one of the main agents of reef dissolution and bioerosion^{1,2}. Their activity in dead carbonates is greatly stimulated by ocean acidification, warming and eutrophication, putting reef resilience at risk^{3,4,5}.
- While effects of global change on corals have received wide-spread attention, much less is known about the dynamics of bioeroding communities driving reef carbonate dissolution over long periods of time, limiting the understanding of reef resilience capacity and projections of reef fate by 2100⁶.
- Only a few studies have investigated dynamics of dead corals colonization by boring flora and their associated dissolution rates over a few months or years⁷. Running experiments with dead coral substrates for more than a few years is difficult.
- Living colonies of slow growing corals are thus an opportunity to study the effects of various factors on microboring flora (corals being natural bio-archives recording environmental variability)^{8,9} over several decades as they are able to colonize skeletons of both dead and living corals.

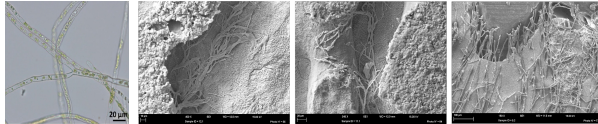


Fig.1 Optical Microscopy image for the green alga of the genus *Ostreobium* (left). Scanning electron microscopes showing the diversity of microborings (ichneumonids) present within the skeleton of the coral (right).

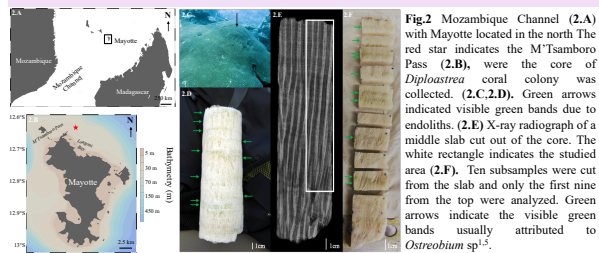
PROJECT OBJECTIVES:

- To develop a new method allowing the study of the abundance of traces left by microborers (microborings; Fig. 1) in the skeleton of living corals relying on a Machine Learning approach
- To apply this innovative method to a coral core of a living massive coral *Diploastrea* sp. collected in Mayotte in October 2018 and covering the last 50 years (Fig.2)
- To determine the possible factors influencing microborings' abundance in the studied coral core

CONCLUSIONS & PERSPECTIVES:

- The new developed approach allowed the analysis of a large number of Scanning electron Microscope (SEM) images (>1500) in a very short time with an accuracy of 93 % (number of good predictions/number of total predictions) (Fig.3).
- This innovative method could be applied to other coral species. It needs to be tested and possibly adapted (ongoing work).
- The analysis of the coral core revealed a significant decrease of microborers' abundance over the last 50 years (Fig.4). No correlation with the coral growth extension rate was found. In contrast, a positive relationship was found with the coral density and SSTs over the last decades ($p < 0.05$; Fig. 5). These trends needs to be confirmed by the study of more coral cores from the Western Indian Ocean.

MACHINE LEARNING : GOAL

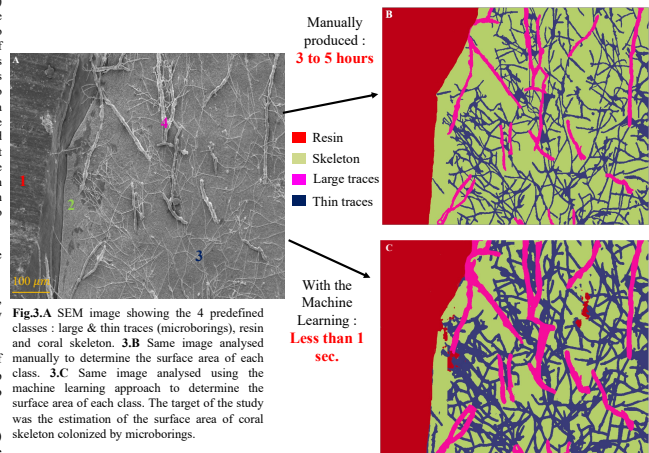


- A 19.5cm long core was collected in a massive coral *Diploastrea* sp. at 15m depth on the outer of the M'Tsambo Pass (NE Mayotte) in October 2018 (Fig.2). Only the first 15 cm were studied.

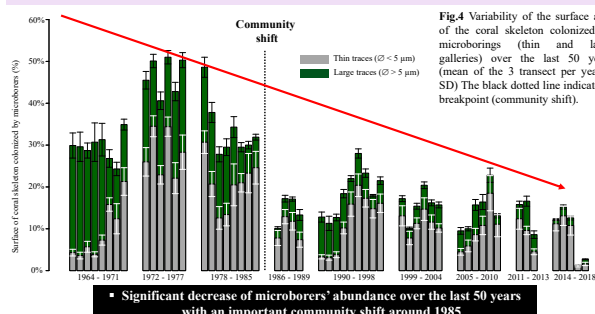
- The core was scanned using computed tomography (GE Discovery CT750 HD, DOSEO-Platform, CEA-Saclay, Paris) to estimate the coral vertical extension rate (manual analysis) and its skeletal density (new image analysis approach, CEA project COR-DENSITÉ). Calcification rate was then calculated.

- The 9 core subsamples (Fig. 2F) were included in resin epoxy for observations of resin casts of microborings under SEM. More than 1500 images were collected along 3 vertical transects from the top to the bottom of the core, with a ZEISS SEM on the Alysés platform (Bondy-LOCEAN; Fig.3) to determine the abundance of microboring traces in the *Diploastrea* sp. over the last decades.

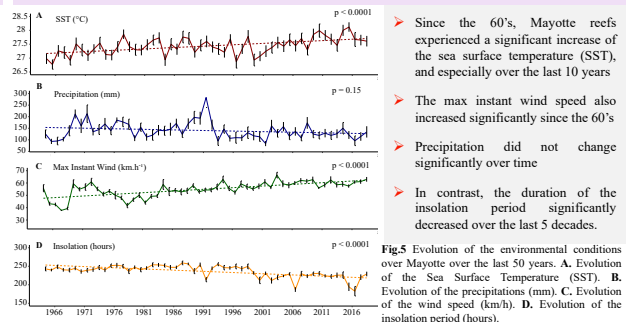
- A machine learning approach (Convolutional Neural Network, U-Net, JupyterLab, Keras library) allowed automatic estimation of the surface areas of 4 predefined classes (resin, coral skeleton, large and thin traces, Fig.3).



VARIABILITY OF MICROBORINGS ABUNDANCE



50 YEARS OF ENVIRONMENTAL CONDITIONS IN MAYOTTE



REFERENCES

1. Tribollet, A. (2008) Current shifts in bioerosion. 2. Tribollet et al. (2019) *Facies*. 3. Carreiro-Silva et al. (2009) *MEPS*. 4. Reyes-Nivia et al. (2013) *GCB*. 5. Schönberg et al. (2017) *JCES*. 6. SROCC (2019) *IPCC*. 7. Grange, J. et al. (2015). *Environ. Sci. Pollut. Res.*. 8. Wu et al. (2018) *Nature Comm.*. 9. Cuny-Guirrice et al. (2019) *Chemical Geol.*. 10. Massé et al. (2018) *Sci. Reports*. 11. Priess et al. (2000) *Mar. Biol.*

CONTACT

➤ Article in Review in *Frontiers in Marine Sciences*
➤ Corresponding author: diego.alaguarda@locean-ipsl.fr



References

- Abdolahpur Monikh, F., Safahieh, A., Savari, A., & Doraghi, A. (2013). Heavy metal concentration in sediment, benthic, benthopelagic, and pelagic fish species from musa estuary (persian gulf). *Environmental monitoring and assessment*, 185(1), 215–222. <https://doi.org/10.1007/s10661-012-2545-9>
- Akhoudas, C., Chevalier, N., Blanc-Valleron, M.-M., Klein, V., Mendez-Millan, M., Demange, J., Dalliah, S., Rommevaux, V., Boudouma, O., Pierre, C., et al. (2018). Methane-derived stromatolitic carbonate crust from an active fluid seepage in the western basin of the sea of marmara: Mineralogical, isotopic and molecular geochemical characterization. *Deep Sea Research Part II: Topical Studies in Oceanography*, 153, 110–120. <https://doi.org/10.1016/j.dsr2.2017.12.022>
- Akpan, E. B., & Farrow, G. E. (1985). Shell bioerosion in high-latitude low-energy environments: Firths of clyde and lorne, scotland. *Marine Geology*, 67(1-2), 139–150. [https://doi.org/10.1016/0025-3227\(85\)90152-5](https://doi.org/10.1016/0025-3227(85)90152-5)
- Alaguarda, D., Brajard, J., Coulibaly, G., Canesi, M., Douville, E., Le Cornec, E., Lelabousse, C., & Tribollet, A. (2022). 54 years of microboring community history explored by machine learning in a massive coral from mayotte (indian ocean). *Frontiers in Marine Science*, 9. <https://doi.org/10.3389/fmars.2022.899398>
- Alfaro, A. C., Thomas, E., Sergeant, L., & Duxbury, M. (2006). Identification of trophic interactions within an estuarine food web (northern new zealand) using fatty acid biomarkers and stable isotopes. *Estuarine, Coastal and Shelf Science*, 70(1-2), 271–286. <https://doi.org/10.1016/j.ecss.2006.06.017>

- Allan, R. P., Hawkins, E., Bellouin, N., & Collins, B. (2021). Ipcc, 2021: Summary for policymakers.
- Allemand, D., Ferrier-Pagès, C., Furla, P., Houlbrèque, E., Puverel, S., Reynaud, S., Tambutté, É., Tambutté, S., & Zoccola, D. (2004). Biomineralisation in reef-building corals: From molecular mechanisms to environmental control. *Comptes Rendus Palevol*, 3(6-7), 453–467. <https://doi.org/10.1016/j.crpv.2004.07.011>
- Alliance, B. N. (2020). *Western Indian Ocean*. Retrieved February 20, 2023, from <https://www.bluenaturealliance.org/where-we-work/western-indian-ocean>
- Alliance, C. R. (2010). *Why care about coral reefs*. Retrieved February 20, 2023, from <https://coral.org/en/coral-reefs-101/why-care-about-reefs/tourism/>
- Al-Moghrabi, S., Allemand, D., Couret, J., & Jaubert, J. (1995). Fatty acids of the scleractinian coral *galaxea fascicularis*: Effect of light and feeding. *Journal of Comparative Physiology B*, 165, 183–192. <https://doi.org/10.1007/BF00260809>
- Andersson, A. J., Bates, N. R., & Mackenzie, F. T. (2007). Dissolution of carbonate sediments under rising p_{CO_2} and ocean acidification: Observations from devil's hole, bermuda. *Aquatic Geochemistry*, 13, 237–264. <https://doi.org/10.1007/s10498-007-9018-8>
- Andersson, A. J., & Gledhill, D. (2013). Ocean acidification and coral reefs: Effects on breakdown, dissolution, and net ecosystem calcification. *Annual review of marine science*, 5, 321–348. <https://doi.org/10.1146/annurev-marine-121211-172241>
- Andréfouët, S., Costello, M., Rast, M., & Sathyendranath, S. (2008). Earth observations for marine and coastal biodiversity and ecosystems. <https://doi.org/10.1016/j.rse.2008.04.006>
- Anthony, K. R., A. Kleypas, J., & Gattuso, J.-P. (2011). Coral reefs modify their seawater carbon chemistry—implications for impacts of ocean acidification. *Global Change Biology*, 17(12), 3655–3666. <https://doi.org/10.1111/j.1365-2486.2011.02510.x>
- Anthony, K. R., Hoogenboom, M. O., & Connolly, S. R. (2005). Adaptive variation in coral geometry and the optimization of internal colony light climates. *Functional Ecology*, 19(1), 17–26. <https://doi.org/10.1111/j.0269-8463.2005.00925.x>
- Anthony, K. R., Hoogenboom, M. O., Maynard, J. A., Grottoli, A. G., & Middlebrook, R. (2009). Energetics approach to predicting mortality risk from environmental

- stress: A case study of coral bleaching. *Functional ecology*, 23(3), 539–550. <https://doi.org/10.1111/j.1365-2435.2008.01531.x>
- Ascasoa, C., Wierzbosch, J., & Castelloa, R. (1998). Study of the biogenic weathering of calcareous litharenite stones caused by lichen and endolithic microorganisms. *International biodeterioration & biodegradation*, 42(1), 29–38. [https://doi.org/10.1016/S0964-8305\(98\)00043-2](https://doi.org/10.1016/S0964-8305(98)00043-2)
- Atkinson, M., Carlson, B., & Crow, G. (1995). Coral growth in high-nutrient, low-ph seawater: A case study of corals cultured at the waikiki aquarium, honolulu, hawaii. *Coral reefs*, 14, 215–223. <https://doi.org/10.1007/BF00334344>
- Ayalon, I., de Barros Marangoni, L. F., Benichou, J. I., Avisar, D., & Levy, O. (2019). Red sea corals under artificial light pollution at night (alan) undergo oxidative stress and photosynthetic impairment. *Global change biology*, 25(12), 4194–4207. <https://doi.org/10.1111/gcb.14795>
- Babcock-Adams, L., Minarro, S., Fitt, W. K., & Medeiros, P. M. (2016). Assessing coral response to a severe bleaching event using mulimolecular biomarkers. *American Geophysical Union*, 2016, PC54B–2250.
- Bachok, Z., Mfilinge, P., & Tsuchiya, M. (2006). Characterization of fatty acid composition in healthy and bleached corals from okinawa, japan. *Coral Reefs*, 25(4), 545–554. <https://doi.org/10.1007/s00338-006-0130-9>
- Backeberg, B., & Reason, C. (2010). A connection between the south equatorial current north of madagascar and mozambique channel eddies. *Geophysical Research Letters*, 37(4). <https://doi.org/10.1029/2009GL041950>
- Badwey, J. A., Curnutte, J., Robinson, J. M., Berde, C., Karnovsky, M., & Karnovsky, M. (1984). Effects of free fatty acids on release of superoxide and on change of shape by human neutrophils. reversibility by albumin. *Journal of Biological Chemistry*, 259(12), 7870–7877. [https://doi.org/10.1016/S0021-9258\(17\)42874-2](https://doi.org/10.1016/S0021-9258(17)42874-2)
- Bagnato, S., Linsley, B. K., Howe, S. S., Wellington, G. M., & Salinger, J. (2004). Evaluating the use of the massive coral *diploastrea heliopora* for paleoclimate reconstruction. *Paleoceanography*, 19(1). <https://doi.org/10.1029/2003PA000935>
- Bak, R., & Laane, R. (1987). Annual black bands in skeletons of reef corals (scleractinia). *Mar Ecol Prog Ser*, 38, 169–175.

- Banin, E., Ben-Haim, Y., Israely, T., Loya, Y., & Rosenberg, E. (2000). Effect of the environment on the bacterial bleaching of corals. *Environmental Challenges*, 337–352. https://doi.org/10.1007/978-94-011-4369-1_27
- Barrett, S. M., Volkman, J. K., Dunstan, G. A., & LeRoi, J.-M. (1995). Sterols of 14 species of marine diatoms (bacillariophyta) 1. *Journal of Phycology*, 31(3), 360–369. <https://doi.org/10.1111/j.0022-3646.1995.00360.x>
- Barrick, R. C., Hedges, J. I., & Peterson, M. L. (1980). Hydrocarbon geochemistry of the puget sound region. sedimentary acyclic hydrocarbons. *Geochimica et Cosmochimica Acta*, 44(9), 1349–1362. [https://doi.org/10.1016/0016-7037\(80\)90094-0](https://doi.org/10.1016/0016-7037(80)90094-0)
- Baumann, J., Grottoli, A. G., Hughes, A. D., & Matsui, Y. (2014). Photoautotrophic and heterotrophic carbon in bleached and non-bleached coral lipid acquisition and storage. *Journal of Experimental Marine Biology and Ecology*, 461, 469–478. <https://doi.org/10.1016/j.jembe.2014.09.017>
- Behrman, E., & Gopalan, V. (2005). Cholesterol and plants. *Journal of chemical Education*, 82(12), 1791.
- Beijbom, O., Edmunds, P. J., Kline, D. I., Mitchell, B. G., & Kriegman, D. (2012). Automated annotation of coral reef survey images. *2012 IEEE conference on computer vision and pattern recognition*, 1170–1177. <https://doi.org/10.1109/CVPR.2012.6247798>
- Bellamy, N., & Risk, M. J. (1982). Coral gas: Oxygen production in millepora on the great barrier reef. *Science*, 215(4540), 1618–1619. <https://doi.org/10.1126/science.215.4540.1618>
- Bentis, C. J., Kaufman, L., & Golubic, S. (2000). Endolithic fungi in reef-building corals (order: Scleractinia) are common, cosmopolitan, and potentially pathogenic. *The Biological Bulletin*, 198(2), 254–260. <https://doi.org/10.2307/1542528>
- Bergé, J.-P., & Barnathan, G. (2005). Fatty acids from lipids of marine organisms: Molecular biodiversity, roles as biomarkers, biologically active compounds, and economical aspects. *Marine biotechnology* 1, 49–125. <https://doi.org/10.1007/b135782>
- Beyan, C., & Browman, H. I. (2020). Setting the stage for the machine intelligence era in marine science. *ICES Journal of Marine Science*, 77(4), 1267–1273. <https://doi.org/10.1093/icesjms/fsaa084>

- Biscere, T., Rodolfo-Metalpa, R., Lorrain, A., Chauvaud, L., Thébault, J., Clavier, J., & Houlbrèque, F. (2015). Responses of two scleractinian corals to cobalt pollution and ocean acidification. *PLoS One*, 10(4), e0122898. <https://doi.org/10.1371/journal.pone.0122898>
- Bishop, C. M., & Nasrabadi, N. M. (2006). *Pattern recognition and machine learning* (Vol. 4). Springer.
- Bornet, E., & Flahault, C. (1888). *Note sur deux nouveaux genres d'algues perforantes*. J. Mersch.
- Bornstein, A. A. (1980). Determination of α -keto adipic acid in aqueous media by gas chromatography. *Journal of Chromatographic Science*, 18(4), 183–185. <https://doi.org/10.1093/chromsci/18.4.183>
- Bouchet, P. (2006). The magnitude of marine biodiversity. *The exploration of marine biodiversity: scientific and technological challenges*, 31–62.
- Bouloubassi, I., & Saliot, A. (1993). Dissolved, particulate and sedimentary naturally derived polycyclic aromatic hydrocarbons in a coastal environment: Geochemical significance. *Marine Chemistry*, 42(2), 127–143. [https://doi.org/10.1016/0304-4203\(93\)90242-G](https://doi.org/10.1016/0304-4203(93)90242-G)
- Bourdin, C., Douville, E., & Genty, D. (2011). Alkaline-earth metal and rare-earth element incorporation control by ionic radius and growth rate on a stalagmite from the Chauvet cave, southeastern France. *Chemical Geology*, 290(1-2), 1–11. <https://doi.org/10.1016/j.chemgeo.2011.08.006>
- Bourne, D., Iida, Y., Uthicke, S., & Smith-Keune, C. (2008). Changes in coral-associated microbial communities during a bleaching event. *The ISME Journal*, 2(4), 350–363. <https://doi.org/10.1038/ismej.2007.112>
- Brooks, J. J., & Banfield, J. (2009). Unravelling ancient microbial history with community proteogenomics and lipid geochemistry. *Nature Reviews Microbiology*, 7(8), 601–609. <https://doi.org/10.1038/nrmicro2167>
- Brown, B., & Bythell, J. (2005). Perspectives on mucus secretion in reef corals. *Marine Ecology Progress Series*, 296, 291–309. <https://doi.org/10.3354/meps296291>
- Brown, D. J., & DuPont, F. M. (1989). Lipid composition of plasma membranes and endomembranes prepared from roots of barley (*Hordeum vulgare* L.) effects of salt. *Plant Physiology*, 90(3), 955–961. <https://doi.org/10.1104/pp.90.3.955>

- Bucher, D. J., Harriott, V. J., & Roberts, L. G. (1998). Skeletal micro-density, porosity and bulk density of acroporid corals. *Journal of experimental marine biology and ecology*, 228(1), 117–136. [https://doi.org/10.1016/S0022-0981\(98\)00020-3](https://doi.org/10.1016/S0022-0981(98)00020-3)
- Budd, A. F., Fukami, H., Smith, N. D., & Knowlton, N. (2012). Taxonomic classification of the reef coral family mussidae (cnidaria: Anthozoa: Scleractinia). *Zoological Journal of the Linnean Society*, 166(3), 465–529. <https://doi.org/10.1111/j.1096-3642.2012.00855.x>
- Budd, A. F., & Stolarski, J. (2011). Corallite wall and septal microstructure in scleractinian reef corals: Comparison of molecular clades within the family faviidae. *Journal of Morphology*, 272(1), 66–88. <https://doi.org/10.1002/jmor.10899>
- Buddemeier, R. W. (1978). Sclerochronology: A data source for reef systems models. *Atoll Research Bulletin*.
- Budge, S. M., & Parrish, C. C. (1998). Lipid biogeochemistry of plankton, settling matter and sediments in trinity bay, newfoundland. ii. fatty acids. *Organic geochemistry*, 29(5-7), 1547–1559. [https://doi.org/10.1016/S0146-6380\(98\)00177-6](https://doi.org/10.1016/S0146-6380(98)00177-6)
- Burke, L., Reyntar, K., Spalding, M., & Perry, A. (2011). *Reefs at risk revisited*. Washington, DC: World Resources Institute.
- Bythell, J. C., & Wild, C. (2011). Biology and ecology of coral mucus release. *Journal of Experimental Marine Biology and Ecology*, 408(1-2), 88–93. <https://doi.org/10.1016/j.jembe.2011.07.028>
- Canesi, M. (2022). Impacts des changements globaux sur les coraux massifs porites et diploastrea de l’océan pacifique.
- Cantin, N. E., & Lough, J. M. (2014). Surviving coral bleaching events: Porites growth anomalies on the great barrier reef. *PloS one*, 9(2), e88720. <https://doi.org/10.1086/BBLv226n3p187>
- Cao, L., & Caldeira, K. (2008). Atmospheric co2 stabilization and ocean acidification. *Geophysical Research Letters*, 35(19). <https://doi.org/10.1029/2008GL035072>
- Cao, L., Caldeira, K., & Jain, A. K. (2007). Effects of carbon dioxide and climate change on ocean acidification and carbonate mineral saturation. *Geophysical Research Letters*, 34(5). <https://doi.org/10.1029/2006GL028605>
- Carilli, J. E., Godfrey, J., Norris, R. D., Sandin, S. A., & Smith, J. E. (2010). Periodic endolithic algal blooms in montastraea faveolata corals may represent periods of low-level stress. *Bulletin of Marine Science*, 86, 709–718.

- Carpenter, K. E., Abrar, M., Aeby, G., Aronson, R. B., Banks, S., Bruckner, A., Chiriboga, A., Cortés, J., Delbeek, J. C., DeVantier, L., et al. (2008). One-third of reef-building corals face elevated extinction risk from climate change and local impacts. *Science*, 321(5888), 560–563. <https://doi.org/10.1126/science.115919>
- Carreiro-Silva, M., & McClanahan, T. (2012). Macrobioerosion of dead branching porites, 4 and 6 years after coral mass mortality. *Marine Ecology Progress Series*, 458, 103–122. <https://doi.org/10.3354/meps09726>
- Carreiro-Silva, M., McClanahan, T., & Kiene, W. (2005). The role of inorganic nutrients and herbivory in controlling microbioerosion of carbonate substratum. *Coral Reefs*, 24(2), 214–221. <https://doi.org/10.1007/s00338-004-0445-3>
- Carreiro-Silva, M., McClanahan, T., & Kiene, W. (2009). Effects of inorganic nutrients and organic matter on microbial euendolithic community composition and microbioerosion rates. *Marine ecology progress series*, 392, 1–15. <https://doi.org/10.3354/meps08251>
- Carreón-Palau, L., Özdemir, N. Ş., Parrish, C. C., & Parzanini, C. (2020). Sterol composition of sponges, cnidarians, arthropods, mollusks, and echinoderms from the deep northwest atlantic: A comparison with shallow coastal gulf of mexico. *Marine drugs*, 18(12), 598. <https://doi.org/10.3390/md18120598>
- Castillo, K. D., & Lima, F. P. (2010). Comparison of in situ and satellite-derived (modis-aqua/terra) methods for assessing temperatures on coral reefs. *Limnology and Oceanography: Methods*, 8(3), 107–117. <https://doi.org/10.4319/lom.2010.8.0107>
- Castro, B. M., Prieto, M., & Silva, L. C. (2014). Ceramide: A simple sphingolipid with unique biophysical properties. *Progress in lipid research*, 54, 53–67. <https://doi.org/10.1016/j.plipres.2014.01.004>
- Caudales, R., & Wells, J. (1991). Fatty acid composition of free-living anabaena and nostoc cyanobacteria and of cyanobionts from different azolla species. *Nitrogen Fixation: Proceedings of the Fifth International Symposium on Nitrogen Fixation with Non-Legumes, Florence, Italy, 10–14 September 1990*, 563–564. https://doi.org/10.1007/978-94-011-3486-6_122
- Chacón, E., Berrendero, E., & Pichel, F. G. (2006). Biogeological signatures of microbor-ing cyanobacterial communities in marine carbonates from cabo rojo, puerto rico. *Sedimentary Geology*, 185(3-4), 215–228. <https://doi.org/10.1016/j.sedgeo.2005.12.014>

- Chan, N. C., & Connolly, S. R. (2013). Sensitivity of coral calcification to ocean acidification: A meta-analysis. *Global change biology*, 19(1), 282–290. <https://doi.org/10.1111/gcb.12011>
- Chazottes, V., Le Campion-Alsumard, T., & Peyrot-Clausade, M. (1995). Bioerosion rates on coral reefs: Interactions between macroborers, microborers and grazers (moorea, french polynesia). *Palaeogeography, Palaeoclimatology, Palaeoecology*, 113(2–4), 189–198. [https://doi.org/10.1016/0031-0182\(95\)00043-L](https://doi.org/10.1016/0031-0182(95)00043-L)
- Chazottes, V., Le Campion-Alsumard, T., Peyrot-Clausade, M., & Cuet, P. (2002). The effects of eutrophication-related alterations to coral reef communities on agents and rates of bioerosion (reunion island, indian ocean). *Coral reefs*, 21, 375–390. <https://doi.org/10.1007/s00338-002-0259-0>
- Chen, P.-Y., Chen, C.-C., Chu, L., & McCarl, B. (2015). Evaluating the economic damage of climate change on global coral reefs. *Global Environmental Change*, 30, 12–20. <https://doi.org/10.1016/j.gloenvcha.2014.10.011>
- Chen, T.-R., Yu, K.-F., Li, S., Price, G. J., Shi, Q., & Wei, G.-J. (2010). Heavy metal pollution recorded in porites corals from daya bay, northern south china sea. *Marine Environmental Research*, 70(3–4), 318–326. <https://doi.org/10.1016/j.marenvres.2010.06.004>
- Chen, X., D’Olivo, J. P., Wei, G., & McCulloch, M. (2019). Anthropogenic ocean warming and acidification recorded by sr/ca, li/mg, $\delta^{11}\text{B}$ and b/ca in porites coral from the kimberley region of northwestern australia. *Palaeogeography, Palaeoclimatology, Palaeoecology*, 528, 50–59. <https://doi.org/10.1016/j.palaeo.2019.04.033>
- Cherchi, A., Buosi, C., Zuddas, P., & De Giudici, G. (2012). Bioerosion by microbial euendoliths in benthic foraminifera from heavy metal-polluted coastal environments of portovesme (south-western sardinia, italy). *Biogeosciences*, 9(11), 4607–4620. <https://doi.org/10.5194/bg-9-4607-2012>
- Cheroske, A. G., Williams, S. L., & Carpenter, R. C. (2000). Effects of physical and biological disturbances on algal turfs in kaneohe bay, hawaii. *Journal of Experimental Marine Biology and Ecology*, 248(1), 1–34. [https://doi.org/10.1016/S0022-0981\(00\)00153-2](https://doi.org/10.1016/S0022-0981(00)00153-2)
- Chevalier, C., Devenon, J., Pagano, M., Rougier, G., Blanchot, J., & Arfi, R. (2017). The atypical hydrodynamics of the mayotte lagoon (indian ocean): Effects on water age and potential impact on plankton productivity. *Estuarine, Coastal and Shelf Science*, 196, 182–197. <https://doi.org/10.1016/j.ecss.2017.06.027>

- Chevalier, N., Savoye, N., Dubois, S., Lama, M. L., David, V., Lecroart, P., Le Ménach, K., & Budzinski, H. (2015). Precise indices based on n-alkane distribution for quantifying sources of sedimentary organic matter in coastal systems. *Organic Geochemistry*, 88, 69–77. <https://doi.org/10.1016/j.orggeochem.2015.07.006>
- Claustre, H., Marty, J.-C., Cassiani, L., & Dagaut, J. (1988). Fatty acid dynamics in phytoplankton and microzooplankton communities during a spring bloom in the coastal ligurian sea: Ecological implications. *Marine Microbial Food Webs*, 3(2), 51–66.
- Clements, K. D., German, D. P., Piché, J., Tribollet, A., & Choat, J. H. (2017). Integrating ecological roles and trophic diversification on coral reefs: Multiple lines of evidence identify parrotfishes as microphages. *Biological Journal of the Linnean Society*, 120(4), 729–751. <https://doi.org/10.1111/bij.12914>
- Cohen, A. L., Layne, G. D., Hart, S. R., & Lobel, P. S. (2001). Kinetic control of skeletal sr/ca in a symbiotic coral: Implications for the paleotemperature proxy. *Paleoceanography*, 16(1), 20–26. <https://doi.org/10.1029/1999PA000478>
- Cohen, A. L., & McConnaughey, T. A. (2003). Geochemical perspectives on coral mineralization. *Reviews in mineralogy and geochemistry*, 54(1), 151–187. <https://doi.org/10.2113/0540151>
- Cohen, A. L., Owens, K. E., Layne, G. D., & Shimizu, N. (2002). The effect of algal symbionts on the accuracy of sr/ca paleotemperatures from coral. *Science*, 296(5566), 331–333. <https://doi.org/10.1126/science.1069330>
- Coles, S. L., & Strathmann, R. (1973). Observations on coral mucus “flocs” and their potential trophic significance 1. *Limnology and Oceanography*, 18(4), 673–678. <https://doi.org/10.4319/lo.1973.18.4.0673>
- Comeau, S., Cornwall, C., Pupier, C., DeCarlo, T., Alessi, C., Trehern, R., & McCulloch, M. (2019). Flow-driven micro-scale ph variability affects the physiology of corals and coralline algae under ocean acidification. *Scientific Reports*, 9(1), 1–12. <https://doi.org/10.1038/s41598-019-49044-w>
- Comeau, S., Tambutté, E., Carpenter, R., Edmunds, P., Evensen, N., Allemand, D., Ferrier-Pagès, C., Tambutté, S., & Venn, A. (2017). Coral calcifying fluid ph is modulated by seawater carbonate chemistry not solely seawater ph. *Proceedings of the Royal Society B: Biological Sciences*, 284(1847), 20161669. <https://doi.org/10.1098/rspb.2016.1669>

- Comeau, S., Carpenter, R. C., Lantz, C. A., & Edmunds, P. J. (2015). Ocean acidification accelerates dissolution of experimental coral reef communities. *Biogeosciences*, 12(2), 365–372. <https://doi.org/10.5194/bg-12-365-2015>
- Comeau, S., Cornwall, C. E., DeCarlo, T. M., Krieger, E., & McCulloch, M. T. (2018). Similar controls on calcification under ocean acidification across unrelated coral reef taxa. *Global Change Biology*, 24(10), 4857–4868. <https://doi.org/10.1111/gcb.14379>
- Conlan, J. A., Rocker, M. M., & Francis, D. S. (2017). A comparison of two common sample preparation techniques for lipid and fatty acid analysis in three different coral morphotypes reveals quantitative and qualitative differences. *PeerJ*, 5, e3645. <https://doi.org/10.7717/peerj.3645>
- Connell, J. H. (1978). Diversity in tropical rain forests and coral reefs: High diversity of trees and corals is maintained only in a nonequilibrium state. *Science*, 199(4335), 1302–1310. <https://doi.org/10.1126/science.199.4335.1302>
- Conte, M. H., & Eglinton, G. (1993). Alkenone and alkenoate distributions within the euphotic zone of the eastern north atlantic: Correlation with production temperature. *Deep Sea Research Part I: Oceanographic Research Papers*, 40(10), 1935–1961. [https://doi.org/10.1016/0967-0637\(93\)90040-A](https://doi.org/10.1016/0967-0637(93)90040-A)
- Corinaldesi, C., Marcellini, F., Nepote, E., Damiani, E., & Danovaro, R. (2018). Impact of inorganic uv filters contained in sunscreen products on tropical stony corals (acropora spp.) *Science of The Total Environment*, 637, 1279–1285. <https://doi.org/10.1016/j.scitotenv.2018.05.108>
- Corrège, T. (2006). Sea surface temperature and salinity reconstruction from coral geochemical tracers. *Palaeogeography, Palaeoclimatology, Palaeoecology*, 232(2-4), 408–428. <https://doi.org/10.1016/j.palaeo.2005.10.014>
- Cox, P. M., Betts, R. A., Jones, C. D., Spall, S. A., & Totterdell, I. J. (2000). Acceleration of global warming due to carbon-cycle feedbacks in a coupled climate model. *Nature*, 408(6809), 184–187. <https://doi.org/10.1038/35041539>
- Crabbe, M. J. C., & Smith, D. J. (2006). Modelling variations in corallite morphology of galaxea fascicularis coral colonies with depth and light on coastal fringing reefs in the wakatobi marine national park (se sulawesi, indonesia). *Computational Biology and Chemistry*, 30(2), 155–159. <https://doi.org/10.1016/j.compbiolchem.2005.11.004>

- Crandall, J., Teece, M., Estes, B., Manfrino, C., & Ciesla, J. (2016). Nutrient acquisition strategies in mesophotic hard corals using compound specific stable isotope analysis of sterols. *Journal of Experimental Marine Biology and Ecology*, 474, 133–141. <https://doi.org/10.1016/j.jembe.2015.10.010>
- Cremen, M. C. M., Leliaert, E., West, J., Lam, D. W., Shimada, S., Lopez-Bautista, J. M., & Verbruggen, H. (2019). Reassessment of the classification of bryopsidales (chlorophyta) based on chloroplast phylogenomic analyses. *Molecular Phylogenetics and Evolution*, 130, 397–405. <https://doi.org/10.1016/j.ympev.2018.09.009>
- Crossland, C. (1987). In situ release of mucus and doc-lipid from the corals *acropora variabilis* and *stylophora pistillata* in different light regimes. *Coral reefs*, 6(1), 35–42. <https://doi.org/10.1007/BF00302210>
- Crossland, C., Barnes, D., & Borowitzka, M. (1980). Diurnal lipid and mucus production in the staghorn coral *acropora acuminata*. *Marine Biology*, 60, 81–90. <https://doi.org/10.1007/BF00389151>
- Cuif, J.-P., Dauphin, Y., Berthet, P., & Jegoudez, J. (2004). Associated water and organic compounds in coral skeletons: Quantitative thermogravimetry coupled to infrared absorption spectrometry. *Geochemistry, Geophysics, Geosystems*, 5(11). <https://doi.org/10.1029/2004GC000783>
- Cuny-Guirriec, K., Douville, E., Reynaud, S., Allemand, D., Bordier, L., Canesi, M., Mazzoli, C., Taviani, M., Canese, S., McCulloch, M., et al. (2019). Coral li/mg thermometry: Caveats and constraints. *Chemical Geology*, 523, 162–178. <https://doi.org/10.1016/j.chemgeo.2019.03.038>
- Darke, W., & Barnes, D. (1993). Growth trajectories of corallites and ages of polyps in massive colonies of reef-building corals of the genus *porites*. *Marine Biology*, 117, 321–326. <https://doi.org/10.1007/BF00345677>
- Daumas, R., Galois, R., & Thomassin, B. A. (1981). Biochemical composition of soft and hard coral mucus on a new caledonian lagoonal reef. *Proceedings of the 4th International Coral Reef Symposium*, 59–67.
- De Carvalho, C. C., & Caramujo, M. J. (2018). The various roles of fatty acids. *Molecules*, 23(10), 2583. <https://doi.org/10.3390/molecules23102583>
- De Los Rios, A., Wierzbos, J., Sancho, L. G., Green, T. A., & Ascaso, C. (2005). Ecology of endolithic lichens colonizing granite in continental antarctica. *The Lichenologist*, 37(5), 383–395. <https://doi.org/10.1017/S0024282905014969>

- De Ruijter, W. P., Ridderinkhof, H., & Schouten, M. W. (2005). Variability of the south-west indian ocean. *Philosophical Transactions of the Royal Society A: Mathematical, Physical and Engineering Sciences*, 363(1826), 63–76. <https://doi.org/10.1098/rsta.2004.1478>
- De Silva, S. S., Gunasekera, R. M., Austin, C. M., & Allinson, G. (1998). Habitat related variations in fatty acids of catadromous galaxias maculatus. *Aquatic Living Resources*, 11(6), 379–385. [https://doi.org/10.1016/S0990-7440\(99\)80003-5](https://doi.org/10.1016/S0990-7440(99)80003-5)
- De Vos, B. D., Wolterink, J. M., De Jong, P. A., Viergever, M. A., & Išgum, I. (2016). 2d image classification for 3d anatomy localization: Employing deep convolutional neural networks. *Medical imaging 2016: Image processing*, 9784, 517–523. <https://doi.org/10.1117/12.2216971>
- De'Ath, G., Fabricius, K. E., Sweatman, H., & Puotinen, M. (2012). The 27 year decline of coral cover on the great barrier reef and its causes. *Proceedings of the National Academy of Sciences*, 109(44), 17995–17999. <https://doi.org/10.1073/pnas.1208909109>
- de Brebisson, A., & Montana, G. (2015). Deep neural networks for anatomical brain segmentation. *Proceedings of the IEEE conference on computer vision and pattern recognition workshops*, 20–28.
- DeCarlo, T. M., Cohen, A. L., Barkley, H. C., Cobban, Q., Young, C., Shamberger, K. E., Brainard, R. E., & Golbuu, Y. (2015). Coral macrobioerosion is accelerated by ocean acidification and nutrients. *Geology*, 43(1), 7–10. <https://doi.org/10.1130/G36147.1>
- DeCarlo, T. M., D'Olivo, J. P., Foster, T., Holcomb, M., Becker, T., & McCulloch, M. T. (2017). Coral calcifying fluid aragonite saturation states derived from raman spectroscopy. *Biogeosciences*, 14(22), 5253–5269. <https://doi.org/10.5194/bg-14-5253-2017>
- DeCarlo, T. M., Gaetani, G. A., Cohen, A. L., Foster, G. L., Alpert, A. E., & Stewart, J. A. (2016). Coral sr-u thermometry. *Paleoceanography*, 31(6), 626–638. <https://doi.org/10.1002/2015PA002908>
- DeCarlo, T. M., Harrison, H. B., Gajdzik, L., Alaguarda, D., Rodolfo-Metalpa, R., D'Olivo, J., Liu, G., Patalwala, D., & McCulloch, M. T. (2019). Acclimatization of massive reef-building corals to consecutive heatwaves. *Proceedings of the Royal Society B*, 286(1898), 20190235. <https://doi.org/10.1098/rspb.2019.0235>

- DeCarlo, T., Comeau, S., Cornwall, C., & McCulloch, M. (2018). Coral resistance to ocean acidification linked to increased calcium at the site of calcification. *Proceedings of the Royal Society B: Biological Sciences*, 285(1878), 20180564. <https://doi.org/10.1098/rspb.2018.0564>
- Del Campo, J., Pombert, J.-F., Šlapeta, J., Larkum, A., & Keeling, P. J. (2017). The ‘other’ coral symbiont: *Ostreobium* diversity and distribution. *The ISME journal*, 11(1), 296–299. <https://doi.org/10.1038/ismej.2016.101>
- DeLong, K. L., Quinn, T. M., & Taylor, F. W. (2007). Reconstructing twentieth-century sea surface temperature variability in the southwest pacific: A replication study using multiple coral sr/ca records from new caledonia. *Paleoceanography*, 22(4). <https://doi.org/10.1029/2007PA001444>
- DeLong, K. L., Quinn, T. M., Taylor, F. W., Shen, C.-C., & Lin, K. (2013). Improving coral-base paleoclimate reconstructions by replicating 350 years of coral sr/ca variations. *Palaeogeography, Palaeoclimatology, Palaeoecology*, 373, 6–24. <https://doi.org/10.1016/j.palaeo.2012.08.019>
- Dembitsky, V. M., & Srebnik, M. (2002). Natural halogenated fatty acids: Their analogues and derivatives. *Progress in Lipid Research*, 41(4), 315–367. [https://doi.org/10.1016/S0163-7827\(02\)00003-6](https://doi.org/10.1016/S0163-7827(02)00003-6)
- Depledge, M., & Fossi, M. (1994). The role of biomarkers in environmental assessment (2). invertebrates. *Ecotoxicology*, 3(3), 161–172. <https://doi.org/10.1007/BF00117081>
- de Ruijter, W. P., van Aken, H. M., Beier, E. J., Lutjeharms, J. R., Matano, R. P., & Schouten, M. W. (2004). Eddies and dipoles around south madagascar: Formation, pathways and large-scale impact. *Deep Sea Research Part I: Oceanographic Research Papers*, 51(3), 383–400. <https://doi.org/10.1016/j.dsr.2003.10.011>
- Desmond, E., & Gribaldo, S. (2009). Phylogenomics of sterol synthesis: Insights into the origin, evolution, and diversity of a key eukaryotic feature. *Genome biology and evolution*, 1, 364–381. <https://doi.org/10.1093/gbe/evp036>
- Dickson, A. G. (1990). Thermodynamics of the dissociation of boric acid in synthetic seawater from 273.15 to 318.15 k. *Deep Sea Research Part A. Oceanographic Research Papers*, 37(5), 755–766. [https://doi.org/10.1016/0198-0149\(90\)90004-F](https://doi.org/10.1016/0198-0149(90)90004-F)
- Dlugokencky, E., & Tans, P. (2020). Trends in atmospheric carbon dioxide, national oceanic & atmospheric administration, earth system research laboratory (noaa/esrl).

- D'Olive, J. P., Ellwood, G., DeCarlo, T. M., & McCulloch, M. T. (2019). Deconvolving the long-term impacts of ocean acidification and warming on coral biomineralisation. *Earth and Planetary Science Letters*, 526, 115785. <https://doi.org/10.1016/j.epsl.2019.115785>
- D'Olive, J. P., Sinclair, D. J., Rankenburg, K., & McCulloch, M. T. (2018). A universal multi-trace element calibration for reconstructing sea surface temperatures from long-lived porites corals: Removing 'vital-effects'. *Geochimica et Cosmochimica Acta*, 239, 109–135. <https://doi.org/10.1016/j.gca.2018.07.035>
- Doney, S. C., Fabry, V. J., Feely, R. A., & Kleypas, J. A. (2009). Ocean acidification: The other co2 problem. *Annual review of marine science*, 1, 169–192. <https://doi.org/10.1146/annurev.marine.010908.163834>
- Druffel, E. R. (1997). Geochemistry of corals: Proxies of past ocean chemistry, ocean circulation, and climate. *Proceedings of the National Academy of Sciences*, 94(16), 8354–8361. <https://doi.org/10.1073/pnas.94.16.8354>
- Dubinsky, Z., & Stambler, N. (1996). Marine pollution and coral reefs. *Global change biology*, 2(6), 511–526. <https://doi.org/10.1111/j.1365-2486.1996.tb00064.x>
- Duerden, J. E. (1902). *Boring algae as agents in the disintegration of corals* (Vol. 16). By Order of the Trustees of the American Museum of Natural History.
- Dufresne, J.-L., Fairhead, L., Le Treut, H., Berthelot, M., Bopp, L., Ciais, P., Friedlingstein, P., & Monfray, P. (2002). On the magnitude of positive feedback between future climate change and the carbon cycle. *Geophysical Research Letters*, 29(10), 43–1. <https://doi.org/10.1029/2001GL013777>
- Eakin, C. M., Morgan, J. A., Heron, S. F., Smith, T. B., Liu, G., Alvarez-Filip, L., Baca, B., Bartels, E., Bastidas, C., Bouchon, C., et al. (2010). Caribbean corals in crisis: Record thermal stress, bleaching, and mortality in 2005. *PloS one*, 5(11), e13969. <https://doi.org/10.1371/journal.pone.0013969>
- Eder, K. (1995). Gas chromatographic analysis of fatty acid methyl esters. *Journal of Chromatography B: Biomedical Sciences and Applications*, 671(1-2), 113–131. [https://doi.org/10.1016/0378-4347\(95\)00142-6](https://doi.org/10.1016/0378-4347(95)00142-6)
- Edinger, E. N., Jompa, J., Limmon, G. V., Widjatmoko, W., & Risk, M. J. (1998). Reef degradation and coral biodiversity in indonesia: Effects of land-based pollution, destructive fishing practices and changes over time. *Marine Pollution Bulletin*, 36(8), 617–630. [https://doi.org/10.1016/S0025-326X\(98\)00047-2](https://doi.org/10.1016/S0025-326X(98)00047-2)

- Edinger, E. N., Limmon, G. V., Jompa, J., Widjatmoko, W., Heikoop, J. M., & Risk, M. J. (2000). Normal coral growth rates on dying reefs: Are coral growth rates good indicators of reef health? *Marine Pollution Bulletin*, 40(5), 404–425. [https://doi.org/10.1016/S0025-326X\(99\)00237-4](https://doi.org/10.1016/S0025-326X(99)00237-4)
- Ellen, J. S., Graff, C. A., & Ohman, M. D. (2019). Improving plankton image classification using context metadata. *Limnology and Oceanography: Methods*, 17(8), 439–461. <https://doi.org/10.1002/lom3.10324>
- Emerson, S., & Hedges, J. (2008). *Chemical oceanography and the marine carbon cycle*. Cambridge University Press.
- Enochs, I. C., Manzello, D. P., Kolodziej, G., Noonan, S. H., Valentino, L., & Fabricius, K. E. (2016). Enhanced macroboring and depressed calcification drive net dissolution at high-co₂ coral reefs. *Proceedings of the Royal Society B: Biological Sciences*, 283(1842), 20161742. <https://doi.org/10.1098/rspb.2016.1742>
- Enochs, I. C., Manzello, D. P., Tribollet, A., Valentino, L., Kolodziej, G., Donham, E. M., Fitchett, M. D., Carlton, R., & Price, N. N. (2016). Elevated colonization of microborers at a volcanically acidified coral reef. *PLoS One*, 11(7), e0159818. <https://doi.org/10.1371/journal.pone.0159818>
- Enriquez, S., Mendez, E. R., Hoegh-Guldberg, O., & Iglesias-Prieto, R. (2017). Key functional role of the optical properties of coral skeletons in coral ecology and evolution. *Proceedings of the Royal Society B: Biological Sciences*, 284(1853), 20161667. <https://doi.org/10.1098/rspb.2016.1667>
- Enriquez, S., Mendez, E. R., & Prieto, R. I. (2005). Multiple scattering on coral skeletons enhances light absorption by symbiotic algae. *Limnology and Oceanography*, 50(4), 1025–1032. <https://doi.org/10.4319/lo.2005.50.4.1025>
- Fabricius, K. E. (2005). Effects of terrestrial runoff on the ecology of corals and coral reefs: Review and synthesis. *Marine pollution bulletin*, 50(2), 125–146. <https://doi.org/10.1016/j.marpolbul.2004.11.028>
- Fabricius, K. E. (2011). Factors determining the resilience of coral reefs to eutrophication: A review and conceptual model. *Coral reefs: an ecosystem in transition*, 493–505.
- Falini, G., Fermani, S., & Goffredo, S. (2015). Coral biomineralization: A focus on intraskeletal organic matrix and calcification. *Seminars in cell & developmental biology*, 46, 17–26. <https://doi.org/10.1016/j.semcdb.2015.09.005>

- Färber, C., Wisshak, M., Pyko, I., Bellou, N., & Freiwald, A. (2015). Effects of water depth, seasonal exposure, and substrate orientation on microbial bioerosion in the ionian sea (eastern mediterranean). *PloS one*, 10(4), e0126495. <https://doi.org/10.1371/journal.pone.0126495>
- Farre, B., Cuif, J.-P., & Dauphin, Y. (2010). Occurrence and diversity of lipids in modern coral skeletons. *Zoology*, 113(4), 250–257. <https://doi.org/10.1016/j.zool.2009.11.004>
- Feely, R. A., Doney, S. C., & Cooley, S. R. (2009). Ocean acidification: Present conditions and future changes in a high-co₂ world. *Oceanography*, 22(4), 36–47. <https://doi.org/10.5670/oceanog.2009.95>
- Feely, R. A., Sabine, C. L., Lee, K., Berelson, W., Kleypas, J., Fabry, V. J., & Millero, F. J. (2004). Impact of anthropogenic co₂ on the caco₃ system in the oceans. *Science*, 305(5682), 362–366. <https://doi.org/10.1126/science.1097329>
- Fel, J.-P., Lacherez, C., Bensetra, A., Mezzache, S., Béraud, E., Léonard, M., Allemand, D., & Ferrier-Pagès, C. (2019). Photochemical response of the scleractinian coral *stylophora pistillata* to some sunscreen ingredients. *Coral Reefs*, 38(1), 109–122. <https://doi.org/10.1007/s00338-018-01759-4>
- Ferrier-Pagès, C., Leal, M. C., Calado, R., Schmid, D. W., Bertucci, F., Lecchini, D., & Allemand, D. (2021). Noise pollution on coral reefs? a yet underestimated threat to coral reef communities. *Marine Pollution Bulletin*, 165, 112129. <https://doi.org/10.1016/j.marpolbul.2021.112129>
- Fine, M., & Loya, Y. (2002). Endolithic algae: An alternative source of photoassimilates during coral bleaching. *Proceedings of the Royal Society of London. Series B: Biological Sciences*, 269(1497), 1205–1210. <https://doi.org/10.1098/rspb.2002.1983>
- Foo, J. L., Ling, H., Lee, Y. S., & Chang, M. W. (2017). Microbiome engineering: Current applications and its future. *Biotechnology journal*, 12(3), 1600099. <https://doi.org/10.1002/biot.201600099>
- Fordyce, A., Ainsworth, T., & Leggat, W. (2020). Microalgae, a boring bivalve and a corala newly described association between two coral reef bioeroders within their coral host. *Integrative Organismal Biology*, 2(1), obaa035. <https://doi.org/10.1093/iob/obaa035>
- Fordyce, A., Ainsworth, T., & Leggat, W. (2021). Light capture, skeletal morphology, and the biomass of corals' boring endoliths. *MSphere*, 6(1), e00060–21. <https://doi.org/10.1128/mSphere.00060-21>

- Forsman, Z., Wellington, G. M., Fox, G. E., & Toonen, R. J. (2015). Clues to unraveling the coral species problem: Distinguishing species from geographic variation in porites across the pacific with molecular markers and microskeletal traits. *PeerJ*, 3, e751. <https://doi.org/10.7717/peerj.751>
- Försterra, G., Beuck, L., Häussermann, V., & Freiwald, A. (2005). Shallow-water desmophyllum dianthus (scleractinia) from chile: Characteristics of the biocoenoses, the bioeroding community, heterotrophic interactions and (paleo)-bathymetric implications. *Cold-water corals and ecosystems*, 937–977. https://doi.org/10.1007/3-540-27673-4_48
- Fowell, S. E., Sandford, K., Stewart, J. A., Castillo, K. D., Ries, J. B., & Foster, G. L. (2016). Intrareef variations in li/mg and sr/ca sea surface temperature proxies in the caribbean reef-building coral siderastrea siderea. *Paleoceanography*, 31(10), 1315–1329. <https://doi.org/10.1002/2016PA002968>
- Fowell, S., Foster, G., Ries, J., Castillo, K., De La Vega, E., Tyrrell, T., Donald, H., & Chalk, T. (2018). Historical trends in ph and carbonate biogeochemistry on the belize mesoamerican barrier reef system. *Geophysical Research Letters*, 45(7), 3228–3237. <https://doi.org/10.1002/2017GL076496>
- Freiwald, A., Fossâ, J. H., Grehan, A., Koslow, T., & Roberts, J. M. (2004). *Cold-water coral reefs: Out of sight-no longer out of mind*. UNEP-WCMC.
- Friedlingstein, P., Dufresne, J.-L., Cox, P., & Rayner, P. (2003). How positive is the feedback between climate change and the carbon cycle? *Tellus B: Chemical and Physical Meteorology*, 55(2), 692–700. <https://doi.org/10.3402/tellusb.v55i2.16765>
- Friedlingstein, P., Jones, M. W., O'Sullivan, M., Andrew, R. M., Bakker, D. C., Hauck, J., Le Quéré, C., Peters, G. P., Peters, W., Pongratz, J., et al. (2022). Global carbon budget 2021. *Earth System Science Data*, 14(4), 1917–2005. <https://doi.org/10.5194/essd-14-1917-2022>
- Friedmann, E. I., Hua, M., & Ocampo-Friedmann, R. (1988). 3.6 cryptoendolithic lichen and cyanobacterial communities of the ross desert, antarctica. *Polarforschung*, 58(2/3), 251–259.
- Fung, I. Y., Doney, S. C., Lindsay, K., & John, J. (2005). Evolution of carbon sinks in a changing climate. *Proceedings of the National Academy of Sciences*, 102(32), 11201–11206. <https://doi.org/10.1073/pnas.050494910>

- Gagan, M., Ayliffe, L., Beck, J. W., Cole, J., Druffel, E., Dunbar, R. B., & Schrag, D. (2000). New views of tropical paleoclimates from corals. *Quaternary Science Reviews*, 19(1-5), 45–64. [https://doi.org/10.1016/S0277-3791\(99\)00054-2](https://doi.org/10.1016/S0277-3791(99)00054-2)
- Gagnon, A. C., Adkins, J. F., & Erez, J. (2012). Seawater transport during coral biomineralization. *Earth and Planetary Science Letters*, 329, 150–161. <https://doi.org/10.1016/j.epsl.2012.03.005>
- Gagnon, A. C., Adkins, J. F., Fernandez, D. P., & Robinson, L. F. (2007). Sr/ca and mg/ca vital effects correlated with skeletal architecture in a scleractinian deep-sea coral and the role of rayleigh fractionation. *Earth and Planetary Science Letters*, 261(1-2), 280–295. <https://doi.org/10.1016/j.epsl.2007.07.013>
- Galindo-Martinez, C. T., Weber, M., Avila-Magana, V., Enriquez, S., Kitano, H., Medina, M., & Iglesias-Prieto, R. (2022). The role of the endolithic alga *ostreobium* spp. during coral bleaching recovery. *Scientific reports*, 12(1), 1–12. <https://doi.org/10.1038/s41598-022-07017-6>
- Galloway, A. W., & Budge, S. M. (2020). The critical importance of experimentation in biomarker-based trophic ecology. <https://doi.org/10.1098/rstb.2019.0638>
- Garrett, J., Donald, P., & Gaston, K. (2020). Skyglow extends into the world's key biodiversity areas. *Animal conservation*, 23(2), 153–159. <https://doi.org/10.1111/acv.12480>
- Gattuso, J.-P., Allemand, D., & Frankignoulle, M. (1999). Photosynthesis and calcification at cellular, organismal and community levels in coral reefs: A review on interactions and control by carbonate chemistry. *American zoologist*, 39(1), 160–183. <https://doi.org/10.1093/icb/39.1.160>
- Gattuso, J.-P., & Hansson, L. (2011). *Ocean acidification*. Oxford university press.
- Gattuso, J.-P., Mach, K. J., & Morgan, G. (2013). Ocean acidification and its impacts: An expert survey. *Climatic change*, 117(4), 725–738. <https://doi.org/10.1007/s10584-012-0591-5>
- Gaylarde, P. M., Jungblut, A.-D., Gaylarde, C. C., & Neilan, B. A. (2006). Endolithic phototrophs from an active geothermal region in new zealand. *Geomicrobiology Journal*, 23(7), 579–587. <https://doi.org/10.1080/01490450600897401>
- Ghirardelli, L. (2002). Endolithic microorganisms in live and dead thalli of coralline red algae (corallinales, rhodophyta) in the northern adriatic sea. *Acta Geologica Hispanica*, 53–60.

- Girshick, R., Donahue, J., Darrell, T., & Malik, J. (2015). Region-based convolutional networks for accurate object detection and segmentation. *IEEE transactions on pattern analysis and machine intelligence*, 38(1), 142–158. <https://doi.org/10.1109/TPAMI.2015.2437384>
- Glynn, P. W., & Manzello, D. P. (2015). Bioerosion and coral reef growth: A dynamic balance. *Coral reefs in the Anthropocene*, 67–97. https://doi.org/10.1007/978-94-017-7249-5_4
- Godinot, C., Tribollet, A., Grover, R., & Ferrier-Pagès, C. (2012). Bioerosion by eueendoliths decreases in phosphate-enriched skeletons of living corals. *Biogeosciences*, 9(7), 2377–2384. <https://doi.org/10.5194/bg-9-2377-2012>
- Golubic, S., & Schneider, J. (1979). Carbonate dissolution. In *Studies in environmental science* (pp. 107–129). Elsevier. [https://doi.org/10.1016/S0166-1116\(08\)71056-2](https://doi.org/10.1016/S0166-1116(08)71056-2)
- Golubic, S., Friedmann, E. I., & Schneider, J. (1981). The lithobiontic ecological niche, with special reference to microorganisms. *Journal of Sedimentary Research*, 51(2), 475–478. <https://doi.org/10.1306/212F7CB6-2B24-11D7-8648000102C1865D>
- Golubic, S., Perkins, R. D., & Lukas, K. J. (1975). Boring microorganisms and microborings in carbonate substrates. In *The study of trace fossils* (pp. 229–259). Springer. https://doi.org/10.1007/978-3-642-65923-2_12
- Golubic, S., Radtke, G., & Le Campion-Alsumard, T. (2005). Endolithic fungi in marine ecosystems. *Trends in microbiology*, 13(5), 229–235. <https://doi.org/10.1016/j.tim.2005.03.007>
- Golubic, S., & Schneider, J. (2003). Microbial endoliths as internal biofilms. *Fossil and recent biofilms: a natural history of life on earth*, 249–263. https://doi.org/10.1007/978-94-017-0193-8_16
- Golubic, S., Schneider, J., Campion-Alsumard, L., Campbell, S. E., Hook, J. E., Radtke, G., et al. (2019). Approaching microbial bioerosion. *Facies*, 65(3), 1–17. <https://doi.org/10.1007/s10347-019-0568-1>
- Gonzalez-Vila, F. J. (1995). Alkane biomarkers. geochemical significance and application in oil shale geochemistry. *Composition, Geochemistry and Conversion of Oil Shales*, 51–68. https://doi.org/10.1007/978-94-011-0317-6_4
- Goutx, M., Acquaviva, M., & Bertrand, J.-C. (1990). Cellular and extracellular carbohydrates and lipids from marine bacteria during growth on soluble substrates and

- hydrocarbons. *Marine ecology progress series*. Oldendorf, 61(3), 291–296. <https://doi.org/10.3354/MEPS061291>
- Gove, J. M., McManus, M. A., Neuheimer, A. B., Polovina, J. J., Drazen, J. C., Smith, C. R., Merrifield, M. A., Friedlander, A. M., Ehses, J. S., Young, C. W., et al. (2016). Near-island biological hotspots in barren ocean basins. *Nature communications*, 7(1), 10581. <https://doi.org/10.1038/ncomms10581>
- Grange, J., Rybarczyk, H., & Tribollet, A. (2015). The three steps of the carbonate biogenic dissolution process by microborers in coral reefs (new caledonia). *Environmental Science and Pollution Research*, 22(18), 13625–13637. <https://doi.org/10.1007/s11356-014-4069-z>
- Grottoli, A., Rodrigues, L., & Juarez, C. (2004). Lipids and stable carbon isotopes in two species of hawaiian corals, *porites compressa* and *montipora verrucosa*, following a bleaching event. *Marine Biology*, 145(3), 621–631. <https://doi.org/10.1007/s00227-004-1337-3>
- Guérin, M., Dolphin, P. J., & Chapman, M. J. (1993). Familial lecithin: Cholesterol acyltransferase deficiency: Further resolution of lipoprotein particle heterogeneity in the low density interval. *Atherosclerosis*, 104(1-2), 195–212. [https://doi.org/10.1016/0021-9150\(93\)90191-V](https://doi.org/10.1016/0021-9150(93)90191-V)
- Guinotte, J. M., & Fabry, V. J. (2008). Ocean acidification and its potential effects on marine ecosystems. *Annals of the New York Academy of Sciences*, 1134(1), 320–342. <https://doi.org/10.1196/annals.1439.013>
- Gutner-Hoch, E., & Fine, M. (2011). Genotypic diversity and distribution of *ostreobium quekettii* within scleractinian corals. *Coral reefs*, 30(3), 643–650. <https://doi.org/10.1007/s00338-011-0750-6>
- Halldal, P. (1968). Photosynthetic capacities and photosynthetic action spectra of endozoic algae of the massive coral *favia*. *The Biological Bulletin*, 134(3), 411–424. <https://doi.org/10.2307/1539860>
- Hall-Spencer, J. M., Rodolfo-Metalpa, R., Martin, S., Ransome, E., Fine, M., Turner, S. M., Rowley, S. J., Tedesco, D., & Buia, M.-C. (2008). Volcanic carbon dioxide vents show ecosystem effects of ocean acidification. *Nature*, 454(7200), 96–99. <https://doi.org/10.1038/nature07051>
- Halo, I., Backeberg, B., Penven, P., Ansorge, I., Reason, C., & Ullgren, J. (2014). Eddy properties in the mozambique channel: A comparison between observations and two numerical ocean circulation models. *Deep Sea Research Part II: Topical*

- Studies in Oceanography*, 100, 38–53. <https://doi.org/10.1016/j.dsr2.2013.10.015>
- Hammar, L., Ehnberg, J., Mavume, A., Cuamba, B. C., & Molander, S. (2012). Renewable ocean energy in the western indian ocean. *Renewable and Sustainable Energy Reviews*, 16(7), 4938–4950. <https://doi.org/10.1016/j.rser.2012.04.026>
- Han, J., McCarthy, E. D., Hoeven, W. V., Calvin, M., & Bradley, W. (1968). Organic geochemical studies, ii. a preliminary report on the distribution of aliphatic hydrocarbons in algae, in bacteria, and in a recent lake sediment. *Proceedings of the National Academy of Sciences*, 59(1), 29–33. <https://doi.org/10.1073/pnas.59.1.29>
- Hannun, Y. A., Obeid, L. M., & Dbaiibo, G. S. (1996). Ceramide: A novel second messenger and lipid mediator. *Lipid Second Messengers*, 177–204. https://doi.org/10.1007/978-1-4899-1361-6_5
- Harland, A., Navarro, J., Spencer Davies, P., & Fixter, L. (1993). Lipids of some caribbean and red sea corals: Total lipid, wax esters, triglycerides and fatty acids. *Marine Biology*, 117, 113–117. <https://doi.org/10.1007/BF00346432>
- Harvey, H. R., Fallon, R. D., & Patton, J. S. (1986). The effect of organic matter and oxygen on the degradation of bacterial membrane lipids in marine sediments. *Geochimica et Cosmochimica Acta*, 50(5), 795–804. [https://doi.org/10.1016/0016-7037\(86\)90355-8](https://doi.org/10.1016/0016-7037(86)90355-8)
- Hashimoto, K. (2019). Global temperature and atmospheric carbon dioxide concentration. In *Global carbon dioxide recycling* (pp. 5–17). Springer. https://doi.org/10.1007/978-981-13-8584-1_3
- Hatcher, B. G. (1990). Coral reef primary productivity. a hierarchy of pattern and process. *Trends in Ecology & Evolution*, 5(5), 149–155. [https://doi.org/10.1016/0169-5347\(90\)90221-X](https://doi.org/10.1016/0169-5347(90)90221-X)
- Hathorne, E. C., Gagnon, A., Felis, T., Adkins, J., Asami, R., Boer, W., Caillon, N., Case, D., Cobb, K. M., Douville, E., et al. (2013). Interlaboratory study for coral sr/ca and other element/ca ratio measurements. *Geochemistry, Geophysics, Geosystems*, 14(9), 3730–3750. <https://doi.org/10.1002/ggge.20230>
- Hattori, T., Adachi, K., & Shizuri, Y. (1998). New ceramide from marine sponge haliclona koremella and related compounds as antifouling substances against macroalgae. *Journal of natural products*, 61(6), 823–826. <https://doi.org/10.1021/np970527y>

- Hemming, N. G., & Hanson, G. N. (1992). Boron isotopic composition and concentration in modern marine carbonates. *Geochimica et Cosmochimica Acta*, 56(1), 537–543. [https://doi.org/10.1016/0016-7037\(92\)90151-8](https://doi.org/10.1016/0016-7037(92)90151-8)
- Hendy, E., Gagan, M., Lough, J., McCulloch, M., & DeMenocal, P. (2007). Impact of skeletal dissolution and secondary aragonite on trace element and isotopic climate proxies in porites corals. *Paleoceanography*, 22(4). <https://doi.org/10.1029/2007PA001462>
- Hernandez-Agreda, A., Gates, R. D., & Ainsworth, T. D. (2017). Defining the core microbiome in corals' microbial soup. *Trends in microbiology*, 25(2), 125–140. <https://doi.org/10.1016/j.tim.2016.11.003>
- Highsmith, R. C. (1981). Lime-boring algae in hermatypic coral skeletons. *Journal of Experimental Marine Biology and Ecology*, 55(2-3), 267–281. [https://doi.org/10.1016/0022-0981\(81\)90117-9](https://doi.org/10.1016/0022-0981(81)90117-9)
- Highsmith, R. C., Lueptow, R. L., & Schonberg, S. C. (1983). Growth and bioerosion of three massive corals on the belize barrier reef. *Marine ecology progress series. Oldendorf*, 13(2), 261–271.
- Hoegh-Guldberg, O. (1999). Climate change, coral bleaching and the future of the world's coral reefs. *Marine and freshwater research*, 50(8), 839–866. <https://doi.org/10.1071/MF99078>
- Hoegh-Guldberg, O., Cai, R., Poloczanska, E. S., Brewer, P. G., Sundby, S., Hilmi, K., Fabry, V. J., Jung, S., Skirving, W., Stone, D. A., et al. (2014). The ocean.
- Hoegh-Guldberg, O., Mumby, P. J., Hooten, A. J., Steneck, R. S., Greenfield, P., Gomez, E., Harvell, C. D., Sale, P. F., Edwards, A. J., Caldeira, K., et al. (2007). Coral reefs under rapid climate change and ocean acidification. *science*, 318(5857), 1737–1742. <https://doi.org/10.1126/science.1152509>
- Hoegh-Guldberg, O., Poloczanska, E. S., Skirving, W., & Dove, S. (2017). Coral reef ecosystems under climate change and ocean acidification. *Frontiers in Marine Science*, 4, 158. <https://doi.org/10.3389/fmars.2017.00158>
- Holcomb, M., McCorkle, D. C., & Cohen, A. L. (2010). Long-term effects of nutrient and co2 enrichment on the temperate coral *astrangia poculata* (ellis and solander, 1786). *Journal of Experimental Marine Biology and Ecology*, 386(1-2), 27–33. <https://doi.org/10.1016/j.jembe.2010.02.007>

- Holcomb, M., Venn, A., Tambutté, E., Tambutté, S., Allemand, D., Trotter, J., & Mcculloch, M. (2014). Coral calcifying fluid ph dictates response to ocean acidification. *Scientific reports*, 4(1), 5207. <https://doi.org/10.1038/srep05207>
- Holmes, K. E., Edinger, E. N., Limmon, G. V., Risk, M. J., et al. (2000). Bioerosion of live massive corals and branching coral rubble on indonesian coral reefs. *Marine Pollution Bulletin*, 40(7), 606–617. [https://doi.org/10.1016/S0025-326X\(00\)00067-9](https://doi.org/10.1016/S0025-326X(00)00067-9)
- Hood, R. R., Beckley, L. E., & Wiggert, J. D. (2017). Biogeochemical and ecological impacts of boundary currents in the indian ocean. *Progress in Oceanography*, 156, 290–325. <https://doi.org/10.1016/j.pocean.2017.04.011>
- Hood, R., Bange, H., Beal, L., Beckley, L., Burkill, P., Cowie, G., D'Adamo, N., Ganssen, G., Hendon, H., Hermes, J., et al. (2015). Science plan of the second international indian ocean expedition (iioe-2): A basin-wide research program.(2015-2020).
- Hopkinson, B. M., King, A. C., Owen, D. P., Johnson-Roberson, M., Long, M. H., & Bhandarkar, S. M. (2020). Automated classification of three-dimensional reconstructions of coral reefs using convolutional neural networks. *PloS one*, 15(3), e0230671. <https://doi.org/10.1371/journal.pone.0230671>
- Huang, B., Banzon, V. F., Freeman, E., Lawrimore, J., Liu, W., Peterson, T. C., Smith, T. M., Thorne, P. W., Woodruff, S. D., & Zhang, H.-M. (2015). Extended reconstructed sea surface temperature version 4 (ersst. v4). part i: Upgrades and intercomparisons. *Journal of climate*, 28(3), 911–930. <https://doi.org/10.1175/JCLI-D-14-00006.1>
- Huang, B., Thorne, P. W., Banzon, V. F., Boyer, T., Chepurin, G., Lawrimore, J. H., Menne, M. J., Smith, T. M., Vose, R. S., & Zhang, H.-M. (2017). Extended reconstructed sea surface temperature, version 5 (ersstv5): Upgrades, validations, and intercomparisons. *Journal of Climate*, 30(20), 8179–8205. <https://doi.org/10.1175/JCLI-D-16-0836.1>
- Huang, D., Benzoni, F., Fukami, H., Knowlton, N., Smith, N. D., & Budd, A. F. (2014). Taxonomic classification of the reef coral families merulinidae, montastraeidae, and diploastraeidae (cnidaria: Anthozoa: Scleractinia). *Zoological Journal of the Linnean Society*, 171(2), 277–355. <https://doi.org/10.1111/ZOJ.12140>

- Hudson, J. H., Shinn, E. A., Halley, R. B., & Lidz, B. (1976). Sclerochronology: A tool for interpreting past environments. *Geology*, 4(6), 361–364. [https://doi.org/10.1130/0091-7613\(1976\)4<361:SATFIP>2.0.CO;2](https://doi.org/10.1130/0091-7613(1976)4<361:SATFIP>2.0.CO;2)
- Hughes, T. P. (1994). Catastrophes, phase shifts, and large-scale degradation of a caribbean coral reef. *Science*, 265(5178), 1547–1551. <https://doi.org/10.1126/science.265.5178.1547>
- Hughes, T. P., Anderson, K. D., Connolly, S. R., Heron, S. F., Kerry, J. T., Lough, J. M., Baird, A. H., Baum, J. K., Berumen, M. L., Bridge, T. C., et al. (2018). Spatial and temporal patterns of mass bleaching of corals in the anthropocene. *Science*, 359(6371), 80–83. <https://doi.org/10.1126/science.aan8048>
- Hughes, T. P., Kerry, J. T., Álvarez-Noriega, M., Álvarez-Romero, J. G., Anderson, K. D., Baird, A. H., Babcock, R. C., Beger, M., Bellwood, D. R., Berkelmans, R., et al. (2017). Global warming and recurrent mass bleaching of corals. *Nature*, 543(7645), 373–377. <https://doi.org/10.1038/nature21707>
- Hutchings, P. (1986). Biological destruction of coral reefs. *Coral reefs*, 4(4), 239–252. <https://doi.org/10.1007/BF00298083>
- Iha, C., Dougan, K. E., Varela, J. A., Avila, V., Jackson, C. J., Bogaert, K. A., Chen, Y., Judd, L. M., Wick, R., Holt, K. E., et al. (2021). Genomic adaptations to an endolithic lifestyle in the coral-associated alga *ostreobium*. *Current Biology*, 31(7), 1393–1402. <https://doi.org/10.1016/j.cub.2021.01.018>
- Imbs, A. (2013). Fatty acids and other lipids of corals: Composition, distribution, and biosynthesis. *Russian Journal of Marine Biology*, 39, 153–168. <https://doi.org/10.1134/S1063074013030061>
- Inagaki, M., Isobe, R., Kawano, Y., Miyamoto, T., Komori, T., & Higuchi, R. (1998). Isolation and structure of three new ceramides from the starfish *acanthaster planci*. *European journal of organic chemistry*, 1998(1), 129–131. [https://doi.org/10.1002/\(SICI\)1099-0690\(199801\)1998:1<129::AID-EJOC129>3.0.CO;2-A](https://doi.org/10.1002/(SICI)1099-0690(199801)1998:1<129::AID-EJOC129>3.0.CO;2-A)
- Ingalls, A. E., Lee, C., & Druffel, E. R. (2003). Preservation of organic matter in mound-forming coral skeletons. *Geochimica et Cosmochimica Acta*, 67(15), 2827–2841. [https://doi.org/10.1016/S0016-7037\(03\)00079-6](https://doi.org/10.1016/S0016-7037(03)00079-6)
- Irisson, J.-O., Ayata, S.-D., Lindsay, D. J., Karp-Boss, L., & Stemmann, L. (2022). Machine learning for the study of plankton and marine snow from images. *Annual review of marine science*, 14, 277–301. <https://doi.org/10.1146/annurev-marine-041921-013023>

- Isa, Y., & Okazaki, M. (1987). Some observations on the Ca^{2+} -binding phospholipid from scleractinian coral skeletons. *Comparative Biochemistry and Physiology Part B: Comparative Biochemistry*, 87(3), 507–512. [https://doi.org/10.1016/0305-0491\(87\)90045-9](https://doi.org/10.1016/0305-0491(87)90045-9)
- Jafarabadi, A. R., Bakhtiyari, A. R., Toosi, A. S., & Jadot, C. (2017). Spatial distribution, ecological and health risk assessment of heavy metals in marine surface sediments and coastal seawaters of fringing coral reefs of the Persian Gulf, Iran. *Chemosphere*, 185, 1090–1111. <https://doi.org/10.1016/j.chemosphere.2017.07.110>
- Jamieson, G., & Reid, E. (1972). The component fatty acids of some marine algal lipids. *Phytochemistry*, 11(4), 1423–1432. [https://doi.org/10.1016/S0031-9422\(00\)90096-7](https://doi.org/10.1016/S0031-9422(00)90096-7)
- Jeanson, M., Anthony, E. J., Dolique, F., & Cremades, C. (2014). Mangrove evolution in Mayotte Island, Indian Ocean: A 60-year synopsis based on aerial photographs. *Wetlands*, 34(3), 459–468. <https://doi.org/10.1007/s13157-014-0512-7>
- Jeffries, H. P. (1970). Seasonal composition of temperate plankton communities: Fatty acids 1. *Limnology and Oceanography*, 15(3), 419–426. <https://doi.org/10.4319/lo.1970.15.3.0419>
- Johannes, R. (1967). Ecology of organic aggregates in the vicinity of a coral reef. *Limnology and Oceanography*, 12(2), 189–195. <https://doi.org/10.4319/lo.1967.12.2.0189>
- Joint, I., & Morris, R. (1982). The role of bacteria in the turnover of organic matter in the sea. *Oceanogr. Mar. Biol.*, 20, 65–118.
- Junior, P. M. G., Molina, W. F., Affonso, P. R. A., & Aguilar, C. T. (2006). Assessing genetic diversity of Brazilian reef fishes by chromosomal and DNA markers. *Genetica*, 126, 161–177. <https://doi.org/10.1007/s10709-005-1446-z>
- Kapsenberg, L., Alliouane, S., Gazeau, F., Mousseau, L., & Gattuso, J.-P. (2017). Coastal ocean acidification and increasing total alkalinity in the northwestern Mediterranean Sea. *Ocean Science*, 13(3), 411–426. <https://doi.org/10.5194/os-13-411-2017>
- Keck, M., Gisch, N., Moll, H., Vorhölter, F.-J., Gerth, K., Kahmann, U., Lissel, M., Lindner, B., Niehaus, K., & Holst, O. (2011). Unusual outer membrane lipid composition of the gram-negative, lipopolysaccharide-lacking myxobacterium *Sorbus*

- rangium cellulosum so ce56. *Journal of biological chemistry*, 286(15), 12850–12859. <https://doi.org/10.1074/jbc.M110.194209>
- Khotimchenko, S., & Svetashev, V. (1987). Fatty acids of marine macrophytes. *BIOLOGIYA MORYA-MARINE BIOLOGY*, (6), 3–15.
- Kitahara, M. V., Fukami, H., Benzoni, F., & Huang, D. (2016). The new systematics of scleractinia: Integrating molecular and morphological evidence. *The Cnidaria, Past, Present and Future: The world of medusa and her sisters*, 41–59. https://doi.org/10.1007/978-3-319-31305-4_4
- Klein, C. J., Ban, N. C., Halpern, B. S., Beger, M., Game, E. T., Grantham, H. S., Green, A., Klein, T. J., Kininmonth, S., Treml, E., et al. (2010). Prioritizing land and sea conservation investments to protect coral reefs. *PLoS One*, 5(8), e12431. <https://doi.org/10.1371/journal.pone.0012431>
- Kleypas, J. A., & Langdon, C. (2006). Coral reefs and changing seawater carbonate chemistry. *Coastal and Estuarine Studies: Coral Reefs and Climate Change Science and Management*, 61, 73–110.
- Kleypas, J. A., McManus, J. W., & Meñez, L. A. (1999). Environmental limits to coral reef development: Where do we draw the line? *American zoologist*, 39(1), 146–159. <https://doi.org/10.1093/icb/39.1.146>
- Klochko, K., Kaufman, A. J., Yao, W., Byrne, R. H., & Tossell, J. A. (2006). Experimental measurement of boron isotope fractionation in seawater. *Earth and Planetary Science Letters*, 248(1-2), 276–285. <https://doi.org/10.1016/j.epsl.2006.05.034>
- Kneeland, J., Huguen, K., Cervino, J., Hauff, B., & Eglinton, T. (2013). Lipid biomarkers in symbiodinium dinoflagellates: New indicators of thermal stress. *Coral Reefs*, 32, 923–934. <https://doi.org/10.1007/s00338-013-1076-3>
- Knutson, D. W., Buddemeier, R. W., & Smith, S. V. (1972). Coral chronometers: Seasonal growth bands in reef corals. *Science*, 177(4045), 270–272. <https://doi.org/10.1126/science.177.4045.27>
- Kołodziej, B., Golubic, S., Bucur, I. I., Radtke, G., & Tribollet, A. (2012). Early cretaceous record of microboring organisms in skeletons of growing corals. *Lethaia*, 45(1), 34–45. <https://doi.org/10.1111/J.1502-3931.2011.00291.X>
- Kramer, N., Guan, J., Chen, S., Wangpraseurt, D., & Loya, Y. (2022). Morpho-functional traits of the coral stylophora pistillata enhance light capture for photosynthesis at mesophotic depths. *Communications Biology*, 5(1), 861. <https://doi.org/10.1038/s42003-022-03829-4>

- Krizhevsky, A., Sutskever, I., & Hinton, G. E. (2017). Imagenet classification with deep convolutional neural networks. *Communications of the ACM*, 60(6), 84–90. <https://doi.org/10.1145/3065386>
- Kubota, K., Yokoyama, Y., Ishikawa, T., Suzuki, A., & Ishii, M. (2017). Rapid decline in ph of coral calcification fluid due to incorporation of anthropogenic co₂. *Scientific reports*, 7(1), 7694. <https://doi.org/10.1038/s41598-017-07680-0>
- Kühl, M., Holst, G., Larkum, A. W., & Ralph, P. J. (2008). Imaging of oxygen dynamics within the endolithic algal community of the massive coral *Porites lobata*. *Journal of Phycology*, 44(3), 541–550.
- Kumar, P., Gupta, V., Misra, A., Modi, D., & Pandey, B. (2009). Potential of molecular markers in plant biotechnology. *Plant omics*, 2(4), 141–162.
- Laborel, J., & Le Campion-Alsumard, T. (1979). Infestation massive du squelette de coraux vivants par des rhodophycées de type conchocelis.
- Lamb, J. B., Willis, B. L., Fiorenza, E. A., Couch, C. S., Howard, R., Rader, D. N., True, J. D., Kelly, L. A., Ahmad, A., Jompa, J., et al. (2018). Plastic waste associated with disease on coral reefs. *Science*, 359(6374), 460–462. <https://doi.org/10.1126/science.aar3320>
- Langdon, C., & Atkinson, M. (2005). Effect of elevated pco₂ on photosynthesis and calcification of corals and interactions with seasonal change in temperature/irradiance and nutrient enrichment. *Journal of Geophysical Research: Oceans*, 110(C9). <https://doi.org/10.1029/2004JC002576>
- Lauvset, S. K., Gruber, N., Landschützer, P., Olsen, A., & Tjiputra, J. (2015). Trends and drivers in global surface ocean ph over the past 3 decades. *Biogeosciences*, 12(5), 1285–1298. <https://doi.org/10.5194/bg-12-1285-2015>
- Lazareth, C. E., Soares-Pereira, C., Douville, E., Brahmi, C., Dissard, D., Le Cornec, E., Thil, F., Gonzalez-Roubaud, C., Caquineau, S., & Cabioch, G. (2016). Intra-skeletal calcite in a live-collected porites sp.: Impact on environmental proxies and potential formation process. *Geochimica et Cosmochimica Acta*, 176, 279–294. <https://doi.org/10.1016/j.gca.2015.12.020>
- Le Campion Alsumard, T., Golubic, S., & Hutchings, P. (1995). Microbial endoliths in skeletons of live and dead corals: *Porites lobata* (moorea, french polynesia). *Marine Ecology Progress Series*, 149–157. <https://doi.org/10.3354/meps117149>
- Le Campion-Alsumard, T. (1979). Les cyanophycées endolithes marines. systématique, ultrastructure, écologie et biodestruction. *Oceanologica Acta*, 2(2), 143–156.

- Le Campion-Alsumard, T., Golubic, S., & Priess, K. (1995). Fungi in corals: Symbiosis or disease? interaction between polyps and fungi causes pearl-like skeleton biomineralization. *Marine Ecology Progress Series*, 137–147. <https://doi.org/10.3354/meps117137>
- Le Corre, M., & Safford, R. (2001). La réunion and iles eparses. *Important Bird Areas in Africa and associated islands: priority sites for conservation*. Pisces Publications, Newbury & BirdLife International, Cambridge, UK, 693–702.
- Lebreton, L., Van Der Zwet, J., Damsteeg, J.-W., Slat, B., Andrady, A., & Reisser, J. (2017). River plastic emissions to the world's oceans. *Nature communications*, 8(1), 1–10. <https://doi.org/10.1038/ncomms15611>
- Leclercq, N., Gattuso, J.-P., & Jaubert, J. (2002). Primary production, respiration, and calcification of a coral reef mesocosm under increased co₂ partial pressure. *Limnology and Oceanography*, 47(2), 558–564. <https://doi.org/10.4319/lo.2002.47.2.0558>
- LeCun, Y., Bengio, Y., & Hinton, G. (2015). Deep learning. *nature*, 521(7553), 436–444. <https://doi.org/10.1038/nature14539>
- Lee, R. F., & Loeblich III, A. (1971). Distribution of 21: 6 hydrocarbon and its relationship to 22: 6 fatty acid in algae. *Phytochemistry*, 10(3), 593–602. [https://doi.org/10.1016/S0031-9422\(00\)94703-4](https://doi.org/10.1016/S0031-9422(00)94703-4)
- Lesser, M. (2013). Using energetic budgets to assess the effects of environmental stress on corals: Are we measuring the right things? *Coral Reefs*, 32(1), 25–33. <https://doi.org/10.1007/s00338-012-0993-x>
- Leuzinger, S., Anthony, K. R., & Willis, B. L. (2003). Reproductive energy investment in corals: Scaling with module size. *Oecologia*, 136, 524–531. <https://doi.org/10.1007/s00442-003-1305-5>
- Liu, G., Strong, A. E., Skirving, W., & Arzayus, L. F. (2006). Overview of noaa coral reef watch program's near-real time satellite global coral bleaching monitoring activities. *Proceedings of the 10th international coral reef symposium*, 1793, 1783–1793.
- Lo, J.-M., Wang, W.-L., Chiang, Y.-M., & Chen, C.-M. (2001). Ceramides from the taiwan red alga ceratodictyon spongiosum and symbiotic sponge sigmadocia symbiotica. *Journal of the Chinese Chemical Society*, 48(4), 821–826. <https://doi.org/10.1002/jccs.200100118>

- Long, J., Shelhamer, E., & Darrell, T. (2015). Fully convolutional networks for semantic segmentation. *Proceedings of the IEEE conference on computer vision and pattern recognition*, 3431–3440. <https://doi.org/arXiv:1411.4038>
- Lorenzen, W., Bozhüyük, K. A., Cortina, N. S., & Bode, H. B. (2014). A comprehensive insight into the lipid composition of myxococcus xanthus by uplc-esi-ms [s]. *Journal of lipid research*, 55(12), 2620–2633. <https://doi.org/10.1194/jlr.M054593>
- Lough, J. (2008). Coral calcification from skeletal records revisited. *Marine Ecology Progress Series*, 373, 257–264. <https://doi.org/10.3354/meps07398>
- Lough, J., & Cantin, N. E. (2014). Perspectives on massive coral growth rates in a changing ocean. *The Biological Bulletin*, 226(3), 187–202. <https://doi.org/10.1086/BBLv226n3p187>
- Lough, J., & Barnes, D. (1997). Several centuries of variation in skeletal extension, density and calcification in massive porites colonies from the great barrier reef: A proxy for seawater temperature and a background of variability against which to identify unnatural change. *Journal of Experimental Marine Biology and Ecology*, 211(1), 29–67. [https://doi.org/10.1016/S0022-0981\(96\)02710-4](https://doi.org/10.1016/S0022-0981(96)02710-4)
- Lukas, K. (1973). Taxonomy and ecology of the endolithic microflora of reef corals, with a review of the literature on endolithic microphytes, 159 pp. *Unpublished PhD Thesis, University of Rhode Island*.
- Lukas, K. (1974). Two species of the chlorophyte genus ostreobium from skeletons of atlantic and caribbean reef corals 1, 2. *Journal of Phycology*, 10(3), 331–335. <https://doi.org/10.1111/j.1529-8817.1974.tb02722.x>
- Luo, G., Yang, H., Algeo, T. J., Hallmann, C., & Xie, S. (2019). Lipid biomarkers for the reconstruction of deep-time environmental conditions. *Earth-Science Reviews*, 189, 99–124. <https://doi.org/10.1016/j.earscirev.2018.03.005>
- Lutjeharms, J. R. (2006). *The agulhas current retroflexion*. Springer.
- Madan, R., Pankhurst, C., Hawke, B., & Smith, S. (2002). Use of fatty acids for identification of am fungi and estimation of the biomass of am spores in soil. *Soil Biology and Biochemistry*, 34(1), 125–128. [https://doi.org/10.1016/S0038-0717\(01\)00151-1](https://doi.org/10.1016/S0038-0717(01)00151-1)
- Madkaiker, K., Valsala, V., Sreeush, M., Mallissery, A., Chakraborty, K., & Deshpande, A. (2023). Understanding the seasonality, trends, and controlling factors of indian ocean acidification over distinctive bio-provinces. *Journal of Geophysical*

- Research: Biogeosciences*, 128(1), e2022JG006926. <https://doi.org/10.1029/2022JG006926>
- Magnusson, M., Heimann, K., Quayle, P., & Negri, A. P. (2010). Additive toxicity of herbicide mixtures and comparative sensitivity of tropical benthic microalgae. *Marine Pollution Bulletin*, 60(11), 1978–1987. <https://doi.org/10.1016/j.marpolbul.2010.07.031>
- Magnusson, S. H., Fine, M., & Kühl, M. (2007). Light microclimate of endolithic phototrophs in the scleractinian corals *Montipora monasteriata* and *Porites cylindrica*. *Marine Ecology Progress Series*, 332, 119–128. <https://doi.org/10.3354/meps332119>
- Mahmood, A., Bennamoun, M., An, S., Sohel, F., Boussaid, F., Hovey, R., Kendrick, G., & Fisher, R. (2016). Automatic annotation of coral reefs using deep learning. *Oceans 2016 mts/IEEE monterey*, 1–5. <https://doi.org/10.1109/OCEANS.2016.7761105>
- Mantoura, R., & Llewellyn, C. (1983). The rapid determination of algal chlorophyll and carotenoid pigments and their breakdown products in natural waters by reverse-phase high-performance liquid chromatography. *Analytica Chimica Acta*, 151, 297–314. [https://doi.org/10.1016/S0003-2670\(00\)80092-6](https://doi.org/10.1016/S0003-2670(00)80092-6)
- Mao Che, L., Campion-Alsumard, L., Boury-Esnault, N., Payri, C., Golubic, S., Bézac, C., et al. (1996). Biodegradation of shells of the black pearl oyster, *Pinctada margaritifera* var. *cumingii*, by microborers and sponges of French Polynesia. *Marine Biology*, 126(3), 509–519. <https://doi.org/10.1007/BF00354633>
- Marcelino, L. A., Westneat, M. W., Stoyneva, V., Henss, J., Rogers, J. D., Radosevich, A., Turzhitsky, V., Siple, M., Fang, A., Swain, T. D., et al. (2013). Modulation of light-enhancement to symbiotic algae by light-scattering in corals and evolutionary trends in bleaching. *PLoS One*, 8(4), e61492. <https://doi.org/10.1371/journal.pone.0061492>
- Marcelino, V. R., & Verbruggen, H. (2016). Multi-marker metabarcoding of coral skeletons reveals a rich microbiome and diverse evolutionary origins of endolithic algae. *Scientific Reports*, 6(1), 1–9. <https://doi.org/10.1038/srep31508>
- Marubini, F., & Thake, B. (1999). Bicarbonate addition promotes coral growth. *Limnology and Oceanography*, 44(3), 716–720. <https://doi.org/10.4319/lo.1999.44.3.0716>

- Massé, A., Domart-Coulon, I., Golubic, S., Duché, D., & Tribollet, A. (2018). Early skeletal colonization of the coral holobiont by the microboring ulvophyceae *ostreobium* sp. *Scientific reports*, 8(1), 1–11. <https://doi.org/10.1038/s41598-018-20196-5>
- Massé, A., Tribollet, A., Meziane, T., Bourguet-Kondracki, M.-L., Yéprémian, C., Sève, C., Thiney, N., Longeon, A., Couté, A., & Domart-Coulon, I. (2020). Functional diversity of microboring *ostreobium* algae isolated from corals. *Environmental Microbiology*, 22(11), 4825–4846. <https://doi.org/10.1111/jmi.13046>
- Maulucci, G., Cohen, O., Daniel, B., Sansone, A., Petropoulou, P., Filou, S., Spyridonidis, A., Pani, G., De Spirito, M., Chatgililoglu, C., et al. (2016). Fatty acid-related modulations of membrane fluidity in cells: Detection and implications. *Free radical research*, 50(sup1), S40–S50. <https://doi.org/10.1080/10715762.2016.1231403>
- Mawren, D., Blamey, R., Hermes, J., & Reason, C. (2022). On the importance of the mozambique channel for the climate of southeastern africa. *Climate Dynamics*, 1–21. <https://doi.org/10.1007/s00382-022-06334-w>
- Mawren, D., Hermes, J., & Reason, C. (2020). Exceptional tropical cyclone kenneth in the far northern mozambique channel and ocean eddy influences. *Geophysical Research Letters*, 47(16), e2020GL088715. <https://doi.org/10.1029/2020GL088715>
- Mawren, D., Hermes, J., & Reason, C. (2022). Marine heatwaves in the mozambique channel. *Climate Dynamics*, 58(1-2), 305–327. <https://doi.org/10.1007/s00382-021-05909-3>
- McClanahan, T. R., Maina, J. M., & Muthiga, N. A. (2011). Associations between climate stress and coral reef diversity in the western indian ocean. *Global Change Biology*, 17(6), 2023–2032. <https://doi.org/10.1111/j.1365-2486.2011.02395.x>
- McClanahan, T., Aronson, R., Precht, W., & Muthiga, N. (1999). Fleshy algae dominate remote coral reefs of belize. *Coral Reefs*, 18, 61–62. <https://doi.org/10.1007/s003380050155>
- McCook, L. J. (1999). Macroalgae, nutrients and phase shifts on coral reefs: Scientific issues and management consequences for the great barrier reef. *Coral reefs*, 18(4), 357–367. <https://doi.org/10.1007/s003380050213>
- McCulloch, M., Falter, J., Trotter, J., & Montagna, P. (2012). Coral resilience to ocean acidification and global warming through ph up-regulation. *Nature Climate Change*, 2(8), 623–627. <https://doi.org/10.1038/nclimate1473>

- McCulloch, M. T., D'Olivo, J. P., Falter, J., Holcomb, M., & Trotter, J. A. (2017). Coral calcification in a changing world and the interactive dynamics of ph and dic upregulation. *Nature Communications*, 8(1), 15686. <https://doi.org/10.1038/ncomms15686>
- McLaughlin, M. J., Bessey, C., Kendrick, G. A., Keesing, J., & Olsen, Y. S. (2023). Production and accumulation of reef framework by calcifying corals and macroalgae on a remote indian ocean cay. *Biogeosciences*, 20(5), 1011–1026. <https://doi.org/10.5194/bg-20-1011-2023>
- Messmer, V., Pratchett, M., & Clark, T. (2013). Capacity for regeneration in crown of thorns starfish, *acanthaster planci*. *Coral Reefs*, 32(2), 461–461. <https://doi.org/10.1007/s00338-013-1017-1>
- Meyers, P. A. (2003). Applications of organic geochemistry to paleolimnological reconstructions: A summary of examples from the laurentian great lakes. *Organic geochemistry*, 34(2), 261–289. [https://doi.org/10.1016/S0146-6380\(02\)00168-7](https://doi.org/10.1016/S0146-6380(02)00168-7)
- Meyers, P. A., Quinn, J. G., & Marshall, N. (1974). A method for analysis of fatty acids in coral. *Limnology and Oceanography*, 19(5), 846–848. <https://doi.org/10.4319/lo.1974.19.5.0846>
- Méziane, T., d'Agata, F., & Lee, S. Y. (2006). Fate of mangrove organic matter along a subtropical estuary: Small-scale exportation and contribution to the food of crab communities. *Marine Ecology Progress Series*, 312, 15–27. <https://doi.org/10.3354/meps312015>
- Mikola, J., & Setälä, H. (1998). No evidence of trophic cascades in an experimental microbial-based soil food web. *Ecology*, 79(1), 153–164. [https://doi.org/10.1890/0012-9658\(1998\)079\[0153:NEOTCI\]2.0.CO;2](https://doi.org/10.1890/0012-9658(1998)079[0153:NEOTCI]2.0.CO;2)
- Min, G. R., Edwards, R. L., Taylor, F. W., Recy, J., Gallup, C. D., & Beck, J. W. (1995). Annual cycles of uca in coral skeletons and uca thermometry. *Geochimica et Cosmochimica Acta*, 59(10), 2025–2042. [https://doi.org/10.1016/0016-7037\(95\)00124-7](https://doi.org/10.1016/0016-7037(95)00124-7)
- Mitchell, T. M., & Mitchell, T. M. (1997). *Machine learning* (Vol. 1). McGraw-hill New York.
- Mitsuguchi, T., Matsumoto, E., Abe, O., Uchida, T., & Isdale, P. J. (1996). Mg/ca thermometry in coral skeletons. *Science*, 274(5289), 961–963. <https://doi.org/10.1126/science.274.5289.961>

- Moberg, F., & Folke, C. (1999). Ecological goods and services of coral reef ecosystems. *Ecological economics*, 29(2), 215–233. [https://doi.org/10.1016/S0921-8009\(99\)00009-9](https://doi.org/10.1016/S0921-8009(99)00009-9)
- Moeskops, P., Viergever, M. A., Mendrik, A. M., De Vries, L. S., Benders, M. J., & Išgum, I. (2016). Automatic segmentation of mr brain images with a convolutional neural network. *IEEE transactions on medical imaging*, 35(5), 1252–1261. <https://doi.org/10.1109/TMI.2016.2548501>
- Moeskops, P., Wolterink, J. M., Van Der Velden, B. H., Gilhuijs, K. G., Leiner, T., Viergever, M. A., & Išgum, I. (2016). Deep learning for multi-task medical image segmentation in multiple modalities. *Medical Image Computing and Computer-Assisted Intervention–MICCAI 2016: 19th International Conference, Athens, Greece, October 17–21, 2016, Proceedings, Part II* 19, 478–486. https://doi.org/10.1007/978-3-319-46723-8_55
- Monaco, C. L., Metzl, N., Fin, J., Mignon, C., Cuët, P., Douville, E., Gehlen, M., Chau, T. T. T., & Tribollet, A. (2021). Distribution and long-term change of the sea surface carbonate system in the mozambique channel (1963–2019). *Deep Sea Research Part II: Topical Studies in Oceanography*, 186, 104936. <https://doi.org/10.1016/j.dsr2.2021.104936>
- Montaggioni, L., & Faure, G. (1980). Les récifs coralliens de l’archipel des mascareignes. *Coll. Trav. Univ. Réunion*.
- Montagna, P., McCulloch, M., Douville, E., Correa, M. L., Trotter, J., Rodolfo-Metalpa, R., Dissard, D., Ferrier-Pagès, C., Frank, N., Freiwald, A., et al. (2014). Li/mg systematics in scleractinian corals: Calibration of the thermometer. *Geochimica et Cosmochimica Acta*, 132, 288–310. <https://doi.org/10.1016/j.gca.2014.02.005>
- Morse, J. W., Arvidson, R. S., & Lüttge, A. (2007). Calcium carbonate formation and dissolution. *Chemical reviews*, 107(2), 342–381. <https://doi.org/10.1021/cr050358j>
- Moss, B. (1968). Studies on the degradation of chlorophyll a and carotenoids in freshwaters. *New Phytologist*, 67(1), 49–59. <https://doi.org/10.1111/j.1469-8137.1968.tb05453.x>
- Mouchi, V., Chapron, L., Peru, E., Pruski, A. M., Meistertzheim, A.-L., Vétion, G., Galand, P. E., & Lartaud, F. (2019). Long-term aquaria study suggests species-specific responses of two cold-water corals to macro-and microplastics exposure. *Environmental Pollution*, 253, 322–329. <https://doi.org/10.1016/j.envpol.2019.07.024>

- Mudge, S. M., & Norris, C. E. (1997). Lipid biomarkers in the conwy estuary (north wales, uk): A comparison between fatty alcohols and sterols. *Marine Chemistry*, 57(1-2), 61–84. [https://doi.org/10.1016/S0304-4203\(97\)00010-8](https://doi.org/10.1016/S0304-4203(97)00010-8)
- Mueller, B., de Goeij, J. M., Vermeij, M. J., Mulders, Y., van der Ent, E., Ribes, M., & van Duyl, F. C. (2014). Natural diet of coral-excavating sponges consists mainly of dissolved organic carbon (doc). *PloS one*, 9(2), e90152. <https://doi.org/10.1371/journal.pone.0090152>
- Muko, S., Kawasaki, K., Sakai, K., Takasu, F., & Shigesada, N. (2000). Morphological plasticity in the coral *Porites sillimaniani* and its adaptive significance. *Bulletin of Marine Science*, 66(1), 225–239.
- Mukwaya, G. M., & Welch, D. F. (1989). Subgrouping of pseudomonas cepacia by cellular fatty acid composition. *Journal of Clinical Microbiology*, 27(12), 2640–2646. <https://doi.org/10.1128/jcm.27.12.2640-2646.1989>
- Mumby, P. J., & Harborne, A. R. (2010). Marine reserves enhance the recovery of corals on caribbean reefs. *Plos one*, 5(1), e8657.
- Muscantine, L., & Porter, J. W. (1977). Reef corals: Mutualistic symbioses adapted to nutrient-poor environments. *Bioscience*, 27(7), 454–460. <https://doi.org/10.2307/1297526>
- Nama, S., Shanmughan, A., Nayak, B. B., Bhushan, S., & Ramteke, K. (2023). Impacts of marine debris on coral reef ecosystem: A review for conservation and ecological monitoring of the coral reef ecosystem. *Marine Pollution Bulletin*, 189, 114755. <https://doi.org/10.1016/j.marpolbul.2023.114755>
- Nes, W. D., Norton, R. A., Crumley, F. G., Madigan, S. J., & Katz, E. R. (1990). Sterol phylogeny and algal evolution. *Proceedings of the National Academy of Sciences*, 87(19), 7565–7569. <https://doi.org/10.1073/pnas.87.19.7565>
- Neumann, A. C. (1966). Observations on coastal erosion in bermuda and measurements of the boring rate of the sponge, *cliona lampa* 1, 2. *Limnology and Oceanography*, 11(1), 92–108. <https://doi.org/10.4319/lo.1966.11.1.0092>
- Nieminen, P., Käkälä, R., Mäkinen, T., Laine, O., Takalo, T., & Mustonen, A.-M. (2018). Preservation of fatty acid signatures in three vertebrate species after six months of storage at various temperatures. *PloS one*, 13(9), e0204207. <https://doi.org/10.1371/journal.pone.0204207>

- Nordby, H. E., & Nagy, S. (1971). Comparative citrus fatty acid profiles of triglycerides, monogalactosyl diglycerides, steryl esters and esterified steryl glucosides. *Lipids*, 6(8), 554–561. <https://doi.org/10.1007/BF02531135>
- Nothdurft, L. D., & Webb, G. E. (2009). Earliest diagenesis in scleractinian coral skeletons: Implications for palaeoclimate-sensitive geochemical archives. *Facies*, 55, 161–201. <https://doi.org/10.1007/s10347-008-0167-z>
- Obura, D., Gudka, M., Abdou Rabi, E., Bacha Gian, S., Bijoux, J., Freed, S., Maharavo, J., Mwaura, J., Porter, S., Sola, E., et al. (2017). Coral reef status report for the western indian ocean. global coral reef monitoring network (gcrmn). *International Coral Reef Initiative (ICRI)*, 144.
- Obura, D., Gudka, M., Samoilys, M., Osuka, K., Mbugua, J., Keith, D. A., Porter, S., Roche, R., van Hooideonk, R., Ahamada, S., et al. (2022). Vulnerability to collapse of coral reef ecosystems in the western indian ocean. *Nature Sustainability*, 5(2), 104–113. <https://doi.org/10.1038/s41893-021-00817-0>
- Obura, D. O. (2005). Resilience and climate change: Lessons from coral reefs and bleaching in the western indian ocean. *Estuarine, coastal and shelf science*, 63(3), 353–372. <https://doi.org/10.1016/j.ecss.2004.11.010>
- Odum, H. T., & Odum, E. P. (1955). Trophic structure and productivity of a windward coral reef community on eniwetok atoll. *Ecological monographs*, 25(3), 291–320. <https://doi.org/10.2307/1943285>
- Orenstein, E. C., Ayata, S.-D., Maps, F., Becker, É. C., Benedetti, F., Biard, T., de Garidel-Thoron, T., Ellen, J. S., Ferrario, F., Giering, S. L., et al. (2022). Machine learning techniques to characterize functional traits of plankton from image data. *Limnology and oceanography*, 67(8), 1647–1669. <https://doi.org/10.1002/lno.12101>
- Ow, Y., & Todd, P. (2010). Light-induced morphological plasticity in the scleractinian coral *goniastrea pectinata* and its functional significance. *Coral reefs*, 29, 797–808. <https://doi.org/10.1007/s00338-010-0631-4>
- Parrish, C., Abrajano, T., Budge, S., Helleur, R., Hudson, E., Pulchan, K., & Ramos, C. (2000). Lipid and phenolic biomarkers in marine ecosystems: Analysis and applications. *Marine chemistry*, 193–223. https://doi.org/10.1007/10683826_8
- Parrish, C. (2013). Lipids in marine ecosystems. *International Scholarly Research Notices*, 2013. <https://doi.org/10.5402/2013/604045>

- Patterson, G. W., & VanValkenburg, S. D. (1991). Sterols of cephalopores (trentepohliaceae), a parasitic green alga. *Journal of phycology*, 27(4), 549–551. <https://doi.org/10.1111/j.0022-3646.1991.00549.x>
- Pereira, H., Barreira, L., Figueiredo, F., Custódio, L., Vizetto-Duarte, C., Polo, C., Rešek, E., Engelen, A., & Varela, J. (2012). Polyunsaturated fatty acids of marine macroalgae: Potential for nutritional and pharmaceutical applications. *Marine drugs*, 10(9), 1920–1935. <https://doi.org/10.3390/md10091920>
- Pernice, M., Raina, J.-B., Räddecker, N., Cárdenas, A., Pogoreutz, C., & Voolstra, C. R. (2020). Down to the bone: The role of overlooked endolithic microbiomes in reef coral health. *The ISME journal*, 14(2), 325–334. <https://doi.org/10.1038/s41396-019-0548-z>
- Perry, C., & Hepburn, L. (2008). Syn-depositional alteration of coral reef framework through bioerosion, encrustation and cementation: Taphonomic signatures of reef accretion and reef depositional events. *Earth-Science Reviews*, 86(1-4), 106–144. <https://doi.org/10.1016/j.earscirev.2007.08.006>
- Perry, C., Spencer, T., & Kench, P. (2008). Carbonate budgets and reef production states: A geomorphic perspective on the ecological phase-shift concept. *Coral Reefs*, 27(4), 853–866. <https://doi.org/10.1007/s00338-008-0418-z>
- Perry, C. T. (1998). Grain susceptibility to the effects of microboring: Implications for the preservation of skeletal carbonates. *Sedimentology*, 45(1), 39–51. <https://doi.org/10.1046/j.1365-3091.1998.00134.x>
- Pica, D., Tribollet, A., Golubic, S., Bo, M., Di Camillo, C. G., Bavestrello, G., & Puce, S. (2016). Microboring organisms in living stylasterid corals (cnidaria, hydrozoa). *Marine Biology Research*, 12(6), 573–582. <https://doi.org/10.1080/17451000.2016.1169298>
- Poole, S. K., & Poole, C. E. (2003). Separation methods for estimating octanol–water partition coefficients. *Journal of Chromatography B*, 797(1-2), 3–19. <https://doi.org/10.1016/j.jchromb.2003.08.032>
- Pressé, G. (2022). Les terres australes et antarctiques françaises: Des territoires au cœur des enjeux de la planète. *Civitas Europa*, (1), 281–312.
- Priess, K., Le Campion-Alsumard, T., Golubic, S., Gadel, F., Thomassin, B., et al. (2000). Fungi in corals: Black bands and density-banding of porites lutea and p. lobata skeleton. *Marine Biology*, 136(1), 19–27. <https://doi.org/10.1007/s002270050003>

- Quod, J.-P., Barrere, A., Chabanet, P., Durville, P., Nicet, J.-B., & Garnier, R. (2007). La situation des récifs coralliens des îles éparses françaises de l'océan indien. *Revue d'Ecologie, Terre et Vie*, 62(1), 3–16.
- Ralph, P., Larkum, A., & Kühl, M. (2007). Photobiology of endolithic microorganisms in living coral skeletons: 1. pigmentation, spectral reflectance and variable chlorophyll fluorescence analysis of endoliths in the massive corals *Cyphastrea serailia*, *Porites lutea* and *Goniastrea australensis*. *Marine Biology*, 152(2), 395–404. <https://doi.org/10.1007/s00227-007-0694-0>
- Ram, S., & Erez, J. (2021). The distribution coefficients of major and minor elements in coral skeletons under variable calcium seawater concentrations. *Frontiers in Earth Science*, 9, 657176. <https://doi.org/10.3389/feart.2021.657176>
- Ranjan, R. K., Routh, J., Klump, J. V., & Ramanathan, A. (2015). Sediment biomarker profiles trace organic matter input in the Pichavaram mangrove complex, south-eastern India. *Marine Chemistry*, 171, 44–57. <https://doi.org/10.1016/j.marchem.2015.02.001>
- Reaka-Kudla, M. L. (1997). The global biodiversity of coral reefs: A comparison with rain forests. *Biodiversity II: Understanding and protecting our biological resources*, 2, 551.
- Reed, E. V., Thompson, D. M., Cole, J. E., Lough, J. M., Cantin, N. E., Cheung, A. H., Tudhope, A., Vetter, L., Jimenez, G., & Edwards, R. L. (2021). Impacts of coral growth on geochemistry: Lessons from the Galápagos Islands. *Paleoceanography and Paleoclimatology*, 36(4), e2020PA004051. <https://doi.org/10.1029/2020PA004051>
- Reichert, J., Schellenberg, J., Schubert, P., & Wilke, T. (2018). Responses of reef building corals to microplastic exposure. *Environmental Pollution*, 237, 955–960. <https://doi.org/10.1016/j.envpol.2017.11.006>
- Reyes-Nivia, C., Diaz-Pulido, G., Kline, D., Guldberg, O.-H., & Dove, S. (2013). Ocean acidification and warming scenarios increase microbioerosion of coral skeletons. *Global Change Biology*, 19(6), 1919–1929. <https://doi.org/10.1111/gcb.12158>
- Ricci, F., Rossetto Marcelino, V., Blackall, L. L., Kühl, M., Medina, M., & Verbruggen, H. (2019). Beneath the surface: Community assembly and functions of the coral skeleton microbiome. *Microbiome*, 7(1), 1–10. <https://doi.org/10.1186/s40168-019-0762-y>

- Ricci, F., Tandon, K., Moßhammer, M., Cho, E. H.-J., Blackall, L. L., Kühl, M., & Verbruggen, H. (2023). Fine-scale mapping of physicochemical and microbial landscapes of the coral skeleton. *Environmental Microbiology*. <https://doi.org/10.1111/1462-2920.16369>
- Richmond, M. (2011). *A field guide to the seashores of eastern africa and the western indian ocean islands*.
- Risk, M., Sammarco, P., & Edinger, E. (1995). Bioerosion in acropora across the continental shelf of the great barrier reef. *Coral reefs*, 14, 79–86. <https://doi.org/10.1007/BF00303427>
- Rix, L., de Goeij, J. M., Mueller, C. E., Struck, U., Middelburg, J. J., van Duyl, F. C., Al-Horani, F. A., Wild, C., Naumann, M. S., & van Oevelen, D. (2016). Coral mucus fuels the sponge loop in warm-and cold-water coral reef ecosystems. *Scientific reports*, 6(1), 18715. <https://doi.org/10.1038/srep18715>
- Roberts, M. J., Ternon, J.-F., & Morris, T. (2014). Interaction of dipole eddies with the western continental slope of the mozambique channel. *Deep Sea Research Part II: Topical Studies in Oceanography*, 100, 54–67. <https://doi.org/10.1016/j.dsr2.2013.10.016>
- Romero, I. C., & Feakins, S. J. (2011). Spatial gradients in plant leaf wax d/h across a coastal salt marsh in southern california. *Organic geochemistry*, 42(6), 618–629. <https://doi.org/10.1016/j.orggeochem.2011.04.001>
- Ronneberger, O., Fischer, P., & Brox, T. (2015). U-net: Convolutional networks for biomedical image segmentation. *Medical Image Computing and Computer Assisted Intervention MICCAI 2015: 18th International Conference, Munich, Germany, October 5-9, 2015, Proceedings, Part III* 18, 234–241. <https://doi.org/10.48550/arXiv.1505.04597>
- Rose, C. S., & Risk, M. J. (1985). Increase in cliona delitrix infestation of montastrea cavernosa heads on an organically polluted portion of the grand cayman fringing reef. *Marine Ecology*, 6(4), 345–363. <https://doi.org/10.1111/j.1439-0485.1985.tb00142.x>
- Ross, C. L., DeCarlo, T. M., & McCulloch, M. T. (2019). Environmental and physiochemical controls on coral calcification along a latitudinal temperature gradient in western australia. *Global change biology*, 25(2), 431–447. <https://doi.org/10.1111/gcb.14488>

- Roxy, M. K., Ritika, K., Terray, P., & Masson, S. (2014). The curious case of indian ocean warming. *Journal of Climate*, 27(22), 8501–8509. <https://doi.org/10.1175/JCLI-D-14-00471.1>
- Russ, G. R., & McCook, L. J. (1999). Potential effects of a cyclone on benthic algal production and yield to grazers on coral reefs across the central great barrier reef. *Journal of Experimental Marine Biology and Ecology*, 235(2), 237–254. [https://doi.org/10.1016/S0022-0981\(98\)00180-4](https://doi.org/10.1016/S0022-0981(98)00180-4)
- Rust, C. M., Aelion, C. M., & Flora, J. R. (2000). Control of ph during denitrification in subsurface sediment microcosms using encapsulated phosphate buffer. *Water Research*, 34(5), 1447–1454. [https://doi.org/10.1016/S0043-1354\(99\)00287-0](https://doi.org/10.1016/S0043-1354(99)00287-0)
- Rütters, H., Sass, H., Cypionka, H., & Rullkötter, J. (2002). Phospholipid analysis as a tool to study complex microbial communities in marine sediments. *Journal of microbiological methods*, 48(2-3), 149–160. [https://doi.org/10.1016/S0167-7012\(01\)00319-0](https://doi.org/10.1016/S0167-7012(01)00319-0)
- Sadler, J., Webb, G. E., Nothdurft, L. D., & Dechnik, B. (2014). Geochemistry-based coral palaeoclimate studies and the potential of ‘non-traditional’ (non-massive porites) corals: Recent developments and future progression. *Earth-Science Reviews*, 139, 291–316. <https://doi.org/10.1016/j.earscirev.2014.10.002>
- Saetre, R., & Da Silva, A. J. (1982). Water masses and circulation of the mozambique channel.
- Saliot, A. (1981). Natural hydrocarbons in sea water alain saliot. In *Elsevier oceanography series* (pp. 327–374). Elsevier. [https://doi.org/10.1016/S0422-9894\(08\)70333-7](https://doi.org/10.1016/S0422-9894(08)70333-7)
- Sallam, A., El-Metwally, M., Sabry, M. A., & Elsbaey, M. (2021). Cladamide: A new ceramide from the endophytic fungus cladosporium cladosporioides. *Natural Product Research*, 1–10. <https://doi.org/10.1080/14786419.2021.1986709>
- Sammarco, P. W. (1982). Echinoid grazing as a structuring force in coral communities: Whole reef manipulations. *Journal of Experimental Marine Biology and Ecology*, 61(1), 31–55. [https://doi.org/10.1016/0022-0981\(82\)90020-X](https://doi.org/10.1016/0022-0981(82)90020-X)
- Sánchez-Baracaldo, P., Bianchini, G., Wilson, J. D., & Knoll, A. H. (2022). Cyanobacteria and biogeochemical cycles through earth history. *Trends in Microbiology*, 30(2), 143–157. <https://doi.org/10.1016/j.tim.2021.05.008>

- Sanger, J. E. (1988). Fossil pigments in paleoecology and paleolimnology. *Palaeogeography, Palaeoclimatology, Palaeoecology*, 62(1-4), 343–359. [https://doi.org/10.1016/0031-0182\(88\)90061-2](https://doi.org/10.1016/0031-0182(88)90061-2)
- Sargent, J., Gatten, R., & McIntosh, R. (1977). Wax esters in the marine environment—their occurrence, formation, transformation and ultimate fates. *Marine Chemistry*, 5(4-6), 573–584. [https://doi.org/10.1016/0304-4203\(77\)90043-3](https://doi.org/10.1016/0304-4203(77)90043-3)
- Sarmiento, J. L., & Sundquist, E. (1992). Revised budget for the oceanic uptake of anthropogenic carbon dioxide. *Nature*, 356(6370), 589–593. <https://doi.org/10.1038/356589a0>
- Sauvage, T., Schmidt, W. E., Suda, S., & Fredericq, S. (2016). A metabarcoding framework for facilitated survey of endolithic phototrophs with tufa. *BMC ecology*, 16(1), 1–21. <https://doi.org/10.1186/s12898-016-0068-x>
- Sayani, H. R., Cobb, K. M., Cohen, A. L., Elliott, W. C., Nurhati, I. S., Dunbar, R. B., Rose, K. A., & Zaunbrecher, L. K. (2011). Effects of diagenesis on paleoclimate reconstructions from modern and young fossil corals. *Geochimica et Cosmochimica Acta*, 75(21), 6361–6373. <https://doi.org/10.1016/j.gca.2011.08.026>
- Schätzle, P.-K., Wisshak, M., Bick, A., Freiwald, A., & Kieneker, A. (2021). Exploring confocal laser scanning microscopy (clsm) and fluorescence staining as a tool for imaging and quantifying traces of marine microbioerosion and their trace-making microendoliths. *Journal of Microscopy*, 284(2), 118–131. <https://doi.org/10.1111/jmi.13046>
- Schlichter, D., Kampmann, H., & Conrad, S. (1997). Trophic potential and photoecology of endolithic algae living within coral skeletons. *Marine Ecology*, 18(4), 299–317. <https://doi.org/10.1111/j.1439-0485.1997.tb00444.x>
- Schlichter, D., Zscharnack, B., & Krisch, H. (1995). Transfer of photoassimilates from endolithic algae to coral tissue. *Naturwissenschaften*, 82(12), 561–564. <https://doi.org/10.1007/BF01140246>
- Schneider, J., & Le Campion-Alsumard, T. (1999). Construction and destruction of carbonates by marine and freshwater cyanobacteria. *European Journal of Phycology*, 34(4), 417–426. <https://doi.org/10.1080/09670269910001736472>
- Schneider, J., & Torunski, H. (1983). Biokarst on limestone coasts, morphogenesis and sediment production. *Marine Ecology*, 4(1), 45–63. <https://doi.org/10.1111/j.1439-0485.1983.tb00287.x>

- Schoepf, V., Carrion, S. A., Pfeifer, S. M., Naugle, M., Dugal, L., Bruyn, J., & McCulloch, M. T. (2019). Stress-resistant corals may not acclimatize to ocean warming but maintain heat tolerance under cooler temperatures. *Nature communications*, 10(1), 4031. <https://doi.org/10.1038/s41467-019-12065-0>
- Schönberg, C. H. (2008). A history of sponge erosion: From past myths and hypotheses to recent approaches. *Current developments in bioerosion*, 165–202. https://doi.org/10.1007/978-3-540-77598-0_9
- Schönberg, C. H., Fang, J. K., Carreiro-Silva, M., Tribollet, A., & Wisshak, M. (2017). Bio-erosion: The other ocean acidification problem. *ICES Journal of Marine Science*, 74(4), 895–925. <https://doi.org/10.1093/icesjms/fsw254>
- Schott, F. A., & McCreary Jr, J. P. (2001). The monsoon circulation of the indian ocean. *Progress in Oceanography*, 51(1), 1–123. [https://doi.org/10.1016/S0079-6611\(01\)00083-0](https://doi.org/10.1016/S0079-6611(01)00083-0)
- Schott, F. A., Xie, S.-P., & McCreary Jr, J. P. (2009). Indian ocean circulation and climate variability. *Reviews of Geophysics*, 47(1). <https://doi.org/10.1029/2007RG000245>
- Schouten, M. W., de Ruijter, W. P., Van Leeuwen, P. J., & Ridderinkhof, H. (2003). Eddies and variability in the mozambique channel. *Deep Sea Research Part II: Topical Studies in Oceanography*, 50(12-13), 1987–2003. [https://doi.org/10.1016/S0967-0645\(03\)00042-0](https://doi.org/10.1016/S0967-0645(03)00042-0)
- Scoffin, T. P. (1993). Microfabrics of carbonate muds in reefs. *Carbonate microfabrics*, 65–74. https://doi.org/10.1007/978-1-4684-9421-1_5
- Scoffin, T. (1992). Taphonomy of coral reefs: A review. *Coral reefs*, 11(2), 57–77. <https://doi.org/10.1007/BF00357423>
- Scoffin, T., CW, S., CM, H., IG, H., et al. (1980). Calcium carbonate budget of a fringing reef on the west coast of barbados. ii. erosion, sediments and internal structure.
- Scott, P., & Risk, M. J. (1988). The effect of lithophaga (bivalvia: Mytilidae) boreholes on the strength of the coral porites lobata. *Coral reefs*, 7(3), 145–151. <https://doi.org/10.1007/BF00300974>
- Seemann, J., Sawall, Y., Auel, H., & Richter, C. (2013). The use of lipids and fatty acids to measure the trophic plasticity of the coral stylophora subseriata. *Lipids*, 48, 275–286. <https://doi.org/10.1007/s11745-012-3747-1>
- Sen Gupta, A., Thomsen, M., Benthuyssen, J. A., Hobday, A. J., Oliver, E., Alexander, L. V., Burrows, M. T., Donat, M. G., Feng, M., Holbrook, N. J., et al. (2020). Drivers and

- impacts of the most extreme marine heatwave events. *Scientific reports*, 10(1), 19359. <https://doi.org/10.1038/s41598-020-75445-3>
- Shashar, N., & Stambler, N. (1992). Endolithic algae within corals-life in an extreme environment. *Journal of Experimental Marine Biology and Ecology*, 163(2), 277–286. [https://doi.org/10.1016/0022-0981\(92\)90055-F](https://doi.org/10.1016/0022-0981(92)90055-F)
- Sheikh, M., Higuchi, T., Fujimura, H., Imo, T., Miyagi, T., & Oomori, T. (2009). Contamination and impacts of new antifouling biocide irgarol-1051 on subtropical coral reef waters. *International Journal of Environmental Science & Technology*, 6(3), 353–358. <https://doi.org/10.1007/BF03326073>
- Shibata, K., & Haxo, F. T. (1969). Light transmission and spectral distribution through epi-and endozoic algal layers in the brain coral, favia. *The Biological Bulletin*, 136(3), 461–468. <https://doi.org/10.2307/1539688>
- Sicre, M.-A., & Ternois, Y. (2006). Les biomarqueurs organiques en paléo-océanographie. *Océanis: Série de documents océanographiques*, 30(2), 229–238.
- Sikes, E. L., & Volkman, J. K. (1993). Calibration of alkenone unsaturation ratios (uk'37) for paleotemperature estimation in cold polar waters. *Geochimica et Cosmochimica Acta*, 57(8), 1883–1889. [https://doi.org/10.1016/0016-7037\(93\)90120-L](https://doi.org/10.1016/0016-7037(93)90120-L)
- Silbiger, N. J., Guadayol, Ò., Thomas, F. I., & Donahue, M. J. (2014). Reefs shift from net accretion to net erosion along a natural environmental gradient. *Marine Ecology Progress Series*, 515, 33–44. <https://doi.org/10.3354/meps10999>
- Silva, L. O., Resende, M., Galhardas, H., Manquinho, V., & Lynce, I. (2022). Deepdata: Machine learning in the marine ecosystems. *Expert Systems with Applications*, 206, 117841. <https://doi.org/10.1016/j.eswa.2022.117841>
- Sinclair, M., Arnason, R., Csirke, J., Karnicki, Z., Sigurjonsson, J., Skjoldal, H. R., & Valdimarsson, G. (2002). Responsible fisheries in the marine ecosystem. *Fisheries Research*, 58(3), 255–265. [https://doi.org/10.1016/S0165-7836\(02\)00168-6](https://doi.org/10.1016/S0165-7836(02)00168-6)
- Song, X.-P., Huang, C., Saatchi, S. S., Hansen, M. C., & Townshend, J. R. (2015). Annual carbon emissions from deforestation in the amazon basin between 2000 and 2010. *PloS one*, 10(5), e0126754. <https://doi.org/10.1371/journal.pone.0126754>
- Spalding, M., Spalding, M. D., Ravilious, C., Green, E. P., et al. (2001). *World atlas of coral reefs*. Univ of California Press.
- Spurgeon, J. P. (1992). The economic valuation of coral reefs. *Marine pollution bulletin*, 24(11), 529–536. [https://doi.org/10.1016/0025-326X\(92\)90704-A](https://doi.org/10.1016/0025-326X(92)90704-A)

- Stanley Jr, G. D., & Fautin, D. G. (2001). The origins of modern corals. *Science*, 291(5510), 1913–1914. <https://doi.org/10.1126/science.1056632>
- Stauber, J. L., & Jeffrey, S. (1988). Photosynthetic pigments in fifty-one species of marine diatoms. *Journal of Phycology*, 24(2), 158–172. <https://doi.org/10.1111/j.1529-8817.1988.tb04230.x>
- Stolarski, J., Kitahara, M. V., Miller, D. J., Cairns, S. D., Mazur, M., & Meibom, A. (2011). The ancient evolutionary origins of scleractinia revealed by azooxanthellate corals. *BMC evolutionary biology*, 11(1), 1–11. <https://doi.org/10.1186/1471-2148-11-316>
- Studivan, M. S., Milstein, G., & Voss, J. D. (2019). *Montastraea cavernosa* corallite structure demonstrates distinct morphotypes across shallow and mesophotic depth zones in the gulf of mexico. *PLoS One*, 14(3), e0203732. <https://doi.org/10.1371/journal.pone.0203732>
- Sully, S., Burkepile, D. E., Donovan, M., Hodgson, G., & Van Woesik, R. (2019). A global analysis of coral bleaching over the past two decades. *Nature communications*, 10(1), 1–5. <https://doi.org/10.1038/s41467-019-09238-2>
- Sun, A. Y., & Scanlon, B. R. (2019). How can big data and machine learning benefit environment and water management: A survey of methods, applications, and future directions. *Environmental Research Letters*, 14(7), 073001. <https://doi.org/10.1088/1748-9326/ab1b7d>
- Sutton, M. D. (2008). Tomographic techniques for the study of exceptionally preserved fossils. *Proceedings of the Royal Society B: Biological Sciences*, 275(1643), 1587–1593. <https://doi.org/10.1098/rspb.2008.0263>
- Swain, T. D., Lax, S., Lake, N., Grooms, H., Backman, V., & Marcelino, L. A. (2018). Relating coral skeletal structures at different length scales to growth, light availability to symbiodinium, and thermal bleaching. *Frontiers in Marine Science*, 5, 450. <https://doi.org/10.3389/fmars.2018.00450>
- Szmant, A. M. (2002). Nutrient enrichment on coral reefs: Is it a major cause of coral reef decline? *Estuaries*, 25(4), 743–766. <https://doi.org/10.1007/BF02804903>
- Tafforeau, P., Boistel, R., Boller, E., Bravin, A., Brunet, M., Chaimanee, Y., Cloetens, P., Feist, M., Hoszowska, J., Jaeger, J.-J., et al. (2006). Applications of x-ray synchrotron microtomography for non-destructive 3d studies of paleontological specimens. *Applied Physics A*, 83(2), 195–202. <https://doi.org/10.1007/s00339-006-3507-2>

- Tambutté, S., Holcomb, M., Ferrier-Pagès, C., Reynaud, S., Tambutté, É., Zoccola, D., & Allemand, D. (2011). Coral biomineralization: From the gene to the environment. *Journal of Experimental Marine Biology and Ecology*, 408(1-2), 58–78. <https://doi.org/10.1016/j.jembe.2011.07.026>
- Tanaka, I., Matsuoka, S., Murata, M., & Tachibana, K. (1998). A new ceramide with a novel branched-chain fatty acid isolated from the epiphytic dinoflagellate *Cochyloea monotis*. *Journal of natural products*, 61(5), 685–688. <https://doi.org/10.1021/np970554o>
- Tandon, K., Pasella, M. M., Iha, C., Ricci, F., Hu, J., O’Kelly, C. J., Medina, M., Kühl, M., & Verbruggen, H. (2022). Every refuge has its price: *Ostreobium* as a model for understanding how algae can live in rock and stay in business. *Seminars in Cell & Developmental Biology*. <https://doi.org/10.1016/j.semcdb.2022.03.010>
- Tandon, K., Ricci, F., Costa, J., Medina, M., Kühl, M., Blackall, L. L., & Verbruggen, H. (2023). Genomic view of the diversity and functional role of archaea and bacteria in the skeleton of the reef-building corals *Porites lutea* and *Isopora palifera*. *GigaScience*, 12, giac127. <https://doi.org/10.1093/gigascience/giac127>
- Tarique, M., & Rahaman, W. (2022). Recent ocean acidification trends from boron isotope ($\delta^{11}\text{B}$) records of coral: Role of oceanographic processes and anthropogenic CO_2 forcing. *Journal of Earth System Science*, 131(3), 165. <https://doi.org/10.1007/s12040-022-01907-z>
- Taylor, J., & Parkes, R. J. (1983). The cellular fatty acids of the sulphate-reducing bacteria, *Desulfobacter* sp., *Desulfobulbus* sp. and *Desulfovibrio desulfuricans*. *Microbiology*, 129(11), 3303–3309. <https://doi.org/10.1099/00221287-129-11-3303>
- Taylor, P. D., & Jones, C. G. (1993). Skeletal ultrastructure in the cyclostome bryozoan *Hornera*. *Acta Zoologica*, 74(2), 135–143. <https://doi.org/10.1111/j.1463-6395.1993.tb01230.x>
- Tchernov, D., Gorbunov, M. Y., De Vargas, C., Narayan Yadav, S., Milligan, A. J., Hägblom, M., & Falkowski, P. G. (2004). Membrane lipids of symbiotic algae are diagnostic of sensitivity to thermal bleaching in corals. *Proceedings of the National Academy of Sciences*, 101(37), 13531–13535. <https://doi.org/10.1073/pnas.0402907101>

- Teh, L. S., Teh, L. C., & Sumaila, U. R. (2013). A global estimate of the number of coral reef fishers. *PLoS One*, 8(6), e65397. <https://doi.org/10.1371/journal.pone.0065397>
- Teran, E., Mendez, E. R., Enriquez, S., & Iglesias-Prieto, R. (2010). Multiple light scattering and absorption in reef-building corals. *Applied optics*, 49(27), 5032–5042. <https://doi.org/10.1364/AO.49.005032>
- Teshima, S. (1991). Sterols of crustaceans, molluscs, and fishes. *Physiology and biochemistry of sterols*, 229–259.
- Tisthammer, K. H., Timmins-Schiffman, E., Seneca, F. O., Nunn, B. L., & Richmond, R. H. (2021). Physiological and molecular responses of lobe coral indicate nearshore adaptations to anthropogenic stressors. *Scientific Reports*, 11(1), 3423. <https://doi.org/10.1038/s41598-021-82569-7>
- Todd, P. A., Ladle, R. J., Lewin-Koh, N., & Chou, L. M. (2004). Genotype × environment interactions in transplanted clones of the massive corals *favia speciosa* and *diploastrea heliopora*. *Marine Ecology Progress Series*, 271, 167–182. <https://doi.org/10.3354/meps271167>
- Tomczak, M., & Godfrey, J. S. (2003). *Regional oceanography: An introduction*. Daya books.
- Towle, E. K., Enochs, I. C., & Langdon, C. (2015). Threatened caribbean coral is able to mitigate the adverse effects of ocean acidification on calcification by increasing feeding rate. *PloS one*, 10(4), e0123394. <https://doi.org/10.1371/journal.pone.0123394>
- Tran, T., Kannoorpatti, K., Padovan, A., & Thennadil, S. (2021). Effect of ph regulation by sulfate-reducing bacteria on corrosion behaviour of duplex stainless steel 2205 in acidic artificial seawater. *Royal Society open science*, 8(1), 200639. <https://doi.org/10.1098/rsos.200639>
- Treignier, C., Grover, R., Ferrier-Pages, C., & Tolosa, I. (2008). Effect of light and feeding on the fatty acid and sterol composition of zooxanthellae and host tissue isolated from the scleractinian coral *turbinaria reniformis*. *Limnology and Oceanography*, 53(6), 2702–2710. <https://doi.org/10.4319/lo.2008.53.6.2702>
- Tribollet, A., Decherf, G., Hutchings, P., & Peyrot-Clausade, M. (2002). Large-scale spatial variability in bioerosion of experimental coral substrates on the great barrier reef (australia): Importance of microborers. *Coral reefs*, 21, 424–432. <https://doi.org/10.1007/s00338-002-0267-0>

- Tribollet, A. (2008). The boring microflora in modern coral reef ecosystems: A review of its roles. *Current developments in bioerosion*, 67–94. https://doi.org/10.1007/978-3-540-77598-0_4
- Tribollet, A., Chauvin, A., & Cuet, P. (2019). Carbonate dissolution by reef microbial borers: A biogeological process producing alkalinity under different pco2 conditions. *Facies*, 65(2), 1–10. <https://doi.org/10.1007/s10347-018-0548-x>
- Tribollet, A., Godinot, C., Atkinson, M., & Langdon, C. (2009). Effects of elevated pco2 on dissolution of coral carbonates by microbial euendoliths. *Global Biogeochemical Cycles*, 23(3). <https://doi.org/10.1029/2008GB003286>
- Tribollet, A., & Golubic, S. (2005). Cross-shelf differences in the pattern and pace of bioerosion of experimental carbonate substrates exposed for 3 years on the northern great barrier reef, australia. *Coral reefs*, 24(3), 422–434. <https://doi.org/10.1007/s00338-005-0003-7>
- Tribollet, A., & Golubic, S. (2011). Reef bioerosion: Agents and processes. In *Coral reefs: An ecosystem in transition* (pp. 435–449). Springer. https://doi.org/10.1007/978-94-007-0114-4_25
- Tribollet, A., Langdon, C., Golubic, S., & Atkinson, M. (2006). Endolithic microflora are major primary producers in dead carbonate substrates of hawaiian coral reefs 1. *Journal of Phycology*, 42(2), 292–303. <https://doi.org/10.1111/j.1529-8817.2006.00198.x>
- Tribollet, A., & Payri, C. (2001). Bioerosion of the coralline alga hydrolithon onkodes by microborers in the coral reefs of moorea, french polynesia. *Oceanologica acta*, 24(4), 329–342. [https://doi.org/10.1016/S0399-1784\(01\)01150-1](https://doi.org/10.1016/S0399-1784(01)01150-1)
- Trotter, J., Montagna, P., McCulloch, M., Silenzi, S., Reynaud, S., Mortimer, G., Martin, S., Ferrier-Pagès, C., Gattuso, J.-P., & Rodolfo-Metalpa, R. (2011). Quantifying the ph ‘vital effect’ in the temperate zooxanthellate coral *cladocora caespitosa*: Validation of the boron seawater ph proxy. *Earth and Planetary Science Letters*, 303(3-4), 163–173. <https://doi.org/10.1016/j.epsl.2011.01.030>
- Trudgill, S. (1976). The marine erosion of limestones on aldabra atoll, indian ocean. *Zeitschrift fur Geomorphologie NF*, 164–200.
- Valsala, V., Maksyutov, S., & Murtugudde, R. (2012). A window for carbon uptake in the southern subtropical indian ocean. *Geophysical research letters*, 39(17). <https://doi.org/10.1029/2012GL052857>

- Van der Werf, G. R., Morton, D. C., DeFries, R. S., Olivier, J. G., Kasibhatla, P. S., Jackson, R. B., Collatz, G. J., & Randerson, J. T. (2009). Co₂ emissions from forest loss. *Nature geoscience*, 2(11), 737–738. <https://doi.org/10.1038/ngeo671>
- Verbruggen, H., Marcelino, V. R., Guiry, M. D., Cremen, M. C. M., & Jackson, C. J. (2017). Phylogenetic position of the coral symbiont *ostreobium* (ulvophyceae) inferred from chloroplast genome data. *Journal of Phycology*, 53(4), 790–803. <https://doi.org/10.1111/jpy.12540>
- Verbruggen, H., & Tribollet, A. (2011). Boring algae. *Current Biology*, 21(21), R876–R877.
- Vermeij, M. J., Van Moorselaar, I., Engelhard, S., Hörnlein, C., Vonk, S. M., & Visser, P. M. (2010). The effects of nutrient enrichment and herbivore abundance on the ability of turf algae to overgrow coral in the caribbean. *PloS one*, 5(12), e14312. <https://doi.org/10.1371/journal.pone.0014312>
- Veron, J. (1986). Corals of australia and the indo-pacific. angus and robertson, north ryde. NSW.
- Veron, J. (1996). Evolution in corals. *The Paleontological Society Papers*, 1, 7–38. <https://doi.org/10.1017/S1089332600000036>
- Vignal, A., Milan, D., SanCristobal, M., & Eggen, A. (2002). A review on snp and other types of molecular markers and their use in animal genetics. *Genetics selection evolution*, 34(3), 275–305. <https://doi.org/10.1051/gse:2002009>
- Vinayachandran, P. N. M., Masumoto, Y., Roberts, M. J., Huggett, J. A., Halo, I., Chatterjee, A., Amol, P., Gupta, G. V., Singh, A., Mukherjee, A., et al. (2021). Reviews and syntheses: Physical and biogeochemical processes associated with upwelling in the indian ocean. *Biogeosciences*, 18(22), 5967–6029. <https://doi.org/10.5194/bg-18-5967-2021>
- Vogel, K., Gektidis, M., Golubic, S., Kiene, W. E., & Radtke, G. (2000). Experimental studies on microbial bioerosion at lee stocking island, bahamas and one tree island, great barrier reef, australia: Implications for paleoecological reconstructions. *Lethaia*, 33(3), 190–204. <https://doi.org/10.1080/00241160025100053>
- Volkman, J., Jeffrey, S., Nichols, P., Rogers, G., & Garland, C. (1989). Fatty acid and lipid composition of 10 species of microalgae used in mariculture. *Journal of experimental marine biology and ecology*, 128(3), 219–240. [https://doi.org/10.1016/0022-0981\(89\)90029-4](https://doi.org/10.1016/0022-0981(89)90029-4)

- Volkman, J. K. (1986). A review of sterol markers for marine and terrigenous organic matter. *Organic geochemistry*, 9(2), 83–99. [https://doi.org/10.1016/0146-6380\(86\)90089-6](https://doi.org/10.1016/0146-6380(86)90089-6)
- Volkman, J. K. (2003). Sterols in microorganisms. *Applied Microbiology & Biotechnology*, 60(5). <https://doi.org/10.1007/s00253-002-1172-8>
- Volkman, J. K. (2006). Lipid markers for marine organic matter. *Marine organic matter: biomarkers, isotopes and DNA*, 27–70. https://doi.org/10.1007/698_2_002
- Voshall, A., Christie, N. T., Rose, S. L., Khasin, M., Van Etten, J. L., Markham, J. E., Riekhof, W. R., & Nickerson, K. W. (2021). Sterol biosynthesis in four green algae: A bioinformatic analysis of the ergosterol versus phytosterol decision point. *Journal of Phycology*, 57(4), 1199–1211. <https://doi.org/10.1111/jpy.13164>
- Wagner, D., Friedlander, A. M., Pyle, R. L., Brooks, C. M., Gjerde, K. M., & Wilhelm, T. (2020). Coral reefs of the high seas: Hidden biodiversity hotspots in need of protection. *Frontiers in Marine Science*, 7, 567428. <https://doi.org/10.3389/fmars.2020.567428>
- Wakeham, S. G., & Canuel, E. A. (1988). Organic geochemistry of particulate matter in the eastern tropical north pacific ocean: Implications for particle dynamics. *Journal of Marine Research*, 46(1), 183–213. <https://doi.org/10.1357/002224088785113748>
- Wanders, J. (1976). The role of benthic algae in the shallow reef of curacao (netherlands antilles). i: Primary productivity in the coral reef. *Aquatic Botany*, 2, 235–270. [https://doi.org/10.1016/0304-3770\(76\)90023-1](https://doi.org/10.1016/0304-3770(76)90023-1)
- Wangpraseurt, D., Larkum, A. W., Ralph, P. J., & Kühl, M. (2012). Light gradients and optical microniches in coral tissues. *Frontiers in microbiology*, 3, 316. <https://doi.org/10.3389/fmicb.2012.00316>
- Watanabe, T., Gagan, M. K., Corrège, T., Scott-Gagan, H., Cowley, J., & Hantoro, W. S. (2003). Oxygen isotope systematics in diploastrea heliopora: New coral archive of tropical paleoclimate. *Geochimica et Cosmochimica Acta*, 67(7), 1349–1358. [https://doi.org/10.1016/S0016-7037\(02\)01221-8](https://doi.org/10.1016/S0016-7037(02)01221-8)
- Watanabe, T., Watanabe, T. K., Yamazaki, A., Yoneta, S., Sowa, K., Sinniger, F., Eyal, G., Loya, Y., & Harii, S. (2019). Coral sclerochronology: Similarities and differences in the coral isotopic signatures between mesophotic and shallow-water reefs. In *Mesophotic coral ecosystems* (pp. 667–681). Springer. https://doi.org/10.1007/978-3-319-92735-0_36

- Weete, J. D., & Weber, D. J. (1980). Lipid metabolism during fungal development. *Lipid biochemistry of fungi and other organisms*, 300–316. https://doi.org/10.1007/978-1-4757-0064-0_11
- Wei, G., Wang, Z., Ke, T., Liu, Y., Deng, W., Chen, X., Xu, J., Zeng, T., & Xie, L. (2015). Decadal variability in seawater pH in the western Pacific: Evidence from coral $\delta^{11}\text{B}$ records. *Journal of Geophysical Research: Oceans*, 120(11), 7166–7181. <https://doi.org/10.1002/2015JC011066>
- Wei, H.-Z., Zhao, Y., Liu, X., Wang, Y.-J., Lei, F., Wang, W.-Q., Li, Y.-C., & Lu, H.-Y. (2021). Evolution of paleo-climate and seawater pH from the late Permian to postindustrial periods recorded by boron isotopes and B/Ca in biogenic carbonates. *Earth-Science Reviews*, 215, 103546. <https://doi.org/10.1016/j.earscirev.2021.103546>
- Wells, S., & Ravilious, C. (2006). *In the front line: Shoreline protection and other ecosystem services from mangroves and coral reefs*. UNEP/Earthprint.
- Wells, S. M. (2008). *National and regional networks of marine protected areas: A review of progress*. UNEP-WCMC/UNEP.
- West, K., & Van Woesik, R. (2001). Spatial and temporal variance of river discharge on Okinawa (Japan): Inferring the temporal impact on adjacent coral reefs. *Marine Pollution Bulletin*, 42(10), 864–872. [https://doi.org/10.1016/S0025-326X\(01\)00040-6](https://doi.org/10.1016/S0025-326X(01)00040-6)
- White, D., Davis, W., Nickels, J., King, J., & Bobbie, R. (1979). Determination of the sedimentary microbial biomass by extractable lipid phosphate. *Oecologia*, 51–62.
- Wijsman-Best, M. (1980). Indo-Pacific coral species belonging to the subfamily Montastreae Vaughan & Wells, 1943 (Scleractinia-Coelenterata) part II. The genera Cyphastrea, Leptastrea, Echinopora and Diploastrea. *Zoologische Mededelingen*, 55(21), 235–263.
- Wisshak, M. (2012). Microbioerosion. In *Developments in sedimentology* (pp. 213–243). Elsevier. <https://doi.org/10.1016/B978-0-444-53813-0.00008-3>
- Wisshak, M., Gektidis, M., Freiwald, A., & Lundälv, T. (2005). Bioerosion along a bathymetric gradient in a cold-temperate setting (Kosterfjord, SW Sweden): An experimental study. *Facies*, 51(1-4), 93–117. <https://doi.org/10.1007/s10347-005-0009-1>

- Wisshak, M., & Rüggeberg, A. (2006). Colonisation and bioerosion of experimental substrates by benthic foraminiferans from euphotic to aphotic depths (kosterfjord, sw sweden). *Facies*, 52(1), 1–17. <https://doi.org/10.1007/s10347-005-0033-1>
- Wisshak, M., Seunß, B., & Nützel, A. (2008). Evolutionary implications of an exceptionally preserved carboniferous microboring assemblage in the buckhorn asphalt lagerstätte (oklahoma, usa). *Current developments in bioerosion*, 21–54. https://doi.org/10.1007/978-3-540-77598-0_2
- Wisshak, M., & Tapanila, L. (2008). *Current developments in bioerosion*. Springer Science & Business Media.
- Woodhead, A. J., Hicks, C. C., Norström, A. V., Williams, G. J., & Graham, N. A. (2019). Coral reef ecosystem services in the anthropocene. *Functional Ecology*, 33(6), 1023–1034. <https://doi.org/10.1111/1365-2435.13331>
- Wu, H. C., Dissard, D., Douville, E., Blamart, D., Bordier, L., Tribollet, A., Le Cornec, F., Pons-Branchu, E., Dapoigny, A., & Lazareth, C. E. (2018). Surface ocean ph variations since 1689 ce and recent ocean acidification in the tropical south pacific. *Nature Communications*, 9(1), 1–13. <https://doi.org/10.1038/s41467-018-04922-1>
- Yahel, G., Marie, D., Beninger, P. G., Eckstein, S., & Genin, A. (2009). In situ evidence for pre-capture qualitative selection in the tropical bivalve lithophaga simplex. *Aquatic Biology*, 6, 235–246. <https://doi.org/10.3354/ab00131>
- Yang, S.-H., & Tang, S.-L. (2019). Endolithic microbes in coral skeletons: Algae or bacteria? In *Symbiotic microbiomes of coral reefs sponges and corals* (pp. 43–53). Springer. https://doi.org/10.1007/978-94-024-1612-1_4
- Yap, H. T. (2004). Differential survival of coral transplants on various substrates under elevated water temperatures. *Marine Pollution Bulletin*, 49(4), 306–312. <https://doi.org/10.1016/j.marpolbul.2004.02.017>
- Yates, K., & Halley, R. (2006). CO_3^{2-} concentration and pCO_2 thresholds for calcification and dissolution on the molokai reef flat, hawaii. *Biogeosciences*, 3(3), 357–369. <https://doi.org/10.5194/bg-3-357-2006>
- Zeebe, R. E., & Wolf-Gladrow, D. (2001). *CO₂ in seawater: Equilibrium, kinetics, isotopes*. Gulf Professional Publishing.
- Zhang, Y., Yang, Q., Ling, J., Long, L., Huang, H., Yin, J., Wu, M., Tang, X., Lin, X., Zhang, Y., et al. (2021). Shifting the microbiome of a coral holobiont and improving host

- physiology by inoculation with a potentially beneficial bacterial consortium. *BMC microbiology*, 21(1), 1–14. <https://doi.org/10.1186/s12866-021-02167-5>
- Zhang, Y., & Golubic, S. (1987). Endolithic microfossils (cyanophyta) from early proterozoic stromatolites, hebei, china. *Acta Micropaleontol. Sin*, 4, 1–3.
- Zhila, N. O., Kalacheva, G. S., & Volova, T. G. (2011). Effect of salinity on the biochemical composition of the alga botryococcus braunii kütz ippas h-252. *Journal of Applied Phycology*, 23(1), 47–52. <https://doi.org/10.1007/s10811-010-9532-8>
- Zhukova, N. V., & Aizdaicher, N. A. (1995). Fatty acid composition of 15 species of marine microalgae. *Phytochemistry*, 39(2), 351–356. [https://doi.org/10.1016/0031-9422\(94\)00913-E](https://doi.org/10.1016/0031-9422(94)00913-E)
- Zhukova, N. V., & Titlyanov, E. A. (2003). Fatty acid variations in symbiotic dinoflagellates from okinawan corals. *Phytochemistry*, 62(2), 191–195. [https://doi.org/10.1016/S0031-9422\(02\)00371-0](https://doi.org/10.1016/S0031-9422(02)00371-0)
- Zinke, J., d’Olivo, J. P., Gey, C. J., McCulloch, M. T., Bruggemann, J. H., Lough, J. M., & Guillaume, M. M. (2019). Multi-trace-element sea surface temperature coral reconstruction for the southern mozambique channel reveals teleconnections with the tropical atlantic. *Biogeosciences*, 16(3), 695–712. <https://doi.org/10.5194/bg-16-695-2019>
- Zinke, J., Pfeiffer, M., Timm, O., Dullo, W.-C., Kroon, D., & Thomassin, B. (2008). Mayotte coral reveals hydrological changes in the western indian ocean between 1881 and 1994. *Geophysical Research Letters*, 35(23). <https://doi.org/10.1029/2008GL035634>
- Zinke, J., Rountrey, A., Feng, M., Xie, S.-P., Dissard, D., Rankenburg, K., Lough, J., & McCulloch, M. (2014). Corals record long-term leeuwin current variability including ningaloo niño/niña since 1795. *Nature Communications*, 5(1), 3607. <https://doi.org/10.1038/ncomms4607>

)